

Fröhlich Polarons

Lecture course including detailed theoretical derivations*

Jozef T. L. Devreese

Theory of Quantum and Complex Systems (TQC), Universiteit Antwerpen,

CDE, Universiteitsplein, 1, B-2610 Antwerpen, Belgium

(Dated: December 3, 2020)

arXiv:1611.06122v5 [cond-mat.other] 2 Dec 2020

Abstract

Based on a course presented by the author at the International School of Physics Enrico Fermi, CLXI Course, "Polarons in Bulk Materials and Systems with Reduced Dimensionality", Varenna, Italy, 21.6. - 1.7.2005, including further developments since 2005.

In the present course, an overview is presented of the fundamentals of continuum-polaron physics, which provide the basis of the analysis of polaron effects in ionic crystals and polar semiconductors. These Lecture Notes deal with "large", or "continuum", polarons, as described by the Fröhlich Hamiltonian. The emphasis is on the polaron optical absorption, with detailed mathematical derivations.

Appendix A treats optical conductivity of a strong-coupling polaron.

Appendix B considers Feynman's path-integral polaron treatment approached using time-ordered operator calculus.

Appendix C is devoted to the many-body large polaron optical conductivity in Nb doped strontium titanate.

Appendix D contains summary of the present state of the problem of the polaron mobility. **It is remarkable that the theory of the polaron mobility developed by Kadanoff [65], which was recognized during a long time, needs a correction factor as found in Ref. [151] and independently confirmed in the recent work [153].**

Appendix E represents the all-coupling analytic description for the optical conductivity of the Fröhlich polaron, with the goal being to bridge the gap in validity range that exists between two complementary methods: on the one hand the memory function formalism and on the other hand the strong-coupling expansion based on the Franck-Condon picture for the polaron response.

Appendix F represents the solution of the large polaron Fröhlich Hamiltonian in 3-dimensions (3D) and 2-dimensions (2D) obtained via the Diagrammatic Monte Carlo (DMC) method. Polaron ground state energies and effective polaron masses are successfully benchmarked with data obtained using Feynman's path integral formalism. By comparing 3D and 2D data, we verify the analytically exact scaling relations for energies and effective masses from 3D→2D, which provides a stringent test for the quality of DMC predictions.

Appendix G lists recent publications on Fröhlich polarons in Nature, Science and Physical Review Letters appeared from 2005 to 2020.

*The printed version of these Lectures is copyrighted by TQC – Departement Fysica – Universiteit Antwerpen, Belgium / Jozef T. L. Devreese.

Contents

<i>Preface</i>	9
References	11
I Single polaron	
I. Introduction. The "standard" theories	13
A. The polaron concept	13
B. Intuitive concepts	14
C. The Fröhlich Hamiltonian	18
D. Infinite mass model ["shift"-operators]	19
E. The "standard" theories	20
1. Weak coupling via a perturbation theory	20
2. Weak coupling via a canonical transformation ["shift"-operators]	21
3. Strong coupling via a canonical transformation ["shift"-operators]	23
4. All-coupling theory. The Feynman path integral	32
5. On Monte Carlo calculations of the polaron free energy	34
6. On the contributions of the N -phonon states to the polaron ground state	36
F. Polaron mobility	39
II. Optical Absorption. Weak coupling	41
A. Optical absorption at weak coupling [within the perturbation theory]	41
B. Optical absorption at weak coupling [within the canonical-transformation method [73] (DHL)]	42
III. Optical absorption. Strong coupling	49
IV. Arbitrary coupling	51
A. Impedance function of large polarons: An alternative derivation of FHIP [76]	51
B. Calculation of the memory function (Devreese <i>et. al.</i> [50])	73
C. Discussion of optical absorption of polarons at arbitrary coupling	76
1. Sum rules for the optical conductivity spectra	80

D. Scaling relations	82
1. Derivation of the scaling relations	82
2. Check of the scaling relation for the path integral Monte Carlo result for the polaron free energy	89
Appendix 1. Weak coupling: LLP approach	91
Appendix 2. Expansion in Stieltjes continuous fractions [54]	104

II Many polarons

V. Optical conductivity of an interacting many-polaron gas	108
A. Kubo formula for the optical conductivity of the many-polaron gas	108
B. Force-force correlation function	111
C. Canonical transformation	113
D. Dynamic structure factor	116
1. Calculation of the dynamic structure factor using the retarded Green's functions	120
2. Plasmon-phonon contribution	124
E. Comparison to the infrared spectrum of $\text{Nd}_{2-x}\text{Ce}_x\text{CuO}_{2-y}$	125
F. Experimental data on the optical absorption in manganites: interpretation in terms of a many-polaron response	126
VI. Interacting polarons in a quantum dot	130
A. The partition function and the free energy of a many-polaron system	130
B. Model system	136
1. Analytical calculation of the model partition function	137
C. Variational functional	141
D. Two-point correlation functions	145
1. The correlation function $\tilde{g}(\mathbf{q}, \tau \{N_\sigma\}, \beta)$	146
E. Many-polaron ground state in a quantum dot: extrapolation to the homogeneous limit and comparison to the results for a polaron gas in bulk [90]	156
F. Optical conductivity	160
1. Selected results: the manifestations of the shell filling in optical conductivity	166

VII. Variational path-integral treatment of a translation invariant N-polaron system	169
A. The many-polaron system	169
B. Variational principle	170
C. Results	172
VIII. Ripplonic polarons in multielectron bubbles	175
A. Ripplon-phonon modes of a MEB	175
B. Electron-ripplon interaction in the MEB	177
C. Locally flat approximation	178
D. Ripplon-polaron in a Wigner lattice: the mean-field approach	178
E. Ripplon-polaron Wigner lattice at finite temperature	180
F. Melting of the ripplon-polaron Wigner lattice	182
Acknowledgments	186
A. Optical conductivity of a strong-coupling Fröhlich polaron [<i>S. N. Klimin and J. T. Devreese, Phys. Rev. B 89, 035201 (2014)</i>]	187
1. Introduction	187
2. Optical conductivity	188
3. Results and discussion	196
4. Conclusions	199
5. Appendix 1. Correlation function	200
6. Appendix 2. Effective phonon modes	202
a. Exact averaging	204
b. Averaging neglecting the Jahn-Teller effect	206
B. Feynman's path-integral polaron treatment approached using time-ordered operator calculus [<i>S. N. Klimin and J. T. Devreese, Solid State Communications 151, 144 (2011)</i>]	211
C. Many-body large polaron optical conductivity in $\text{SrTi}_{1-x}\text{Nb}_x\text{O}_3$ [<i>J. T. Devreese, S. N. Klimin, J. L. M. van Mechelen, and D. van der Marel, Phys. Rev. B 81, 125119 (2010)</i>]	222

1. Introduction	222
2. Optical conductivity of a gas of large polarons	226
a. Theory and experiment	231
b. Material parameters	231
3. Optical conductivity spectra	233
4. Conclusions	237
References	238
D. Notes on the polaron mobility	242
E. All-coupling polaron optical response: analytic approaches beyond the adiabatic approximation [<i>S. N. Klimin, J. Tempere, and J. T. Devreese, Phys. Rev. B 94, 125206 (2016)</i>]	251
1. Introduction	251
2. Analytic methods for the polaron optical conductivity	254
a. Memory function formalism with a non-parabolic trial action	254
b. Non-adiabatic strong coupling expansion	261
3. Results and discussions	267
4. Conclusions	270
Appendix 1: Analytic summations	272
References	273
F. Diagrammatic Monte Carlo study of the Fröhlich polaron dispersion in 2D and 3D [<i>T. Hahn, S. N. Klimin, J. Tempere, J. T. Devreese, and C. Franchini, Phys. Rev. B 97, 134305 (2018)</i>]	284
1. Introduction	284
2. Theory and Methodology	287
a. Green's functions and Feynman diagrams	287
b. Diagrammatic Monte Carlo	289
c. DMC for the Fröhlich polaron	291
3. Results and discussion	294
a. Polaron ground state energy and effective mass	294

b. Polaron dispersion	299
4. Summary and Conclusion	302
References	303
G. Selected publications on polarons in high-rating journals (Nature, Science, Physical Review Letters – 2005-2020)	
	305
References	346

Preface

Since 2005, when the first edition of the present Lecture Course was prepared, polaron physics continued to intensely develop, involving new areas and testing new powerful methods. In subsequent editions, these new developments are included in order to emphasize which of them we consider important.

Renewed interest in large (Fröhlich) polarons has been inspired by recent experimental advances in the determination of the band structure of highly polar oxides [1]. The optical response of complex oxides clearly reveals the polaron features and can shed light on the band structure of a crystal and its polaron characteristics. The interpretation of the measured data is essential to achieve a comprehensive understanding and to optimize practical application of functional materials. In particular, the question whether the polarons are large or small is often a subject of intense discussions, for example, in the case of SrTiO₃ and TiO₂, key materials in many technological sectors.

In the recent ARPES measurements [1] no clear signatures of small-polaron phenomena in *n*-doped strontium titanate were found, and the conclusion was reached that small polarons are not formed in strontium titanate. The electron-phonon coupling strength in strontium titanate $\alpha \approx 3.6$ obtained in Ref. [2] is typical for a rather moderate coupling that makes the formation of small polarons in the conduction band of SrTiO₃ hardly possible. On the contrary, recent density functional calculations [3, 4] show that excess electrons form small polarons if the density of electronic carriers is sufficiently high. This opens the interesting possibility to study an interplay of small and large polarons in SrTiO₃ and other oxides. In Ref. [5], the many-large-polaron model gives then a convincing interpretation of the experimentally observed mid-infrared band of SrTi_{1-x}Nb_xO₃.

The polaron theory is a testing field for new powerful theoretical quantum field methods, such as the Diagrammatic Quantum Monte Carlo (DQMC) method. Applied first to the calculation of the ground-state energy of a Fröhlich polaron [6], DQMC has been successful in the calculation of the optical conductivity of the Fröhlich polaron [7]. This inspired attempts to develop analytical methods for the polaron optical response. The recent work on the strong-coupling large-polaron optical conductivity [8] shows a good agreement with DQMC in the strong-coupling limit. In Ref. [9], the momentum average approximation is applied to derive an analytic expression for the optical conductivity of a small polaron, that

very well matches the DQMC data.

The polaron theory has found recently several new interesting applications. One of them is the theoretical interpretation of the physics of an impurity immersed in an atomic Bose-Einstein condensate. In Refs. [10, 11], the ground-state energy of the BEC polaron has been studied on the basis of a Fröhlich type Hamiltonian using the Feynman variational technique and the DQMC method. In Ref. [12], the problem of the BEC polaron has been treated using the renormalization group method. It successfully retrieves the DQMC results in the whole (available for the comparison) range of the particle-phonon coupling strength.

Very recently, interesting works appeared which confirmed new trends in the polaron physics. These studies are devoted to polaron manifestations in real systems, e. g., quantum atomic gases [13–16]. In Ref. [13], an impurity embedded in a quasi-two-dimensional Bose-Einstein atomic condensate is realized as a dark-state polariton. It is demonstrated show that the interaction of the impurity with phonons lead to photonic polarons, described by the Bogoliubov-Fröhlich Hamiltonian. The theoretical study in Ref. [13] is performed extending a renormalization group approach, developed for Fröhlich polarons in Ref. [17]. The study in Ref. [14] is devoted to the problem of a mobile impurity moving through a Bose-Einstein atomic condensate. The radio frequency spectroscopy of ultracold bosonic atoms is used to experimentally demonstrate the existence of a well-defined quasiparticle state of an impurity interacting with a BEC. Both attractive and repulsive polaron-type quasiparticles in BEC are realized. The experimental work [15] is devoted to Bose polarons in atomic condensates in the strongly interacting regime. This is, at the moment, the first measurement of the Bose polaron in a three-dimensional trapped atom gas, which probed the energies and lifetimes for both the attractive and repulsive polaron branches. In Ref. [16], the dynamics of Bose polarons in the vicinity of a Feshbach resonance between the impurity and host atoms is studied in the specific setting of radio-frequency spectroscopy of impurity atoms immersed in a Bose-Einstein condensate. The authors demonstrate the disappearance of the sharp quasiparticle spectral feature at strong coupling and the presence of a novel type of excitations in which several Bogoliubov quasiparticles are bound to the impurity. This work represents a particular interest for studying nonperturbative phenomena in Bose polarons at strong coupling.

We may consider at least two remarkable achievements as the most important recent progress in the polaron physics. First, the numerically accurate solutions of the polaron

problem using the Diagrammatic Quantum Monte Carlo method allowed theorists to verify and compare different analytic approximations, what has significance far beyond the polaron theory itself, because the polaron is a classic example of the problem of a particle interacting with a quantum field, where nonperturbative solutions are extremely valuable. Second, the discovery of polarons in quantum gases demonstrates the universality of the polaron concept, which can embrace a lot of new unexpected areas of manifestations. In summary, polaron physics recently demonstrated new fascinating developments, that makes the present lecture course timely and relevant.

-
- [1] W. Meevasana, X. J. Zhou, B. Moritz, C.-C. Chen, R. H. He, S.-I. Fujimori, D. H. Lu, S.-K. Mo, R. G. Moore, F. Baumberger, T. P. Devereaux, D. van der Marel, N. Nagaosa, J. Zaanen and Z.-X. Shen, *New Journal of Physics* **12**, 023004 (2010).
 - [2] J. L. M. van Mechelen, D. van der Marel, C. Grimaldi, A. B. Kuzmenko, N. P. Armitage, N. Reyren, H. Hagemann, and I. I. Mazin, *Phys. Rev. Lett.* **100**, 226403 (2008).
 - [3] M. Setvin, C. Franchini, X. Hao, M. Schmid, A. Janotti, M. Kaltak, C. G. Van de Walle, G. Kresse, and U. Diebold, *Phys. Rev. Lett.* **113**, 086402 (2014).
 - [4] X. Hao, Z. Wang, M. Schmid, U. Diebold, and C. Franchini, *Phys. Rev. B* **91**, 085204 (2015).
 - [5] J. T. Devreese, S. N. Klimin, J. L. M. van Mechelen, and D. van der Marel, *Phys. Rev. B* **81**, 125119 (2010).
 - [6] A. S. Mishchenko, N. V. Prokof'ev, A. Sakamoto, and B. V. Svistunov, *Phys. Rev. B* **62**, 6317 (2000).
 - [7] A. S. Mishchenko, N. Nagaosa, N. V. Prokof'ev, A. Sakamoto, and B. V. Svistunov, *Phys. Rev. Lett.* **91**, 236401 (2003).
 - [8] S. N. Klimin and J. T. Devreese, *Phys. Rev. B* **89**, 035201 (2014).
 - [9] G. L. Goodvin, A. S. Mishchenko, and M. Berciu, *Phys. Rev. Lett.* **107**, 076403 (2011).
 - [10] J. Tempere, W. Casteels, M. K. Oberthaler, S. Knoop, E. Timmermans, and J. T. Devreese, *Phys. Rev. B* **80**, 184504 (2009); **87**, 099903 (2013).
 - [11] J. Vlietinck, W. Casteels, K. Van Houcke, J. Tempere, J. Ryckebusch, and J. T. Devreese, *New J. Phys.* **17**, 033023 (2015).
 - [12] F. Grusdt, Y. E. Shchadilova, A. N. Rubtsov, and E. Demler, *Sci. Rep.* **5**, 12124 (2015).

- [13] F. Grusdt and M. Fleischhauer, Phys. Rev. Lett. **116**, 053602 (2016).
- [14] N. B. Jorgensen, L. Wacker, K. T. Skalmstang, M. M. Parish, J. Levinsen, R. S. Christensen, G. M. Bruun, and Jan J. Arlt, Phys. Rev. Lett. **117**, 055302 (2016).
- [15] M.-G. Hu, M. J. Van de Graaff, D. Kedar, J. P. Corson, E. A. Cornell, and D. S. Jin, Phys. Rev. Lett. **117**, 055301 (2016).
- [16] Y. E. Shchadilova, R. Schmidt, F. Grusdt, and E. Demler, Phys. Rev. Lett. **117**, 113002 (2016).
- [17] F. Grusdt, Phys. Rev. B **93**, 144302 (2016).

The most cited articles devoted to Fröhlich polarons

1. *Polarons In Crystalline And Non-Crystalline Materials*. By: Austin, I. G; Mott, N. F., Advances In Physics **18**, 41 (1969).
Times cited: 2322
2. *Slow Electrons in a Polar Crystal*. By: Feynman, R. P., Physical Review **97**, 660 (1955).
Times cited: 970
3. *The Motion of Slow Electrons in a Polar Crystal*. By: T. D. Lee, F. E. Low, and D. Pines, Phys. Rev. **90**, 297 (1953).
Times cited: 950

Part I

Single polaron

I. INTRODUCTION. THE "STANDARD" THEORIES

A. The polaron concept

A charge placed in a polarizable medium is screened. Dielectric theory describes the phenomenon by the induction of a polarization around the charge carrier. The idea of the autolocalization of an electron due to the induced lattice polarization was first proposed by L. D. Landau [1]. In the further development of this concept, the induced polarization can follow the charge carrier when it is moving through the medium. The carrier together with the induced polarization is considered as one entity (see Fig. 1). It was called a *polaron* by S. I. Pekar [2, 3]. The physical properties of a polaron differ from those of a band-carrier. A polaron is characterized by its *binding (or self-) energy* E_0 , an *effective mass* m^* and by its characteristic *response* to external electric and magnetic fields (e. g. dc mobility and optical absorption coefficient).

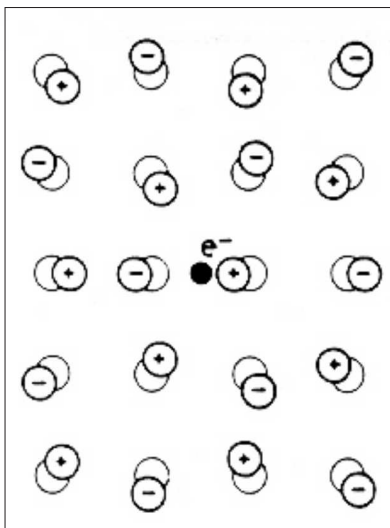


FIG. 1: Artist view of a polaron. A conduction electron in an ionic crystal or a polar semiconductor repels the negative ions and attracts the positive ions. A self-induced potential arises, which acts back on the electron and modifies its physical properties. (From [4].)

If the spatial extension of a polaron is large compared to the lattice parameter of the solid, the latter can be treated as a polarizable continuum. This is the case of a *large (Fröhlich)* polaron. When the self-induced polarization caused by an electron or hole becomes of the order of the lattice parameter, a *small (Holstein)* polaron can arise [136]. As distinct from large polarons, small polarons are governed by short-range interactions.

B. Intuitive concepts

a. The polaron radius. Large polarons vs small polarons Consider the LO phonon field with frequency ω_{LO} interacting with an electron. Denote by $\Delta\nu$ the quadratic mean square deviation of the electron velocity. In the electron-phonon interaction is weak, the electron can travel a distance

$$\Delta x \approx \frac{\Delta\nu}{\omega_{\text{LO}}} \quad (1.1)$$

during a time ω_{LO}^{-1} , characteristic for the lattice period, because it is the distance within which the electron can be localized using the phonon field as measuring device. From the uncertainty relations it follows

$$\begin{aligned} \Delta p \Delta x &= \frac{m}{\omega_{\text{LO}}} (\Delta\nu)^2 \approx \hbar \\ \Delta\nu &\sim \sqrt{\frac{\hbar\omega_{\text{LO}}}{m}}, \\ \Delta x &\sim \sqrt{\frac{\hbar}{m\omega_{\text{LO}}}}. \end{aligned} \quad (1.2)$$

At weak coupling Δx is a measure of the polaron radius r_p . To be consistent, the polaron radius r_p must be considerably larger than the lattice parameter a . (this is a criterion of a “large polaron”). Experimental evaluation of the polaron radius leads to the following typical values: $r_p \approx 10\text{\AA}$ for alkali halides, $r_p \approx 20\text{\AA}$ for silver halides, $r_p \approx 100\text{\AA}$ for II-VI, II-V semiconductors. The continuum approximation is not satisfied for transition metal oxides (NiO, CaO, MnO), in other oxides (UO₂, NbO₂...). For those solids the “small polaron” concept is used. In some substances (e.g. perovskites) some intermediate region between large and small polarons is realized.

b. The coupling constant [5] Consider the case of *strong electron-phonon interaction* in a polar crystal. The electron of mass m is then localized and can - to a first approximation - be considered as a static charge distribution within a sphere with radius l_1 . The medium is characterized by an average dielectric constant $\bar{\epsilon}$, which will be defined below.

The potential energy of a sphere of radius l_1 uniformly charged with the charge e in a vacuum is (see Eq. (8.6) of Ref. [6])

$$U_{vac} = \frac{3}{5} \frac{e^2}{l_1}. \quad (1.3)$$

The potential energy of a uniformly charged sphere in a medium with the high-frequency dielectric constant ϵ_∞ is

$$U_1 = \frac{3}{5} \frac{e^2}{\epsilon_\infty l_1}. \quad (1.4)$$

This is the potential energy of the *self-interaction* of the charge e uniformly spread over the sphere of radius l_1 in a medium with the dielectric constant ϵ_∞ . In a medium with an inertial polarization field (due to LO phonons), the potential energy of the uniformly charged sphere is

$$U_2 = \frac{3}{5} \frac{e^2}{\epsilon_0 l_1}, \quad (1.5)$$

where ϵ_0 is the static dielectric constant. The polaron effect is then related to the change of the potential energy of the interaction of the charged sphere due to the inertial polarization field. This change is the potential energy U_2 of the uniformly charged sphere in the presence of the inertial polarization field minus the potential energy of the *self-interaction* U_1 of the charge e uniformly spread over the sphere in a medium without the inertial polarization:

$$U_{pol} \equiv U_2 - U_1 = \frac{3}{5} \frac{e^2}{l_1} \left(\frac{1}{\epsilon_0} - \frac{1}{\epsilon_\infty} \right) = -\frac{3}{5} \frac{e^2}{\bar{\epsilon} l_1}, \quad (1.6)$$

with

$$\frac{1}{\bar{\epsilon}} = \frac{1}{\epsilon_\infty} - \frac{1}{\epsilon_0}.$$

The electron distribution in a sphere may be non-uniform, what may influence the numerical coefficient in Eqs. (1.4) to (1.6). In this connection one can use the estimate [5]

$$U_{pol} \sim -\frac{e^2}{\bar{\epsilon} l_1}. \quad (1.7)$$

The restriction of the electron in space requires its de Broglie wave length to be of the order l_1 , so that its kinetic energy is of the order $4\pi^2 \hbar^2 / 2ml_1^2$. Minimizing the total energy with respect to l_1 leads to

$$\frac{\partial}{\partial l_1} \left(-\frac{e^2}{l_1 \bar{\epsilon}} + \frac{4\pi^2 \hbar^2}{2ml_1^2} \right) = 0 \implies \frac{1}{l_1} = \frac{e^2 m}{4\pi^2 \hbar^2 \bar{\epsilon}},$$

wherefrom the binding energy is

$$U_1 = -\frac{e^4 m}{8\pi^2 \hbar^2 \bar{\epsilon}^2}. \quad (1.8)$$

For *weak coupling*, one can neglect the kinetic energy of the electron. Taking the polaron radius according to (1.2), $r_p = \sqrt{2\hbar/m\omega_{\text{LO}}}$, the binding energy is

$$U_2 = -\frac{e^2}{r_p \bar{\epsilon}} = -\frac{e^2}{\bar{\epsilon}} \sqrt{\frac{m\omega_{\text{LO}}}{2\hbar}}. \quad (1.9)$$

We note that

$$\frac{U_1}{\hbar\omega_{\text{LO}}} = -\frac{e^4 m}{8\pi^2 \hbar^3 \bar{\epsilon}^2 \omega_{\text{LO}}} = -\frac{1}{4\pi^2} \left(\frac{U_2}{\hbar\omega_{\text{LO}}} \right)^2. \quad (1.10)$$

Following the conventions of the field theory, the self energy at weak coupling is written as

$$U_2 = -\alpha \hbar\omega_{\text{LO}}.$$

Therefore the so-called Fröhlich polaron coupling constant is

$$\begin{aligned} \alpha &= \frac{e^2}{\bar{\epsilon}} \sqrt{\frac{m}{2\hbar^3 \omega_{\text{LO}}}} \\ &\equiv \frac{e^2}{\hbar c} \sqrt{\frac{mc^2}{2\hbar\omega_{\text{LO}}}} \frac{1}{\bar{\epsilon}}. \end{aligned} \quad (1.11)$$

For the average dielectric constant one shows that

$$\frac{1}{\bar{\epsilon}} = \frac{1}{\epsilon_\infty} - \frac{1}{\epsilon_0},$$

where ϵ_∞ and ϵ_0 are, respectively, the electronic and the static dielectric constant of the polar crystal. The difference $1/\epsilon_\infty - 1/\epsilon_0$ arises because the ionic vibrations occur in the infrared spectrum and the electrons in the shells can follow the conduction electron adiabatically.

*c. Polaron mobility*¹ Here we give a simple derivation leading to the gross features of the mobility behavior, especially its temperature dependence. The key idea is that the mobility will change because the number of phonons in the lattice, with which the polaron interacts, is changing with temperature.

The phonon density is given by

$$n = \frac{1}{e^{\frac{\hbar\omega_{\text{LO}}}{kT}} - 1}.$$

The mobility for large polaron is proportional to the inverse of the number of phonons:

$$\mu \approx \frac{1}{n} = e^{\frac{\hbar\omega_{\text{LO}}}{kT}} - 1$$

and for low temperatures $kT \ll \hbar\omega_{\text{LO}}$

$$\mu \approx e^{\frac{\hbar\omega_{\text{LO}}}{kT}}. \quad (1.12)$$

The mobility of continuum polarons decreases with increasing temperature following an exponential law. The slope of the straight line in $\ln \mu$ vs $1/T$ is characterized by the LO phonon frequency. Systematic study performed, in particular, by Fröhlich and Kadanoff, gives

$$\mu = \frac{e}{2m\omega_{\text{LO}}} e^{\frac{\hbar\omega_{\text{LO}}}{kT}}. \quad (1.13)$$

The small polaron will jump from ion to ion under the influence of optical phonons. The larger the number of phonons, the larger the mobility. The behavior of the small polaron is the opposite of that of the large polaron. One expects:

$$\mu \approx n = \frac{1}{e^{\frac{\hbar\omega_{\text{LO}}}{kT}} - 1}.$$

For low temperatures $kT \ll \hbar\omega_{\text{LO}}$ one has:

$$\mu \approx e^{-\frac{\hbar\omega_{\text{LO}}}{kT}} : \quad (1.14)$$

the mobility of small polaron is thermally activated. Systematic analysis within the small-polaron theory shows that

¹See also Appendix D “Notes on the polaron mobility”.

$$\mu \approx e^{-\gamma \frac{\hbar\omega_{\text{LO}}}{kT}} : \quad (1.15)$$

with $\gamma \sim 5$.

C. The Fröhlich Hamiltonian

Fröhlich proposed a model Hamiltonian for the “large” polaron through which its dynamics is treated quantum mechanically (“Fröhlich Hamiltonian”). The polarization, carried by the longitudinal optical (LO) phonons, is represented by a set of quantum oscillators with frequency ω_{LO} , the long-wavelength LO-phonon frequency, and the interaction between the charge and the polarization field is linear in the field [5]:

$$H = \frac{\mathbf{p}^2}{2m_b} + \sum_{\mathbf{k}} \hbar\omega_{\text{LO}} a_{\mathbf{k}}^\dagger a_{\mathbf{k}} + \sum_{\mathbf{k}} (V_k a_{\mathbf{k}} e^{i\mathbf{k}\cdot\mathbf{r}} + V_k^* a_{\mathbf{k}}^\dagger e^{-i\mathbf{k}\cdot\mathbf{r}}), \quad (1.16)$$

where \mathbf{r} is the position coordinate operator of the electron with band mass m_b , \mathbf{p} is its canonically conjugate momentum operator; $a_{\mathbf{k}}^\dagger$ and $a_{\mathbf{k}}$ are the creation (and annihilation) operators for longitudinal optical phonons of wave vector \mathbf{k} and energy $\hbar\omega_{\text{LO}}$. The V_k are Fourier components of the electron-phonon interaction

$$V_k = -i \frac{\hbar\omega_{\text{LO}}}{k} \left(\frac{4\pi\alpha}{V} \right)^{\frac{1}{2}} \left(\frac{\hbar}{2m_b\omega_{\text{LO}}} \right)^{\frac{1}{4}}. \quad (1.17)$$

The strength of the electron–phonon interaction is expressed by a dimensionless coupling constant α , which is defined as:

$$\alpha = \frac{e^2}{\hbar} \sqrt{\frac{m_b}{2\hbar\omega_{\text{LO}}}} \left(\frac{1}{\varepsilon_\infty} - \frac{1}{\varepsilon_0} \right). \quad (1.18)$$

In this definition, ε_∞ and ε_0 are, respectively, the electronic and the static dielectric constant of the polar crystal.

In Table I the Fröhlich coupling constant is given for a few solids².

In deriving the form of V_k , expressions (1.17) and (1.18), it was assumed that (i) the spatial extension of the polaron is large compared to the lattice parameter of the solid (“continuum”

²In some cases, due to lack of reliable experimental data to determine the electron band mass, the values of α are not well established.

approximation), (ii) spin and relativistic effects can be neglected, (iii) the band-electron has parabolic dispersion, (iv) in line with the first approximation it is also assumed that the LO-phonons of interest for the interaction, are the long-wavelength phonons with constant frequency ω_{LO} .

The model, represented by the Hamiltonian (1.16) (which up to now could not be solved exactly) has been the subject of extensive investigations, see, e. g., Refs. [23–30]. In what follows the key approaches of the Fröhlich-polaron theory are briefly reviewed with indication of their relevance for the polaron problems in nanostructures.

D. Infinite mass model [“shift”-operators]

Here some insight will be given in the type of transformation that might be useful to study the Fröhlich Hamiltonian (1.16). For this purpose the Hamiltonian will be treated for a particle with infinite mass $m_b \rightarrow \infty$, (which is at $\mathbf{r} = 0$) :

$$H^\infty = \sum_{\mathbf{k}} \hbar\omega_{\text{LO}} a_{\mathbf{k}}^\dagger a_{\mathbf{k}} + \sum_{\mathbf{k}} (V_{\mathbf{k}} a_{\mathbf{k}} + V_{\mathbf{k}}^* a_{\mathbf{k}}^\dagger), \quad (1.19)$$

TABLE I: *Electron-phonon coupling constants* (After Ref. [4])

Material	α	Ref.	Material	α	Ref.
InSb	0.023	[7]	AgCl	1.84	[13]
InAs	0.052	[7]	KI	2.5	[7]
GaAs	0.068	[7]	TlBr	2.55	[7]
GaP	0.20	[7]	KBr	3.05	[7]
CdTe	0.29	[8]	Bi ₁₂ SiO ₂₀	3.18	[21]
ZnSe	0.43	[7]	CdF ₂	3.2	[7]
CdS	0.53	[7]	KCl	3.44	[7]
α -Al ₂ O ₃	1.25	[9]	CsI	3.67	[7]
AgBr	1.53	[13]	SrTiO ₃	3.77	[22]
α -SiO ₂	1.59	[14]	RbCl	3.81	[7]

which can be transformed into the following expression with “shifted” phonon operators:

$$H^\infty = \sum_{\mathbf{k}} \hbar\omega_{\text{LO}} \left(a_{\mathbf{k}}^\dagger + \frac{V_{\mathbf{k}}}{\hbar\omega_{\text{LO}}} \right) \left(a_{\mathbf{k}} + \frac{V_{\mathbf{k}}^*}{\hbar\omega_{\text{LO}}} \right) - \sum_{\mathbf{k}} \frac{|V_{\mathbf{k}}|^2}{\hbar\omega_{\text{LO}}}. \quad (1.20)$$

To determine the eigenstates of this Hamiltonian, one can perform a unitary transformation which produces the following “shift” of the phonon operators:

$$a_{\mathbf{k}} \rightarrow b_{\mathbf{k}} = a_{\mathbf{k}} + \frac{V_{\mathbf{k}}^*}{\hbar\omega_{\text{LO}}}, a_{\mathbf{k}}^\dagger \rightarrow b_{\mathbf{k}}^\dagger = a_{\mathbf{k}}^\dagger + \frac{V_{\mathbf{k}}}{\hbar\omega_{\text{LO}}}.$$

The transformation

$$S = \exp \left[- \sum_{\mathbf{k}} a_{\mathbf{k}}^\dagger \frac{V_{\mathbf{k}}^*}{\hbar\omega_{\text{LO}}} + \sum_{\mathbf{k}} \frac{V_{\mathbf{k}}}{\hbar\omega_{\text{LO}}} a_{\mathbf{k}} \right] \quad (1.21)$$

is canonical:

$$S^\dagger = \exp \left[- \sum_{\mathbf{k}} a_{\mathbf{k}} \frac{V_{\mathbf{k}}}{\hbar\omega_{\text{LO}}} + \sum_{\mathbf{k}} \frac{V_{\mathbf{k}}^*}{\hbar\omega_{\text{LO}}} a_{\mathbf{k}}^\dagger \right] = S^{-1}$$

and has the desired property:

$$S^{-1} a_{\mathbf{k}} S = a_{\mathbf{k}} - \frac{V_{\mathbf{k}}^*}{\hbar\omega_{\text{LO}}}, S^{-1} a_{\mathbf{k}}^\dagger S = a_{\mathbf{k}}^\dagger - \frac{V_{\mathbf{k}}}{\hbar\omega_{\text{LO}}}.$$

The transformed Hamiltonian is now:

$$S^{-1} H^\infty S = \sum_{\mathbf{k}} \hbar\omega_{\text{LO}} a_{\mathbf{k}}^\dagger a_{\mathbf{k}} - \sum_{\mathbf{k}} \frac{|V_{\mathbf{k}}|^2}{\hbar\omega_{\text{LO}}}.$$

The eigenstates of the Hamiltonian contain an integer number of phonons ($|n_{\mathbf{k}}\rangle$). The eigenenergies are evidently:

$$E = \sum_{\mathbf{k}} n_{\mathbf{k}} \hbar\omega_{\text{LO}} - \sum_{\mathbf{k}} \frac{|V_{\mathbf{k}}|^2}{\hbar\omega_{\text{LO}}}.$$

This expression is divergent as it is often the case in field theory of point charges are considered. A transformation of the type S has been of great interest in developing weak coupling theory as shown below.

E. The “standard” theories

1. Weak coupling via a perturbation theory

For actual crystals α -values typically range from $\alpha = 0.02$ (InSb) up to $\alpha \sim 3$ to 4 (alkali halides, some oxides), see Table 1. A weak-coupling theory of the polaron was developed

originally by Fröhlich [5]. He derived the first weak-coupling perturbation-theory results:

$$E_0 = -\alpha\hbar\omega_{\text{LO}} \quad (1.22)$$

and

$$m^* = \frac{m_b}{1 - \alpha/6}. \quad (1.23)$$

Expressions (1.22) and (1.23) are rigorous to order α .

2. Weak coupling via a canonical transformation [“shift”-operators]

Inspired by the work of Tomonaga on quantum electrodynamics (Q. E. D.), Lee, Low and Pines (LLP) [31] analyzed the properties of a weak-coupling polaron starting from a formulation based on canonical transformations (cp. the results of the subsection ID). As shown by them, the unitary transformation

$$U = \exp \left\{ \frac{i}{\hbar} \left(\mathbf{P} - \sum_{\mathbf{k}} \hbar \mathbf{k} a_{\mathbf{k}}^{\dagger} a_{\mathbf{k}} \right) \cdot \mathbf{r} \right\}, \quad (1.24)$$

where \mathbf{P} is a “c”-number representing the *total system momentum* allows to eliminate the electron co-ordinates from the system. Intuitively one might guess this transformation by writing the exact wave function in the form

$$\Psi_{\text{total } H} = \exp \left(\frac{i}{\hbar} \mathbf{p} \cdot \mathbf{r} \right) |\Phi\rangle.$$

It is plausible that the “Bloch” factor $\exp(i/\hbar \mathbf{p} \cdot \mathbf{r})$ attaches the system to the electron as origin of the co-ordinates. After this transformation the Hamiltonian (1.16) becomes:

$$\mathcal{H} = U^{-1} H U = \frac{\left(\mathbf{P} - \sum_{\mathbf{k}} \hbar \mathbf{k} a_{\mathbf{k}}^{\dagger} a_{\mathbf{k}} \right)^2}{2m_b} + \sum_{\mathbf{k}} \hbar \omega_{\text{LO}} a_{\mathbf{k}}^{\dagger} a_{\mathbf{k}} + \sum_{\mathbf{k}} (V_{\mathbf{k}} a_{\mathbf{k}} + V_{\mathbf{k}}^* a_{\mathbf{k}}^{\dagger}). \quad (1.25)$$

If, for the sake of simplicity, the case of total momentum equal to zero is considered, this expression becomes:

$$\mathcal{H} = \sum_{\mathbf{k}, \mathbf{k}'} \frac{\hbar^2 \mathbf{k} \cdot \mathbf{k}' a_{\mathbf{k}}^{\dagger} a_{\mathbf{k}'}^{\dagger} a_{\mathbf{k}} a_{\mathbf{k}'}}{2m_b} + \sum_{\mathbf{k}} \left(\hbar \omega_{\text{LO}} + \frac{\hbar^2 k^2}{2m_b} \right) a_{\mathbf{k}}^{\dagger} a_{\mathbf{k}} + \sum_{\mathbf{k}} (V_{\mathbf{k}} a_{\mathbf{k}} + V_{\mathbf{k}}^* a_{\mathbf{k}}^{\dagger}). \quad (1.26)$$

The first term of this Hamiltonian is the correlation energy term involving different values for \mathbf{k} and \mathbf{k}' . If one diagonalizes the second and the third term of the Hamiltonian (1.26)

(this can be done exactly by means of the "shifted-oscillator canonical transformation" S (1.21)), the result of LLP is found. The expectation value of the first term is zero for the wave function $S|0\rangle$. Therefore one is sure to obtain a variational result. It is remarkable that merely extracting the $\mathbf{k} = \mathbf{k}'$ term from the expression

$$\sum_{\mathbf{k}, \mathbf{k}'} \frac{\hbar^2 \mathbf{k} \cdot \mathbf{k}' a_{\mathbf{k}}^\dagger a_{\mathbf{k}'}^\dagger a_{\mathbf{k}} a_{\mathbf{k}'}}{2m_b} \quad (1.27)$$

eliminates the divergency from the problem (cp. with the case $m_b \rightarrow \infty$) and is equivalent to the sophisticated theory by Lee, Low and Pines (LLP), which corresponds thus to neglect of the term (1.27). The details of the LLP theory are given in Appendix 1. The explicit form for the energy is now

$$E = - \sum_{\mathbf{k}} \frac{|V_{\mathbf{k}}|^2}{\hbar\omega_{\text{LO}} + \frac{\hbar^2 k^2}{2m_b}} = -\alpha \hbar\omega.$$

This self energy is no longer divergent. The divergence is eliminated by the quantum cut-off occurring at $k = \sqrt{2m_b\omega_{\text{LO}}}/\hbar$.

For the self energy the LLP result is equivalent to the perturbation result. The effective mass however is now given by

$$m^* = m_b \left(1 + \frac{\alpha}{6}\right),$$

a result, which follows if one considers the case $\mathbf{P} \neq 0$ and which is also exact for $\alpha \rightarrow 0$. However, the LLP effective mass is different from the perturbation result if α increases.

The LLP approximation has often been called "intermediate-coupling approximation". However its range of validity is the same as that of perturbation theory to order α . The significance of the LLP approximation consists of the flexibility of the canonical transformations together with the fact that it puts the Fröhlich result on a variational basis.

To order α^2 , the analytical expressions for the coefficients are $\alpha^2: 2 \ln(\sqrt{2} + 1) - \frac{3}{2} \ln 2 - \frac{\sqrt{2}}{2} \approx -0.01591962$ for the energy and $\frac{4}{3} \ln(\sqrt{2} + 1) - \frac{2}{3} \ln 2 - \frac{5\sqrt{2}}{8} + \frac{7}{36} \approx 0.02362763$ for the polaron mass [32].

At present the following weak-coupling expansions are known: for the energy [33, 34]

$$\frac{E_0}{\hbar\omega_{\text{LO}}} = -\alpha - 0.0159196220\alpha^2 - 0.000806070048\alpha^3 - \dots, \quad (1.28)$$

and for the polaron mass [32]

$$\frac{m^*}{m_b} = 1 + \frac{\alpha}{6} + 0.02362763\alpha^2 + \dots \quad (1.29)$$

3. Strong coupling via a canonical transformation [“shift”-operators]

Historically, the strong coupling limit was studied before all other treatments (Landau, Pekar [23, 35]). Although it is only a formal case because the actual crystals seems to have α values smaller than 5, it is very interesting because it contains some indication of the intermediate coupling too: approach the excitations from the strong coupling limit and extrapolate to intermediate coupling is interesting because it is expected that some specific strong coupling properties “survive” at intermediate coupling. In what follows, a treatment, equivalent to that of Pekar, but in second quantization and written with as much analogy to the LLP treatment as possible is given.

We start from the Fröhlich Hamiltonian (1.16). At strong coupling one makes the assumption (a “Produkt-Ansatz”) for the polaron wave-function

$$|\Phi\rangle = |\varphi\rangle|f\rangle \quad (1.30)$$

where $|\varphi\rangle$ is the “electron-component” of the wave function ($\langle\varphi|\varphi\rangle = 1$). The “field-component” of the wave function $|f\rangle$ ($\langle f|f\rangle = 1$) parametrically depends on $|\varphi\rangle$. The Produkt-Ansatz (1.30) — or Born-Oppenheimer approximation — implies that the electron adiabatically follows the motion of the atoms, while the field cannot follow the instantaneous motion of the electron. Fröhlich showed that the approximation (1.30) leads to results, which are only valid for sufficiently large $\alpha \rightarrow \infty$, i. e. in the strong-coupling regime. A more systematic analysis of strong-coupling polarons based on canonical transformations applied to the Hamiltonian (1.16) was performed in Refs. [36–38].

The expectation value for the energy is now:

$$\langle H \rangle = \langle \varphi | \frac{\mathbf{p}^2}{2m_b} | \varphi \rangle + \langle f | \left[\sum_{\mathbf{k}} \hbar \omega_{\text{LO}} a_{\mathbf{k}}^{\dagger} a_{\mathbf{k}} + \sum_{\mathbf{k}} (V_{\mathbf{k}} a_{\mathbf{k}} \rho_{\mathbf{k}} e^{i\mathbf{k}\cdot\mathbf{r}} + V_{\mathbf{k}}^* a_{\mathbf{k}}^{\dagger} \rho_{\mathbf{k}}^*) \right] | f \rangle$$

with

$$\rho_{\mathbf{k}} = \langle \varphi | e^{i\mathbf{k}\cdot\mathbf{r}} | \varphi \rangle.$$

We wish to minimize $\langle H \rangle$, but also

$$\langle f | \left[\sum_{\mathbf{k}} \hbar \omega_{\text{LO}} a_{\mathbf{k}}^{\dagger} a_{\mathbf{k}} + \sum_{\mathbf{k}} (V_{\mathbf{k}} a_{\mathbf{k}} \rho_{\mathbf{k}} e^{i\mathbf{k}\cdot\mathbf{r}} + V_{\mathbf{k}}^* a_{\mathbf{k}}^{\dagger} \rho_{\mathbf{k}}^*) \right] | f \rangle$$

has to be minimized. This expression will be minimized if $|f\rangle$ is the ground state wave function of the “shifted” oscillator-type Hamiltonian. As we can diagonalize this Hamiltonian

exactly:

$$\sum_{\mathbf{k}} \hbar\omega_{\text{LO}} a_{\mathbf{k}}^{\dagger} a_{\mathbf{k}} + \sum_{\mathbf{k}} (V_k a_{\mathbf{k}} \rho_{\mathbf{k}} e^{i\mathbf{k}\cdot\mathbf{r}} + V_k^* a_{\mathbf{k}}^{\dagger} \rho_{\mathbf{k}}^*) \quad (1.31)$$

$$= \sum_{\mathbf{k}} \hbar\omega_{\text{LO}} \left(a_{\mathbf{k}}^{\dagger} + \frac{V_k \rho_{\mathbf{k}}}{\hbar\omega_{\text{LO}}} \right) \left(a_{\mathbf{k}} + \frac{V_k^* \rho_{\mathbf{k}}^*}{\hbar\omega_{\text{LO}}} \right) - \sum_{\mathbf{k}} \frac{|V_k|^2 |\rho_{\mathbf{k}}|^2}{\hbar\omega_{\text{LO}}}, \quad (1.32)$$

we can apply a canonical transformation similar to (1.21):

$$S = \exp \left[\sum_{\mathbf{k}} \left(\frac{V_k \rho_{\mathbf{k}}}{\hbar\omega_{\text{LO}}} a_{\mathbf{k}} - \frac{V_k^* \rho_{\mathbf{k}}^*}{\hbar\omega_{\text{LO}}} a_{\mathbf{k}}^{\dagger} \right) \right], \quad (1.33)$$

which has the property:

$$S^{-1} a_{\mathbf{k}} S = a_{\mathbf{k}} - \frac{V_k^* \rho_{\mathbf{k}}}{\hbar\omega_{\text{LO}}}, \quad S^{-1} a_{\mathbf{k}}^{\dagger} S = a_{\mathbf{k}}^{\dagger} - \frac{V_k \rho_{\mathbf{k}}^*}{\hbar\omega_{\text{LO}}}.$$

The transformed Hamiltonian is now:

$$\begin{aligned} & S^{-1} \left[\sum_{\mathbf{k}} \hbar\omega_{\text{LO}} a_{\mathbf{k}}^{\dagger} a_{\mathbf{k}} + \sum_{\mathbf{k}} (V_k a_{\mathbf{k}} \rho_{\mathbf{k}} e^{i\mathbf{k}\cdot\mathbf{r}} + V_k^* a_{\mathbf{k}}^{\dagger} \rho_{\mathbf{k}}^*) \right] S \\ &= \sum_{\mathbf{k}} \hbar\omega_{\text{LO}} a_{\mathbf{k}}^{\dagger} a_{\mathbf{k}} - \sum_{\mathbf{k}} \frac{|V_k|^2 |\rho_{\mathbf{k}}|^2}{\hbar\omega_{\text{LO}}}. \end{aligned}$$

The phonon vacuum $|0\rangle$ provides a minimum:

$$\langle 0 | S^{-1} \left[\sum_{\mathbf{k}} \hbar\omega_{\text{LO}} a_{\mathbf{k}}^{\dagger} a_{\mathbf{k}} + \sum_{\mathbf{k}} (V_k a_{\mathbf{k}} \rho_{\mathbf{k}} e^{i\mathbf{k}\cdot\mathbf{r}} + V_k^* a_{\mathbf{k}}^{\dagger} \rho_{\mathbf{k}}^*) \right] S | 0 \rangle = - \sum_{\mathbf{k}} \frac{|V_k|^2 |\rho_{\mathbf{k}}|^2}{\hbar\omega_{\text{LO}}}.$$

Hence, the Hamiltonian (1.31) is minimized by the ground state wave function

$$S | 0 \rangle = \exp \left[\sum_{\mathbf{k}} \left(\frac{V_k \rho_{\mathbf{k}}}{\hbar\omega_{\text{LO}}} a_{\mathbf{k}} - \frac{V_k^* \rho_{\mathbf{k}}^*}{\hbar\omega_{\text{LO}}} a_{\mathbf{k}}^{\dagger} \right) \right] | 0 \rangle. \quad (1.34)$$

It gives the ground state energy

$$E_0 = \langle \varphi | \frac{\mathbf{p}^2}{2m_b} | \varphi \rangle - \sum_{\mathbf{k}} \frac{|V_k|^2 |\rho_{\mathbf{k}}|^2}{\hbar\omega_{\text{LO}}}, \quad (1.35)$$

which is still a functional of $|\varphi\rangle$. The functionals $\rho_{\mathbf{k}}$ are different for different excitations.

a. *Ground state of strong-coupling polarons* For the ground state one considers a Gaussian wave function:

$$|\varphi^{1s}\rangle = C \exp\left(-\frac{m_b\Omega_0}{2\hbar}r^2\right)$$

with a variational parameter Ω_0 .

$$\begin{aligned} \langle\varphi^{1s}|\varphi^{1s}\rangle &= C^2 \int d^3r \exp\left(-\frac{m_b\Omega_0}{\hbar}r^2\right) = C^2 \left[\int_{-\infty}^{\infty} dx \exp\left(-\frac{m_b\Omega_0}{\hbar}x^2\right)\right]^3 \\ &= C^2 \left(\frac{\sqrt{\pi}}{\frac{m_b\Omega_0}{\hbar}}\right)^3 = C^2 \left(\frac{\pi\hbar}{m_b\Omega_0}\right)^{3/2} = 1 \Rightarrow C^2 = \left(\frac{m_b\Omega_0}{\pi\hbar}\right)^{3/2} \\ |\varphi^{1s}\rangle &= \left(\frac{m_b\Omega_0}{\pi\hbar}\right)^{3/4} \exp\left(-\frac{m_b\Omega_0}{2\hbar}r^2\right). \end{aligned}$$

For the further use, we introduce a notation $C_1^2 = \left(\frac{m_b\Omega_0}{\pi\hbar}\right)^{1/2}$. Such a wave function is consistent with the localization of the electron, which we expect for large α . The kinetic energy in (1.35) for this function is calculated using the representation of the operator $\mathbf{p}^2 = -\hbar^2\nabla^2 = -\hbar^2(\nabla_x^2 + \nabla_x^2 + \nabla_x^2)$:

$$\begin{aligned} \langle\varphi^{1s}|\frac{\mathbf{p}^2}{2m_b}|\varphi^{1s}\rangle &= -\frac{\hbar^2}{2m_b}C^2 \int d^3r \exp\left(-\frac{m_b\Omega_0}{2\hbar}r^2\right) \\ &\quad \times (\nabla_x^2 + \nabla_x^2 + \nabla_x^2) \exp\left(-\frac{m_b\Omega_0}{2\hbar}r^2\right) \\ &= -3\frac{\hbar^2}{2m_b}C^2 \int_{-\infty}^{\infty} dx \exp\left(-\frac{m_b\Omega_0}{2\hbar}x^2\right) \nabla_x^2 \exp\left(-\frac{m_b\Omega_0}{2\hbar}x^2\right) \\ &\quad \times \int_{-\infty}^{\infty} dy \exp\left(-\frac{m_b\Omega_0}{\hbar}y^2\right) \int_{-\infty}^{\infty} dz \exp\left(-\frac{m_b\Omega_0}{\hbar}z^2\right) \\ &= -3\frac{\hbar^2}{2m_b}C_1^2 \int_{-\infty}^{\infty} dx \exp\left(-\frac{m_b\Omega_0}{2\hbar}x^2\right) \\ &\quad \times \nabla_x \left[-\frac{m_b\Omega_0}{\hbar}x \exp\left(-\frac{m_b\Omega_0}{2\hbar}x^2\right)\right] \\ &= 3\frac{\hbar^2}{2m_b}C_1^2 \frac{m_b\Omega_0}{\hbar} \int_{-\infty}^{\infty} dx \left(1 - \frac{m_b\Omega_0}{\hbar}x^2\right) \exp\left(-\frac{m_b\Omega_0}{\hbar}x^2\right) \\ &== 3\frac{\hbar^2}{m_b}C_1^2 \frac{m_b\Omega_0}{\hbar} \int_0^{\infty} dx \left(1 - \frac{m_b\Omega_0}{\hbar}x^2\right) \exp\left(-\frac{m_b\Omega_0}{\hbar}x^2\right) \\ &= 3\frac{\hbar^2}{m_b}C_1^2 \frac{m_b\Omega_0}{\hbar} \left[\frac{\sqrt{\pi}}{2\sqrt{\frac{m_b\Omega_0}{\hbar}}} - \frac{m_b\Omega_0}{\hbar} \frac{\sqrt{\pi}}{4\sqrt{\left(\frac{m_b\Omega_0}{\hbar}\right)^3}}\right] \\ &= 3\frac{\hbar\Omega_0}{4}C_1^2 \sqrt{\frac{\pi\hbar}{m_b\Omega_0}} = 3\frac{\hbar\Omega_0}{4} \sqrt{\frac{m_b\Omega_0}{\pi\hbar}} \sqrt{\frac{\pi\hbar}{m_b\Omega_0}} = \frac{3}{4}\hbar\Omega_0. \end{aligned}$$

The functional

$$\begin{aligned}
\rho_{\mathbf{k}''1s''} &= \langle \varphi_{''1s''} | e^{i\mathbf{k} \cdot \mathbf{r}} | \varphi_{''1s''} \rangle = C^2 \int d^3r \exp \left(-\frac{m_b \Omega_0}{\hbar} r^2 + i\mathbf{k} \cdot \mathbf{r} \right) \\
&= C^2 \int d^3r \exp \left(-\frac{m_b \Omega_0}{\hbar} \left[r^2 + i \frac{\hbar}{m_b \Omega_0} \mathbf{k} \cdot \mathbf{r} - \frac{\hbar^2 k^2}{4m_b^2 \Omega_0^2} + \frac{\hbar^2 k^2}{4m_b^2 \Omega_0^2} \right] \right) \\
&= C^2 \exp \left(-\frac{m_b \Omega_0}{\hbar} \frac{\hbar^2 k^2}{4m_b^2 \Omega_0^2} \right) \int d^3r \exp \left(-\frac{m_b \Omega_0}{\hbar} \left[\mathbf{r} + i \frac{\hbar}{2m_b \Omega_0} \mathbf{k} \right]^2 \right) \Rightarrow \\
\rho_{\mathbf{k}''1s''} &= \exp \left(-\frac{\hbar k^2}{4m_b \Omega_0} \right). \tag{1.36}
\end{aligned}$$

The second term in (1.35) is then

$$\begin{aligned}
-\sum_{\mathbf{k}} \frac{|V_{\mathbf{k}}|^2 |\rho_{\mathbf{k}''1s''}|^2}{\hbar \omega_{\text{LO}}} &= -\frac{V}{(2\pi)^3} \int d^3k \frac{\hbar \omega_{\text{LO}}}{k^2} \frac{4\pi\alpha}{V} \left(\frac{\hbar}{2m_b \omega_{\text{LO}}} \right)^{\frac{1}{2}} \exp \left(-\frac{\hbar k^2}{2m_b \Omega_0} \right) \\
&= -\frac{\alpha \hbar \omega_{\text{LO}}}{2\pi^2} \cdot 4\pi \left(\frac{\hbar}{2m_b \omega_{\text{LO}}} \right)^{\frac{1}{2}} \int_0^\infty dk \exp \left(-\frac{\hbar k^2}{2m_b \Omega_0} \right) \\
&= -\frac{2\alpha \hbar \omega_{\text{LO}}}{\pi} \left(\frac{\hbar}{2m_b \omega_{\text{LO}}} \right)^{\frac{1}{2}} \frac{\sqrt{\pi}}{2} \sqrt{\frac{2m_b \Omega_0}{\hbar}} = -\frac{\alpha \hbar}{\sqrt{\pi}} \sqrt{\Omega_0 \omega_{\text{LO}}}. \tag{1.37}
\end{aligned}$$

The variational energy (1.35) thus becomes

$$E_0 = \frac{3}{4} \hbar \Omega_0 - \frac{\hbar \omega_{\text{LO}} \alpha}{\sqrt{\pi}} \sqrt{\frac{\Omega_0}{\omega_{\text{LO}}}}. \tag{1.38}$$

Putting

$$\frac{\partial E_0}{\partial \Omega_0} = 0,$$

one obtains

$$\begin{aligned}
\frac{3}{4} &= \frac{\alpha}{2\sqrt{\pi}} \sqrt{\frac{\omega_{\text{LO}}}{\Omega_0}} \Rightarrow \sqrt{\frac{\Omega_0}{\omega_{\text{LO}}}} = \frac{2\alpha}{3\sqrt{\pi}} \Rightarrow \frac{\Omega_0}{\omega_{\text{LO}}} = \frac{4}{9} \frac{\alpha^2}{\pi} \Rightarrow \\
\Omega_0 &= \frac{4}{9} \frac{\alpha^2}{\pi} \omega_{\text{LO}}. \tag{1.39}
\end{aligned}$$

Substituting (1.39) in (1.38), we find the ground state energy of the polaron E_0 (calculated with the energy of the uncoupled electron-phonon system as zero energy):

$$\begin{aligned}
E_0 &= \frac{3}{4} \hbar \frac{4}{9} \frac{\alpha^2}{\pi} \omega_{\text{LO}} - \frac{\hbar \omega_{\text{LO}} \alpha}{\sqrt{\pi}} \frac{2\alpha}{3\sqrt{\pi}} = \left(\frac{1}{3} - \frac{2}{3} \right) \frac{\alpha^2}{\pi} \hbar \omega_{\text{LO}} \Rightarrow \\
E_0 &= -\frac{1}{3} \frac{\alpha^2}{\pi} \hbar \omega_{\text{LO}} = -0.106 \alpha^2 \hbar \omega_{\text{LO}}. \tag{1.40}
\end{aligned}$$

The strong-coupling mass of the polaron, resulting again from the approximation (1.30), is given [39] as:

$$m_0^* = 0.0200 \alpha^4 m_b. \tag{1.41}$$

More rigorous strong-coupling expansions for E_0 and m^* have been presented in the literature [40]:

$$\frac{E_0}{\hbar\omega_{\text{LO}}} = -0.108513\alpha^2 - 2.836, \quad (1.42)$$

$$\frac{m_0^*}{m_b} = 1 + 0.0227019\alpha^4. \quad (1.43)$$

The strong-coupling ground state energy (1.40) is lower than the LLP ground state energy for $\alpha > 10$.

b. The excited states of the polaron: SS, FC, RES In principle, excited states of the polaron exist at all coupling. In the general case, and for simplicity for $\mathbf{P} = 0$, a continuum of states starts at $\hbar\omega_{\text{LO}}$ above the ground state of the polaron. This continuum physically corresponds to the scattering of free phonons on the polaron. Those “scattering states” (SS) were studied in [41] and for the first time more generally in [39] are not the only excitations of the polaron. There are also *internal* excitation states corresponding to the excitations of the electron in the potential it created itself. By analogy with the excited states of colour centers, the following terminology is used.

- (i) The states where the electron is excited in the potential belonging to the ground state configuration of the lattice are called *Franck-Condon* (FC) states
- (ii) Excitations of the electron in which the lattice polarization is adapted to the electronic configuration of the excited electron (which itself then adapts its wave function to the new potential, etc. ...leading to a self-consistent final state), are called *relaxed excited state* (RES) [23].

c. Calculation of the lowest FC state The formalism used until now is well adapted to treat the polaron excitations at strong coupling. The field dependence of the wave function is (1.34). For the FC state the $\rho_{\mathbf{k}}$ are the same as for the ground state (1.36). Physically $\rho_{\mathbf{k}}$ tells us, to what electronic distribution the field is adapted. The electronic part of the excited wave function is *2p*-like:

$$|\varphi_{2p}\rangle = C_{2p} z \exp\left(-\frac{m_b\Omega_p}{2\hbar}r^2\right) \quad (1.44)$$

with a parameter Ω_p , which is equal to Ω_0 :

$$\begin{aligned}
\langle \varphi_{2p''} | \varphi_{2p''} \rangle &= C_{2p''}^2 \int_{-\infty}^{\infty} dz z^2 \exp\left(-\frac{m_b \Omega_p}{\hbar} z^2\right) \left[\int_{-\infty}^{\infty} dx \exp\left(-\frac{m_b \Omega_p}{\hbar} x^2\right) \right]^2 \\
&= C_{2p''}^2 \left(\frac{\sqrt{\pi}}{\frac{m_b \Omega_p}{\hbar}} \right)^2 \frac{\sqrt{\pi}}{2 \left(\frac{m_b \Omega_p}{\hbar} \right)^{3/2}} = C_{2p''}^2 \left(\frac{\pi \hbar}{m_b \Omega_p} \right)^{3/2} \frac{\hbar}{2 m_b \Omega_p} = 1 \Rightarrow \\
C_{2p''}^2 &= \left(\frac{m_b \Omega_p}{\pi \hbar} \right)^{3/2} \frac{2 m_b \Omega_p}{\hbar} \\
|\varphi_{2p''}\rangle &= \left(\frac{m_b \Omega_0}{\pi \hbar} \right)^{3/4} \left(\frac{2 m_b \Omega_p}{\hbar} \right)^{1/2} z \exp\left(-\frac{m_b \Omega_0}{2 \hbar} r^2\right).
\end{aligned}$$

We introduce still a notation

$$C_2^2 = \frac{2}{\sqrt{\pi}} \left(\frac{m_b \Omega_p}{\hbar} \right)^{3/2}$$

The FC state energy is, similarly to (1.35),

$$E_{FC} = \langle \varphi_{2p''} | \frac{\mathbf{p}^2}{2m_b} | \varphi_{2p''} \rangle - \sum_{\mathbf{k}} \frac{|V_{\mathbf{k}}|^2 |\rho_{\mathbf{k}''1s''}|^2}{\hbar \omega_{\text{LO}}}. \quad (1.45)$$

The kinetic energy term is

$$\begin{aligned}
\langle \varphi_{"2p"} | \frac{\mathbf{p}^2}{2m_b} | \varphi_{"2p"} \rangle &= -\frac{\hbar^2}{2m_b} C_{"2p"}^2 \int d^3r z \exp\left(-\frac{m_b \Omega_p}{2\hbar} r^2\right) \\
&\quad \times (\nabla_x^2 + \nabla_x^2 + \nabla_x^2) \left[z \exp\left(-\frac{m_b \Omega_p}{2\hbar} r^2\right) \right] \\
&= -\frac{\hbar^2}{2m_b} C_{"2p"}^2 \int_{-\infty}^{\infty} dz z \exp\left(-\frac{m_b \Omega_p}{2\hbar} z^2\right) \nabla_z^2 \left[z \exp\left(-\frac{m_b \Omega_p}{2\hbar} z^2\right) \right] \\
&\quad \times \int_{-\infty}^{\infty} dy \exp\left(-\frac{m_b \Omega_p}{\hbar} y^2\right) \int_{-\infty}^{\infty} dz \exp\left(-\frac{m_b \Omega_p}{\hbar} z^2\right) + \frac{2}{4} \hbar \Omega_p \\
&= -\frac{\hbar^2}{2m_b} C_2^2 \int_{-\infty}^{\infty} dz z \exp\left(-\frac{m_b \Omega_p}{2\hbar} z^2\right) \\
&\quad \times \nabla_z \left[\left(1 - \frac{m_b \Omega_p}{\hbar} z^2\right) \exp\left(-\frac{m_b \Omega_p}{2\hbar} z^2\right) \right] + \frac{1}{2} \hbar \Omega_p \\
&= \frac{\hbar^2}{2m_b} C_2^2 \int_{-\infty}^{\infty} dz z \exp\left(-\frac{m_b \Omega_p}{2\hbar} z^2\right) \\
&\quad \times \left[\frac{2m_b \Omega_p}{\hbar} z + \left(1 - \frac{m_b \Omega_p}{\hbar} z^2\right) \frac{m_b \Omega_p}{\hbar} z \right] \exp\left(-\frac{m_b \Omega_p}{2\hbar} z^2\right) \\
+ \frac{1}{2} \hbar \Omega_p &= \frac{\hbar^2}{2m_b} C_2^2 \int_{-\infty}^{\infty} dz \left(3 - \frac{m_b \Omega_p}{\hbar} z^2\right) \frac{m_b \Omega_p}{\hbar} z^2 \exp\left(-\frac{m_b \Omega_p}{\hbar} z^2\right) \\
+ \frac{1}{2} \hbar \Omega_p &= \frac{\hbar \Omega_p}{2} C_2^2 \left[\frac{3\sqrt{\pi}}{2 \left(\frac{m_b \Omega_p}{\hbar}\right)^{3/2}} - \frac{m_b \Omega_p}{\hbar} \frac{3\sqrt{\pi}}{4 \left(\frac{m_b \Omega_p}{\hbar}\right)^{5/2}} \right] + \frac{1}{2} \hbar \Omega_p \\
&= \frac{\hbar \Omega_p}{2} C_2^2 \frac{3\sqrt{\pi}}{4 \left(\frac{m_b \Omega_p}{\hbar}\right)^{3/2}} + \frac{1}{2} \hbar \Omega_p \\
&= \frac{\hbar \Omega_p}{2} \frac{2}{\sqrt{\pi}} \left(\frac{m_b \Omega_p}{\hbar}\right)^{3/2} \frac{3\sqrt{\pi}}{4 \left(\frac{m_b \Omega_p}{\hbar}\right)^{3/2}} + \frac{1}{2} \hbar \Omega_p \\
&= \frac{3}{4} \hbar \Omega_p + \frac{1}{2} \hbar \Omega_p = \frac{5}{4} \hbar \Omega_p. \tag{1.46}
\end{aligned}$$

For the FC state, $\Omega_p = \Omega_0$. The second term in (1.45) is precisely (1.37),

$$-\sum_{\mathbf{k}} \frac{|V_{\mathbf{k}}|^2 |\rho_{\mathbf{k}''1s''}|^2}{\hbar \omega_{\text{LO}}} = -\frac{\hbar}{\sqrt{\pi}} \sqrt{\Omega_0 \omega_{\text{LO}}},$$

and the FC energy (1.45) becomes

$$\begin{aligned}
E_{FC} &= \frac{5}{4} \hbar \Omega_0 - \frac{\hbar \omega_{\text{LO}} \alpha}{\sqrt{\pi}} \sqrt{\frac{\Omega_0}{\omega_{\text{LO}}}} \\
&= \frac{5}{4} \hbar \frac{4}{9} \frac{\alpha^2}{\pi} \omega_{\text{LO}} - \frac{2}{3} \frac{\alpha^2}{\pi} \hbar \omega_{\text{LO}} = \left(\frac{5}{9} - \frac{2}{3}\right) \frac{\alpha^2}{\pi} \hbar \omega_{\text{LO}} \implies
\end{aligned}$$

The energy of the lowest FC state is, within the Produkt-Ansatz [42]:

$$E_{\text{FC}} = \frac{\alpha^2}{9\pi} \hbar\omega_{\text{LO}} = 0.0354\alpha^2 \hbar\omega_{\text{LO}}. \quad (1.47)$$

The fact that this energy is positive, is presumably due to the choice of a harmonic potential. The real potential the electron sees is anharmonic, and a bound state may be expected.

d. Calculation of RES The electronic part of the excited wave function is (1.44) with a variational parameter Ω_p , which is determined below. The variational RES energy is, similarly to (1.35),

$$E_{\text{RES}} = \langle \varphi_{2p}'' | \frac{\mathbf{p}^2}{2m_b} | \varphi_{2p}'' \rangle - \sum_{\mathbf{k}} \frac{|V_{\mathbf{k}}|^2 |\rho_{\mathbf{k}''2p}''|^2}{\hbar\omega_{\text{LO}}}. \quad (1.48)$$

Here the kinetic energy term is given by Eq. (1.46). The functional, which is now needed, is

$$\begin{aligned} \rho_{\mathbf{k}''2p}'' &= \langle \varphi_{2p}'' | e^{i\mathbf{k} \cdot \mathbf{r}} | \varphi_{2p}'' \rangle = C_{2p}''^2 \int d^3r z^2 \exp\left(-\frac{m_b\Omega_p}{\hbar} r^2 + i\mathbf{k} \cdot \mathbf{r}\right) \\ &= C_{2p}''^2 \int d^3r z^2 \exp\left(-\frac{m_b\Omega_p}{\hbar} \left[r^2 + i\frac{\hbar}{m_b\Omega_p} \mathbf{k} \cdot \mathbf{r} - \frac{\hbar^2 k^2}{4m_b^2\Omega_p^2} + \frac{\hbar^2 k^2}{4m_b^2\Omega_p^2}\right]\right) \\ &= C_{2p}''^2 \exp\left(-\frac{m_b\Omega_p}{\hbar} \frac{\hbar^2 k^2}{4m_b^2\Omega_p^2}\right) \int d^3r z^2 \exp\left(-\frac{m_b\Omega_p}{\hbar} \left[\mathbf{r} + i\frac{\hbar}{2m_b\Omega_p} \mathbf{k}\right]^2\right) \Rightarrow \\ \rho_{\mathbf{k}''2p}'' &= \exp\left(-\frac{\hbar k^2}{4m_b\Omega_p}\right) C_2^2 \int_{-\infty}^{\infty} dz z^2 \exp\left(-\frac{m_b\Omega_p}{\hbar} \left[z + i\frac{\hbar}{2m_b\Omega_p} k_z\right]^2\right) \\ &= \exp\left(-\frac{\hbar k^2}{4m_b\Omega_p}\right) C_2^2 \int_{-\infty}^{\infty} dz \left(z - i\frac{\hbar}{2m_b\Omega_p} k_z\right)^2 \exp\left(-\frac{m_b\Omega_p}{\hbar} z^2\right) \\ &= \exp\left(-\frac{\hbar k^2}{4m_b\Omega_p}\right) C_2^2 \int_{-\infty}^{\infty} dz \left[z^2 - \left(\frac{\hbar}{2m_b\Omega_p} k_z\right)^2\right]^2 \exp\left(-\frac{m_b\Omega_p}{\hbar} z^2\right) \\ &= \exp\left(-\frac{\hbar k^2}{4m_b\Omega_p}\right) C_2^2 \left\{ \frac{\sqrt{\pi}}{2 \left(\frac{m_b\Omega_p}{\hbar}\right)^{3/2}} - \left(\frac{\hbar}{2m_b\Omega_p} k_z\right)^2 \frac{\sqrt{\pi}}{\left(\frac{m_b\Omega_p}{\hbar}\right)^{1/2}} \right\} \\ &= \left(1 - \frac{\hbar k_z^2}{2m_b\Omega_p}\right) \exp\left(-\frac{\hbar k^2}{4m_b\Omega_p}\right). \end{aligned} \quad (1.49)$$

Further, we substitute (1.49) in the second term in the r.h.s. of Eq. (1.48):

$$\begin{aligned}
-\sum_{\mathbf{k}} \frac{|V_{\mathbf{k}}|^2 |\rho_{\mathbf{k}''1s''}|^2}{\hbar\omega_{\text{LO}}} &= -\frac{V}{(2\pi)^3} \int d^3k \frac{\hbar\omega_{\text{LO}}}{k^2} \frac{4\pi\alpha}{V} \left(\frac{\hbar}{2m_b\omega_{\text{LO}}} \right)^{\frac{1}{2}} \\
&\times \left(1 - \frac{\hbar k_z^2}{2m_b\Omega_p} \right)^2 \exp\left(-\frac{\hbar k^2}{2m_b\Omega_p} \right) \\
&= -\frac{\alpha\hbar\omega_{\text{LO}}}{2\pi^2} \left(\frac{\hbar}{2m_b\omega_{\text{LO}}} \right)^{\frac{1}{2}} 2\pi \int_{-1}^1 dx \\
&\times \int_0^\infty dk \left(1 - \frac{\hbar k^2 x^2}{m_b\Omega_p} + \frac{\hbar^2 k^4 x^4}{4m_b^2\Omega_p^2} \right) \exp\left(-\frac{\hbar k^2}{2m_b\Omega_p} \right) \\
&= -\frac{\alpha\hbar\omega_{\text{LO}}}{\pi} \left(\frac{\hbar}{2m_b\omega_{\text{LO}}} \right)^{\frac{1}{2}} \\
&\times \int_0^\infty dk \left(2 - \frac{2}{3} \frac{\hbar k^2}{m_b\Omega_p} + \frac{2}{5} \frac{\hbar^2 k^4}{4m_b^2\Omega_p^2} \right) \exp\left(-\frac{\hbar k^2}{2m_b\Omega_p} \right) \\
&= -\frac{\alpha\hbar\omega_{\text{LO}}}{\pi} \left(\frac{\hbar}{2m_b\omega_{\text{LO}}} \right)^{\frac{1}{2}} \\
&\times \left[\frac{\sqrt{\pi}}{\left(\frac{\hbar}{2m_b\Omega_p} \right)^{1/2}} - \frac{1}{3} \frac{\hbar}{m_b\Omega_p} \frac{\sqrt{\pi}}{2 \left(\frac{\hbar}{2m_b\Omega_p} \right)^{3/2}} + \frac{1}{5} \frac{\hbar^2}{4m_b^2\Omega_p^2} \frac{3\sqrt{\pi}}{4 \left(\frac{\hbar}{2m_b\Omega_p} \right)^{5/2}} \right] \\
&= -\frac{\alpha\hbar}{\sqrt{\pi}} \sqrt{\omega_{\text{LO}}\Omega_p} \left[1 - \frac{1}{3} + \frac{3}{20} \right] \\
&= -\frac{\alpha\hbar}{\sqrt{\pi}} \sqrt{\omega_{\text{LO}}\Omega_p} \frac{60 - 20 + 9}{60} = -\frac{49}{60} \frac{\alpha\hbar}{\sqrt{\pi}} \sqrt{\omega_{\text{LO}}\Omega_p}
\end{aligned}$$

The variational energy (1.48) becomes

$$E_{RES} = \frac{5}{4} \hbar\Omega_p - \frac{49}{60} \frac{\alpha\hbar}{\sqrt{\pi}} \sqrt{\omega_{\text{LO}}\Omega_p}.$$

Putting

$$\frac{\partial E_{RES}}{\partial \Omega_p} = 0,$$

one obtains

$$\frac{5}{4} = \frac{49\alpha}{120\sqrt{\pi}} \sqrt{\frac{\omega_{\text{LO}}}{\Omega_p}} \implies \sqrt{\frac{\Omega_p}{\omega_{\text{LO}}}} = \frac{49\alpha}{150\sqrt{\pi}} \implies \frac{\Omega_p}{\omega_{\text{LO}}} = \left(\frac{49}{150} \right)^2 \frac{\alpha^2}{\pi} \implies$$

$$\begin{aligned}
E_{RES} &= \frac{5}{4} \hbar \left(\frac{49}{150} \right)^2 \frac{\alpha^2}{\pi} \omega_{\text{LO}} - \frac{\hbar\omega_{\text{LO}}\alpha}{\sqrt{\pi}} \frac{49}{60} \frac{49\alpha}{150\sqrt{\pi}} = \left(\frac{5}{4} - \frac{5}{2} \right) \left(\frac{49}{150} \right)^2 \frac{\alpha^2}{\pi} \hbar\omega_{\text{LO}} \\
&= -\frac{5}{4} \left(\frac{49}{150} \right)^2 \frac{\alpha^2}{\pi} \hbar\omega_{\text{LO}} = -\frac{49^2}{120 \times 150} \frac{\alpha^2}{\pi} \hbar\omega_{\text{LO}} \implies
\end{aligned}$$

The energy of the RES is (see Refs. [39, 41]):

$$E_{RES} = -0.042\alpha^2\hbar\omega_{LO}. \quad (1.50)$$

The effective mass of the polaron in the RES is given [39] as:

$$m_{RES}^* = 0.621\frac{\alpha^4}{81\pi^2}m_b = 0.0200\alpha^4m_b. \quad (1.51)$$

The structure of the energy spectrum of the strong-coupling polaron is shown in Fig. 2.

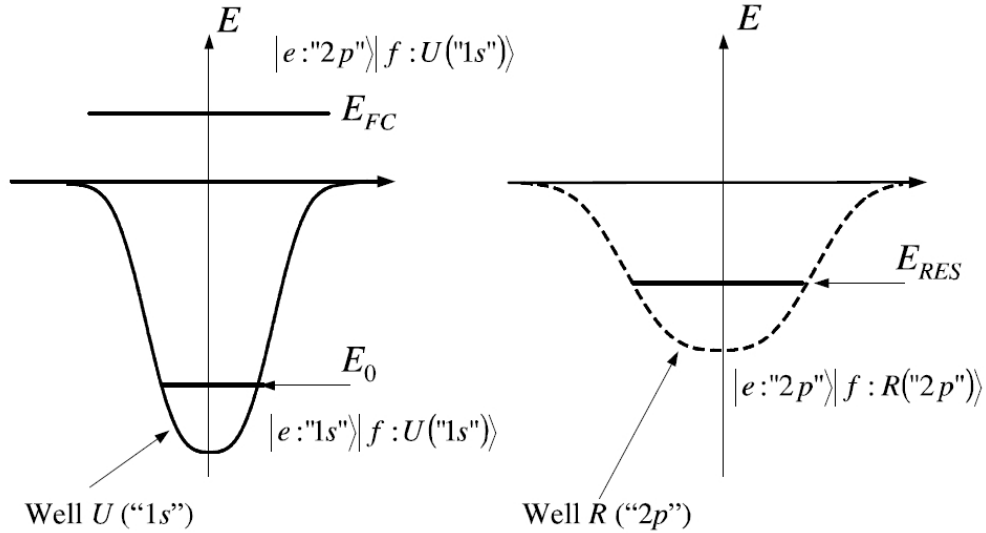


FIG. 2: Structure of the energy spectrum of a polaron at strong coupling: E_0 — the ground state, E_{RES} — the (first) relaxed excited state; the Franck-Condon states (E_{FC}). In fact, both the Franck-Condon states and the relaxed excited states lie in the continuum and, strictly speaking, are resonances.

The significance of the strong-coupling large polaron theory is formal only: it allows to test “all-coupling” theories in the limit $\alpha \rightarrow \infty$. Remarkably, the effective electron-phonon coupling strength significantly increases in systems of low dimension and low dimensionality.

4. All-coupling theory. The Feynman path integral

Feynman developed a superior all-coupling polaron theory using his path-integral formalism [43]. He studied first the self-energy E_0 and the effective mass m^* of polarons [43].

Feynman got the idea to formulate the polaron problem into the Lagrangian form of quantum mechanics and then eliminate the field oscillators, “. . . in exact analogy to Q. E. D. . . . (resulting in) . . . a sum over all trajectories . . .”. The resulting path integral (here limited to the ground-state properties) is of the form (Ref. [43]):

$$\langle 0, \beta | 0, 0 \rangle = \int \mathcal{D}\mathbf{r}(\tau) \exp \left[-\frac{1}{2} \int_0^\beta \dot{\mathbf{r}}^2 d\tau + \frac{\alpha}{2^{\frac{3}{2}}} \int_0^\beta \int_0^\beta \frac{e^{-|\tau-\sigma|}}{|\mathbf{r}(\tau) - \mathbf{r}(\sigma)|} d\tau d\sigma \right], \quad (1.52)$$

where $\beta = 1/(k_B T)$. (1.52) gives the amplitude that an electron found at a point in space at time zero will appear at the same point at the (imaginary) time β . This path integral (1.52) has a great intuitive appeal: it shows the polaron problem as an equivalent one-particle problem in which the interaction, non-local in time or “retarded”, occurs between the electron and itself. Subsequently Feynman showed how the variational principle of quantum mechanics could be adapted to the path-integral formalism and he introduced a quadratic trial action (non-local in time) to simulate (1.52).

Applying the variational principle for path integrals then results in an upper bound for the polaron self-energy at all α , which at weak and strong coupling gives accurate expressions. Feynman obtained smooth interpolation between a weak and strong coupling (for the ground state energy). The weak-coupling expansions of Feynman for the ground-state energy and the effective mass of the polaron are:

$$\frac{E_0}{\hbar\omega_{\text{LO}}} = -\alpha - 0.0123\alpha^2 - 0.00064\alpha^3 - \dots \quad (\alpha \rightarrow 0), \quad (1.53)$$

$$\frac{m^*}{m_b} = 1 + \frac{\alpha}{6} + 0.025\alpha^2 + \dots \quad (\alpha \rightarrow 0). \quad (1.54)$$

In the strong-coupling limit Feynman found for the ground-state energy energy:

$$\frac{E_0}{\hbar\omega_{\text{LO}}} \equiv \frac{E_{3D}(\alpha)}{\hbar\omega_{\text{LO}}} = -0.106\alpha^2 - 2.83 - \dots \quad (\alpha \rightarrow \infty) \quad (1.55)$$

and for the polaron mass:

$$\frac{m^*}{m_b} \equiv \frac{m_{3D}^*(\alpha)}{m_b} = 0.0202\alpha^4 + \dots \quad (\alpha \rightarrow \infty). \quad (1.56)$$

Over the years the Feynman model for the polaron has remained the most successful approach to this problem. The analysis of an exactly solvable (“symmetrical”) 1D-polaron model [41, 44], Monte Carlo schemes [30, 45] and other numerical schemes [46] demonstrate the remarkable accuracy of Feynman’s path-integral approach to the polaron ground-state

energy. Experimentally more directly accessible properties of the polaron, such as its mobility and optical absorption, have been investigated subsequently. Within the path-integral approach, Feynman et al. studied later the mobility of polarons [47, 48]. Subsequently the path-integral approach to the polaron problem was generalized and developed to become a powerful tool to study optical absorption, magnetophonon resonance and cyclotron resonance [49–53].

In Ref. [54], a self-consistent treatment for the polaron problem at all α was presented, which is based on the Heisenberg equations of motion starting from a trial expression for the electron position. It was used to derive the effective mass and the optical properties of the polaron at arbitrary coupling. A variational justification of the approximation used in Ref. [54] (through a Stiltjes continuous fraction) is reproduced in Appendix 2.

5. On Monte Carlo calculations of the polaron free energy

In Ref. [55], using a Monte Carlo calculation, the ground-state energy of a polaron was derived as $E_0 = \lim_{\beta \rightarrow \infty} \Delta F$, where $\Delta F = F_\beta - F_\beta^0$ with F_β the free energy per polaron and $F_\beta^0 = [3/(2\beta)] \ln(2\pi\beta)$ the free energy per electron. The value $\beta\hbar\omega_{\text{LO}} = 25$, used for the actual computation in Ref. [55], corresponds to $T/T_D = 0.04$ ($T_D = \hbar\omega_{\text{LO}}/k_B$; $\hbar\omega_{\text{LO}}$ is the LO phonon energy). So, as pointed out in Ref. [56], the authors of Ref. [55] actually calculated the *free energy* ΔF , rather than the polaron *ground-state energy*.

To investigate the importance of temperature effects on ΔF , the authors of Ref. [56] considered the polaron energy as obtained by Osaka [57], who generalized the Feynman [43] polaron theory to nonzero temperatures:

$$\begin{aligned} \frac{\Delta F}{\hbar\omega} = & \frac{3}{\beta} \ln \left(\frac{w \sinh \frac{\beta_0 v}{2}}{v \sinh \frac{\beta_0 w}{2}} \right) - \frac{3}{4} \frac{v^2 - w^2}{v} \left(\coth \frac{\beta_0 v}{2} - \frac{2}{\beta_0 v} \right) \\ & - \frac{\alpha}{\sqrt{2\pi}} [1 + n(\omega_{\text{LO}})] \int_0^{\beta_0} du \frac{e^{-u}}{\sqrt{D(u)}}, \end{aligned} \quad (1.57)$$

where $\beta_0 = \beta\hbar\omega_{\text{LO}}$, $n(\omega) = 1/(e^{\beta\hbar\omega} - 1)$, and

$$D(u) = \frac{w^2 u}{v^2} \left(1 - \frac{u}{\beta_0} \right) + \frac{v^2 - w^2}{2v^3} \left(1 - e^{-vu} - 4n(v) \sinh^2 \frac{vu}{2} \right). \quad (1.58)$$

This result is variational, with variational parameters v and w , and gives an upper bound to the exact polaron free energy.

The results of a numerical-variational calculation of Eq. (1.57) are shown in Fig. 3, where the free energy $-\Delta F$ is plotted (in units of $\hbar\omega_{\text{LO}}$) as a function of α for different values of the lattice temperature. As seen from Fig. 3, (i) $-\Delta F$ increases with increasing temperature and (ii) the effect of temperature on ΔF increases with increasing α .

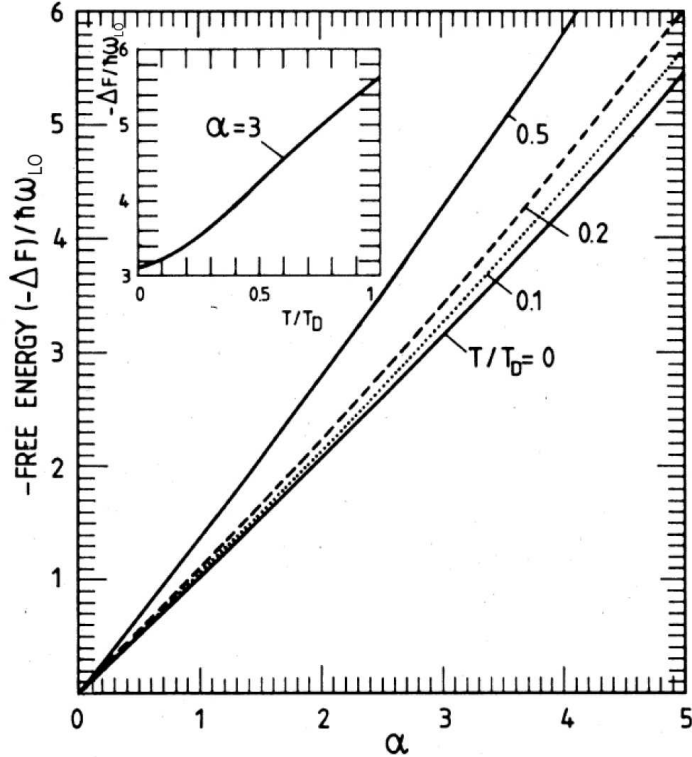


FIG. 3: Contribution of the electron-phonon interaction to the free energy of the Feynman polaron as a function of the electron-phonon coupling constant α for different values of the lattice temperature. Inset: temperature dependence of the free energy for $\alpha = 3$. (From Ref. [56].)

In Table II, the Monte Carlo results [55], $(\Delta F)_{\text{MC}}$, are compared with the free energy of the Feynman polaron, $(\Delta F)_{\text{F}}$, calculated in [56]. The values for the free energy obtained from the Feynman polaron model are *lower* than the MC results for $\alpha \lesssim 2$ and $\alpha \geq 4$ (but lie within the 1% error of the Monte Carlo results). Since the Feynman result for the polaron free energy is an upper bound to the exact result, we conclude that for $\alpha \lesssim 2$ and $\alpha \geq 4$ the results of the Feynman model are closer to the exact result than the MC results of [55].

TABLE II: Comparison between the free energy of the Feynman polaron theory, $-(\Delta F)_F$, and the Monte Carlo results of Ref. [55], $-(\Delta F)_{MC}$, for $T/T_D = 0.04$. The relative difference is defined as $\Delta = 100 \times [(\Delta F)_F - (\Delta F)_{MC}] / (\Delta F)_{MC}$. (From Ref. [56])

α	$-(\Delta F)_F$	$-(\Delta F)_{MC}$	Δ (%)
0.5	0.50860	0.505	0.71
1.0	1.02429	1.020	0.42
1.5	1.54776	1.545	0.18
2.0	2.07979	2.080	-0.010
2.5	2.62137	2.627	-0.21
3.0	3.17365	3.184	-0.32
3.5	3.73814	3.747	-0.24
4.0	4.31670	4.314	0.063

6. On the contributions of the N -phonon states to the polaron ground state

The analysis of an exactly solvable (“symmetric”) 1D-polaron model was performed in Refs. [41, 58, 59]. The model consists of an electron interacting with two oscillators possessing the opposite wave vectors: \mathbf{k} and $-\mathbf{k}$. The parity operator, which changes $a_{\mathbf{k}}$ and $a_{-\mathbf{k}}$ (and also $a_{\mathbf{k}}^\dagger$ and $a_{-\mathbf{k}}^\dagger$), commutes with the Hamiltonian of the system. Hence, the polaron states are classified into the even and odd ones with the eigenvalues of the parity operator $+1$ and -1 , respectively. For the lowest even and odd states, the phonon distribution functions W_N are plotted in Fig. 4, upper panel, at some values of the effective coupling constant λ of the “symmetric” model. The value of the parameter

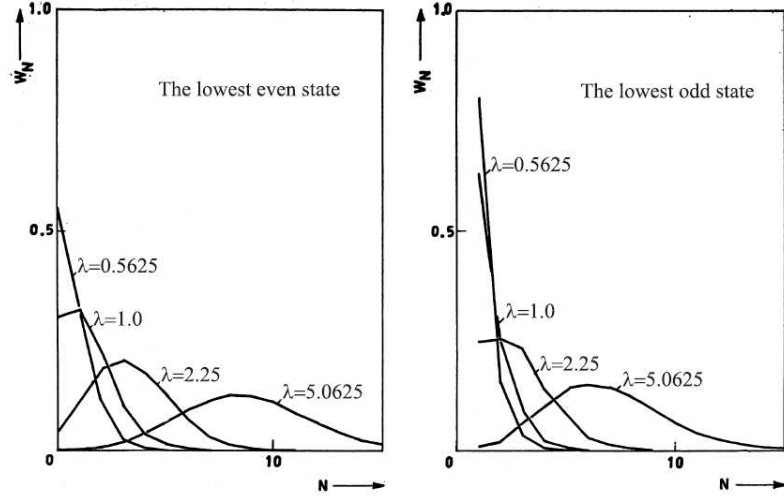
$$\varkappa = \sqrt{\frac{(\hbar k)^2}{m_b \hbar \omega_{LO}}}$$

for these graphs was taken 1, while the total polaron momentum $\mathbf{P} = 0$. In the weak-coupling case ($\lambda \approx 0.6$) W_N is a decaying function of N . When increasing λ , W_N acquires a maximum, e.g. at $N = 8$ for the lowest even state at $\lambda \approx 5.1$. The phonon distribution function W_N has the same character for the lowest even and the lowest odd states at all values of the number of the virtual phonons in the ground state. (as distinct from the

higher states). This led to the conclusion that the lowest odd state is an internal excited state of the polaron.

In Ref [30], the structure of the polaron cloud was investigated using the diagrammatic quantum Monte Carlo (DQMC) method. In particular, partial contributions of N -phonon states to the polaron ground state were found as a function of N for a few values of the coupling constant α , see Fig. 4, lower panel. It was shown to gradually evolve from the weak-coupling case ($\alpha = 1$) into the strong-coupling regime ($\alpha = 17$). Comparison of the lower panel to the upper panel in Fig. 4 clearly shows that the evolution of the shape and the scale of the distribution of the N -phonon states with increasing α as derived for a large polaron within DQMC method [30] is *in remarkable agreement* with the results obtained within the "symmetric" 1D polaron model [41, 58, 59].

The “symmetric” polaron model (Devreese 1964)



DQMC (Mishchenko et al. 2000)

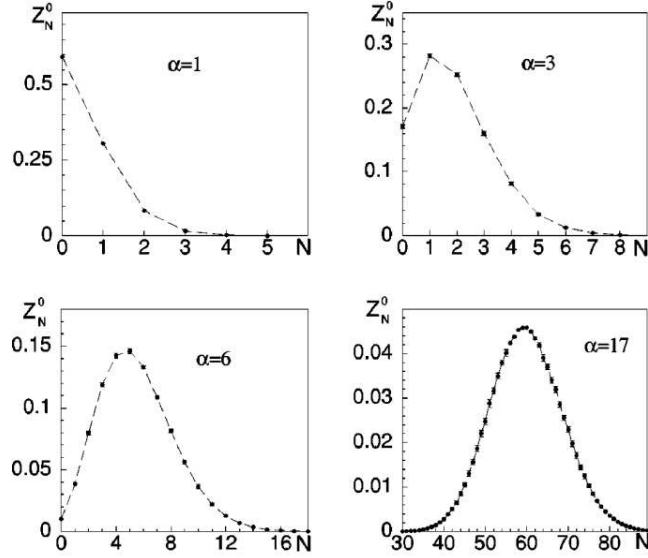


FIG. 4: *Upper panel*: The phonon distribution functions W_N in the “symmetric” polaron model for various values of the effective coupling constant λ at $\kappa = 1, \mathbf{P} = 0$ (from [58], Fig. 23). *Lower panel*: Distribution of multiphonon states in the polaron cloud within DQMC method for various values of α (from [30], Fig. 7).

F. Polaron mobility ³

The mobility of large polarons was studied within various theoretical approaches (see Ref. [60] for the detailed references). Fröhlich [61] pointed out the typical behavior of the large-polaron mobility

$$\mu \propto \exp(\hbar\omega_{\text{LO}}\beta), \quad (1.59)$$

which is characteristic for weak coupling. Here, $\beta = 1/k_B T$, T is the temperature. Within the weak-coupling regime, the mobility of the polaron was then derived, e. g., using the Boltzmann equation in Refs. [62, 63] and starting from the LLP-transformation in Ref. [64].

A nonperturbative analysis was embodied in the Feynman polaron theory, where the mobility μ of the polaron using the path-integral formalism was derived by Feynman et al. (usually referred to as FHIP) as a static limit starting from a frequency-dependent impedance function. For sufficiently low temperature T the mobility then takes the form [47]

$$\mu = \left(\frac{w}{v}\right)^3 \frac{3e}{4m_b\hbar\omega_{\text{LO}}^2\alpha\beta} e^{\hbar\omega_{\text{LO}}\beta} \exp\{(v^2 - w^2)/w^2v\}, \quad (1.60)$$

where v and w are (variational) functions of α obtained from the Feynman polaron model.

Using the Boltzmann equation for the Feynman polaron model, Kadanoff [65] found the mobility, which for low temperatures can be represented as follows:

$$\mu = \left(\frac{w}{v}\right)^3 \frac{e}{2m_b\omega_{\text{LO}}\alpha} e^{\hbar\omega_{\text{LO}}\beta} \exp\{(v^2 - w^2)/w^2v\}, \quad (1.61)$$

The weak-coupling perturbation expansion of the low-temperature polaron mobility as found using the Green's function technique [66] has confirmed that the mobility derived from the Boltzmann equation is exceedingly exact for weak coupling ($\alpha/6 \ll 1$) and at low temperatures ($k_B T \ll \hbar\omega_{\text{LO}}$). As shown in Ref. [65], the mobility of Eq. (1.60) differs by the factor of $3/(2\beta\hbar\omega_{\text{LO}})$ from that derived using the polaron Boltzmann equation as given by Eq. (1.61).

In the limit of weak electron-phonon coupling and low temperature, the FHIP polaron mobility of Eq. (1.60) differs by the factor of $3/(2\beta\hbar\omega_{\text{LO}})$ from the previous result [62–64], which, as pointed out in Ref. [47] and in later publications (see, e.g., Refs.[60, 65, 66]), is

³See also Appendix D “Notes on the polaron mobility”.

correct for $\beta \gg 1$. As follows from this comparison, the result of Ref. [47] is not valid when $T \rightarrow 0$. As argued in Ref. [47] and later confirmed, in particular, in Ref. [67] the above discrepancy can be attributed to an interchange of two limits in calculating the impedance. In FHIP, for weak electron-phonon coupling, one takes $\lim_{\Omega \rightarrow 0} \lim_{\alpha \rightarrow 0}$, whereas the correct order is $\lim_{\alpha \rightarrow 0} \lim_{\Omega \rightarrow 0}$ (Ω is the frequency of the applied electric field). It turns out that for the correct result the mobility at low temperatures is predominantly limited by the absorption of phonons, while in the theory of FHIP it is the emission of phonons which gives the dominant contribution as T goes to zero [67].

The analysis based on the Boltzmann equation takes into account the phonon emission processes whenever the energy of the polaron is above the emission threshold. The independent-collision model, which underlies the Boltzmann-equation approach, however, fails in the “strong coupling regime” of the large polaron, when the thermal mean free path becomes less than the de Broglie wavelength; in this case, the Boltzmann equation cannot be expected to be adequate [47, 68].⁴

In fact, the expression (1.60) for the polaron mobility was reported to adequately describe the experimental data in several polar materials (see, e.g., Refs. [68–70]). Experimental work on alkali halides and silver halides indicates that the mobility obtained from Eq. (1.60) describes the experimental results quite accurately [69]. Measurements of mobility as a function of temperature for photoexcited electrons in cubic n -type $\text{Bi}_{12}\text{SiO}_{20}$ are explained well in terms of large polarons within the Feynman approach [68]. The experimental findings on electron transport in crystalline TiO_2 (rutile phase) probed by THz time-domain spectroscopy are quantitatively interpreted within the Feynman model [70]. One of the reasons for the agreement between theory based on Eq. (1.60) and experiment is that in the path-integral approximation to the polaron mobility, a Maxwellian distribution for the electron velocities is assumed, when applying the adiabatic switching on of the Fröhlich interaction. Although such a distribution is not inherent in the Fröhlich interaction, its incorporation tends to favor agreement with experiment because other mechanisms (interaction with acoustic phonons etc.) cause a Gaussian distribution.

⁴For the polaron mobility in the weak- and strong-coupling regimes, see also Appendix D “Notes on the polaron mobility”.

II. OPTICAL ABSORPTION. WEAK COUPLING

A. Optical absorption at weak coupling [within the perturbation theory]

At zero temperature and in the weak-coupling limit, the optical absorption is due to the elementary polaron scattering process, schematically shown in Fig. 5.

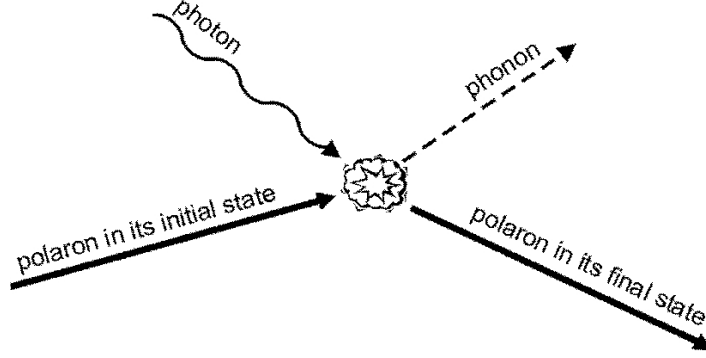


FIG. 5: Elementary polaron scattering process describing the absorption of an incoming photon and the generation of an outgoing phonon.

In the weak-coupling limit ($\alpha \ll 1$) the polaron absorption coefficient was first obtained by V. Gurevich, I. Lang and Yu. Firsov [71], who started from the Kubo formula. Their optical-absorption coefficient is equivalent to a particular case of the result of J. Tempere and J. T. Devreese (Ref. [53]), with the dynamic structure factor $S(\mathbf{q}, \omega)$ corresponding to the Hartree-Fock approximation (see also [72], p. 585). At zero temperature, the absorption coefficient for absorption of light with frequency Ω can be expressed in terms of elementary functions in two limiting cases: in the region of comparatively high polaron densities ($\hbar(\Omega - \omega_{\text{LO}})/\zeta \ll 1$)

$$\Gamma(\omega) = \frac{1}{\epsilon_0 n c} \frac{2^{1/2} N^{2/3} \alpha}{(3\pi^2)^{1/3}} \frac{e^2}{(\hbar m_b \omega_{\text{LO}})^{1/2}} \frac{\omega - 1}{\omega^3} \Theta(\omega - 1), \quad (2.1)$$

and in the low-concentration region ($\hbar(\Omega - \omega_{\text{LO}})/\zeta \gg 1$)

$$\Gamma(\omega) = \frac{1}{\epsilon_0 n c} \frac{2N e^2 \alpha}{3m_b \omega_{\text{LO}}} \frac{(\omega - 1)^{1/2}}{\omega^3} \Theta(\omega - 1), \quad (2.2)$$

where $\omega = \Omega/\omega_{\text{LO}}$, ϵ_0 is the dielectric permittivity of the vacuum, n is the refractive index of the medium, N is the concentration of polarons and ζ is the Fermi level for the electrons.

A step function

$$\Theta(\omega - 1) = \begin{cases} 1 & \text{if } \omega > 1, \\ 0 & \text{if } \omega < 1 \end{cases}$$

reflects the fact that at zero temperature the absorption of light accompanied by the emission of a phonon can occur only if the energy of the incident photon is larger than that of a phonon ($\omega > 1$). In the weak-coupling limit, according to Eqs. (2.1), (2.2), the absorption spectrum consists of a “one-phonon line”.

At nonzero temperature, the absorption of a photon can be accompanied not only by emission, but also by absorption of one or more phonons.

A simple derivation in Ref. [73] using a canonical transformation method gives the absorption coefficient of free polarons, which coincides with the result (2.2) of Ref. [71].

B. Optical absorption at weak coupling [within the canonical-transformation method [73] (DHL)]

The optical absorption of large polarons as a function of the frequency of the incident light is calculated using the canonical-transformation formalism by Devreese, Huybrechts and Lemmens (DHL) Ref. [73]. A simple calculation, which is developed below in full detail, gives a result for the absorption coefficient, which is exact to order α .

We start from the Hamiltonian of the electron-phonon system interacting with light is written down using the vector potential of an electromagnetic field $\mathbf{A}(t)$:

$$H = \frac{1}{2m_b} \left(\mathbf{p} + \frac{e}{c} \mathbf{A}(t) \right)^2 + \sum_{\mathbf{k}} \omega_{\text{LO}} a_{\mathbf{k}}^\dagger a_{\mathbf{k}} + \sum_{\mathbf{k}} (V_{\mathbf{k}} a_{\mathbf{k}} e^{i\mathbf{k}\cdot\mathbf{r}} + V_{\mathbf{k}}^* a_{\mathbf{k}}^\dagger e^{-i\mathbf{k}\cdot\mathbf{r}}). \quad (2.3)$$

The electric field is related to the vector potential as

$$\mathbf{E}(t) = -\frac{1}{c} \frac{\partial \mathbf{A}(t)}{\partial t}. \quad (2.4)$$

Within the electric dipole interaction the electric field with frequency Ω is

$$\mathbf{E}(t) = \mathbf{E} \cos(\Omega t) \Rightarrow \quad (2.5)$$

$$\mathbf{A} = -\frac{c}{\Omega} \mathbf{E} \sin(\Omega t). \quad (2.6)$$

When expanding $\frac{1}{2m_b} \left(\mathbf{p} + \frac{e}{c} \mathbf{A}(t) \right)^2$ in the Hamiltonian, we find

$$\frac{1}{2m_b} \left(\mathbf{p} + \frac{e}{c} \mathbf{A}(t) \right)^2 = \frac{\mathbf{p}^2}{2m_b} + \frac{e}{m_b c} \mathbf{A}(t) \cdot \mathbf{p} + \frac{e^2}{2m_b c^2} A^2(t) \quad (2.7)$$

where the first term is the kinetic energy of the electron, and the second term describes the interaction of the electron-phonon system with light

$$V_t = \frac{e}{m_b c} \mathbf{A}(t) \cdot \mathbf{p} = -\frac{e}{m_b \Omega} \mathbf{E} \cdot \mathbf{p} \sin \Omega t \quad (2.8)$$

$$V_t \equiv V \sin \Omega t, \quad (2.9)$$

$$V \equiv -\frac{e}{m_b \Omega} \mathbf{E} \cdot \mathbf{p}. \quad (2.10)$$

Since $\mathbf{A}(t)$ does not depend on the electron coordinates, the term $\frac{e^2}{2m_b c^2} A^2(t)$ in (2.7) does not play a role in our description of the optical absorption. The total Hamiltonian for the system of a continuum polaron interacting with light is thus

$$H_{tot} = H_{pol} + V_t,$$

where H_{pol} is Fröhlich's Hamiltonian (1.16).

The absorption coefficient for absorption of light with frequency Ω by free polarons is proportional to the probability $P(\Omega)$ that a photon is absorbed by these polarons in their ground state,

$$\Gamma_p(\Omega) = \frac{N}{\varepsilon_0 c n 2 E^2} \Omega P(\Omega). \quad (2.11)$$

Here N is number of polarons, which are considered as independent from each other, ε_0 is the permittivity of vacuum, c is the velocity of light, n is the refractive index of the medium in which the polarons move, E is the modulus of the electric field vector of the incident photon. If the incident light can be treated as a perturbation, the transition probability $P(\Omega)$ is given by the Golden Rule of Fermi:

$$P(\Omega) = 2\pi \sum_f \langle \Phi_0 | V | f \rangle \langle f | V | \Phi_0 \rangle \delta(E_0 + \Omega - E_f). \quad (2.12)$$

V is the amplitude of the time-dependent perturbation given by (2.10). The ground state wave function of a free polaron is $|\Phi_0\rangle$ and its energy is E_0 . The wave functions of all possible final states are $|f\rangle$ and the corresponding energies are E_f . The possible final states are all the excited states of the polaron. The main idea of the present calculation is to avoid the explicit summation over the final polaron states, which are poorly known, by eliminating all the excited state wave functions $|f\rangle$ from the expression (2.12).

With this aim, the representation of the δ -function is used:

$$\delta(x) = \frac{1}{\pi} \operatorname{Re} \int_{-\infty}^0 dt \exp[-i(x + i\varepsilon)t].$$

This leads to:

$$\begin{aligned} P(\Omega) &= 2 \operatorname{Re} \sum_f \int_{-\infty}^0 dt \langle \Phi_0 | V | f \rangle \langle f | V | \Phi_0 \rangle \exp[-i(\Omega + i\varepsilon + E_0 - E_f)t] \\ &= 2 \operatorname{Re} \sum_f \int_{-\infty}^0 dt \exp[-i(\Omega + i\varepsilon)t] \langle \Phi_0 | V | f \rangle \langle f | e^{iHt} V e^{-iHt} | \Phi_0 \rangle. \end{aligned}$$

Using the fact that

$$\sum_f |f\rangle \langle f| = 1$$

and the notation

$$\begin{aligned} e^{iHt} V(0) e^{-iHt} &= V(t), \\ \frac{dV(t)}{dt} &= i[H, V(t)] \end{aligned}$$

we find

$$P(\Omega) = 2 \operatorname{Re} \int_{-\infty}^0 dt \exp[-i(\Omega + i\varepsilon)t] \langle \Phi_0 | V(0) V(t) | \Phi_0 \rangle. \quad (2.13)$$

Defining

$$R(\Omega) = \int_{-\infty}^0 dt \exp[-i(\Omega + i\varepsilon)t] \langle \Phi_0 | V(0) V(t) | \Phi_0 \rangle, \quad (2.14)$$

one has

$$P(\Omega) = 2 \operatorname{Re} R(\Omega). \quad (2.15)$$

Substituting (2.10) to (2.14), we find that

$$R(\Omega) = \left(\frac{e}{m_b \Omega} \right)^2 \int_{-\infty}^0 dt e^{-i(\Omega + i\varepsilon)t} \langle \Phi_0 | (\mathbf{E} \cdot \mathbf{p}(0)) (\mathbf{E} \cdot \mathbf{p}(t)) | \Phi_0 \rangle \quad (2.16)$$

and hence

$$P(\Omega) = 2 \left(\frac{e}{m_b \Omega} \right)^2 \operatorname{Re} \int_{-\infty}^0 dt e^{-i(\Omega + i\varepsilon)t} \langle \Phi_0 | (\mathbf{E} \cdot \mathbf{p}(0)) (\mathbf{E} \cdot \mathbf{p}(t)) | \Phi_0 \rangle. \quad (2.17)$$

It is convenient to apply the first LLP transformation S_1 (4.187), which eliminates the electron operators from the polaron Hamiltonian:

$$\begin{aligned} H &\longrightarrow \mathcal{H} = S_1^{-1} H_{pol} S_1 = \mathcal{H}_0 + \mathcal{H}_1 : \\ \mathcal{H}_0 &= \frac{\mathbf{P}^2}{2m_b} + \sum_{\mathbf{k}} \left(\omega_{LO} + \frac{k^2}{2m_b} - \frac{\mathbf{k} \cdot \mathbf{P}}{m_b} \right) a_{\mathbf{k}}^\dagger a_{\mathbf{k}} + \sum_{\mathbf{k}} (V_{\mathbf{k}} a_{\mathbf{k}} + V_{\mathbf{k}}^* a_{\mathbf{k}}^\dagger), \\ \mathcal{H}_1 &= \frac{1}{2m_b} \sum_{\mathbf{k}} \mathbf{k} \cdot \mathbf{k}' a_{\mathbf{k}}^\dagger a_{\mathbf{k}'}^\dagger a_{\mathbf{k}} a_{\mathbf{k}'}, \end{aligned}$$

where \mathcal{H}_0 can be diagonalized exactly and gives rise to the self-energy $E = -\alpha\omega_{\text{LO}}$, and \mathcal{H}_1 contains the correlation effects between the phonons. The optical absorption will be calculated here for the total momentum of the system $\mathbf{P} = \mathbf{0}$.

In the LLP approximation the explicit form of the matrix element in (2.16) is

$$\langle \Phi_0 | (\mathbf{E} \cdot \mathbf{p}(0)) (\mathbf{E} \cdot \mathbf{p}(t)) | \Phi_0 \rangle = \langle 0 | S_2^{-1} S_1^{-1} \mathbf{E} \cdot \mathbf{p} S_1 S_1^{-1} \mathbf{E} \cdot \mathbf{p}(t) S_1 S_2 | 0 \rangle, \quad (2.18)$$

where S_1 and S_2 are the first (4.187) and the second (4.196) LLP transformations. The application of S_1 gives:

$$S_1^{-1} \mathbf{p}(t) S_1 = S_1^{-1} e^{i\mathcal{H}t} \mathbf{p} e^{-i\mathcal{H}t} S_1 = S_1^{-1} e^{i\mathcal{H}t} S_1 S_1^{-1} \mathbf{p} S_1 S_1^{-1} e^{-i\mathcal{H}t} S_1.$$

Using $\mathcal{H} = S_1^{-1} H S_1$, we arrive at $S_1^{-1} e^{i\mathcal{H}t} S_1 = e^{iHt}$. Further we recall $S_1^{-1} \mathbf{p} S_1 = \mathbf{P} - \sum_{\mathbf{k}} \hbar \mathbf{k} a_{\mathbf{k}}^\dagger a_{\mathbf{k}} + \mathbf{p}$, where $\mathbf{P} = \mathbf{0}$ and \mathbf{p} is set 0 (see Appendix 1). This results in

$$S_1^{-1} \mathbf{p}(t) S_1 = e^{i\mathcal{H}t} \mathbf{p} e^{-i\mathcal{H}t} = - \sum_{\mathbf{k}} \hbar \mathbf{k} e^{i\mathcal{H}t} a_{\mathbf{k}}^\dagger a_{\mathbf{k}} e^{-i\mathcal{H}t} = - \sum_{\mathbf{k}} \hbar \mathbf{k} a_{\mathbf{k}}^\dagger(t) a_{\mathbf{k}}(t).$$

Then (2.18) takes the form

$$\langle \Phi_0 | (\mathbf{E} \cdot \mathbf{p}(0)) (\mathbf{E} \cdot \mathbf{p}(t)) | \Phi_0 \rangle = \left\langle 0 \left| S_2^{-1} \left(\sum_{\mathbf{k}} \mathbf{E} \cdot \mathbf{k} a_{\mathbf{k}}^\dagger a_{\mathbf{k}} \right) \left(\sum_{\mathbf{k}} \mathbf{E} \cdot \mathbf{k} a_{\mathbf{k}}^\dagger(t) a_{\mathbf{k}}(t) \right) S_2 \right| 0 \right\rangle. \quad (2.19)$$

Here the second LLP transformation is given by (4.196) with

$$f_{\mathbf{k}} = - \frac{V_{\mathbf{k}}^*}{\omega_{\text{LO}} + \frac{k^2}{2m_b}} \quad (2.20)$$

and the vacuum is defined by $a_{\mathbf{k}} |0\rangle = 0$. The calculation of the matrix element (2.19) proceeds as follows:

$$\begin{aligned} & \left\langle 0 \left| S_2^{-1} \left(\sum_{\mathbf{k}} \mathbf{E} \cdot \mathbf{k} a_{\mathbf{k}}^\dagger a_{\mathbf{k}} \right) \left(\sum_{\mathbf{k}} \mathbf{E} \cdot \mathbf{k} a_{\mathbf{k}}^\dagger(t) a_{\mathbf{k}}(t) \right) S_2 \right| 0 \right\rangle \\ &= \left\langle 0 \left| S_2^{-1} \left(\sum_{\mathbf{k}} \mathbf{E} \cdot \mathbf{k} a_{\mathbf{k}}^\dagger a_{\mathbf{k}} \right) S_2 S_2^{-1} e^{i\mathcal{H}t} S_2 S_2^{-1} \left(\sum_{\mathbf{k}} \mathbf{E} \cdot \mathbf{k} a_{\mathbf{k}}^\dagger a_{\mathbf{k}} \right) S_2 S_2^{-1} e^{-i\mathcal{H}t} S_2 \right| 0 \right\rangle \\ &= \left\langle 0 \left| S_2^{-1} \left(\sum_{\mathbf{k}} \mathbf{E} \cdot \mathbf{k} a_{\mathbf{k}}^\dagger a_{\mathbf{k}} \right) S_2 e^{iS_2^{-1} \mathcal{H} S_2 t} S_2^{-1} \left(\sum_{\mathbf{k}} \mathbf{E} \cdot \mathbf{k} a_{\mathbf{k}}^\dagger a_{\mathbf{k}} \right) S_2 e^{-iS_2^{-1} \mathcal{H} S_2 t} \right| 0 \right\rangle. \quad (2.21) \end{aligned}$$

Further on, we calculate

$$S_2^{-1} \mathcal{H} S_2 = H_0 + H_1$$

where

$$H_0 = S_2^{-1} \mathcal{H}_0 S_2 = S_2^{-1} \left[\sum_{\mathbf{k}} \left(\omega_{\text{LO}} + \frac{k^2}{2m_b} \right) a_{\mathbf{k}}^\dagger a_{\mathbf{k}} + \sum_{\mathbf{k}} (V_{\mathbf{k}} a_{\mathbf{k}} + V_{\mathbf{k}}^* a_{\mathbf{k}}^\dagger) \right] S_2$$

Further we use $S_2^{-1} a_{\mathbf{k}} S_2 = a_{\mathbf{k}} + f_{\mathbf{k}}$:

$$\begin{aligned} H_0 &= \sum_{\mathbf{k}} \left(\omega_{\text{LO}} + \frac{k^2}{2m_b} \right) a_{\mathbf{k}}^\dagger a_{\mathbf{k}} + \sum_{\mathbf{k}} \left(\omega_{\text{LO}} + \frac{k^2}{2m_b} \right) |f_{\mathbf{k}}|^2 \\ &+ \sum_{\mathbf{k}} \left(\omega_{\text{LO}} + \frac{k^2}{2m_b} \right) (a_{\mathbf{k}}^\dagger f_{\mathbf{k}} + a_{\mathbf{k}} f_{\mathbf{k}}^*) + \sum_{\mathbf{k}} [V_{\mathbf{k}} (a_{\mathbf{k}} + f_{\mathbf{k}}) + V_{\mathbf{k}}^* (a_{\mathbf{k}}^\dagger + f_{\mathbf{k}}^*)] \\ &= \sum_{\mathbf{k}} \left(\omega_{\text{LO}} + \frac{k^2}{2m_b} \right) a_{\mathbf{k}}^\dagger a_{\mathbf{k}} + \sum_{\mathbf{k}} \frac{|V_{\mathbf{k}}|^2}{\left(\omega_{\text{LO}} + \frac{k^2}{2m_b} \right)} - 2 \sum_{\mathbf{k}} \frac{|V_{\mathbf{k}}|^2}{\left(\omega_{\text{LO}} + \frac{k^2}{2m_b} \right)} \\ &= \sum_{\mathbf{k}} \left(\omega_{\text{LO}} + \frac{k^2}{2m_b} \right) a_{\mathbf{k}}^\dagger a_{\mathbf{k}} - \sum_{\mathbf{k}} \frac{|V_{\mathbf{k}}|^2}{\left(\omega_{\text{LO}} + \frac{k^2}{2m_b} \right)}. \end{aligned}$$

The last term can be calculated analytically:

$$\begin{aligned} \sum_{\mathbf{k}} \frac{|V_{\mathbf{k}}|^2}{\omega_{\text{LO}} + \frac{k^2}{2m_b}} &= \frac{V}{(2\pi)^3} \int d^3k \left(\frac{\omega_{\text{LO}}}{k} \right)^2 \frac{4\pi\alpha}{V} \left(\frac{1}{2m_b\omega_{\text{LO}}} \right)^{\frac{1}{2}} \cdot \frac{1}{\omega_{\text{LO}} + \frac{k^2}{2m_b}} \\ &= \frac{\alpha\omega_{\text{LO}}}{2\pi^2} 4\pi \int_0^\infty dk \left(\frac{1}{2m_b\omega_{\text{LO}}} \right)^{\frac{1}{2}} \frac{1}{1 + \frac{k^2}{2m_b\omega_{\text{LO}}}} \\ &= \frac{2\alpha\omega_{\text{LO}}}{\pi} \int_0^\infty d\kappa \frac{1}{1 + \kappa^2} = \frac{2\alpha\omega_{\text{LO}}}{\pi} \arctan \kappa \Big|_0^\infty = \alpha\omega_{\text{LO}}, \end{aligned}$$

$$H_0 = -\alpha\omega_{\text{LO}} + \sum_{\mathbf{k}} \left(\omega_{\text{LO}} + \frac{k^2}{2m_b} \right) a_{\mathbf{k}}^\dagger a_{\mathbf{k}}.$$

The term

$$H_1 = S_2^{-1} \mathcal{H}_1 S_2$$

will be neglected:

$$e^{iS_2^{-1} \mathcal{H} S_2 t} \approx e^{iH_0 t}.$$

Neglecting H_1 , consistent with the LLP description, introduces no error in order α . Therefore (2.21) becomes

$$\left\langle 0 \left| \sum_{\mathbf{k}} \mathbf{E} \cdot \mathbf{k} \left(a_{\mathbf{k}}^\dagger a_{\mathbf{k}} + f_{\mathbf{k}} a_{\mathbf{k}}^\dagger + f_{\mathbf{k}}^* a_{\mathbf{k}} + f_{\mathbf{k}} f_{\mathbf{k}}^* \right) e^{iH_0 t} \right. \right. \\ \left. \left. \times \sum_{\mathbf{k}} \mathbf{E} \cdot \mathbf{k} \left(a_{\mathbf{k}}^\dagger a_{\mathbf{k}} + f_{\mathbf{k}} a_{\mathbf{k}}^\dagger + f_{\mathbf{k}}^* a_{\mathbf{k}} + f_{\mathbf{k}} f_{\mathbf{k}}^* \right) e^{-iH_0 t} \right| 0 \right\rangle. \quad (2.22)$$

For $\mathbf{P} = 0$ there is no privileged direction and $\sum_{\mathbf{k}} \mathbf{E} \cdot \mathbf{k} f_{\mathbf{k}} f_{\mathbf{k}}^* = 0$, (2.22) reduces to:

$$\left\langle 0 \left| \sum_{\mathbf{k}} \mathbf{E} \cdot \mathbf{k} f_{\mathbf{k}}^* a_{\mathbf{k}} e^{iH_0 t} \sum_{\mathbf{k}} \mathbf{E} \cdot \mathbf{k} f_{\mathbf{k}} a_{\mathbf{k}}^\dagger e^{-iH_0 t} \right| 0 \right\rangle.$$

From the equation of motion for $a_{\mathbf{k}}^\dagger$:

$$\frac{da_{\mathbf{k}}^\dagger(t)}{dt} = i [H_0, a_{\mathbf{k}}^\dagger] = i \left(\omega_{\text{LO}} + \frac{k^2}{2m_b} \right) a_{\mathbf{k}}^\dagger,$$

it is easy now to calculate

$$e^{iH_0 t} a_{\mathbf{k}}^\dagger e^{-iH_0 t} = a_{\mathbf{k}}^\dagger \exp \left[i \left(\omega_{\text{LO}} + \frac{k^2}{2m_b} \right) t \right].$$

The matrix element (2.19) now becomes

$$\langle \Phi_0 | (\mathbf{E} \cdot \mathbf{p}(0)) (\mathbf{E} \cdot \mathbf{p}(t)) | \Phi_0 \rangle = \sum_{\mathbf{k}} (\mathbf{E} \cdot \mathbf{k})^2 f_{\mathbf{k}}^* f_{\mathbf{k}} \exp \left[i \left(\omega_{\text{LO}} + \frac{k^2}{2m_b} \right) t \right] + O(\alpha^2).$$

The transition probability (2.13) is then given by the expression

$$\begin{aligned} P(\Omega) &= 2 \operatorname{Re} \frac{e^2}{m_b^2 \Omega^2} \sum_{\mathbf{k}} (\mathbf{E} \cdot \mathbf{k})^2 f_{\mathbf{k}}^* f_{\mathbf{k}} \int_{-\infty}^0 dt \exp \left[-i \left(\Omega + i\varepsilon - \omega_{\text{LO}} - \frac{k^2}{2m_b} \right) t \right] \\ &= 2\pi \frac{e^2}{m_b^2 \Omega^2} \sum_{\mathbf{k}} (\mathbf{E} \cdot \mathbf{k})^2 |f_{\mathbf{k}}|^2 \delta \left(\Omega - \omega_{\text{LO}} - \frac{k^2}{2m_b} \right). \end{aligned}$$

Using (2.20), we obtain

$$\begin{aligned}
P(\Omega) &= \frac{2\pi e^2}{m_b^2 \Omega^2} \sum_{\mathbf{k}} \frac{(\mathbf{E} \cdot \mathbf{k})^2}{\left(\omega_{\text{LO}} + \frac{k^2}{2m_b}\right)^2} |V_{\mathbf{k}}|^2 \delta\left(\Omega - \omega_{\text{LO}} - \frac{k^2}{2m_b}\right) \\
&= \frac{2\pi e^2}{m_b^2 \Omega^2} \frac{V}{(2\pi)^3} \int d^3k \left(\frac{\omega_{\text{LO}}}{k}\right)^2 \frac{4\pi\alpha}{V} \left(\frac{1}{2m_b\omega_{\text{LO}}}\right)^{\frac{1}{2}} \\
&\quad \times \frac{(\mathbf{E} \cdot \mathbf{k})^2}{\left(\omega_{\text{LO}} + \frac{k^2}{2m_b}\right)^2} \delta\left(\Omega - \omega_{\text{LO}} - \frac{k^2}{2m_b}\right) \\
&= \frac{e^2 \alpha E^2}{m_b^2 \Omega^2 \pi} 2\pi \int_{-1}^1 dx x^2 \int_0^\infty dk \left(\frac{1}{2m_b\omega_{\text{LO}}}\right)^{\frac{1}{2}} \\
&\quad \times \frac{k^2}{\left(1 + \frac{k^2}{2m_b\omega_{\text{LO}}}\right)^2} \frac{1}{\omega_{\text{LO}}} \delta\left(\frac{\Omega}{\omega_{\text{LO}}} - 1 - \frac{k^2}{2m_b\omega_{\text{LO}}}\right) \\
&= \frac{8e^2 \alpha E^2}{3m_b \Omega^2} \int_0^\infty d\kappa \frac{\kappa^2}{(1 + \kappa^2)^2} \delta\left(\frac{\Omega}{\omega_{\text{LO}}} - 1 - \kappa^2\right) \\
&= \frac{4e^2 \alpha E^2}{3m_b \Omega^2} \int_0^\infty d\zeta \frac{\sqrt{\zeta}}{(1 + \zeta)^2} \delta\left(\frac{\Omega}{\omega_{\text{LO}}} - 1 - \zeta\right) \\
&= \frac{4e^2 \alpha E^2}{3m_b \Omega^2} \Theta\left(\frac{\Omega}{\omega_{\text{LO}}} - 1\right) \frac{\sqrt{\frac{\Omega}{\omega_{\text{LO}}} - 1}}{\left(\frac{\Omega}{\omega_{\text{LO}}}\right)^2} = \frac{4e^2 \alpha E^2 \omega_{\text{LO}}^2}{3m_b \Omega^4} \sqrt{\frac{\Omega}{\omega_{\text{LO}}} - 1} \Theta\left(\frac{\Omega}{\omega_{\text{LO}}} - 1\right),
\end{aligned}$$

where

$$\Theta\left(\frac{\Omega}{\omega_{\text{LO}}} - 1\right) = \begin{cases} 1 & \text{if } \frac{\Omega}{\omega_{\text{LO}}} > 1 \\ 0 & \text{if } \frac{\Omega}{\omega_{\text{LO}}} < 1 \end{cases}.$$

The absorption coefficient (2.11) for absorption by free polarons for $\alpha \rightarrow 0$ finally takes the form

$$\Gamma_p(\Omega) = \frac{1}{\varepsilon_0 c n} \frac{2N e^2 \alpha \omega_{\text{LO}}^2}{3m_b \Omega^3} \sqrt{\frac{\Omega}{\omega_{\text{LO}}} - 1} \Theta\left(\frac{\Omega}{\omega_{\text{LO}}} - 1\right). \quad (2.23)$$

The behavior of $\Gamma_p(\Omega)$ (2.23) as a function of Ω is as follows. For $\Omega < \omega_{\text{LO}}$ there is no absorption. The threshold for absorption is at $\Omega = \omega_{\text{LO}}$. From $\Omega = \omega_{\text{LO}}$ up to $\Omega = \frac{6}{5}\omega_{\text{LO}}$, Γ_p increases to a maximum and for $\Omega > \frac{6}{5}\omega_{\text{LO}}$ the absorption coefficient decreases slowly with increasing Ω .

Experimentally, this one-phonon line has been observed for free polarons in the infrared absorption spectra of CdO-films, see Fig. 6. In CdO, which is a weakly polar material with $\alpha \approx 0.74$, the polaron absorption band is observed in the spectral region between 6 and 20 μm (above the LO phonon frequency). The difference between theory and experiment in the

wavelength region where polaron absorption dominates the spectrum is due to many-polaron effects.

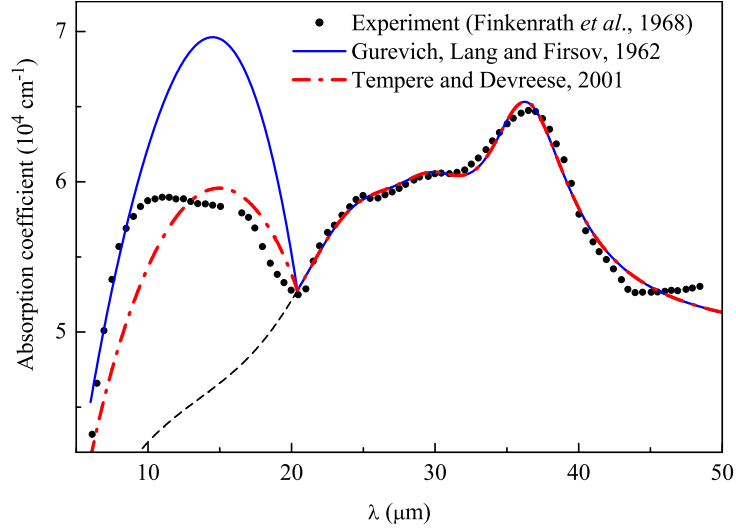


FIG. 6: Optical absorption spectrum of a CdO-film with the carrier concentration $n = 5.9 \times 10^{19} \text{ cm}^{-3}$ at $T = 300 \text{ K}$. The experimental data (solid dots) of Ref. [74] are compared to different theoretical results: with (solid curve) and without (dashed line) the one-polaron contribution of Ref. [71] and for many polarons (dash-dotted curve) of Ref. [53].

III. OPTICAL ABSORPTION. STRONG COUPLING

The absorption of light by free large polarons was treated in Ref. [49] using the polaron states obtained within the adiabatic strong-coupling approximation, which was considered above in subsection IE 3.

It was argued in Ref. [49], that for sufficiently large α ($\alpha > 3$), the (first) RES of a polaron is a relatively stable state, which can participate in optical absorption transitions. This idea was necessary to understand the polaron optical absorption spectrum in the strong-coupling regime. The following scenario of a transition, which leads to a “zero-phonon” peak in the absorption by a strong-coupling polaron, can then be suggested. If the frequency of the incoming photon is equal to

$$\Omega_{\text{RES}} \equiv \frac{E_{\text{RES}} - E_0}{\hbar} = 0.065\alpha^2\omega_{\text{LO}},$$

then the electron jumps from the ground state (which, at large coupling, is well-characterized by "s"-symmetry for the electron) to an excited state ("2p"), while the lattice polarization in the final state is adapted to the "2p" electronic state of the polaron. In Ref. [49] considering the decay of the RES with emission of one real phonon it is demonstrated, that the "zero-phonon" peak can be described using the Wigner-Weisskopf formula valid when the linewidth of that peak is much smaller than $\hbar\omega_{\text{LO}}$.

For photon energies larger than

$$\Omega_{\text{RES}} + \omega_{\text{LO}},$$

a transition of the polaron towards the first scattering state, belonging to the RES, becomes possible. The final state of the optical absorption process then consists of a polaron in its lowest RES plus a free phonon. A "one-phonon sideband" then appears in the polaron absorption spectrum. This process is called *one-phonon sideband absorption*.

The one-, two-, ... K -, ... phonon sidebands of the zero-phonon peak give rise to a broad structure in the absorption spectrum. It turns that the *first moment* of the phonon sidebands corresponds to the FC frequency Ω_{FC} :

$$\Omega_{\text{FC}} \equiv \frac{E_{\text{FC}} - E_0}{\hbar} = 0.141\alpha^2\omega_{\text{LO}}.$$

To summarize, the polaron optical absorption spectrum at strong coupling is characterized by the following features ($T = 0$):

- a) An intense absorption peak ("zero-phonon line") appears, which corresponds to a transition from the ground state to the first RES at Ω_{RES} .
- b) For $\Omega > \Omega_{\text{RES}} + \omega_{\text{LO}}$, a phonon sideband structure arises. This sideband structure peaks around Ω_{FC} .

The qualitative behaviour predicted in Ref. [49], namely, an intense zero-phonon (RES) line with a broader sideband at the high-frequency side, was confirmed after an all-coupling expression for the polaron optical absorption coefficient at $\alpha = 5, 6, 7$ had been studied [50].

In what precedes, the low-frequency end of the polaron absorption spectrum was discussed; at higher frequencies, transitions to higher RES and their scattering states can appear. The two-phonon sidebands in the optical absorption of free polarons in the strong-coupling limit were numerically studied in Ref. [75].

The study of the optical absorption of polarons at large coupling is mainly of formal interest because all reported coupling constants of polar semiconductors and ionic crystals are smaller than 5 (see Table 1).

IV. ARBITRARY COUPLING

A. Impedance function of large polarons: An alternative derivation of FHIP [76]

a. Definitions We derive here the linear response of the Fröhlich polaron, described by the Hamiltonian

$$H = \frac{\mathbf{p}^2}{2m_b} + \sum_{\mathbf{k}} \hbar\omega_{\mathbf{k}} a_{\mathbf{k}}^{\dagger} a_{\mathbf{k}} + \sum_{\mathbf{k}} (V_{\mathbf{k}} a_{\mathbf{k}} e^{i\mathbf{k}\cdot\mathbf{r}} + V_{\mathbf{k}}^* a_{\mathbf{k}}^{\dagger} e^{-i\mathbf{k}\cdot\mathbf{r}}), \quad (4.1)$$

to a spatially uniform, time-varying electric field

$$\mathbf{E}_{\Omega}(t) = E_0 \exp(i\Omega t) \mathbf{e}_x. \quad (4.2)$$

This field induces a current in the x -direction

$$j_{\Omega}(t) = \frac{1}{Z(\Omega)} E_{\Omega}(t). \quad (4.3)$$

The complex function $Z(\Omega)$ is called the impedance function. The frequency-dependent mobility is defined by

$$\mu(\Omega) = \text{Re} \frac{1}{Z(\Omega)}. \quad (4.4)$$

For nonzero frequencies (in the case of polarons the frequencies of interest are in the infrared) one defines the absorption coefficient [50]

$$\Gamma(\Omega) = \frac{1}{n\epsilon_0 c} \text{Re} \frac{1}{Z(\Omega)}, \quad (4.5)$$

where ϵ_0 is the dielectric constant of the vacuum, n the refractive index of the crystal, and c the velocity of light. In the following the amplitude of the electric field E_0 is taken sufficiently small so that linear-response theory can be applied.

The impedance function can be expressed via a frequency-dependent conductivity of a single polaron in a unit volume

$$\frac{1}{Z(\Omega)} = \sigma(\Omega) \quad (4.6)$$

using *the standard Kubo formula* (cf. Eq. (3.8.8) from Ref. [72]):

$$\sigma(\Omega) = i \frac{e^2}{Vm_b\Omega} + \frac{1}{V\hbar\Omega} \int_0^\infty e^{i\Omega t} \langle [j_x(t), j_x] \rangle dt. \quad (4.7)$$

In order to introduce a convenient representation of the impedance function, we give in the next subsection a definition and discuss properties of a scalar product of two operators [cf. [77], Chapter 5].

b. Definition and properties of the scalar product For two operators A and B (i.e., elements of the Hilbert space of operators) the scalar product is defined as

$$(A, B) = \int_0^\beta d\lambda \langle (e^{\lambda h L} A^\dagger) B \rangle. \quad (4.8)$$

The notation $(e^{\lambda h L} A^\dagger)$ is used in order to indicate that the operator $e^{\lambda h L}$ acts on the operator A^\dagger . The time evolution of the operator A is determined by the Liouville operator L :

$$-i \frac{\partial A}{\partial t} = LA \equiv \frac{1}{\hbar} [H, A] \quad (4.9)$$

with a commutator $[H, A]$, wherefrom

$$A(t) = e^{iLt} A(0) \equiv e^{iHt/\hbar} A(0) e^{-iHt/\hbar}. \quad (4.10)$$

The expectation value in (4.8) is taken over the Gibbs' ensemble:

$$\langle A \rangle = \text{Tr}(\rho_0(H) A) \quad (4.11)$$

with the equilibrium density matrix when the electric field is absent

$$\rho_0(H) = e^{-\beta H} / \text{Tr}(e^{-\beta H}). \quad (4.12)$$

One can show that (4.8) defines a positive definite scalar product with the following properties

$$(i) \quad (A, B) = (B^\dagger, A^\dagger), \quad (4.13)$$

$$(ii) \quad (A, LB) = (LA, B), \quad (4.14)$$

$$(iii) \quad (A, LB) = \frac{1}{\hbar} \langle [A^\dagger, B] \rangle, \quad (4.15)$$

and [cf. Eq. (5.11) of [77]]

$$(iv) \quad (A, B)^* = (B, A) \quad (4.16)$$

Demonstration of the property (4.13). Starting from the definition (4.8) and using (4.10), we obtain

$$(A, B) = \int_0^\beta d\lambda \langle e^{\lambda H} A^\dagger e^{-\lambda H} B \rangle. \quad (4.17)$$

Substituting here (4.11) with (4.12), one finds

$$(A, B) = \int_0^\beta d\lambda \text{Tr} [e^{-(\beta-\lambda)H} A^\dagger e^{-\lambda H} B] / \text{Tr}(e^{-\beta H}).$$

Change of the variable $\lambda' = \beta - \lambda$ allows us to represent this integral as

$$(A, B) = \int_0^\beta d\lambda' \text{Tr} [e^{-\lambda' H} A^\dagger e^{-(\beta-\lambda')H} B] / \text{Tr}(e^{-\beta H}).$$

Further, a cyclic permutation of the operators under the trace Tr sign gives

$$\begin{aligned} (A, B) &= \int_0^\beta d\lambda \text{Tr} [e^{-(\beta-\lambda)H} B e^{-\lambda H} A^\dagger] / \text{Tr}(e^{-\beta H}) \\ &= \int_0^\beta d\lambda \langle e^{\lambda H} B e^{-\lambda H} A^\dagger \rangle = \int_0^\beta d\lambda \langle (e^{\lambda h L} B) A^\dagger \rangle \\ &= \int_0^\beta d\lambda \langle [e^{\lambda h L} (B^\dagger)^\dagger] A^\dagger \rangle. \end{aligned}$$

According to the definition (4.8), this finalizes the demonstration of (4.13).

Demonstration of the property (4.14). Starting from (4.17) and using (4.9), we obtain

$$\begin{aligned} (A, LB) &= \int_0^\beta d\lambda \langle e^{\lambda H} A^\dagger e^{-\lambda H} LB \rangle \\ &= \frac{1}{\hbar} \int_0^\beta d\lambda \langle e^{\lambda H} A^\dagger e^{-\lambda H} (HB - BH) \rangle. \end{aligned}$$

A cyclic permutation of the operators under the average $\langle \bullet \rangle$ sign gives

$$(A, LB) = \frac{1}{\hbar} \int_0^\beta d\lambda \langle e^{\lambda H} A^\dagger e^{-\lambda H} HB - He^{\lambda H} A^\dagger e^{-\lambda H} B \rangle. \quad (4.18)$$

Using the commutation of H and $e^{\pm\lambda H}$, one finds

$$(A, LB) = \frac{1}{\hbar} \int_0^\beta d\lambda \langle e^{\lambda H} A^\dagger H e^{-\lambda H} B - e^{\lambda H} H A^\dagger e^{-\lambda H} B \rangle \quad (4.19)$$

$$= \frac{1}{\hbar} \int_0^\beta d\lambda \langle e^{\lambda H} (A^\dagger H - H A^\dagger) e^{-\lambda H} B \rangle \quad (4.20)$$

$$= \frac{1}{\hbar} \int_0^\beta d\lambda \langle e^{\lambda H} (HA - AH)^\dagger e^{-\lambda H} B \rangle \quad (4.21)$$

$$= \int_0^\beta d\lambda \left\langle e^{\lambda H} \left(\frac{1}{\hbar} [H, A] \right)^\dagger e^{-\lambda H} B \right\rangle. \quad (4.22)$$

With the definition (4.9), this gives

$$(A, LB) = \int_0^\beta d\lambda \left\langle e^{\lambda H} (LA)^\dagger e^{-\lambda H} B \right\rangle = \int_0^\beta d\lambda \left\langle \left[e^{\lambda \hbar L} (LA)^\dagger \right] B \right\rangle.$$

According to the definition (4.8), this finalizes the demonstration of (4.14).

Demonstration of the property (4.15). Starting from (4.20) and performing a cyclic permutation of the operators under the average $\langle \bullet \rangle$, we find

$$(A, LB) = \frac{1}{\hbar} \int_0^\beta d\lambda \left\langle e^{\lambda H} (A^\dagger H - H A^\dagger) e^{-\lambda H} B \right\rangle$$

Further we notice that

$$e^{\lambda H} (A^\dagger H - H A^\dagger) e^{-\lambda H} = -\frac{d(e^{\lambda H} A^\dagger e^{-\lambda H})}{d\lambda},$$

consequently,

$$\begin{aligned} (A, LB) &= -\frac{1}{\hbar} \int_0^\beta d\lambda \left\langle \frac{d(e^{\lambda H} A^\dagger e^{-\lambda H})}{d\lambda} B \right\rangle \\ &= -\frac{1}{\hbar} \left\langle \int_0^\beta d\lambda \frac{d(e^{\lambda H} A^\dagger e^{-\lambda H})}{d\lambda} B \right\rangle \\ &= -\frac{1}{\hbar} \left\langle e^{\lambda H} A^\dagger e^{-\lambda H} B \Big|_0^\beta \right\rangle = \frac{1}{\hbar} \langle (A^\dagger B - e^{\beta H} A^\dagger e^{-\beta H} B) \rangle \\ &= \frac{1}{\hbar} \text{Tr} [e^{-\beta H} (A^\dagger B - e^{\beta H} A^\dagger e^{-\beta H} B)] / \text{Tr}(e^{-\beta H}) \\ &= \frac{1}{\hbar} \text{Tr} [e^{-\beta H} A^\dagger B - A^\dagger e^{-\beta H} B] / \text{Tr}(e^{-\beta H}). \end{aligned} \quad (4.23)$$

Further, a cyclic permutation of the operators in the second term under the trace Tr sign gives

$$\begin{aligned} (A, LB) &= \frac{1}{\hbar} \text{Tr} [e^{-\beta H} A^\dagger B - e^{-\beta H} B A^\dagger] / \text{Tr}(e^{-\beta H}) \\ &= \frac{1}{\hbar} \text{Tr} [e^{-\beta H} (A^\dagger B - B A^\dagger)] / \text{Tr}(e^{-\beta H}) \\ &= \frac{1}{\hbar} \langle A^\dagger B - B A^\dagger \rangle = \frac{1}{\hbar} \langle [A^\dagger, B] \rangle. \end{aligned}$$

Thus, the property (4.15) has been demonstrated.

Demonstration of the property (4.16). We start from the representation of the scalar product (4.17) and take a complex conjugate:

$$(A, B)^* = \int_0^\beta d\lambda \langle e^{\lambda H} A^\dagger e^{-\lambda H} B \rangle^* = \int_0^\beta d\lambda \langle B^\dagger e^{-\lambda H} A e^{\lambda H} \rangle.$$

A cyclic permutation of the operators under the average $\langle \bullet \rangle$ sign gives then

$$\begin{aligned} (A, B)^* &= \int_0^\beta d\lambda \langle e^{\lambda H} B^\dagger e^{-\lambda H} A \rangle = \int_0^\beta d\lambda \langle e^{\lambda H} B^\dagger e^{-\lambda H} A \rangle \\ &= \int_0^\beta d\lambda \langle (e^{\lambda h L} B^\dagger) A \rangle. \end{aligned} \quad (4.24)$$

According to the definition (4.8), this finalizes the demonstration of (4.16).

The above scalar product allows one to represent different dynamical quantities in a rather simple way. For example, let us consider a scalar product

$$\Phi_{AB}(z) = \left(A, \frac{1}{z-L} B \right) \quad (4.25)$$

$$\begin{aligned} &= \int_0^\beta d\lambda \left\langle (e^{\lambda h L} A^\dagger) \frac{1}{z-L} B \right\rangle \\ &= -i \int_0^\beta d\lambda \left\langle e^{\lambda h L} A^\dagger \left[\int_0^\infty dt e^{i(z-L)t} \right] B \right\rangle \end{aligned} \quad (4.26)$$

$$\begin{aligned} &= -i \int_0^\infty dt e^{izt} \int_0^\beta d\lambda \langle e^{\lambda h L} A^\dagger e^{-iLt} B \rangle \\ &= -i \int_0^\infty dt e^{izt} \int_0^\beta d\lambda \langle e^{\lambda H} A^\dagger e^{-\lambda H} e^{-iHt/\hbar} B e^{iHt/\hbar} \rangle \\ &= -i \int_0^\infty dt e^{izt} \int_0^\beta d\lambda \langle e^{iHt/\hbar + \lambda H} A^\dagger e^{-iHt/\hbar - \lambda H} B \rangle \\ &= -i \int_0^\infty dt e^{izt} \int_0^\beta d\lambda \langle e^{iH(t-i\lambda\hbar)/\hbar} A^\dagger e^{-iH(t-i\lambda\hbar)/\hbar} B \rangle \\ &= -i \int_0^\infty dt e^{izt} \int_0^\beta d\lambda \langle e^{iL(t-i\lambda\hbar)} A^\dagger B \rangle \end{aligned} \quad (4.27)$$

$$= -i \int_0^\infty dt e^{izt} \int_0^\beta d\lambda \langle A^\dagger(t - i\hbar\lambda) B(0) \rangle. \quad (4.28)$$

c. Representation of the impedance function in terms of the relaxation function The impedance function is related to the relaxation function

$$\Phi(z) \equiv \Phi_{\dot{x}\dot{x}}(z) = \left(\dot{x}, \frac{1}{z-L} \dot{x} \right), \quad (4.29)$$

where \dot{x} is the velocity operator, by the following expression:

$$\frac{1}{Z(\Omega)} = ie^2 \lim_{\epsilon \rightarrow 0} \Phi(\Omega + i\epsilon) \quad (4.30)$$

($z = \Omega + i\epsilon, \epsilon > 0$).

Demonstration of the representation (4.29). Apply (4.27) to the relaxation function entering (4.30):

$$\Phi(z) = -i \int_0^\beta d\lambda \int_0^\infty dt e^{izt} \langle (e^{i(t-i\hbar\lambda)L} \dot{x}) \dot{x} \rangle$$

and perform the integration by parts using the formula

$$\begin{aligned} \int_0^\infty e^{izt} f(t) dt &= -\frac{i}{z} f(t) e^{izt} \Big|_{t=0}^\infty + \frac{i}{z} \int_0^\infty \frac{\partial f(t)}{\partial t} e^{izt} dt \\ &= \frac{i}{z} f(0) + \frac{i}{z} \int_0^\infty \frac{\partial f(t)}{\partial t} e^{izt} dt : \end{aligned}$$

$$\begin{aligned} \int_0^\infty e^{izt} \langle (e^{i(t-i\hbar\lambda)L} \dot{x}) \dot{x} \rangle dt &= \frac{i}{z} \langle (e^{\hbar\lambda L} \dot{x}) \dot{x} \rangle + \frac{i}{z} \int_0^\infty e^{izt} \frac{\partial}{\partial t} \langle (e^{i(t-i\hbar\lambda)L} \dot{x}) \dot{x} \rangle dt \\ &= \frac{i}{z} \langle (e^{\hbar\lambda L} \dot{x}) \dot{x} \rangle - \frac{1}{z} \int_0^\infty e^{izt} \langle L (e^{i(t-i\hbar\lambda)L} \dot{x}) \dot{x} \rangle dt. \end{aligned}$$

This allows us to represent the relaxation function in the form

$$\begin{aligned} \Phi(z) &= -i \int_0^\beta d\lambda \left(\frac{i}{z} \langle (e^{\hbar\lambda L} \dot{x}) \dot{x} \rangle - \frac{1}{z} \int_0^\infty e^{izt} \langle L (e^{i(t-i\hbar\lambda)L} \dot{x}) \dot{x} \rangle dt \right) \\ &= \frac{1}{z} \int_0^\beta d\lambda \langle (e^{\hbar\lambda L} \dot{x}) \dot{x} \rangle + \frac{i}{z} \int_0^\beta d\lambda \int_0^\infty e^{izt} \langle L (e^{i(t-i\hbar\lambda)L} \dot{x}) \dot{x} \rangle dt \\ &= \frac{1}{m_b z} + \frac{i}{z} \int_0^\beta d\lambda \int_0^\infty e^{izt} \langle L (e^{i(t-i\hbar\lambda)L} \dot{x}) \dot{x} \rangle dt, \end{aligned}$$

where the expression (4.55) is inserted in the first term. Further on, the integral over λ is taken as follows:

$$\begin{aligned} \int_0^\beta d\lambda \langle L (e^{i(t-i\hbar\lambda)L} \dot{x}) \dot{x} \rangle &= \left\langle \left(L \int_0^\beta e^{i(t-i\hbar\lambda)L} d\lambda \dot{x} \right) \dot{x} \right\rangle \\ &= \frac{1}{\hbar} \langle (e^{iLt} (e^{\hbar\beta L} - 1) \dot{x}) \dot{x} \rangle \\ &= \frac{1}{\hbar} \langle e^{iLt} (e^{\hbar\beta L} \dot{x} - \dot{x}) \dot{x} \rangle \\ &= \frac{1}{\hbar} \langle (e^{\hbar\beta L} \dot{x}(t) - \dot{x}(t)) \dot{x} \rangle \\ &= \frac{1}{\hbar} \langle (e^{\beta H} \dot{x}(t) e^{-\beta H} - \dot{x}(t)) \dot{x} \rangle \\ &= \frac{1}{\hbar \text{Tr} e^{-\beta H}} \text{Tr} [e^{-\beta H} (e^{\beta H} \dot{x}(t) e^{-\beta H} - \dot{x}(t)) \dot{x}] \\ &= \frac{1}{\hbar \text{Tr} e^{-\beta H}} \text{Tr} [(\dot{x}(t) e^{-\beta H} - e^{-\beta H} \dot{x}(t)) \dot{x}] \\ &= \frac{1}{\hbar \text{Tr} e^{-\beta H}} \text{Tr} [e^{-\beta H} (\dot{x} \dot{x}(t) - \dot{x}(t) \dot{x})] \\ &= \frac{1}{\hbar} \langle \dot{x} \dot{x}(t) - \dot{x}(t) \dot{x} \rangle = -\frac{1}{\hbar} \langle \dot{x}(t), \dot{x} \rangle. \end{aligned}$$

Hence,

$$\Phi(z) = \frac{1}{m_b z} - \frac{i}{\hbar z} \int_0^\infty dt e^{izt} \langle [\dot{x}(t), \dot{x}] \rangle. \quad (4.31)$$

When setting $z = \Omega + i\varepsilon$ with $\varepsilon \rightarrow +0$, we have

$$\Phi(\Omega + i\varepsilon) = \frac{1}{m_b} \frac{1}{\Omega + i\varepsilon} - \frac{i}{\hbar(\Omega + i\varepsilon)} \int_0^\infty e^{i(\Omega+i\varepsilon)t} \langle [\dot{x}(t), \dot{x}] \rangle dt. \quad (4.32)$$

For $\Omega \neq 0$, we can set

$$\Phi(\Omega + i\varepsilon) = \frac{1}{m_b} \frac{1}{\Omega} - \frac{i}{\hbar\Omega} \int_0^\infty e^{i(\Omega+i\varepsilon)t} \langle [\dot{x}(t), \dot{x}] \rangle dt. \quad (4.33)$$

Multiplying $\Phi(\Omega + i\varepsilon)$ by ie^2 , we find that

$$\begin{aligned} ie^2\Phi(\Omega + i\varepsilon) &= ie^2 \left(\frac{1}{m_b} \frac{1}{\Omega} - \frac{i}{\hbar\Omega} \int_0^\infty e^{i(\Omega+i\varepsilon)t} \langle [\dot{x}(t), \dot{x}] \rangle dt \right) \\ &= i \frac{e^2}{m_b\Omega} + \frac{e^2}{\hbar\Omega} \int_0^\infty e^{i(\Omega+i\varepsilon)t} \langle [\dot{x}(t), \dot{x}] \rangle dt \\ &= i \frac{e^2}{m_b\Omega} + \frac{1}{\hbar\Omega} \int_0^\infty e^{i(\Omega+i\varepsilon)t} \langle [j_x(t), j_x] \rangle dt, \end{aligned} \quad (4.34)$$

where the electric current density is

$$j_x = -e\dot{x}.$$

Substituting further (4.34) in (4.30), we arrive at

$$\frac{1}{Z(\Omega)} = i \frac{e^2}{m_b\Omega} + \lim_{\varepsilon \rightarrow 0} \frac{1}{\hbar\Omega} \int_0^\infty e^{i(\Omega+i\varepsilon)t} \langle [j_x(t), j_x] \rangle dt,$$

what coincides with the expression of the impedance function (4.6) through a frequency-dependent conductivity given by the Kubo formula (4.7), q.e.d.

d. Application of the projection operator technique Using the Mori-Zwanzig projection operator technique (cf. [77], Chapter 5), the relaxation function (4.29)

$$\Phi(z) = \left(\dot{x}, \frac{1}{z - L} \dot{x} \right)$$

can be represented in a form, which is especially convenient for the application in the theory of the optical absorption of polarons.

The projection operator P ($Q = 1 - P$) is defined as

$$PA = \frac{\dot{x}(\dot{x}, A)}{\chi} \quad (4.35)$$

with A an operator and

$$\chi = (\dot{x}, \dot{x}). \quad (4.36)$$

The projection operator $Q = 1 - P$ projects an operator onto the space orthogonal to the space containing \dot{x} . Here we give some examples of the action of the projection operators:

$$P\dot{x} = \dot{x}, \quad Q\dot{x} = (1 - P)\dot{x} = 0; \quad (4.37)$$

$$Px = \frac{\dot{x}(\dot{x}, x)}{\chi} = \frac{\dot{x}(iLx, x)}{\chi} = -\frac{i\dot{x}(x, Lx)}{\chi} = -\frac{i\dot{x}}{\chi} \langle [x, x] \rangle = 0, \quad (4.38)$$

$$Qx = (1 - P)x = x. \quad (4.39)$$

$$Pa_{\mathbf{k}} = \frac{\dot{x}(\dot{x}, a_{\mathbf{k}})}{\chi} = \frac{\dot{x}(iLx, a_{\mathbf{k}})}{\chi} = -\frac{i\dot{x}(a_{\mathbf{k}}, Lx)}{\chi} = -\frac{i\dot{x}}{\chi} \langle [a_{\mathbf{k}}^\dagger, x] \rangle = 0, \quad (4.40)$$

$$Qa_{\mathbf{k}} = (1 - P)a_{\mathbf{k}} = a_{\mathbf{k}} \quad (4.41)$$

The projection operators P and Q are idempotent:

$$P^2A = \frac{\dot{x}\left(\dot{x}, \frac{\dot{x}(\dot{x}, A)}{\chi}\right)}{\chi} = \frac{\dot{x}(\dot{x}, A)}{\chi} = PA;$$

$$Q^2 = (1 - P)^2 = 1 - 2P + P^2 = 1 - P = Q.$$

The Liouville operator can be identically represented as $L = LP + LQ$. Then the operator $\frac{1}{z-L}$ in the relaxation function (4.29) can be represented as follows:

$$\frac{1}{z-L} = \frac{1}{z-LQ-LP}.$$

We use the algebraic operator identity:

$$\frac{1}{x+y} = \frac{1}{x} - \frac{1}{x}y\frac{1}{x+y}$$

with $x = z - LQ$ and $y = -LP$:

$$\frac{1}{z-L} = \frac{1}{z-LQ} + \frac{1}{z-LQ}LP\frac{1}{z-L}.$$

Consequently, the relaxation function (4.29) takes the form

$$\Phi(z) = \left(\dot{x}, \frac{1}{z-LQ}\dot{x}\right) + \left(\dot{x}, \frac{1}{z-LQ}LP\frac{1}{z-L}\dot{x}\right). \quad (4.42)$$

The first term in the r.h.s. of (4.42) simplifies as follows:

$$\left(\dot{x}, \frac{1}{z-LQ}\dot{x}\right) = \left(\dot{x}, \left[\frac{1}{z} + \frac{1}{z^2}LQ + \frac{1}{z^3}LQLQ + \dots\right]\dot{x}\right) = \left(\dot{x}, \frac{1}{z}\dot{x}\right)$$

because $Q\dot{x} = 0$. Using the quantity (4.36) we obtain:

$$\left(\dot{x}, \frac{1}{z-LQ}\dot{x}\right) = \frac{\chi}{z}. \quad (4.43)$$

The second term in the r.h.s. of (4.42) contains the operator

$$P \frac{1}{z-L} \dot{x}$$

which according to the definition of the projection operator P (4.35) can be transformed as

$$P \frac{1}{z-L} \dot{x} = \frac{\dot{x}}{\chi} \left(\dot{x}, \frac{1}{z-L} \dot{x} \right) = \frac{\dot{x}}{\chi} \Phi(z). \quad (4.44)$$

It is remarkable that this term is exactly expressed in terms of the sought relaxation function (4.29). Substituting (4.43) and (4.44) in (4.42), we find

$$\begin{aligned} \Phi(z) &= \frac{\chi}{z} + \left(\dot{x}, \frac{1}{z-LQ} L \frac{\dot{x}}{\chi} \right) \Phi(z) \Rightarrow \\ z\Phi(z) &= \chi + \left(\dot{x}, \frac{z}{z-LQ} L \frac{\dot{x}}{\chi} \right) \Phi(z) \\ &= \chi + \left(\dot{x}, \frac{z-LQ+LQ}{z-LQ} L \frac{\dot{x}}{\chi} \right) \Phi(z) \\ &= \chi + \left(\dot{x}, \left[1 + \frac{LQ}{z-LQ} \right] L \frac{\dot{x}}{\chi} \right) \Phi(z) \Rightarrow \\ z\Phi(z) &= \chi + \left[\frac{(\dot{x}, L\dot{x})}{\chi} + \frac{1}{\chi} \left(\dot{x}, \frac{LQ}{z-LQ} L\dot{x} \right) \right] \Phi(z). \end{aligned} \quad (4.45)$$

Introducing the quantity

$$O = \frac{(\dot{x}, L\dot{x})}{\chi} \quad (4.46)$$

and the function called the *memory function*

$$\Sigma(z) = \frac{1}{\chi} \left(\dot{x}, LQ \frac{1}{z-LQ} L\dot{x} \right), \quad (4.47)$$

we represent (4.45) in the form of the equation

$$[z - O - \Sigma(z)] \Phi(z) = \chi.$$

A solution of this equation gives the relaxation function $\Phi(z)$ represented within the Mori-Zwanzig projection operator technique:

$$\Phi(z) = \frac{\chi}{z - O - \Sigma(z)}. \quad (4.48)$$

The memory function (4.47) can be still transformed to another useful form. First of all, we apply the property of a scalar product (4.14):

$$\Sigma(z) = \frac{1}{\chi} \left(L\dot{x}, Q \frac{1}{z - LQ} L\dot{x} \right) \quad (4.49)$$

$$= \frac{1}{\chi} \left((P + Q)L\dot{x}, Q \frac{1}{z - LQ} L\dot{x} \right) \quad (4.50)$$

$$= \frac{1}{\chi} \left(PL\dot{x}, Q \frac{1}{z - LQ} L\dot{x} \right) + \frac{1}{\chi} \left(QL\dot{x}, Q \frac{1}{z - LQ} L\dot{x} \right). \quad (4.51)$$

For any two operators A and B

$$\begin{aligned} (PA, QB) &= \left(\frac{\dot{x}(\dot{x}, A)}{\chi}, \left[B - \frac{\dot{x}(\dot{x}, B)}{\chi} \right] \right) \\ &= \frac{(\dot{x}, A)}{\chi} \left[(\dot{x}, B) - \frac{(\dot{x}, \dot{x})(\dot{x}, B)}{\chi} \right] \\ &= \frac{(\dot{x}, A)}{\chi} [(\dot{x}, B) - (\dot{x}, B)] = 0, \end{aligned}$$

therefore the first term on the r.h.s. in (4.49) vanishes, and we obtain

$$\Sigma(z) = \frac{1}{\chi} \left(QL\dot{x}, Q \frac{1}{z - LQ} L\dot{x} \right). \quad (4.52)$$

In this expression, the operator $Q \frac{1}{z - LQ}$ can be represented in the following form, using the fact that Q is the idempotent operator:

$$\begin{aligned} Q \frac{1}{z - LQ} &= Q \left[\frac{1}{z} + \frac{1}{z^2} LQ + \frac{1}{z^3} LQLQ + \dots \right] \\ &= \frac{1}{z} Q + \frac{1}{z^2} QLQ + \frac{1}{z^3} QLQLQ + \dots \\ &= \frac{1}{z} Q + \frac{1}{z^2} QLQ^2 + \frac{1}{z^3} QLQ^2LQ^2 + \dots \\ &= \left[\frac{1}{z} + \frac{1}{z^2} QLQ + \frac{1}{z^3} QLQQLQ + \dots \right] Q \Rightarrow \\ Q \frac{1}{z - LQ} &= \frac{1}{z - QLQ} Q. \end{aligned} \quad (4.53)$$

A new Liouville operator can be defined, $\mathcal{L} = QLQ$, which describes the time evolution in the Hilbert space of operators, which is orthogonal complement of \dot{x} . Substituting then (4.53) with the operator \mathcal{L} into (4.52), we bring it to the form, which will be used in what follows.

$$\Sigma(z) = \frac{1}{\chi} \left(QL\dot{x}, \frac{1}{z - \mathcal{L}} QL\dot{x} \right). \quad (4.54)$$

For the Hamiltonian (1.16) we obtain the following quantities:

$$\chi = (\dot{x}, \dot{x}) = \left(\frac{p_x}{m_b}, iLx \right) = \frac{i}{m_b \hbar} (p_x, Lx)$$

Using (4.15), we find

$$\chi = \frac{i}{m_b \hbar} \langle [p_x, x] \rangle = \frac{i}{m_b \hbar} \langle (-i\hbar) \rangle = \frac{1}{m_b} \quad (4.55)$$

and

$$O = \frac{(\dot{x}, L\dot{x})}{\chi} = m_b \frac{1}{\hbar} \langle [\dot{x}, \dot{x}] \rangle = 0. \quad (4.56)$$

Substituting (4.55) and (4.56) in (4.48), one obtains

$$\Phi(z) = \frac{1}{m_b} \frac{1}{z - \Sigma(z)}. \quad (4.57)$$

The operator

$$\begin{aligned} L\dot{x} &= L \frac{p_x}{m_b} = \frac{1}{m_b \hbar} [H, p_x] = \\ &= -\frac{1}{m_b \hbar} \left[p_x, \sum_{\mathbf{k}} (V_k a_{\mathbf{k}} e^{i\mathbf{k}\cdot\mathbf{r}} + V_k^* a_{\mathbf{k}}^\dagger e^{-i\mathbf{k}\cdot\mathbf{r}}) \right] \\ &= \frac{i}{m_b} \sum_{\mathbf{k}} k_x (V_k a_{\mathbf{k}} e^{i\mathbf{k}\cdot\mathbf{r}} - V_k^* a_{\mathbf{k}}^\dagger e^{-i\mathbf{k}\cdot\mathbf{r}}) \Rightarrow \\ L\dot{x} &= -\frac{1}{m_b} \sum_{\mathbf{k}} k_x (V_k a_{\mathbf{k}} e^{i\mathbf{k}\cdot\mathbf{r}} - V_k^* a_{\mathbf{k}}^\dagger e^{-i\mathbf{k}\cdot\mathbf{r}}) \end{aligned} \quad (4.58)$$

does not depend on the velocities. Therefore, multiplying both parts of (4.58) with Q and taking into account (4.39) and (4.41), we obtain

$$QL\dot{x} = -\frac{1}{m_b} \sum_{\mathbf{k}} k_x (V_k a_{\mathbf{k}} e^{i\mathbf{k}\cdot\mathbf{r}} - V_k^* a_{\mathbf{k}}^\dagger e^{-i\mathbf{k}\cdot\mathbf{r}}),$$

what allows us to represent the memory function in the form

$$\begin{aligned} \Sigma(z) &= \frac{1}{\chi} \left(QL\dot{x}, \frac{1}{z - \mathcal{L}} QL\dot{x} \right) \\ &= \frac{1}{m_b} \sum_{\mathbf{k}} \sum_{\mathbf{k}'} \left(\begin{array}{c} k_x (V_k a_{\mathbf{k}} e^{i\mathbf{k}\cdot\mathbf{r}} - V_k^* a_{\mathbf{k}}^\dagger e^{-i\mathbf{k}\cdot\mathbf{r}}), \\ \frac{1}{z - \mathcal{L}} k'_x (V_{k'} a_{\mathbf{k}'} e^{i\mathbf{k}'\cdot\mathbf{r}} - V_{k'}^* a_{\mathbf{k}'}^\dagger e^{-i\mathbf{k}'\cdot\mathbf{r}}) \end{array} \right) \\ &= \frac{1}{m_b} \sum_{\mathbf{k}} \sum_{\mathbf{k}'} k_x k'_x V_k V_{k'}^* \left(\begin{array}{c} (a_{\mathbf{k}} e^{i\mathbf{k}\cdot\mathbf{r}} + a_{\mathbf{k}}^\dagger e^{-i\mathbf{k}\cdot\mathbf{r}}), \\ \frac{1}{z - \mathcal{L}} (a_{\mathbf{k}'} e^{i\mathbf{k}'\cdot\mathbf{r}} + a_{\mathbf{k}'}^\dagger e^{-i\mathbf{k}'\cdot\mathbf{r}}) \end{array} \right). \end{aligned} \quad (4.59)$$

In transition to (4.59) we have used the property of the amplitude (1.17): $V_k^* = -V_k$ and taken into account that according to the definition (4.8), the first operator enters a scalar product in the hermitian conjugate form. Introducing the operators

$$b_{\mathbf{k}} = a_{\mathbf{k}} e^{i\mathbf{k}\cdot\mathbf{r}}; b_{\mathbf{k}}^\dagger = a_{\mathbf{k}}^\dagger e^{-i\mathbf{k}\cdot\mathbf{r}},$$

we represent the memory function as

$$\Sigma(z) = \frac{1}{m_b} \sum_{\mathbf{k}} \sum_{\mathbf{k}'} k_x k'_x V_{\mathbf{k}} V_{\mathbf{k}'}^* \left((b_{\mathbf{k}} + b_{\mathbf{k}}^\dagger), \frac{1}{z - \mathcal{L}} (b_{\mathbf{k}'} + b_{\mathbf{k}'}^\dagger) \right). \quad (4.60)$$

We notice that $Qb_{\mathbf{k}} = Q(a_{\mathbf{k}}e^{i\mathbf{k}\cdot\mathbf{r}}) = a_{\mathbf{k}}e^{i\mathbf{k}\cdot\mathbf{r}} = b_{\mathbf{k}}$. It will be represented through the four relaxation functions:

$$\Sigma(z) = \frac{1}{m_b} \sum_{\mathbf{k}} \sum_{\mathbf{k}'} k_x k'_x V_{\mathbf{k}} V_{\mathbf{k}'}^* [\Phi_{\mathbf{k}\mathbf{k}'}^{++}(z) + \Phi_{\mathbf{k}\mathbf{k}'}^{--}(z) + \Phi_{\mathbf{k}\mathbf{k}'}^{+-}(z) + \Phi_{\mathbf{k}\mathbf{k}'}^{-+}(z)], \quad (4.61)$$

$$\Phi_{\mathbf{k}\mathbf{k}'}^{++}(z) = \left(b_{\mathbf{k}}^\dagger, \frac{1}{z - \mathcal{L}} b_{\mathbf{k}'}^\dagger \right), \quad (4.62)$$

$$\Phi_{\mathbf{k}\mathbf{k}'}^{--}(z) = \left(b_{\mathbf{k}}, \frac{1}{z - \mathcal{L}} b_{\mathbf{k}'} \right), \quad (4.63)$$

$$\Phi_{\mathbf{k}\mathbf{k}'}^{+-}(z) = \left(b_{\mathbf{k}}^\dagger, \frac{1}{z - \mathcal{L}} b_{\mathbf{k}'} \right), \quad (4.64)$$

$$\Phi_{\mathbf{k}\mathbf{k}'}^{-+}(z) = \left(b_{\mathbf{k}}, \frac{1}{z - \mathcal{L}} b_{\mathbf{k}'}^\dagger \right). \quad (4.65)$$

There exist relations between the above relaxation functions. For example, the relaxation function (4.63), takes the form

$$\begin{aligned} \Phi_{\mathbf{k}\mathbf{k}'}^{--}(z) &= \left(b_{\mathbf{k}}, \frac{1}{z - \mathcal{L}} b_{\mathbf{k}'} \right) \\ &= -i \int_0^\infty dt e^{izt} (e^{i\mathcal{L}t} b_{\mathbf{k}}(0), b_{\mathbf{k}'}(0)). \end{aligned}$$

Then the complex conjugate of this relaxation function:

$$\begin{aligned} [\Phi_{\mathbf{k}\mathbf{k}'}^{--}(z)]^* &= i \int_0^\infty dt e^{-iz^*t} (e^{i\mathcal{L}t} b_{\mathbf{k}}(0), b_{\mathbf{k}'}(0))^* \\ &= i \int_0^\infty dt e^{-iz^*t} (b_{\mathbf{k}'}(0), e^{i\mathcal{L}t} b_{\mathbf{k}}(0)), \end{aligned}$$

where the property (4.16) has been used. The property (4.13) gives

$$\begin{aligned} [\Phi_{\mathbf{k}\mathbf{k}'}^{--}(z)]^* &= i \int_0^\infty dt e^{-iz^*t} (b_{\mathbf{k}'}(0), e^{i\mathcal{H}t/\hbar} b_{\mathbf{k}}(0) e^{-i\mathcal{H}t/\hbar}) \\ &= i \int_0^\infty dt e^{-iz^*t} (e^{i\mathcal{H}t/\hbar} b_{\mathbf{k}}^\dagger(0) e^{i\mathcal{H}t/\hbar}, b_{\mathbf{k}'}^\dagger(0)) \\ &= i \int_0^\infty dt e^{-iz^*t} (e^{i\mathcal{L}t} b_{\mathbf{k}}^\dagger(0), b_{\mathbf{k}'}^\dagger(0)) \\ &= i \int_0^\infty dt e^{-iz^*t} (b_{\mathbf{k}}^\dagger(t), b_{\mathbf{k}'}^\dagger(0)) = -\Phi_{\mathbf{k}\mathbf{k}'}^{++}(-z^*), \end{aligned}$$

wherefrom it follows that

$$\Phi_{\mathbf{k}\mathbf{k}'}^{--}(z) = - [\Phi_{\mathbf{k}\mathbf{k}'}^{++}(-z^*)]^*. \quad (4.66)$$

Similarly, the relation

$$\Phi_{\mathbf{k}\mathbf{k}'}^{-+}(z) = - [\Phi_{\mathbf{k}\mathbf{k}'}^{+-}(-z^*)]^* \quad (4.67)$$

is proven.

e. Memory function In this subsection we indicate which approximations must be made in the calculation of the relaxation functions in order to obtain the FHIP results for the impedance function. Consider the relaxation function (4.62):

$$\begin{aligned} \Phi_{\mathbf{k}\mathbf{k}'}^{++}(z) &= \left(b_{\mathbf{k}}^\dagger, \frac{1}{z - \mathcal{L}} b_{\mathbf{k}'}^\dagger \right) \\ &= -i \int_0^\infty dt e^{izt} \left(e^{i\mathcal{L}t} b_{\mathbf{k}}^\dagger(0), b_{\mathbf{k}'}^\dagger(0) \right) = -i \int_0^\infty dt e^{izt} \left(b_{\mathbf{k}}^\dagger(t), b_{\mathbf{k}'}^\dagger(0) \right), \end{aligned}$$

where $b_{\mathbf{k}}^\dagger(t) = e^{i\mathcal{L}t} b_{\mathbf{k}}^\dagger(0)$, and perform a partial integration:

$$\begin{aligned} \Phi_{\mathbf{k}\mathbf{k}'}^{++}(z) &= -\frac{1}{z} \int_0^\infty d(e^{izt}) \left(b_{\mathbf{k}}^\dagger(t), b_{\mathbf{k}'}^\dagger(0) \right) \\ &= -\frac{1}{z} e^{izt} \left(b_{\mathbf{k}}^\dagger(t), b_{\mathbf{k}'}^\dagger(0) \right) \Big|_0^\infty + \frac{1}{z} \int_0^\infty dt e^{izt} \left(\frac{db_{\mathbf{k}}^\dagger(t)}{dt}, b_{\mathbf{k}'}^\dagger(0) \right) \\ &= \frac{1}{z} \left(b_{\mathbf{k}}^\dagger(0), b_{\mathbf{k}'}^\dagger(0) \right) + \frac{1}{z} \int_0^\infty dt e^{izt} \left(i\mathcal{L} b_{\mathbf{k}}^\dagger(t), b_{\mathbf{k}'}^\dagger(0) \right) \\ &= \frac{1}{z} \left(b_{\mathbf{k}}^\dagger(0), b_{\mathbf{k}'}^\dagger(0) \right) - \frac{i}{z} \int_0^\infty dt e^{izt} \left(\mathcal{L} b_{\mathbf{k}}^\dagger(t), b_{\mathbf{k}'}^\dagger(0) \right). \end{aligned} \quad (4.68)$$

Here we supposed that

$$\lim_{t \rightarrow \infty} e^{izt} \left(b_{\mathbf{k}}^\dagger(t), b_{\mathbf{k}'}^\dagger(0) \right) = 0.$$

In the second term in (4.68),

$$\begin{aligned} \left(\mathcal{L} b_{\mathbf{k}}^\dagger(t), b_{\mathbf{k}'}^\dagger(0) \right) &= \left(\mathcal{L} e^{i\mathcal{L}t} b_{\mathbf{k}}^\dagger, b_{\mathbf{k}'}^\dagger \right) = \left(QLQ e^{iQLQt} b_{\mathbf{k}}^\dagger, b_{\mathbf{k}'}^\dagger(0) \right) \\ &= \left(QLQ e^{iQHQt/\hbar} b_{\mathbf{k}}^\dagger e^{-iQHQt/\hbar}, b_{\mathbf{k}'}^\dagger \right) \\ &= \left(QL e^{iQHQt/\hbar} b_{\mathbf{k}}^\dagger e^{-iQHQt/\hbar}, b_{\mathbf{k}'}^\dagger \right) \end{aligned}$$

because $Qb_{\mathbf{k}}^\dagger = b_{\mathbf{k}}^\dagger$ and $Q^2 = Q$. Further on, we have

$$\begin{aligned}
(\mathcal{L}b_{\mathbf{k}}^\dagger(t), b_{\mathbf{k}'}^\dagger(0)) &= \int_0^\beta d\lambda \left\langle e^{\lambda hL} e^{iQHQt/\hbar} b_{\mathbf{k}} e^{-iQHQt/\hbar} LQb_{\mathbf{k}'}^\dagger \right\rangle \\
&= \int_0^\beta d\lambda \left\langle e^{\lambda hL} e^{iQHQt/\hbar} b_{\mathbf{k}} e^{-iQHQt/\hbar} Lb_{\mathbf{k}'}^\dagger \right\rangle \\
&= \left(L e^{iQHQt/\hbar} b_{\mathbf{k}}^\dagger e^{-iQHQt/\hbar}, b_{\mathbf{k}'}^\dagger \right) \\
&= \left(Lb_{\mathbf{k}}^\dagger(t), b_{\mathbf{k}'}^\dagger(0) \right).
\end{aligned}$$

So, we find from (4.68)

$$\begin{aligned}
\Phi_{\mathbf{k}\mathbf{k}'}^{++}(z) &= \frac{1}{z} \left(b_{\mathbf{k}}^\dagger(0), b_{\mathbf{k}'}^\dagger(0) \right) - \frac{i}{z} \int_0^\infty dt e^{izt} \left(Lb_{\mathbf{k}}^\dagger(t), b_{\mathbf{k}'}^\dagger(0) \right) \\
&= \frac{1}{z} \left(b_{\mathbf{k}}^\dagger(0), b_{\mathbf{k}'}^\dagger(0) \right) - \frac{i}{z} \int_0^\infty dt e^{izt} \left(b_{\mathbf{k}}^\dagger(t), Lb_{\mathbf{k}'}^\dagger(0) \right) \\
&= \frac{1}{z} \left(b_{\mathbf{k}}^\dagger(0), b_{\mathbf{k}'}^\dagger(0) \right) - \frac{i}{z\hbar} \int_0^\infty dt e^{izt} \left\langle \left[b_{\mathbf{k}}(t), b_{\mathbf{k}'}^\dagger(0) \right] \right\rangle.
\end{aligned} \tag{4.69}$$

The first term in the r.h.s. of this expression can be represented as follows:

$$\begin{aligned}
\frac{1}{z} \left(b_{\mathbf{k}}^\dagger(0), b_{\mathbf{k}'}^\dagger(0) \right) &= \frac{1}{z} \int_0^\beta d\lambda \left\langle \left(e^{\lambda hL} b_{\mathbf{k}} \right) b_{\mathbf{k}'}^\dagger \right\rangle = \frac{1}{z} \left\langle \int_0^\beta d\lambda \left(e^{\lambda hL} b_{\mathbf{k}} \right) b_{\mathbf{k}'}^\dagger \right\rangle \\
&= \frac{1}{z} \left\langle \left(\frac{e^{\beta hL} - 1}{\hbar L} b_{\mathbf{k}} \right) b_{\mathbf{k}'}^\dagger \right\rangle = \frac{1}{z\hbar} \left\langle e^{\beta H} \frac{1}{L} b_{\mathbf{k}} e^{-\beta H} b_{\mathbf{k}'}^\dagger - \frac{1}{L} b_{\mathbf{k}} b_{\mathbf{k}'}^\dagger \right\rangle \\
&= \frac{1}{z\hbar} \frac{1}{\text{Tr} e^{-\beta H}} \text{Tr} \left\{ e^{-\beta H} \left[e^{\beta H} \frac{1}{L} b_{\mathbf{k}} e^{-\beta H} b_{\mathbf{k}'}^\dagger - \frac{1}{L} b_{\mathbf{k}} b_{\mathbf{k}'}^\dagger \right] \right\} \\
&= \frac{1}{z\hbar} \frac{1}{\text{Tr} e^{-\beta H}} \text{Tr} \left\{ b_{\mathbf{k}'}^\dagger \frac{1}{L} b_{\mathbf{k}} e^{-\beta H} - e^{-\beta H} \frac{1}{L} b_{\mathbf{k}} b_{\mathbf{k}'}^\dagger \right\} \\
&= \frac{1}{z\hbar} \left\langle b_{\mathbf{k}'}^\dagger \frac{1}{L} b_{\mathbf{k}} - \frac{1}{L} b_{\mathbf{k}} b_{\mathbf{k}'}^\dagger \right\rangle \\
&= \frac{i}{z\hbar} \left\langle b_{\mathbf{k}'}^\dagger \frac{1}{iL} b_{\mathbf{k}} - \frac{1}{iL} b_{\mathbf{k}} b_{\mathbf{k}'}^\dagger \right\rangle \\
&= \frac{i}{z\hbar} \left\langle \int_0^\infty dt e^{iLt} b_{\mathbf{k}} b_{\mathbf{k}'}^\dagger - \int_0^\infty dt b_{\mathbf{k}'}^\dagger e^{iLt} b_{\mathbf{k}} \right\rangle \\
&= \frac{i}{z\hbar} \left\langle \int_0^\infty dt b_{\mathbf{k}}(t) b_{\mathbf{k}'}^\dagger - \int_0^\infty dt b_{\mathbf{k}'}^\dagger b_{\mathbf{k}}(t) \right\rangle \\
&= \frac{i}{z\hbar} \int_0^\infty dt \left\langle \left[b_{\mathbf{k}}(t), b_{\mathbf{k}'}^\dagger(0) \right] \right\rangle.
\end{aligned}$$

Substituting it in the r.h.s. of (4.69), we find

$$\begin{aligned}
\Phi_{\mathbf{k}\mathbf{k}'}^{++}(z) &= \frac{i}{z\hbar} \int_0^\infty dt \left\langle \left[b_{\mathbf{k}}(t), b_{\mathbf{k}'}^\dagger(0) \right] \right\rangle - \frac{i}{z\hbar} \int_0^\infty dt e^{izt} \left\langle \left[b_{\mathbf{k}}(t), b_{\mathbf{k}'}^\dagger(0) \right] \right\rangle \\
&= \frac{i}{z\hbar} \int_0^\infty dt \left(1 - e^{izt} \right) \left\langle \left[b_{\mathbf{k}}(t), b_{\mathbf{k}'}^\dagger(0) \right] \right\rangle.
\end{aligned} \tag{4.70}$$

In a similar way one obtains

$$\Phi_{\mathbf{k}\mathbf{k}'}^{+-}(z) = \frac{i}{z\hbar} \int_0^\infty dt (1 - e^{izt}) \langle [b_{\mathbf{k}}(t), b_{\mathbf{k}'}(0)] \rangle. \quad (4.71)$$

Inserting the relaxation functions (4.70), (4.71), (4.66) and (4.67), we find the memory function (4.61)

$$\begin{aligned} \Sigma(z) &= \frac{1}{m_b} \sum_{\mathbf{k}} \sum_{\mathbf{k}'} k_x k'_x V_{\mathbf{k}} V_{\mathbf{k}'}^* \frac{i}{z\hbar} \int_0^\infty dt (1 - e^{izt}) \\ &\quad \times \left[\begin{aligned} &\left\langle [b_{\mathbf{k}}(t), b_{\mathbf{k}'}^\dagger(0)] \right\rangle + \langle [b_{\mathbf{k}}(t), b_{\mathbf{k}'}(0)] \rangle \\ &- \left\langle [b_{\mathbf{k}}(t), b_{\mathbf{k}'}^\dagger(0)] \right\rangle^* - \langle [b_{\mathbf{k}}(t), b_{\mathbf{k}'}(0)] \rangle^* \end{aligned} \right] \\ &= -\frac{1}{m_b} \sum_{\mathbf{k}} \sum_{\mathbf{k}'} k_x k'_x V_{\mathbf{k}} V_{\mathbf{k}'}^* \frac{2}{z\hbar} \int_0^\infty dt (1 - e^{izt}) \\ &\quad \times \text{Im} \left[\left\langle [b_{\mathbf{k}}(t), b_{\mathbf{k}'}^\dagger(0)] \right\rangle + \langle [b_{\mathbf{k}}(t), b_{\mathbf{k}'}(0)] \rangle \right], \end{aligned}$$

wherefrom

$$\Sigma(z) = \frac{1}{z} \int_0^\infty dt (1 - e^{izt}) \text{Im} F(t) \quad (4.72)$$

with

$$F(t) = -\frac{2}{m_b \hbar} \sum_{\mathbf{k}} \sum_{\mathbf{k}'} k_x k'_x V_{\mathbf{k}} V_{\mathbf{k}'}^* \left\{ \left\langle [b_{\mathbf{k}}(t), b_{\mathbf{k}'}^\dagger(0)] \right\rangle + \langle [b_{\mathbf{k}}(t), b_{\mathbf{k}'}(0)] \rangle \right\}. \quad (4.73)$$

f. Derivation of the memory function To calculate the expectation values in Eq. (4.73), we shall make the following approximations (cf. Ref. [78]). The Liouville operator \mathcal{L} , which determines the time evolution of the operator $b_{\mathbf{k}}^\dagger(t) = e^{i\mathcal{L}t} b_{\mathbf{k}}^\dagger(0)$, is replaced by $L_{ph} + L_F$, where L_{ph} is the Liouville operator for free phonons and L_F is the Liouville operator for the Feynman polaron model [43]. The Fröhlich Hamiltonian appearing in the statistical average $\langle \bullet \rangle$ is similarly replaced by $H_{ph} + H_F$, with H_{ph} the Hamiltonian of free phonons and H_F the Hamiltonian of the Feynman polaron model. With this approximation, e.g., the average

$$\left\langle b_{\mathbf{k}}(t) b_{\mathbf{k}'}^\dagger(0) \right\rangle = \left\langle a_{\mathbf{k}}(t) a_{\mathbf{k}'}^\dagger(0) \right\rangle \left\langle e^{i\mathbf{k}\cdot\mathbf{r}(t)} e^{-i\mathbf{k}'\cdot\mathbf{r}} \right\rangle = \delta_{\mathbf{k},\mathbf{k}'} \left\langle a_{\mathbf{k}}(t) a_{\mathbf{k}}^\dagger(0) \right\rangle \left\langle e^{i\mathbf{k}\cdot\mathbf{r}(t)} e^{-i\mathbf{k}\cdot\mathbf{r}} \right\rangle. \quad (4.74)$$

The time evolution of the free-phonon annihilation operator (4.10),

$$a_{\mathbf{k}}(t) = e^{iH_{ph}t/\hbar} a_{\mathbf{k}} e^{-iH_{ph}t/\hbar} = \exp(i\omega_{\mathbf{k}} a_{\mathbf{k}}^+ a_{\mathbf{k}} t) a_{\mathbf{k}} \exp(-i\omega_{\mathbf{k}} a_{\mathbf{k}}^+ a_{\mathbf{k}} t)$$

according to (4.9) is

$$\begin{aligned}
-i\frac{da_{\mathbf{k}}(t)}{dt} &= \omega_{\mathbf{k}} \exp(i\omega_{\mathbf{k}}a_{\mathbf{k}}^{\dagger}a_{\mathbf{k}}t) [a_{\mathbf{k}}^{\dagger}a_{\mathbf{k}}, a_{\mathbf{k}}] \exp(-i\omega_{\mathbf{k}}a_{\mathbf{k}}^{\dagger}a_{\mathbf{k}}t) \\
&= \omega_{\mathbf{k}} \exp(i\omega_{\mathbf{k}}a_{\mathbf{k}}^{\dagger}a_{\mathbf{k}}t) [a_{\mathbf{k}}^{\dagger}, a_{\mathbf{k}}] a_{\mathbf{k}} \exp(-i\omega_{\mathbf{k}}a_{\mathbf{k}}^{\dagger}a_{\mathbf{k}}t) \\
&= -\omega_{\mathbf{k}} \exp(i\omega_{\mathbf{k}}a_{\mathbf{k}}^{\dagger}a_{\mathbf{k}}t) a_{\mathbf{k}} \exp(-i\omega_{\mathbf{k}}a_{\mathbf{k}}^{\dagger}a_{\mathbf{k}}t) \Rightarrow \\
a_{\mathbf{k}}(t) &= \exp(-i\omega_{\mathbf{k}}t) a_{\mathbf{k}}.
\end{aligned}$$

Similarly,

$$a_{\mathbf{k}}^{\dagger}(t) = \exp(i\omega_{\mathbf{k}}t) a_{\mathbf{k}}^{\dagger}.$$

Hence, we have

$$\langle a_{\mathbf{k}}(t)a_{\mathbf{k}}^{\dagger} \rangle = \exp(-i\omega_{\mathbf{k}}t) \langle a_{\mathbf{k}}a_{\mathbf{k}}^{\dagger} \rangle = \exp(-i\omega_{\mathbf{k}}t) \langle 1 + a_{\mathbf{k}}^{\dagger}a_{\mathbf{k}} \rangle = \exp(-i\omega_{\mathbf{k}}t) [1 + n(\omega_{\mathbf{k}})],$$

where $n(\omega_{\mathbf{k}}) = [\exp(\beta\hbar\omega_{\mathbf{k}}) - 1]^{-1}$ is the average number of phonons with energy $\hbar\omega_{\mathbf{k}}$.

The calculation of the Fourier component of the electron density-density correlation function $\langle e^{i\mathbf{k}\cdot\mathbf{r}(t)}e^{-i\mathbf{k}\cdot\mathbf{r}} \rangle$ in Eq. (4.74) for an electron described by the Feynman polaron model is given below following the approach of Ref. [78].

We calculate the correlation function

$$\langle e^{i\mathbf{k}\cdot\mathbf{r}(t)}e^{-i\mathbf{k}\cdot\mathbf{r}(\tau)} \rangle = \frac{\text{Tr}(e^{-\beta H_F} e^{i\mathbf{k}\cdot\mathbf{r}(t)} e^{i\mathbf{k}\cdot\mathbf{r}(\tau)})}{\text{Tr}(e^{-\beta H_F})} \quad (4.75)$$

with the Feynman trial Hamiltonian

$$H_F = \frac{\mathbf{p}^2}{2m} + \frac{\mathbf{p}_f^2}{2m_f} + \frac{1}{2}\chi(\mathbf{r} - \mathbf{r}_f)^2. \quad (4.76)$$

Here, $\mathbf{r}(t)$ denotes the operator in the Heisenberg representation

$$\mathbf{r}(t) = e^{\frac{it}{\hbar}H_F} \mathbf{r} e^{-\frac{it}{\hbar}H_F}. \quad (4.77)$$

We show that the correlation function $\langle e^{i\mathbf{k}\cdot\mathbf{r}(t)}e^{-i\mathbf{k}\cdot\mathbf{r}(\tau)} \rangle$ depends on $(\tau - t)$ rather than on t and τ independently:

$$\begin{aligned}
\langle e^{i\mathbf{k}\cdot\mathbf{r}(t)}e^{-i\mathbf{k}\cdot\mathbf{r}(\tau)} \rangle &= \frac{\text{Tr}\left(e^{-\beta H_F} e^{\frac{it}{\hbar}H_F} e^{i\mathbf{k}\cdot\mathbf{r}} e^{-\frac{it}{\hbar}H_F} e^{\frac{i\tau}{\hbar}H_F} e^{i\mathbf{k}\cdot\mathbf{r}} e^{-\frac{i\tau}{\hbar}H_F}\right)}{\text{Tr}(e^{-\beta H_F})} \\
&= \frac{\text{Tr}\left(e^{-\beta H_F} e^{i\mathbf{k}\cdot\mathbf{r}} e^{\frac{i(\tau-t)}{\hbar}H_F} e^{i\mathbf{k}\cdot\mathbf{r}} e^{-\frac{i(\tau-t)}{\hbar}H_F}\right)}{\text{Tr}(e^{-\beta H_F})} \\
&= \langle e^{i\mathbf{k}\cdot\mathbf{r}} e^{-i\mathbf{k}\cdot\mathbf{r}(\tau-t)} \rangle = \langle e^{i\mathbf{k}\cdot\mathbf{r}} e^{-i\mathbf{k}\cdot\mathbf{r}(\sigma)} \rangle, \quad (4.78)
\end{aligned}$$

where $\sigma = \tau - t$.

The normal coordinates are the center-of-mass vector \mathbf{R} and the vector of the relative motion ρ :

$$\begin{cases} \mathbf{R} = \frac{m\mathbf{r} + m_f\mathbf{r}_f}{m + m_f} \\ \rho = \mathbf{r} - \mathbf{r}_f \end{cases} \quad (4.79)$$

The inverse transformation is:

$$\begin{cases} \mathbf{r} = \mathbf{R} + \frac{m_f}{m + m_f}\rho \\ \mathbf{r}_f = \mathbf{R} - \frac{m}{m + m_f}\rho \end{cases} \quad (4.80)$$

The same transformation as (4.79) takes place for velocities:

$$\begin{cases} \dot{\mathbf{r}} = \dot{\mathbf{R}} + \frac{m_f}{m + m_f}\dot{\rho} \\ \dot{\mathbf{r}}_f = \dot{\mathbf{R}} - \frac{m}{m + m_f}\dot{\rho} \end{cases} \quad (4.81)$$

From (4.79) we derive the transformation for moments

$$\begin{cases} \frac{\mathbf{p}}{m} = \frac{\mathbf{P}}{m + m_f} + \frac{m_f}{m + m_f} \frac{\mathbf{p}_\rho}{\frac{mm_f}{m + m_f}} \\ \frac{\mathbf{p}_f}{m_f} = \frac{\mathbf{P}}{m + m_f} - \frac{m}{m + m_f} \frac{\mathbf{p}_\rho}{\frac{mm_f}{m + m_f}} \end{cases} \\ \Downarrow \\ \begin{cases} \mathbf{p} = \frac{m}{m + m_f}\mathbf{P} + \mathbf{p}_\rho \\ \mathbf{p}_f = \frac{m_f}{m + m_f}\mathbf{P} - \mathbf{p}_\rho \end{cases} \quad (4.82)$$

The Hamiltonian (4.76) then takes the form

$$H_F = \frac{\mathbf{P}^2}{2M} + \frac{\mathbf{p}_\rho^2}{2\mu} + \frac{1}{2}\mu\bar{\Omega}^2\rho^2 \quad (4.83)$$

with the masses

$$M = m + m_f, \quad \mu = \frac{mm_f}{m + m_f} \quad (4.84)$$

and with the frequency

$$\bar{\Omega} = \sqrt{\frac{\chi}{\mu}}. \quad (4.85)$$

The Cartesian coordinates and moments corresponding to the relative motion can be in the standard way expressed in terms of the second quantization operators:

$$\begin{aligned} \rho_j &= \left(\frac{\hbar}{2\mu\bar{\Omega}}\right)^{1/2} (C_j + C_j^\dagger), \\ p_{\rho,j} &= -i \left(\frac{\mu\hbar\bar{\Omega}}{2}\right)^{1/2} (C_j - C_j^\dagger). \end{aligned} \quad (4.86)$$

$(j = 1, 2, 3)$

In these notations, the Hamiltonian (4.83) takes the form

$$H_F = \frac{\mathbf{P}^2}{2M} + \sum_{j=1}^3 \hbar \bar{\Omega} \left(C_j^\dagger C_j + \frac{1}{2} \right). \quad (4.87)$$

Using (4.87), we find the operators in the Heisenberg representation, (i) for the center-of-mass coordinates

$$\begin{aligned} X_j(\sigma) &= e^{\frac{i\sigma}{\hbar} H_F} X_j e^{-\frac{i\sigma}{\hbar} H_F} = e^{i\frac{\sigma}{2M\hbar} P_j^2} X_j e^{-i\frac{\sigma}{2M\hbar} P_j^2} \\ &= X_j + i\frac{\sigma}{2M\hbar} [P_j^2, X_j] \\ &= X_j + i\frac{\sigma}{2M\hbar} (P_j^2 X_j - P_j X_j P_j + P_j X_j P_j - X_j P_j^2) \\ &= X_j + i\frac{\sigma}{2M\hbar} (P_j [P_j, X_j] + [P_j, X_j] P_j) \\ &= X_j + i\frac{\sigma}{2M\hbar} P_j (-2i\hbar) = X_j + \frac{\sigma}{M} P_j, \\ X_j(\sigma) &= X_j + \frac{\sigma}{M} P_j, \end{aligned} \quad (4.88)$$

(ii) for the operators C_j and C_j^\dagger

$$C_j(\sigma) = C_j e^{-i\bar{\Omega}\sigma}, \quad C_j^\dagger(\sigma) = C_j^\dagger e^{i\bar{\Omega}\sigma}. \quad (4.89)$$

Using the first formula of (4.80) we find

$$\begin{aligned} \mathbf{r}(\sigma) &= \mathbf{R}(\sigma) + \frac{m_f}{m+m_f} \rho(\sigma) \\ &\quad \downarrow \\ \mathbf{r}(\sigma) &= \mathbf{R} + \frac{\sigma}{M} \mathbf{P} + \frac{m_f}{M} \left(\frac{\hbar}{2\mu\bar{\Omega}} \right)^{1/2} \left(\mathbf{C} e^{-i\bar{\Omega}\sigma} + \mathbf{C}^\dagger e^{i\bar{\Omega}\sigma} \right). \end{aligned} \quad (4.90)$$

We denote

$$\begin{aligned} a &\equiv \frac{m_f}{M} \left(\frac{\hbar}{2\mu\bar{\Omega}} \right)^{1/2} = \left(\frac{\hbar m_f^2}{2M^2 \mu \bar{\Omega}} \right)^{1/2} \\ &= \left(\frac{\hbar m_f^2}{2(m+m_f)^2 \frac{mm_f}{m+m_f} \bar{\Omega}} \right)^{1/2} = \left(\frac{\hbar m_f}{2mM\bar{\Omega}} \right)^{1/2} \\ \mathbf{r}(\sigma) &= \mathbf{R} + \frac{\sigma}{M} \mathbf{P} + a \left(\mathbf{C} e^{-i\bar{\Omega}\sigma} + \mathbf{C}^\dagger e^{i\bar{\Omega}\sigma} \right). \end{aligned} \quad (4.91)$$

Therefore, we obtain

$$\begin{aligned} e^{i\mathbf{k}\cdot\mathbf{r}} &= \exp(i\mathbf{k}\cdot\mathbf{R}) \exp(i\mathbf{k}\cdot\mathbf{C} + i\mathbf{k}\cdot\mathbf{C}^\dagger) \\ &= \prod_{j=1}^3 \exp(ik_j X_j) \exp\left(iak_j C_j - iak_j C_j^\dagger \right) \end{aligned}$$

$$\begin{aligned}
e^{-i\mathbf{k}\cdot\mathbf{r}(\sigma)} &= \exp \left[-i\mathbf{k}\cdot\mathbf{R} - i\frac{\sigma}{M}\mathbf{k}\cdot\mathbf{P} - i\mathbf{a}\mathbf{k}\cdot\left(\mathbf{C}e^{-i\bar{\Omega}\sigma} + \mathbf{C}^\dagger e^{i\bar{\Omega}\sigma}\right) \right] \\
&= \exp \left(-i\mathbf{k}\cdot\mathbf{R} - i\frac{\sigma}{M}\mathbf{k}\cdot\mathbf{P} \right) \exp \left(-i\mathbf{a}\mathbf{k}\cdot\mathbf{C}e^{-i\bar{\Omega}\sigma} - i\mathbf{a}\mathbf{k}\cdot\mathbf{C}^\dagger e^{i\bar{\Omega}\sigma} \right) \\
&= \prod_{j=1}^3 \exp \left(-ik_j X_j - i\frac{\sigma}{M}k_j P_j \right) \exp \left(-iak_j C_j e^{-i\bar{\Omega}\sigma} - iak_j C_j^\dagger e^{i\bar{\Omega}\sigma} \right). \tag{4.92}
\end{aligned}$$

The disentangling of the exponents is performed using the formula

$$e^{A+B} = e^A T \exp \left(\int_0^1 d\lambda e^{-\lambda A} B e^{\lambda A} \right). \tag{4.93}$$

In the case when $[A, B]$ commutes with both A and B , this formula is reduced to

$$e^{A+B} = e^A e^B e^{-\frac{1}{2}[A, B]}. \tag{4.94}$$

We perform the necessary commutations:

$$\begin{aligned}
-\frac{1}{2} \left[-ik_j X_j, -i\frac{\sigma}{M}k_j P_j \right] &= \frac{1}{2}k_j^2 \frac{\sigma}{M} [X_j, P_j] = i\frac{\hbar k_j^2}{2M}\sigma, \\
-\frac{1}{2} \left[iak_j C_j^\dagger, iak_j C_j \right] &= \frac{1}{2}a^2 k_j^2 [C_j^\dagger, C_j] = -\frac{1}{2}a^2 k_j^2 \\
-\frac{1}{2} \left[-iak_j C_j^\dagger e^{i\bar{\Omega}\sigma}, -iak_j C_j e^{-i\bar{\Omega}\sigma} \right] &= \frac{1}{2}a^2 k_j^2 [C_j^\dagger, C_j] = -\frac{1}{2}a^2 k_j^2 \\
&\Downarrow \\
e^{i\mathbf{k}\cdot\mathbf{r}} &= e^{i\mathbf{k}\cdot\mathbf{R}} e^{i\mathbf{a}\mathbf{k}\cdot\mathbf{C}^\dagger} e^{i\mathbf{a}\mathbf{k}\cdot\mathbf{C}} e^{-\frac{1}{2}a^2 k^2}, \\
e^{-i\mathbf{k}\cdot\mathbf{r}(\sigma)} &= e^{-i\mathbf{k}\cdot\mathbf{R}} e^{-i\frac{\sigma}{M}\mathbf{k}\cdot\mathbf{P}} e^{-i\mathbf{a}\mathbf{k}\cdot\mathbf{C}^\dagger e^{i\bar{\Omega}\sigma}} e^{-i\mathbf{a}\mathbf{k}\cdot\mathbf{C} e^{-i\bar{\Omega}\sigma}} e^{i\frac{\hbar k^2}{2M}\sigma - \frac{1}{2}a^2 k^2} \\
&\Downarrow \\
e^{i\mathbf{k}\cdot\mathbf{r}} e^{-i\mathbf{k}\cdot\mathbf{r}(\sigma)} &= e^{-i\frac{\sigma}{M}\mathbf{k}\cdot\mathbf{P}} e^{i\mathbf{a}\mathbf{k}\cdot\mathbf{C}^\dagger} e^{i\mathbf{a}\mathbf{k}\cdot\mathbf{C}} e^{-i\mathbf{a}\mathbf{k}\cdot\mathbf{C}^\dagger e^{i\bar{\Omega}\sigma}} e^{-i\mathbf{a}\mathbf{k}\cdot\mathbf{C} e^{-i\bar{\Omega}\sigma}} e^{i\frac{\hbar k^2}{2M}\sigma - a^2 k^2}.
\end{aligned}$$

It follows from Eq. (4.94) that when $[A, B]$ commutes with both A and B ,

$$e^A e^B = e^B e^A e^{[A, B]}. \tag{4.95}$$

Using (4.95), we find

$$\begin{aligned}
e^{iak_j \cdot C_j} e^{-iak_j \cdot C_j^\dagger e^{i\bar{\Omega}\sigma}} &= e^{-iak_j \cdot C_j^\dagger e^{i\bar{\Omega}\sigma}} e^{iak_j \cdot C_j} e^{[iak_j \cdot C_j, -iak_j \cdot C_j^\dagger e^{i\bar{\Omega}\sigma}]} \\
&= e^{-iak_j \cdot C_j^\dagger e^{i\bar{\Omega}\sigma}} e^{iak_j \cdot C_j} e^{a^2 k_j^2 e^{i\bar{\Omega}\sigma}}.
\end{aligned}$$

Herefrom, we find

$$e^{i\mathbf{k}\cdot\mathbf{r}} e^{-i\mathbf{k}\cdot\mathbf{r}(\sigma)} = e^{-i\frac{\sigma}{M}\mathbf{k}\cdot\mathbf{P}} e^{i\mathbf{a}\mathbf{k}\cdot\mathbf{C}^\dagger(1-e^{i\bar{\Omega}\sigma})} e^{i\mathbf{a}\mathbf{k}\cdot\mathbf{C}(1-e^{-i\bar{\Omega}\sigma})} e^{i\frac{\hbar k^2}{2M}\sigma - a^2 k^2(1-e^{i\bar{\Omega}\sigma})}. \quad (4.96)$$

The correlation function then is

$$\langle e^{i\mathbf{k}\cdot\mathbf{r}} e^{-i\mathbf{k}\cdot\mathbf{r}(\sigma)} \rangle = \langle e^{-i\frac{\sigma}{M}\mathbf{k}\cdot\mathbf{P}} \rangle \langle e^{i\mathbf{a}\mathbf{k}\cdot\mathbf{C}^\dagger(1-e^{i\bar{\Omega}\sigma})} e^{i\mathbf{a}\mathbf{k}\cdot\mathbf{C}(1-e^{-i\bar{\Omega}\sigma})} \rangle e^{i\frac{\hbar k^2}{2M}\sigma - a^2 k^2(1-e^{i\bar{\Omega}\sigma})}, \quad (4.97)$$

since the variables of the center-of mass motion and of the relative motion are averaged independently.

$$\begin{aligned} \langle e^{i\mathbf{a}\mathbf{k}\cdot\mathbf{C}^\dagger(1-e^{i\bar{\Omega}\sigma})} e^{i\mathbf{a}\mathbf{k}\cdot\mathbf{C}(1-e^{-i\bar{\Omega}\sigma})} \rangle &= \langle e^{i\mathbf{Q}\cdot\mathbf{C}^\dagger} e^{i\mathbf{Q}^*\cdot\mathbf{C}} \rangle \\ &= \frac{\text{Tr} \left(e^{-\beta\hbar\bar{\Omega}\mathbf{C}^\dagger\cdot\mathbf{C}} e^{i\mathbf{Q}\cdot\mathbf{C}^\dagger} e^{i\mathbf{Q}^*\cdot\mathbf{C}} \right)}{\text{Tr} \left(e^{-\beta\hbar\bar{\Omega}\mathbf{C}^\dagger\cdot\mathbf{C}} \right)} \end{aligned}$$

with

$$\mathbf{Q} = a \left(1 - e^{i\bar{\Omega}\sigma} \right) \mathbf{k}.$$

Let us consider the auxiliary expectation value

$$\begin{aligned} \langle e^{i\mathbf{Q}\cdot\mathbf{C}^\dagger} e^{i\mathbf{Q}^*\cdot\mathbf{C}} \rangle &\equiv \frac{\text{Tr} \left(e^{-\beta\hbar\bar{\Omega}\mathbf{C}^\dagger\mathbf{C}} e^{i\mathbf{Q}\cdot\mathbf{C}^\dagger} e^{i\mathbf{Q}^*\cdot\mathbf{C}} \right)}{\text{Tr} \left(e^{-\beta\hbar\bar{\Omega}\mathbf{C}^\dagger\mathbf{C}} \right)} \\ &= \frac{1}{\text{Tr} \left(e^{-\beta\hbar\bar{\Omega}\mathbf{C}^\dagger\mathbf{C}} \right)} \sum_{n=0}^{\infty} \frac{(i\mathbf{Q})^n}{n!} \sum_{m=0}^{\infty} \frac{(i\mathbf{Q}^*)^m}{m!} \text{Tr} \left(e^{-\beta\hbar\bar{\Omega}\mathbf{C}^\dagger\mathbf{C}} (C^\dagger)^n C^m \right) \\ &= \frac{1}{\text{Tr} \left(e^{-\beta\hbar\bar{\Omega}\mathbf{C}^\dagger\mathbf{C}} \right)} \sum_{n=0}^{\infty} \frac{(-1)^n |\mathbf{Q}|^{2n}}{(n!)^2} \text{Tr} \left(e^{-\beta\hbar\bar{\Omega}\mathbf{C}^\dagger\mathbf{C}} (C^\dagger)^n C^n \right). \end{aligned}$$

$$\begin{aligned} \text{Tr} \left(e^{-\beta\hbar\bar{\Omega}\mathbf{C}^\dagger\mathbf{C}} (C^\dagger)^n C^n \right) &= \sum_{m=0}^{\infty} \langle m | e^{-\beta\hbar\bar{\Omega}\mathbf{C}^\dagger\mathbf{C}} (C^\dagger)^n C^n | m \rangle \\ &= \sum_{m=0}^{\infty} e^{-\beta\hbar\bar{\Omega}m} \langle m | (C^\dagger)^n C^n | m \rangle, \end{aligned}$$

where $|m\rangle$ are the eigenstates of $(C^\dagger C)$. The operators C act on these states as follows:

$$\begin{aligned} C |m\rangle &= \sqrt{m} |m-1\rangle, \\ C |0\rangle &= 0. \end{aligned}$$

Therefore, we find

$$\langle m | (C^\dagger)^n C^n | m \rangle = m(m-1)\dots(m-n+1) = \frac{m!}{(m-n)!} \text{ for } n \leq m,$$

$$\langle m | (C^\dagger)^n C^n | m \rangle = 0 \text{ for } n > m.$$

$$\Downarrow$$

$$\text{Tr} \left(e^{-\beta\hbar\bar{\Omega}C^\dagger C} (C^\dagger)^n C^n \right) = \sum_{m=n}^{\infty} e^{-\beta\hbar\bar{\Omega}m} \frac{m!}{(m-n)!},$$

and

$$\begin{aligned} \text{Tr} \left(e^{-\beta\hbar\Omega C^\dagger C} e^{iQC^\dagger} e^{iQ^*C} \right) &= \sum_{n=0}^{\infty} \frac{(-1)^n |Q|^{2n}}{(n!)^2} \sum_{m=n}^{\infty} e^{-\beta\hbar\bar{\Omega}m} \frac{m!}{(m-n)!} \\ &= \sum_{n=0}^{\infty} \frac{(-1)^n |Q|^{2n}}{n!} \sum_{m=n}^{\infty} e^{-\beta\hbar\bar{\Omega}m} \binom{m}{n} \\ &= \sum_{n=0}^{\infty} \frac{(-1)^n |Q|^{2n}}{n!} e^{-\beta\hbar\bar{\Omega}n} \sum_{k=0}^{\infty} e^{-\beta\hbar\bar{\Omega}k} \binom{k+n}{n} \\ &= \sum_{n=0}^{\infty} \frac{(-1)^n |Q|^{2n}}{n!} e^{-\beta\hbar\bar{\Omega}n} \frac{1}{(1 - e^{-\beta\hbar\bar{\Omega}})^{n+1}} \\ &= \frac{1}{1 - e^{-\beta\hbar\bar{\Omega}}} \sum_{n=0}^{\infty} \frac{(-1)^n |Q|^{2n}}{n!} \frac{1}{(e^{\beta\hbar\bar{\Omega}} - 1)^n} \\ &= \frac{1}{1 - e^{-\beta\hbar\bar{\Omega}}} \exp \left(-\frac{|Q|^2}{e^{\beta\hbar\bar{\Omega}} - 1} \right). \end{aligned}$$

In particular, for $Q = Q^* = 0$, we have

$$\text{Tr} \left(e^{-\beta\hbar\Omega C^\dagger C} \right) = \frac{1}{1 - e^{-\beta\hbar\Omega}}. \quad (4.98)$$

As a result, the expectation value $\langle e^{iQC^\dagger} e^{iQ^*C} \rangle$ is

$$\langle e^{iQC^\dagger} e^{iQ^*C} \rangle = \exp \left[-n(\Omega) |Q|^2 \right], \quad (4.99)$$

with

$$n(\Omega) \equiv \frac{1}{e^{\beta\hbar\Omega} - 1}.$$

Using this result, we obtain the expression

$$\begin{aligned} \langle e^{i\mathbf{Q}\cdot\mathbf{C}^\dagger} e^{i\mathbf{Q}^*\cdot\mathbf{C}} \rangle &= \exp \left[-n(\Omega) \mathbf{Q} \cdot \mathbf{Q}^* \right] \\ &= \exp \left[-n(\Omega) a^2 k^2 \left(1 - e^{i\bar{\Omega}\sigma} \right) \left(1 - e^{-i\bar{\Omega}\sigma} \right) \right] \\ &= \exp \left[-4n(\Omega) a^2 k^2 \sin^2 \left(\frac{1}{2} \bar{\Omega}\sigma \right) \right]. \end{aligned}$$

The expectation value $\langle e^{-i\frac{\sigma}{M}\mathbf{k}\cdot\mathbf{P}} \rangle$ is

$$\begin{aligned}\langle e^{-i\frac{\sigma}{M}\mathbf{k}\cdot\mathbf{P}} \rangle &= \frac{\int d\mathbf{P} \exp\left(-\beta\frac{P^2}{2M} - i\frac{\sigma}{M}\mathbf{k}\cdot\mathbf{P}\right)}{\int d\mathbf{P} \exp\left(-\beta\frac{P^2}{2M}\right)} \\ &= \frac{\int d\mathbf{P} \exp\left(\frac{(-i\mathbf{P}\beta+\mathbf{k}\sigma)^2}{2M\beta} - \frac{k^2\sigma^2}{2M\beta}\right)}{\int d\mathbf{P} \exp\left(-\beta\frac{P^2}{2M}\right)} \\ &= \exp\left(-\frac{k^2\sigma^2}{2M\beta}\right).\end{aligned}$$

Collecting all factors in Eq. (4.97) together, we find

$$\begin{aligned}\langle e^{i\mathbf{k}\cdot\mathbf{r}} e^{-i\mathbf{k}\cdot\mathbf{r}(\sigma)} \rangle &= \exp\left[i\frac{\hbar k^2}{2M}\sigma - \frac{k^2\sigma^2}{2M\beta} - 4n(\bar{\Omega}) a^2 k^2 \sin^2\left(\frac{1}{2}\bar{\Omega}\sigma\right) - a^2 k^2 (1 - e^{i\bar{\Omega}\sigma})\right] \Rightarrow . \\ \langle e^{i\mathbf{k}\cdot\mathbf{r}(t)} e^{-i\mathbf{k}\cdot\mathbf{r}(\sigma+t)} \rangle &= e^{-k^2 D(\sigma)}\end{aligned}\quad (4.100)$$

with the function

$$D(t) = \frac{\hbar}{2M} \left(-it + \frac{t^2}{\beta\hbar}\right) + a^2 \left[1 - \exp(i\bar{\Omega}t) + 4n(\bar{\Omega}) \sin^2\left(\frac{\bar{\Omega}t}{2}\right)\right], \quad (4.101)$$

where

$$M = \left(\frac{v}{w}\right)^2 m_b, \bar{\Omega} = v\omega_{\text{LO}}, a^2 = \frac{\hbar}{2m_b\omega_{\text{LO}}} \frac{v^2 - w^2}{v^3}. \quad (4.102)$$

According to (4.78),

$$\langle e^{i\mathbf{k}\cdot\mathbf{r}(t)} e^{-i\mathbf{k}\cdot\mathbf{r}(\sigma+t)} \rangle = \langle e^{i\mathbf{k}\cdot\mathbf{r}} e^{-i\mathbf{k}\cdot\mathbf{r}(\sigma)} \rangle.$$

Taking $\sigma = -t$ in (4.100) we finally find the Fourier component of the electron density-density correlation function $\langle e^{i\mathbf{k}\cdot\mathbf{r}(t)} e^{-i\mathbf{k}\cdot\mathbf{r}} \rangle$ which enters Eq. (4.74):

$$\langle e^{i\mathbf{k}\cdot\mathbf{r}(t)} e^{-i\mathbf{k}\cdot\mathbf{r}} \rangle = \exp[-k^2 D(-t)] \quad (4.103)$$

Finally, the correlation functions in (4.73) reduce to

$$\begin{aligned}\langle b_{\mathbf{k}}(t) b_{\mathbf{k}}^\dagger(0) \rangle &= [1 + n(\omega_{\mathbf{k}})] \exp(-i\omega_{\mathbf{k}}t) \exp[-k^2 D(-t)], \\ \langle b_{\mathbf{k}}^\dagger(0) b_{\mathbf{k}}(t) \rangle &= n(\omega_{\mathbf{k}}) \exp(-i\omega_{\mathbf{k}}t) \exp[-k^2 D(t)], \\ \langle b_{\mathbf{k}}(t) b_{\mathbf{k}}(0) \rangle &= 0, \\ \langle b_{\mathbf{k}}(0) b_{\mathbf{k}}(t) \rangle &= 0.\end{aligned}$$

Inserting these equations into Eqs. (4.72) and (4.73), one obtains

$$\Sigma(z) = \frac{1}{z} \int_0^\infty dt (1 - e^{izt}) \text{Im} S(t) \quad (4.104)$$

with

$$\text{Im } S(t) = \frac{2}{m_b \hbar} \sum_{\mathbf{k}} k_x^2 |V_k|^2 \text{Im} \left\{ \begin{array}{l} -[1 + n(\omega_{\mathbf{k}})] \exp(-i\omega_{\mathbf{k}}t) \exp[-k^2 D(-t)] \\ +n(\omega_{\mathbf{k}}) \exp(-i\omega_{\mathbf{k}}t) \exp[-k^2 D(t)] \end{array} \right\}.$$

Using the property $D(-t)^* = D(t)$ for real values of t , one obtains

$$\begin{aligned} -\text{Im} \exp(-i\omega_{\mathbf{k}}t) \exp[-k^2 D(-t)] &= \text{Im} \exp(i\omega_{\mathbf{k}}t) \exp[-k^2 D(-t)^*] \\ &= \text{Im} \exp(i\omega_{\mathbf{k}}t) \exp[-k^2 D(t)] \end{aligned}$$

and consequently

$$S(t) = \frac{2}{m_b \hbar} \sum_{\mathbf{k}} k_x^2 |V_k|^2 \exp[-k^2 D(t)] \{ [1 + n(\omega_{\mathbf{k}})] \exp(i\omega_{\mathbf{k}}t) + n(\omega_{\mathbf{k}}) \exp(-i\omega_{\mathbf{k}}t) \}. \quad (4.105)$$

Owing to the rotational invariance of $|V_k|^2$ and $\omega_{\mathbf{k}}$, we can substitute in (4.105)

$$k_x^2 \rightarrow \frac{k^2}{3}.$$

The resulting expression for

$$S(t) = \frac{2}{3m_b \hbar} \sum_{\mathbf{k}} k^2 |V_k|^2 \exp[-k^2 D(t)] \{ [1 + n(\omega_{\mathbf{k}})] \exp(i\omega_{\mathbf{k}}t) + n(\omega_{\mathbf{k}}) \exp(-i\omega_{\mathbf{k}}t) \} \quad (4.106)$$

is identical with Eq. (35) of FHIP [47]. In the case of Fröhlich polarons, taking into account (1.17), Eq. (4.106) simplifies to

$$S(t) = \left(\frac{\hbar\omega_{\text{LO}}}{m_b} \right)^{3/2} \frac{\alpha}{3\sqrt{2\pi}} \left\{ \begin{array}{l} [1 + n(\omega_{\text{LO}})] \exp(i\omega_{\text{LO}}t) \\ +n(\omega_{\text{LO}}) \exp(-i\omega_{\text{LO}}t) \end{array} \right\} [D(t)]^{-3/2}. \quad (4.107)$$

B. Calculation of the memory function (Devreese *et. al.* [50])

Upon substitution of (4.30) and (4.57) into Eq. (4.5), we find the absorption coefficient

$$\begin{aligned} \Gamma(\Omega) &= \frac{1}{n\epsilon_0 c} \text{Re} \left[\frac{ie^2}{m_b} \frac{1}{\Omega - \Sigma(\Omega)} \right] = -\frac{1}{n\epsilon_0 c} \frac{e^2}{m_b} \text{Im} \left[\frac{1}{\Omega - \Sigma(\Omega)} \right] \\ &= -\frac{1}{n\epsilon_0 c} \frac{e^2}{m_b} \text{Im} \left\{ \frac{\Omega - \Sigma^*(\Omega)}{[\Omega - \text{Re} \Sigma(\Omega)]^2 + [\text{Im} \Sigma(\Omega)]^2} \right\} \\ &= \frac{1}{n\epsilon_0 c} \frac{e^2}{m_b} \frac{\text{Im} \Sigma^*(\Omega)}{[\Omega - \text{Re} \Sigma(\Omega)]^2 + [\text{Im} \Sigma(\Omega)]^2} \Rightarrow \end{aligned}$$

$$\Gamma(\Omega) = -\frac{1}{n\epsilon_0 c} \frac{e^2}{m_b} \frac{\text{Im } \Sigma(\Omega)}{[\Omega - \text{Re } \Sigma(\Omega)]^2 + [\text{Im } \Sigma(\Omega)]^2}. \quad (4.108)$$

This general expression was the starting point for a derivation of the theoretical optical absorption spectrum of a single large polaron, at *all electron-phonon coupling strengths* by Devreese et al. in Ref. [50]. The memory function $\Sigma(\Omega)$ as given by Eq. (4.104) with (4.107) contains the dynamics of the polaron and depends on α , temperature and Ω . Following the notation, introduced in Ref. [47],

$$\Sigma(\Omega) = \frac{\chi^*(\Omega)}{\Omega} \quad (4.109)$$

we represent Eq. (4.108) in the form used in Ref. [50]:

$$\Gamma(\Omega) = \frac{1}{n\epsilon_0 c} \frac{e^2}{m_b} \frac{\Omega \text{Im } \chi(\Omega)}{[\Omega^2 - \text{Re } \chi(\Omega)]^2 + [\text{Im } \chi(\Omega)]^2}. \quad (4.110)$$

According to (4.104) and (4.109),

$$\text{Im } \chi(\Omega) = \text{Im} \int_0^\infty dt \sin(\Omega t) S(t), \quad \text{Re } \chi(\Omega) = \text{Im} \int_0^\infty dt [1 - \cos(\Omega t)] S(t). \quad (4.111)$$

In the present Notes we limit our attention to the case $T = 0$ ($\beta \rightarrow \infty$). It was demonstrated in Ref.[50] that the exact zero-temperature limit arises if the limit $\beta \rightarrow \infty$ is taken directly in the expressions (4.111) (see Appendices A and B of Ref.[50]). As follows from (4.107),

$$S(t) = \left(\frac{\hbar\omega_{\text{LO}}}{m_b} \right)^{3/2} \frac{\alpha}{3\sqrt{2}\pi} \exp(i\omega_{\text{LO}}t) [D(t)]^{-3/2} \quad (\beta \rightarrow \infty). \quad (4.112)$$

According to (4.101)

$$D(t) = -i \frac{\hbar t}{2M} + a^2 [1 - \exp(i\bar{\Omega}t)] \quad (\beta \rightarrow \infty).$$

Using the Feynman units (where $\hbar = 1, \omega_{\text{LO}} = 1$ and $m_b = 1$), we obtain from (4.102):

$$M = \left(\frac{v}{w} \right)^2, \quad \bar{\Omega} = v, \quad a^2 = \frac{1}{2} \frac{v^2 - w^2}{v^3},$$

and consequently

$$D(t) = \frac{1}{2} \frac{v^2 - w^2}{v^3} (1 - e^{ivt}) - i \frac{1}{2} \left(\frac{w}{v} \right)^2 t = \frac{1}{2} \left(\frac{w}{v} \right)^2 \{ R(1 - e^{ivt}) - it \} \quad (\beta \rightarrow \infty) \quad (4.113)$$

with

$$R = \frac{v^2 - w^2}{w^2 v}.$$

and according to (4.112)

$$S(t) = \frac{2\alpha}{3\sqrt{\pi}} \left(\frac{v}{w}\right)^3 e^{it} [R(1 - e^{ivt}) - it]^{-3/2} \quad (\beta \rightarrow \infty). \quad (4.114)$$

From (4.111) one obtains immediately

$$\text{Im } \chi(\Omega) = \frac{2\alpha}{3\sqrt{\pi}} \left(\frac{v}{w}\right)^3 \text{Im} \int_0^\infty dt \frac{\sin(\Omega t) e^{it}}{[R(1 - e^{ivt}) - it]^{3/2}}, \quad (4.115)$$

$$\text{Re } \chi(\Omega) = \frac{2\alpha}{3\sqrt{\pi}} \left(\frac{v}{w}\right)^3 \text{Im} \int_0^\infty dt \frac{[1 - \cos(\Omega t)] e^{it}}{[R(1 - e^{ivt}) - it]^{3/2}}. \quad (4.116)$$

In the limit $\beta \rightarrow \infty$ the function $\text{Im } \chi(\Omega)$ was calculated by FHIP [47]. However, to study the optical absorption to the same approximation as FHIP's treatment of the impedance, we have also to calculate $\text{Re } \chi(\Omega)$ and use this result in (4.110). The calculation of $\text{Re } \chi(\Omega)$, which is a Kramers-Kronig-type transform of $\text{Im } \chi(\Omega)$, is a key ingredient in Ref. [50]. The details of those calculations are presented in the Appendices A, B and C to Ref. [50].

Developing the denominator of both integrals on the right-hand side of (4.115) and (4.116), the calculations are reduced to the evaluation of a sum of integrals of the type

$$\text{Im} \int_0^\infty dt \frac{\sin(\Omega t) e^{i(1+nv)t}}{(R - it)^{3/2+n}}, \quad \text{Im} \int_0^\infty dt \frac{\cos(\Omega t) e^{i(1+nv)t}}{(R - it)^{3/2+n}}. \quad (4.117)$$

In Appendix B to Ref. [50] it is shown how such integrals are evaluated using a recurrence formula. For $\text{Im } \chi(\Omega)$ a very convenient result was found in [50]:

$$\begin{aligned} \text{Im } \chi(\Omega) = & \frac{2\alpha}{3} \left(\frac{v}{w}\right)^3 \sum_{n=0}^{\infty} C_{-3/2}^n (-1)^n \frac{R^n 2^n}{(2n+1)\dots 3 \cdot 1} \\ & \times |\Omega - 1 - nv|^{n+1/2} e^{-|\Omega-1-nv|R} \frac{1 + \text{sgn}(\Omega - 1 - nv)}{2}. \end{aligned} \quad (4.118)$$

This expression is a finite sum and not an infinite series. FHIP gave the first two terms of (4.118) explicitly.

Using the same recurrence relation it is seen the analytical expression (see Appendix B to Ref. [50]), which was found for $\text{Re } \chi(\Omega)$ is far more complicated. To circumvent the difficulty with the numerical treatment of $\text{Re } \chi(\Omega)$, the corresponding integrals in (4.117) have been

transformed in [50] to integrals with rapidly convergent integrands:

$$\begin{aligned}
& \text{Im} \int_0^\infty dt \frac{[1 - \cos(\Omega t)] e^{i(1+nv)t}}{(R - it)^{3/2+n}} \\
&= -\frac{1}{\Gamma(n + \frac{3}{2})} \int_0^\infty dx \left[\left(n + \frac{1}{2}\right) x^{n-1/2} e^{-Rx} - R x^{n+1/2} e^{-Rx} \right] \\
&\times \ln \left| \left(\frac{(1 + nv + x)^2}{\Omega^2 - (1 + nv + x)^2} \right) \right|^{1/2}. \tag{4.119}
\end{aligned}$$

The integral on the right-hand side of (4.119) is adequate for computer calculations. In Appendix C to Ref. [50] some supplementary details of the computation of (4.119) are given. Another analytical representation for the memory function (4.104) was derived in Ref. [76].

C. Discussion of optical absorption of polarons at arbitrary coupling

At weak coupling, the optical absorption spectrum (4.108) of the polaron is determined by the absorption of radiation energy, which is reemitted in the form of LO phonons. For $\alpha \gtrsim 5.9$, the polaron can undergo transitions toward a relatively stable RES (see Fig. 7). The RES peak in the optical absorption spectrum also has a phonon sideband-structure, whose average transition frequency can be related to a FC-type transition. Furthermore, at zero temperature, the optical absorption spectrum of one polaron exhibits also a zero-frequency “central peak” [$\sim \delta(\Omega)$]. For non-zero temperature, this “central peak” smears out and gives rise to an “anomalous” Drude-type low-frequency component of the optical absorption spectrum.

For example, in Fig. 7 from Ref. [50], the main peak of the polaron optical absorption for $\alpha = 5$ at $\Omega = 3.51\omega_{\text{LO}}$ is interpreted as due to transitions to a RES. A “shoulder” at the low-frequency side of the main peak is attributed to one-phonon transitions to polaron-“scattering states”. The broad structure centered at about $\Omega = 6.3\omega_{\text{LO}}$ is interpreted as a FC band. As seen from Fig. 7, when increasing the electron-phonon coupling constant to $\alpha=6$, the RES peak at $\Omega = 4.3\omega_{\text{LO}}$ stabilizes. It is in Ref. [50] that the all-coupling optical absorption spectrum of a Fröhlich polaron, together with the role of RES-states, FC-states and scattering states, was first presented.

Recent interesting numerical calculations of the optical conductivity for the Fröhlich polaron performed within the diagrammatic Quantum Monte Carlo method [79], see Fig. 8,

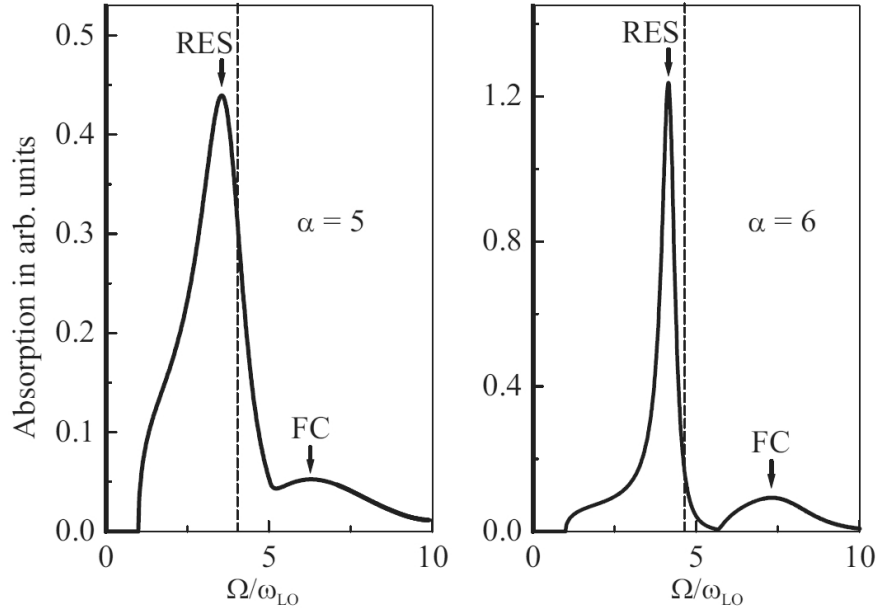


FIG. 7: Optical absorption spectrum of a polaron calculated by Devreese *et al.* [50] $\alpha = 5$ and 6. The RES peak is very intense compared with the FC peak. The frequency $\Omega/\omega_{\text{LO}} = v$ is indicated by the dashed lines.)

fully confirm the essential analytical results derived by Devreese *et al.* in Ref. [50] for $\alpha \lesssim 3$. In the intermediate coupling regime $3 < \alpha < 6$, the low-energy behavior and the position of the RES-peak in the optical conductivity spectrum of Ref. [79] follow closely the prediction of Ref. [50]. There are some minor qualitative differences between the two approaches in the intermediate coupling regime: in Ref. [79], the dominant (“RES”) peak is less intense in the Monte-Carlo numerical simulations and the second (“FC”) peak develops less prominently. There are the following qualitative differences between the two approaches in the strong coupling regime: in Ref.[79], the dominant peak broadens and the second peak does not develop, giving instead rise to a flat shoulder in the optical conductivity spectrum at $\alpha = 6$. This behavior has been tentatively attributed to the optical processes with participation of two [75] or more phonons. The above differences can arise also due to the fact that, within the Feynman polaron model, one-phonon processes are assigned more oscillator strength and the RES tends to be more stable as compared to the Monte-Carlo result. The nature of the excited states of a polaron needs further study. An independent numerical simulation might be called for.

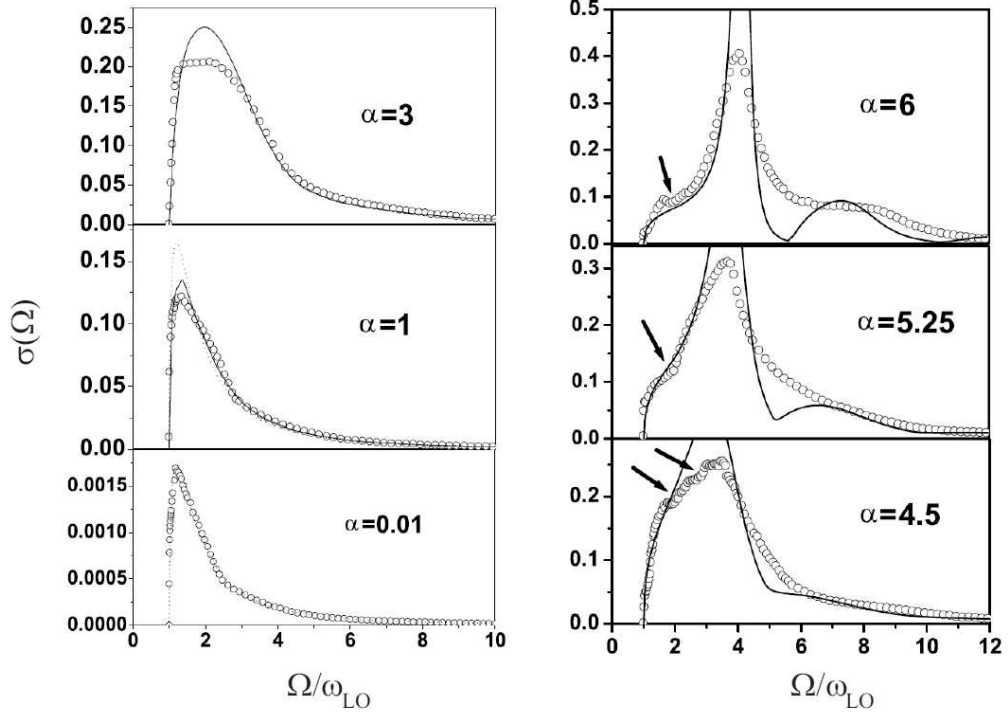


FIG. 8: *Left-hand panel*: Monte Carlo optical conductivity spectra of one polaron for the weak-coupling regime (open circles) compared to the second-order perturbation theory (dotted lines) for $\alpha = 0.01$ and $\alpha = 1$ and to the analytical DSG calculations [50] (solid lines). *Right-hand panel*: Monte Carlo optical conductivity spectra for the intermediate coupling regime (open circles) compared to the analytical DSG approach [50] (solid lines). Arrows point to the two- and three-phonon thresholds. (From Ref. [79].)

In Fig. 9, Monte-Carlo optical conductivity spectrum of one polaron for $\alpha = 1$ compares well with that obtained in Ref. [80] within the canonical-transformation formalism taking into account correlation in processes involving two LO phonons. The difference between the results of these two approaches becomes less pronounced when decreasing the value of $\alpha = 1$ and might be indicative of a possible precision loss, which requires an independent check.

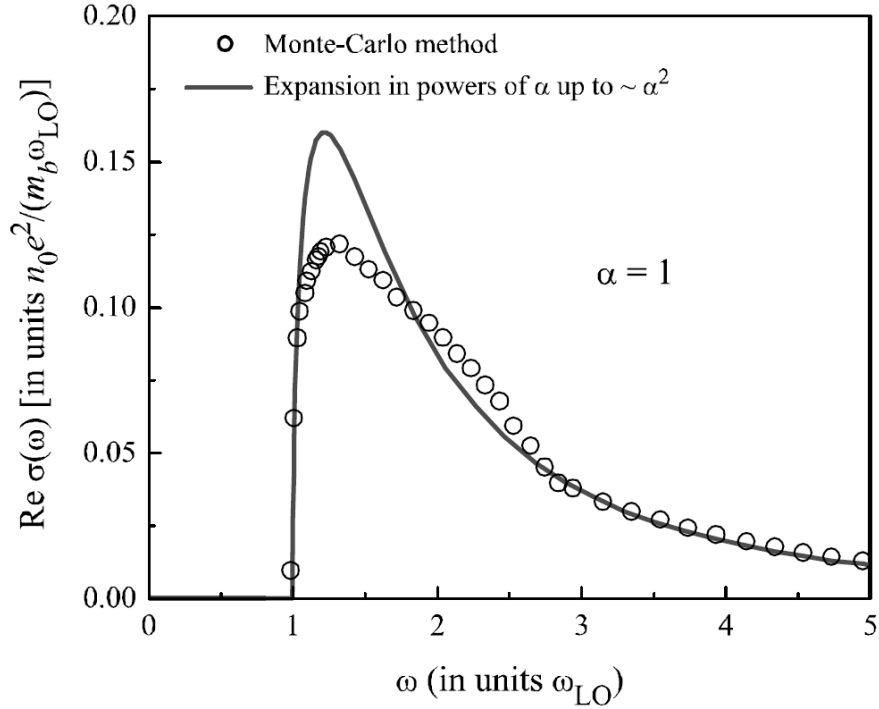


FIG. 9: One-polaron optical conductivity $\text{Re } \sigma(\omega)$ for $\alpha = 1$ calculated within the Monte Carlo approach [79] (open circles) and derived using the expansion in powers of α up to α^2 [80] (solid curve).

The coupling constant α of the known ionic crystals is too small ($\alpha < 5$) to allow for the experimental detection of sharp RES peaks, and the resonance condition $\Omega = \text{Re}\Sigma(\Omega)$ cannot be satisfied for $\alpha \lesssim 5.9$ as shown in Ref. [50]. Nevertheless, for $3 \lesssim \alpha \lesssim 5.9$ the development of RES is already reflected in a broad optical absorption peak. Such a peak, predicted in Ref. [50], was identified, e. g., in the optical absorption of $\text{Pr}_2\text{NiO}_{4.22}$ in Ref. [81]. Also, the resonance condition can be fulfilled if an external magnetic field is applied; the magnetic field stabilizes the RES, which then can be detected in a cyclotron resonance peak.

1. *Sum rules for the optical conductivity spectra*

In this section, we analyze the sum rules for the optical conductivity spectra obtained within the DSG approach [50] with those obtained within the diagrammatic Monte Carlo calculation [79]. The values of the polaron effective mass for the Monte Carlo approach are taken from Ref. [30]. In Tables 3 and 4, we represent the polaron ground-state E_0 and the following parameters calculated using the optical conductivity spectra:

$$M_0 \equiv \int_1^{\omega_{\max}} \text{Re } \sigma(\omega) d\omega, \quad (4.120)$$

$$M_1 \equiv \int_1^{\omega_{\max}} \omega \text{Re } \sigma(\omega) d\omega, \quad (4.121)$$

where ω_{\max} is the upper value of the frequency available from Ref. [79],

$$\tilde{M}_0 \equiv \frac{\pi}{2m^*} + \int_1^{\omega_{\max}} \text{Re } \sigma(\omega) d\omega, \quad (4.122)$$

where m^* is the polaron mass, the optical conductivity is calculated in units $\frac{n_0 e^2}{m_b \omega_{\text{LO}}}$, m^* is measured in units of the band mass m_b , and the frequency is measured in units of ω_{LO} . The values of ω_{\max} are: $\omega_{\max} = 10$ for $\alpha = 0.01, 1$ and 3 , $\omega_{\max} = 12$ for $\alpha = 4.5, 5.25$ and 6 , $\omega_{\max} = 18$ for $\alpha = 6.5, 7$ and 8 .

Table 3. Polaron parameters obtained within the diagrammatic Monte Carlo approach

α	$M_0^{(\text{MC})}$	$m^{*(\text{MC})}$	$\tilde{M}_0^{(\text{MC})}$	$M_1^{(\text{MC})}/\alpha$	$E_0^{(\text{MC})}$
0.01	0.00249	1.0017	1.5706	0.634	-0.010
1	0.24179	1.1865	1.5657	0.65789	-1.013
3	0.67743	1.8467	1.5280	0.73123	-3.18
4.5	0.97540	2.8742	1.5219	0.862	-4.97
5.25	1.0904	3.8148	1.5022	0.90181	-5.68
6	1.1994	5.3708	1.4919	0.98248	-6.79
6.5	1.30	6.4989	1.5417	1.1356	-7.44
7	1.3558	9.7158	1.5175	1.2163	-8.31
8	1.4195	19.991	1.4981	1.3774	-9.85

Table 4. Polaron parameters obtained within the path-integral approach

α	$M_0^{(\text{DSG})}$	$m^{*(\text{Feynman})}$	$\tilde{M}_0^{(\text{DSG})}$	$M_1^{(\text{DSG})}/\alpha$	$E_0^{(\text{Feynman})}$
0.01	0.00248	1.0017	1.5706	0.633	-0.010
1	0.24318	1.1957	1.5569	0.65468	-1.0130
3	0.69696	1.8912	1.5275	0.71572	-3.1333
4.5	1.0162	3.1202	1.5196	0.83184	-4.8394
5.25	1.1504	4.3969	1.5077	0.88595	-5.7482
6	1.2608	6.8367	1.4906	0.95384	-6.7108
6.5	1.3657	9.7449	1.5269	1.1192	-7.3920
7	1.4278	14.395	1.5369	1.2170	-8.1127
8	1.4741	31.569	1.5239	1.4340	-9.6953

The parameters corresponding to the Monte Carlo calculation are obtained using the numerical data kindly provided by A. Mishchenko. The comparison of the zero frequency moments $\tilde{M}_0^{(\text{MC})}$ and $\tilde{M}_0^{(\text{DSG})}$ with each other and with the value $\pi/2$ corresponding to the sum rule [82]

$$\frac{\pi}{2m^*} + \int_1^\infty \text{Re } \sigma(\omega) d\omega = \frac{\pi}{2} \quad (4.123)$$

shows that $\left| \tilde{M}_0^{(\text{MC})} - \tilde{M}_0^{(\text{DSG})} \right|$ is smaller than each of the differences $\frac{\pi}{2} - \tilde{M}_0^{(\text{MC})}$, $\frac{\pi}{2} - \tilde{M}_0^{(\text{DSG})}$, which appear due to a finite interval of the integration in (4.120), (4.121).

We analyze also the fulfilment of the ground-state theorem [83]

$$E_0(\alpha) - E_0(0) = -\frac{3}{\pi} \int_0^\alpha \frac{d\alpha'}{\alpha'} \int_0^\infty \omega \text{Re } \sigma(\omega, \alpha') d\omega \quad (4.124)$$

using the first-frequency moments $M_1^{(\text{MC})}$ and $M_1^{(\text{DSG})}$. The results of this comparison are presented in Fig. 10. The dots indicate the polaron ground-state energy calculated using the Feynman variational principle. The solid curve is the value of $E_0(\alpha)$ calculated numerically using the optical conductivity spectra and the ground-state theorem with the DSG optical conductivity [50] for a polaron,

$$E_0^{(\text{DSG})}(\alpha) \equiv -\frac{3}{\pi} \int_0^\alpha \frac{d\alpha'}{\alpha'} \int_0^\infty \omega \text{Re } \sigma^{(\text{DSG})}(\omega, \alpha') d\omega. \quad (4.125)$$

The dashed and the dot-dashed curves are the values obtained using $M_1^{(\text{DSG})}(\alpha)$ and

$M_1^{(\text{MC})}(\alpha)$, respectively:

$$\tilde{E}_0^{(\text{DSG})}(\alpha) \equiv -\frac{3}{\pi} \int_0^\alpha \frac{d\alpha'}{\alpha'} \int_0^{\omega_{\text{max}}} \omega \text{Re} \sigma^{(\text{DSG})}(\omega, \alpha') d\omega = -\frac{3}{\pi} \int_0^\alpha d\alpha' \frac{M_1^{(\text{DSG})}(\alpha')}{\alpha'}, \quad (4.126)$$

$$\tilde{E}_0^{(\text{MC})}(\alpha) \equiv -\frac{3}{\pi} \int_0^\alpha \frac{d\alpha'}{\alpha'} \int_0^{\omega_{\text{max}}} \omega \text{Re} \sigma^{(\text{MC})}(\omega, \alpha') d\omega = -\frac{3}{\pi} \int_0^\alpha d\alpha' \frac{M_1^{(\text{MC})}(\alpha')}{\alpha'}. \quad (4.127)$$

As seen from the figure, $E_0^{(\text{DSG})}(\alpha)$ to a high degree of accuracy coincides with the variational polaron ground-state energy. Both $\tilde{E}_0^{(\text{DSG})}(\alpha)$ and $\tilde{E}_0^{(\text{MC})}(\alpha)$ differ from $E_0^{(\text{DSG})}(\alpha)$ due to the integration over a finite interval of frequencies. However, $\tilde{E}_0^{(\text{DSG})}(\alpha)$ and $\tilde{E}_0^{(\text{MC})}(\alpha)$ are very close to each other. Herefrom, a conclusion follows that for integrals over the finite frequency region characteristic for the polaron optical absorption (i. e., except the ‘‘tails’’), the function $\tilde{E}_0^{(\text{MC})}(\alpha)$ (4.127) reproduces very well the function $\tilde{E}_0^{(\text{DSG})}(\alpha)$.

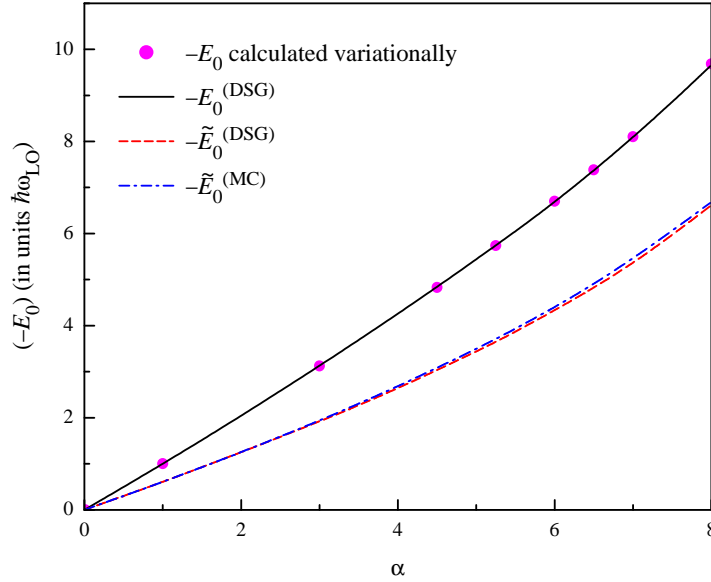


FIG. 10: The ground-state theorem for a polaron using different data for the optical conductivity spectra, DSG from Ref. [50] and MC from Ref. [79]. The notations are explained in the text.

D. Scaling relations

1. Derivation of the scaling relations

The form of the Fröhlich Hamiltonian in n dimensions is the same as in 3D,

$$H = \frac{\mathbf{p}^2}{2m_b} + \sum_{\mathbf{k}} \hbar\omega_{\mathbf{k}} a_{\mathbf{k}}^\dagger a_{\mathbf{k}} + \sum_{\mathbf{k}} \left(V_{\mathbf{k}} a_{\mathbf{k}} e^{i\mathbf{k}\cdot\mathbf{r}} + V_{\mathbf{k}}^* a_{\mathbf{k}}^\dagger e^{-i\mathbf{k}\cdot\mathbf{r}} \right), \quad (4.128)$$

except that now all vectors are n -dimensional. In this subsection, dispersionless longitudinal phonons are considered, i.e., $\omega_{\mathbf{k}} = \omega_{\text{LO}}$, and units are chosen such that $\hbar = m_b = \omega_{\text{LO}} = 1$.

The electron-phonon interaction is a representation in second quantization of the electron interaction with the lattice polarization, which in 3D is essentially the Coulomb potential $1/r$. $|V_{\mathbf{k}}|^2$ is proportional to the Fourier transform of this potential, and as a consequence we have in n dimensions

$$|V_{\mathbf{k}}|^2 = \frac{A_n}{L_n k^{n-1}}, \quad (4.129)$$

where L_n is the volume of the n -dimensional crystal. Note that $|V_{\tilde{\mathbf{k}}}|^2$, where $\tilde{\mathbf{k}}$ is an $(n-1)$ -dimensional vector, can be obtained from $|V_{\mathbf{k}}|^2$, where $\mathbf{k} = (\tilde{\mathbf{k}}, k_n)$ is an n -dimensional vector, by summing out one of the dimensions explicitly:

$$|V_{\tilde{\mathbf{k}}}|^2 = \sum_{k_n} |V_{\mathbf{k}}|^2. \quad (4.130)$$

Inserting Eq. (4.129) into Eq. (4.130), we have

$$\frac{A_{n-1}}{L_{n-1} \tilde{k}^{n-2}} = \sum_{k_n} \frac{A_n}{L_n (\tilde{k}^2 + k_n^2)^{(n-1)/2}}. \quad (4.131)$$

Replacing the sum in Eq. (4.131) by an integral, i.e.,

$$\frac{L_{n-1}}{L_n} \sum_{k_n} \longrightarrow \frac{1}{2\pi} \int dk_n, \quad (4.132)$$

we obtain

$$\frac{A_{n-1}}{\tilde{k}^{n-2}} = \frac{A_n}{2\pi} \int_{-\infty}^{\infty} \frac{dk_n}{(\tilde{k}^2 + k_n^2)^{(n-1)/2}}. \quad (4.133)$$

Since

$$\int_{-\infty}^{\infty} \frac{dx}{(z^\mu + x^\mu)^\rho} = z^{1-\mu\rho} \frac{\Gamma\left(\frac{1}{\mu}\right) \Gamma\left(\rho - \frac{1}{\mu}\right)}{\Gamma(\rho)}, \quad (4.134)$$

we have

$$\int_{-\infty}^{\infty} \frac{dk_n}{(\tilde{k}^2 + k_n^2)^{(n-1)/2}} = \frac{1}{\tilde{k}^{n-2}} \frac{\Gamma\left(\frac{1}{2}\right) \Gamma\left(\frac{n-2}{2}\right)}{\Gamma\left(\frac{n-1}{2}\right)} = \frac{\sqrt{\pi}}{\tilde{k}^{n-2}} \frac{\Gamma\left(\frac{n-2}{2}\right)}{\Gamma\left(\frac{n-1}{2}\right)}, \quad (4.135)$$

where $\Gamma(x)$ is the Γ function. Inserting Eq. (4.135) into Eq. (4.133), we obtain

$$A_n = \frac{2\sqrt{\pi}\Gamma\left(\frac{n-1}{2}\right)}{\Gamma\left(\frac{n-2}{2}\right)} A_{n-1}. \quad (4.136)$$

In 3D the interaction coefficient is well known, $|V_{\mathbf{k}}|^2 = 2\sqrt{2}\pi\alpha/L_3k^2$, so that

$$A_3 = 2\sqrt{2}\pi\alpha. \quad (4.137)$$

Inserting Eq. (4.137) into Eq. (4.136), we immediately obtain

$$A_2 = 2\sqrt{2}\pi\alpha \frac{\Gamma(\frac{1}{2})}{2\sqrt{\pi}\Gamma(1)} = \sqrt{2}\pi\alpha. \quad (4.138)$$

Applying Eq. (4.136) $n - 2$ times, we further obtain for $n > 3$

$$\begin{aligned} A_n &= \frac{(2\sqrt{\pi})^{n-2} \prod_{j=2}^{n-1} \Gamma(\frac{j}{2})}{\prod_{j=1}^{n-2} \Gamma(\frac{j}{2})} A_2 = \frac{(2\sqrt{\pi})^{n-2} \Gamma(\frac{n-1}{2})}{\Gamma(\frac{1}{2})} A_2 = 2^{n-2} \pi^{(n-3)/2} \Gamma\left(\frac{n-1}{2}\right) A_2 \\ &= 2^{n-3/2} \pi^{(n-1)/2} \Gamma\left(\frac{n-1}{2}\right) \alpha. \end{aligned} \quad (4.139)$$

So, the interaction coefficient in n dimensions becomes [84]

$$|V_{\mathbf{k}}|^2 = \frac{2^{n-3/2} \pi^{(n-1)/2} \Gamma\left(\frac{n-1}{2}\right) \alpha}{L_n k^{n-1}}. \quad (4.140)$$

Following the Feynman approach [43], the upper bound for the polaron ground-state energy can be written down as

$$E = E_0 - \lim_{\beta \rightarrow \infty} \frac{1}{\beta} \langle S - S_0 \rangle_0, \quad (4.141)$$

where S is the exact action functional of the polaron problem, while S_0 is the trial action functional, which corresponds to a model system where an electron is coupled by an elastic force to a fictitious particle (i.e., the model system describes a harmonic oscillator). E_0 is the ground-state energy of the above model system, and

$$\langle F \rangle_0 \equiv \frac{\int F e^{S_0} \mathcal{D}\mathbf{r}(t)}{\int e^{S_0} \mathcal{D}\mathbf{r}(t)}. \quad (4.142)$$

As indicated above, the Fröhlich Hamiltonian in n dimensions is the same as in 3D, except that now all vectors are n -dimensional [and the coupling coefficient $|V_{\mathbf{k}}|^2$ is modified in accordance with Eq. (4.140)]. Similarly, the only difference of the model system in n dimensions from the model system in 3D is that now one deals with an n -dimensional harmonic oscillator. So, directly following [43], one can represent $\lim_{\beta \rightarrow \infty} \langle S - S_0 \rangle_0 / \beta$ as

$$\lim_{\beta \rightarrow \infty} \frac{1}{\beta} \langle S - S_0 \rangle_0 = A + B, \quad (4.143)$$

where

$$A = \sum_{\mathbf{k}} |V_{\mathbf{k}}|^2 \int_0^\infty \langle e^{i\mathbf{k}\cdot[\mathbf{r}(t)-\mathbf{r}(0)]} \rangle_0 e^{-t} dt, \quad (4.144)$$

$$B = \frac{w(v^2 - w^2)}{4} \int_0^\infty \langle [\mathbf{r}(t) - \mathbf{r}(0)]^2 \rangle_0 e^{-wt} dt, \quad (4.145)$$

w and v are variational parameters, which should be determined by minimizing E of Eq. (4.141). Since the averaging $\langle \dots \rangle_0$ in Eq. (4.144) is performed with the trial action, which corresponds to a harmonic oscillator, components of the electron coordinates, r_j ($j = 1, \dots, n$), in $\langle e^{i\mathbf{k}\cdot[\mathbf{r}(t)-\mathbf{r}(0)]} \rangle_0$ separate [43]:

$$\langle e^{i\mathbf{k}\cdot[\mathbf{r}(t)-\mathbf{r}(0)]} \rangle_0 = \prod_{j=1}^n \langle e^{ik_j[r_j(t)-r_j(0)]} \rangle_0. \quad (4.146)$$

For the average $\langle e^{ik_j[r_j(t)-r_j(0)]} \rangle_0$, Feynman obtained [43]

$$\langle e^{ik_j[r_j(t)-r_j(0)]} \rangle_0 = e^{-k_j^2 D_0(t)}, \quad (4.147)$$

where

$$D_0(t) = \frac{w^2}{2v^2} t + \frac{v^2 - w^2}{2v^3} (1 - e^{-vt}). \quad (4.148)$$

Inserting Eq. (4.146) with Eq. (4.147) into Eq. (4.144), we obtain

$$A = \int_0^\infty e^{-t} dt \sum_{\mathbf{k}} |V_{\mathbf{k}}|^2 e^{-k^2 D_0(t)}. \quad (4.149)$$

Inserting expression (4.140) for $|V_{\mathbf{k}}|^2$ into Eq. (4.149) and replacing the sum over \mathbf{k} by an integral [see (4.132)], we have

$$\begin{aligned} A &= 2^{n-3/2} \pi^{(n-1)/2} \Gamma\left(\frac{n-1}{2}\right) \alpha \int_0^\infty e^{-t} dt \int \frac{e^{-k^2 D_0(t)} d\mathbf{k}}{k^{n-1} (2\pi)^n} \\ &= 2^{n-3/2} \pi^{(n-1)/2} \Gamma\left(\frac{n-1}{2}\right) \alpha \int_0^\infty e^{-t} dt \int d\Omega_n \int_0^\infty \frac{e^{-k^2 D_0(t)} k^{n-1} dk}{k^{n-1} (2\pi)^n}, \end{aligned} \quad (4.150)$$

where $d\Omega_n$ is the elemental solid angle in n dimensions. Since the integrand in Eq. (4.150) depends only on the modulus k of \mathbf{k} , one have simply $\int d\Omega_n = \Omega_n$ with

$$\Omega_n = \frac{2\pi^{n/2}}{\Gamma\left(\frac{n}{2}\right)}. \quad (4.151)$$

So, we obtain for A the result

$$\begin{aligned} A &= \frac{2^{-1/2} \pi^{-1/2} \Gamma\left(\frac{n-1}{2}\right) \alpha}{\Gamma\left(\frac{n}{2}\right)} \int_0^\infty e^{-t} dt \int_0^\infty e^{-k^2 D_0(t)} dk = \frac{2^{-1/2} \pi^{-1/2} \Gamma\left(\frac{n-1}{2}\right) \alpha}{\Gamma\left(\frac{n}{2}\right)} \int_0^\infty \frac{\sqrt{\pi} e^{-t}}{2\sqrt{D_0(t)}} dt \\ &= \frac{2^{-3/2} \Gamma\left(\frac{n-1}{2}\right) \alpha}{\Gamma\left(\frac{n}{2}\right)} \int_0^\infty \frac{e^{-t}}{\sqrt{D_0(t)}} dt. \end{aligned} \quad (4.152)$$

Like in Ref. [43], B can be easily calculated by noticing that

$$\begin{aligned}\langle [\mathbf{r}(t) - \mathbf{r}(0)]^2 \rangle_0 &= \sum_{j=1}^n \langle [r_j(t) - r_j(0)]^2 \rangle_0 = \sum_{j=1}^n \left[-\frac{\partial^2}{\partial k_j^2} \langle e^{i\mathbf{k} \cdot [\mathbf{r}(t) - \mathbf{r}(0)]} \rangle_0 \right] \Big|_{\mathbf{k}=0} \\ &= \sum_{j=1}^n 2D_0(t) = 2nD_0(t),\end{aligned}\tag{4.153}$$

so that

$$\begin{aligned}B &= \frac{nw(v^2 - w^2)}{2} \int_0^\infty D_0(t) e^{-wt} dt \\ &= \frac{nw(v^2 - w^2)}{2} \int_0^\infty \left[\frac{w^2}{2v^2} t e^{-wt} + \frac{v^2 - w^2}{2v^3} (e^{-wt} - e^{-(v+w)t}) \right] dt \\ &= \frac{nw(v^2 - w^2)}{2} \left[\frac{w^2}{2v^2} \frac{1}{v^2} + \frac{v^2 - w^2}{2v^3} \left(\frac{1}{w} - \frac{1}{v+w} \right) \right] \\ &= \frac{n(v^2 - w^2)}{4v}.\end{aligned}\tag{4.154}$$

Inserting Eq. (4.140) with A and B , given by Eqs. (4.152) and (4.154), together with the ground-state energy of the model system [43] (an isotropic n -dimensional harmonic oscillator),

$$E_0 = \frac{n(v-w)}{2},\tag{4.155}$$

into Eq. (4.141), we obtain

$$\begin{aligned}E &= \frac{n(v-w)}{2} - \frac{n(v^2 - w^2)}{4v} - \frac{2^{-3/2} \Gamma(\frac{n-1}{2}) \alpha}{\Gamma(\frac{n}{2})} \int_0^\infty \frac{e^{-t}}{\sqrt{D_0(t)}} dt \\ &= \frac{n(v-w)^2}{4v} - \frac{\Gamma(\frac{n-1}{2}) \alpha}{2\sqrt{2}\Gamma(\frac{n}{2})} \int_0^\infty \frac{e^{-t}}{\sqrt{D_0(t)}} dt.\end{aligned}\tag{4.156}$$

In order to make easier a comparison of E for n dimensions with the Feynman result [43] for 3D,

$$E_{3D}(\alpha) = \frac{3(v-w)^2}{4v} - \frac{1}{\sqrt{2\pi}} \alpha \int_0^\infty \frac{e^{-t}}{\sqrt{D_0(t)}} dt,\tag{4.157}$$

it is convenient to rewrite Eq. (4.156) in the form

$$E_{nD}(\alpha) = \frac{n}{3} \left[\frac{3(v-w)^2}{4v} - \frac{1}{\sqrt{2\pi}} \frac{3\sqrt{\pi}\Gamma(\frac{n-1}{2})}{2n\Gamma(\frac{n}{2})} \alpha \int_0^\infty \frac{e^{-t}}{\sqrt{D_0(t)}} dt \right].\tag{4.158}$$

It is worth recalling that the parameters w and v must be determined by minimizing E . Thus, in the case of Eq. (4.158) one has to minimize the expression in the square brackets.

The only difference of this expression from the r.h.s. of Eq. (4.157) is that α is multiplied by the factor

$$a_n = \frac{3\sqrt{\pi}\Gamma\left(\frac{n-1}{2}\right)}{2n\Gamma\left(\frac{n}{2}\right)}. \quad (4.159)$$

This means that the minimizing parameters w and v in n D at a given α will be exactly the same as those calculated in 3D for the Fröhlich constant as large as $a_n\alpha$:

$$v_{nD}(\alpha) = v_{3D}(a_n\alpha), \quad w_{nD}(\alpha) = w_{3D}(a_n\alpha). \quad (4.160)$$

Therefore, comparing Eq. (4.158) to Eq. (4.157), we obtain the scaling relation [84–86]

$$E_{nD}(\alpha) = \frac{n}{3}E_{3D}(a_n\alpha), \quad (4.161)$$

where a_n is given by Eq. (4.159). As discussed in Ref. [84], the above scaling relation is not an exact relation. It is valid for the Feynman polaron energy and also for the ground-state energy to order α . The next-order term (i.e., α^2) no longer satisfies Eq. (4.161). The reason is that in the exact calculation (to order α^2) the electron motion in the different space directions is coupled by the electron-phonon interaction. No such a coupling appears in the Feynman polaron model [see, e.g., Eq. (4.146)]; and this is the underlying reason for the validity of the scaling relation for the Feynman approximation.

In Refs. [84, 86], scaling relations are obtained also for the impedance function, the effective mass and the mobility of a polaron. The inverse of the impedance function $Z(\omega)$ is given by

$$\frac{1}{Z(\omega)} = \frac{i}{\omega - \Sigma(\omega)}, \quad (4.162)$$

where the memory function $\Sigma(\omega)$ can be expressed as [87]

$$\Sigma(z) = \frac{1}{z} \int_0^\infty dt (1 - e^{izt}) \text{Im}S(t), \quad (4.163)$$

with $z = \omega + i0^+$ and

$$S(t) = \sum_{\mathbf{k}} 2k_1^2 |V_{\mathbf{k}}|^2 e^{-k^2 D(t)} T(t), \quad (4.164)$$

$$T(t) = [1 + n(1)] e^t + n(1) e^{-it}, \quad (4.165)$$

$$D(t) = \frac{w^2}{2v^2} \left(-it + \frac{t^2}{\beta} \right) + \frac{v^2 - w^2}{2v^3} \left[1 - e^{-ivt} + 4n(v) \sin^2 \left(\frac{vt}{2} \right) \right]. \quad (4.166)$$

Here, β is the inverse temperature and $n(\omega)$ is the occupation number of phonons with frequency ω (recall that in our units $\omega_{LO} = 1$).

As implied from Eqs. (4.162) and (4.163), scaling of $\Sigma(\omega)$ and $Z(\omega)$ is determined by scaling of $S(t)$. For an isotropic crystal, since $|V_{\mathbf{k}}|^2$, $D(t)$ and $T(t)$ do not depend on the direction of \mathbf{k} , one can write $\sum_{\mathbf{k}} k_1^2 |V_{\mathbf{k}}|^2 e^{-k^2 D(t)} T(t) = \sum_{\mathbf{k}} k_2^2 |V_{\mathbf{k}}|^2 e^{-k^2 D(t)} T(t) = \dots = \sum_{\mathbf{k}} k_n^2 |V_{\mathbf{k}}|^2 e^{-k^2 D(t)} T(t)$, so that

$$S(t) = \frac{2}{n} \sum_{\mathbf{k}} k^2 |V_{\mathbf{k}}|^2 e^{-k^2 D(t)} T(t). \quad (4.167)$$

Inserting expression (4.140) for $|V_{\mathbf{k}}|^2$ and replacing the sum over \mathbf{k} by an integral, we have

$$\begin{aligned} S(t) &= \frac{2}{n} \frac{2^{n-3/2} \pi^{(n-1)/2} \Gamma\left(\frac{n-1}{2}\right) \alpha}{(2\pi)^n} \int d\Omega_n \int_0^\infty k^2 e^{-k^2 D(t)} T(t) dk \\ &= \frac{2}{n} \frac{2^{n-3/2} \pi^{(n-1)/2} \Gamma\left(\frac{n-1}{2}\right) \alpha}{(2\pi)^n} \frac{2\pi^{n/2}}{\Gamma\left(\frac{n}{2}\right)} \int_0^\infty k^2 e^{-k^2 D(t)} T(t) dk \\ &= \sqrt{\frac{2}{\pi}} \frac{\Gamma\left(\frac{n-1}{2}\right) \alpha}{n \Gamma\left(\frac{n}{2}\right)} \int_0^\infty k^2 e^{-k^2 D(t)} T(t) dk. \end{aligned} \quad (4.168)$$

In particular, for 3D one has from Eq. (4.168)

$$S_{3D}(\alpha; t) = \frac{2\sqrt{2}}{3\pi} \alpha \int_0^\infty k^2 e^{-k^2 D(t)} T(t) dk. \quad (4.169)$$

For nD , Eq. (4.168) can be rewritten in the form

$$\begin{aligned} S_{nD}(\alpha; t) &= \frac{2\sqrt{2}}{3\pi} \frac{3\sqrt{\pi} \Gamma\left(\frac{n-1}{2}\right)}{2n \Gamma\left(\frac{n}{2}\right)} \alpha \int_0^\infty k^2 e^{-k^2 D(t)} T(t) dk \\ &= \frac{2\sqrt{2}}{3\pi} a_n \alpha \int_0^\infty k^2 e^{-k^2 D(t)} T(t) dk. \end{aligned} \quad (4.170)$$

So, the only difference of the expression for $S_{nD}(t)$ from $S_{3D}(t)$ is that α is multiplied by a_n . Since for the minimizing parameters w and v , which enter $D(t)$, scaling is determined by the same product α with a_n [see Eq. (4.160)], we can write

$$S_{nD}(\alpha; t) = S_{3D}(a_n \alpha; t), \quad (4.171)$$

so that [86]

$$\Sigma_{nD}(\alpha; \omega) = \Sigma_{3D}(a_n \alpha; \omega), \quad (4.172)$$

and

$$Z_{nD}(\alpha; \omega) = Z_{3D}(a_n \alpha; \omega). \quad (4.173)$$

The polaron mass at zero temperature can be obtained from the impedance function as [87, 88]

$$\frac{m^*}{m_b} = 1 - \lim_{\omega \rightarrow 0} \frac{\text{Re}\Sigma(\omega)}{\omega}, \quad (4.174)$$

so that from the scaling relation (4.172) for the memory function we also have a scaling relation for the polaron mass [86]:

$$\frac{m_{nD}^*(\alpha)}{(m_b)_{nD}} = \frac{m_{3D}^*(a_n\alpha)}{(m_b)_{3D}}. \quad (4.175)$$

Since the mobility can be obtained from the memory function as [89]

$$\frac{1}{\mu} = -\frac{m_b}{e} \lim_{\omega \rightarrow 0} \frac{\text{Im}\Sigma(\omega)}{\omega}, \quad (4.176)$$

fulfilment of the scaling relation (4.172) implies also a scaling relation for the mobility [86]:

$$\mu_{nD}(\alpha) = \mu_{3D}(a_n\alpha). \quad (4.177)$$

In the important particular case of 2D, the above scaling relations take the form [84–86]:

$$E_{2D}(\alpha) = \frac{2}{3}E_{3D}\left(\frac{3\pi}{4}\alpha\right), \quad (4.178)$$

$$Z_{2D}(\alpha; \omega) = Z_{3D}\left(\frac{3\pi}{4}\alpha; \omega\right), \quad (4.179)$$

$$\frac{m_{2D}^*(\alpha)}{(m_b)_{2D}} = \frac{m_{3D}^*\left(\frac{3\pi}{4}\alpha\right)}{(m_b)_{3D}}, \quad (4.180)$$

$$\mu_{2D}(\alpha) = \mu_{3D}\left(\frac{3\pi}{4}\alpha\right). \quad (4.181)$$

2. Check of the scaling relation for the path integral Monte Carlo result for the polaron free energy

The fulfilment of the PD-scaling relation [86] is checked for the path integral Monte Carlo results [45] for the polaron free energy.

The path integral Monte Carlo results of Ref.[45] for the polaron free energy in 3D and in 2D are given for a few values of temperature and for some selected values of α . For a check of the scaling relation, the values of the polaron free energy at $\beta = 10$ are taken from Ref.

[45] in 3D (Table I, for 4 values of α) and in 2D (Table II, for 2 values of α) and plotted in Fig. 11, upper panel, with squares and open circles, correspondingly.

The PD-scaling relation for the polaron ground-state energy as derived in Ref. [86] reads:

$$E_{2D}(\alpha) \equiv \frac{2}{3} E_{3D} \left(\frac{3\pi\alpha}{4} \right). \quad (4.182)$$

In Fig. 11, lower panel, the available data for the free energy from Ref [45] are plotted in the following form *inspired by the l.h.s. and the r.h.s parts of Eq. (1)*: $F_{2D}(\alpha)$ (squares) and $\frac{2}{3}F_{3D}(\frac{3\pi\alpha}{4})$ (open triangles). As follows from the figure, *the path integral Monte Carlo results for the polaron free energy in 2D and 3D very closely follow the PD-scaling relation of the form given by Eq. (4.182)*:

$$F_{2D}(\alpha) \equiv \frac{2}{3} F_{3D} \left(\frac{3\pi\alpha}{4} \right). \quad (4.183)$$

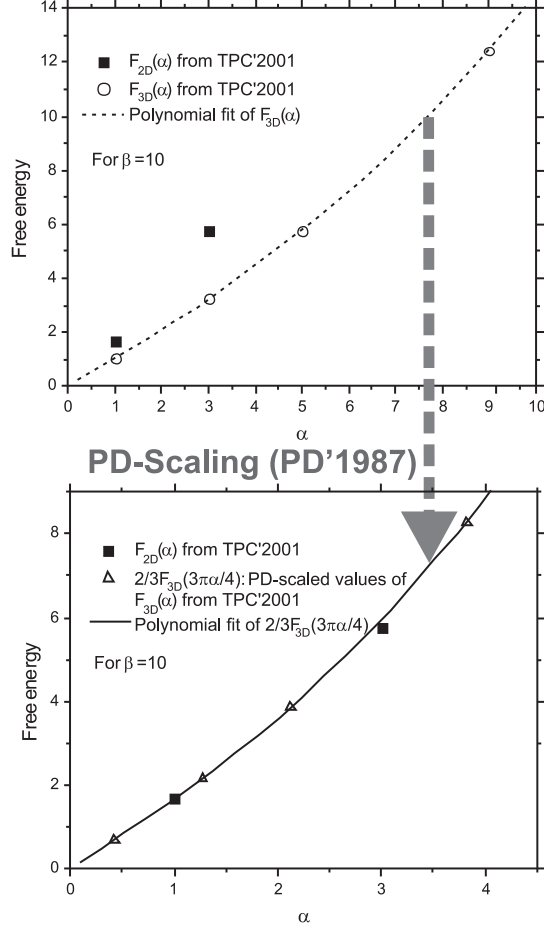


FIG. 11: *Upper panel:* The values of the polaron free energy in 3D (squares) and 2D (open circles) obtained by Ciuchi'2001 [45] for $\beta = 10$. The data for $F_{3D}(\alpha)$ are interpolated using a polynomial fit to the available four points (dotted line). *Lower panel:* Demonstration of the PD-scaling cf. PD'1987: the values of the polaron free energy in 2D obtained by Ciuchi'2001 [45] for $\beta = 10$ (squares) are very close to the **PD-scaled** according to PD'1987 [86] values of the polaron free energy in 3D from Ciuchi'2001 for $\beta = 10$ (open triangles). The data for $\frac{2}{3}F_{3D}(\frac{3\pi\alpha}{4})$ are interpolated using a polynomial fit to the available four points (solid line).

Appendix 1. Weak coupling: LLP approach

Inspired by the work of Tomonaga on quantum electrodynamics (Q. E. D.), Lee, Low and Pines (L.L.P.) [31] derived (1.22) and $m^* = m_b(1 + \alpha/6)$ from a canonical transformation formulation, which establishes (1.22) as a variational upper bound for the ground-state energy.

The wave equation corresponding to the Fröhlich Hamiltonian (1.16) is

$$H\Phi = E\Phi. \quad (4.184)$$

We shall take advantage of the fact that the total momentum of the system

$$\mathbf{P}_{op} = \sum_{\mathbf{k}} \hbar \mathbf{k} a_{\mathbf{k}}^{\dagger} a_{\mathbf{k}} + \mathbf{p} \quad (4.185)$$

(where $\mathbf{p} = -i\hbar\nabla$ is the momentum of the electron) is a constant of motion because it commutes with the Hamiltonian (1.16)

Indeed,

$$\begin{aligned} [\mathbf{p}, H] &= [\mathbf{p}, \sum_{\mathbf{k}} (V_{\mathbf{k}} a_{\mathbf{k}} e^{i\mathbf{k}\cdot\mathbf{r}} + V_{\mathbf{k}}^* a_{\mathbf{k}}^{\dagger} e^{-i\mathbf{k}\cdot\mathbf{r}})] = \sum_{\mathbf{k}} (V_{\mathbf{k}} a_{\mathbf{k}} [\mathbf{p}, e^{i\mathbf{k}\cdot\mathbf{r}}] + V_{\mathbf{k}}^* a_{\mathbf{k}}^{\dagger} [\mathbf{p}, e^{-i\mathbf{k}\cdot\mathbf{r}}]) \\ &= \sum_{\mathbf{k}} \hbar \mathbf{k} (V_{\mathbf{k}} a_{\mathbf{k}} e^{i\mathbf{k}\cdot\mathbf{r}} - V_{\mathbf{k}}^* a_{\mathbf{k}}^{\dagger} e^{-i\mathbf{k}\cdot\mathbf{r}}); \end{aligned}$$

$$\begin{aligned} \left[\sum_{\mathbf{k}} \hbar \mathbf{k} a_{\mathbf{k}}^{\dagger} a_{\mathbf{k}}, H \right] &= \left[\sum_{\mathbf{k}} \hbar \mathbf{k} a_{\mathbf{k}}^{\dagger} a_{\mathbf{k}}, \sum_{\mathbf{k}'} (V_{\mathbf{k}'} a_{\mathbf{k}'} e^{i\mathbf{k}'\cdot\mathbf{r}} + V_{\mathbf{k}'}^* a_{\mathbf{k}'}^{\dagger} e^{-i\mathbf{k}'\cdot\mathbf{r}}) \right] = \\ &= \sum_{\mathbf{k}} \hbar \mathbf{k} \left[a_{\mathbf{k}}^{\dagger} a_{\mathbf{k}}, (V_{\mathbf{k}} a_{\mathbf{k}} e^{i\mathbf{k}\cdot\mathbf{r}} + V_{\mathbf{k}}^* a_{\mathbf{k}}^{\dagger} e^{-i\mathbf{k}\cdot\mathbf{r}}) \right] = \\ &= \sum_{\mathbf{k}} \hbar \mathbf{k} \left\{ V_{\mathbf{k}} \left[a_{\mathbf{k}}^{\dagger} a_{\mathbf{k}}, a_{\mathbf{k}} \right] e^{i\mathbf{k}\cdot\mathbf{r}} + V_{\mathbf{k}}^* \left[a_{\mathbf{k}}^{\dagger} a_{\mathbf{k}}, a_{\mathbf{k}}^{\dagger} \right] e^{-i\mathbf{k}\cdot\mathbf{r}} \right\} = \\ &= - \sum_{\mathbf{k}} \hbar \mathbf{k} \left(V_{\mathbf{k}} a_{\mathbf{k}} e^{i\mathbf{k}\cdot\mathbf{r}} - V_{\mathbf{k}}^* a_{\mathbf{k}}^{\dagger} e^{-i\mathbf{k}\cdot\mathbf{r}} \right); \end{aligned}$$

$$[\mathbf{P}_{op}, H] = \left[\sum_{\mathbf{k}} \hbar \mathbf{k} a_{\mathbf{k}}^{\dagger} a_{\mathbf{k}} + \mathbf{p}, H \right] = 0. \quad (4.186)$$

Because of the commutation (4.186), the operators H and \mathbf{P}_{op} have a common set of basis functions: $H\Phi = E\Phi$ and $\mathbf{P}_{op}\Phi = \mathbf{P}\Phi$.

It is possible to transform to a representation in which \mathbf{P}_{op} becomes a “c” number \mathbf{P} , and in which the Hamiltonian no longer contains the electron coordinates. The unitary (canonical) transformation required is $\Phi = S_1\psi$, where

$$S_1 = \exp \left[\frac{i}{\hbar} (\mathbf{P} - \sum_{\mathbf{k}} \hbar \mathbf{k} a_{\mathbf{k}}^{\dagger} a_{\mathbf{k}}) \cdot \mathbf{r} \right]. \quad (4.187)$$

Derivation of the transformations of the operators.

$$\begin{aligned}
\mathbf{p} &\longrightarrow S_1^{-1} \mathbf{p} S_1 = \\
&= \exp \left[-\frac{i}{\hbar} (\mathbf{P} - \sum_{\mathbf{k}} \hbar \mathbf{k} a_{\mathbf{k}}^\dagger a_{\mathbf{k}}) \cdot \mathbf{r} \right] \mathbf{p} \exp \left[\frac{i}{\hbar} (\mathbf{P} - \sum_{\mathbf{k}} \hbar \mathbf{k} a_{\mathbf{k}}^\dagger a_{\mathbf{k}}) \cdot \mathbf{r} \right] \\
&= \exp \left[-\frac{i}{\hbar} (\mathbf{P} - \sum_{\mathbf{k}} \hbar \mathbf{k} a_{\mathbf{k}}^\dagger a_{\mathbf{k}}) \cdot \mathbf{r} \right] (-i\hbar \nabla) \exp \left[\frac{i}{\hbar} (\mathbf{P} - \sum_{\mathbf{k}} \hbar \mathbf{k} a_{\mathbf{k}}^\dagger a_{\mathbf{k}}) \cdot \mathbf{r} \right] \\
&= \exp \left[-\frac{i}{\hbar} (\mathbf{P} - \sum_{\mathbf{k}} \hbar \mathbf{k} a_{\mathbf{k}}^\dagger a_{\mathbf{k}}) \cdot \mathbf{r} \right] \left\{ (\mathbf{P} - \sum_{\mathbf{k}} \hbar \mathbf{k} a_{\mathbf{k}}^\dagger a_{\mathbf{k}}) \exp \left[\frac{i}{\hbar} (\mathbf{P} - \sum_{\mathbf{k}} \hbar \mathbf{k} a_{\mathbf{k}}^\dagger a_{\mathbf{k}}) \cdot \mathbf{r} \right] \right. \\
&\quad \left. + \exp \left[\frac{i}{\hbar} (\mathbf{P} - \sum_{\mathbf{k}} \hbar \mathbf{k} a_{\mathbf{k}}^\dagger a_{\mathbf{k}}) \cdot \mathbf{r} \right] (-i\hbar \nabla) \right\} \\
&= \mathbf{P} - \sum_{\mathbf{k}} \hbar \mathbf{k} a_{\mathbf{k}}^\dagger a_{\mathbf{k}} + \mathbf{p}, \tag{4.188}
\end{aligned}$$

$$\begin{aligned}
\mathbf{P}_{op} &\longrightarrow S_1^{-1} \mathbf{P}_{op} S_1 = \\
&= \exp \left[-\frac{i}{\hbar} (\mathbf{P} - \sum_{\mathbf{k}} \hbar \mathbf{k} a_{\mathbf{k}}^\dagger a_{\mathbf{k}}) \cdot \mathbf{r} \right] \left(\sum_{\mathbf{k}} \hbar \mathbf{k} a_{\mathbf{k}}^\dagger a_{\mathbf{k}} + \mathbf{p} \right) \exp \left[\frac{i}{\hbar} (\mathbf{P} - \sum_{\mathbf{k}} \hbar \mathbf{k} a_{\mathbf{k}}^\dagger a_{\mathbf{k}}) \cdot \mathbf{r} \right] \\
&= \exp \left[\frac{i}{\hbar} \sum_{\mathbf{k}} \hbar \mathbf{k} a_{\mathbf{k}}^\dagger a_{\mathbf{k}} \cdot \mathbf{r} \right] \sum_{\mathbf{k}} \hbar \mathbf{k} a_{\mathbf{k}}^\dagger a_{\mathbf{k}} \exp \left[-\frac{i}{\hbar} \sum_{\mathbf{k}} \hbar \mathbf{k} a_{\mathbf{k}}^\dagger a_{\mathbf{k}} \cdot \mathbf{r} \right] + S_1^{-1} \mathbf{p} S_1 \\
&= \sum_{\mathbf{k}} \hbar \mathbf{k} a_{\mathbf{k}}^\dagger a_{\mathbf{k}} + \mathbf{P} - \sum_{\mathbf{k}} \hbar \mathbf{k} a_{\mathbf{k}}^\dagger a_{\mathbf{k}} + \mathbf{p} = \mathbf{P} + \mathbf{p}, \tag{4.189}
\end{aligned}$$

$$\begin{aligned}
a_{\mathbf{k}} &\longrightarrow S_1^{-1} a_{\mathbf{k}} S_1 = \\
&= \exp \left[-\frac{i}{\hbar} (\mathbf{P} - \sum_{\mathbf{k}} \hbar \mathbf{k} a_{\mathbf{k}}^\dagger a_{\mathbf{k}}) \cdot \mathbf{r} \right] a_{\mathbf{k}} \exp \left[\frac{i}{\hbar} (\mathbf{P} - \sum_{\mathbf{k}} \hbar \mathbf{k} a_{\mathbf{k}}^\dagger a_{\mathbf{k}}) \cdot \mathbf{r} \right] \\
&= \exp \left[\frac{i}{\hbar} \sum_{\mathbf{k}} \hbar \mathbf{k} a_{\mathbf{k}}^\dagger a_{\mathbf{k}} \cdot \mathbf{r} \right] a_{\mathbf{k}} \exp \left[-\frac{i}{\hbar} \sum_{\mathbf{k}} \hbar \mathbf{k} a_{\mathbf{k}}^\dagger a_{\mathbf{k}} \cdot \mathbf{r} \right] \\
&= \exp \left[i \mathbf{k} a_{\mathbf{k}}^\dagger a_{\mathbf{k}} \cdot \mathbf{r} \right] a_{\mathbf{k}} \exp \left[-i \mathbf{k} a_{\mathbf{k}}^\dagger a_{\mathbf{k}} \cdot \mathbf{r} \right] \\
&= \exp \left[i \mathbf{k} a_{\mathbf{k}}^\dagger a_{\mathbf{k}} \cdot \mathbf{r} \right] a_{\mathbf{k}} \sum_{n=0}^{\infty} \frac{1}{n!} \left(-i \mathbf{k} a_{\mathbf{k}}^\dagger a_{\mathbf{k}} \cdot \mathbf{r} \right)^n \\
&= \exp \left[i \mathbf{k} a_{\mathbf{k}}^\dagger a_{\mathbf{k}} \cdot \mathbf{r} \right] \sum_{n=0}^{\infty} \frac{1}{n!} a_{\mathbf{k}} \left(-i \mathbf{k} a_{\mathbf{k}}^\dagger a_{\mathbf{k}} \cdot \mathbf{r} \right)^n \\
&= \exp \left[i \mathbf{k} \cdot \mathbf{r} a_{\mathbf{k}}^\dagger a_{\mathbf{k}} \right] \sum_{n=0}^{\infty} \frac{1}{n!} (-i \mathbf{k} \cdot \mathbf{r})^n a_{\mathbf{k}} \left(a_{\mathbf{k}}^\dagger a_{\mathbf{k}} \right)^n \stackrel{\text{see} (*)}{=} \\
&= \exp \left[i \mathbf{k} \cdot \mathbf{r} a_{\mathbf{k}}^\dagger a_{\mathbf{k}} \right] \sum_{n=0}^{\infty} \frac{1}{n!} [-i \mathbf{k} \cdot \mathbf{r} \left(a_{\mathbf{k}}^\dagger a_{\mathbf{k}} + 1 \right)]^n a_{\mathbf{k}} \\
&= \exp \left[i \mathbf{k} \cdot \mathbf{r} a_{\mathbf{k}}^\dagger a_{\mathbf{k}} \right] \exp \left[-i \mathbf{k} \cdot \mathbf{r} \left(a_{\mathbf{k}}^\dagger a_{\mathbf{k}} + 1 \right) \right] a_{\mathbf{k}} \\
&= a_{\mathbf{k}} \exp \left(-i \mathbf{k} \cdot \mathbf{r} \right). \tag{4.190}
\end{aligned}$$

Here the property was used:

$$a_{\mathbf{k}} \left(a_{\mathbf{k}}^\dagger a_{\mathbf{k}} \right)^n = \left(a_{\mathbf{k}}^\dagger a_{\mathbf{k}} + 1 \right)^n a_{\mathbf{k}}. \tag{*}$$

It is evident for $n = 0$. For $n = 1$ it is demonstrated as follows:

$$a_{\mathbf{k}} a_{\mathbf{k}}^\dagger = a_{\mathbf{k}}^\dagger a_{\mathbf{k}} + 1 \implies a_{\mathbf{k}} a_{\mathbf{k}}^\dagger a_{\mathbf{k}} = \left(a_{\mathbf{k}}^\dagger a_{\mathbf{k}} + 1 \right) a_{\mathbf{k}};$$

then for $n \geq 2$ the validity of (*) is straightforwardly demonstrated by induction.

Finally,

$$a_{\mathbf{k}}^\dagger \longrightarrow S_1^{-1} a_{\mathbf{k}}^\dagger S_1 = [S_1^{-1} a_{\mathbf{k}} S_1]^\dagger = a_{\mathbf{k}}^\dagger \exp \left(i \mathbf{k} \cdot \mathbf{r} \right). \tag{4.191}$$

Using (4.188), (4.189), (4.190) and (4.191), one arrives at

$$H \longrightarrow \mathcal{H} = S_1^{-1} H S_1 = \frac{\left(\mathbf{P} - \sum_{\mathbf{k}} \hbar \mathbf{k} a_{\mathbf{k}}^\dagger a_{\mathbf{k}} \right)^2}{2m_b} + \sum_{\mathbf{k}} \hbar \omega_{\text{LO}} a_{\mathbf{k}}^\dagger a_{\mathbf{k}} + \sum_{\mathbf{k}} (V_{\mathbf{k}} a_{\mathbf{k}} + V_{\mathbf{k}}^* a_{\mathbf{k}}^\dagger), \tag{4.192}$$

where \mathbf{p} is set 0.⁵ The wave equation (4.184) takes the form

$$HS_1\psi = ES_1\psi \implies \mathcal{H}\psi = E\psi. \quad (4.193)$$

Our aim is to calculate for a given momentum \mathbf{P} the lowest eigenvalue $E(P)$ of the Hamiltonian (4.192). For the low-lying energy levels of the electron $E(P)$ may be well represented by the first two terms of a power series expansion in P^2 : $E(P) = E_0 + P^2/2m_p + O(P^4)$, where m_p is the effective mass of the polaron.

The canonical transformation (4.187) formally eliminates the electron operators from the Hamiltonian. LLP use further a variational method of calculation. The trial wave function is chosen as

$$\psi = S_2\psi_0 \quad (4.194)$$

where ψ_0 is the eigenstate of the unperturbed Hamiltonian with no phonons present (vacuum state). Specifically, ψ_0 is defined by

$$a_{\mathbf{k}}\psi_0 = 0, \quad (\psi_0, \psi_0) = 1 \quad (4.195)$$

and the second canonical transformation:

$$S_2 = \exp \left[\sum_{\mathbf{k}} (a_{\mathbf{k}}^\dagger f_{\mathbf{k}} - a_{\mathbf{k}} f_{\mathbf{k}}^*) \right], \quad (4.196)$$

where $f_{\mathbf{k}}$ are treated as variational functions and will be chosen to minimize the energy. The physical significance of Eq. (4.196) is that it “dresses” the electron with the virtual phonon field, which describes the polarization. Viewed as a unitary transformation, S_2 is a *displacement* operator on $a_{\mathbf{k}}$ and $a_{\mathbf{k}}^\dagger$:

⁵Transformation of the equation $\mathbf{P}_{op}\Phi = \mathbf{P}\Phi$ leads to $S_1^{-1}\mathbf{P}_{op}S_1\psi = \mathbf{P}\psi$. At the same time, applying Eq. (4.189), we obtain $S_1^{-1}\mathbf{P}_{op}S_1 = \mathbf{P} + \mathbf{p}$. Setting the gauge $\mathbf{p}\psi = 0$ eliminates the operator \mathbf{p} from the problem.

$$\begin{aligned}
a_{\mathbf{k}} &\longrightarrow S_2^{-1} a_{\mathbf{k}} S_2 = \\
&= \exp \left[- \sum_{\mathbf{k}} (a_{\mathbf{k}}^\dagger f_{\mathbf{k}} - a_{\mathbf{k}} f_{\mathbf{k}}^*) \right] a_{\mathbf{k}} \exp \left[\sum_{\mathbf{k}} (a_{\mathbf{k}}^\dagger f_{\mathbf{k}} - a_{\mathbf{k}} f_{\mathbf{k}}^*) \right] \\
&= \exp \left[-(a_{\mathbf{k}}^\dagger f_{\mathbf{k}} - a_{\mathbf{k}} f_{\mathbf{k}}^*) \right] a_{\mathbf{k}} \exp \left[(a_{\mathbf{k}}^\dagger f_{\mathbf{k}} - a_{\mathbf{k}} f_{\mathbf{k}}^*) \right] \stackrel{\text{see(**)}}{=} \\
&= a_{\mathbf{k}} + \left[a_{\mathbf{k}}, (a_{\mathbf{k}}^\dagger f_{\mathbf{k}} - a_{\mathbf{k}} f_{\mathbf{k}}^*) \right] + \frac{1}{2} \left[\left[a_{\mathbf{k}}, (a_{\mathbf{k}}^\dagger f_{\mathbf{k}} - a_{\mathbf{k}} f_{\mathbf{k}}^*) \right], (a_{\mathbf{k}}^\dagger f_{\mathbf{k}} - a_{\mathbf{k}} f_{\mathbf{k}}^*) \right] + \dots \\
&= a_{\mathbf{k}} + f_{\mathbf{k}}, \tag{4.197}
\end{aligned}$$

$$a_{\mathbf{k}}^\dagger \longrightarrow S_2^{-1} a_{\mathbf{k}}^\dagger S_2 = a_{\mathbf{k}}^\dagger + f_{\mathbf{k}}^*. \tag{4.198}$$

Here the relation was used

$$\exp[-V] a \exp[V] = a + [a, V] + \frac{1}{2} [[a, V], V] + \frac{1}{3!} [[[a, V], V], V] + \dots \tag{**}$$

Further we seek to minimize the expression for the energy,

$$E = (\psi, H\psi) = (\psi_0, S_2^{-1} \mathcal{H} S_2 \psi_0). \tag{4.199}$$

In virtue of (4.197) and (4.198), we obtain:

$$\begin{aligned}
S_2^{-1} \mathcal{H} S_2 &= \frac{\left[\mathbf{P} - \sum_{\mathbf{k}} \hbar \mathbf{k} (a_{\mathbf{k}}^\dagger + f_{\mathbf{k}}^*) (a_{\mathbf{k}} + f_{\mathbf{k}}) \right]^2}{2m_b} \\
&+ \sum_{\mathbf{k}} \hbar \omega_{\text{LO}} (a_{\mathbf{k}}^\dagger + f_{\mathbf{k}}^*) (a_{\mathbf{k}} + f_{\mathbf{k}}) + \sum_{\mathbf{k}} \left[V_{\mathbf{k}} (a_{\mathbf{k}} + f_{\mathbf{k}}) + V_{\mathbf{k}}^* (a_{\mathbf{k}}^\dagger + f_{\mathbf{k}}^*) \right] \\
&= \frac{\left[(\mathbf{P} - \sum_{\mathbf{k}} \hbar \mathbf{k} a_{\mathbf{k}}^\dagger a_{\mathbf{k}}) - \sum_{\mathbf{k}} \hbar \mathbf{k} |f_{\mathbf{k}}|^2 - \sum_{\mathbf{k}} \hbar \mathbf{k} (a_{\mathbf{k}}^\dagger f_{\mathbf{k}} + a_{\mathbf{k}} f_{\mathbf{k}}^*) \right]^2}{2m_b} \\
&+ \sum_{\mathbf{k}} \hbar \omega_{\text{LO}} (a_{\mathbf{k}}^\dagger a_{\mathbf{k}} + |f_{\mathbf{k}}|^2 + a_{\mathbf{k}}^\dagger f_{\mathbf{k}} + a_{\mathbf{k}} f_{\mathbf{k}}^*) \\
&+ \sum_{\mathbf{k}} \left[V_{\mathbf{k}} (a_{\mathbf{k}} + f_{\mathbf{k}}) + V_{\mathbf{k}}^* (a_{\mathbf{k}}^\dagger + f_{\mathbf{k}}^*) \right] \\
&= H_0 + H_1,
\end{aligned}$$

where

$$\begin{aligned}
H_0 = & \frac{\left[(\mathbf{P} - \sum_{\mathbf{k}} \hbar \mathbf{k} a_{\mathbf{k}}^\dagger a_{\mathbf{k}}) \right]^2 + \left[\sum_{\mathbf{k}} \hbar \mathbf{k} |f_{\mathbf{k}}|^2 \right]^2}{2m_b} + \sum_{\mathbf{k}} [V_{\mathbf{k}} f_{\mathbf{k}} + V_{\mathbf{k}}^* f_{\mathbf{k}}^*] \\
& + \sum_{\mathbf{k}} |f_{\mathbf{k}}|^2 \left\{ \hbar \omega_{\text{LO}} - \frac{\hbar \mathbf{k} \cdot \mathbf{P}}{m_b} + \frac{\hbar^2 k^2}{2m_b} \right\} + \frac{\hbar^2}{m_b} \sum_{\mathbf{k}} \mathbf{k} a_{\mathbf{k}}^\dagger a_{\mathbf{k}} \cdot \sum_{\mathbf{k}'} \mathbf{k}' |f_{\mathbf{k}'}|^2 \\
& + \sum_{\mathbf{k}} a_{\mathbf{k}} \left\{ V_{\mathbf{k}} + f_{\mathbf{k}}^* \left[\hbar \omega_{\text{LO}} - \frac{\hbar \mathbf{k} \cdot \mathbf{P}}{m_b} + \frac{\hbar^2 k^2}{2m_b} + \frac{\hbar^2 \mathbf{k}}{m_b} \cdot \sum_{\mathbf{k}'} \mathbf{k}' |f_{\mathbf{k}'}|^2 \right] \right\} \\
& + \sum_{\mathbf{k}} a_{\mathbf{k}}^\dagger \left\{ V_{\mathbf{k}}^* + f_{\mathbf{k}} \left[\hbar \omega_{\text{LO}} - \frac{\hbar \mathbf{k} \cdot \mathbf{P}}{m_b} + \frac{\hbar^2 k^2}{2m_b} + \frac{\hbar^2 \mathbf{k}}{m_b} \cdot \sum_{\mathbf{k}'} \mathbf{k}' |f_{\mathbf{k}'}|^2 \right] \right\} \\
& + \sum_{\mathbf{k}} \hbar \omega_{\text{LO}} a_{\mathbf{k}}^\dagger a_{\mathbf{k}}; \tag{4.200}
\end{aligned}$$

$$\begin{aligned}
H_1 = & \sum_{\mathbf{k}, \mathbf{k}'} \frac{\hbar^2 \mathbf{k} \cdot \mathbf{k}'}{2m_b} \left\{ a_{\mathbf{k}} a_{\mathbf{k}'} f_{\mathbf{k}}^* f_{\mathbf{k}'}^* + 2a_{\mathbf{k}}^\dagger a_{\mathbf{k}'} f_{\mathbf{k}} f_{\mathbf{k}'}^* + a_{\mathbf{k}}^\dagger a_{\mathbf{k}'}^\dagger f_{\mathbf{k}} f_{\mathbf{k}'} \right\} + \\
& + \sum_{\mathbf{k}, \mathbf{k}'} \frac{\hbar^2 \mathbf{k} \cdot \mathbf{k}'}{2m_b} \left\{ a_{\mathbf{k}}^\dagger a_{\mathbf{k}} a_{\mathbf{k}'} f_{\mathbf{k}'}^* + a_{\mathbf{k}'}^\dagger a_{\mathbf{k}}^\dagger a_{\mathbf{k}} f_{\mathbf{k}'} \right\}.
\end{aligned}$$

Using (4.195), we obtain from (4.199) that

$$\begin{aligned}
E = H_0 = & \frac{P^2 + \left[\sum_{\mathbf{k}} \hbar \mathbf{k} |f_{\mathbf{k}}|^2 \right]^2}{2m_b} + \sum_{\mathbf{k}} [V_{\mathbf{k}} f_{\mathbf{k}} + V_{\mathbf{k}}^* f_{\mathbf{k}}^*] \\
& + \sum_{\mathbf{k}} |f_{\mathbf{k}}|^2 \left\{ \hbar \omega_{\text{LO}} - \frac{\hbar \mathbf{k} \cdot \mathbf{P}}{m_b} + \frac{\hbar^2 k^2}{2m_b} \right\}. \tag{4.201}
\end{aligned}$$

We minimize (4.201) by imposing

$$\frac{\delta E}{\delta f_{\mathbf{k}}} = 0, \quad \frac{\delta E}{\delta f_{\mathbf{k}}^\dagger} = 0.$$

This results in

$$V_{\mathbf{k}} + f_{\mathbf{k}}^* \left\{ \hbar \omega_{\text{LO}} - \frac{\hbar \mathbf{k} \cdot \mathbf{P}}{m_b} + \frac{\hbar^2 k^2}{2m_b} + \frac{\hbar^2}{m_b} \left[\sum_{\mathbf{k}'} \hbar \mathbf{k}' |f_{\mathbf{k}'}|^2 \right] \cdot \mathbf{k} \right\} = 0 \tag{4.202}$$

and the appropriate complex conjugate equation for $f_{\mathbf{k}}$. Upon comparing (4.202) and (4.200), we see that the linear terms in $a_{\mathbf{k}}^\dagger$ and $a_{\mathbf{k}}$ are identically zero if (4.202) is satisfied, and hence that H_0 is diagonal in a representation in which $a_{\mathbf{k}}^\dagger a_{\mathbf{k}}$ is diagonal. So, the variational calculation by LLP is equivalent to the use of (4.200) as the total Hamiltonian provided $f_{\mathbf{k}}^*$

satisfies (4.202). An estimate of the accuracy of the LLP variational procedure was obtained by an estimate of the effect of H_1 using a perturbation theory.

Now we evaluate the energy of the ground state of the system, which is given by Eq. (4.201) with $f_{\mathbf{k}}^*$ satisfying Eq. (4.202). The only preferred direction in this problem is \mathbf{P} . Therefore one may introduce the parameter η defined as

$$\eta\mathbf{P} = \sum_{\mathbf{k}} \hbar\mathbf{k} |f_{\mathbf{k}}|^2. \quad (4.203)$$

Then Eq. (4.202) leads to

$$f_{\mathbf{k}}^* = -V_k \left/ \left[\hbar\omega_{\text{LO}} - \frac{\hbar\mathbf{k} \cdot \mathbf{P}}{m_b} (1 - \eta) + \frac{\hbar^2 k^2}{2m_b} \right] \right., \quad (4.204)$$

and we obtain the following implicit equation for η :

$$\begin{aligned} \eta\mathbf{P} &= \sum_{\mathbf{k}} \hbar\mathbf{k} |V_k|^2 \left/ \left[\hbar\omega_{\text{LO}} - \frac{\hbar\mathbf{k} \cdot \mathbf{P}}{m_b} (1 - \eta) + \frac{\hbar^2 k^2}{2m_b} \right]^2 \right. \\ &= \frac{V}{(2\pi)^3} \int d^3k \hbar\mathbf{k} \left(\frac{\hbar\omega_{\text{LO}}}{k} \right)^2 \frac{4\pi\alpha}{V} \left(\frac{\hbar}{2m_b\omega_{\text{LO}}} \right)^{\frac{1}{2}} \left/ \left[\hbar\omega_{\text{LO}} - \frac{\hbar\mathbf{k} \cdot \mathbf{P}}{m_b} (1 - \eta) + \frac{\hbar^2 k^2}{2m_b} \right]^2 \right. . \end{aligned}$$

Let us introduce spherical coordinates with a polar axis along \mathbf{P} and denote $x = \cos(\hat{\mathbf{k}} \cdot \mathbf{P})$:

$$\begin{aligned} \eta P &= \frac{\alpha \hbar^3 \omega_{\text{LO}}^2}{2\pi^2} \left(\frac{\hbar}{2m_b\omega_{\text{LO}}} \right)^{\frac{1}{2}} 2\pi \int_{-1}^1 dx x \int_0^\infty dk k \left/ \left[\hbar\omega_{\text{LO}} - \frac{\hbar k P x}{m_b} (1 - \eta) + \frac{\hbar^2 k^2}{2m_b} \right]^2 \right. \\ &= \frac{\alpha \hbar}{2\pi^2} \left(\frac{\hbar}{2m_b\omega_{\text{LO}}} \right)^{\frac{1}{2}} 2\pi \int_{-1}^1 dx x \int_0^\infty dk k \left/ \left[1 - 2 \frac{\hbar k P x}{2m_b \hbar\omega_{\text{LO}}} (1 - \eta) + \frac{\hbar^2 k^2}{2m_b \hbar\omega_{\text{LO}}} \right]^2 \right. . \end{aligned}$$

Further, we introduce the parameter

$$q = \frac{P}{(2m_b \hbar\omega_{\text{LO}})^{1/2}} (1 - \eta) \quad (4.205)$$

and a new variable

$$\kappa = \frac{\hbar k}{(2m_b \hbar\omega_{\text{LO}})^{1/2}}.$$

This gives

$$\begin{aligned}
\eta &= \frac{\alpha \hbar}{\pi} \left(\frac{\hbar}{2m_b \omega_{\text{LO}}} \right)^{\frac{1}{2}} \frac{2m_b \hbar \omega_{\text{LO}}}{\hbar^2 P} \int_{-1}^1 dx \int_0^\infty d\kappa \kappa / [1 - 2q\kappa x + \kappa^2]^2 \\
&= \frac{\alpha (2m_b \hbar \omega_{\text{LO}})^{1/2}}{\pi P} \int_{-1}^1 dx \int_0^\infty d\kappa \kappa / [(\kappa - qx)^2 + (1 - q^2 x^2)]^2 \\
&= \frac{\alpha (2m_b \hbar \omega_{\text{LO}})^{1/2}}{\pi P} \int_{-1}^1 dx \int_{-qx}^\infty d\kappa (\kappa + qx) / [\kappa^2 + (1 - q^2 x^2)]^2 \\
&= \frac{\alpha (2m_b \hbar \omega_{\text{LO}})^{1/2}}{\pi P} \int_{-1}^1 dx \left\{ \begin{aligned} & -\frac{1}{2[\kappa^2 + (1 - q^2 x^2)]} \\ & + qx \left[\frac{\kappa}{2(1 - q^2 x^2)[\kappa^2 + (1 - q^2 x^2)]} + \frac{1}{2(1 - q^2 x^2)^{3/2}} \arctan \left(\frac{\kappa}{[1 - q^2 x^2]^{1/2}} \right) \right] \end{aligned} \right\}_{-qx}^\infty \\
&= \frac{\alpha (2m_b \hbar \omega_{\text{LO}})^{1/2}}{\pi P} \int_{-1}^1 dx \left\{ \frac{1}{2} + \frac{qx\pi}{4(1 - q^2 x^2)^{3/2}} + \frac{q^2 x^2}{2(1 - q^2 x^2)} + \frac{qx}{2(1 - q^2 x^2)^{3/2}} \arcsin(qx) \right\}.
\end{aligned}$$

↓

$$\begin{aligned}
\eta &= \frac{\alpha (2m_b \hbar \omega_{\text{LO}})^{1/2} q\pi}{\pi P} \int_{-1}^1 \frac{x^2}{(1 - q^2 x^2)^{3/2}} dx \\
&= \frac{\alpha}{4} (1 - \eta) \int_{-1}^1 \frac{x^2}{(1 - q^2 x^2)^{3/2}} dx \\
&= \frac{\alpha}{2} (1 - \eta) \frac{q - \sqrt{1 - q^2} \arcsin(q)}{q^3 \sqrt{1 - q^2}} \\
&= \frac{\alpha (1 - \eta)}{2 \left(\frac{P}{(2m_b \hbar \omega_{\text{LO}})^{1/2}} (1 - \eta) \right)^3} \left(\frac{q}{\sqrt{1 - q^2}} - \arcsin(q) \right) \\
&= \frac{\alpha}{2 (1 - \eta)^2} \left(\frac{2m_b \hbar \omega_{\text{LO}}}{P^2} \right)^{3/2} \left(\frac{q}{\sqrt{1 - q^2}} - \arcsin(q) \right)
\end{aligned}$$

So, we have arrived at the equation

$$\eta (1 - \eta)^2 = \frac{\alpha}{2} \left(\frac{2m_b \hbar \omega_{\text{LO}}}{P^2} \right)^{3/2} \left(\frac{q}{\sqrt{1 - q^2}} - \arcsin(q) \right), \quad (4.206)$$

or equivalently, using the definition (4.205),

$$\frac{\eta}{1 - \eta} = \frac{\alpha}{2q^3} \left(\frac{q}{\sqrt{1 - q^2}} - \arcsin(q) \right). \quad (4.207)$$

Using Eqs. (4.203) and (4.204), we can simplify the energy (4.201) as follows:

$$\begin{aligned}
E &= \frac{P^2 + (\eta \mathbf{P})^2}{2m_b} - 2 \sum_{\mathbf{k}} \frac{|V_{\mathbf{k}}|^2}{\hbar \omega_{\text{LO}} - \frac{\hbar \mathbf{k} \cdot \mathbf{P}}{m_b} (1 - \eta) + \frac{\hbar^2 k^2}{2m_b}} \\
&+ \sum_{\mathbf{k}} \frac{|V_{\mathbf{k}}|^2}{\left(\hbar \omega_{\text{LO}} - \frac{\hbar \mathbf{k} \cdot \mathbf{P}}{m_b} (1 - \eta) + \frac{\hbar^2 k^2}{2m_b} \right)^2} \left(\hbar \omega_{\text{LO}} - \frac{\hbar \mathbf{k} \cdot \mathbf{P}}{m_b} + \frac{\hbar^2 k^2}{2m_b} \right)
\end{aligned}$$

$$\begin{aligned}
&= \frac{(1 + \eta^2) P^2}{2m_b} - 2 \sum_{\mathbf{k}} \frac{|V_{\mathbf{k}}|^2}{\hbar\omega_{\text{LO}} - \frac{\hbar\mathbf{k}\cdot\mathbf{P}}{m_b}(1 - \eta) + \frac{\hbar^2 k^2}{2m_b}} \\
&+ \sum_{\mathbf{k}} \frac{|V_{\mathbf{k}}|^2}{\left(\hbar\omega_{\text{LO}} - \frac{\hbar\mathbf{k}\cdot\mathbf{P}}{m_b}(1 - \eta) + \frac{\hbar^2 k^2}{2m_b}\right)^2} \left(\hbar\omega_{\text{LO}} - \frac{\hbar\mathbf{k}\cdot\mathbf{P}}{m_b}(1 - \eta + \eta) + \frac{\hbar^2 k^2}{2m_b} \right) \\
&= \frac{(1 + \eta^2) P^2}{2m_b} - 2 \sum_{\mathbf{k}} \frac{|V_{\mathbf{k}}|^2}{\hbar\omega_{\text{LO}} - \frac{\hbar\mathbf{k}\cdot\mathbf{P}}{m_b}(1 - \eta) + \frac{\hbar^2 k^2}{2m_b}} \\
&+ \sum_{\mathbf{k}} \frac{|V_{\mathbf{k}}|^2}{\left(\hbar\omega_{\text{LO}} - \frac{\hbar\mathbf{k}\cdot\mathbf{P}}{m_b}(1 - \eta) + \frac{\hbar^2 k^2}{2m_b}\right)^2} \left(\hbar\omega_{\text{LO}} - \frac{\hbar\mathbf{k}\cdot\mathbf{P}}{m_b}(1 - \eta) + \frac{\hbar^2 k^2}{2m_b} \right) \\
&- \sum_{\mathbf{k}} \frac{|V_{\mathbf{k}}|^2}{\left(\hbar\omega_{\text{LO}} - \frac{\hbar\mathbf{k}\cdot\mathbf{P}}{m_b}(1 - \eta) + \frac{\hbar^2 k^2}{2m_b}\right)^2} \left(\frac{\hbar\mathbf{k}\cdot\mathbf{P}}{m_b} \eta \right) \\
&= \frac{(1 + \eta^2) P^2}{2m_b} - 2 \sum_{\mathbf{k}} \frac{|V_{\mathbf{k}}|^2}{\hbar\omega_{\text{LO}} - \frac{\hbar\mathbf{k}\cdot\mathbf{P}}{m_b}(1 - \eta) + \frac{\hbar^2 k^2}{2m_b}} \\
&+ \sum_{\mathbf{k}} \frac{|V_{\mathbf{k}}|^2}{\hbar\omega_{\text{LO}} - \frac{\hbar\mathbf{k}\cdot\mathbf{P}}{m_b}(1 - \eta) + \frac{\hbar^2 k^2}{2m_b}} \\
&- \left(\frac{\mathbf{P}}{m_b} \eta \right) \cdot \sum_{\mathbf{k}} \frac{\hbar\mathbf{k} |V_{\mathbf{k}}|^2}{\left(\hbar\omega_{\text{LO}} - \frac{\hbar\mathbf{k}\cdot\mathbf{P}}{m_b}(1 - \eta) + \frac{\hbar^2 k^2}{2m_b}\right)^2} \\
&= \frac{(1 + \eta^2) P^2}{2m_b} - \sum_{\mathbf{k}} \frac{|V_{\mathbf{k}}|^2}{\hbar\omega_{\text{LO}} - \frac{\hbar\mathbf{k}\cdot\mathbf{P}}{m_b}(1 - \eta) + \frac{\hbar^2 k^2}{2m_b}} - \left(\frac{\mathbf{P}}{m_b} \eta \right) \cdot \sum_{\mathbf{k}} \hbar\mathbf{k} |f_{\mathbf{k}}|^2 \\
&= \frac{(1 + \eta^2) P^2}{2m_b} - \left(\frac{\mathbf{P}}{m_b} \eta \right) \cdot \eta \mathbf{P} - \sum_{\mathbf{k}} \frac{|V_{\mathbf{k}}|^2}{\hbar\omega_{\text{LO}} - \frac{\hbar\mathbf{k}\cdot\mathbf{P}}{m_b}(1 - \eta) + \frac{\hbar^2 k^2}{2m_b}} \\
&\quad \downarrow \\
&E = \frac{P^2}{2m_b} (1 - \eta^2) - \sum_{\mathbf{k}} \frac{|V_{\mathbf{k}}|^2}{\hbar\omega_{\text{LO}} - \frac{\hbar\mathbf{k}\cdot\mathbf{P}}{m_b}(1 - \eta) + \frac{\hbar^2 k^2}{2m_b}}. \tag{4.208}
\end{aligned}$$

The sum over \mathbf{k} in Eq. (4.208) is calculated as follows:

$$\begin{aligned}
& \sum_{\mathbf{k}} \frac{|V_{\mathbf{k}}|^2}{\hbar\omega_{\text{LO}} - \frac{\hbar\mathbf{k}\cdot\mathbf{P}}{m_b}(1-\eta) + \frac{\hbar^2k^2}{2m_b}} \\
&= \frac{V}{(2\pi)^3} \int d\mathbf{k} \frac{\left(\frac{\hbar\omega_{\text{LO}}}{k} \left(\frac{4\pi\alpha}{V}\right)^{\frac{1}{2}} \left(\frac{\hbar}{2m_b\omega_{\text{LO}}}\right)^{\frac{1}{4}}\right)^2}{\hbar\omega_{\text{LO}} - \frac{\hbar\mathbf{k}\cdot\mathbf{P}}{m_b}(1-\eta) + \frac{\hbar^2k^2}{2m_b}} \\
&= \frac{V}{(2\pi)^3} \hbar^2\omega_{\text{LO}}^2 \left(\frac{4\pi\alpha}{V}\right) \left(\frac{\hbar}{2m_b\omega_{\text{LO}}}\right)^{\frac{1}{2}} \int d\mathbf{k} \frac{1}{k^2 \left[\hbar\omega_{\text{LO}} - \frac{\hbar\mathbf{k}\cdot\mathbf{P}}{m_b}(1-\eta) + \frac{\hbar^2k^2}{2m_b}\right]} \\
&= \frac{m_b\omega_{\text{LO}}^2\alpha}{\pi^2} \left(\frac{\hbar}{2m_b\omega_{\text{LO}}}\right)^{\frac{1}{2}} \int d\mathbf{k} \frac{1}{k^2 \left(k^2 - 2\frac{\mathbf{k}\cdot\mathbf{P}}{\hbar}(1-\eta) + \frac{2m_b\omega_{\text{LO}}}{\hbar}\right)}.
\end{aligned}$$

For the calculation of this integral, we can use the auxiliary identity

$$\frac{1}{ab} = \int_0^1 \frac{1}{[ax + b(1-x)]^2}. \quad (4.209)$$

Setting

$$\begin{aligned}
a &= k^2 - 2\frac{\mathbf{k}\cdot\mathbf{P}}{\hbar}(1-\eta) + \frac{2m_b\omega_{\text{LO}}}{\hbar}, \\
b &= k^2,
\end{aligned}$$

we find

$$\begin{aligned}
& \sum_{\mathbf{k}} \frac{|V_{\mathbf{k}}|^2}{\hbar\omega_{\text{LO}} - \frac{\hbar\mathbf{k}\cdot\mathbf{P}}{m_b}(1-\eta) + \frac{\hbar^2k^2}{2m_b}} \\
&= \frac{m_b\omega_{\text{LO}}^2\alpha}{\pi^2} \left(\frac{\hbar}{2m_b\omega_{\text{LO}}}\right)^{\frac{1}{2}} \int_0^1 dx \int d\mathbf{k} \frac{1}{\left[x \left(k^2 - 2\frac{\mathbf{k}\cdot\mathbf{P}}{\hbar}(1-\eta) + \frac{2m_b\omega_{\text{LO}}}{\hbar}\right) + (1-x)k^2\right]^2} \\
&= \frac{m_b\omega_{\text{LO}}^2\alpha}{\pi^2} \left(\frac{\hbar}{2m_b\omega_{\text{LO}}}\right)^{\frac{1}{2}} \int_0^1 dx \int d\mathbf{k} \frac{1}{\left(k^2 - 2\frac{\mathbf{k}\cdot\mathbf{P}}{\hbar}(1-\eta)x + \frac{2m_b\omega_{\text{LO}}}{\hbar}x\right)^2} \\
&= \frac{m_b\omega_{\text{LO}}^2\alpha}{\pi^2} \left(\frac{\hbar}{2m_b\omega_{\text{LO}}}\right)^{\frac{1}{2}} \int_0^1 dx \int d\mathbf{k} \frac{1}{\left(\left(\mathbf{k} - \frac{\mathbf{P}}{\hbar}(1-\eta)x\right)^2 + \frac{2m_b\omega_{\text{LO}}}{\hbar}x - \frac{P^2}{\hbar^2}(1-\eta)^2x^2\right)^2} \\
&= \frac{m_b\omega_{\text{LO}}^2\alpha}{\pi^2} \left(\frac{\hbar}{2m_b\omega_{\text{LO}}}\right)^{\frac{1}{2}} \int_0^1 dx \int d\mathbf{k} \frac{1}{\left(k^2 + \frac{2m_b\omega_{\text{LO}}}{\hbar}x - \frac{P^2}{\hbar^2}(1-\eta)^2x^2\right)^2}
\end{aligned}$$

As long as $P^2/(2m_b)$ is sufficiently small so that no spontaneous emission can occur (roughly $P^2/(2m_b) \lesssim \hbar\omega_{\text{LO}}$), the quantity

$$A \equiv \frac{2m_b\omega_{\text{LO}}}{\hbar}x - \frac{P^2}{\hbar^2}(1-\eta)^2x^2$$

is supposed to be positive for $0 < x < 1$. Therefore, we can use the integral

$$\int \frac{1}{(k^2 + A)^2} d\mathbf{k} = \frac{\pi^2}{\sqrt{A}},$$

what gives

$$\begin{aligned} & \sum_{\mathbf{k}} \frac{|V_{\mathbf{k}}|^2}{\hbar\omega_{\text{LO}} - \frac{\hbar\mathbf{k}\cdot\mathbf{P}}{m_b}(1-\eta) + \frac{\hbar^2k^2}{2m_b}} \\ &= \frac{m_b\omega_{\text{LO}}^2\alpha}{\pi^2} \left(\frac{\hbar}{2m_b\omega_{\text{LO}}}\right)^{\frac{1}{2}} \int_0^1 dx \frac{\pi^2}{\sqrt{\frac{2m_b\omega_{\text{LO}}}{\hbar}x - \frac{P^2}{\hbar^2}(1-\eta)^2x^2}} \\ &= \frac{1}{2}\alpha\hbar\omega_{\text{LO}} \int_0^1 dx \frac{1}{\sqrt{x - \frac{(1-\eta)^2P^2}{2m_b\hbar\omega_{\text{LO}}}x^2}} \\ &= \frac{1}{2}\alpha\hbar\omega_{\text{LO}} \int_0^1 dx \frac{1}{\sqrt{x - q^2x^2}}. \end{aligned}$$

We change the variable $x = t^2$, what gives

$$\int_0^1 \frac{1}{\sqrt{x - q^2x^2}} dx = 2 \int_0^1 \frac{1}{\sqrt{1 - q^2t^2}} dt = \frac{2}{q} \arcsin q,$$

and hence

$$\sum_{\mathbf{k}} \frac{|V_{\mathbf{k}}|^2}{\hbar\omega_{\text{LO}} - \frac{\hbar\mathbf{k}\cdot\mathbf{P}}{m_b}(1-\eta) + \frac{\hbar^2k^2}{2m_b}} = \frac{\alpha\hbar\omega_{\text{LO}}}{q} \arcsin q. \quad (4.210)$$

As a result, the energy (4.208) is expressed in a closed form

$$E = \frac{P^2}{2m_b} (1 - \eta^2) - \frac{\alpha\hbar\omega_{\text{LO}}}{q} \arcsin q. \quad (4.211)$$

Further, we expand the r.h.s. of Eq. (4.207) to the second order in powers of P (or, what is the same, in powers of q) using the relation

$$\frac{q}{\sqrt{1 - q^2}} - \arcsin(q) = \frac{1}{3}q^3 + O(q^5) \quad (4.212)$$

what results in

$$\frac{\eta}{1 - \eta} = \frac{\alpha}{2q^3} \left[\frac{1}{3}q^3 + O(q^5) \right] = \frac{\alpha}{6} + O(q^2).$$

Solving this equation for η , we find

$$\eta = \frac{\alpha/6}{1 + \alpha/6} + O\left(\frac{P^2}{2m_b\hbar\omega_{\text{LO}}}\right). \quad (4.213)$$

We also apply the expansion in powers of q up to $\sim q^2$ to the energy (4.211):

$$\begin{aligned}
E &= \frac{P^2}{2m_b} (1 - \eta^2) - \frac{\alpha \hbar \omega_{\text{LO}}}{q} \left(q + \frac{1}{6} q^3 + O(q^5) \right) \\
&= \frac{P^2}{2m_b} (1 - \eta^2) - \alpha \hbar \omega_{\text{LO}} - \frac{1}{6} \alpha \hbar \omega_{\text{LO}} q^2 + \hbar \omega_{\text{LO}} O(q^4) \\
&= -\alpha \hbar \omega_{\text{LO}} + \frac{P^2}{2m_b} (1 - \eta^2) - \frac{\alpha P^2 (1 - \eta)^2}{12m_b} + \hbar \omega_{\text{LO}} O(q^4) \\
&= -\alpha \hbar \omega_{\text{LO}} + \frac{P^2}{2m_b} (1 - \eta^2) - \frac{\alpha P^2 (1 - \eta)^2}{12m_b} + \hbar \omega_{\text{LO}} O(q^4) \\
&= -\alpha \hbar \omega_{\text{LO}} + \frac{P^2}{12m_b} (1 - \eta) ((6 + \alpha) \eta - \alpha + 6) + \hbar \omega_{\text{LO}} O(q^4) \\
&= -\alpha \hbar \omega_{\text{LO}} + \frac{P^2}{12m_b} \left(1 - \frac{\alpha/6}{1 + \alpha/6} \right) \left((6 + \alpha) \frac{\alpha/6}{1 + \alpha/6} - \alpha + 6 \right) + \hbar \omega_{\text{LO}} O(q^4) \\
&= -\alpha \hbar \omega_{\text{LO}} + \frac{P^2}{2m_b (1 + \alpha/6)} + \hbar \omega_{\text{LO}} O(q^4).
\end{aligned}$$

Finally, we have arrived at the LLP polaron energy

$$E = -\alpha \hbar \omega_{\text{LO}} + \frac{P^2}{2m_b (1 + \alpha/6)} + \hbar \omega_{\text{LO}} O \left(\left(\frac{P^2}{2m_b \hbar \omega_{\text{LO}}} \right)^2 \right). \quad (4.214)$$

Appendix 2. Expansion in Stieltjes continuous fractions [54]

In this derivation it is shown that the approximation used in the evaluation of the function, which determines the polaron mass [see Eqs. (40) and (B1) from Ref. [54]]

$$g(k, z) = \int_{-\infty}^0 d\tau e^{iz\tau} \exp[-k^2 C(0)] \exp[k^2 C(\tau)] \quad (4.215)$$

with

$$C(\tau) = \frac{1}{3} \sum_{k'} \frac{k'^2}{m^2} |f_{k'}|^2 \frac{e^{i\gamma_{k'} \tau}}{\gamma_{k'}^2} \quad (4.216)$$

is equivalent to an expansion in a continued fraction limited to the first step. Moreover, it is proved that the choice of the coefficients of the continued fraction can be justified by a variational principle, at least when z is real and positive.

Expanding the last exponential of Eq. (4.215) in a power series leads to

$$\begin{aligned} g(k, z) &= \exp[-k^2 C(0)] \int_{-\infty}^0 d\tau e^{iz\tau} \sum_{n=0}^{\infty} \frac{1}{n!} \left(\frac{1}{3m^2} \right)^n \\ &\times \sum_{\vec{k}_1, \dots, \vec{k}_n} \frac{k_1^2 k_2^2 \dots k_n^2 |f_{k_1}|^2 |f_{k_2}|^2 \dots |f_{k_n}|^2}{\gamma_{k_1}^2 \gamma_{k_2}^2 \dots \gamma_{k_n}^2} \\ &\times \exp[i(\gamma_{k_1} + \gamma_{k_2} + \dots + \gamma_{k_n})\tau] \\ &= -i \exp[-k^2 C(0)] \sum_{n=0}^{\infty} \frac{(3m^2)^{-n}}{n!} \\ &\times \sum_{\vec{k}_1, \dots, \vec{k}_n} \frac{k_1^2 k_2^2 \dots k_n^2 |f_{k_1}|^2 |f_{k_2}|^2 \dots |f_{k_n}|^2}{\gamma_{k_1}^2 \gamma_{k_2}^2 \dots \gamma_{k_n}^2} \frac{1}{\gamma_{k_1} + \gamma_{k_2} + \dots + \gamma_{k_n} + z}. \end{aligned} \quad (4.217)$$

The multiple sum over the k 's is in fact an integral with $3n$ variables. It is possible to change the variables in that one of the new variables is

$$x_n = \gamma_{k_1} + \gamma_{k_2} + \dots + \gamma_{k_n}. \quad (4.218)$$

Then the multiple sum which appears in the last term of Eq. (4.217) is of the following type:

$$J(z) = \int_{n\omega}^{\infty} \frac{L(x_n)}{x_n + z} dx_n, \quad (4.219)$$

where

$$L(x_n) = 0$$

is the result of the integration over the $n - 1$ other variables. An expansion of integrals of the type (4.219) into Stieltjes continued fractions is known to give good results when z is real and not located on the cut of $J(z)$, i.e., when

$$z > -n\omega. \quad (4.220)$$

The first nontrivial step in the continued fraction expansion is

$$J(z) = \frac{a_0}{a_1 + z} \quad (4.221)$$

with

$$a_0 = \int_{n\omega}^{\infty} L(x_n) dx_n, \quad (4.222)$$

$$a_1 = \frac{\int_{n\omega}^{\infty} x_n L(x_n) dx_n}{\int_{n\omega}^{\infty} L(x_n) dx_n}. \quad (4.223)$$

A *variational principle* can be established, which gives a rather strong argument in favour of the approximation (4.221). Let us introduce a variational parameter \bar{x} writing

$$J(z) = \int_{n\omega}^{\infty} \frac{L(x_n)}{(x_n - \bar{x}) + (z + \bar{x})} dx_n. \quad (4.224)$$

Performing two steps of the division, this relation becomes

$$\begin{aligned} J(z) &= \frac{1}{z + \bar{x}} \int_{n\omega}^{\infty} L(x_n) dx_n \\ &\quad - \frac{1}{(z + \bar{x})^2} \int_{n\omega}^{\infty} (x_n - \bar{x}) L(x_n) dx_n + K(z, \bar{x}) \end{aligned} \quad (4.225)$$

with

$$K(z, \bar{x}) = \frac{1}{(z + \bar{x})^2} \int_{n\omega}^{\infty} \frac{(x_n - \bar{x})^2 L(x_n)}{x_n + z} dx_n. \quad (4.226)$$

The approximation consists of neglecting the term $K(z, \bar{x})$ in Eq. (4.225). As this term is positive [cf. (4.220)], the best approximation is obtained when it is minimum. Therefore let us use the freedom in the choice of \bar{x} to minimize the expression (4.226),

$$\begin{aligned} \frac{\partial K(z, \bar{x})}{\partial \bar{x}} &= -2 \frac{K(z, \bar{x})}{z + \bar{x}} \\ -2 \frac{1}{(z + \bar{x})^2} \int_{n\omega}^{\infty} \frac{(x_n - \bar{x})^2 L(x_n)}{x_n + z} dx_n &= 0, \end{aligned} \quad (4.227)$$

which gives

$$-2 \frac{1}{(z + \bar{x})^2} \int_{n\omega}^{\infty} \left(\frac{x_n - \bar{x}}{z + \bar{x}} + 1 \right) \frac{x_n - \bar{x}}{x_n + z} L(x_n) dx_n = 0 \quad (4.228)$$

or

$$-2 \frac{1}{(z + \bar{x})^3} \int_{n\omega}^{\infty} (x_n - \bar{x}) L(x_n) dx_n = 0. \quad (4.229)$$

This provides us with the best value of the variational parameter

$$\bar{x} = \frac{\int_{n\omega}^{\infty} x_n L(x_n) dx_n}{\int_{n\omega}^{\infty} L(x_n) dx_n}, \quad (4.230)$$

which is a_1 [cf. Eq. (4.223)].

With this value of \bar{x} and neglecting $K(z, \bar{x})$, the expression (4.225) of the calculated quantity $J(z)$ becomes

$$J(z) = \frac{1}{z + \bar{x}} \int_{n\omega}^{\infty} L(x_n) dx_n = J(z) = \frac{a_0}{a_1 + z}, \quad (4.231)$$

which is the first step (4.221) of a Stieltjes continued fraction.

To prove that this value of \bar{x} gives a minimum of $K(z, \bar{x})$, let us calculate the second derivative

$$\begin{aligned} \frac{\partial^2 K(z, \bar{x})}{\partial \bar{x}^2} &= \frac{6}{(z + \bar{x})^3} \int_{n\omega}^{\infty} (x_n - \bar{x}) L(x_n) dx_n \\ &+ \frac{2}{(z + \bar{x})^3} \int_{n\omega}^{\infty} L(x_n) dx_n. \end{aligned} \quad (4.232)$$

Now the parameter \bar{x} is replaced by its expression (4.230). The relation (4.232) becomes

$$\frac{\partial^2 K(z, \bar{x})}{\partial \bar{x}^2} = \frac{2}{(z + a_1)^3} \int_{n\omega}^{\infty} L(x_n) dx_n, \quad (4.233)$$

which is positive of $z \geq -n\omega$, since it follows from relation (4.230) that $a_1 > n\omega$.

Our approximation is related to that used by Feynman which is based on the following inequality:

$$\langle e^{-sx} \rangle \geq e^{-s\langle x \rangle}, \quad (4.234)$$

where the brackets denote the expectation value of the random variable x . For instance,

$$\langle e^{-sx} \rangle = \frac{\int_a^{\infty} L(x) e^{-sx} dx}{\int_a^{\infty} L(x) dx}, \quad (4.235)$$

where $L(x)$ is the non-normalized probability density of x . The Laplace transform of Eq. (4.234) gives

$$\int_0^{\infty} e^{-sz} \langle e^{-sx} \rangle ds \geq \int_0^{\infty} e^{-sz} e^{-s\langle x \rangle} ds, \quad (4.236)$$

which after integration becomes

$$\int_a^{\infty} \frac{L(x)}{x+z} dx \geq \frac{\int_a^{\infty} L(x) dx}{\langle x \rangle + z} = \frac{a_0}{a_1 + z}. \quad (4.237)$$

The last inequality shows the relation with our procedure.

Part II

Many polarons

V. OPTICAL CONDUCTIVITY OF AN INTERACTING MANY-POLARON GAS

A. Kubo formula for the optical conductivity of the many-polaron gas

The derivations in the present section are based on Ref. [53]. The Hamiltonian of a system of N interacting continuum polarons is given by:

$$\begin{aligned}
 H_0 = & \sum_{j=1}^N \frac{p_j^2}{2m_b} + \sum_{\mathbf{q}} \hbar\omega_{\text{LO}} b_{\mathbf{q}}^+ b_{\mathbf{q}} \\
 & + \sum_{\mathbf{q}} \sum_{j=1}^N (e^{i\mathbf{q}\cdot\mathbf{r}_j} b_{\mathbf{q}} V_{\mathbf{q}} + e^{-i\mathbf{q}\cdot\mathbf{r}_j} b_{\mathbf{q}}^+ V_{\mathbf{q}}^*) + \frac{e^2}{2\varepsilon_{\infty}} \sum_{j=1}^N \sum_{\ell(\neq j)=1}^N \frac{1}{|\mathbf{r}_i - \mathbf{r}_j|}, \quad (5.1)
 \end{aligned}$$

where $\mathbf{r}_j, \mathbf{p}_j$ represent the position and momentum of the N constituent electrons (or holes) with band mass m_b ; $b_{\mathbf{q}}^+, b_{\mathbf{q}}$ denote the creation and annihilation operators for longitudinal optical (LO) phonons with wave vector \mathbf{q} and frequency ω_{LO} ; $V_{\mathbf{q}}$ describes the amplitude of the interaction between the electrons and the phonons; and e is the elementary electron charge. This Hamiltonian can be subdivided into the following parts:

$$H = H_e + H_{e-e} + H_{ph} + H_{e-ph} \quad (5.2)$$

where

$$H_e = \sum_{j=1}^N \frac{p_j^2}{2m_b} \quad (5.3)$$

is the kinetic energy of electrons,

$$H_{e-e} = \frac{e^2}{2\varepsilon_{\infty}} \sum_{j=1}^N \sum_{\ell(\neq j)=1}^N \frac{1}{|\mathbf{r}_i - \mathbf{r}_j|} \quad (5.4)$$

is the potential energy of the Coulomb electron-electron interaction,

$$H_{ph} = \sum_{\mathbf{q}} \hbar\omega_{\text{LO}} b_{\mathbf{q}}^+ b_{\mathbf{q}} \quad (5.5)$$

is the Hamiltonian of phonons, and

$$H_{e-ph} = \sum_{\mathbf{q}} \sum_{j=1}^N (e^{i\mathbf{q}\cdot\mathbf{r}_j} b_{\mathbf{q}} V_{\mathbf{q}} + e^{-i\mathbf{q}\cdot\mathbf{r}_j} b_{\mathbf{q}}^{\dagger} V_{\mathbf{q}}^*) \quad (5.6)$$

is the Hamiltonian of the electron-phonon interaction. Further on, we use the second quantization formalism for electrons, in which the terms H_e , H_{e-e} and H_{e-ph} are

$$H_e = \sum_{\mathbf{k},\sigma} \frac{\hbar^2 k^2}{2m_b} a_{\mathbf{k},\sigma}^{\dagger} a_{\mathbf{k},\sigma}, \quad (5.7)$$

$$H_{e-e} = \frac{1}{2} \sum_{\mathbf{q} \neq 0} v_{\mathbf{q}} \sum_{\substack{\mathbf{k},\sigma \\ \mathbf{k}',\sigma'}} a_{\mathbf{k}+\mathbf{q},\sigma}^{\dagger} a_{\mathbf{k}'-\mathbf{q},\sigma'}^{\dagger} a_{\mathbf{k}',\sigma'} a_{\mathbf{k},\sigma} = \frac{1}{2} \sum_{\mathbf{q} \neq 0} v_{\mathbf{q}} : \rho_{\mathbf{q}} \rho_{-\mathbf{q}} :, \quad (5.8)$$

$$H_{e-ph} = \sum_{\mathbf{q}} (V_{\mathbf{q}} b_{\mathbf{q}} \rho_{\mathbf{q}} + V_{\mathbf{q}}^* b_{\mathbf{q}}^{\dagger} \rho_{-\mathbf{q}}), \quad (5.9)$$

where $: \dots :$ is the symbol of the normal product of operators,

$$v_{\mathbf{q}} = \frac{4\pi e^2}{\varepsilon_{\infty} q^2 V} \quad (5.10)$$

is the Fourier component of the Coulomb potential, and

$$\rho_{\mathbf{q}} = \sum_{j=1}^N e^{i\mathbf{q}\cdot\mathbf{r}_j} = \sum_{\mathbf{k},\sigma} a_{\mathbf{k}+\mathbf{q},\sigma}^{\dagger} a_{\mathbf{k},\sigma} \quad (5.11)$$

is the Fourier component of the electron density.

The ground state energy of the many-polaron Hamiltonian (5.1) has been studied by L. Lemmens, J. T. Devreese and F. Brosens (LDB) [91], for weak and intermediate strength of the electron-phonon coupling. They introduce a variational wave function:

$$|\psi_{\text{LDB}}\rangle = U |\phi\rangle \left| \psi_{el}^{(0)} \right\rangle, \quad (5.12)$$

where $\left| \psi_{el}^{(0)} \right\rangle$ represents the ground-state many-body wave function for the electron (or hole) system and $|\phi\rangle$ is the phonon vacuum, U is a many-body unitary operator which determines a canonical transformation for a fermion gas interacting with a boson field:

$$U = \exp \left\{ \sum_{j=1}^N \sum_{\mathbf{q}} (f_{\mathbf{q}} a_{\mathbf{q}} e^{i\mathbf{q}\cdot\mathbf{r}_j} - f_{\mathbf{q}}^* a_{\mathbf{q}}^{\dagger} e^{-i\mathbf{q}\cdot\mathbf{r}_j}) \right\}. \quad (5.13)$$

In Ref. [91], this canonical transformation was used to establish a many-fermion theory. The $f_{\mathbf{q}}$ were determined variationally [91] resulting in

$$f_{\mathbf{q}} = \frac{V_{\mathbf{q}}}{\hbar\omega_{\text{LO}} + \frac{\hbar^2 q^2}{2m_b S(\mathbf{q})}}, \quad (5.14)$$

for a system with total momentum $\mathbf{P} = \sum_j \mathbf{p}_j = 0$. In this expression, $S(\mathbf{q})$ represents the static structure factor of the constituent interacting many electron or hole system :

$$NS(\mathbf{q}) = \left\langle \sum_{j=1}^N \sum_{j'=1}^N e^{i\mathbf{q}\cdot(\mathbf{r}_j - \mathbf{r}_{j'})} \right\rangle. \quad (5.15)$$

The angular brackets $\langle \dots \rangle$ represent the expectation value with respect to the ground state.

The many-polaron optical conductivity is the response of the current-density, in the system described by the Hamiltonian (5.1), to an applied electric field (along the x -axis) with frequency ω . This applied electric field introduces a perturbation term in the Hamiltonian (5.1), which couples the vector potential of the incident electromagnetic field to the current-density. Within linear response theory, the optical conductivity can be expressed through the Kubo formula as a current-current correlation function:

$$\sigma(\omega) = i \frac{Ne^2}{Vm_b\omega} + \frac{1}{V\hbar\omega} \int_0^\infty e^{i\omega t} \langle [J_x(t), J_x(0)] \rangle dt. \quad (5.16)$$

In this expression, V is the volume of the system, and J_x is the x -component of the current operator \mathbf{J} , which is related to the momentum operators of the charge carriers:

$$\mathbf{J} = \frac{q}{m_b} \sum_{j=1}^N \mathbf{p}_j = \frac{q}{m_b} \mathbf{P}, \quad (5.17)$$

with q the charge of the charge carriers ($+e$ for holes, $-e$ for electrons) and \mathbf{P} the total momentum operator of the charge carriers. The real part of the optical conductivity at temperature zero, which is proportional to the optical absorption coefficient, can be written as a function of the total momentum operator of the charge carriers as follows :

$$\text{Re } \sigma(\omega) = \frac{1}{V\hbar\omega} \frac{e^2}{m_b^2} \text{Re} \left\{ \int_0^\infty e^{i\omega t} \langle [P_x(t), P_x(0)] \rangle dt \right\}. \quad (5.18)$$

B. Force-force correlation function

Let us integrate over time in (5.18) twice by parts as follows:

$$\begin{aligned}
& \int_0^\infty dt \langle [P_x(t), P_x] \rangle e^{i\omega t - \delta t} \\
&= \frac{1}{i\omega - \delta} \left\{ \langle [P_x(t), P_x] \rangle e^{i\omega t - \delta t} \Big|_{t=0}^\infty - \int_0^\infty dt \left\langle \left[\frac{d}{dt} P_x(t), P_x \right] \right\rangle e^{i\omega t - \delta t} \right\} \\
&= -\frac{1}{i\omega - \delta} \int_0^\infty dt \left\langle \left[\frac{d}{dt} \left(e^{\frac{it}{\hbar} H} P_x e^{-\frac{it}{\hbar} H} \right), P_x \right] \right\rangle e^{i\omega t - \delta t} \\
&= -\frac{1}{i\omega - \delta} \int_0^\infty dt \left\langle \left[\left(e^{\frac{it}{\hbar} H} \frac{i}{\hbar} [H, P_x] e^{-\frac{it}{\hbar} H} \right), P_x \right] \right\rangle e^{i\omega t - \delta t} \\
&= -\frac{1}{i\omega - \delta} \int_0^\infty dt \left\langle \left[\frac{i}{\hbar} [H, P_x], e^{-\frac{it}{\hbar} H} P_x e^{\frac{it}{\hbar} H} \right] \right\rangle e^{i\omega t - \delta t} \\
&= -\frac{1}{i\omega - \delta} \int_0^\infty dt \left\langle \left[F_x(0), e^{-\frac{it}{\hbar} H} P_x e^{\frac{it}{\hbar} H} \right] \right\rangle e^{i\omega t - \delta t} \\
&= -\left(\frac{1}{i\omega - \delta} \right)^2 \left\{ \left\langle \left[F_x(0), e^{-\frac{it}{\hbar} H} P_x e^{\frac{it}{\hbar} H} \right] \right\rangle e^{i\omega t - \delta t} \Big|_{t=0}^\infty \right. \\
&\quad \left. - \int_0^\infty dt \left\langle \left[F_x(0), \frac{d}{dt} e^{-\frac{it}{\hbar} H} P_x e^{\frac{it}{\hbar} H} \right] \right\rangle e^{i\omega t - \delta t} \right\} \\
&= -\left(\frac{1}{i\omega - \delta} \right)^2 \left\{ -\langle [F_x, P_x] \rangle + \int_0^\infty dt \left\langle \left[F_x(0), e^{-\frac{it}{\hbar} H} \left(\frac{i}{\hbar} [H, P_x] \right) e^{\frac{it}{\hbar} H} \right] \right\rangle e^{i\omega t - \delta t} \right\} \\
&= -\left(\frac{1}{i\omega - \delta} \right)^2 \left\{ -\langle [F_x, P_x] \rangle + \int_0^\infty dt \left\langle \left[F_x(0), e^{-\frac{it}{\hbar} H} F_x(0) e^{\frac{it}{\hbar} H} \right] \right\rangle e^{i\omega t - \delta t} \right\} \\
&= -\left(\frac{1}{i\omega - \delta} \right)^2 \left\{ -\langle [F_x, P_x] \rangle + \int_0^\infty dt \left\langle \left[e^{\frac{it}{\hbar} H} F_x(0) e^{-\frac{it}{\hbar} H}, F_x(0) \right] \right\rangle e^{i\omega t - \delta t} \right\} \\
&= \frac{1}{(\omega + i\delta)^2} \left\{ -\langle [F_x, P_x] \rangle + \int_0^\infty dt \langle [F_x(t), F_x(0)] \rangle e^{i\omega t - \delta t} \right\},
\end{aligned}$$

where $\mathbf{F} \equiv \frac{i}{\hbar} [H, \mathbf{P}]$ is the operator of the force applied to the center of mass of the electrons.

Since both F_x and P_x are hermitian operators, the average $\langle [F_x, P_x] \rangle$ is imaginary. Hence, for $\omega \neq 0$, this term does not give a contribution into $\text{Re } \sigma(\omega)$. As a result, integrating by parts twice, the real part of the optical conductivity of the many-polaron system is written with a force-force correlation function:

$$\text{Re } \sigma(\omega) = \frac{1}{V \hbar \omega^3} \frac{e^2}{m_b^2} \text{Re} \left\{ \int_0^\infty e^{i\omega t} \langle [F_x(t), F_x(0)] \rangle dt \right\}. \quad (5.19)$$

The force operator is determined as

$$F_x = \frac{i}{\hbar} [H, P_x] = \frac{i}{\hbar} [H_e + H_{e-e} + H_{ph} + H_{e-ph}, P_x].$$

Further, we use the commutators:

$$\begin{aligned}
[a_{\mathbf{k}+\mathbf{q},\sigma}^+ a_{\mathbf{k},\sigma}, P_x] &= \sum_{\mathbf{k}'} \hbar k'_x [a_{\mathbf{k}+\mathbf{q},\sigma}^+ a_{\mathbf{k},\sigma}, a_{\mathbf{k}',\sigma}^+ a_{\mathbf{k}',\sigma}] \\
&= \sum_{\mathbf{k}'} \hbar k'_x \left(\begin{aligned} &a_{\mathbf{k}+\mathbf{q},\sigma}^+ a_{\mathbf{k},\sigma} a_{\mathbf{k}',\sigma}^+ a_{\mathbf{k}',\sigma} + a_{\mathbf{k}+\mathbf{q},\sigma}^+ a_{\mathbf{k}',\sigma}^+ a_{\mathbf{k},\sigma} a_{\mathbf{k}',\sigma} \\ &- a_{\mathbf{k}',\sigma}^+ a_{\mathbf{k}+\mathbf{q},\sigma}^+ a_{\mathbf{k}',\sigma} a_{\mathbf{k},\sigma} - a_{\mathbf{k}',\sigma}^+ a_{\mathbf{k}',\sigma} a_{\mathbf{k}+\mathbf{q},\sigma}^+ a_{\mathbf{k},\sigma} \end{aligned} \right) \\
&= \sum_{\mathbf{k}'} \hbar k'_x (\delta_{\mathbf{k}\mathbf{k}'} a_{\mathbf{k}+\mathbf{q},\sigma}^+ a_{\mathbf{k}',\sigma} - \delta_{\mathbf{k}',\mathbf{k}+\mathbf{q}} a_{\mathbf{k}',\sigma}^+ a_{\mathbf{k},\sigma}) \\
&= \sum_{\mathbf{k}'} \hbar k'_x (\delta_{\mathbf{k}\mathbf{k}'} a_{\mathbf{k}+\mathbf{q},\sigma}^+ a_{\mathbf{k},\sigma} - \delta_{\mathbf{k}',\mathbf{k}+\mathbf{q}} a_{\mathbf{k}+\mathbf{q},\sigma}^+ a_{\mathbf{k},\sigma}) \\
&= a_{\mathbf{k}+\mathbf{q},\sigma}^+ a_{\mathbf{k},\sigma} \sum_{\mathbf{k}'} \hbar k'_x (\delta_{\mathbf{k}\mathbf{k}'} - \delta_{\mathbf{k}',\mathbf{k}+\mathbf{q}}) = -\hbar q_x a_{\mathbf{k}+\mathbf{q},\sigma}^+ a_{\mathbf{k},\sigma},
\end{aligned}$$

$$[\rho_{\mathbf{q}}, P_x] = -\hbar q_x \rho_{\mathbf{q}}.$$

Hence, $[H_e, P_x] = 0$, $[H_{e-e}, P_x] = 0$,

$$\begin{aligned}
[H_{e-ph}, P_x] &= \sum_{\mathbf{q}} (V_{\mathbf{q}} b_{\mathbf{q}} [\rho_{\mathbf{q}}, P_x] + V_{\mathbf{q}}^* b_{\mathbf{q}}^+ [\rho_{-\mathbf{q}}, P_x]) \\
&= -\hbar \sum_{\mathbf{q}} q_x (V_{\mathbf{q}} b_{\mathbf{q}} \rho_{\mathbf{q}} - V_{\mathbf{q}}^* b_{\mathbf{q}}^+ \rho_{-\mathbf{q}}),
\end{aligned}$$

So, the commutator of the Hamiltonian (5.1) with the total momentum operator of the charge carriers leads to the expression for the force

$$\mathbf{F} = -i \sum_{\mathbf{q}} \mathbf{q} (V_{\mathbf{q}} b_{\mathbf{q}} \rho_{\mathbf{q}} - V_{\mathbf{q}}^* b_{\mathbf{q}}^+ \rho_{-\mathbf{q}}). \quad (5.20)$$

This result for the force operator clarifies the significance of using the force-force correlation function rather than the momentum-momentum correlation function. The operator product $F_x(t)F_x(0)$ is proportional to $|V_{\mathbf{k}}|^2$, the charge carrier - phonon interaction strength. This will be a distinct advantage for any expansion of the final result in the charge carrier - phonon interaction strength, since one power of $|V_{\mathbf{k}}|^2$ is factored out beforehand. Substituting (5.20) into (5.19), the real part of the optical conductivity then takes the form:

$$\begin{aligned}
\text{Re } \sigma(\omega) &= \frac{1}{V \hbar \omega^3} \frac{e^2}{m_b^2} \text{Re} \int_0^\infty dt e^{i\omega t - \delta t} \sum_{\mathbf{q}, \mathbf{q}'} q_x q'_x \\
&\times \langle [[V_{\mathbf{q}} b_{\mathbf{q}}(t) + V_{-\mathbf{q}}^* b_{-\mathbf{q}}^+(t)] \rho_{\mathbf{q}}(t), (V_{-\mathbf{q}'} b_{-\mathbf{q}'} + V_{\mathbf{q}'}^* b_{\mathbf{q}'}^+) \rho_{-\mathbf{q}'}] \rangle. \quad (5.21)
\end{aligned}$$

Up to this point, no approximations other than *linear response theory* have been made.

C. Canonical transformation

The expectation value appearing in the right hand side of expression (5.21) for the real part of the optical conductivity is calculated now with respect to the LDB many-polaron wave function (5.12). The unitary operator (5.13) can be written as

$$U = \exp \sum_{\mathbf{q}} A_{\mathbf{q}} \rho_{\mathbf{q}}, \quad A_{\mathbf{q}} = f_{\mathbf{q}} b_{\mathbf{q}} - f_{-\mathbf{q}}^* b_{-\mathbf{q}}^+, \quad (5.22)$$

The transformed Hamiltonian (5.2) is denoted as

$$\tilde{H} = U^{-1} H U. \quad (5.23)$$

The momentum operator of an electron \mathbf{p}_j , the operator of the total momentum of electrons \mathbf{P} and the phonon creation and annihilation operators are transformed by the unitary transformation (5.22) as follows:

$$U^{-1} \mathbf{p}_j U = \mathbf{p}_j + \sum_{\mathbf{q}} \hbar \mathbf{q} A_{\mathbf{q}} e^{i\mathbf{q} \cdot \mathbf{r}_j}, \quad (5.24)$$

$$U^{-1} \mathbf{P} U = \mathbf{P} + \sum_{\mathbf{q}} \hbar \mathbf{q} A_{\mathbf{q}} \rho_{\mathbf{q}}, \quad (5.25)$$

$$U^{-1} b_{\mathbf{q}} U = b_{\mathbf{q}} - f_{\mathbf{q}}^* \rho_{-\mathbf{q}}, \quad U^{-1} b_{\mathbf{q}}^+ U = b_{\mathbf{q}}^+ - f_{\mathbf{q}} \rho_{\mathbf{q}}. \quad (5.26)$$

As a result, after the transformation (5.22), the Hamiltonian takes the form (see Ref. [91]):

$$\tilde{H} = H_e + \tilde{H}_{e-e} + H_{ph} + \tilde{H}_{e-ph} + H_N + H_{ppe}, \quad (5.27)$$

where the terms are

$$\tilde{H}_{e-e} = \frac{1}{2} \sum_{\mathbf{q} \neq 0} \tilde{v}_{\mathbf{q}} : \rho_{\mathbf{q}} \rho_{-\mathbf{q}} :, \quad \tilde{v}_{\mathbf{q}} = v_{\mathbf{q}} + 2 (\hbar \omega_{\text{LO}} |f_{\mathbf{q}}|^2 - V_{\mathbf{q}} f_{\mathbf{q}}^* - V_{\mathbf{q}}^* f_{\mathbf{q}}), \quad (5.28)$$

$$\begin{aligned} \tilde{H}_{e-ph} = & \sum_{\mathbf{q}} [(V_{\mathbf{q}} - \hbar \omega_{\text{LO}} f_{\mathbf{q}}) b_{\mathbf{q}} \rho_{\mathbf{q}} + (V_{\mathbf{q}}^* - \hbar \omega_{\text{LO}} f_{\mathbf{q}}^*) b_{\mathbf{q}}^+ \rho_{-\mathbf{q}}] \\ & + \frac{\hbar^2}{2m_b} \sum_{\mathbf{q}} A_{\mathbf{q}} \sum_{\mathbf{k}, \sigma} (\mathbf{q}^2 + 2\mathbf{k} \cdot \mathbf{q}) a_{\mathbf{k}+\mathbf{q}, \sigma}^+ a_{\mathbf{k}, \sigma}, \end{aligned} \quad (5.29)$$

$$H_N = \hat{N} \sum_{\mathbf{q}} (\hbar \omega_{\text{LO}} |f_{\mathbf{q}}|^2 - V_{\mathbf{q}} f_{\mathbf{q}}^* - V_{\mathbf{q}}^* f_{\mathbf{q}}), \quad \left(\hat{N} \equiv \sum_{\mathbf{k}, \sigma} a_{\mathbf{k}, \sigma}^+ a_{\mathbf{k}, \sigma} \right), \quad (5.30)$$

$$H_{ppe} = \frac{\hbar^2}{2m_b} \sum_{\mathbf{q}\mathbf{q}'} \mathbf{q} \cdot \mathbf{q}' A_{\mathbf{q}} A_{\mathbf{q}'} \rho_{\mathbf{q}+\mathbf{q}'}. \quad (5.31)$$

The exact expression for the real part of the conductivity (5.21) after the replacement of $|\Psi_0\rangle$ by $|\Psi_{LDB}\rangle = U|\phi\rangle|\psi_{el}^{(0)}\rangle$ is transformed to the approximate one

$$\begin{aligned} & \text{Re } \sigma(\omega) \\ &= \frac{1}{V\hbar\omega^3} \frac{e^2}{m_b^2} \text{Re} \int_0^\infty dt e^{i\omega t - \delta t} \sum_{\mathbf{q}, \mathbf{q}'} q_x q'_x \\ & \times \left\langle \psi_{el}^{(0)} \left| \left\langle \phi \left| U^{-1} \begin{bmatrix} e^{\frac{i\hbar}{\hbar} H} [V_{\mathbf{q}} b_{\mathbf{q}} + V_{-\mathbf{q}}^* b_{-\mathbf{q}}^+] \rho_{\mathbf{q}} e^{-\frac{i\hbar}{\hbar} H}, \\ (V_{-\mathbf{q}'} b_{-\mathbf{q}'} + V_{\mathbf{q}'}^* b_{\mathbf{q}'}^+) \rho_{-\mathbf{q}'} \end{bmatrix} U \right| \phi \right\rangle \right| \psi_{el}^{(0)} \rangle \\ &= \frac{1}{V\hbar\omega^3} \frac{e^2}{m_b^2} \text{Re} \int_0^\infty dt e^{i\omega t - \delta t} \sum_{\mathbf{q}, \mathbf{q}'} q_x q'_x \\ & \times \left\langle \psi_{el}^{(0)} \left| \left\langle \phi \left| \begin{bmatrix} e^{\frac{i\hbar}{\hbar} \tilde{H}} U^{-1} [V_{\mathbf{q}} b_{\mathbf{q}} + V_{-\mathbf{q}}^* b_{-\mathbf{q}}^+] U \rho_{\mathbf{q}} e^{-\frac{i\hbar}{\hbar} \tilde{H}}, \\ U^{-1} (V_{-\mathbf{q}'} b_{-\mathbf{q}'} + V_{\mathbf{q}'}^* b_{\mathbf{q}'}^+) U \rho_{-\mathbf{q}'} \end{bmatrix} \right| \phi \right\rangle \right| \psi_{el}^{(0)} \rangle \\ &= \frac{1}{V\hbar\omega^3} \frac{e^2}{m_b^2} \text{Re} \int_0^\infty dt e^{i\omega t - \delta t} \sum_{\mathbf{q}, \mathbf{q}'} q_x q'_x \\ & \times \left\langle \psi_{el}^{(0)} \left| \left\langle \phi \left| \left[e^{\frac{i\hbar}{\hbar} \tilde{H}} (V_{\mathbf{q}} (b_{\mathbf{q}} - f_{\mathbf{q}}^* \rho_{-\mathbf{q}}) + V_{-\mathbf{q}}^* (b_{-\mathbf{q}}^+ - f_{-\mathbf{q}} \rho_{-\mathbf{q}})) \rho_{\mathbf{q}} e^{-\frac{i\hbar}{\hbar} \tilde{H}}, \right. \right. \right. \\ & \left. \left. \left. (V_{-\mathbf{q}'} (b_{-\mathbf{q}'} - f_{-\mathbf{q}'}^* \rho_{\mathbf{q}'}) + V_{\mathbf{q}'}^* (b_{\mathbf{q}'}^+ - f_{\mathbf{q}'} \rho_{\mathbf{q}'}) \right) \rho_{-\mathbf{q}'} \right] \right| \phi \right\rangle \left| \psi_{el}^{(0)} \right\rangle. \end{aligned}$$

So, we have arrived at the expression

$$\begin{aligned} & \text{Re } \sigma(\omega) = \frac{1}{V\hbar\omega^3} \frac{e^2}{m_b^2} \text{Re} \int_0^\infty dt e^{i\omega t - \delta t} \sum_{\mathbf{q}, \mathbf{q}'} q_x q'_x \\ & \times \left\langle \psi_{el}^{(0)} \left| \left\langle \phi \left| \left[e^{\frac{i\hbar}{\hbar} \tilde{H}} (V_{\mathbf{q}} (b_{\mathbf{q}} - f_{\mathbf{q}}^* \rho_{-\mathbf{q}}) + V_{-\mathbf{q}}^* (b_{-\mathbf{q}}^+ - f_{-\mathbf{q}} \rho_{-\mathbf{q}})) \rho_{\mathbf{q}} e^{-\frac{i\hbar}{\hbar} \tilde{H}}, \right. \right. \right. \\ & \left. \left. \left. (V_{-\mathbf{q}'} (b_{-\mathbf{q}'} - f_{-\mathbf{q}'}^* \rho_{\mathbf{q}'}) + V_{\mathbf{q}'}^* (b_{\mathbf{q}'}^+ - f_{\mathbf{q}'} \rho_{\mathbf{q}'}) \right) \rho_{-\mathbf{q}'} \right] \right| \phi \right\rangle \left| \psi_{el}^{(0)} \right\rangle. \end{aligned}$$

Since $\rho_{\mathbf{q}} \rho_{-\mathbf{q}} = \rho_{-\mathbf{q}} \rho_{\mathbf{q}}$, and $V_{\mathbf{q}} f_{\mathbf{q}}^* = V_{-\mathbf{q}} f_{-\mathbf{q}}^*$, the terms proportional to $\rho_{-\mathbf{q}} \rho_{\mathbf{q}}$ vanish after the summation over \mathbf{q} :

$$\sum_{\mathbf{q}} q_x V_{\mathbf{q}} f_{\mathbf{q}}^* \rho_{-\mathbf{q}} \rho_{\mathbf{q}} \stackrel{\mathbf{q} \rightarrow -\mathbf{q}}{=} - \sum_{\mathbf{q}} q_x V_{\mathbf{q}} f_{\mathbf{q}}^* \rho_{-\mathbf{q}} \rho_{\mathbf{q}} = 0. \quad (5.32)$$

Hence we obtain the real part of the optical conductivity in the form

$$\begin{aligned} \text{Re } \sigma(\omega) &= \frac{1}{V\hbar\omega^3} \frac{e^2}{m_b^2} \text{Re} \int_0^\infty dt e^{i\omega t - \delta t} \sum_{\mathbf{q}, \mathbf{q}'} q_x q'_x \\ &\times \left\langle \psi_{el}^{(0)} \left| \left\langle \phi \left| \left[e^{\frac{i\hbar}{\hbar} \tilde{H}} (V_{\mathbf{q}} b_{\mathbf{q}} + V_{-\mathbf{q}}^* b_{-\mathbf{q}}^+) \rho_{\mathbf{q}} e^{-\frac{i\hbar}{\hbar} \tilde{H}}, \right. \right. \right. \\ &\quad \left. \left. \left. (V_{-\mathbf{q}'} b_{-\mathbf{q}'} + V_{\mathbf{q}'}^* b_{\mathbf{q}'}^+) \rho_{-\mathbf{q}'} \right] \right| \phi \right\rangle \left| \psi_{el}^{(0)} \right\rangle. \end{aligned} \quad (5.33)$$

Introducing the factor

$$\begin{aligned} \mathcal{J}(\mathbf{q}, \mathbf{q}') &= \left\langle \psi_{el}^{(0)} \left| \left\langle \phi \left| \left[e^{\frac{i\hbar}{\hbar} \tilde{H}} (V_{\mathbf{q}} b_{\mathbf{q}} + V_{-\mathbf{q}}^* b_{-\mathbf{q}}^+) \rho_{\mathbf{q}} e^{-\frac{i\hbar}{\hbar} \tilde{H}}, \right. \right. \right. \\ &\quad \left. \left. \left. (V_{-\mathbf{q}'} b_{-\mathbf{q}'} + V_{\mathbf{q}'}^* b_{\mathbf{q}'}^+) \rho_{-\mathbf{q}'} \right] \right| \phi \right\rangle \left| \psi_{el}^{(0)} \right\rangle, \end{aligned} \quad (5.34)$$

the optical conductivity can be written as

$$\text{Re } \sigma(\omega) = \frac{1}{V\hbar\omega^3} \frac{e^2}{m_b^2} \text{Re} \int_0^\infty dt e^{i\omega t - \delta t} \sum_{\mathbf{q}, \mathbf{q}'} q_x q'_x \mathcal{J}(\mathbf{q}, \mathbf{q}'). \quad (5.35)$$

In the case of a weak electron-phonon coupling, we can neglect in the exponent $e^{-\frac{i\hbar}{\hbar} \tilde{H}}$ of (5.33) the terms \tilde{H}_{e-ph} and H_{ppe} [i. e., the renormalized Hamiltonian of the electron-phonon interaction (5.28) and (5.31)]. Namely, we replace \tilde{H} in Eq. (5.33) by the Hamiltonian

$$\tilde{H}_0 = H_e + \tilde{H}_{e-e} + H_{ph} + H_N. \quad (5.36)$$

In this case, we find

$$\begin{aligned} \mathcal{J}(\mathbf{q}, \mathbf{q}') &= \left\langle \psi_{el}^{(0)} \left| \left\langle \phi \left| \left[e^{\frac{i\hbar}{\hbar} \tilde{H}_0} (V_{\mathbf{q}} b_{\mathbf{q}} + V_{-\mathbf{q}}^* b_{-\mathbf{q}}^+) \rho_{\mathbf{q}} e^{-\frac{i\hbar}{\hbar} \tilde{H}_0}, \right. \right. \right. \\ &\quad \left. \left. \left. (V_{-\mathbf{q}'} b_{-\mathbf{q}'} + V_{\mathbf{q}'}^* b_{\mathbf{q}'}^+) \rho_{-\mathbf{q}'} \right] \right| \phi \right\rangle \left| \psi_{el}^{(0)} \right\rangle \\ &= |V_{\mathbf{q}}|^2 \delta_{\mathbf{q}\mathbf{q}'} \left\langle \psi_{el}^{(0)} \left| \left\langle \phi \left| e^{i\tilde{H}_0 t/\hbar} \rho_{\mathbf{q}} b_{\mathbf{q}} e^{-i\tilde{H}_0 t/\hbar} \rho_{-\mathbf{q}} b_{\mathbf{q}}^+ \right. \right. \right. \\ &\quad \left. \left. \left. - \rho_{\mathbf{q}} b_{\mathbf{q}} e^{i\tilde{H}_0 t/\hbar} \rho_{-\mathbf{q}} b_{\mathbf{q}}^+ e^{-i\tilde{H}_0 t/\hbar} \right| \phi \right\rangle \left| \psi_{el}^{(0)} \right\rangle \right. \\ &= 2i |V_{\mathbf{q}}|^2 \delta_{\mathbf{q}\mathbf{q}'} \text{Im} \left[\left\langle \psi_{el}^{(0)} \left| \left\langle \phi \left| e^{i\tilde{H}_0 t/\hbar} \rho_{\mathbf{q}} b_{\mathbf{q}} e^{-i\tilde{H}_0 t/\hbar} \rho_{-\mathbf{q}} b_{\mathbf{q}}^+ \right| \phi \right\rangle \left| \psi_{el}^{(0)} \right\rangle \right] \right]. \end{aligned}$$

The time-dependent phonon operators are

$$e^{i\tilde{H}_0 t/\hbar} b_{\mathbf{q}} e^{-i\tilde{H}_0 t/\hbar} = b_{\mathbf{q}} e^{-i\omega_{\text{LO}} t},$$

so that we have

$$\begin{aligned}\mathcal{J}(\mathbf{q}, \mathbf{q}') &= 2i|V_{\mathbf{q}}|^2 \delta_{\mathbf{q}\mathbf{q}'} \text{Im} \left[e^{-i\omega_{\text{LO}}t} \left\langle \psi_{el}^{(0)} \left| \left\langle \phi \left| e^{i\tilde{H}_0t/\hbar} \rho_{\mathbf{q}} e^{-i\tilde{H}_0t/\hbar} \rho_{-\mathbf{q}} b_{\mathbf{q}} b_{\mathbf{q}}^+ \right| \phi \right\rangle \right| \psi_{el}^{(0)} \right\rangle \right] \\ &= 2i|V_{\mathbf{q}}|^2 \delta_{\mathbf{q}\mathbf{q}'} \text{Im} \left[\left\langle \psi_{el}^{(0)} \left| e^{i\tilde{H}_e t/\hbar} \rho_{\mathbf{q}} e^{-i\tilde{H}_e t/\hbar} \rho_{-\mathbf{q}} \right| \psi_{el}^{(0)} \right\rangle \left\langle \phi \left| b_{\mathbf{q}} b_{\mathbf{q}}^+ \right| \phi \right\rangle \right],\end{aligned}$$

where $\tilde{H}_e = H_e + \tilde{H}_{e-e} + H_N$.

Taking the expectation value with respect to the phonon vacuum, we find

$$\mathcal{J}(\mathbf{q}, \mathbf{q}') = 2i|V_{\mathbf{q}}|^2 \delta_{\mathbf{q}\mathbf{q}'} \text{Im} \left[e^{-i\omega_{\text{LO}}t} \left\langle \psi_{el}^{(0)} \left| e^{i\tilde{H}_e t/\hbar} \rho_{\mathbf{q}} e^{-i\tilde{H}_e t/\hbar} \rho_{-\mathbf{q}} \right| \psi_{el}^{(0)} \right\rangle \right]. \quad (5.37)$$

The optical conductivity (5.33) then takes the form:

$$\begin{aligned}\text{Re } \sigma(\omega) &= -\frac{2e^2}{V\hbar m_b^2 \omega^3} \text{Im} \int_0^\infty dt e^{i\omega t - \delta t} \sum_{\mathbf{q}} q_x^2 |V_{\mathbf{q}}|^2 \\ &\quad \times \text{Im} \left[e^{-i\omega_{\text{LO}}t} \left\langle \psi_{el}^{(0)} \left| e^{i\tilde{H}_e t/\hbar} \rho_{\mathbf{q}} e^{-i\tilde{H}_e t/\hbar} \rho_{-\mathbf{q}} \right| \psi_{el}^{(0)} \right\rangle \right]\end{aligned} \quad (5.38)$$

For an isotropic electron-phonon system, q_x^2 in 3D can be replaced by $\frac{1}{3}(q_x^2 + q_y^2 + q_z^2) = \frac{1}{3}q^2$, what gives us the result

$$\text{Re } \sigma_{3\text{D}}(\omega) = -\frac{2}{3V\hbar\omega^3} \frac{e^2}{m_b^2} \sum_{\mathbf{q}} q^2 |V_{\mathbf{q}}|^2 \text{Im} \int_0^\infty dt e^{i\omega t - \delta t} \text{Im} \left[e^{-i\omega_{\text{LO}}t} F(\mathbf{q}, t) \right], \quad (5.39)$$

where the two-point correlation function is

$$F(\mathbf{q}, t) = \left\langle \psi_{el}^{(0)} \left| e^{\frac{it}{\hbar}\tilde{H}_e} \rho_{\mathbf{q}} e^{-\frac{it}{\hbar}\tilde{H}_e} \rho_{-\mathbf{q}} \right| \psi_{el}^{(0)} \right\rangle. \quad (5.40)$$

The same derivation for the 2D case, provides the expression

$$\text{Re } \sigma_{2\text{D}}(\omega) = -\frac{1}{A\hbar\omega^3} \frac{e^2}{m_b^2} \sum_{\mathbf{q}} q^2 |V_{\mathbf{q}}|^2 \text{Im} \int_0^\infty dt e^{i\omega t - \delta t} \text{Im} \left[e^{-i\omega_{\text{LO}}t} F(\mathbf{q}, t) \right], \quad (5.41)$$

where A is the surface of the 2D system.

D. Dynamic structure factor

To find the formula for the real part of the optical conductivity in its final form, we introduce the standard expression for the dynamic structure factor of the system of charge carriers interacting through a Coulomb potential,

$$S(\mathbf{q}, \omega) = \frac{1}{2N} \int_{-\infty}^{\infty} \left\langle \psi_{el}^{(0)} \left| \sum_{j,\ell} e^{i\mathbf{q}\cdot(\mathbf{r}_j(t) - \mathbf{r}_\ell(0))} \right| \psi_{el}^{(0)} \right\rangle e^{i\omega t} dt. \quad (5.42)$$

The dynamic structure factor is expressed in terms of the two-point correlation function as follows:

$$\begin{aligned}
S(\mathbf{q}, \omega) &= \frac{1}{2N} \int_{-\infty}^{\infty} \left\langle \psi_{el}^{(0)} \left| e^{\frac{it}{\hbar} \tilde{H}_e} \rho_{\mathbf{q}} e^{-\frac{it}{\hbar} \tilde{H}_e} \rho_{-\mathbf{q}} \right| \psi_{el}^{(0)} \right\rangle e^{i\omega t} dt \\
&= \frac{1}{2N} \int_{-\infty}^{\infty} F(\mathbf{q}, t) e^{i\omega t} dt = \frac{1}{2N} F(\mathbf{q}, \omega) \\
&\quad \Downarrow \\
S(\mathbf{q}, \omega) &= \frac{1}{2N} F(\mathbf{q}, \omega), \tag{5.43}
\end{aligned}$$

where $F(\mathbf{q}, \omega)$ is the Fourier image of $F(\mathbf{q}, t)$:

$$F(\mathbf{q}, \omega) = \int_{-\infty}^{\infty} F(\mathbf{q}, t) e^{i\omega t} dt. \tag{5.44}$$

The function $F(\mathbf{q}, t)$ obeys the following property:

$$\begin{aligned}
F^*(\mathbf{q}, t) &= \left\langle \psi_{el}^{(0)} \left| \rho_{-\mathbf{q}}^+ e^{\frac{it}{\hbar} \tilde{H}_e} \rho_{\mathbf{q}}^+ e^{-\frac{it}{\hbar} \tilde{H}_e} \right| \psi_{el}^{(0)} \right\rangle \\
&= \left\langle \psi_{el}^{(0)} \left| \rho_{\mathbf{q}} e^{\frac{it}{\hbar} \tilde{H}_e} \rho_{-\mathbf{q}} e^{-\frac{it}{\hbar} \tilde{H}_e} \right| \psi_{el}^{(0)} \right\rangle \\
&= \left\langle \psi_{el}^{(0)} \left| \rho_{\mathbf{q}} e^{\frac{it}{\hbar} \tilde{H}_e} \rho_{-\mathbf{q}} \right| \psi_{el}^{(0)} \right\rangle e^{-\frac{it}{\hbar} \tilde{E}_0},
\end{aligned}$$

where \tilde{E}_0 is the eigenvalue of the Hamiltonian \tilde{H}_e :

$$\tilde{H}_e \left| \psi_{el}^{(0)} \right\rangle = \tilde{E}_0 \left| \psi_{el}^{(0)} \right\rangle.$$

Herefrom, we find that

$$\begin{aligned}
F^*(\mathbf{q}, t) &= e^{-\frac{it}{\hbar} \tilde{E}_0} \left\langle \psi_{el}^{(0)} \left| \rho_{\mathbf{q}} e^{\frac{it}{\hbar} \tilde{H}_e} \rho_{-\mathbf{q}} \right| \psi_{el}^{(0)} \right\rangle \\
&= \left\langle \psi_{el}^{(0)} \left| e^{-\frac{it}{\hbar} \tilde{H}_e} \rho_{\mathbf{q}} e^{\frac{it}{\hbar} \tilde{H}_e} \rho_{-\mathbf{q}} \right| \psi_{el}^{(0)} \right\rangle = F(\mathbf{q}, -t). \tag{5.45}
\end{aligned}$$

From (5.45), for the function

$$B(\mathbf{q}, t) \equiv \text{Im} [e^{-i\omega_{\text{LO}} t} F(\mathbf{q}, t)] \tag{5.46}$$

the following equality is derived:

$$\begin{aligned}
B(\mathbf{q}, -t) &= \text{Im} [e^{i\omega_{\text{LO}} t} F(\mathbf{q}, -t)] \\
&= \text{Im} [e^{i\omega_{\text{LO}} t} F^*(\mathbf{q}, t)] \\
&= -\text{Im} [e^{-i\omega_{\text{LO}} t} F(\mathbf{q}, t)] = -B(\mathbf{q}, t),
\end{aligned}$$

$$B(\mathbf{q}, -t) = -B(\mathbf{q}, t). \quad (5.47)$$

The integral in Eq. (5.39)

$$\text{Im} \int_0^\infty dt e^{i\omega t - \delta t} \text{Im} [e^{-i\omega_{\text{LO}} t} F(\mathbf{q}, t)] = \text{Im} \int_0^\infty dt e^{i\omega t - \delta t} B(\mathbf{q}, t)$$

is then transformed as follows:

$$\begin{aligned} \text{Im} \int_0^\infty dt e^{i\omega t - \delta t} B(\mathbf{q}, t) &= \frac{1}{2i} \left[\int_0^\infty dt e^{i\omega t - \delta t} B(\mathbf{q}, t) - \int_0^\infty dt e^{-i\omega t - \delta t} B(\mathbf{q}, t) \right] \\ &= \frac{1}{2i} \left[\int_0^\infty dt e^{i\omega t - \delta t} B(\mathbf{q}, t) - \int_{-\infty}^0 dt e^{i\omega t + \delta t} B(\mathbf{q}, -t) \right] \\ &= \frac{1}{2i} \left[\int_0^\infty dt e^{i\omega t - \delta t} B(\mathbf{q}, t) + \int_{-\infty}^0 dt e^{i\omega t + \delta t} B(\mathbf{q}, t) \right] \\ &= \frac{1}{2i} \int_{-\infty}^\infty dt e^{i\omega t - \delta|t|} B(\mathbf{q}, t) \\ &= \frac{1}{2i} \int_{-\infty}^\infty dt e^{i\omega t - \delta|t|} \frac{1}{2i} [e^{-i\omega_{\text{LO}} t} F(\mathbf{q}, t) - e^{i\omega_{\text{LO}} t} F^*(\mathbf{q}, t)] \\ &= -\frac{1}{4} \int_{-\infty}^\infty dt e^{i\omega t - \delta|t|} [e^{-i\omega_{\text{LO}} t} F(\mathbf{q}, t) - e^{i\omega_{\text{LO}} t} F(\mathbf{q}, -t)]. \end{aligned}$$

We can show that, as far as $|\psi_{el}^{(0)}\rangle$ is the *ground* state, the integral $\int_{-\infty}^\infty dt e^{i\omega t - \delta|t|} F(\mathbf{q}, -t)$ for positive ω is equal to zero. Let $\{|\psi_{el}^{(n)}\rangle\}$ is the total basis set of the eigenfunctions of the Hamiltonian \tilde{H}_e . Using these functions we expand $F(\mathbf{q}, t)$:

$$\begin{aligned} F(\mathbf{q}, t) &= \sum_n \langle \psi_{el}^{(0)} | e^{\frac{i}{\hbar} \tilde{H}_e} \rho_{\mathbf{q}} e^{-\frac{i}{\hbar} \tilde{H}_e} | \psi_{el}^{(n)} \rangle \langle \psi_{el}^{(n)} | \rho_{-\mathbf{q}} | \psi_{el}^{(0)} \rangle \\ &= \sum_n \left| \langle \psi_{el}^{(n)} | \rho_{-\mathbf{q}} | \psi_{el}^{(0)} \rangle \right|^2 e^{\frac{i}{\hbar} (\tilde{E}_0 - \tilde{E}_n) t}, \\ \int_{-\infty}^\infty dt e^{i\omega t - \delta|t|} F(\mathbf{q}, -t) &= \sum_n \left| \langle \psi_{el}^{(n)} | \rho_{-\mathbf{q}} | \psi_{el}^{(0)} \rangle \right|^2 \int_{-\infty}^\infty dt e^{i\omega t + \frac{i}{\hbar} (\tilde{E}_n - \tilde{E}_0) t - \delta|t|} \\ &= \sum_n \left| \langle \psi_{el}^{(n)} | \rho_{-\mathbf{q}} | \psi_{el}^{(0)} \rangle \right|^2 2\pi \delta \left(\omega + \frac{\tilde{E}_n - \tilde{E}_0}{\hbar} \right) = 0, \end{aligned}$$

because for $\omega > 0$, $\omega + \frac{\tilde{E}_n - \tilde{E}_0}{\hbar}$ is never equal to zero.

So, rewriting expression (5.39) with the dynamic structure factor of the electron (or hole) gas results in:

$$\begin{aligned} \text{Re} \sigma_{3\text{D}}(\omega) &= \frac{1}{6V\hbar\omega^3} \frac{e^2}{m_b^2} \sum_{\mathbf{q}} q^2 |V_{\mathbf{q}}|^2 \int_{-\infty}^\infty dt e^{i(\omega - \omega_{\text{LO}})t - \delta|t|} F(\mathbf{q}, t), \\ \text{Re} \sigma_{2\text{D}}(\omega) &= \frac{1}{4A\hbar\omega^3} \frac{e^2}{m_b^2} \sum_{\mathbf{q}} q^2 |V_{\mathbf{q}}|^2 \int_{-\infty}^\infty dt e^{i(\omega - \omega_{\text{LO}})t - \delta|t|} F(\mathbf{q}, t), \end{aligned}$$

and we obtain

$$\text{Re } \sigma_{3\text{D}}(\omega) = \frac{n_0}{3\hbar\omega^3} \frac{e^2}{m_b^2} \sum_{\mathbf{q}} q^2 |V_{\mathbf{q}}|^2 S(\mathbf{q}, \omega - \omega_{\text{LO}}), \quad (5.48\text{a})$$

$$\text{Re } \sigma_{2\text{D}}(\omega) = \frac{n_0}{2\hbar\omega^3} \frac{e^2}{m_b^2} \sum_{\mathbf{q}} q^2 |V_{\mathbf{q}}|^2 S(\mathbf{q}, \omega - \omega_{\text{LO}}), \quad (5.48\text{b})$$

where

$$n_0 = \begin{cases} N/V & \text{in 3D,} \\ N/A & \text{in 2D} \end{cases}$$

is the density of charge carriers.

For an isotropic medium, the dynamic structure factor does not depend on the direction of \mathbf{q} , so that $S(\mathbf{q}, \omega) = S(q, \omega)$, where $q = |\mathbf{q}|$. Let us simplify the expression (5.48a) using explicitly the amplitudes of the Fröhlich electron-phonon interaction. The modulus squared of the Fröhlich electron-phonon interaction amplitude is given by

$$|V_{\mathbf{q}}|^2 = \begin{cases} \frac{(\hbar\omega_{\text{LO}})^2}{q^2} \frac{4\pi\alpha}{V} \left(\frac{\hbar}{2m_b\omega_{\text{LO}}} \right)^{1/2} & \text{in 3D} \\ \frac{(\hbar\omega_{\text{LO}})^2}{q} \frac{2\pi\alpha}{A} \left(\frac{\hbar}{2m_b\omega_{\text{LO}}} \right)^{1/2} & \text{in 2D,} \end{cases} \quad (5.49)$$

where α is the (dimensionless) Fröhlich coupling constant determining the coupling strength between the charge carriers and the longitudinal optical phonons [85, 86]. In 3D and 2D, respectively, the sums over \mathbf{q} is transformed to the integrals as follows:

$$\text{3D: } \sum_{\mathbf{q}} \dots = \frac{V}{(2\pi)^3} \int d\mathbf{q} \dots$$

$$\text{2D: } \sum_{\mathbf{q}} \dots = \frac{A}{(2\pi)^2} \int d\mathbf{q} \dots$$

↓

$$\text{Re } \sigma_{3\text{D}}(\omega) = \frac{n_0}{3\hbar\omega^3} \frac{e^2}{m_b^2} \frac{V}{(2\pi)^3} \int d\mathbf{q} q^2 \left| \frac{\hbar\omega_{\text{LO}}}{iq} \left(\frac{4\pi\alpha}{V} \right)^{1/2} \left(\frac{\hbar}{2m_b\omega_{\text{LO}}} \right)^{1/4} \right|^2 S(q, \omega - \omega_{\text{LO}})$$

↓

$$\text{Re } \sigma_{3\text{D}}(\omega) = \frac{n_0 e^2}{m_b^2} \frac{2\alpha}{3\pi} \frac{\hbar\omega_{\text{LO}}^2}{\omega^3} \left(\frac{\hbar}{2m_b\omega_{\text{LO}}} \right)^{1/2} \int_0^\infty q^2 S(q, \omega - \omega_{\text{LO}}) dq. \quad (5.51)$$

In the same way, we transform $\text{Re } \sigma_{2\text{D}}(\omega)$:

$$\text{Re } \sigma_{2\text{D}}(\omega) = \frac{n_0 e^2}{m_b^2} \frac{\alpha}{2} \frac{\hbar\omega_{\text{LO}}^2}{\omega^3} \left(\frac{\hbar}{2m_b\omega_{\text{LO}}} \right)^{1/2} \int_0^\infty q^2 S(q, \omega - \omega_{\text{LO}}) dq.$$

Using the Feynman units ($\hbar = 1$, $m_b = 1$, $\omega_{\text{LO}} = 1$), $\text{Re } \sigma(\omega)$ is

$$\text{Re } \sigma_{3\text{D}}(\omega) = n_0 e^2 \frac{\sqrt{2}\alpha}{3\pi} \frac{1}{\omega^3} \int_0^\infty q^2 S(q, \omega - 1) dq, \quad (5.52)$$

$$\text{Re } \sigma_{2\text{D}}(\omega) = n_0 e^2 \frac{\alpha}{2\sqrt{2}} \frac{1}{\omega^3} \int_0^\infty q^2 S(q, \omega - 1) dq. \quad (5.53)$$

From these expressions, it is clear that the scaling relation

$$\text{Re } \sigma_{2\text{D}}(\omega, \alpha) = \text{Re } \sigma_{3\text{D}}(\omega, \frac{3\pi}{4}\alpha) \quad (5.54)$$

which holds for the one-polaron case introduced in ref. [85, 86], is also valid for the many-polaron case if the corresponding 2D or 3D dynamic structure factor is used.

1. Calculation of the dynamic structure factor using the retarded Green's functions

The dynamic structure factor $S(\mathbf{q}, \omega)$ is expressed through the two-point correlation function by Eq. (5.43). The correlation function $F(\mathbf{q}, \omega)$ can be found using the retarded Green's function of the density operators

$$G^R(\mathbf{q}, t) = -i\Theta(t) \left\langle \psi_{el}^{(0)} \left| \left[e^{\frac{it}{\hbar}\tilde{H}_0} \rho_{\mathbf{q}} e^{-\frac{it}{\hbar}\tilde{H}_0}, \rho_{-\mathbf{q}} \right] \right| \psi_{el}^{(0)} \right\rangle, \quad (5.55)$$

where $\Theta(t)$ is the step function. Let us consider the more general case of a finite temperature,

$$G^R(\mathbf{q}, t) = -i\Theta(t) \left\langle \left[e^{\frac{it}{\hbar}\tilde{H}_0} \rho_{\mathbf{q}} e^{-\frac{it}{\hbar}\tilde{H}_0}, \rho_{-\mathbf{q}} \right] \right\rangle, \quad (5.56)$$

where the average is

$$\langle \dots \rangle \equiv \frac{\text{Tr} \left(e^{-\beta\tilde{H}_0} \dots \right)}{\text{Tr} \left(e^{-\beta\tilde{H}_0} \right)}, \quad \beta = \frac{1}{k_B T}. \quad (5.57)$$

The Fourier image $G^R(\mathbf{q}, \omega)$ of the retarded Green's function $G^R(\mathbf{q}, t)$ is

$$\begin{aligned} G^R(\mathbf{q}, \omega) &= \int_{-\infty}^{\infty} G^R(\mathbf{q}, t) e^{i\omega t} dt \\ &= -i \int_0^{\infty} \left\langle \left[e^{\frac{it}{\hbar}\tilde{H}_0} \rho_{\mathbf{q}} e^{-\frac{it}{\hbar}\tilde{H}_0}, \rho_{-\mathbf{q}} \right] \right\rangle e^{i\omega t} dt \\ &= -i \int_0^{\infty} \left(\left\langle e^{\frac{it}{\hbar}\tilde{H}_0} \rho_{\mathbf{q}} e^{-\frac{it}{\hbar}\tilde{H}_0} \rho_{-\mathbf{q}} \right\rangle - \left\langle \rho_{-\mathbf{q}} e^{\frac{it}{\hbar}\tilde{H}_0} \rho_{\mathbf{q}} e^{-\frac{it}{\hbar}\tilde{H}_0} \right\rangle \right) e^{i\omega t} dt \end{aligned}$$

The imaginary part of $G^R(\mathbf{q}, \omega)$ then is

$$\begin{aligned}
\text{Im } G^R(\mathbf{q}, \omega) &= -\text{Re} \int_0^\infty \left(\left\langle e^{\frac{it}{\hbar} \tilde{H}_0} \rho_{\mathbf{q}} e^{-\frac{it}{\hbar} \tilde{H}_0} \rho_{-\mathbf{q}} \right\rangle - \left\langle \rho_{-\mathbf{q}} e^{\frac{it}{\hbar} \tilde{H}_0} \rho_{\mathbf{q}} e^{-\frac{it}{\hbar} \tilde{H}_0} \right\rangle \right) e^{i\omega t} dt \\
&= -\frac{1}{2} \int_0^\infty \left(\left\langle e^{\frac{it}{\hbar} \tilde{H}_0} \rho_{\mathbf{q}} e^{-\frac{it}{\hbar} \tilde{H}_0} \rho_{-\mathbf{q}} \right\rangle - \left\langle \rho_{-\mathbf{q}} e^{\frac{it}{\hbar} \tilde{H}_0} \rho_{\mathbf{q}} e^{-\frac{it}{\hbar} \tilde{H}_0} \right\rangle \right) e^{i\omega t} dt \\
&\quad - \frac{1}{2} \int_0^\infty \left(\left\langle \rho_{\mathbf{q}} e^{\frac{it}{\hbar} \tilde{H}_0} \rho_{-\mathbf{q}} e^{-\frac{it}{\hbar} \tilde{H}_0} \right\rangle - \left\langle e^{\frac{it}{\hbar} \tilde{H}_0} \rho_{-\mathbf{q}} e^{-\frac{it}{\hbar} \tilde{H}_0} \rho_{\mathbf{q}} \right\rangle \right) e^{-i\omega t} dt \\
&= -\frac{1}{2} \int_{-\infty}^\infty \left\langle e^{\frac{it}{\hbar} \tilde{H}_0} \rho_{\mathbf{q}} e^{-\frac{it}{\hbar} \tilde{H}_0} \rho_{-\mathbf{q}} \right\rangle e^{i\omega t} dt + \frac{1}{2} \int_{-\infty}^\infty \left\langle \rho_{-\mathbf{q}} e^{\frac{it}{\hbar} \tilde{H}_0} \rho_{\mathbf{q}} e^{-\frac{it}{\hbar} \tilde{H}_0} \right\rangle e^{i\omega t} dt.
\end{aligned}$$

In the second integral here, we replace t by $(t' + i\hbar\beta)$:

$$\begin{aligned}
&\int_{-\infty}^\infty \frac{\text{Tr} \left(e^{-\beta \tilde{H}_0} \rho_{-\mathbf{q}} e^{\frac{it}{\hbar} \tilde{H}_0} \rho_{\mathbf{q}} e^{-\frac{it}{\hbar} \tilde{H}_0} \right)}{\text{Tr} \left(e^{-\beta \tilde{H}_0} \right)} e^{i\omega t} dt \\
&= \int_{-\infty - i\hbar\beta}^{\infty - i\hbar\beta} \frac{\text{Tr} \left(e^{-\beta \tilde{H}_0} \rho_{-\mathbf{q}} e^{\frac{it'}{\hbar} \tilde{H}_0 - \beta \tilde{H}_0} \rho_{\mathbf{q}} e^{-\frac{it'}{\hbar} \tilde{H}_0 + \beta \tilde{H}_0} \right)}{\text{Tr} \left(e^{-\beta \tilde{H}_0} \right)} e^{i\omega(t' + i\hbar\beta)} dt' \\
&= e^{-\beta\hbar\omega} \int_{-\infty - i\hbar\beta}^{\infty - i\hbar\beta} \frac{\text{Tr} \left(e^{\frac{it'}{\hbar} \tilde{H}_0 - \beta \tilde{H}_0} \rho_{\mathbf{q}} e^{-\frac{it'}{\hbar} \tilde{H}_0} \rho_{-\mathbf{q}} \right)}{\text{Tr} \left(e^{-\beta \tilde{H}_0} \right)} e^{i\omega t'} dt'.
\end{aligned}$$

As far as the integral over t converges (i. e., $\left\langle e^{\frac{it}{\hbar} \tilde{H}_0} \rho_{\mathbf{q}} e^{-\frac{it}{\hbar} \tilde{H}_0} \rho_{-\mathbf{q}} \right\rangle$ tends to zero at $|t| \rightarrow \infty$), we can shift the integration contour to the real axis, what gives us the result

$$\begin{aligned}
&\int_{-\infty}^\infty \frac{\text{Tr} \left(e^{-\beta \tilde{H}_0} \rho_{-\mathbf{q}} e^{\frac{it}{\hbar} \tilde{H}_0} \rho_{\mathbf{q}} e^{-\frac{it}{\hbar} \tilde{H}_0} \right)}{\text{Tr} \left(e^{-\beta \tilde{H}_0} \right)} e^{i\omega t} dt \\
&= e^{-\beta\hbar\omega} \int_{-\infty}^\infty \frac{\text{Tr} \left(e^{\frac{it}{\hbar} \tilde{H}_0 - \beta \tilde{H}_0} \rho_{\mathbf{q}} e^{-\frac{it}{\hbar} \tilde{H}_0} \rho_{-\mathbf{q}} \right)}{\text{Tr} \left(e^{-\beta \tilde{H}_0} \right)} e^{i\omega t} dt, \\
&\Updownarrow \\
&\int_{-\infty}^\infty \left\langle \rho_{-\mathbf{q}} e^{\frac{it}{\hbar} \tilde{H}_0} \rho_{\mathbf{q}} e^{-\frac{it}{\hbar} \tilde{H}_0} \right\rangle e^{i\omega t} dt \\
&= e^{-\beta\hbar\omega} \int_{-\infty}^\infty \left\langle e^{\frac{it}{\hbar} \tilde{H}_0} \rho_{\mathbf{q}} e^{-\frac{it}{\hbar} \tilde{H}_0} \rho_{-\mathbf{q}} \right\rangle e^{i\omega t} dt.
\end{aligned}$$

Herefrom, we find that

$$\begin{aligned}
\text{Im } G^R(\mathbf{q}, \omega) &= -\frac{1}{2} (1 - e^{-\beta\hbar\omega}) \int_{-\infty}^\infty \left\langle e^{\frac{it}{\hbar} \tilde{H}_0} \rho_{\mathbf{q}} e^{-\frac{it}{\hbar} \tilde{H}_0} \rho_{-\mathbf{q}} \right\rangle e^{i\omega t} dt \\
&\quad \Downarrow \\
\text{Im } G^R(\mathbf{q}, \omega) &= -\frac{1}{2} (1 - e^{-\beta\hbar\omega}) F(\mathbf{q}, \omega).
\end{aligned}$$

So, the equation follows from the analytical properties of the Green's functions:

$$F(\mathbf{q}, \omega) = -\frac{2 \operatorname{Im} G^R(\mathbf{q}, \omega)}{1 - e^{-\beta \hbar \omega}}. \quad (5.58)$$

The formula (5.58) is related to arbitrary temperatures. In the zero-temperature limit ($\beta \rightarrow \infty$), the factor $(1 - e^{-\beta \hbar \omega})^{-1}$ (5.58) turns into the Heavicide step function $\Theta(\omega)$, what leads to the formula

$$F(\mathbf{q}, \omega)|_{T=0} = -2\Theta(\omega) \operatorname{Im} G^R(\mathbf{q}, \omega)|_{T=0} \quad (5.59)$$

\Downarrow

$$S(\mathbf{q}, \omega)|_{T=0} = -\frac{1}{N}\Theta(\omega) \operatorname{Im} G^R(\mathbf{q}, \omega)|_{T=0} \quad (5.60)$$

The retarded Green function is related to the dielectric function of the electron gas by the following equation:

$$G^R(\mathbf{q}, \omega) = \frac{1}{v_{\mathbf{q}}} \left[\frac{1}{\varepsilon(\mathbf{q}, \omega)} - 1 \right]. \quad (5.61)$$

Within the random phase approximation (RPA), following [72], the expression for $G^R(\mathbf{q}, \omega)$ is

$$G^R(\mathbf{q}, \omega) = [1 - v_{\mathbf{q}}P(\mathbf{q}, \omega)]^{-1} \hbar P(\mathbf{q}, \omega), \quad (5.62)$$

where the polarization function $P(\mathbf{q}, \omega)$ is (see, e. g., p. 434 of [72])

$$P(\mathbf{q}, \omega) = \frac{1}{\hbar} \sum_{\mathbf{k}, \sigma} \frac{f_{\mathbf{k}+\mathbf{q}, \sigma} - f_{\mathbf{k}, \sigma}}{\omega - \frac{\hbar \mathbf{k}^2}{2m_b} + \frac{\hbar(\mathbf{k}+\mathbf{q})^2}{2m_b} + i\delta}, \quad \delta \rightarrow +0 \quad (5.63)$$

with the Fermi distribution function of electrons $f_{\mathbf{k}, \sigma}$.

For a finite temperature, the explicit analytic expression for the imaginary part of the structure factor $P_{3D}(\mathbf{q}, \omega)$ is obtained (see [72]),

$$\begin{aligned} \operatorname{Im} P_{3D}(\mathbf{q}, \omega) &= \frac{V m_b^2}{2\pi \hbar^4 \beta q} \ln \frac{1 + \exp \{ \beta [\mu - E^{(+)}(q, \omega)] \}}{1 + \exp \{ \beta [\mu - E^{(-)}(q, \omega)] \}}, \\ E^{(\pm)}(q, \omega) &\equiv \frac{\left(\hbar \omega \pm \frac{\hbar^2 q^2}{2m_b} \right)^2}{4 \frac{\hbar^2 q^2}{2m_b}}, \end{aligned} \quad (5.64)$$

with the chemical potential μ . The real part of the structure factor is obtained using the Kramers-Kronig dispersion relation:

$$\operatorname{Re} P(\mathbf{q}, \omega) = \frac{1}{\pi} \int_{-\infty}^{\infty} \mathcal{P} \left(\frac{1}{\omega' - \omega} \right) \operatorname{Im} P(\mathbf{q}, \omega') d\omega'. \quad (5.65)$$

Analytical expressions for both real and imaginary parts of $P(\mathbf{q}, \omega)$ can be written down for the zero temperature (see [72]),

$$\begin{aligned} \text{Re } P_{3\text{D}}(q, \omega) &= -\frac{Vm_b}{4\pi^2\hbar^2q} \left\{ \begin{aligned} &\left[k_F^2 - \frac{m_b^2}{\hbar^2q^2} \left(\omega - \frac{\hbar q^2}{2m_b} \right)^2 \right] \ln \left| \frac{\omega - \frac{\hbar q^2}{2m_b} - \frac{\hbar k_F q}{m_b}}{\omega - \frac{\hbar q^2}{2m_b} + \frac{\hbar k_F q}{m_b}} \right| \\ &+ \left[k_F^2 - \frac{m_b^2}{\hbar^2q^2} \left(\omega + \frac{\hbar q^2}{2m_b} \right)^2 \right] \ln \left| \frac{\omega + \frac{\hbar q^2}{2m_b} + \frac{\hbar k_F q}{m_b}}{\omega + \frac{\hbar q^2}{2m_b} - \frac{\hbar k_F q}{m_b}} \right| \\ &+ 2k_F q \end{aligned} \right\}, \\ \text{Im } P_{3\text{D}}(q, \omega) &= -\frac{Vm_b}{4\pi\hbar^2q} \left\{ \begin{aligned} &\left[k_F^2 - \frac{m_b^2}{\hbar^2q^2} \left(\omega - \frac{\hbar q^2}{2m_b} \right)^2 \right] \Theta \left(k_F^2 - \frac{m_b^2}{\hbar^2q^2} \left(\omega - \frac{\hbar q^2}{2m_b} \right)^2 \right) \\ &- \left[k_F^2 - \frac{m_b^2}{\hbar^2q^2} \left(\omega + \frac{\hbar q^2}{2m_b} \right)^2 \right] \Theta \left(k_F^2 - \frac{m_b^2}{\hbar^2q^2} \left(\omega + \frac{\hbar q^2}{2m_b} \right)^2 \right) \end{aligned} \right\}, \end{aligned} \quad (5.66)$$

where $k_F = (3\pi^2 N/V)^{1/3}$ is the Fermi wave number.

After substituting into Eq. (5.58) the retarded Green's function (5.62) in terms of the polarization function we arrive at the formula

$$F(\mathbf{q}, \omega) = -\frac{2\hbar}{1 - e^{-\beta\hbar\omega}} \text{Im} \frac{P(\mathbf{q}, \omega)}{1 - v_{\mathbf{q}} P(\mathbf{q}, \omega)}$$

↓

$$S(\mathbf{q}, \omega) = -\frac{\hbar}{N(1 - e^{-\beta\hbar\omega})} \frac{\text{Im } P(\mathbf{q}, \omega)}{[1 - v_{\mathbf{q}} \text{Re } P(\mathbf{q}, \omega)]^2 + [v_{\mathbf{q}} \text{Im } P(\mathbf{q}, \omega)]^2}, \quad (5.67)$$

$$S(\mathbf{q}, \omega)|_{T=0} = -\frac{\hbar}{N} \Theta(\omega) \frac{\text{Im } P(\mathbf{q}, \omega)}{[1 - v_{\mathbf{q}} \text{Re } P(\mathbf{q}, \omega)]^2 + [v_{\mathbf{q}} \text{Im } P(\mathbf{q}, \omega)]^2}. \quad (5.68)$$

With this dynamic structure factor, the optical conductivity (5.52) (in the Feynman units) takes the form

$$\begin{aligned} \text{Re } \sigma_{3\text{D}}(\omega) &= -e^2 \frac{\sqrt{2}\alpha}{3\pi V} \frac{1}{\omega^3} \Theta(\omega - 1) \\ &\times \int_0^\infty \frac{\text{Im } P_{3\text{D}}(q, \omega - 1)}{[1 - v_q \text{Re } P_{3\text{D}}(q, \omega - 1)]^2 + [v_q \text{Im } P_{3\text{D}}(q, \omega - 1)]^2} q^2 dq. \end{aligned} \quad (5.69)$$

Correspondingly, in the 2D case we obtain the expression

$$\begin{aligned} \text{Re } \sigma_{2\text{D}}(\omega) &= -e^2 \frac{\alpha}{2\sqrt{2}V} \frac{1}{\omega^3} \Theta(\omega - 1) \\ &\times \int_0^\infty \frac{\text{Im } P_{2\text{D}}(q, \omega - 1)}{[1 - v_q \text{Re } P_{2\text{D}}(q, \omega - 1)]^2 + [v_q \text{Im } P_{2\text{D}}(q, \omega - 1)]^2} q^2 dq. \end{aligned} \quad (5.70)$$

2. Plasmon-phonon contribution

The RPA dynamic structure factor for the electron (or hole) system can be separated in two parts, one related to continuum excitations of the electrons (or holes) S_{cont} , and one related to the undamped plasmon branch:

$$S_{\text{RPA}}(q, \omega) = A_{\text{pl}}(q)\delta(\omega - \omega_{\text{pl}}(q)) + S_{\text{cont}}(q, \omega), \quad (5.71)$$

where $\omega_{\text{pl}}(q)$ is the wave number dependent plasmon frequency and A_{pl} is the strength of the undamped plasmon branch.

In Eqs. (5.69), (5.70), the contribution of the continuum excitations corresponds to the region (q, ω) where $\text{Im} P(q, \omega) \neq 0$. The contribution related to the undamped plasmons is provided by a region of (q, ω) , where the equations

$$\begin{cases} \text{Im} P(q, \omega) = 0 \\ 1 - v_q \text{Re} P(q, \omega) = 0 \end{cases}. \quad (5.72)$$

are fulfilled simultaneously. Using (5.61), we find that Eqs. (5.73) are equivalent to

$$\text{Im} \frac{1}{\varepsilon(q, \omega)} = 0, \quad \text{Re} \frac{1}{\varepsilon(q, \omega)} = 0. \quad (5.73)$$

In the region where $\text{Im} P(q, \omega) = 0$, the expression $\frac{\text{Im} P(q, \omega)}{[1 - v_q \text{Re} P(q, \omega)]^2 + [v_q \text{Im} P(q, \omega)]^2}$ is proportional to the delta function, which gives a finite contribution to the memory function after the integration over q :

$$\begin{aligned} & \left. \frac{\text{Im} P(q, \omega)}{[1 - v_q \text{Re} P(q, \omega)]^2 + [v_q \text{Im} P(q, \omega)]^2} \right|_{\text{Im} P(q, \omega) = 0} \\ &= \frac{1}{\pi v_q} \delta(1 - v_q \text{Re} P(q, \omega)). \end{aligned} \quad (5.74)$$

Using Eq. (5.74), the coefficients $A_{\text{pl}}(q)$ in Eq. (5.71) can be expressed in terms of the polarization function $P(q, \omega)$ as follows:

$$\begin{aligned} & \left. \frac{\text{Im} P(q, \omega)}{[1 - v_q \text{Re} P(q, \omega)]^2 + [v_q \text{Im} P(q, \omega)]^2} \right|_{\text{Im} P(q, \omega) = 0} \\ &= \frac{1}{\pi v_q^2 \left| \frac{\partial}{\partial \omega} \text{Re} P(q, \omega) \right|} \Bigg|_{\omega = \omega_{\text{pl}}(q)} \delta(\omega - \omega_{\text{pl}}(q)) \end{aligned}$$

↓

$$A_{\text{pl}}(q) = \frac{1}{\pi v_q^2 \left| \frac{\partial}{\partial \omega} \text{Re} P(q, \omega) \right|} \Bigg|_{\omega=\omega_{\text{pl}}(q)}. \quad (5.75)$$

The contribution derived from the undamped plasmon branch $A_{\text{pl}}(q)\delta(\omega - \omega_{\text{pl}}(q))$ is denoted in Ref. [53] as the ‘*plasmon-phonon*’ contribution. The physical process related to this contribution is the emission of both a phonon and a plasmon in the scattering process.

E. Comparison to the infrared spectrum of $\text{Nd}_{2-x}\text{Ce}_x\text{CuO}_{2-y}$

Calvani and collaborators have performed doping-dependent measurements of the infrared absorption spectra of the high- T_c material $\text{Nd}_{2-x}\text{Ce}_x\text{CuO}_{2-y}$ (NCCO). The region of the spectrum examined by these authors (50-10000 cm^{-1}) is very rich in absorption features: they observe is a “Drude-like” component at the lowest frequencies, and a set of sharp absorption peaks related to phonons and infrared active modes (up to about 1000 cm^{-1}) possibly associated to small (Holstein) polarons. Three distinct absorption bands can be distinguished: the ‘*d*-band’ (around 1000 cm^{-1}), the Mid-Infrared band (MIR, around 5000 cm^{-1}) and the Charge-Transfer band (around 10^4 cm^{-1}). Of all these features, the *d*-band and, at a higher temperatures, the Drude-like component have (hypothetically) been associated with large polaron optical absorption [92].

For the lowest levels of Ce doping, the *d*-band can be most clearly distinguished from the other features. The experimental optical absorption spectrum (up to 3000 cm^{-1}) of $\text{Nd}_2\text{CuO}_{2-\delta}$ ($\delta < 0.004$), obtained by Calvani and co-workers [92], is shown in Fig. 12 (shaded area) together with the theoretical curve obtained by the present method (full, bold curve) and, for reference, the one-polaron optical absorption result (dotted curve). At lower frequencies (600-1000 cm^{-1}) a marked difference between the single polaron optical absorption and the many-polaron result is manifest. The experimental *d*-band can be clearly identified, rising in intensity at about 600 cm^{-1} , peaking around 1000 cm^{-1} , and then decreasing in intensity above that frequency. At a density of $n_0 = 1.5 \times 10^{17} \text{ cm}^{-3}$, we found a remarkable agreement between our theoretical predictions and the experimental curve.

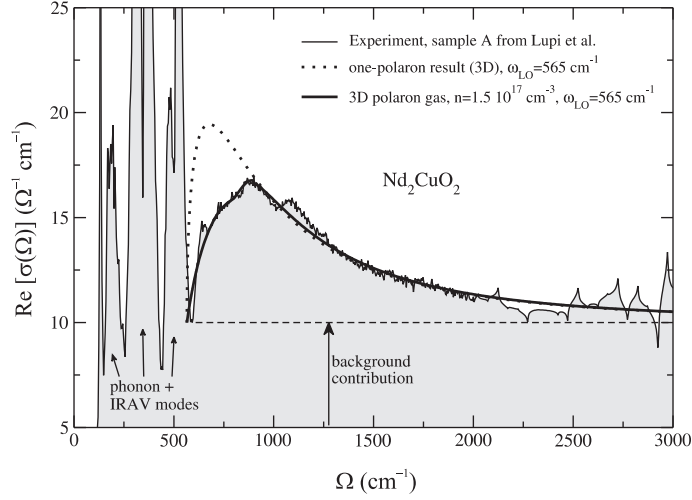


FIG. 12: The infrared absorption of $\text{Nd}_2\text{CuO}_{2-\delta}$ ($\delta < 0.004$) is shown as a function of frequency, up to 3000 cm^{-1} . The experimental results of Calvani and co-workers [92] is represented by the thin black curve and by the shaded area. The so-called ‘d-band’ rises in intensity around 600 cm^{-1} and increases in intensity up to a maximum around 1000 cm^{-1} . The dotted curve shows the single polaron result. The full black curve represents the theoretical results obtained in the present work for the interacting many-polaron gas with $n_0 = 1.5 \times 10^{17} \text{ cm}^{-3}$, $\alpha = 2.1$ and $m_b = 0.5 m_e$. (From Ref. [53].)

F. Experimental data on the optical absorption in manganites: interpretation in terms of a many-polaron response

In Refs. [93, 94], the experimental results on the optical spectroscopy of $\text{La}_{2/3}\text{Sr}_{1/3}\text{MnO}_3$ (LSMO) and $\text{La}_{2/3}\text{Ca}_{1/3}\text{MnO}_3$ (LCMO) thin films in the mid-infrared frequency region are presented. The optical conductivity spectra of LCMO films are interpreted in [93, 94] in terms of the optical response of small polarons, while the optical conductivity spectra of LSMO films are explained using the large-polaron picture (see Fig. 13).

The real part of the optical conductivity $\text{Re } \sigma(\omega)$ is expressed in Ref. [94] by the formula

$$\text{Re } \sigma(\omega) = \alpha n_p \frac{2 e^2 (\hbar\omega_0)^2}{3 m^2 \pi \hbar \omega^3} \sqrt{\frac{\hbar}{2m\omega_0}} \int_0^\infty q^2 S^{(H)}(q, \omega - \omega_0) dq, \quad (5.76a)$$

where α is the electron-phonon coupling constant, n_p is the polaron density, m is the electron band mass, ω_0 is the LO-phonon frequency, and $S^{(H)}(q, \omega)$ is the dynamic structure factor,

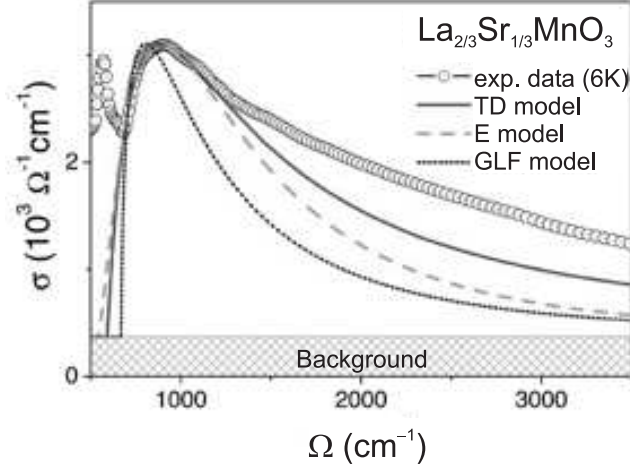


FIG. 13: Comparison of the low-temperature MIR optical conductivity to $\sigma(\omega)$ from various model calculations: the solid line refers to the weak-coupling approach of Tempere and Devreese [53] modified for an on-site Hubbard interaction, the dashed line is the result of the phenomenological approach for self-trapped large polarons by Emin [95], the dotted curve is the weak-coupling single-polaron result [71]. (From Ref. [93].)

determined in Ref. [94] through the dielectric function of an electron gas $\varepsilon(\mathbf{q}, \omega)$:

$$S^{(H)}(\mathbf{q}, \omega) = \frac{\hbar}{n_p} \frac{q^2}{4\pi e^2} \text{Im} \left[-\frac{1}{\varepsilon(\mathbf{q}, \omega)} \right]. \quad (5.77)$$

In Ref. [53], the other definition for the dynamic structure factor is used, which is equivalent to that given by (5.77) (see Ref. [72]) with the factor N (the number of electrons)

$$S^{(TD)}(\mathbf{q}, \omega) = \frac{1}{2} \int_{-\infty}^{+\infty} \langle \varphi_{\text{el}} | \rho_{\mathbf{q}}(t) \rho_{-\mathbf{q}}(0) | \varphi_{\text{el}} \rangle e^{i\omega t} dt = N S^{(H)}(\mathbf{q}, \omega). \quad (5.78)$$

Here, φ_{el} denotes the ground state of the electron subsystem (without the electron-phonon interaction), $\rho_{\mathbf{q}} = \sum_{j=1}^N e^{i\mathbf{q}\cdot\mathbf{r}_j}$ is the Fourier component of the electron density.

In Ref. [53], the dynamic structure factor is calculated within the random-phase approximation (RPA) taking into account the Coulomb interaction between electrons with the Fourier component of the Coulomb potential

$$v_{\mathbf{q}} = \frac{4\pi e^2}{q^2 \varepsilon_{\infty}}, \quad (5.79)$$

where ε_{∞} is the high-frequency dielectric constant of the crystal. In Refs. [93, 94], the dynamic structure factor is calculated taking into account the local Hubbard electron-electron

interaction instead of the Coulomb interaction. The local Hubbard interaction is used in the small-polaron formalism and describes the potential energy of two electrons on one and the same site (see, e. g., Refs. [96, 97]). In its simplest form the Hubbard interaction is (see Eq. (1) of Ref. [96])

$$V_H = U \sum_i n_{i\uparrow} n_{i\downarrow}, \quad (5.80)$$

where U is the coupling constant of the Hubbard interaction, $n_{i\uparrow}$ is the electron occupation number for the i -th site.

In Refs. [93, 94], there are no details of the calculation using the interaction term (5.80). The following procedure can be supposed. The transition from the summation over the lattice sites to the integral over the crystal volume V is performed taking into account the normalization condition

$$N_{\uparrow(\downarrow)} = \sum_i n_{i\uparrow(\downarrow)} = \int_V \tilde{n}_{\uparrow(\downarrow)}(\mathbf{r}) d\mathbf{r},$$

where the density $\tilde{n}_{\uparrow(\downarrow)}(\mathbf{r})$ is to be determined through $n_{i\uparrow(\downarrow)}$. As far as the lattice cell volume $\Omega_0 \ll V$, the integral $\int_V n_{\uparrow(\downarrow)}(\mathbf{r}) d\mathbf{r}$ can be written as the sum over the lattice sites:

$$\int_V n_{\uparrow(\downarrow)}(\mathbf{r}) d\mathbf{r} = \Omega_0 \sum_i \tilde{n}_{\uparrow(\downarrow)}(\mathbf{r}_i),$$

where $\{\mathbf{r}_i\}$ are the vectors of the lattice. Therefore, from the equality

$$\sum_i n_{i\uparrow(\downarrow)} = \Omega_0 \sum_i \tilde{n}_{\uparrow(\downarrow)}(\mathbf{r}_i)$$

we find that

$$n_{i\uparrow(\downarrow)} = \tilde{n}_{\uparrow(\downarrow)}(\mathbf{r}_i).$$

The potential (5.80) is then transformed from the sum over sites to the integral:

$$V_H = \frac{U}{\Omega_0} \sum_i n_{i\uparrow} n_{i\downarrow} \Omega_0 = \int_V U \Omega_0 \delta(\mathbf{r} - \mathbf{r}') \tilde{n}_{\uparrow}(\mathbf{r}) \tilde{n}_{\downarrow}(\mathbf{r}') d\mathbf{r} d\mathbf{r}'. \quad (5.81)$$

Consequently, in the continuum approach the Hubbard model is described by the δ -like interparticle potential $U \Omega_0 \delta(\mathbf{r} - \mathbf{r}')$.

This development of the approach [53] performed in Refs. [93, 94] seems to be contradictory by the following reason. For a many-polaron system, both the electron-phonon and electron-electron interactions are provided by the electrostatic potentials. Therefore, it would be consistent to consider them both within one and the same approach. Namely,

the Coulomb electron-electron interaction with the potential (5.79) is relevant for large and small polarons with the Fröhlich electron-phonon interaction, while the Hubbard electron-electron interaction is relevant for small Holstein polarons. Nevertheless, as recognized in Ref. [93], this model “reproduces the observed shape of the polaron peak quite convincingly” and provides a better agreement with the experiment [93, 94] than the phenomenological approach [95] and the one-polaron theory [71].

VI. INTERACTING POLARONS IN A QUANTUM DOT

A. The partition function and the free energy of a many-polaron system

We consider a system of N electrons with mutual Coulomb repulsion and interacting with the lattice vibrations following Ref. [98]. The system is assumed to be confined by a parabolic potential characterized by the frequency parameter Ω_0 . The total number of electrons is represented as $N = \sum_{\sigma} N_{\sigma}$, where N_{σ} is the number of electrons with the spin projection $\sigma = \pm 1/2$. The electron 3D (2D) coordinates are denoted by $\mathbf{x}_{j,\sigma}$ with $j = 1, \dots, N_{\sigma}$. The bulk phonons (characterized by 3D wave vectors \mathbf{k} and frequencies $\omega_{\mathbf{k}}$) are described by the complex coordinates $Q_{\mathbf{k}}$, which possess the property [43]

$$Q_{\mathbf{k}}^* = Q_{-\mathbf{k}}. \quad (6.1)$$

The full set of the electron and phonon coordinates are denoted by $\bar{\mathbf{x}} \equiv \{\mathbf{x}_{j,\sigma}\}$ and $\bar{Q} \equiv \{Q_{\mathbf{k}}\}$.

Throughout the present treatment, the Euclidean time variable $\tau = it$ is used, where t is the real time variable. In this representation the Lagrangian of the system is

$$L\left(\dot{\bar{\mathbf{x}}}, \dot{\bar{Q}}; \bar{\mathbf{x}}, \bar{Q}\right) = L_e\left(\dot{\bar{\mathbf{x}}}, \bar{\mathbf{x}}\right) - V_C\left(\bar{\mathbf{x}}\right) - U_b\left(\bar{\mathbf{x}}\right) + L_{ph}\left(\dot{\bar{Q}}, \bar{Q}\right) + L_{e-ph}\left(\bar{\mathbf{x}}, \bar{Q}\right), \quad (6.2)$$

where $L_e\left(\dot{\bar{\mathbf{x}}}, \bar{\mathbf{x}}\right)$ is the Lagrangian of an electron with band mass m_b in a quantum dot:

$$L_e\left(\dot{\bar{\mathbf{x}}}, \bar{\mathbf{x}}\right) = - \sum_{\sigma=\pm 1/2} \sum_{j=1}^{N_{\sigma}} \frac{m_b}{2} \left(\dot{\mathbf{x}}_{j,\sigma}^2 + \Omega_0^2 \mathbf{x}_{j,\sigma}^2\right), \quad \dot{\mathbf{x}} \equiv \frac{d\mathbf{x}}{d\tau}, \quad (6.3)$$

Ω_0 is the confinement frequency, $V_b\left(\bar{\mathbf{x}}\right)$ is the potential of a background charge (supposed to be static and uniformly distributed with the charge density en_b in a sphere of a radius R),

$$U_b\left(\bar{\mathbf{x}}\right) = \sum_{\sigma} \sum_{j=1}^N V_b\left(r_{j,\sigma}\right), \quad r \equiv |\mathbf{x}|, \quad (6.4)$$

$$V_b\left(r\right) = -\frac{4\pi e^2 n_b}{3\varepsilon_0} \left[\Theta\left(r < R\right) \frac{3R^2 - r^2}{2} + \Theta\left(R \leq r\right) \frac{R^3}{r} \right], \quad (6.5)$$

where ε_0 is the static dielectric constant of a crystal, $V_C\left(\bar{\mathbf{x}}\right)$ is the potential energy of the electron-electron Coulomb repulsion in the medium with the high-frequency dielectric constant ε_{∞} :

$$V_C\left(\bar{\mathbf{x}}\right) = \sum_{\sigma, \sigma'=\pm 1/2} \sum_{j=1}^{N_{\sigma}} \sum_{l=1}^{N_{\sigma'}} \frac{e^2}{2\varepsilon_{\infty}} \frac{1}{|\mathbf{x}_{j,\sigma} - \mathbf{x}_{l,\sigma'}|}, \quad (j,\sigma) \neq (l,\sigma'), \quad (6.6)$$

$L_{ph}(\dot{\bar{Q}}, \dot{\bar{Q}}^*; \bar{Q}, \bar{Q}^*)$ is the Lagrangian of free phonons:

$$L_{ph}(\dot{\bar{Q}}, \dot{\bar{Q}}) = -\frac{1}{2} \sum_{\mathbf{k}} (\dot{\bar{Q}}_{\mathbf{k}}^* \dot{\bar{Q}}_{\mathbf{k}} + \omega_{\mathbf{k}}^2 \bar{Q}_{\mathbf{k}}^* \bar{Q}_{\mathbf{k}}), \quad \dot{\bar{Q}} \equiv \frac{d\bar{Q}}{d\tau}. \quad (6.7)$$

Further, $L_{e-ph}(\bar{\mathbf{x}}, \bar{Q}, \bar{Q}^*)$ is the Lagrangian of the electron-phonon interaction:

$$L_{e-ph}(\bar{\mathbf{x}}, \bar{Q}) = - \sum_{\mathbf{k}} \left(\frac{2\omega_{\mathbf{k}}}{\hbar} \right)^{1/2} V_{\mathbf{k}} \bar{Q}_{-\mathbf{k}} \rho_{\mathbf{k}}, \quad (6.8)$$

where $\rho_{\mathbf{k}}$ is the Fourier transform of the electron density operator:

$$\rho_{\mathbf{k}} = \sum_{\sigma=\pm 1/2} \sum_{j=1}^{N_{\sigma}} e^{i\mathbf{k}\cdot\mathbf{x}_{j,\sigma}}. \quad (6.9)$$

$V_{\mathbf{k}}$ is the amplitude of the electron-phonon interaction. Here, we consider electrons interacting with the long-wavelength longitudinal optical (LO) phonons with a dispersionless frequency $\omega_{\mathbf{k}} = \omega_{\text{LO}}$, for which the amplitude $V_{\mathbf{k}}$ is [26]

$$V_{\mathbf{k}} = \frac{\hbar\omega_{\text{LO}}}{q} \left(\frac{2\sqrt{2}\pi\alpha}{V} \right)^{1/2} \left(\frac{\hbar}{m_b\omega_{\text{LO}}} \right)^{1/4}, \quad (6.10)$$

where α is the electron-phonon coupling constant and V is the volume of the crystal.

We consider a *canonical* ensemble, where the numbers N_{σ} are fixed. The partition function $Z(\{N_{\sigma}\}, \beta)$ of the system can be expressed as a path integral over the electron and phonon coordinates:

$$Z(\{N_{\sigma}\}, \beta) = \sum_P \frac{(-1)^{\xi_P}}{N_{1/2}! N_{-1/2}!} \int d\bar{\mathbf{x}} \int_{\bar{\mathbf{x}}}^{P\bar{\mathbf{x}}} D\bar{\mathbf{x}}(\tau) \int d\bar{Q} \int_{\bar{Q}}^{\bar{Q}} D\bar{Q}(\tau) e^{-S[\bar{\mathbf{x}}(\tau), \bar{Q}(\tau)]}, \quad (6.11)$$

where $S[\bar{\mathbf{x}}(\tau), \bar{Q}(\tau)]$ is the ‘‘action’’ functional:

$$S[\bar{\mathbf{x}}(\tau), \bar{Q}(\tau)] = -\frac{1}{\hbar} \int_0^{\hbar\beta} L(\dot{\bar{\mathbf{x}}}, \dot{\bar{Q}}; \bar{\mathbf{x}}, \bar{Q}) d\tau. \quad (6.12)$$

The parameter $\beta \equiv 1/(k_B T)$ is inversely proportional to the temperature T . In order to take the Fermi-Dirac statistics into account, the integral over the electron paths $\{\bar{\mathbf{x}}(\tau)\}$ in Eq. (6.11) contains a sum over all permutations P of the electrons with the same spin projection, and ξ_P denotes the parity of a permutation P .

The action functional (6.12) is quadratic in the phonon coordinates \bar{Q} . Therefore, *the path integral over the phonon variables in $Z(\{N_{\sigma}\}, \beta)$ can be calculated analytically* following

Ref. [43]. Let us describe this path integration in detail. First, we introduce the real phonon coordinates through the real and imaginary parts of the complex phonon coordinates $Q'_\mathbf{k} \equiv \text{Re} Q_\mathbf{k}$, $Q''_\mathbf{k} \equiv \text{Im} Q_\mathbf{k}$. According to the symmetry property (6.1), they obey the equalities

$$Q'_{-\mathbf{k}} = Q'_\mathbf{k}, \quad Q''_{-\mathbf{k}} = -Q''_\mathbf{k}. \quad (6.13)$$

$$q_\mathbf{k} \equiv \begin{cases} \sqrt{2}Q'_\mathbf{k}, & k_x \geq 0, \\ \sqrt{2}Q''_\mathbf{k}, & k_x < 0. \end{cases} \quad (6.14)$$

In this representation, the sum over phonon coordinates $\sum_{\mathbf{k}} |Q_\mathbf{k}|^2$ is transformed in the following way using the symmetry property (6.13):

$$\begin{aligned} \sum_{\mathbf{k}} |Q_\mathbf{k}|^2 &= \sum_{\mathbf{k}} \left[(Q'_\mathbf{k})^2 + (Q''_\mathbf{k})^2 \right] \\ &= 2 \sum_{\substack{\mathbf{k} \\ (k_x \geq 0)}} (Q'_\mathbf{k})^2 + 2 \sum_{\substack{\mathbf{k} \\ (k_x < 0)}} (Q''_\mathbf{k})^2 \\ &= \sum_{\substack{\mathbf{k} \\ (k_x \geq 0)}} q_\mathbf{k}^2 + \sum_{\substack{\mathbf{k} \\ (k_x < 0)}} q_\mathbf{k}^2 = \sum_{\mathbf{k}} q_\mathbf{k}^2. \end{aligned}$$

Therefore, the phonon Lagrangian (6.7) with the real phonon coordinates is

$$L_{ph} = -\frac{1}{2} \sum_{\mathbf{k}} (\dot{q}_\mathbf{k}^2 + \omega_\mathbf{k}^2 q_\mathbf{k}^2). \quad (6.15)$$

The Lagrangian of the electron-phonon interaction (6.8) with the real phonon coordinates is transformed in the following way using (6.13):

$$\begin{aligned} L_{e-ph} &= - \sum_{\mathbf{k}} \left(\frac{2\omega_\mathbf{k}}{\hbar} \right)^{1/2} V_{\mathbf{k}\rho\mathbf{k}} (Q'_\mathbf{k} - iQ''_\mathbf{k}) \\ &= - \sum_{\substack{\mathbf{k} \\ (k_x \geq 0)}} \left(\frac{2\omega_\mathbf{k}}{\hbar} \right)^{1/2} (V_{\mathbf{k}\rho\mathbf{k}} + V_{-\mathbf{k}\rho-\mathbf{k}}) Q'_\mathbf{k} \\ &\quad + i \sum_{\substack{\mathbf{k} \\ (k_x < 0)}} \left(\frac{2\omega_\mathbf{k}}{\hbar} \right)^{1/2} (V_{\mathbf{k}\rho\mathbf{k}} - V_{-\mathbf{k}\rho-\mathbf{k}}) Q''_\mathbf{k}. \end{aligned}$$

Let us introduce the real forces:

$$\gamma_\mathbf{k} \equiv \begin{cases} \frac{1}{\sqrt{2}} \left(\frac{2\omega_\mathbf{k}}{\hbar} \right)^{1/2} (V_{\mathbf{k}\rho\mathbf{k}} + V_{-\mathbf{k}\rho-\mathbf{k}}), & k_x \geq 0, \\ \frac{1}{i\sqrt{2}} \left(\frac{2\omega_\mathbf{k}}{\hbar} \right)^{1/2} (V_{\mathbf{k}\rho\mathbf{k}} - V_{-\mathbf{k}\rho-\mathbf{k}}), & k_x < 0. \end{cases} \quad (6.16)$$

This gives us the Lagrangian of the electron-phonon interaction in terms of the real forces and real phonon coordinates:

$$L_{e-ph} = - \sum_{\mathbf{k}} \gamma_{\mathbf{k}} q_{\mathbf{k}}. \quad (6.17)$$

So, the sum of the Lagrangians of phonons and of the electron-phonon interaction is expressed through ordinary real oscillator variables:

$$L_{ph} + L_{e-ph} = -\frac{1}{2} \sum_{\mathbf{k}} (\dot{q}_{\mathbf{k}}^2 + \omega_{\mathbf{k}}^2 q_{\mathbf{k}}^2 + \gamma_{\mathbf{k}} q_{\mathbf{k}}). \quad (6.18)$$

The path integration for each phonon mode with the coordinate $q_{\mathbf{k}}$ is performed independently as described in Sec. 2 of Ref. [43] and gives the result

$$\begin{aligned} & \int_{-\infty}^{\infty} dq_{\mathbf{k}} \int_{q_{\mathbf{k}}}^{q_{\mathbf{k}}} Dq_{\mathbf{k}}(\tau) \exp \left[-\frac{1}{\hbar} \int_0^{\hbar\beta} d\tau \frac{1}{2} (\dot{q}_{\mathbf{k}}^2 + \omega_{\mathbf{k}}^2 q_{\mathbf{k}}^2 + \gamma_{\mathbf{k}} q_{\mathbf{k}}) \right] \\ &= \frac{1}{2 \sinh \left(\frac{\beta \hbar \omega_{\mathbf{k}}}{2} \right)} \\ & \times \exp \left\{ \frac{1}{4\hbar} \int_0^{\hbar\beta} d\tau \int_0^{\hbar\beta} d\tau' \frac{\cosh [\omega_{\mathbf{k}} (|\tau - \tau'| - \hbar\beta/2)]}{\omega_{\mathbf{k}} \sinh (\beta \hbar \omega_{\mathbf{k}}/2)} \gamma_{\mathbf{k}}(\tau) \gamma_{\mathbf{k}}(\tau') \right\} \end{aligned}$$

where the exponential is the influence functional of a driven oscillator { [43], Eq. (3.43)}.

Therefore, the path integral over all phonon modes is

$$\begin{aligned} & \int d\{q_{\mathbf{k}}\} \int_{\{q_{\mathbf{k}}\}}^{\{q_{\mathbf{k}}\}} D\{q_{\mathbf{k}}(\tau)\} \exp \left[-\frac{1}{\hbar} \int_0^{\hbar\beta} d\tau \sum_{\mathbf{k}} \frac{1}{2} (\dot{q}_{\mathbf{k}}^2 + \omega_{\mathbf{k}}^2 q_{\mathbf{k}}^2 + \gamma_{\mathbf{k}} q_{\mathbf{k}}) \right] \\ &= \left(\prod_{\mathbf{k}} \frac{1}{2 \sinh \left(\frac{\beta \hbar \omega_{\mathbf{k}}}{2} \right)} \right) \\ & \times \exp \left\{ \frac{1}{4\hbar} \int_0^{\hbar\beta} d\tau \int_0^{\hbar\beta} d\tau' \sum_{\mathbf{k}} \frac{\cosh [\omega_{\mathbf{k}} (|\tau - \tau'| - \hbar\beta/2)]}{\omega_{\mathbf{k}} \sinh (\beta \hbar \omega_{\mathbf{k}}/2)} \gamma_{\mathbf{k}}(\tau) \gamma_{\mathbf{k}}(\tau') \right\} \end{aligned}$$

Here, the product $\prod_{\mathbf{k}} \dots$ is the partition function of free phonons, and the exponential is the influence functional of the phonon subsystem on the electron subsystem. This influence functional results from the above described *elimination of the phonon coordinates* and is usually written down as $e^{-\Phi}$, where Φ is

$$\Phi = -\frac{1}{4\hbar} \int_0^{\hbar\beta} d\tau \int_0^{\hbar\beta} d\tau' \sum_{\mathbf{k}} \frac{\cosh [\omega_{\mathbf{k}} (|\tau - \tau'| - \hbar\beta/2)]}{\omega_{\mathbf{k}} \sinh (\beta \hbar \omega_{\mathbf{k}}/2)} \gamma_{\mathbf{k}}(\tau) \gamma_{\mathbf{k}}(\tau'). \quad (6.19)$$

The sum over the phonon wave vectors \mathbf{k} can be simplified as follows:

$$\begin{aligned}
& \sum_{\mathbf{k}} \frac{\cosh [\omega_{\mathbf{k}} (|\tau - \tau'| - \hbar\beta/2)]}{\omega_{\mathbf{k}} \sinh (\beta\hbar\omega_{\mathbf{k}}/2)} \gamma_{\mathbf{k}}(\tau) \gamma_{\mathbf{k}}(\tau') \\
&= \frac{1}{\hbar} \sum_{\substack{\mathbf{k} \\ (k_x \geq 0)}} \frac{\cosh [\omega_{\mathbf{k}} (|\tau - \tau'| - \hbar\beta/2)]}{\sinh (\beta\hbar\omega_{\mathbf{k}}/2)} \\
&\quad \times [V_{\mathbf{k}}\rho_{\mathbf{k}}(\tau) + V_{-\mathbf{k}}\rho_{-\mathbf{k}}(\tau)] [V_{\mathbf{k}}\rho_{\mathbf{k}}(\tau') + V_{-\mathbf{k}}\rho_{-\mathbf{k}}(\tau')] \\
&\quad - \frac{1}{\hbar} \sum_{\substack{\mathbf{k} \\ (k_x < 0)}} \frac{\cosh [\omega_{\mathbf{k}} (|\tau - \tau'| - \hbar\beta/2)]}{\sinh (\beta\hbar\omega_{\mathbf{k}}/2)} \\
&\quad \times [V_{\mathbf{k}}\rho_{\mathbf{k}}(\tau) - V_{-\mathbf{k}}\rho_{-\mathbf{k}}(\tau)] [V_{\mathbf{k}}\rho_{\mathbf{k}}(\tau') - V_{-\mathbf{k}}\rho_{-\mathbf{k}}(\tau')] \\
&= \frac{2}{\hbar} \sum_{\substack{\mathbf{k} \\ (k_x \geq 0)}} \frac{\cosh [\omega_{\mathbf{k}} (|\tau - \tau'| - \hbar\beta/2)]}{\sinh (\beta\hbar\omega_{\mathbf{k}}/2)} V_{\mathbf{k}} V_{-\mathbf{k}} \\
&\quad \times [\rho_{\mathbf{k}}(\tau) \rho_{-\mathbf{k}}(\tau') + \rho_{-\mathbf{k}}(\tau) \rho_{\mathbf{k}}(\tau')] \\
&= \frac{2}{\hbar} \sum_{\mathbf{k}} \frac{\cosh [\omega_{\mathbf{k}} (|\tau - \tau'| - \hbar\beta/2)]}{\sinh (\beta\hbar\omega_{\mathbf{k}}/2)} |V_{\mathbf{k}}|^2 \rho_{\mathbf{k}}(\tau) \rho_{-\mathbf{k}}(\tau').
\end{aligned}$$

Herefrom, we find that

$$\Phi = - \sum_{\mathbf{k}} \frac{|V_{\mathbf{k}}|^2}{2\hbar^2} \int_0^{\hbar\beta} d\tau \int_0^{\hbar\beta} d\tau' \frac{\cosh [\omega_{\mathbf{k}} (|\tau - \tau'| - \frac{\hbar\beta}{2})]}{\sinh (\frac{\beta\hbar\omega_{\mathbf{k}}}{2})} \rho_{\mathbf{k}}(\tau) \rho_{-\mathbf{k}}(\tau'). \quad (6.20)$$

As a result, the partition function of the electron-phonon system (6.11) factorizes into a product

$$Z(\{N_{\sigma}\}, \beta) = Z_p(\{N_{\sigma}\}, \beta) \prod_{\mathbf{k}} \frac{1}{2 \sinh (\beta\hbar\omega_{\mathbf{k}}/2)} \quad (6.21)$$

of the partition function of free phonons with a partition function $Z_p(\{N_{\sigma}\}, \beta)$ of interacting polarons, which is a path integral over the electron coordinates only:

$$Z_p(\{N_{\sigma}\}, \beta) = \sum_P \frac{(-1)^{\xi_P}}{N_{1/2}! N_{-1/2}!} \int d\bar{\mathbf{x}} \int_{\bar{\mathbf{x}}}^{P\bar{\mathbf{x}}} D\bar{\mathbf{x}}(\tau) e^{-S_p[\bar{\mathbf{x}}(\tau)]}. \quad (6.22)$$

The functional

$$S_p[\bar{\mathbf{x}}(\tau)] = -\frac{1}{\hbar} \int_0^{\hbar\beta} [L_e(\dot{\bar{\mathbf{x}}}(\tau), \bar{\mathbf{x}}(\tau)) - V_C(\bar{\mathbf{x}}(\tau))] d\tau + \Phi[\bar{\mathbf{x}}(\tau)] \quad (6.23)$$

describes the phonon-induced retarded interaction between the electrons, including the retarded self-interaction of each electron.

Using (6.3) and (6.6) we write down $S_p[\bar{\mathbf{x}}(\tau)]$ explicitly:

$$S_p[\bar{\mathbf{x}}(\tau)] = \frac{1}{\hbar} \int_0^{\hbar\beta} \left[\sum_{\sigma} \sum_{j=1}^{N_{\sigma}} \frac{m_b}{2} (\dot{\mathbf{x}}_{j,\sigma}^2 + \Omega_0^2 \mathbf{x}_{j,\sigma}^2) + \sum_{\substack{\sigma,\sigma' \\ (j,\sigma) \neq (l,\sigma')}} \sum_{j=1}^{N_{\sigma}} \sum_{l=1}^{N_{\sigma'}} \frac{e^2}{2\varepsilon_{\infty} |\mathbf{x}_{j,\sigma} - \mathbf{x}_{l,\sigma'}|} \right] d\tau \\ - \sum_{\mathbf{q}} \frac{|V_{\mathbf{q}}|^2}{2\hbar^2} \int_0^{\hbar\beta} d\tau \int_0^{\hbar\beta} d\tau' \frac{\cosh[\omega_{\text{LO}}(|\tau - \tau'| - \hbar\beta/2)]}{\sinh(\beta\hbar\omega_{\text{LO}}/2)} \rho_{\mathbf{q}}(\tau) \rho_{-\mathbf{q}}(\tau'). \quad (6.24)$$

The free energy of a system of interacting polarons $F_p(\{N_{\sigma}\}, \beta)$ is related to their partition function (6.22) by the equation:

$$F_p(\{N_{\sigma}\}, \beta) = -\frac{1}{\beta} \ln Z_p(\{N_{\sigma}\}, \beta). \quad (6.25)$$

At present no method is known to calculate the non-gaussian path integral (6.22) analytically. For *distinguishable* particles, the Jensen-Feynman variational principle [43] provides a convenient approximation technique. It yields a lower bound to the partition function, and hence an upper bound to the free energy.

It can be shown [99] that the path-integral approach to the many-body problem for a fixed number of identical particles can be formulated as a Feynman-Kac functional on a state space for N indistinguishable particles, by imposing an ordering on the configuration space and by the introduction of a set of boundary conditions at the boundaries of this state space. The resulting variational inequality for identical particles takes the same form as the Jensen-Feynman variational principle:

$$F_p \leq F_{var}, \quad (6.26)$$

$$F_{var} = F_0 + \frac{1}{\beta} \langle S_p - S_0 \rangle_{S_0}, \quad (6.27)$$

where S_0 is a model action with the corresponding free energy F_0 . The angular brackets mean a weighted average over the paths

$$\langle (\bullet) \rangle_{S_0} = \frac{\sum_P \frac{(-1)^{\xi_P}}{N_{1/2}! N_{-1/2}!} \int d\bar{\mathbf{x}} \int_{\bar{\mathbf{x}}}^{P\bar{\mathbf{x}}} D\bar{\mathbf{x}}(\tau) (\bullet) e^{-S_0[\bar{\mathbf{x}}(\tau)]}}{\sum_P \frac{(-1)^{\xi_P}}{N_{1/2}! N_{-1/2}!} \int d\bar{\mathbf{x}} \int_{\bar{\mathbf{x}}}^{P\bar{\mathbf{x}}} D\bar{\mathbf{x}}(\tau) e^{-S_0[\bar{\mathbf{x}}(\tau)]}}. \quad (6.28)$$

In the zero-temperature limit, the polaron ground-state energy

$$E_p^0 = \lim_{\beta \rightarrow \infty} F_p \quad (6.29)$$

obeys the inequality following from (6.26) with (6.27):

$$E_p^0 \leq E_{var}$$

with

$$E_{var} = E_0^0 + \lim_{\beta \rightarrow \infty} \left(\frac{1}{\beta} \langle S_p - S_0 \rangle_{S_0} \right), \quad (6.30)$$

$$E_0^0 = \lim_{\beta \rightarrow \infty} F_0. \quad (6.31)$$

B. Model system

We consider a model system consisting of N electrons with coordinates $\bar{\mathbf{x}} \equiv \{\mathbf{x}_{j,\sigma}\}$ and N_f fictitious particles with coordinates $\bar{\mathbf{y}} \equiv \{\mathbf{y}_j\}$ in a harmonic confinement potential with elastic interparticle interactions as studied in Refs. [98, 100]. The Lagrangian of this model system takes the form

$$\begin{aligned} L_M(\dot{\bar{\mathbf{x}}}, \dot{\bar{\mathbf{y}}}; \bar{\mathbf{x}}, \bar{\mathbf{y}}) = & -\frac{m_b}{2} \sum_{\sigma} \sum_{j=1}^{N_{\sigma}} (\dot{\mathbf{x}}_{j,\sigma}^2 + \Omega^2 \mathbf{x}_{j,\sigma}^2) + \frac{m_b \omega^2}{4} \sum_{\sigma, \sigma'} \sum_{j=1}^{N_{\sigma}} \sum_{l=1}^{N_{\sigma'}} (\mathbf{x}_{j,\sigma} - \mathbf{x}_{l,\sigma'})^2 \\ & - \frac{m_f}{2} \sum_{j=1}^{N_f} (\dot{\mathbf{y}}_j^2 + \Omega_f^2 \mathbf{y}_j^2) - \frac{k}{2} \sum_{\sigma} \sum_{j=1}^{N_{\sigma}} \sum_{l=1}^{N_f} (\mathbf{x}_{j,\sigma} - \mathbf{y}_l)^2. \end{aligned} \quad (6.32)$$

The frequencies Ω , ω , Ω_f , the mass of a fictitious particle m_f , and the force constant k are variational parameters. Clearly, this Lagrangian is symmetric with respect to electron permutations. Performing the path integral over the coordinates of the fictitious particles in the same way as described above for phonons, the partition function $Z_0(\{N_{\sigma}\}, \beta)$ of the model system of interacting polarons becomes a path integral over the electron coordinates:

$$Z_0(\{N_{\sigma}\}, \beta) = \sum_P \frac{(-1)^{\xi_P}}{N_{1/2}! N_{-1/2}!} \int d\bar{\mathbf{x}} \int_{\bar{\mathbf{x}}}^{P\bar{\mathbf{x}}} D\bar{\mathbf{x}}(\tau) e^{-S_0[\bar{\mathbf{x}}(\tau)]}, \quad (6.33)$$

with the action functional $S_0[\bar{\mathbf{x}}(\tau)]$ given by

$$\begin{aligned} S_0[\bar{\mathbf{x}}(\tau)] = & \frac{1}{\hbar} \int_0^{\hbar\beta} \sum_{\sigma} \sum_{j=1}^{N_{\sigma}} \frac{m_b}{2} [\dot{\mathbf{x}}_{j,\sigma}^2(\tau) + \Omega^2 \mathbf{x}_{j,\sigma}^2(\tau)] d\tau \\ & - \frac{1}{\hbar} \int_0^{\hbar\beta} \sum_{\sigma, \sigma'} \sum_{j=1}^{N_{\sigma}} \sum_{l=1}^{N_{\sigma'}} \frac{m_b \omega^2}{4} [\mathbf{x}_{j,\sigma}(\tau) - \mathbf{x}_{l,\sigma'}(\tau)]^2 d\tau \\ & - \frac{k^2 N^2 N_f}{4m_f \hbar \Omega_f} \int_0^{\hbar\beta} d\tau \int_0^{\hbar\beta} d\tau' \frac{\cosh[\Omega_f(|\tau - \tau'| - \hbar\beta/2)]}{\sinh(\beta\hbar\Omega_f/2)} \mathbf{X}(\tau) \cdot \mathbf{X}(\tau'), \end{aligned} \quad (6.34)$$

where \mathbf{X} is the center-of-mass coordinate of the electrons,

$$\mathbf{X} = \frac{1}{N} \sum_{\sigma} \sum_{j=1}^{N_{\sigma}} \mathbf{x}_{j,\sigma}. \quad (6.35)$$

1. *Analytical calculation of the model partition function*

The partition function $Z_0(\{N_{\sigma}\}, \beta)$ [Eq. (6.33)] for the model system of interacting polarons can be expressed in terms of the partition function $Z_M(\{N_{\sigma}\}, N_f, \beta)$ of the model system of interacting electrons and fictitious particles with the Lagrangian L_M [Eq. (6.32)] as follows:

$$Z_0(\{N_{\sigma}\}, \beta) = \frac{Z_M(\{N_{\sigma}\}, N_f, \beta)}{Z_f(N_f, w_f, \beta)}, \quad (6.36)$$

where $Z_f(N_f, w_f, \beta)$ is the partition function of fictitious particles,

$$Z_f(N_f, \beta) = \frac{1}{(2 \sinh \frac{1}{2} \beta \hbar w_f)^{DN_f}}, \quad (6.37)$$

with the frequency

$$w_f = \sqrt{\Omega_f^2 + kN/m_f} \quad (6.38)$$

and $D=3(2)$ for 3D(2D) systems. The partition function $Z_M(\{N_{\sigma}\}, N_f, \beta)$ is the path integral for both the electrons and the fictitious particles:

$$Z_M(\{N_{\sigma}\}, N_f, \beta) = \sum_P \frac{(-1)^{\xi_P}}{N_{1/2}! N_{-1/2}!} \int d\bar{\mathbf{x}} \int_{\bar{\mathbf{x}}}^{P\bar{\mathbf{x}}} D\bar{\mathbf{x}}(\tau) \int d\bar{\mathbf{y}} \int_{\bar{\mathbf{y}}}^{\bar{\mathbf{y}}} D\bar{\mathbf{y}}(\tau) e^{-S_M[\bar{\mathbf{x}}(\tau), \bar{\mathbf{y}}(\tau)]} \quad (6.39)$$

with the ‘‘action’’ functional

$$S_M[\bar{\mathbf{x}}(\tau), \bar{\mathbf{y}}(\tau)] = -\frac{1}{\hbar} \int_0^{\hbar\beta} L_M(\dot{\bar{\mathbf{x}}}, \dot{\bar{\mathbf{y}}}; \bar{\mathbf{x}}, \bar{\mathbf{y}}) d\tau, \quad (6.40)$$

where the Lagrangian is given by Eq. (6.32).

Let us consider an auxiliary ‘‘ghost’’ subsystem with the Lagrangian

$$L_g(\dot{\mathbf{X}}_g, \dot{\mathbf{Y}}_g, \mathbf{X}_g, \mathbf{Y}_g) = -\frac{m_b N}{2} (\dot{\mathbf{X}}_g^2 + w^2 \mathbf{X}_g^2) - \frac{m_f N_f}{2} (\dot{\mathbf{Y}}_g^2 + w_f^2 \mathbf{Y}_g^2) \quad (6.41)$$

with two frequencies w and w_f , where w is given by

$$w = \sqrt{\Omega^2 - N\omega^2 + kN_f/m_b}. \quad (6.42)$$

The partition function Z_g of this subsystem

$$Z_g = \int d\mathbf{X}_g \int d\mathbf{Y}_g \int_{\mathbf{X}_g}^{\mathbf{X}_g} D\mathbf{X}_g(\tau) \int_{\mathbf{Y}_g}^{\mathbf{Y}_g} D\mathbf{Y}_g(\tau) \exp\{-S_g[\mathbf{X}_g(\tau), \mathbf{Y}_g(\tau)]\}, \quad (6.43)$$

with the “action” functional

$$S_g[\mathbf{X}_g(\tau), \mathbf{Y}_g(\tau)] = -\frac{1}{\hbar} \int_0^{\hbar\beta} L_g(\dot{\mathbf{X}}_g, \mathbf{X}_g, \dot{\mathbf{Y}}_g, \mathbf{Y}_g) d\tau \quad (6.44)$$

is calculated in the standard way, because its Lagrangian (6.41) has a simple oscillator form. Consequently, the partition function Z_g is

$$Z_g = \frac{1}{[2 \sinh(\frac{\beta\hbar\omega}{2})]^D} \frac{1}{[2 \sinh(\frac{\beta\hbar\omega_f}{2})]^D}. \quad (6.45)$$

The product $Z_g Z_M$ of the two partition functions Z_g and $Z_M(\{N_\sigma\}, N_f, \beta)$ is a path integral in the state space of N electrons, N_f fictitious particles and two “ghost” particles with the coordinate vectors \mathbf{X}_g and \mathbf{Y}_g . The Lagrangian \tilde{L}_M of this system is a sum of L_M and L_g ,

$$\tilde{L}_M(\dot{\bar{\mathbf{x}}}, \dot{\bar{\mathbf{y}}}, \dot{\mathbf{X}}_g, \dot{\mathbf{Y}}_g; \bar{\mathbf{x}}, \bar{\mathbf{y}}, \mathbf{X}_g, \mathbf{Y}_g) \equiv L_M(\dot{\bar{\mathbf{x}}}, \dot{\bar{\mathbf{y}}}; \bar{\mathbf{x}}, \bar{\mathbf{y}}) + L_g(\dot{\mathbf{X}}_g, \dot{\mathbf{Y}}_g, \mathbf{X}_g, \mathbf{Y}_g). \quad (6.46)$$

The “ghost” subsystem is introduced because the center-of-mass coordinates in \tilde{L}_M can be explicitly separated much more transparently than in L_M . This separation is realized by the linear transformation of coordinates,

$$\begin{cases} \mathbf{x}_{j,\sigma} = \mathbf{x}'_{j,\sigma} + \mathbf{X} - \mathbf{X}_g, \\ \mathbf{y}_{j\sigma} = \mathbf{y}'_{j\sigma} + \mathbf{Y} - \mathbf{Y}_g, \end{cases} \quad (6.47)$$

where \mathbf{X} and \mathbf{Y} are the center-of-mass coordinate vectors of the electrons and of the fictitious particles, correspondingly:

$$\mathbf{X} = \frac{1}{N} \sum_{\sigma} \sum_{j=1}^{N_{\sigma}} \mathbf{x}_{j,\sigma}, \quad \mathbf{Y} = \frac{1}{N_f} \sum_{j=1}^{N_f} \mathbf{y}_j. \quad (6.48)$$

Before the transformation (6.47), the independent variables are $(\bar{\mathbf{x}}, \bar{\mathbf{y}}, \mathbf{X}_g, \mathbf{Y}_g)$, with the center-of-mass coordinates \mathbf{X} and \mathbf{Y} determined by Eq. (6.48). When applying the trans-

formation (6.47) to the centers of mass (6.48), we find that

$$\mathbf{X} = \frac{1}{N} \sum_{\sigma} \sum_{j=1}^{N_{\sigma}} (\mathbf{x}'_{j,\sigma} + \mathbf{X} - \mathbf{X}_g) = \frac{1}{N} \sum_{\sigma} \sum_{j=1}^{N_{\sigma}} \mathbf{x}'_{j,\sigma} + \mathbf{X} - \mathbf{X}_g, \quad (6.49)$$

$$\mathbf{Y} = \frac{1}{N_f} \sum_{j=1}^{N_f} (\mathbf{y}'_{j\sigma} + \mathbf{Y} - \mathbf{Y}_g) = \frac{1}{N_f} \sum_{j=1}^{N_f} \mathbf{y}'_{j\sigma} + \mathbf{Y} - \mathbf{Y}_g. \quad (6.50)$$

As seen from Eqs. (6.49), (6.50), after the transformation (6.47) the independent variables are $(\bar{\mathbf{x}}', \bar{\mathbf{y}}', \mathbf{X}, \mathbf{Y})$, while the coordinates $(\mathbf{X}_g, \mathbf{Y}_g)$ obey the equations

$$\mathbf{X}_g = \frac{1}{N} \sum_{\sigma} \sum_{j=1}^{N_{\sigma}} \mathbf{x}'_{j,\sigma}, \quad \mathbf{Y}_g = \frac{1}{N_f} \sum_{j=1}^{N_f} \mathbf{y}'_j. \quad (6.51)$$

In order to find the explicit form of the Lagrangian (6.46) after the transformation (6.47), we use the following relations for the quadratic sums of coordinates:

$$\begin{aligned} \sum_{\sigma} \sum_{j=1}^{N_{\sigma}} \mathbf{x}_{j,\sigma}^2 &= \sum_{\sigma} \sum_{j=1}^{N_{\sigma}} (\mathbf{x}'_{j,\sigma})^2 + N (\mathbf{X}^2 - \mathbf{X}_g^2), & \sum_{j=1}^{N_f} \mathbf{y}_j^2 &= \sum_{j=1}^{N_f} (\mathbf{y}'_j)^2 + N_f (\mathbf{Y}^2 - \mathbf{Y}_g^2), \\ \sum_{\sigma, \sigma'} \sum_{j=1}^{N_{\sigma}} \sum_{l=1}^{N_{\sigma'}} (\mathbf{x}_{j,\sigma} - \mathbf{x}_{l,\sigma'})^2 &= 2N \sum_{\sigma} \sum_{j=1}^{N_{\sigma}} (\mathbf{x}'_{j,\sigma})^2 - 2N_f^2 \mathbf{X}_g^2, \\ \sum_{j=1}^{N_f} \sum_{l=1}^{N_f} (\mathbf{y}_j - \mathbf{y}_l)^2 &= 2N_f \sum_{j=1}^{N_f} (\mathbf{y}'_j)^2 - 2N_f^2 \mathbf{Y}_g^2, \\ \sum_{\sigma} \sum_{j=1}^{N_{\sigma}} \sum_{l=1}^{N_f} (\mathbf{x}_{j,\sigma} - \mathbf{y}_l)^2 &= N_f \sum_{\sigma} \sum_{j=1}^{N_{\sigma}} (\mathbf{x}'_{j,\sigma})^2 + N \sum_{j=1}^{N_f} (\mathbf{y}'_j)^2 + \\ &NN_f (\mathbf{X}^2 + \mathbf{Y}^2 - 2\mathbf{X} \cdot \mathbf{Y} - \mathbf{X}_g^2 - \mathbf{Y}_g^2). \end{aligned} \quad (6.52)$$

The substitution of Eq. (6.48) into Eq. (6.46) then results in the following 3 terms:

$$\tilde{L}_M (\dot{\bar{\mathbf{x}}}', \dot{\bar{\mathbf{y}}}', \dot{\mathbf{X}}, \dot{\mathbf{Y}}; \bar{\mathbf{x}}', \bar{\mathbf{y}}', \mathbf{X}, \mathbf{Y}) = L_w (\dot{\bar{\mathbf{x}}}', \bar{\mathbf{x}}') + L_{w_f} (\dot{\bar{\mathbf{y}}}', \bar{\mathbf{y}}') + L_C (\dot{\mathbf{X}}, \mathbf{X}; \dot{\mathbf{Y}}, \mathbf{Y}), \quad (6.53)$$

where $L_w (\dot{\bar{\mathbf{x}}}', \bar{\mathbf{x}}')$ and $L_{w_f} (\dot{\bar{\mathbf{y}}}', \bar{\mathbf{y}}')$ are Lagrangians of non-interacting identical oscillators with the frequencies w and w_f , respectively,

$$L_w (\dot{\bar{\mathbf{x}}}', \bar{\mathbf{x}}') = -\frac{m_b}{2} \sum_{\sigma=\pm 1/2} \sum_{j=1}^{N_{\sigma}} [(\dot{\mathbf{x}}'_{j,\sigma})^2 + w^2 (\mathbf{x}'_{j,\sigma})^2], \quad (6.54)$$

$$L_{w_f} (\dot{\bar{\mathbf{y}}}', \bar{\mathbf{y}}') = -\frac{m_f}{2} \sum_{j=1}^{N_f} [(\dot{\mathbf{y}}'_{j,\sigma})^2 + w_f^2 (\mathbf{y}'_{j,\sigma})^2]. \quad (6.55)$$

The Lagrangian $L_C(\dot{\mathbf{X}}, \mathbf{X}; \dot{\mathbf{Y}}, \mathbf{Y})$ describes the combined motion of the centers-of-mass of the electrons and of the fictitious particles,

$$L_C(\dot{\mathbf{X}}, \mathbf{X}; \dot{\mathbf{Y}}, \mathbf{Y}) = -\frac{m_b N}{2} (\dot{\mathbf{X}}^2 + \tilde{\Omega}^2 \mathbf{X}^2) - \frac{m_f N_f}{2} (\dot{\mathbf{Y}}^2 + w_f^2 \mathbf{Y}^2) + k N N_f \mathbf{X} \cdot \mathbf{Y}, \quad (6.56)$$

with

$$\tilde{\Omega} = \sqrt{\Omega^2 + k N_f / m_b}. \quad (6.57)$$

The Lagrangian (6.56) is reduced to a diagonal quadratic form in the coordinates and the velocities by a unitary transformation for two interacting oscillators using the following replacement of variables:

$$\begin{aligned} \mathbf{X} &= \frac{1}{\sqrt{m_b N}} (a_1 \mathbf{r} + a_2 \mathbf{R}), \\ \mathbf{Y} &= \frac{1}{\sqrt{m_f N_f}} (-a_2 \mathbf{r} + a_1 \mathbf{R}) \end{aligned} \quad (6.58)$$

with the coefficients

$$a_1 = \left[\frac{1 + \chi}{2} \right]^{1/2}, \quad a_2 = \left[\frac{1 - \chi}{2} \right]^{1/2}, \quad (6.59)$$

$$\chi \equiv \frac{\tilde{\Omega}^2 - \tilde{\Omega}_f^2}{\left[(\tilde{\Omega}^2 - \tilde{\Omega}_f^2)^2 + 4\gamma^2 \right]^{1/2}}, \quad \gamma \equiv k \sqrt{\frac{N N_f}{m_b m_f}}. \quad (6.60)$$

The eigenfrequencies of the center-of-mass subsystem are then given by the expression

$$\begin{cases} \Omega_1 = \sqrt{\frac{1}{2} \left[\tilde{\Omega}^2 + \tilde{\Omega}_f^2 + \sqrt{(\tilde{\Omega}^2 - \tilde{\Omega}_f^2)^2 + 4\gamma^2} \right]}, \\ \Omega_2 = \sqrt{\frac{1}{2} \left[\tilde{\Omega}^2 + \tilde{\Omega}_f^2 - \sqrt{(\tilde{\Omega}^2 - \tilde{\Omega}_f^2)^2 + 4\gamma^2} \right]}. \end{cases} \quad (6.61)$$

As a result, four independent frequencies Ω_1 , Ω_2 , w and w_f appear in the problem. Three of them (Ω_1 , Ω_2 , w) are the eigenfrequencies of the model system. Ω_1 is the frequency of the relative motion of the center of mass of the electrons with respect to the center of mass of the fictitious particles; Ω_2 is the frequency related to the center of mass of the model system as a whole; w is the frequency of the relative motion of the electrons with respect to their center of mass. The parameter w_f is an analog of the second variational parameter w of the one-polaron Feynman model. Further, the Lagrangian (6.56) takes the form

$$L_C = -\frac{1}{2} (\dot{\mathbf{r}}^2 + \Omega_1^2 \mathbf{r}^2) - \frac{1}{2} (\dot{\mathbf{R}}^2 + \Omega_2^2 \mathbf{R}^2), \quad (6.62)$$

leading to the partition function corresponding to the combined motion of the centers-of-mass of the electrons and of the fictitious particles

$$Z_C = \frac{1}{[2 \sinh(\frac{\beta \hbar \Omega_1}{2})]^D} \frac{1}{[2 \sinh(\frac{\beta \hbar \Omega_2}{2})]^D}. \quad (6.63)$$

Taking into account Eqs. (6.45) and (6.63), we obtain finally the partition function of the model system for interacting polarons

$$Z_0(\{N_\sigma\}, \beta) = \left[\frac{\sinh(\frac{\beta \hbar w}{2}) \sinh(\frac{\beta \hbar w_f}{2})}{\sinh(\frac{\beta \hbar \Omega_1}{2}) \sinh(\frac{\beta \hbar \Omega_2}{2})} \right]^D \tilde{Z}_F(\{N_\sigma\}, w, \beta). \quad (6.64)$$

Here

$$\tilde{Z}_F(\{N_\sigma\}, w, \beta) = Z_F(N_{1/2}, w, \beta) Z_F(N_{-1/2}, w, \beta) \quad (6.65)$$

is the partition function of $N = N_{1/2} + N_{-1/2}$ non-interacting fermions in a parabolic confinement potential with the frequency w . The analytical expressions for the partition function of N_σ spin-polarized fermions $Z_F(N_\sigma, w, \beta)$ were derived in Ref. [101].

C. Variational functional

In order to obtain an upper bound to the free energy E_{var} , we substitute the model action functional (6.34) into the right-hand side of the variational inequality (6.26) and consider the limit $\beta \rightarrow \infty$:

$$\begin{aligned} & E_{var}(\{N_\sigma\}) \\ &= \mathbb{E}_F(\{N_\sigma\}, w) + \frac{m_b}{2} (\Omega_0^2 - \Omega^2 + N\omega^2) \left\langle \sum_{j=1}^N \mathbf{x}_j^2(0) \right\rangle_{S_0} \\ &- \frac{m_b \omega^2 N^2}{2} \langle \mathbf{X}^2(0) \rangle_{S_0} + \langle U_b(\bar{\mathbf{x}}) \rangle_{S_0} + \sum_{\mathbf{q} \neq 0} \frac{2\pi e^2}{V \varepsilon_\infty q^2} [\mathcal{G}(\mathbf{q}, 0 | \{N_\sigma\}, \beta \rightarrow \infty) - N] \\ &+ \lim_{\beta \rightarrow \infty} \frac{k^2 N^2 N_f}{4m_f \beta \hbar \Omega_f} \int_0^{\hbar\beta} d\tau \int_0^{\hbar\beta} d\tau' \frac{\cosh[\Omega_f(|\tau - \tau'| - \hbar\beta/2)]}{\sinh(\beta \hbar \Omega_f/2)} \langle \mathbf{X}(\tau) \cdot \mathbf{X}(\tau') \rangle_{S_0} \\ &- \lim_{\beta \rightarrow \infty} \sum_{\mathbf{q}} \frac{|V_{\mathbf{q}}|^2}{2\hbar^2 \beta} \int_0^{\hbar\beta} d\tau \int_0^{\hbar\beta} d\tau' \frac{\cosh[\omega_{LO}(|\tau - \tau'| - \hbar\beta/2)]}{\sinh(\beta \hbar \omega_{LO}/2)} \mathcal{G}(\mathbf{q}, \tau - \tau' | \{N_\sigma\}, \beta). \quad (6.66) \end{aligned}$$

Here, $\mathbb{E}_F(N, w)$ is the energy of N non-interacting fermions in a parabolic confinement potential with the confinement frequency w ,

$$\begin{aligned} \mathbb{E}_F(\{N_\sigma\}, w) = \hbar w \sum_{\sigma=\pm 1/2} \left\{ \sum_{n=0}^{L_\sigma-1} \left(n + \frac{3}{2} \right) g(n) \right. \\ \left. + (N_\sigma - N_{L_\sigma}) \left(L_\sigma + \frac{3}{2} \right) \right\}, \end{aligned} \quad (6.67)$$

where σ is the spin of an electron, L_σ is the lower partly filled or empty level for N_σ electrons with the spin projection σ . The first term in the curly brackets of Eq. (6.94) (the upper line) is the number of electrons at fully filled energy levels, while the second term (square brackets) is the number of electrons at the next upper level (which can be empty or filled partially). The energy levels of a 3D oscillator are degenerate, so that

$$g(n) = \frac{1}{2} (n+1)(n+2) \quad (6.68)$$

is the degeneracy of the n -th energy level. The parameter

$$N_{L_\sigma} = \frac{1}{6} L_\sigma (L_\sigma + 1) (L_\sigma + 2) \quad (6.69)$$

is the number of electrons at all fully filled levels. The summation in Eq. (6.67) is performed explicitly, what gives us the result

$$\mathbb{E}_F(\{N_\sigma\}, w) = \hbar w \sum_{\sigma} \left[\frac{1}{8} L_\sigma (L_\sigma + 1)^2 (L_\sigma + 2) + (N_\sigma - N_{L_\sigma}) \left(L_\sigma + \frac{3}{2} \right) \right]. \quad (6.70)$$

In Eq. (6.66), $\mathcal{G}(\mathbf{q}, \tau - \tau' | \{N_\sigma\}, \beta)$ is the two-point correlation function for the electron density operators:

$$\mathcal{G}(\mathbf{q}, \tau | \{N_\sigma\}, \beta) = \langle \rho_{\mathbf{q}}(\tau) \rho_{-\mathbf{q}}(0) \rangle_{S_0}. \quad (6.71)$$

The averages $\langle \mathbf{X}(\tau) \cdot \mathbf{X}(\tau') \rangle_{S_0}$ are calculated using the generating function method:

$$\langle X_k(\tau) X_k(\tau') \rangle_{S_0} = - \frac{\partial^2}{\partial \xi_k \partial \eta_k} \langle \exp [i(\xi \cdot \mathbf{X}(\tau) + \eta \cdot \mathbf{X}(\tau'))] \rangle_{S_0} \Big|_{\xi=0, \eta=0}, \quad (6.72)$$

$$\implies \langle \mathbf{X}(\tau) \cdot \mathbf{X}(\tau') \rangle_{S_0} = \frac{3\hbar}{2mN} \sum_{i=1}^2 \frac{a_i^2 \cosh [\Omega_i (|\tau - \sigma| - \hbar\beta/2)]}{\Omega_i \sinh (\hbar\beta\Omega_i/2)}. \quad (6.73)$$

Substituting this expression into Eq. (6.66) and performing integrations over τ and σ analytically, we obtain the result

$$\begin{aligned} & \frac{k^2 N^2 N_f}{4m_f \beta \hbar \Omega_f} \int_0^{\hbar\beta} d\tau \int_0^{\hbar\beta} d\tau' \frac{\cosh[\Omega_f (|\tau - \tau'| - \hbar\beta/2)]}{\sinh(\beta \hbar \Omega_f/2)} \langle \mathbf{X}(\tau) \cdot \mathbf{X}(\tau') \rangle_{S_0} \\ &= \frac{3\hbar\gamma}{4} \sum_{i=1}^2 \frac{a_i^2}{\Omega_f^2 - \Omega_i^2} \left[\frac{\coth(\beta\Omega_i/2)}{\Omega_i} - \frac{\coth(\beta\Omega_f/2)}{\Omega_f} \right], \end{aligned} \quad (6.74)$$

and in the zero-temperature limit we have

$$\begin{aligned} & \lim_{\beta \rightarrow \infty} \frac{k^2 N^2 N_f}{4m_f \beta \hbar \Omega_f} \int_0^{\hbar\beta} d\tau \int_0^{\hbar\beta} d\tau' \frac{\cosh[\Omega_f (|\tau - \tau'| - \hbar\beta/2)]}{\sinh(\beta \hbar \Omega_f/2)} \langle \mathbf{X}(\tau) \cdot \mathbf{X}(\tau') \rangle_{S_0} \\ &= \frac{3\hbar\gamma}{4} \sum_{i=1}^2 \frac{a_i^2}{\Omega_f^2 - \Omega_i^2} \left(\frac{1}{\Omega_i} - \frac{1}{\Omega_f} \right). \end{aligned} \quad (6.75)$$

The average $\left\langle \sum_{j=1}^N \mathbf{x}_j^2 \right\rangle_{S_0}$ is transformed, using the described above operations with the “ghost” subsystem,

$$\mathbf{x}_j = \mathbf{x}'_j + \mathbf{X} - \mathbf{X}_g, \quad (6.76)$$

and taking into account the first of equations (6.52)

$$\sum_{j=1}^N \mathbf{x}_j^2 = \sum_{j=1}^N (\mathbf{x}'_j)^2 + N (\mathbf{X}^2 - \mathbf{X}_g^2). \quad (6.77)$$

Consequently, averaging the left-hand side of Eq. (6.77) on the model action functional S_0 , one obtains

$$\begin{aligned} \left\langle \sum_{j=1}^N \mathbf{x}_j^2 \right\rangle_{S_0} &= \left\langle \sum_{j=1}^N \mathbf{x}_j^2 \right\rangle_{S_M} = \left\langle \sum_{j=1}^N \mathbf{x}_j^2 \right\rangle_{S_M+S_g} \\ &= \left\langle \sum_{j=1}^N \mathbf{x}_j^2 \right\rangle_{S_w} + N \left(\langle \mathbf{X}^2 \rangle_{S_C} - \langle \mathbf{X}_g^2 \rangle_{S_g} \right). \end{aligned} \quad (6.78)$$

The term $\left\langle \sum_{j=1}^N \mathbf{x}_j^2 \right\rangle_{S_w}$ is expressed using the virial theorem through the ground-state energy $\mathbb{E}_F(N, w)$ of N independent 3D fermion oscillators with the frequency w and with the mass m_b ,

$$\left\langle \sum_{j=1}^N \mathbf{x}_j^2 \right\rangle_{S_w} = \frac{\mathbb{E}_F(N, w)}{m_b w^2} = -\frac{1}{m_b w^2} \frac{\partial}{\partial \lambda} \ln \mathbb{Z}_I(N), \quad (6.79)$$

Two other terms in Eq. (6.78) are [cf. Eq. (6.73)]:

$$\begin{aligned}\langle \mathbf{X}^2 \rangle_{S_C} &= \frac{3\hbar}{2m_b N} \sum_{i=1}^2 \frac{a_i^2 \coth(\beta\Omega_i/2)}{\Omega_i}, \\ \langle \mathbf{X}_g^2 \rangle_{S_g} &= \frac{3\hbar}{2m_b N} \frac{\coth(\beta w/2)}{w}.\end{aligned}\quad (6.80)$$

So, we obtain

$$\left\langle \sum_{j=1}^N \mathbf{x}_j^2 \right\rangle_{S_0} = \frac{\mathbb{E}_F(\{N_\sigma\}, w)}{m_b w^2} + \frac{3\hbar}{2m_b} \left(\sum_{i=1}^2 \frac{a_i^2}{\Omega_i} - \frac{1}{w} \right).\quad (6.81)$$

The averaging of the background-charge potential gives us the result

$$\begin{aligned}\langle U_b(\bar{\mathbf{x}}) \rangle_{S_0} &= \frac{3\sqrt{2}\alpha\eta}{\pi(1-\eta)} \sum_{\sigma} \sum_{n=0}^{\infty} f_1(n, \sigma | \beta, N_\sigma) |_{\beta \rightarrow \infty} \sum_{k=0}^n \frac{(-1)^k}{k!} \binom{n+2}{n-k} \left(\frac{1}{2w} \right)^k \\ &\times \left\{ \frac{\Gamma(k - \frac{1}{2})}{A^{k-1/2}} \left[{}_1F_1\left(k - \frac{1}{2}; \frac{1}{2}; -\frac{R^2}{4A}\right) - {}_1F_1\left(k - \frac{1}{2}; \frac{3}{2}; -\frac{R^2}{4A}\right) \right] \right\}, \\ \eta &\equiv \varepsilon_\infty/\varepsilon_0, \quad A \equiv \frac{\hbar}{4m_b N} \left(\sum_{i=1}^2 \frac{a_i^2}{\Omega_i} + \frac{N-1}{w} \right),\end{aligned}\quad (6.82)$$

where $f_1(n, \sigma | \beta, N_\sigma)$ is the one-particle distribution function of fermions (the distribution functions are considered in more details in the next subsection).

Collecting all terms together, we arrive at the variational functional

$$\begin{aligned}E_{var}(\Omega_1, \Omega_2, w, \Omega_f) &= \hbar \left\{ \frac{\Omega_0^2 + w^2}{2w^2} \left[\frac{\tilde{E}(w, N)}{\hbar} - \frac{3}{2}w \right] + \frac{3}{2}(\Omega_1 + \Omega_2 - \Omega_f) \right. \\ &+ \left. \frac{3}{4}(\Omega_0^2 - \Omega_1^2 - \Omega_2^2 + \Omega_f^2) \sum_{i=1}^2 \frac{a_i^2}{\Omega_i} + \frac{3\gamma^2}{4\Omega_f} \sum_{i=1}^2 \frac{a_i^2}{\Omega_i(\Omega_i + \Omega_f)} \right\} \\ &+ \langle U_b(\bar{\mathbf{x}}) \rangle_{S_0} + E_C + E_{e-ph},\end{aligned}\quad (6.83)$$

where E_C and E_{e-ph} are the Coulomb and polaron contributions, respectively:

$$E_C = \frac{e^2}{4\pi^2\varepsilon_\infty} \int d\mathbf{q} \frac{1}{q^2} \left[\mathcal{G}(\mathbf{q}, 0 | \{N_\sigma\}, \beta) |_{\beta \rightarrow \infty} - N \right],\quad (6.84)$$

$$E_{e-ph} = -\frac{\sqrt{2}\alpha}{4\pi^2\hbar} \int d\mathbf{q} \frac{1}{q^2} \int_0^\infty d\tau \exp(-\omega_{LO}\tau) \mathcal{G}(\mathbf{q}, \tau | \{N_\sigma\}, \beta) |_{\beta \rightarrow \infty}.\quad (6.85)$$

The correlation function (6.71) is calculated analytically in the next subsection. With this correlation function, the variational ground-state energy is calculated and minimized numerically.

D. Two-point correlation functions

The two-point correlation function (6.71) is represented as the following path integral:

$$\begin{aligned} \mathcal{G}(\mathbf{q}, \tau | \{N_\sigma\}, \beta) &= \frac{1}{Z_0(\{N_\sigma\}, \beta)} \sum_P \frac{(-1)^{\xi_P}}{N_{1/2}! N_{-1/2}!} \\ &\times \int d\bar{\mathbf{x}} \int_{\bar{\mathbf{x}}}^{P\bar{\mathbf{x}}} D\bar{\mathbf{x}}(\tau) e^{-S_0[\bar{\mathbf{x}}(\tau)]} \rho_{\mathbf{q}}(\tau) \rho_{-\mathbf{q}}(0). \end{aligned} \quad (6.86)$$

We observe that $\mathcal{G}(\mathbf{q}, \tau | \{N_\sigma\}, \beta)$ can be rewritten as an average within the model ‘‘action’’ $S_M[\bar{\mathbf{x}}(\tau), \bar{\mathbf{y}}(\tau)]$ of interacting electrons and fictitious particles:

$$\begin{aligned} \mathcal{G}(\mathbf{q}, \tau | \{N_\sigma\}, \beta) &= \frac{1}{Z_M(\{N_\sigma\}, N_f, \beta)} \sum_P \frac{(-1)^{\xi_P}}{N_{1/2}! N_{-1/2}!} \\ &\times \int d\bar{\mathbf{x}} \int_{\bar{\mathbf{x}}}^{P\bar{\mathbf{x}}} D\bar{\mathbf{x}}(\tau) \int d\bar{\mathbf{y}} \int_{\bar{\mathbf{y}}}^{\bar{\mathbf{y}}} D\bar{\mathbf{y}}(\tau) e^{-S_M[\bar{\mathbf{x}}(\tau), \bar{\mathbf{y}}(\tau)]} \\ &\times \rho_{\mathbf{q}}(\tau) \rho_{-\mathbf{q}}(0). \end{aligned} \quad (6.87)$$

Indeed, one readily derives that the elimination of the fictitious particles in (6.87) leads to (6.86). The representation (6.87) allows one to calculate the correlation function $\mathcal{G}(\mathbf{q}, \tau | \{N_\sigma\}, \beta)$ in a much simpler way than through Eq. (6.86), using the separation of the coordinates of the centers of mass of the electrons and of the fictitious particles. This separation is performed for the two-point correlation function (6.87) by the same method as it has been done for the partition function (6.39). As a result, one obtains

$$\mathcal{G}(\mathbf{q}, \tau | \{N_\sigma\}, \beta) = \tilde{g}(\mathbf{q}, \tau | \{N_\sigma\}, \beta) \frac{\langle \exp[i\mathbf{q} \cdot (\mathbf{X}(\tau) - \mathbf{X}(\sigma))] \rangle_{S_C}}{\langle \exp[i\mathbf{q} \cdot (\mathbf{X}_g(\tau) - \mathbf{X}_g(\sigma))] \rangle_{S_g}}, \quad (6.88)$$

where $\tilde{g}(\mathbf{q}, \tau | \{N_\sigma\}, \beta)$ is the time-dependent correlation function of N non-interacting electrons in a parabolic confinement potential with the frequency w ,

$$\tilde{g}(\mathbf{q}, \tau | \{N_\sigma\}, \beta) = \langle \rho_{\mathbf{q}}(\tau) \rho_{-\mathbf{q}}(0) \rangle_{S_w}. \quad (6.89)$$

The action functional $S_w[\bar{\mathbf{x}}_\tau]$ is related to the Lagrangian $L_w(\dot{\bar{\mathbf{x}}}, \bar{\mathbf{x}})$ [Eq. (6.54)]

$$S_w[\bar{\mathbf{x}}_\tau] = \frac{1}{\hbar} \int_0^{\hbar\beta} L_w(\dot{\bar{\mathbf{x}}}, \bar{\mathbf{x}}) d\tau. \quad (6.90)$$

The averages in (6.88) are calculated using Feynman’s method of generating functions [43]. Namely, according to [43], the average

$$G[f(\tau)] \equiv \left\langle \exp \left\{ \frac{i}{\hbar} \int_0^\beta f(\tau) x_\tau d\tau \right\} \right\rangle_{S_w}, \quad (6.91)$$

where S_ω is the action functional of a one-dimensional harmonic oscillator with the frequency ω and with the mass m , results in

$$G[f(\tau)] = \exp \left\{ -\frac{1}{4m\hbar\omega} \int_0^\beta d\tau \int_0^\beta d\sigma \frac{\cosh[\omega(|\tau - \sigma| - \beta/2)]}{\sinh(\beta\omega/2)} f(\tau) f(\sigma) \right\}. \quad (6.92)$$

The diagonalization procedure for the Lagrangian L_C (6.56) allows us to represent that Lagrangian as a sum of Lagrangians of independent harmonic oscillators, what gives the following explicit expressions for averages in Eq. (6.88):

$$\begin{aligned} & \langle \exp [i\mathbf{q} \cdot (\mathbf{X}(\tau) - \mathbf{X}(\sigma))] \rangle_{S_C} \\ &= \exp \left\{ -\frac{\hbar q^2}{Nm_b} \left[\sum_{i=1}^2 a_i^2 \frac{\sinh\left(\frac{\Omega_i|\tau-\sigma|}{2}\right) \sinh\left(\frac{\Omega_i(\hbar\beta-|\tau-\sigma|)}{2}\right)}{\Omega_i \sinh\left(\frac{\beta\hbar\Omega_i}{2}\right)} \right] \right\}, \\ & \langle \exp [i\mathbf{q} \cdot (\mathbf{X}_g(\tau) - \mathbf{X}_g(\sigma))] \rangle_{S_g} \\ &= \exp \left[-\frac{\hbar q^2}{Nm_b} \frac{\sinh\left(\frac{w|\tau-\sigma|}{2}\right) \sinh\left(\frac{w(\hbar\beta-|\tau-\sigma|)}{2}\right)}{w \sinh\left(\frac{\beta\hbar w}{2}\right)} \right]. \end{aligned}$$

1. *The correlation function $\tilde{g}(\mathbf{q}, \tau | \{N_\sigma\}, \beta)$*

As seen from the formula (6.89), $\tilde{g}(\mathbf{q}, \tau | \{N_\sigma\}, \beta)$ is the time-dependent correlation function of N non-interacting fermions in a parabolic confinement potential with the frequency w . Let us consider first of all a system of N identical spin-polarized oscillators with the Lagrangian

$$L = \frac{m}{2} \sum_{j=1}^N (\dot{\mathbf{x}}_j^2 - \omega^2 \mathbf{x}_j^2). \quad (6.93)$$

The corresponding Hamiltonian is

$$\hat{H} = \sum_{j=1}^N \left(\frac{\hat{\mathbf{p}}_j^2}{2m} + \frac{m\omega^2 \hat{\mathbf{x}}_j^2}{2} \right), \quad (6.94)$$

$$\hat{H} = \sum_{j=1}^N \hat{h}_j, \quad \hat{h} \equiv \frac{\hat{\mathbf{p}}^2}{2m} + \frac{m\omega^2 \hat{\mathbf{x}}^2}{2}. \quad (6.95)$$

A set of eigenfunctions of the one-particle Hamiltonian \hat{h} is determined as follows:

$$\hat{h}\psi_{\mathbf{n}}(\mathbf{x}) = \varepsilon_{\mathbf{n}}\psi_{\mathbf{n}}(\mathbf{x}), \quad (6.96)$$

where

$$\begin{aligned} \mathbf{n} &\equiv (n_1, n_2, n_3), \quad n \equiv n_1 + n_2 + n_3, \\ \varepsilon_{\mathbf{n}} = \varepsilon_n &= \hbar\omega \left(n + \frac{3}{2} \right), \quad \psi_{\mathbf{n}}(\mathbf{x}) = \varphi_{n_1}(x_1) \varphi_{n_2}(x_2) \varphi_{n_3}(x_3), \end{aligned} \quad (6.97)$$

$\varphi_n(x)$ is the n -th eigenfunction of a one-dimensional oscillator with the frequency ω .

The Hamiltonian (6.94) can be written down in terms of the annihilation ($\hat{a}_{\mathbf{n}}$) and creation ($\hat{a}_{\mathbf{n}}^+$) operators:

$$\hat{H} = \sum_{\mathbf{n}} \varepsilon_{\mathbf{n}} \hat{a}_{\mathbf{n}}^+ \hat{a}_{\mathbf{n}} = \sum_{\mathbf{n}} \varepsilon_{\mathbf{n}} \hat{N}_{\mathbf{n}}, \quad \hat{N}_{\mathbf{n}} \equiv \hat{a}_{\mathbf{n}}^+ \hat{a}_{\mathbf{n}}. \quad (6.98)$$

The many-particle quantum states in the representation of ‘‘occupation numbers’’ are written down as $|\dots N_{\mathbf{n}} \dots\rangle$, where $N_{\mathbf{n}}$ is the number of particles in the \mathbf{n} -th one-particle quantum state. The states $|\dots N_{\mathbf{n}} \dots\rangle$ are defined as the eigenstates of the operator of the number of particles in the \mathbf{n} -th state $\hat{N}_{\mathbf{n}}$:

$$\hat{N}_{\mathbf{n}} |\dots N_{\mathbf{n}} \dots\rangle = N_{\mathbf{n}} |\dots N_{\mathbf{n}} \dots\rangle. \quad (6.99)$$

Let us determine a set of quantum states with a *finite* total number of particles

$$\sum_{\mathbf{n}} N_{\mathbf{n}} = N \quad (6.100)$$

as follows:

$$|\dots N_{\mathbf{n}} \dots\rangle_{\sum_{\mathbf{n}} N_{\mathbf{n}}=N} \equiv |\Psi_{N, \{N_{\mathbf{n}}\}}\rangle. \quad (6.101)$$

Further on, we use the basis set of quantum states (6.101) for the derivation of the partition function, of the density function and of the two-point correlation function.

Partition function

The density matrix of the *canonical* Hibbs ensemble is

$$\hat{\rho} = \exp\left(-\beta \hat{H}\right), \quad \beta \equiv \frac{1}{k_B T}.$$

The partition function of this ensemble is the trace of the density matrix on the set of quantum states (6.101):

$$\begin{aligned} \mathbb{Z}_I(\beta|N) &= \sum_{\{N_{\mathbf{n}}\}} \left\langle \Psi_{N, \{N_{\mathbf{n}}\}} \left| \exp\left(-\beta \hat{H}\right) \right| \Psi_{N, \{N_{\mathbf{n}}\}} \right\rangle \\ &= \left[\sum_{\{N_{\mathbf{n}}\}} \exp\left(-\beta \sum_{\mathbf{n}} \varepsilon_{\mathbf{n}} N_{\mathbf{n}}\right) \right]_{\sum_{\mathbf{n}} N_{\mathbf{n}}=N}. \end{aligned} \quad (6.102)$$

This expression can be written down also in the form

$$\mathbb{Z}_I(\beta|N) = \sum_{\{N_{\mathbf{n}}\}} \exp\left(-\beta \sum_{\mathbf{n}} \varepsilon_{\mathbf{n}} N_{\mathbf{n}}\right) \delta_{N, \sum_{\mathbf{n}} N_{\mathbf{n}}}, \quad (6.103)$$

where

$$\delta_{j,k} = \begin{cases} 1, & j = k \\ 0, & j \neq k \end{cases}$$

is the delta symbol.

Let us introduce the generating function for the partition function in the same way as in Ref. [101]:

$$\begin{aligned} \Xi(\beta, u) &= \sum_{N=0}^{\infty} u^N \mathbb{Z}_I(\beta|N) = \sum_{N=0}^{\infty} u^N \sum_{\{N_{\mathbf{n}}\}} \exp\left(-\beta \sum_{\mathbf{n}} \varepsilon_{\mathbf{n}} N_{\mathbf{n}}\right) \delta_{N, \sum_{\mathbf{n}} N_{\mathbf{n}}} \\ &= \sum_{\{N_{\mathbf{n}}\}} \exp\left(-\beta \sum_{\mathbf{n}} \varepsilon_{\mathbf{n}} N_{\mathbf{n}}\right) \sum_{N=0}^{\infty} u^{\sum_{\mathbf{n}} N_{\mathbf{n}}} \delta_{N, \sum_{\mathbf{n}} N_{\mathbf{n}}} \\ &= \sum_{\{N_{\mathbf{n}}\}} \exp\left(-\beta \sum_{\mathbf{n}} \varepsilon_{\mathbf{n}} N_{\mathbf{n}}\right) u^{\sum_{\mathbf{n}} N_{\mathbf{n}}} \implies \\ \Xi(\beta, u) &= \prod_{\mathbf{n}} \left\{ \sum_{N_{\mathbf{n}}} [u \exp(-\beta \varepsilon_{\mathbf{n}})]^{N_{\mathbf{n}}} \right\}. \end{aligned} \quad (6.104)$$

Fermions

For fermions, the number $N_{\mathbf{n}}$ can take only values $N_{\mathbf{n}} = 0$ and $N_{\mathbf{n}} = 1$. Hence, for fermions (denoted by the index F), we obtain:

$$\Xi_F(\beta, u) = \prod_{\mathbf{n}} [1 + u \exp(-\beta \varepsilon_{\mathbf{n}})].$$

Since the n -th level of a 3D oscillator is degenerate with the degeneracy

$$g(n) = \frac{(n+1)(n+2)}{2},$$

we find that the generating function $\Xi_F(\beta, u)$ is given by

$$\Xi_F(\beta, u) = \prod_{n=0}^{\infty} [1 + u \exp(-\beta \varepsilon_n)]^{g(n)}. \quad (6.105)$$

Bosons

For bosons (denoted by the index B), $N_{\mathbf{n}} = 0, 1, \dots, \infty$. The summations over $\{N_{\mathbf{n}}\}$ in Eq. (6.104) gives:

$$\Xi_B(\beta, u) = \prod_{n=0}^{\infty} \left[\frac{1}{1 - u \exp(-\beta \varepsilon_n)} \right]^{g(n)}. \quad (6.106)$$

The results (6.104) and (6.106) prove (for the partition function) the equivalence of the path-integral approach for identical particles [101] and of the second-quantization method.

Integral representation

Let us use the Fourier representation for the delta symbol:

$$\delta_{N, \sum_{\mathbf{n}} N_{\mathbf{n}}} = \frac{1}{2\pi} \int_0^{2\pi} \exp \left[i \left(\sum_{\mathbf{n}} N_{\mathbf{n}} - N \right) (\theta - i\zeta) \right] d\theta, \quad (6.107)$$

where ζ is an arbitrary constant. Substituting Eq. (6.107) into Eq. (6.103) we obtain

$$\begin{aligned} \mathbb{Z}_I(\beta|N) &= \sum_{\{N_{\mathbf{n}}\}} \exp \left(-\beta \sum_{\mathbf{n}} \varepsilon_{\mathbf{n}} N_{\mathbf{n}} \right) \frac{1}{2\pi} \int_0^{2\pi} \exp \left[i \left(\sum_{\mathbf{n}} N_{\mathbf{n}} - N \right) (\theta - i\zeta) \right] d\theta \\ &= \frac{1}{2\pi} \int_0^{2\pi} d\theta \exp [-iN(\theta - i\zeta)] \sum_{\{N_{\mathbf{n}}\}} \exp \left(-\beta \sum_{\mathbf{n}} \varepsilon_{\mathbf{n}} N_{\mathbf{n}} + i \sum_{\mathbf{n}} N_{\mathbf{n}} (\theta - i\zeta) \right) \\ &= \frac{1}{2\pi} \int_0^{2\pi} d\theta \exp (-iN\theta - N\zeta) \Xi(\beta, e^{i\theta+\zeta}) \implies \\ \mathbb{Z}_I(\beta|N) &= \frac{1}{2\pi} \int_0^{2\pi} d\theta \exp [\ln \Xi(\beta, e^{i\theta+\zeta}) - N\zeta - iN\theta]. \end{aligned} \quad (6.108)$$

The partition function for a finite number of particles can be obtained from the generation function also by the inversion formula [102]

$$\mathbb{Z}_I(\beta|N) = \frac{1}{2\pi i} \oint \frac{\Xi(\beta, z)}{z^{N+1}} dz \quad (6.109)$$

$$= \frac{1}{2\pi} \int_0^{2\pi} e^{[\ln \Xi(\beta, u e^{i\theta}) - N \ln u]} e^{-iN\theta} d\theta. \quad (6.110)$$

Let us denote in Eq. (6.108):

$$\zeta \equiv \ln u. \quad (6.111)$$

In these notations, Eqs. (6.108) and (6.110) are *identical*. For the numerical calculation, it is more convenient to choose in Eq. (6.107) the interval of the integration over θ as $[-\pi, \pi]$

instead of $[0, 2\pi]$, what gives:

$$\mathbb{Z}_I(\beta|N) = \frac{1}{2\pi} \int_{-\pi}^{\pi} \Phi_N(\theta) d\theta, \quad (6.112)$$

with the function

$$\Phi_N(\theta) = \exp[\ln \Xi(\beta, ue^{i\theta}) - N \ln u - iN\theta]. \quad (6.113)$$

The aforesaid method of derivation of the partition function [Eqs. (6.107) to (6.108)] is heuristically useful, because it allows a simple generalization to spin-mixed systems with various polarization distributions.

The two-point density-density correlation function in the operator formalism is

$$\tilde{g}(\mathbf{q}, \tau | \{N_\sigma\}, \beta) = \langle \hat{\rho}_{\mathbf{q}}(\tau) \hat{\rho}_{-\mathbf{q}}(0) \rangle, \quad (6.114)$$

where $\hat{\rho}_{\mathbf{q}}(t)$ is the density operator in the Heisenberg representation:

$$\hat{\rho}_{\mathbf{q}}(\tau) = \exp\left(\frac{\tau}{\hbar} \hat{H}\right) \rho_{\mathbf{q}} \exp\left(-\frac{\tau}{\hbar} \hat{H}\right). \quad (6.115)$$

In the ‘‘second-quantization’’ representation, $\hat{\rho}_{\mathbf{q}}(t)$ is

$$\begin{aligned} \hat{\rho}_{\mathbf{q}}(\tau) &= \sum_{\mathbf{n}, \mathbf{n}'} (e^{i\mathbf{q} \cdot \hat{\mathbf{x}}})_{\mathbf{nn}'} \hat{a}_{\mathbf{n}}^+(\tau) \hat{a}_{\mathbf{n}'}(\tau) \\ &= \sum_{\mathbf{n}, \mathbf{n}'} (e^{i\mathbf{q} \cdot \hat{\mathbf{x}}})_{\mathbf{nn}'} \hat{a}_{\mathbf{n}}^+ \hat{a}_{\mathbf{n}'} \exp\left[\frac{\tau}{\hbar} (\varepsilon_{\mathbf{n}} - \varepsilon_{\mathbf{n}'})\right]. \end{aligned} \quad (6.116)$$

After substituting Eq. (6.116) into (6.114), we find that

$$\tilde{g}(\mathbf{q}, \tau | \{N_\sigma\}, \beta) = \sum_{\mathbf{n}, \mathbf{n}'} \sum_{\mathbf{m}, \mathbf{m}'} (e^{i\mathbf{q} \cdot \hat{\mathbf{x}}})_{\mathbf{nn}'} (e^{-i\mathbf{q} \cdot \hat{\mathbf{x}}})_{\mathbf{mm}'} \exp\left[\frac{\tau}{\hbar} (\varepsilon_{\mathbf{n}} - \varepsilon_{\mathbf{n}'})\right] \langle \hat{a}_{\mathbf{n}}^+ \hat{a}_{\mathbf{n}'} \hat{a}_{\mathbf{m}}^+ \hat{a}_{\mathbf{m}'} \rangle. \quad (6.117)$$

The operator $\hat{a}_{\mathbf{n}}^+ \hat{a}_{\mathbf{n}'} \hat{a}_{\mathbf{m}}^+ \hat{a}_{\mathbf{m}'}$ has non-zero diagonal matrix elements in the basis of quantum states $|\Psi_{N, \{N_{\mathbf{n}}\}}\rangle$ only in the cases

$$\left\{ \begin{array}{l} \mathbf{n} = \mathbf{n}' \\ \mathbf{m} = \mathbf{m}' \end{array} \right\} \quad \text{or} \quad \left\{ \begin{array}{l} \mathbf{n} = \mathbf{m}' \\ \mathbf{m} = \mathbf{n}' \end{array} \right\}. \quad (6.118)$$

Hence, the average

$$\langle \hat{a}_{\mathbf{n}}^+ \hat{a}_{\mathbf{n}'} \hat{a}_{\mathbf{m}}^+ \hat{a}_{\mathbf{m}'} \rangle = \frac{1}{\mathbb{Z}_I(\beta|N)} \sum_{\{N_{\mathbf{n}}\}} \langle \Psi_{N, \{N_{\mathbf{n}}\}} | \exp(-\beta \hat{H}) \hat{a}_{\mathbf{n}}^+ \hat{a}_{\mathbf{n}'} \hat{a}_{\mathbf{m}}^+ \hat{a}_{\mathbf{m}'} | \Psi_{N, \{N_{\mathbf{n}}\}} \rangle \quad (6.119)$$

is not equal to zero only when the condition (6.118) is fulfilled. This allows us to write down the average (6.119) as

$$\begin{aligned}
\langle \hat{a}_{\mathbf{n}}^+ \hat{a}_{\mathbf{n}'} \hat{a}_{\mathbf{m}}^+ \hat{a}_{\mathbf{m}'} \rangle &= \delta_{\mathbf{n}'\mathbf{n}} \delta_{\mathbf{m}'\mathbf{m}} (1 - \delta_{\mathbf{mn}}) \langle \hat{a}_{\mathbf{n}}^+ \hat{a}_{\mathbf{n}} \hat{a}_{\mathbf{m}}^+ \hat{a}_{\mathbf{m}} \rangle + \delta_{\mathbf{m}'\mathbf{n}} \delta_{\mathbf{n}'\mathbf{m}} (1 - \delta_{\mathbf{mn}}) \langle \hat{a}_{\mathbf{n}}^+ \hat{a}_{\mathbf{m}} \hat{a}_{\mathbf{m}}^+ \hat{a}_{\mathbf{n}} \rangle \\
&+ \delta_{\mathbf{n}'\mathbf{n}} \delta_{\mathbf{m}'\mathbf{m}} \delta_{\mathbf{mn}} \langle \hat{a}_{\mathbf{n}}^+ \hat{a}_{\mathbf{n}} \hat{a}_{\mathbf{n}}^+ \hat{a}_{\mathbf{n}} \rangle \\
&= \delta_{\mathbf{n}'\mathbf{n}} \delta_{\mathbf{m}'\mathbf{m}} (1 - \delta_{\mathbf{mn}}) \langle \hat{N}_{\mathbf{n}} \hat{N}_{\mathbf{m}} \rangle + \delta_{\mathbf{m}'\mathbf{n}} \delta_{\mathbf{n}'\mathbf{m}} (1 - \delta_{\mathbf{mn}}) \left(\langle \hat{N}_{\mathbf{n}} \rangle - \langle \hat{N}_{\mathbf{n}} \hat{N}_{\mathbf{m}} \rangle \right) \\
&+ \delta_{\mathbf{n}'\mathbf{n}} \delta_{\mathbf{m}'\mathbf{m}} \delta_{\mathbf{mn}} \bar{N}_{\mathbf{n}} \\
&= \delta_{\mathbf{n}'\mathbf{n}} \delta_{\mathbf{m}'\mathbf{m}} \langle \hat{N}_{\mathbf{n}} \hat{N}_{\mathbf{m}} \rangle + \delta_{\mathbf{m}'\mathbf{n}} \delta_{\mathbf{n}'\mathbf{m}} \langle \hat{N}_{\mathbf{n}} (1 - \hat{N}_{\mathbf{m}}) \rangle.
\end{aligned} \tag{6.120}$$

Here, the notation is used for the average occupation number $\bar{N}_{\mathbf{n}}$:

$$\langle \hat{N}_{\mathbf{n}} \rangle = \frac{1}{\mathbb{Z}_I(\beta|N)} \sum_{\{N_{\mathbf{n}}\}} \langle \Psi_{N, \{N_{\mathbf{n}}\}} | \exp(-\beta \hat{H}) \hat{N}_{\mathbf{n}} | \Psi_{N, \{N_{\mathbf{n}}\}} \rangle. \tag{6.121}$$

$$\begin{aligned}
\mathbb{Z}_I(\beta|N) &= \sum_{\{N_{\mathbf{n}}\}} \langle \Psi_{N, \{N_{\mathbf{n}}\}} | \exp(-\beta \hat{H}) | \Psi_{N, \{N_{\mathbf{n}}\}} \rangle \\
&= \left[\sum_{\{N_{\mathbf{n}}\}} \exp\left(-\beta \sum_{\mathbf{n}} \varepsilon_{\mathbf{n}} N_{\mathbf{n}}\right) \right]_{\sum_{\mathbf{n}} N_{\mathbf{n}}=N}.
\end{aligned} \tag{6.122}$$

In the same way as Eq. (6.102), the average (6.121) can be written down in the form

$$\begin{aligned}
\langle \hat{N}_{\mathbf{n}} \rangle &= \frac{1}{\mathbb{Z}_I(\beta|N)} \left[\sum_{\{N_{\mathbf{n}'}\}} N_{\mathbf{n}} \exp\left(-\beta \sum_{\mathbf{n}'} \varepsilon_{\mathbf{n}'} N_{\mathbf{n}'}\right) \right]_{\sum_{\mathbf{n}'} N_{\mathbf{n}'}=N}. \\
\langle \hat{N}_{\mathbf{n}} \rangle &= -\frac{1}{\beta \mathbb{Z}_I(\beta|N)} \frac{\delta \mathbb{Z}_I(\beta|N)}{\delta \varepsilon_{\mathbf{n}}}, \\
\langle \hat{N}_{\mathbf{n}} \rangle &= \frac{1}{2\pi \mathbb{Z}_I(\beta|N)} \int_{-\pi}^{\pi} \frac{\Phi_N(\theta)}{\exp(\beta \varepsilon_{\mathbf{n}} - \zeta - i\theta) + 1} d\theta.
\end{aligned} \tag{6.123}$$

Since $\varepsilon_{\mathbf{n}} = \varepsilon_n$, $\langle \hat{N}_{\mathbf{n}} \rangle$ depends only on n .

Using Eq. (6.111), we can write \bar{N}_n as

$$\begin{aligned}
\langle \hat{N}_{\mathbf{n}} \rangle &= \frac{1}{2\pi \mathbb{Z}_I(\beta|N)} \int_{-\pi}^{\pi} \frac{\Phi_N(\theta)}{\frac{1}{u} \exp(\beta \varepsilon_n - i\theta) + 1} d\theta \\
&= \frac{1}{2\pi \mathbb{Z}_I(\beta|N)} \int_{-\pi}^{\pi} \frac{\exp[\ln \Xi(\beta, u e^{i\theta}) - N \ln u - iN\theta]}{\frac{1}{u} \exp(\beta \varepsilon_n - i\theta) + 1} d\theta \\
&= \frac{1}{2\pi \mathbb{Z}_I(\beta|N)} \int_{-\pi}^{\pi} \frac{\Xi(\beta, u e^{i\theta}) \exp[-i\theta(N-1) - \beta \varepsilon_n]}{u^{N-1} (1 + u \exp(i\theta - \beta \varepsilon_n))} d\theta.
\end{aligned} \tag{6.124}$$

The averages $\langle \hat{N}_{\mathbf{n}} \hat{N}_{\mathbf{m}} \rangle$ for $\mathbf{m} \neq \mathbf{n}$ can be also expressed in terms of the integral representation:

$$\begin{aligned}
\langle \hat{N}_{\mathbf{n}} \hat{N}_{\mathbf{m}} \rangle \Big|_{\mathbf{m} \neq \mathbf{n}} &= \frac{1}{\mathbb{Z}_I(\beta|N)} \sum_{\{N_{\mathbf{n}}\}} \left\langle \Psi_{N, \{N_{\mathbf{n}}\}} \left| \exp(-\beta \hat{H}) \hat{N}_{\mathbf{n}} \hat{N}_{\mathbf{m}} \right| \Psi_{N, \{N_{\mathbf{n}}\}} \right\rangle \Big|_{\mathbf{m} \neq \mathbf{n}} \\
&= \frac{1}{\mathbb{Z}_I(\beta|N)} \left[\sum_{\{N_{\mathbf{n}'}\}} N_{\mathbf{n}} N_{\mathbf{m}} \exp\left(-\beta \sum_{\mathbf{n}'} \varepsilon_{\mathbf{n}'} N_{\mathbf{n}'}\right) \right]_{\sum_{\mathbf{n}'} N_{\mathbf{n}'} = N, \quad \mathbf{m} \neq \mathbf{n}} \\
&= \frac{1}{\mathbb{Z}_I(\beta|N) \beta^2} \frac{\delta^2 \mathbb{Z}_I(\beta|N)}{\delta \varepsilon_{\mathbf{m}} \delta \varepsilon_{\mathbf{n}}} \\
&= \frac{1}{\mathbb{Z}_I(\beta|N) \beta^2} \frac{\delta^2}{\delta \varepsilon_{\mathbf{m}} \delta \varepsilon_{\mathbf{n}}} \left(\frac{1}{2\pi} \int_0^{2\pi} d\theta \exp[\ln \Xi(\beta, e^{i\theta+\zeta}) - N\zeta - iN\theta] \right) \Rightarrow
\end{aligned}$$

We obtain the integral representation for the average of the product of operators $\hat{N}_{\mathbf{n}} \hat{N}_{\mathbf{m}}$ for $\mathbf{m} \neq \mathbf{n}$:

$$\langle \hat{N}_{\mathbf{n}} \hat{N}_{\mathbf{m}} \rangle \Big|_{\mathbf{m} \neq \mathbf{n}} = \frac{1}{2\pi \mathbb{Z}_I(N)} \int_{-\pi}^{\pi} \frac{\Phi_N(\theta)}{[\exp(\beta \varepsilon_{\mathbf{n}} - \zeta - i\theta) + 1][\exp(\beta \varepsilon_{\mathbf{m}} - \zeta - i\theta) + 1]} d\theta. \quad (6.125)$$

Let us introduce the notation

$$f(\varepsilon, \theta) \equiv \frac{1}{\exp(\beta \varepsilon - \zeta - i\theta) + 1}, \quad (6.126)$$

which formally coincides with the Fermi distribution function of the energy ε with the “chemical potential” $(\zeta + i\theta)/\beta$. Using this notation, the averages (6.123) and (6.125) can be written down in the form

$$\langle \hat{N}_{\mathbf{n}} \rangle = \frac{1}{2\pi \mathbb{Z}_I(\beta|N)} \int_{-\pi}^{\pi} f(\varepsilon_{\mathbf{n}}, \theta) \Phi_N(\theta) d\theta, \quad (6.127)$$

$$\langle \hat{N}_{\mathbf{n}} \hat{N}_{\mathbf{m}} \rangle \Big|_{\mathbf{m} \neq \mathbf{n}} = \frac{1}{2\pi \mathbb{Z}_I(N)} \int_{-\pi}^{\pi} f(\varepsilon_{\mathbf{n}}, \theta) f(\varepsilon_{\mathbf{m}}, \theta) \Phi_N(\theta) d\theta. \quad (6.128)$$

We can develop the aforesaid procedure for the average of a product of any number of operators $\hat{N}_{\mathbf{n}_1} \hat{N}_{\mathbf{n}_2} \dots \hat{N}_{\mathbf{n}_K}$, where all quantum numbers $\mathbf{n}_1, \mathbf{n}_2, \dots, \mathbf{n}_K$ are *different*. The result is:

$$\langle \hat{N}_{\mathbf{n}_1} \hat{N}_{\mathbf{n}_2} \dots \hat{N}_{\mathbf{n}_K} \rangle \Big|_{\mathbf{n}_j \neq \mathbf{n}_l} = \frac{1}{2\pi \mathbb{Z}_I(N)} \int_{-\pi}^{\pi} f(\varepsilon_{\mathbf{n}_1}, \theta) f(\varepsilon_{\mathbf{n}_2}, \theta) \dots f(\varepsilon_{\mathbf{n}_K}, \theta) \Phi_N(\theta) d\theta. \quad (6.129)$$

It should be emphasized, that all expressions above [including Eq. (6.129)] are derived for a *canonical* Hibbs ensemble (i. e., for a fixed number of particles) and for both closed-shell and open-shell systems.

Let us substitute the average (6.120) into the correlation function $\tilde{g}(\mathbf{q}, \tau | \{N_\sigma\}, \beta)$:

$$\begin{aligned} \tilde{g}(\mathbf{q}, \tau | \{N_\sigma\}, \beta) &= \sum_{\mathbf{n}, \mathbf{n}'} \sum_{\mathbf{m}, \mathbf{m}'} (e^{i\mathbf{q}\cdot\hat{\mathbf{x}}})_{\mathbf{nn}'} (e^{-i\mathbf{q}\cdot\hat{\mathbf{x}}})_{\mathbf{mm}'} \exp\left[\frac{\tau}{\hbar}(\varepsilon_{\mathbf{n}} - \varepsilon_{\mathbf{n}'})\right] \\ &\quad \times \left(\delta_{\mathbf{n}'\mathbf{n}} \delta_{\mathbf{m}'\mathbf{m}} \langle \hat{N}_{\mathbf{n}} \hat{N}_{\mathbf{m}} \rangle + \delta_{\mathbf{m}'\mathbf{n}} \delta_{\mathbf{n}'\mathbf{m}} \langle \hat{N}_{\mathbf{n}} (1 - \hat{N}_{\mathbf{m}}) \rangle \right) \end{aligned}$$

\Rightarrow

$$\begin{aligned} \tilde{g}(\mathbf{q}, \tau | \{N_\sigma\}, \beta) &= \sum_{\mathbf{n}, \mathbf{m}} (e^{i\mathbf{q}\cdot\hat{\mathbf{x}}})_{\mathbf{nn}} (e^{-i\mathbf{q}\cdot\hat{\mathbf{x}}})_{\mathbf{mm}} \langle \hat{N}_{\mathbf{n}} \hat{N}_{\mathbf{m}} \rangle \\ &\quad + \sum_{\mathbf{n}, \mathbf{m}} |(e^{i\mathbf{q}\cdot\hat{\mathbf{x}}})_{\mathbf{nm}}|^2 \exp\left[\frac{\tau}{\hbar}(\varepsilon_{\mathbf{n}} - \varepsilon_{\mathbf{m}})\right] \langle \hat{N}_{\mathbf{n}} (1 - \hat{N}_{\mathbf{m}}) \rangle. \end{aligned} \quad (6.130)$$

The matrix elements $(e^{i\mathbf{q}\cdot\hat{\mathbf{x}}})_{\mathbf{nm}}$ has the following form

$$(e^{i\mathbf{q}\cdot\hat{\mathbf{x}}})_{\mathbf{nm}} = \langle m_1 | e^{iq_1 \hat{x}_1} | n_1 \rangle \langle m_2 | e^{iq_2 \hat{x}_2} | n_2 \rangle \langle m_3 | e^{iq_3 \hat{x}_3} | n_3 \rangle,$$

where $\langle m | e^{iq\hat{x}} | n \rangle$ is the matrix element of a one-dimensional oscillator with the frequency w :

$$\begin{aligned} \langle m | e^{iq\hat{x}} | n \rangle &= \exp\left(-\frac{\gamma^2}{2}\right) (i\gamma)^{n_>-n_<} \sqrt{\frac{n_<!}{n_>!}} L_{n_<}^{(n_>-n_<)}(\gamma^2), \\ &\quad \begin{cases} n_> \equiv \max(n, m); \\ n_< \equiv \min(n, m), \end{cases} \end{aligned} \quad (6.131)$$

$\gamma \equiv q\sqrt{\frac{\hbar}{2mw}}$, $|n\rangle$ are the quantum states of the one-dimensional oscillator with the frequency w , $L_n^{(\alpha)}(z)$ is the generalized Laguerre polynomial.

System with mixed spins

The correlation functions for a system with mixed spins can be explicitly derived by the generalization of Eqs. (6.112) and (6.129) to the case of the particles with the non-zero spin. We use the fact, that the derivation of Eqs. (6.112) and (6.129), performed in this section,

does not depend on the concrete form of the energy spectrum $\varepsilon_{\mathbf{n}}$. Hence, in the formulae, derived above, the replacement should be made:

$$|\mathbf{n}\rangle \rightarrow |\mathbf{n}, \sigma\rangle, \quad \hat{N}_{\mathbf{n}} \rightarrow \hat{N}_{\mathbf{n}, \sigma} = a_{\mathbf{n}, \sigma}^+ a_{\mathbf{n}, \sigma}, \quad (6.132)$$

where σ is the electron spin projection. Consequently, the matrix elements $(e^{i\mathbf{q}\cdot\hat{\mathbf{x}}})_{\mathbf{mn}}$ are replaced by

$$(e^{i\mathbf{q}\cdot\hat{\mathbf{x}}})_{\mathbf{mn}} \rightarrow \langle \mathbf{m}, \sigma | e^{i\mathbf{q}\cdot\hat{\mathbf{x}}} | \mathbf{n}, \sigma' \rangle = \delta_{\sigma\sigma'} (e^{i\mathbf{q}\cdot\hat{\mathbf{x}}})_{\mathbf{mn}}. \quad (6.133)$$

Taking into account Eqs. (6.132) and (6.133), the two-point correlation function (6.130) becomes

$$\begin{aligned} \tilde{g}(\mathbf{q}, \tau | \{N_{\sigma}\}, \beta) &= \sum_{\mathbf{n}, \mathbf{m}} \sum_{\sigma_1, \sigma_2} (e^{i\mathbf{q}\cdot\hat{\mathbf{x}}})_{\mathbf{mn}} (e^{-i\mathbf{q}\cdot\hat{\mathbf{x}}})_{\mathbf{mm}} \langle \hat{N}_{\mathbf{n}, \sigma_1} \hat{N}_{\mathbf{m}, \sigma_2} \rangle \\ &+ \sum_{\mathbf{n}, \mathbf{m}} \sum_{\sigma} |(e^{i\mathbf{q}\cdot\hat{\mathbf{x}}})_{\mathbf{nm}}|^2 \exp\left[\frac{\tau}{\hbar}(\varepsilon_{\mathbf{n}} - \varepsilon_{\mathbf{m}})\right] \langle \hat{N}_{\mathbf{n}, \sigma} (1 - \hat{N}_{\mathbf{m}, \sigma}) \rangle. \end{aligned} \quad (6.134)$$

The averages $\langle \hat{N}_{\mathbf{n}, \sigma} \rangle$ and $\langle \hat{N}_{\mathbf{n}, \sigma_1} \hat{N}_{\mathbf{m}, \sigma_2} \rangle$ are, respectively, one-particle and two-particle distribution functions,

$$\langle \hat{N}_{\mathbf{n}, \sigma} \rangle \equiv f_1(n, \sigma | N_{\sigma}, \beta), \quad (6.135)$$

$$\langle \hat{N}_{\mathbf{n}, \sigma} \hat{N}_{\mathbf{n}', \sigma'} \rangle \equiv f_2(n, \sigma; n', \sigma' | \{N_{\sigma}\}, \beta). \quad (6.136)$$

The one-electron distribution function $f_1(n, \sigma | N_{\sigma}, \beta)$ is the average number of electrons with the spin projection σ at the n -th energy level, while the two-electron distribution function $f_2(n, \sigma; n', \sigma' | \{N_{\sigma}\}, \beta)$ is the average product of the numbers of electrons with the spin projections σ and σ' at the levels n and n' . These functions are expressed through the following integrals [see (6.127), (6.128)]:

$$f_1(n, \sigma | N_{\sigma}, \beta) = \frac{1}{2\pi\mathcal{Z}_F(N_{\sigma}, w, \beta)} \int_{-\pi}^{\pi} f(\varepsilon_n, \theta) \Phi(\theta, \beta, N_{\sigma}) d\theta, \quad (6.137)$$

$$f_2(n, \sigma; n', \sigma' | \{N_{\sigma}\}, \beta) = \begin{cases} \frac{1}{2\pi\mathcal{Z}_F(N_{\sigma}, w, \beta)} \int_{-\pi}^{\pi} f(\varepsilon_n, \theta) f(\varepsilon_{n'}, \theta) \Phi(\theta, \beta, N_{\sigma}) d\theta, & \text{if } \sigma' = \sigma; \\ f_1(n, \sigma | N_{\sigma}, \beta) f_1(n, \sigma' | N_{\sigma'}, \beta), & \text{if } \sigma' \neq \sigma \end{cases} \quad (6.138)$$

with the notations

$$\Phi(\theta, \beta, N_{\sigma}) = \exp\left[\sum_{n=0}^{\infty} \ln(1 + e^{i\theta + \xi - \beta\varepsilon_n}) - N_{\sigma}(\xi + i\theta)\right], \quad (6.139)$$

$$f(\varepsilon, \theta) \equiv \frac{1}{\exp(\beta\varepsilon - \xi - i\theta) + 1}. \quad (6.140)$$

The function $f(\varepsilon, \theta)$ formally coincides with the Fermi-Dirac distribution function of the energy ε with the “chemical potential” $(\xi + i\theta)/\beta$.

Here we consider the zero-temperature limit, for which the integrals (6.137) and (6.138) can be calculated analytically. The result for the one-electron distribution function is

$$f_1(n, \sigma | \beta, N_\sigma) |_{\beta \rightarrow \infty} = \begin{cases} 1, & n < L_\sigma; \\ 0, & n > L_\sigma; \\ \frac{N_\sigma - N_{L_\sigma}}{g_{L_\sigma}}, & n = L_\sigma. \end{cases} \quad (6.141)$$

According to (6.141), L_σ is the number of the lowest open shell, and

$$g_n = \begin{cases} \frac{1}{2}(n+1)(n+2) & (3D), \\ n+1 & (2D). \end{cases}$$

is the degeneracy of the n -th shell. N_{L_σ} is the number of electrons in all the closed shells with the spin projection σ ,

$$N_{L_\sigma} \equiv \sum_{n=0}^{L_\sigma-1} g_n = \begin{cases} \frac{1}{6}L_\sigma(L_\sigma+1)(L_\sigma+2) & (3D), \\ \frac{1}{2}L_\sigma(L_\sigma+1) & (2D). \end{cases} \quad (6.142)$$

The two-electron distribution function $f_2(n, \sigma; n', \sigma' | \{N_\sigma\}, \beta)$ at $T = 0$ takes the form

$$f_2(n, \sigma; n', \sigma' | \beta, \{N_\sigma\}) |_{\beta \rightarrow \infty} = \begin{cases} f_1(n, \sigma | \beta, N_\sigma) |_{\beta \rightarrow \infty} f_1(n', \sigma' | \beta, N_{\sigma'}) |_{\beta \rightarrow \infty}, & n \neq n' \text{ or } \sigma \neq \sigma' \\ 1, & \sigma = \sigma' \text{ and } n = n' < L_\sigma; \\ 0, & \sigma = \sigma' \text{ and } n = n' > L_\sigma; \\ \frac{N_\sigma - N_{L_\sigma}}{g_{L_\sigma}} \frac{N_\sigma - N_{L_\sigma} - 1}{g_{L_\sigma - 1}}, & \sigma = \sigma' \text{ and } n = n' = L_\sigma. \end{cases} \quad (6.143)$$

In summary, we have obtained the following expression for $\tilde{g}(\mathbf{q}, \tau | \{N_\sigma\}, \beta)$:

$$\begin{aligned} \tilde{g}(\mathbf{q}, \tau | \{N_\sigma\}, \beta) &= \sum_{\mathbf{n}, \sigma, \mathbf{n}', \sigma'} (e^{i\mathbf{q}\cdot\mathbf{x}})_{\mathbf{nn}} (e^{-i\mathbf{q}\cdot\mathbf{x}})_{\mathbf{n}'\mathbf{n}'} f_2(n, \sigma; n', \sigma' | \{N_\sigma\}, \beta) \\ &+ \sum_{\mathbf{n}, \mathbf{n}', \sigma} |(e^{i\mathbf{q}\cdot\mathbf{x}})_{\mathbf{nn}'}|^2 \exp\left[\frac{\tau}{\hbar}(\varepsilon_n - \varepsilon_{n'})\right] \\ &\times [f_1(n, \sigma | \{N_\sigma\}, \beta) - f_2(n, \sigma; n', \sigma' | \{N_\sigma\}, \beta)]. \end{aligned} \quad (6.144)$$

This formula is valid for both closed and open shells. The correlation functions derived in this subsection are used both for the calculation of the ground-state energy and, as shown

below, for the calculation of the optical conductivity of an N -polaron system in a quantum dot.

E. Many-polaron ground state in a quantum dot: extrapolation to the homogeneous limit and comparison to the results for a polaron gas in bulk [90]

The correlation function given by Eq. (6.144) can be subdivided as

$$\tilde{g}(\mathbf{q}, \tau | \{N_\sigma\}, \beta) = \tilde{g}_1(\mathbf{q}, \tau | \{N_\sigma\}, \beta) + \tilde{g}_2(\mathbf{q}, \tau | \{N_\sigma\}, \beta), \quad (6.145)$$

with

$$\begin{aligned} \tilde{g}_1(\mathbf{q}, \tau | \{N_\sigma\}, \beta) &\equiv \sum_{\mathbf{n}, \mathbf{n}', \sigma} |(e^{i\mathbf{q}\cdot\mathbf{x}})_{\mathbf{nn}'}|^2 \exp\left[\frac{\tau}{\hbar}(\varepsilon_n - \varepsilon_{n'})\right] \\ &\times [f_1(n, \sigma | \{N_\sigma\}, \beta) - f_2(n, \sigma; n', \sigma' | \{N_\sigma\}, \beta)], \end{aligned} \quad (6.146)$$

$$\tilde{g}_2(\mathbf{q}, \tau | \{N_\sigma\}, \beta) \equiv \sum_{\mathbf{n}, \sigma, \mathbf{n}', \sigma'} (e^{i\mathbf{q}\cdot\mathbf{x}})_{\mathbf{nn}'} (e^{-i\mathbf{q}\cdot\mathbf{x}})_{\mathbf{n}'\mathbf{n}'} f_2(n, \sigma; n', \sigma' | \{N_\sigma\}, \beta). \quad (6.147)$$

In accordance with the subdivision (6.145) of the correlation function, we subdivide the Coulomb and polaron contributions:

$$E_C = E_C^{(1)} + E_C^{(2)}, \quad (6.148)$$

$$E_{e-ph} = E_{e-ph}^{(1)} + E_{e-ph}^{(2)}. \quad (6.149)$$

We have numerically checked whether the polaron contribution per particle $E_{e-ph}^{(1)}/N$ tends to a finite value at $N \rightarrow \infty$. In Figs. 14 and 15, we have plotted the polaron contributions $E_{e-ph}^{(1)}/N$ as a function of N for a quantum dot in ZnO and in a polar medium with $\alpha = 5$, $\eta = 0.3$, respectively.⁶ As seen from Fig. 14, the polaron contribution $E_{e-ph}^{(1)}/N$ in ZnO as a function of N oscillates taking expressed maxima for N corresponding to the closed shells $N = 2, 8, 20, 40, \dots$. There exist kinks of $E_{e-ph}^{(1)}/N$ at N corresponding to the half-filled shells, but these kinks are extremely small. In the case of the medium with $\alpha = 5$, $\eta = 0.3$, for $r_s^* = 20$ (what corresponds to the density $n_0 \approx 1.14 \times 10^{18} \text{ cm}^{-3}$), the polaron

⁶Since, as discussed above, for a single polaron only the whole polaron contribution $E_{e-ph} = E_{e-ph}^{(1)} + E_{e-ph}^{(2)}$ has a physical meaning, the plots for $E_{e-ph}^{(1)}$ in Figs. 3 and 4 start from $N = 2$. The total polaron contribution E_{e-ph} for $N = 1$ is plotted below, in Fig. 9.

contribution $E_{e-ph}^{(1)}/N$ oscillates taking maximal values at the numbers of fermions, which correspond to the closed shells for a spin-polarized system with parallel spins.

In Figs. 14 and 15, the dashed curves are the envelopes for local maxima (closed shells) and local minima of $E_{e-ph}^{(1)}/N$. We see that when these envelopes are *extrapolated* to larger number of fermions, the distance between the envelopes decreases. Therefore, the magnitude of the variations of $E_{e-ph}^{(1)}/N$ related to the shell filling diminishes with increasing N , and it is safe to suppose that in the limit of large N , the envelopes tend to one and the same value. That value corresponds to the *homogeneous* (“bulk”) limit $\lim_{N \rightarrow \infty} \left(E_{e-ph}^{(1)}/N \right)$.

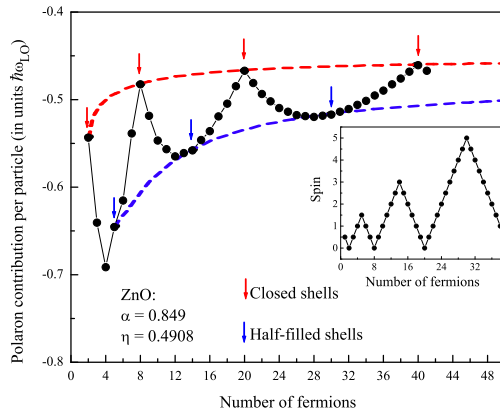


FIG. 14: Polaron contribution $E_{e-ph}^{(1)}/N$ as a function of N for a ZnO quantum dot. The material parameters for ZnO are taken from Ref. [91]. The value $r_s^* = 2$ corresponds to $n_0 = 4.34 \times 10^{19} \text{ cm}^{-2}$. Inset: the total spin as a function of N .

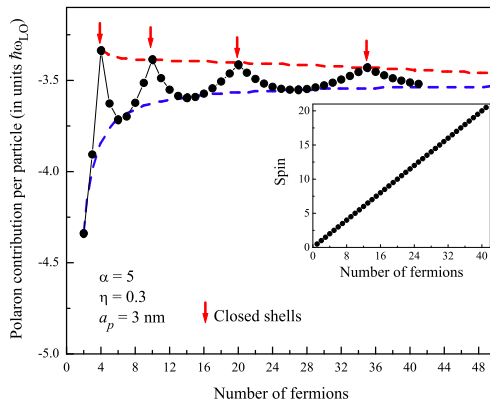


FIG. 15: Polaron contribution $E_{e-ph}^{(1)}/N$ as a function of N for a quantum dot of a polar medium with $\alpha = 5$, $\eta = 0.3$. The value $r_s^* = 20$ corresponds to $n_0 = 1.14 \times 10^{18} \text{ cm}^{-3}$. Inset: the total spin as a function of N .

In Fig. 16, we compare the polaron contribution $E_{e-ph}^{(1)}/N$ calculated within our variational path-integral method for different numbers of fermions with the polaron contribution to the ground-state energy per particle for a polaron gas in bulk, calculated (i) in Ref. [103] within an intermediate-coupling approach (the thin solid curve), (ii) in Ref. [104], using a variational approach developed first in Ref. [91]. As seen from this figure, our all-coupling

variational method provides lower values for the polaron contribution than those obtained in Refs. [103, 104]. The difference between the polaron contribution calculated within our method and that of Ref. [103] is smaller at low densities and increases in magnitude with increasing density. The difference between the polaron contribution calculated within our method and that of Ref. [104] very slightly depends on the density. The result of Ref. [104] becomes closer to our result only at high densities.

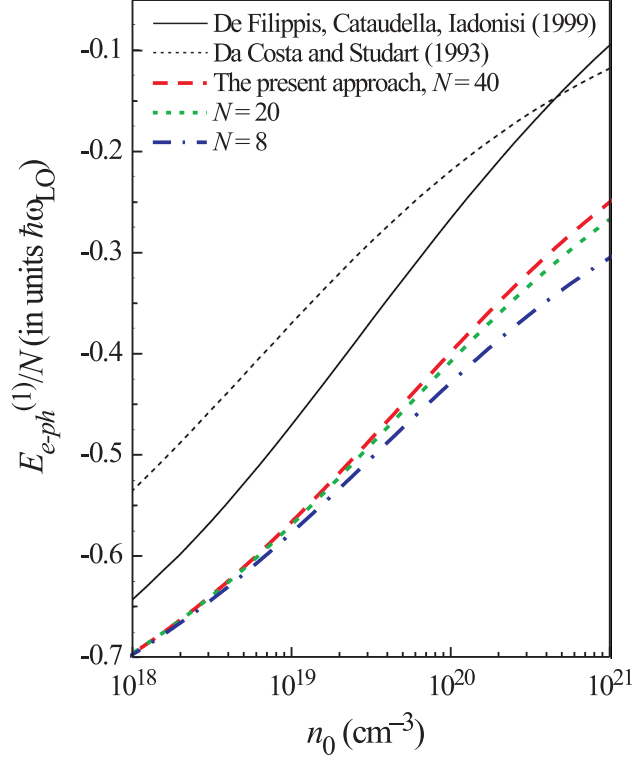


FIG. 16: Polaron contribution to the polaron ground-state energy per particle $E_{e-ph}^{(1)}$ in an N -polaron quantum dot as a function of the effective density. The parameters are taken for ZnO (see Ref. [91]): $\alpha = 0.849$, $\varepsilon_0 = 8.15$, $\varepsilon_\infty = 4.0$, $\hbar\omega_{LO} = 73.27$ meV, $m_b = 0.24m_e$, where m_e is the electron mass in the vacuum. This polaron contribution is compared with the polaron contribution to the ground-state energy of a polaron gas in bulk calculated in Refs. [103, 104].

F. Optical conductivity

In Ref. [98] we have extended the memory-function approach to a system of arbitrary-coupling interacting polarons confined to a parabolic confinement potential. The optical conductivity relates the current $\mathbf{J}(t)$ per electron to a time-dependent uniform electric field $\mathbf{E}(t)$ in the framework of linear response theory. Further on, the Fourier components of the electric field are denoted by $\mathbf{E}(\omega)$:

$$\mathbf{E}(t) = \frac{1}{2\pi} \int_{-\infty}^{\infty} \mathbf{E}(\omega) e^{-i\omega t} d\omega, \quad (6.150)$$

and the similar denotations are used for other time-dependent quantities. The electric current per electron $\mathbf{J}(t)$ is related to the mean electron coordinate response $\mathbf{R}(t)$ by

$$\mathbf{J}(t) = -e \frac{d\mathbf{R}(t)}{dt}, \quad (6.151)$$

and hence

$$\mathbf{J}(\omega) = i e \omega \mathbf{R}(\omega). \quad (6.152)$$

Within the linear-response theory, both the electric current and the coordinate response are proportional to $\mathbf{E}(\omega)$:

$$\mathbf{J}(\omega) = \sigma(\omega) \mathbf{E}(\omega), \quad \mathbf{R}(\omega) = \frac{\sigma(\omega)}{i e \omega} \mathbf{E}(\omega), \quad (6.153)$$

where $\sigma(\omega)$ is the conductivity per electron. Because we treat an isotropic electron-phonon system, $\sigma(\omega)$ is a scalar function. It is determined from the time evolution of the center-of-mass coordinate:

$$\mathbf{R}(t) \equiv \frac{1}{N} \left\langle \left\langle \sum_{j=1}^N \mathbf{x}_j(t) \right\rangle \right\rangle_S. \quad (6.154)$$

The symbol $\langle\langle(\bullet)\rangle\rangle_S$ denotes an average in the *real-time* representation for a system with action functional S :

$$\langle\langle(\bullet)\rangle\rangle_S \equiv \int d\bar{\mathbf{x}} \int d\bar{\mathbf{x}}_0 \int_{\bar{\mathbf{x}}_0}^{\bar{\mathbf{x}}} d\bar{\mathbf{x}}'_0 \int_{\bar{\mathbf{x}}'_0}^{\bar{\mathbf{x}}} D\bar{\mathbf{x}}(t) \int_{\bar{\mathbf{x}}'_0}^{\bar{\mathbf{x}}} D\bar{\mathbf{x}}'(t) e^{\frac{i}{\hbar} S[\bar{\mathbf{x}}(t), \bar{\mathbf{x}}'(t)]} (\bullet) \left\langle \bar{\mathbf{x}}_0 | \hat{\rho}(t_0) | \bar{\mathbf{x}}'_0 \right\rangle \Big|_{t_0 \rightarrow -\infty}, \quad (6.155)$$

where $\langle \bar{\mathbf{x}}_0 | \hat{\rho}(t_0) | \bar{\mathbf{x}}'_0 \rangle$ is the density matrix before the onset of the electric field in the infinite past ($t_0 \rightarrow -\infty$). The corresponding action functional is

$$S[\bar{\mathbf{x}}(t), \bar{\mathbf{x}}'(t)] = \int_{-\infty}^t \left[L_e(\dot{\bar{\mathbf{x}}}(t), \bar{\mathbf{x}}(t), t) - L_e(\dot{\bar{\mathbf{x}}}'(t), \bar{\mathbf{x}}'(t), t) \right] dt' - i\hbar\Phi[\bar{\mathbf{x}}(t), \bar{\mathbf{x}}'(t)], \quad (6.156)$$

where $L_e(\dot{\bar{\mathbf{x}}}, \bar{\mathbf{x}}, t)$ is the Lagrangian of N interacting electrons in a time-dependent uniform electric field $\mathbf{E}(t)$

$$L_e(\dot{\bar{\mathbf{x}}}, \bar{\mathbf{x}}, t) = \sum_{\sigma} \sum_{j=1}^{N_{\sigma}} \left(\frac{m_b \dot{\mathbf{x}}_{j,\sigma}^2}{2} - \frac{m_b \Omega_0^2 \mathbf{x}_{j,\sigma}^2}{2} - e \mathbf{x}_{j,\sigma} \cdot \mathbf{E}(t) \right) - \sum_{\substack{\sigma, \sigma' \\ (j,\sigma) \neq (l,\sigma')}} \sum_{j=1}^{N_{\sigma}} \sum_{l=1}^{N_{\sigma'}} \frac{e^2}{2\epsilon_{\infty} |\mathbf{x}_{j,\sigma} - \mathbf{x}_{l,\sigma'}|}. \quad (6.157)$$

The influence phase of the phonons

$$\begin{aligned} \Phi[\bar{\mathbf{x}}(s), \bar{\mathbf{x}}'(s)] &= - \sum_{\mathbf{q}} \frac{|V_{\mathbf{q}}|^2}{\hbar^2} \int_{-\infty}^t ds \int_{-\infty}^s ds' [\rho_{\mathbf{q}}(s) - \rho'_{\mathbf{q}}(s)] \\ &\quad \times \left[T_{\omega_{\mathbf{q}}}^*(s-s') \rho_{\mathbf{q}}(s') - T_{\omega_{\mathbf{q}}}(s-s') \rho'_{\mathbf{q}}(s') \right] \end{aligned} \quad (6.158)$$

describes both a retarded interaction between different electrons and a retarded self-interaction of each electron due to the elimination of the phonon coordinates. This functional contains the free-phonon Green's function:

$$T_{\omega}(t) = \frac{e^{i\omega t}}{1 - e^{-\beta\hbar\omega}} + \frac{e^{-i\omega t}}{e^{\beta\hbar\omega} - 1}. \quad (6.159)$$

The equation of motion for $\mathbf{R}(t)$ is

$$m_b \frac{d^2 \mathbf{R}(t)}{dt^2} + m_b \Omega_0^2 \mathbf{R}(t) + e \mathbf{E}(t) = \mathbf{F}_{ph}(t), \quad (6.160)$$

where $\mathbf{F}_{ph}(t)$ is the average force due to the electron-phonon interaction,

$$\mathbf{F}_{ph}(t) = - \text{Re} \sum_{\mathbf{q}} \frac{2|V_{\mathbf{q}}|^2 \mathbf{q}}{N\hbar} \int_{-\infty}^t ds T_{\omega_{\mathbf{LO}}}^*(t-s) \langle\langle \rho_{\mathbf{q}}(t) \rho_{-\mathbf{q}}(s) \rangle\rangle_S. \quad (6.161)$$

The two-point correlation function $\langle\langle \rho_{\mathbf{q}}(t) \rho_{-\mathbf{q}}(s) \rangle\rangle_S$ should be calculated from Eq. (6.155) using the exact action (6.156), but like for the free energy above, this path integral cannot be calculated analytically. Instead, we perform an approximate calculation, replacing the two-point correlation function in Eq. (6.161) by $\langle\langle \rho_{\mathbf{q}}(t) \rho_{-\mathbf{q}}(s) \rangle\rangle_{S_0}$, where $S_0[\bar{\mathbf{x}}(t), \bar{\mathbf{x}}'(t)]$ is the action functional with the optimal values of the variational parameters for the model system considered in the previous section in the presence of the electric field $\mathbf{E}(t)$. The functional $S_0[\bar{\mathbf{x}}(t), \bar{\mathbf{x}}'(t)]$ is quadratic and describes a system of coupled harmonic oscillators in the uniform electric field $\mathbf{E}(t)$. This field enters the term $-e \mathbf{E}(t) \cdot \sum_{\sigma} \sum_{j=1}^{N_{\sigma}} \mathbf{x}_{j,\sigma}$ in the

Lagrangian, which only affects the center-of-mass coordinate. Hence, a shift of variables to the frame of reference with the origin at the center of mass

$$\begin{cases} \mathbf{x}_n(t) = \tilde{\mathbf{x}}_n(t) + \mathbf{R}(t), \\ \mathbf{x}'_n(t) = \tilde{\mathbf{x}}'_n(t) + \dot{\mathbf{R}}(t), \end{cases} \quad (6.162)$$

results in

$$\langle\langle \rho_{\mathbf{q}}(t) \rho_{-\mathbf{q}}(s) \rangle\rangle_{S_0} = \langle\langle \rho_{\mathbf{q}}(t) \rho_{-\mathbf{q}}(s) \rangle\rangle_{S_0} \Big|_{E=0} e^{i\mathbf{q} \cdot [\mathbf{R}(t) - \mathbf{R}(s)]}. \quad (6.163)$$

This result (6.163) is valid for any *quadratic* model action S_0 .

The applicability of the parabolic approximation is confirmed by the fact that a self-induced polaronic potential, created by the polarization cloud around an electron, is rather well described by a parabolic potential whose parameters are determined by a variational method. For weak coupling, our variational method is at least of the same accuracy as the perturbation theory, which results from our approach at a special choice of the variational parameters. For strong coupling, an interplay of the electron-phonon interaction and the Coulomb correlations within a confinement potential can lead to the assemblage of polarons in multi-polaron systems. Our choice of the model variational system is reasonable because of this trend, apparently occurring in a many-polaron system with arbitrary N for a finite confinement strength.

The correlation function $\langle \rho_{\mathbf{q}}(t) \rho_{-\mathbf{q}}(s) \rangle_{S_0} \Big|_{\mathbf{E}=0}$ corresponds to the model system in the absence of an electric field. For $t > s$, this function is related to the imaginary-time correlation function $\mathcal{G}(\mathbf{q}, \tau | \{N_\sigma\}, \beta)$, described in the previous section:

$$\langle\langle \rho_{\mathbf{q}}(t) \rho_{-\mathbf{q}}(s) \rangle\rangle_{S_0} \Big|_{\mathbf{E}=0, t>s} = \mathcal{G}(\mathbf{q}, i(t-s) | \{N_\sigma\}, \beta). \quad (6.164)$$

Using the transformation (6.162) and the relation (6.164), we obtain from Eq. (6.161)

$$\mathbf{F}_{ph}(t) = -\text{Re} \sum_{\mathbf{q}} \frac{2|V_{\mathbf{q}}|^2 \mathbf{q}}{N\hbar} \int_{-\infty}^t T_{\omega_{LO}}^*(t-s) e^{i\mathbf{q} \cdot [\mathbf{R}(t) - \mathbf{R}(s)]} \mathcal{G}(\mathbf{q}, i(t-s) | \{N_\sigma\}, \beta) ds. \quad (6.165)$$

Within the linear-response theory, we expand the function $e^{i\mathbf{q} \cdot [\mathbf{R}(t) - \mathbf{R}(s)]}$ in Eq. (6.165) as a Taylor series in $[\mathbf{R}(t) - \mathbf{R}(s)]$ up to the first-order term. The zeroth-order term gives no contribution into $\mathbf{F}_{ph}(t)$ due to the symmetry of $|V_{\mathbf{q}}|^2$ and of $f_{\mathbf{q}}(t-s)$ with respect to the inversion $\mathbf{q} \rightarrow -\mathbf{q}$. In this approach, the Cartesian coordinates of the force ($j = 1, 2, 3$)

become

$$\begin{aligned}
(\mathbf{F}_{ph}(t))_j &= \sum_{k=1}^3 \sum_{\mathbf{q}} \frac{2|V_{\mathbf{q}}|^2 q_j q_k}{N\hbar} \int_{-\infty}^t [R_k(t) - R_k(s)] \\
&\quad \times \text{Im} [T_{\omega_{\text{LO}}}^*(t-s) \mathcal{G}(\mathbf{q}, i(t-s) | \{N_{\sigma}\}, \beta)] ds.
\end{aligned} \tag{6.166}$$

Further on, we perform the Fourier expansion:

$$\mathbf{R}(t) = \frac{1}{2\pi} \int_{-\infty}^{\infty} \mathbf{R}(\omega) e^{-i\omega t} d\omega. \tag{6.167}$$

In Eq. (6.166), we make the replacement

$$\tau \equiv t - s, \quad \implies \quad s = t - \tau,$$

what gives

$$\begin{aligned}
(\mathbf{F}_{ph}(t))_j &= \sum_{k=1}^3 \sum_{\mathbf{q}} \frac{2|V_{\mathbf{q}}|^2 q_j q_k}{N\hbar} \int_0^{\infty} d\tau [R_k(t) - R_k(t-\tau)] \text{Im} [T_{\omega_{\text{LO}}}^*(\tau) \mathcal{G}(\mathbf{q}, i\tau | \{N_{\sigma}\}, \beta)] \\
&= \sum_{k=1}^3 \sum_{\mathbf{q}} \frac{2|V_{\mathbf{q}}|^2 q_j q_k}{N\hbar} \frac{1}{2\pi} \int_{-\infty}^{\infty} d\omega R_k(\omega) e^{-i\omega t} \int_0^{\infty} d\tau (1 - e^{i\omega\tau}) \text{Im} [T_{\omega_{\text{LO}}}^*(\tau) f_{\mathbf{q}}(\tau)] \\
&= \frac{1}{2\pi} \int_{-\infty}^{\infty} d\omega F_j(\omega) e^{-i\omega t},
\end{aligned}$$

where the Fourier component of the force is

$$(\mathbf{F}_{ph}(\omega))_j = \sum_{k=1}^3 \sum_{\mathbf{q}} \frac{2|V_{\mathbf{q}}|^2 q_j q_k}{N\hbar} \int_0^{\infty} dt (1 - e^{i\omega t}) \text{Im} [T_{\omega_{\text{LO}}}^*(\tau) \mathcal{G}(\mathbf{q}, i\tau | \{N_{\sigma}\}, \beta)] R_k(\omega). \tag{6.168}$$

The expression (6.168) can be written down as

$$(\mathbf{F}_{ph}(\omega))_j = -m_b \sum_{k=1}^3 \chi_{jk}(\omega) R_k(\omega), \tag{6.169}$$

where $\chi_{jk}(\omega)$ are components of the tensor

$$\chi_{jk}(\omega) = \sum_{\mathbf{q}} \frac{2|V_{\mathbf{q}}|^2 q_j q_k}{N\hbar m_b} \int_0^{\infty} dt (e^{i\omega t} - 1) \text{Im} [T_{\omega_{\text{LO}}}^*(t) \mathcal{G}(\mathbf{q}, it | \{N_{\sigma}\}, \beta)]. \tag{6.170}$$

In the abstract tensor form, Eq. (6.169) is

$$\mathbf{F}(\omega) = -\overleftrightarrow{\chi}(\omega) \mathbf{R}(\omega). \tag{6.171}$$

In particular, for the isotropic electron-phonon interaction and in the absence of the magnetic field, the tensor $\overleftrightarrow{\chi}(\omega)$ is proportional to the unity tensor \mathbb{I} ,

$$\overleftrightarrow{\chi}(\omega) = \chi(\omega) \mathbb{I}, \quad (6.172)$$

where $\chi(\omega)$ is the scalar memory function:

$$\chi(\omega) = \sum_{\mathbf{q}} \frac{2|V_{\mathbf{q}}|^2 q^2}{3N\hbar m_b} \int_0^{\infty} dt (e^{i\omega t} - 1) \text{Im} [T_{\omega_{\text{LO}}}^*(t) \mathcal{G}(\mathbf{q}, it | \{N_{\sigma}\}, \beta)]. \quad (6.173)$$

Let us perform the Fourier transformation of the equation of motion (6.160):

$$m_b (\Omega_0^2 - \omega^2) \mathbf{R}(\omega) + e\mathbf{E}(\omega) = \mathbf{F}_{ph}(\omega). \quad (6.174)$$

With Eq. (6.171), this equation takes the form

$$\begin{aligned} m_b (\Omega_0^2 - \omega^2) \mathbf{R}(\omega) + e\mathbf{E}(\omega) &= -m_b \overleftrightarrow{\chi}(\omega) \mathbf{R}(\omega) \\ &\Downarrow \\ m_b [\omega^2 - \Omega_0^2 - \overleftrightarrow{\chi}(\omega)] \mathbf{R}(\omega) &= e\mathbf{E}(\omega). \end{aligned} \quad (6.175)$$

Comparing Eqs. (6.153) and (6.175) between each other, we find that

$$m_b [\omega^2 - \Omega_0^2 - \overleftrightarrow{\chi}(\omega)] \frac{\sigma(\omega)}{ie\omega} \mathbf{E}(\omega) = e\mathbf{E}(\omega),$$

so that

$$\sigma(\omega) = \frac{ie^2\omega}{m_b} [\omega^2 - \Omega_0^2 - \overleftrightarrow{\chi}(\omega)]^{-1}.$$

In the case when Eq. (6.172) is valid, we obtain the conductivity in the scalar form

$$\sigma(\omega) = \frac{ie^2\omega}{m_b [\omega^2 - \Omega_0^2 - \chi(\omega)]}.$$

The real part of the conductivity is

$$\begin{aligned} \text{Re } \sigma(\omega) &= \text{Re} \frac{ie^2\omega [(\omega^2 - \Omega_0^2) - \text{Re } \chi(\omega) + i \text{Im } \chi(\omega)]}{m_b \left\{ [(\omega^2 - \Omega_0^2) - \text{Re } \chi(\omega)]^2 + [\text{Im } \chi(\omega)]^2 \right\}} \\ &= -\frac{e^2\omega}{m_b} \frac{\text{Im } \chi(\omega)}{[(\omega^2 - \Omega_0^2) - \text{Re } \chi(\omega)]^2 + [\text{Im } \chi(\omega)]^2}. \end{aligned}$$

In summary, the optical conductivity can be expressed in terms of the memory function $\chi(\omega)$ (cf. Ref. [50]),

$$\text{Re } \sigma(\omega) = -\frac{e^2}{m_b} \frac{\omega \text{Im } \chi(\omega)}{[\omega^2 - \Omega_0^2 - \text{Re } \chi(\omega)]^2 + [\text{Im } \chi(\omega)]^2}, \quad (6.176)$$

where $\chi(\omega)$ is given by

$$\chi(\omega) = \sum_{\mathbf{q}} \frac{2|V_{\mathbf{q}}|^2 q^2}{3N\hbar m_b} \int_0^{\infty} dt (e^{i\omega t} - 1) \text{Im} [T_{\omega_{\text{LO}}}^*(t) \mathcal{G}(\mathbf{q}, it | \{N_{\sigma}\}, \beta)]. \quad (6.177)$$

It is worth noting that the optical conductivity (6.176) differs from that for a translationally invariant polaron system both by the explicit form of $\chi(\omega)$ and by the presence of the term Ω_0^2 in the denominator. For $\alpha \rightarrow 0$, the optical conductivity tends to a δ -like peak at $\omega = \Omega_0$,

$$\lim_{\alpha \rightarrow 0} \text{Re} \sigma(\omega) = \frac{\pi e^2}{2m_b} \delta(\omega - \Omega_0). \quad (6.178)$$

For a translationally invariant system $\Omega_0 \rightarrow 0$, and this weak-coupling expression (6.178) reproduces the ‘‘central peak’’ of the polaron optical conductivity [82].

The further simplification of the memory function (6.177) is performed in the following way. With the Fröhlich amplitudes of the electron-phonon interaction, we transform the summation over \mathbf{q} to the integral and use the Feynman units ($\hbar = 1$, $\omega_{\text{LO}} = 1$, $m_b = 1$), in which $|V_{\mathbf{q}}|^2 = \frac{2\sqrt{2}\pi\alpha}{q^2V}$. We also use the fact that in an isotropic crystal, $\mathcal{G}(\mathbf{q}, it | \{N_{\sigma}\}, \beta) = \mathcal{G}(q, it | \{N_{\sigma}\}, \beta)$. As a result, we find

$$\begin{aligned} \chi(\omega) &= \frac{V}{(2\pi)^3} \int_0^{\infty} 4\pi q^2 dq \frac{2q^2}{3N} \frac{2\sqrt{2}\pi\alpha}{q^2V} \\ &\quad \times \int_0^{\infty} dt (e^{i\omega t} - 1) \text{Im} [T_{\omega_{\text{LO}}}^*(t) \mathcal{G}(q, it | \{N_{\sigma}\}, \beta)] \\ &= \frac{2\sqrt{2}\alpha}{3\pi N} \int_0^{\infty} q^2 dq \int_0^{\infty} dt (e^{i\omega t} - 1) \text{Im} [T_{\omega_{\text{LO}}}^*(t) \mathcal{G}(q, it | \{N_{\sigma}\}, \beta)]. \end{aligned}$$

In the zero-temperature case, $T_{\omega_{\text{LO}}}^*(t) \rightarrow e^{-it}$, and we arrive at the expression

$$\chi(\omega) = \frac{2\sqrt{2}\alpha}{3\pi N} \int_0^{\infty} q^2 dq \int_0^{\infty} dt (e^{i\omega t} - 1) \text{Im} [e^{-it} \mathcal{G}(q, it | \{N_{\sigma}\}, \beta)]. \quad (6.179)$$

Substituting the two-point correlation function $\mathcal{G}(q, it | \{N_{\sigma}\}, \beta)$ with the one-electron (6.141) and the two-electron (6.143) distribution functions into the memory function (6.179) and expanding $\mathcal{G}(q, it | \{N_{\sigma}\}, \beta)$ in powers of $e^{-i\omega t}$, $e^{-i\Omega_1 t}$ and $e^{-i\Omega_2 t}$, the integrations over q and t in Eq. (6.179) are performed analytically. The similar transformations are performed also in the 2D case. As a result, the memory function (6.177) is represented in the unified

form for 3D and 2D interacting polarons:

$$\begin{aligned}
\chi(\omega) = & \lim_{\varepsilon \rightarrow +0} \frac{2\alpha}{3\pi N} \left(\frac{3\pi}{4}\right)^{3-D} \left(\frac{\omega_{\text{LO}}}{A}\right)^{3/2} \\
& \times \sum_{p_1=0}^{\infty} \sum_{p_2=0}^{\infty} \sum_{p_3=0}^{\infty} \frac{(-1)^{p_3}}{p_1! p_2! p_3!} \left(\frac{a_1^2}{N\Omega_1 A}\right)^{p_1} \left(\frac{a_2^2}{N\Omega_2 A}\right)^{p_2} \left(\frac{1}{NwA}\right)^{p_3} \\
& \times \left\{ \left[\sum_{m=0}^{\infty} \sum_{n=0}^{\infty} \sum_{\sigma} [f_1(n, \sigma | \{N_{\sigma}\}, \beta) - f_2(n, \sigma; m, \sigma | \{N_{\sigma}\}, \beta)] \right]_{\beta \rightarrow \infty} \right. \\
& \times \left(\frac{1}{\omega - \omega_{\text{LO}} - [p_1\Omega_1 + p_2\Omega_2 + (p_3 - m + n)w] + i\varepsilon} - \frac{1}{\omega + \omega_{\text{LO}} + p_1\Omega_1 + p_2\Omega_2 + (p_3 - m + n)w + i\varepsilon} \right. \\
& \quad \left. \left. + \mathcal{P} \left(\frac{2}{\omega_{\text{LO}} + p_1\Omega_1 + p_2\Omega_2 + (p_3 - m + n)w} \right) \right) \right. \\
& \times \sum_{l=0}^m \sum_{k=n-m+l}^n \frac{(-1)^{n-m+l+k} \Gamma(p_1 + p_2 + p_3 + k + l + \frac{3}{2})}{k! l!} \left(\frac{1}{wA}\right)^{l+k} \\
& \times \left. \left(\binom{n+D-1}{n-k} \binom{2k}{k-l-n+m} \right) \right] \\
& + \left[\left(\frac{1}{\omega - \omega_{\text{LO}} - (p_1\Omega_1 + p_2\Omega_2 + p_3w) + i\varepsilon} - \frac{1}{\omega + \omega_{\text{LO}} + p_1\Omega_1 + p_2\Omega_2 + p_3w + i\varepsilon} \right) \right. \\
& \quad \left. + \mathcal{P} \left(\frac{2}{\omega_{\text{LO}} + p_1\Omega_1 + p_2\Omega_2 + p_3w} \right) \right) \\
& \times \sum_{m=0}^{\infty} \sum_{n=0}^{\infty} \sum_{\sigma, \sigma'} f_2(n, \sigma; m, \sigma' | \{N_{\sigma}\}, \beta) \Big|_{\beta \rightarrow \infty} \\
& \times \sum_{k=0}^n \sum_{l=0}^m \frac{(-1)^{k+l} \Gamma(p_1 + p_2 + p_3 + k + l + \frac{3}{2})}{k! l!} \left(\frac{1}{wA}\right)^{k+l} \\
& \times \left. \left(\binom{n+D-1}{n-k} \binom{m+D-1}{m-l} \right) \right] \Big\}, \tag{6.180}
\end{aligned}$$

where $D = 2, 3$ is the dimensionality of the space, \mathcal{P} denotes the principal value, A is defined as $A \equiv [\sum_{i=1}^2 a_i^2 / \Omega_i + (N-1)/w] / N$, Ω_1, Ω_2 , and w are the eigenfrequencies of the model system, a_1 and a_2 are the coefficients of the canonical transformation which diagonalizes the model Lagrangian (6.32).

1. Selected results: the manifestations of the shell filling in optical conductivity

The shell filling schemes for an N -polaron system in a quantum dot can manifest themselves in the spectra of the optical conductivity. In Fig. 17, optical conductivity spectra for $N = 20$ polarons are presented for a quantum dot with the parameters of CdSe: $\alpha = 0.46$,

$\eta = 0.656$ [7] and with different values of the confinement energy $\hbar\Omega_0$.⁷ In this case, the spin-polarized ground state changes to the ground state satisfying Hund's rule with increasing $\hbar\Omega_0$ in the interval $0.0421H^* < \hbar\Omega_0 < 0.0422H^*$.

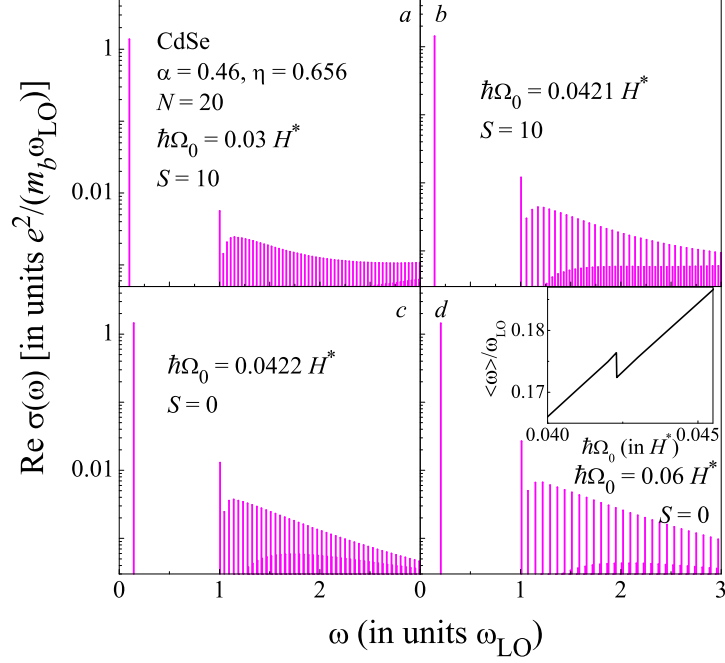


FIG. 17: Optical conductivity spectra of $N = 20$ interacting polarons in CdSe quantum dots with $\alpha = 0.46$, $\eta = 0.656$ for different confinement energies close to the transition from a spin-polarized ground state to a ground state obeying Hund's rule. *Inset*: the first frequency moment $\langle\omega\rangle$ of the optical conductivity as a function of the confinement energy. (From Ref. [98].)

In the inset to Fig. 17, the first frequency moment of the optical conductivity

$$\langle\omega\rangle \equiv \frac{\int_0^\infty \omega \operatorname{Re} \sigma(\omega) d\omega}{\int_0^\infty \operatorname{Re} \sigma(\omega) d\omega}, \quad (6.181)$$

as a function of $\hbar\Omega_0$ shows a *discontinuity*, at the value of the confinement energy corresponding to the change of the shell filling schemes from the spin-polarized ground state to the ground state obeying Hund's rule. This discontinuity might be observable in optical measurements.

⁷For the numerical calculations, we use effective atomic units, where \hbar , the electron band mass m_b and $e/\sqrt{\epsilon_\infty}$ have the numerical value of 1. This means that the unit of length is the effective Bohr radius $a_B^* = \hbar^2 \epsilon_\infty / (m_b e^2)$, while the unit of energy is the effective Hartree $H^* = m_b e^4 / (\hbar^2 \epsilon_\infty^2)$.

The shell structure for a system of interacting polarons in a quantum dot is clearly revealed when analyzing the addition energy and the first frequency moment of the optical conductivity in parallel. In Fig 18, we show both the function

$$\Theta(N) \equiv \langle \omega \rangle|_{N+1} - 2 \langle \omega \rangle|_N + \langle \omega \rangle|_{N-1}, \quad (6.182)$$

and the addition energy

$$\Delta(N) = E^0(N+1) - 2E^0(N) + E^0(N-1). \quad (6.183)$$

for interacting polarons in a 3D CdSe quantum dot.

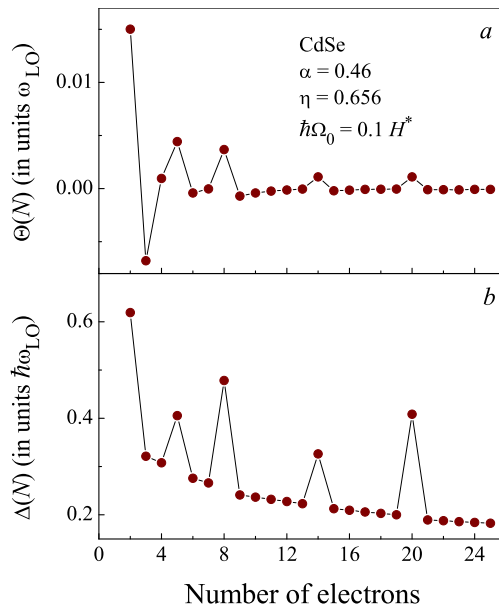


FIG. 18: The function $\Theta(N)$ and the addition energy $\Delta(N)$ for systems of interacting polarons in CdSe quantum dots with $\alpha = 0.46$, $\eta = 0.656$ for $\hbar\Omega_0 = 0.1H^*$. (From Ref. [98].)

As seen from Fig 18, distinct peaks appear in $\Theta(N)$ and $\Delta(N)$ at the “magic numbers” corresponding to closed-shell configurations at $N = 8, 20$ and to half-filled-shell configurations at $N = 5, 14$. We see that each of the peaks of $\Theta(N)$ corresponds to a peak of the addition energy. The filling patterns for a many-polaron system in a quantum dot can be therefore determined from the analysis of the first moment of the optical absorption for different numbers of polarons.

VII. VARIATIONAL PATH-INTEGRAL TREATMENT OF A TRANSLATION INVARIANT N -POLARON SYSTEM

A. The many-polaron system

In the present section, the ground-state properties of a translation invariant N -polaron system are theoretically studied in the framework of the variational path-integral method for identical particles, using a further development [105] of the model introduced in Refs. [98, 100, 106].

In order to describe a many-polaron system, we start from the translation invariant N -polaron Hamiltonian

$$H = \sum_{j=1}^N \frac{\mathbf{p}_j^2}{2m} + \frac{1}{2} \sum_{j=1}^N \sum_{l=1, \neq j}^N \frac{e^2}{\epsilon_\infty |\mathbf{r}_j - \mathbf{r}_l|} + \sum_{\mathbf{k}} \hbar \omega_{\text{LO}} a_{\mathbf{k}}^\dagger a_{\mathbf{k}} + \left(\sum_{j=1}^N \sum_{\mathbf{k}} V_{\mathbf{k}} a_{\mathbf{k}} e^{i\mathbf{k} \cdot \mathbf{r}_j} + H.c. \right), \quad (7.1)$$

where m is the band mass, e is the electron charge, ω_{LO} is the longitudinal optical (LO) phonon frequency, and $V_{\mathbf{k}}$ are the amplitudes of the Fröhlich electron-LO-phonon interaction

$$V_{\mathbf{k}} = i \frac{\hbar \omega_{\text{LO}}}{k} \left(\frac{4\pi\alpha}{V} \right)^{1/2} \left(\frac{\hbar}{2m\omega_{\text{LO}}} \right)^{1/4}, \quad \alpha = \frac{e^2}{2\hbar\omega_{\text{LO}}} \left(\frac{2m\omega_{\text{LO}}}{\hbar} \right)^{1/2} \left(\frac{1}{\epsilon_\infty} - \frac{1}{\epsilon_0} \right), \quad (7.2)$$

with the electron-phonon coupling constant $\alpha > 0$, the high-frequency dielectric constant $\epsilon_\infty > 0$ and the static dielectric constant $\epsilon_0 > 0$, and consequently

$$\frac{e^2}{\epsilon_\infty} > \hbar \left(\frac{2\hbar\omega_{\text{LO}}}{m} \right)^{1/2} \alpha \iff \alpha\sqrt{2} < \left(\frac{H^*}{\hbar\omega_{\text{LO}}} \right)^{1/2} \equiv U. \quad (7.3)$$

In the expression (7.3), H^* is the effective Hartree

$$H^* = \frac{e^2}{\epsilon_\infty a_B^*}, \quad a_B^* = \frac{\hbar^2}{m e^2 / \epsilon_\infty} \quad (7.4)$$

where a_B^* is the effective Bohr radius. The partition function of the system can be expressed as a path integral over all electron and phonon coordinates. The path integral over the phonon variables can be calculated analytically [43]. Feynman's phonon elimination technique for this system is well known and leads to the partition function, which is a path integral over the electron coordinates only:

$$Z = \left(\prod_{\mathbf{k}} \frac{e^{\frac{1}{2}\beta\hbar\omega_{\text{LO}}}}{2 \sinh \frac{1}{2}\beta\hbar\omega_{\text{LO}}} \right) \oint e^S \mathcal{D}\bar{\mathbf{r}} \quad (7.5)$$

where $\bar{\mathbf{r}} = \{\mathbf{r}_1, \dots, \mathbf{r}_N\}$ denotes the set of electron coordinates, and $\oint \mathcal{D}\bar{\mathbf{r}}$ denotes the path integral over all the electron coordinates, integrated over equal initial and final points, i.e.

$$\oint e^S \mathcal{D}\bar{\mathbf{r}} \equiv \int d\bar{\mathbf{r}} \int_{\bar{\mathbf{r}}(0)=\bar{\mathbf{r}}}^{\bar{\mathbf{r}}(\beta)=\bar{\mathbf{r}}} e^S \mathcal{D}\bar{\mathbf{r}}(\tau).$$

Throughout this paper, imaginary time variables are used. The effective action for the N -polaron system is retarded and given by

$$\begin{aligned} S = & - \int_0^\beta \left(\frac{m}{2} \sum_{j=1}^N \left(\frac{d\mathbf{r}_j(\tau)}{d\tau} \right)^2 + \frac{1}{2} \sum_{j=1}^N \sum_{l=1, \neq j}^N \frac{e^2}{\epsilon_\infty |\mathbf{r}_j(\tau) - \mathbf{r}_l(\tau)|} \right) d\tau \\ & + \frac{1}{2} \int_0^\beta \int_0^\beta \sum_{j,l=1}^N \sum_{\mathbf{k}} |V_{\mathbf{k}}|^2 e^{i\mathbf{k} \cdot (\mathbf{r}_j(\tau) - \mathbf{r}_l(\sigma))} \frac{\cosh \hbar\omega_{\text{LO}} \left(\frac{1}{2}\beta - |\tau - \sigma| \right)}{\sinh \frac{1}{2}\beta \hbar\omega_{\text{LO}}} d\sigma d\tau. \end{aligned} \quad (7.6)$$

Note that the electrons are fermions. Therefore the path integral for the electrons with parallel spin has to be interpreted as the required antisymmetric projection of the propagators for distinguishable particles.

We below use units in which $\hbar = 1$, $m = 1$, and $\omega_{\text{LO}} = 1$. The units of distance and energy are thus the effective polaron radius $[\hbar / (m\omega_{\text{LO}})]^{1/2}$ and the LO-phonon energy $\hbar\omega_{\text{LO}}$.

B. Variational principle

For distinguishable particles, it is well known that the Jensen-Feynman inequality [43] provides a lower bound on the partition function Z (and consequently an upper bound on the free energy F)

$$Z = \oint e^S \mathcal{D}\bar{\mathbf{r}} = \left(\oint e^{S_0} \mathcal{D}\bar{\mathbf{r}} \right) \langle e^{S-S_0} \rangle_0 \geq \left(\oint e^{S_0} \mathcal{D}\bar{\mathbf{r}} \right) e^{\langle S-S_0 \rangle_0} \quad \text{with} \quad \langle A \rangle_0 \equiv \frac{\oint A(\bar{\mathbf{r}}) e^{S_0} \mathcal{D}\bar{\mathbf{r}}}{\oint e^{S_0} \mathcal{D}\bar{\mathbf{r}}}, \quad (7.7)$$

$$e^{-\beta F} \geq e^{-\beta F_0} e^{\langle S-S_0 \rangle_0} \implies F \leq F_0 - \frac{\langle S - S_0 \rangle_0}{\beta} \quad (7.8)$$

for a system with real action S and a real trial action S_0 . The many-body extension (Ref. [99, 107]) of the Jensen-Feynman inequality, requires that the potentials are symmetric with respect to all particle permutations, and that the exact propagator as well as the model propagator are defined on the same state space. Within this interpretation we consider the

following generalization of Feynman's trial action

$$\begin{aligned}
S_0 = & - \int_0^\beta \left(\frac{1}{2} \sum_{j=1}^N \left(\frac{d\mathbf{r}_j(\tau)}{d\tau} \right)^2 + \frac{\omega^2 + w^2 - v^2}{4N} \sum_{j,l=1}^N (\mathbf{r}_j(\tau) - \mathbf{r}_l(\tau))^2 \right) d\tau \\
& - \frac{w v^2 - w^2}{8} \frac{1}{N} \sum_{j,l=1}^N \int_0^\beta \int_0^\beta (\mathbf{r}_j(\tau) - \mathbf{r}_l(\sigma))^2 \frac{\cosh w \left(\frac{1}{2}\beta - |\tau - \sigma| \right)}{\sinh \frac{1}{2}\beta w} d\sigma d\tau \quad (7.9)
\end{aligned}$$

with the variational frequency parameters v, w, ω .

Using the explicit forms of the exact (7.6) and the trial (7.9) actions, the variational inequality (7.8) takes the form

$$\begin{aligned}
F(\beta | N_\uparrow, N_\downarrow) \leq & F_0(\beta | N_\uparrow, N_\downarrow) + \frac{U}{2\beta} \int_0^\beta \left\langle \sum_{j,l=1, \neq j}^N \frac{1}{|\mathbf{r}_j(\tau) - \mathbf{r}_l(\tau)|} \right\rangle_0 d\tau \\
& - \frac{\omega^2 + w^2 - v^2}{4N\beta} \int_0^\beta \left\langle \sum_{j,l=1}^N (\mathbf{r}_j(\tau) - \mathbf{r}_l(\tau))^2 \right\rangle_0 d\tau \\
& - \frac{w v^2 - w^2}{8} \frac{1}{N\beta} \int_0^\beta \int_0^\beta \left\langle \sum_{j,l=1}^N (\mathbf{r}_j(\tau) - \mathbf{r}_l(\sigma))^2 \right\rangle_0 \frac{\cosh w \left(\frac{1}{2}\beta - |\tau - \sigma| \right)}{\sinh \frac{1}{2}\beta w} d\sigma d\tau \\
& - \frac{1}{2\beta} \int_0^\beta \int_0^\beta \sum_{\mathbf{k}} |V_{\mathbf{k}}|^2 \left\langle \sum_{j,l=1}^N e^{i\mathbf{k} \cdot (\mathbf{r}_j(\tau) - \mathbf{r}_l(\sigma))} \right\rangle_0 \frac{\cosh \omega_{\text{LO}} \left(\frac{1}{2}\beta - |\tau - \sigma| \right)}{\sinh \frac{1}{2}\beta \omega_{\text{LO}}} d\sigma d\tau. \quad (7.10)
\end{aligned}$$

In the zero-temperature limit ($\beta \rightarrow \infty$), we arrive at the following upper bound for the ground-state energy $E^0(N_\uparrow, N_\downarrow)$ of a translation invariant N -polaron system

$$E^0(N_\uparrow, N_\downarrow) \leq E_{\text{var}}(N_\uparrow, N_\downarrow | v, w, \omega),$$

with

$$\begin{aligned}
E_{\text{var}}(N_\uparrow, N_\downarrow | v, w, \omega) = & \frac{3(v-w)^2}{4v} - \frac{3}{4}\omega + \frac{1}{2}\mathbb{E}_F(N_\downarrow) + \frac{1}{2}\mathbb{E}_F(N_\uparrow) \\
& + E_{C\parallel}(N_\uparrow) + E_{C\parallel}(N_\downarrow) + E_{C\uparrow\downarrow}(N_\uparrow, N_\downarrow) \\
& + E_{\alpha\parallel}(N_\uparrow) + E_{\alpha\parallel}(N_\downarrow) + E_{\alpha\uparrow\downarrow}(N_\uparrow, N_\downarrow), \quad (7.11)
\end{aligned}$$

where $\mathbb{E}_F(N)$ is the energy of N spin-polarized fermions confined to a parabolic potential with the confinement frequency ω , $E_{C\parallel}(N_{\uparrow(\downarrow)})$ is the Coulomb energy of the electrons with parallel spins, $E_{C\uparrow\downarrow}(N_\uparrow, N_\downarrow)$ is the Coulomb energy of the electrons with opposite spins, $E_{\alpha\parallel}(N_{\uparrow(\downarrow)})$ is the electron-phonon energy of the electrons with parallel spins, and $E_{\alpha\uparrow\downarrow}(N_\uparrow, N_\downarrow)$ is the electron-phonon energy of the electrons with opposite spins.

C. Results

Here, we discuss some results of the numerical minimization of $E_{var}(N_{\uparrow}, N_{\downarrow}|v, w, \omega)$ with respect to the three variational parameters v , w , and ω . The Fröhlich constant α and the Coulomb parameter

$$\alpha_0 \equiv \frac{U}{\sqrt{2}} \equiv \frac{\alpha}{1-\eta} \quad \text{with} \quad \frac{1}{\eta} = \frac{\varepsilon_0}{\varepsilon_{\infty}} \quad (7.12)$$

characterize the strength of the electron-phonon and of the Coulomb interaction, obeying the physical condition $\alpha \geq \alpha_0$ [see (7.3)]. The optimal values of the variational parameters $v, w,$ and ω are denoted $v_{op}, w_{op},$ and ω_{op} , respectively. The optimal value of the total spin was always determined by choosing the combination $(N_{\uparrow}, N_{\downarrow})$ for fixed $N = N_{\uparrow} + N_{\downarrow}$ which corresponds to the lowest value $E^0(N)$ of the variational functional

$$E^0(N) \equiv \min_{N_{\uparrow}} E_{var}(N_{\uparrow}, N - N_{\uparrow}|v_{op}, w_{op}, \omega_{op}). \quad (7.13)$$

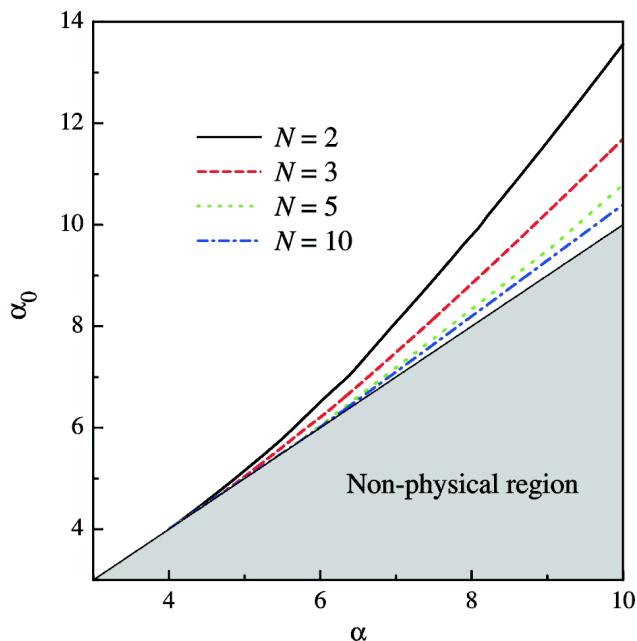


FIG. 19: The “phase diagrams” of a translation invariant N -polaron system. The grey area is the non-physical region, for which $\alpha > \alpha_0$. The stability region for each number of electrons is determined by the equation $\alpha_c < \alpha < \alpha_0$. (From Ref. [105].)

In Fig. 19, the “phase diagrams” analogous to the bipolaron “phase diagram” of Ref. [108] are plotted for an N -polaron system in bulk with $N = 2, 3, 5,$ and 10 . The area where $\alpha_0 \leq \alpha$ is the non-physical region. For $\alpha > \alpha_0$, each sector between a curve corresponding

to a well defined N and the line indicating $\alpha_0 = \alpha$ shows the stability region where $\omega_{op} \neq 0$, while the white area corresponds to the regime with $\omega_{op} = 0$. When comparing the stability region for $N = 2$ from Fig. 19 with the bipolaron “phase diagram” of Ref. [108], the stability region in the present work starts from the value $\alpha_c \approx 4.1$ (instead of $\alpha_c \approx 6.9$ in Ref. [108]). The width of the stability region within the present model is also larger than the width of the stability region within the model of Ref. [108]. Also, the absolute values of the ground-state energy of a two-polaron system given by the present model are smaller than those given by the approach of Ref. [108].

The difference between the numerical results of the present work and of Ref. [108] is due to the following distinction between the used model systems. The model system of Ref. [108] consists of two electrons interacting with two fictitious particles and with each other through quadratic interactions. But the trial Hamiltonian given by Eq. (6) of Ref. [108] is not symmetric with respect to the permutation of the electrons. It is only symmetric under the permutation of the pairs “electron + fictitious particle”. As a consequence, this trial system is only applicable if the electrons are distinguishable, i.e. have opposite spin. In contrast to the model of Ref. [108], the model used in the present paper is described by the trial action (9), which is fully symmetric with respect to the permutations of the electrons, as is required to describe identical particles.

The “phase diagrams” for $N > 2$ demonstrate the existence of stable multipolaron states (see Ref. [109]). As distinct from Ref. [109], here the ground state of an N -polaron system is investigated supposing that the electrons are fermions. As seen from Fig. 20, for $N > 2$, the stability region for a multipolaron state is narrower than the stability region for $N = 2$, and its width decreases with increasing N .

A consequence of the Fermi statistics is the dependence of the polaron characteristics and of the total spin of an N -polaron system on the parameters (α, α_0, N) . In Fig. 20, we present the ground-state energy per particle, the confinement frequency ω_{op} and the total spin S as a function of the coupling constant α for $\alpha_0/\alpha = 1.05$ and for a different numbers of polarons. The ground-state energy turns out to be a continuous function of α , while ω_{op} and S reveal jumps. For $N = 2$ (the case of a bipolaron), we see from Fig. 20 that the ground state has a total spin $S = 0$ for all values of α , i. e., the ground state of a bipolaron is a singlet. This result is in agreement with earlier investigations on the large-bipolaron problem (see, e. g., [110]).

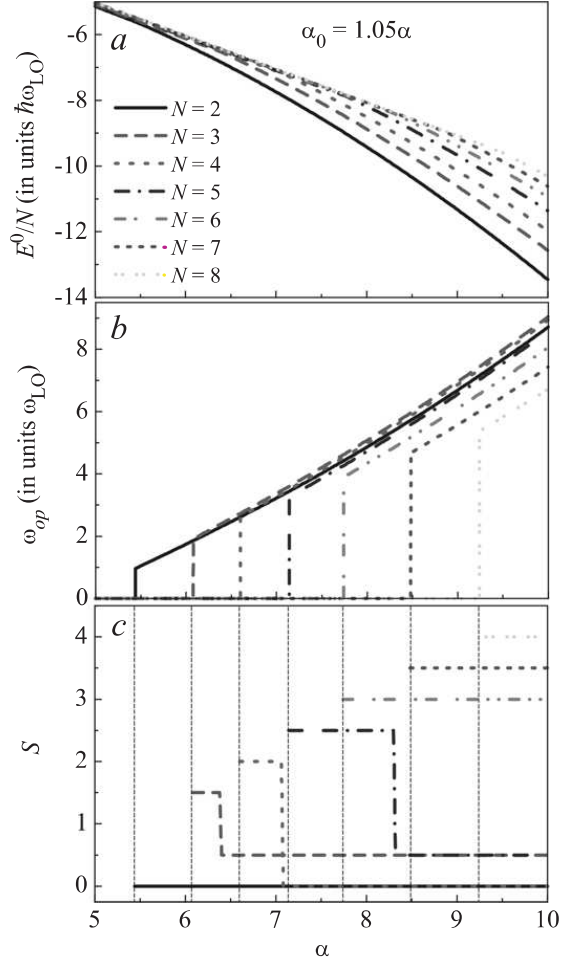


FIG. 20: The ground-state energy per particle (a), the optimal value ω_{op} of the confinement frequency (b), and the total spin (c) of a translation invariant N -polaron system as a function of the coupling strength α for $\alpha_0/\alpha = 0.5$. The vertical dashed lines in the panel c indicate the critical values α_c separating the regimes of $\alpha > \alpha_c$, where the multipolaron ground state with $\omega_{op} \neq 0$ exists, and $\alpha < \alpha_c$, where $\omega_{op} = 0$. (From Ref. [105].)

In summary, using the extension of the Jensen-Feynman variational principle to the systems of identical particles, we have derived a rigorous upper bound for the free energy of a translation invariant system of N interacting polarons. The developed approach is valid for an arbitrary coupling strength. The resulting ground-state energy is obtained taking into account the Fermi statistics of electrons.

VIII. RIPPLONIC POLARONS IN MULTIELECTRON BUBBLES

A. Ripplon-phonon modes of a MEB

Spherical shells of charged particles appear in a variety of physical systems, such as fullerenes, metallic nanoshells, charged droplets and neutron stars. A particularly interesting physical realization of the spherical electron gas is found in multielectron bubbles (MEBs) in liquid helium-4. These MEBs are $0.1 \mu\text{m} - 100 \mu\text{m}$ sized cavities inside liquid helium, that contain helium vapor at vapor pressure and a nanometer-thick electron layer anchored to the surface of the bubble [112]. They exist as a result of equilibrium between the surface tension of liquid helium and the Coulomb repulsion of the electrons [113]. Recently proposed experimental schemes to stabilize MEBs [114] have stimulated theoretical investigation of their properties.

We describe the dynamical modes of an MEB by considering the motion of the helium surface (“rippbons”) and the vibrational modes of the electrons together. In particular, we analyze the case when the ripplon-polarons form a Wigner lattice [111].

First, we derive the Lagrangian of interacting ripples and phonons within a continuum approach. The shape of the surface of a bubble is described by the function $R(\theta, \varphi) = R_b + u(\theta, \varphi)$, where $u(\theta, \varphi)$ is the deformation of the surface from a sphere with radius R_b . The deformation can be expanded in a series of spherical harmonics $Y_{lm}(\theta, \varphi)$ with amplitudes Q_{lm} ,

$$u(\theta, \varphi) = \sum_{l=1}^{\infty} \sum_{m=-l}^l Q_{lm} Y_{lm}(\theta, \varphi). \quad (8.1)$$

We suppose that the amplitudes are small in such a way that $\sqrt{l(l+1)}|Q_{lm}| \ll R_b$.

The ripplon contribution (T_r) to the kinetic energy of an MEB, and the contributions to the potential energy due to the surface tension (U_σ) and due to the pressure (U_V) were described in Ref. [115]:

$$\begin{aligned} T_r &= \frac{\rho}{2} R_b^3 \sum_{l=1}^{\infty} \sum_{m=-l}^l \frac{1}{l+1} |\dot{Q}_{lm}|^2, \\ U_\sigma &= 4\pi\sigma R_b^2 + \frac{\sigma}{2} \sum_{l=1}^{\infty} \sum_{m=-l}^l (l^2 + l + 2) |Q_{lm}|^2, \\ U_V &= \frac{4\pi}{3} p R_b^3 + p R_b \sum_{l=1}^{\infty} \sum_{m=-l}^l |Q_{lm}|^2. \end{aligned} \quad (8.2)$$

Here $\rho \approx 145 \text{ kg/m}^3$ is the density of liquid helium, $\sigma \approx 3.6 \times 10^{-4} \text{ J/m}^2$ is its surface tension, and p is the difference of pressures outside and inside the bubble.

Expanding the surface electron density $n(\theta, \varphi)$ in a series of spherical harmonics with amplitudes n_{lm} ,

$$n(\theta, \varphi) = \sum_{l=0}^{\infty} \sum_{m=-l}^l n_{lm} Y_{lm}(\theta, \varphi), \quad (8.3)$$

the kinetic energy of the motion of electrons can be written as

$$T_p = \frac{1}{2} \sum_{l=1}^{\infty} \sum_{m=-l}^l \frac{4\pi m_e R_b^6}{l(l+1)N} |\dot{n}_{lm}|^2, \quad (8.4)$$

where m_e is the bare electron mass and N is the number of electrons. Finally, the electrostatic energy (U_C) of the deformed MEB with a non-uniform surface electron density (8.3) is calculated using the Maxwell equations and the electrostatic boundary conditions at the surface. The result is:

$$\begin{aligned} U_C = & \frac{e^2 N^2}{2\varepsilon R_b} + 2\pi e^2 R_b^3 \sum_{l=1}^{\infty} \sum_{m=-l}^l \frac{|n_{lm}|^2}{l + \varepsilon(l+1)} \\ & - \frac{e^2 N^2}{8\pi\varepsilon R_b^3} \sum_{l=1}^{\infty} \sum_{m=-l}^l \frac{l^2 - \varepsilon(l+1)}{l + \varepsilon(l+1)} |Q_{lm}|^2 \\ & - e^2 N \sum_{l=1}^{\infty} \sum_{m=-l}^l \frac{l+1}{l + \varepsilon(l+1)} n_{lm} Q_{lm}^*, \end{aligned} \quad (8.5)$$

with the dielectric constant of liquid helium $\varepsilon \approx 1.0572$. The last term in Eq. (8.5) describes the ripplon-phonon mixing. Only ripplon and phonon modes which have the same angular momentum couple to each other. After the diagonalization of the Lagrangian of this ripplon-phonon system, we arrive at the eigenfrequencies:

$$\begin{aligned} \Omega_{1,2}(l) = & \left\{ \frac{1}{2} \left[\omega_p^2(l) + \omega_r^2(l) \right. \right. \\ & \left. \left. \pm \sqrt{[\omega_p^2(l) - \omega_r^2(l)]^2 + 4\gamma^2(l)} \right] \right\}^{1/2}, \end{aligned} \quad (8.6)$$

where $\omega_r(l)$ is the bare ripplon frequency,

$$\begin{aligned} \omega_r(l) = & \left\{ \frac{l+1}{\rho R_b^3} \left[\sigma(l^2 + l + 2) \right. \right. \\ & \left. \left. - \frac{e^2 N^2}{4\pi\varepsilon R_b^3} \frac{l^2 - \varepsilon(l+1)}{l + \varepsilon(l+1)} + 2pR_b \right] \right\}^{1/2}, \end{aligned} \quad (8.7)$$

while $\omega_p(l)$ is the bare phonon frequency,

$$\omega_p(l) = \left(\frac{e^2 N}{m_e R_b^3} \frac{l(l+1)}{l + \varepsilon(l+1)} \right)^{1/2}, \quad (8.8)$$

and $\gamma(l)$ describes the ripplon-phonon coupling:

$$\gamma(l) = \frac{e^2 N}{R_b^3} \left(\frac{Nl}{4\pi m_e \rho R_b^3} \right)^{1/2} \frac{(l+1)^2}{l + \varepsilon(l+1)}. \quad (8.9)$$

B. Electron-ripplon interaction in the MEB

The interaction energy between the riplons and the electrons in the multielectron bubble can be derived from the following considerations: (i) the distance between the layer electrons and the helium surface is fixed (the electrons find themselves confined to an effectively 2D surface anchored to the helium surface) and (ii) the electrons are subjected to a force field, arising from the electric field of the other electrons. For a spherical bubble, this electric field lies along the radial direction and equals

$$\mathbf{E} = -\frac{Ne}{2R_b^2} \mathbf{e}_r. \quad (8.10)$$

A bubble shape oscillation will displace the layer of electrons anchored to the surface. The interaction energy which arises from this, equals the displacement of the electrons times the force $e\mathbf{E}$ acting on them. Thus, we get for the interaction Hamiltonian

$$\hat{H}_{int} = \sum_j e|\mathbf{E}| \times u(\hat{\Omega}_j). \quad (8.11)$$

Here $u(\Omega)$ is the radial displacement of the surface in the direction given by the spherical angle Ω ; and $\hat{\Omega}_j$ is the (angular) position operator for electron j . The displacement can be rewritten using (8.1) and we find

$$\hat{H}_{int} = \sum_j e|\mathbf{E}| \sum_{\ell,m} \hat{Q}_{\ell m} Y_{\ell m}(\hat{\Omega}_j). \quad (8.12)$$

Using the relation

$$\hat{Q}_{\ell,m} = (-1)^{(m-|m|)/2} \sqrt{\frac{\hbar(\ell+1)}{2\rho R_b^3 \omega_\ell}} (\hat{a}_{\ell,m} + \hat{a}_{\ell,-m}^+), \quad (8.13)$$

the interaction Hamiltonian can be written in the suggestive form

$$\hat{H}_{int} = \sum_{\ell,m} \sum_j M_{\ell,m} Y_{\ell,m}(\hat{\Omega}_j) (\hat{a}_{\ell,m} + \hat{a}_{\ell,-m}^+), \quad (8.14)$$

with the electron-rippion coupling amplitude for a MEB given by

$$M_{\ell,m} = (-1)^{(m-|m|)/2} \frac{Ne^2}{2R_b^2} \sqrt{\frac{\hbar(\ell+1)}{2\rho R_b^3 \omega_\ell}} \quad (8.15)$$

C. Locally flat approximation

Substituting $M_{\ell,m}$ into (8.14), we get

$$\begin{aligned} \hat{H}_{int} &= \sum_{\ell,m} \sum_j \frac{Ne^2}{2R_b^2} \sqrt{\frac{\hbar(\ell+1)}{2\rho R_b^3 \omega_\ell}} \\ &\times \left[(-1)^{(m-|m|)/2} \frac{Y_{\ell,m}(\hat{\Omega}_j)}{R_b} \right] (\hat{a}_{\ell,m} + \hat{a}_{\ell,-m}^+). \end{aligned} \quad (8.16)$$

In this expression, we consider the limit of a bubble so large that the surface becomes flat on all length scales of interest. Hence we let $R_b \rightarrow \infty$ but keep $\ell/R_b = q$ a constant. This means we have to let $\ell \rightarrow \infty$ as well. In this limit,

$$\lim_{\ell \rightarrow \infty} Y_{\ell,0}(\theta) = \frac{i^\ell}{\pi \sqrt{\sin \theta}} \sin[(\ell + 1/2)\theta + \pi/4], \quad (8.17)$$

and $Y_{\ell,0}(\theta)$ varies locally as a plane wave with wave vector $q = \ell/R_b$. The wave function $Y_{\ell,m}(\hat{\Omega}_j)/R_b$ is furthermore normalized with respect to integration over the surface (with total area $4\pi R_b^2$). Thus, we get in the locally flat approximation

$$\hat{H}_{int} = \sum_{\mathbf{q}} \sum_j \frac{Ne^2}{2R_b^2} \sqrt{\frac{\hbar q}{2\rho\omega(q)}} e^{i\mathbf{q}\cdot\hat{\mathbf{r}}_j} (\hat{a}_{\mathbf{q}} + \hat{a}_{-\mathbf{q}}^+), \quad (8.18)$$

or

$$\begin{aligned} \hat{H}_{int} &= \sum_{\mathbf{q}} \sum_j M_q e^{i\mathbf{q}\cdot\hat{\mathbf{r}}_j} (\hat{a}_{\mathbf{q}} + \hat{a}_{-\mathbf{q}}^+), \\ M_q &= e|\mathbf{E}| \sqrt{\frac{\hbar q}{2\rho\omega(q)}}. \end{aligned} \quad (8.19)$$

This corresponds in the limit of large bubbles to the interaction Hamiltonian expected for a flat surface.

D. Ripplipolaron in a Wigner lattice: the mean-field approach

In their treatment of the electron Wigner lattice embedded in a polarizable medium such as a semiconductors or an ionic solid, Fratini and Quémerais [116] described the effect of

the electrons on a particular electron through a mean-field lattice potential. The (classical) lattice potential V_{lat} is obtained by approximating all the electrons acting on one particular electron by a homogenous charge density in which a hole is punched out; this hole is centered in the lattice point of the particular electron under investigation and has a radius given by the lattice distance d .

Within this particular mean-field approximation, the lattice potential can be calculated from classical electrostatics and we find that for a 2D electron gas it can be expressed in terms of the elliptic functions of first and second kind, $E(x)$ and $K(x)$,

$$V_{lat}(\mathbf{r}) = -\frac{2e^2}{\pi d^2} \left\{ |d-r| E \left[-\frac{4rd}{(d-r)^2} \right] + (d+r) \operatorname{sgn}(d-r) K \left[-\frac{4rd}{(d-r)^2} \right] \right\}. \quad (8.20)$$

Here, \mathbf{r} is the position vector measured from the lattice position. We can expand this potential around the origin to find the small-amplitude oscillation frequency of the electron lattice:

$$\lim_{r \ll d} V_{lat}(\mathbf{r}) = -\frac{2e^2}{d} + \frac{1}{2} m_e \omega_{lat}^2 r^2 + \mathcal{O}(r^4), \quad (8.21)$$

with the confinement frequency

$$\omega_{lat} = \sqrt{\frac{e^2}{m_e d^3}}. \quad (8.22)$$

In the mean-field approximation, the Hamiltonian for a ripplon-polaron in a lattice on a *locally flat* helium surface is given by

$$\hat{H} = \frac{\hat{p}^2}{2m_e} + V_{lat}(\hat{\mathbf{r}}) + \sum_{\mathbf{q}} \hbar \omega(q) \hat{a}_{\mathbf{q}}^+ \hat{a}_{\mathbf{q}} + \sum_{\mathbf{q}} M_q e^{-i\mathbf{q} \cdot \mathbf{r}} (\hat{a}_{\mathbf{q}} + \hat{a}_{-\mathbf{q}}^+), \quad (8.23)$$

where $\hat{\mathbf{r}}$ is the electron position operator.

Now that the lattice potential has been introduced, we can move on and include effects of the bubble geometry. If we restrict our treatment to the case of large bubbles (with $N > 10^5$ electrons), then both the ripplon-polaron radius and the inter-electron distance d are much smaller than the radius of the bubble R_b . This gives us ground to use the locally flat approximation using the auxiliary model of a ripplonic polaron in a planar system described by (8.23), but with a modified ripplon dispersion relation and an modified pressing field.

We find for the modified ripplon dispersion relation in the MEB:

$$\omega(q) = \sqrt{\frac{\sigma}{\rho}q^3 + \frac{p}{\rho R_b}q}, \quad (8.24)$$

where R_b is the equilibrium bubble radius which depends on the pressure and the number of electrons. The bubble radius is found by balancing the surface tension and the pressure with the Coulomb repulsion. The modified electron-riplon interaction amplitude in an MEB is given by

$$M_{\mathbf{q}} = e|\mathbf{E}|\sqrt{\frac{\hbar q}{2\rho\omega(q)}}. \quad (8.25)$$

The effective electric pressing field pushing the electrons against the helium surface and determining the strength of the electron-riplon interaction is

$$\mathbf{E} = -\frac{Ne}{2R_b^2}\mathbf{e}_r. \quad (8.26)$$

E. Ripplon Wigner lattice at finite temperature

To study the ripplon Wigner lattice at finite temperature and for any value of the electron-riplon coupling, we use the variational path-integral approach [43]. This variational principle distinguishes itself from Rayleigh-Ritz variation in that it uses a trial action functional S_{trial} instead of a trial wave function.

The action functional of the system described by Hamiltonian (8.23), becomes, after elimination of the ripplon degrees of freedom,

$$\begin{aligned} S = & -\frac{1}{\hbar} \int_0^{\hbar\beta} d\tau \left\{ \frac{m_e}{2} \dot{r}^2(\tau) + V_{lat}[r(\tau)] \right\} + \sum_{\mathbf{q}} |M_{\mathbf{q}}|^2 \\ & \times \int_0^{\hbar\beta} d\tau \int_0^{\hbar\beta} d\sigma G_{\omega(q)}(\tau - \sigma) e^{i\mathbf{q} \cdot [\mathbf{r}(\tau) - \mathbf{r}(\sigma)]}, \end{aligned} \quad (8.27)$$

with

$$G_{\nu}(\tau - \sigma) = \frac{\cosh[\nu(|\tau - \sigma| - \hbar\beta/2)]}{\sinh(\beta\hbar\nu/2)}. \quad (8.28)$$

In preparation of its customary use in the Jensen-Feynman inequality, the action functional (8.27) is written in imaginary time $t = i\tau$ with $\beta = 1/(k_B T)$ where T is the temperature.

We introduce a quadratic trial action of the form

$$S_{trial} = -\frac{1}{\hbar} \int_0^{\hbar\beta} d\tau \left[\frac{m_e}{2} \dot{r}^2(\tau) + \frac{m_e \Omega^2}{2} r^2(\tau) \right] - \frac{Mw^2}{4\hbar} \int_0^{\hbar\beta} d\tau \int_0^{\hbar\beta} d\sigma G_w(\tau - \sigma) \mathbf{r}(\tau) \cdot \mathbf{r}(\sigma). \quad (8.29)$$

where M , w , and Ω are the variationally adjustable parameters. This trial action corresponds to the Lagrangian

$$\mathcal{L}_0 = \frac{m_e}{2} \dot{r}^2 + \frac{M}{2} \dot{R}^2 - \frac{\kappa}{2} r^2 - \frac{K}{2} (\mathbf{r} - \mathbf{R})^2, \quad (8.30)$$

from which the degrees of freedom associated with \mathbf{R} have been integrated out. This Lagrangian can be interpreted as describing an electron with mass m_e at position \mathbf{r} , coupled through a spring with spring constant κ to its lattice site, and to which a fictitious mass M at position \mathbf{R} has been attached with another spring, with spring constant K . The relation between the spring constants in (8.30) and the variational parameters w, Ω is given by

$$w = \sqrt{K/m_e}, \quad (8.31)$$

$$\Omega = \sqrt{(\kappa + K)/m_e}. \quad (8.32)$$

Based on the trial action S_{trial} , Feynman's variational method allows one to obtain an upper bound for the free energy F of the system (at temperature T) described by the action functional S by minimizing the following function:

$$F = F_0 - \frac{1}{\beta} \langle S - S_{trial} \rangle, \quad (8.33)$$

with respect to the variational parameters of the trial action. In this expression, F_0 is the free energy of the trial system characterized by the Lagrangian \mathcal{L}_0 , $\beta = 1/(k_b T)$ is the inverse temperature, and the expectation value $\langle S - S_{trial} \rangle$ is to be taken with respect to the ground state of this trial system. The evaluation of expression (8.33) is straightforward

though lengthy. We find

$$\begin{aligned}
F &= \frac{2}{\beta} \ln \left[2 \sinh \left(\frac{\beta \hbar \Omega_1}{2} \right) \right] + \frac{2}{\beta} \ln \left[2 \sinh \left(\frac{\beta \hbar \Omega_2}{2} \right) \right] \\
&- \frac{2}{\beta} \ln \left[2 \sinh \left(\frac{\beta \hbar w}{2} \right) \right] - \frac{\hbar}{2} \sum_{i=1}^2 a_i^2 \Omega_i \coth \left(\frac{\beta \hbar \Omega_i}{2} \right) \\
&- \frac{\sqrt{\pi} e^2}{D} e^{-d^2/(2D)} \left[I_0 \left(\frac{d^2}{2D} \right) + I_1 \left(\frac{d^2}{2D} \right) \right] \\
&- \frac{1}{2\pi \hbar \beta} \int_{1/R_b}^{\infty} dq q |M_q|^2 \int_0^{\hbar \beta/2} d\tau \frac{\cosh[\omega(q)(\tau - \hbar \beta/2)]}{\sinh[\beta \hbar \omega(q)/2]} \\
&\times \exp \left[-\frac{\hbar q^2}{2m_e} \sum_{j=1}^2 a_j^2 \frac{\cosh(\hbar \Omega_j \beta/2) - \cosh[\hbar \Omega_j (\tau - \beta/2)]}{\Omega_j \sinh(\hbar \Omega_j \beta/2)} \right].
\end{aligned} \tag{8.34}$$

In this expression, I_0 and I_1 are Bessel functions of imaginary argument, and

$$D = \frac{\hbar}{m_e} \sum_{j=1}^2 \frac{a_j^2}{\Omega_j} \coth(\hbar \Omega_j \beta/2), \tag{8.35}$$

$$a_1 = \sqrt{\frac{\Omega_1^2 - w^2}{\Omega_1^2 - \Omega_2^2}}; a_2 = \sqrt{\frac{w^2 - \Omega_2^2}{\Omega_1^2 - \Omega_2^2}}. \tag{8.36}$$

Finally, Ω_1 and Ω_2 are the eigenfrequencies of the trial system, given by

$$\Omega_{1,2}^2 = \frac{1}{2} \left[\Omega^2 + w^2 \pm \sqrt{(\Omega^2 - w^2)^2 + 4K/(Mm_e)} \right]. \tag{8.37}$$

Optimal values of the variational parameters are determined by the numerical minimization of the variational functional F as given by expression (8.34).

F. Melting of the ripplopolaron Wigner lattice

The Lindemann melting criterion [117] states in general that a crystal lattice of objects (be it atoms, molecules, electrons, or ripplopolarons) will melt when the average motion of the objects around their lattice site is larger than a critical fraction δ_0 of the lattice parameter d . It would be a strenuous task to calculate from first principles the exact value of the critical fraction δ_0 , but for the particular case of electrons on a helium surface, we can make use of an experimental determination. Grimes and Adams [118] found that the Wigner lattice melts when $\Gamma = 137 \pm 15$, where Γ is the ratio of potential energy to the kinetic energy per electron. At temperature T the average kinetic energy in a lattice potential V_{lat} is

$$E_{kin} = \frac{\hbar \omega_{lat}}{2} \coth \left(\frac{\hbar \omega_{lat}}{2k_B T} \right), \tag{8.38}$$

and the average distance that an electron moves out of the lattice site is determined by

$$\langle \mathbf{r}^2 \rangle = \frac{\hbar}{m_e \omega_{lat}} \coth \left(\frac{\hbar \omega_{lat}}{2k_B T} \right) = \frac{2E_{kin}}{m_e \omega_{lat}^2}. \quad (8.39)$$

From this we find that for the melting transition in Grimes and Adams' experiment [118], the critical fraction equals $\delta_0 \approx 0.13$. This estimate is in agreement with previous (empirical) estimates yielding $\delta_0 \approx 0.1$ [119], and we shall use it in the rest of this section.

Within the approach of Fratini and Qu  merais [116], the Wigner lattice of (rip-
plo)polarens melts when at least one of the two following Lindemann criteria are met:

$$\delta_r = \frac{\sqrt{\langle \mathbf{R}_{cms}^2 \rangle}}{d} > \delta_0, \quad (8.40)$$

$$\delta_\rho = \frac{\sqrt{\langle \rho^2 \rangle}}{d} > \delta_0. \quad (8.41)$$

where ρ and \mathbf{R}_{cms} are, respectively, the relative coordinate and the center of mass coordinate of the model system (8.30): if \mathbf{r} is the electron coordinate and \mathbf{R} is the position coordinate of the fictitious ripplon mass M , this is

$$\mathbf{R}_{cms} = \frac{m_e \mathbf{r} + M \mathbf{R}}{m_e + M}; \rho = \mathbf{r} - \mathbf{R}. \quad (8.42)$$

The appearance of two Lindemann criteria takes into account the composite nature of (rip-
plo)polarens. As follows from the physical sense of the coordinates ρ and \mathbf{R}_{cms} , the first criterion (8.40) is related to the melting of the ripplon Wigner lattice towards a rip-
plopolarens liquid, where the ripplonpolarens move as a whole, the electron together with its dimple. The second criterion (8.41) is related to the dissociation of ripplonpolarens: the electrons shed their dimple.

The path-integral variational formalism allows us to calculate the expectation values $\langle \mathbf{R}_{cms}^2 \rangle$ and $\langle \rho^2 \rangle$ with respect to the ground state of the variationally optimal model system. We find

$$\begin{aligned} \langle \mathbf{R}_{cms}^2 \rangle &= \frac{\hbar w^4}{m_e [w^2(\Omega_1^2 + \Omega_2^2) - \Omega_1^2 \Omega_2^2] (\Omega_1^2 - \Omega_2^2)} \\ &\times [\Omega_2^4 (\Omega_1^2 - w^2) \coth(\hbar \Omega_1 \beta / 2) / \Omega_1 \\ &+ \Omega_1^4 (w^2 - \Omega_2^2) \coth(\hbar \Omega_2 \beta / 2) / \Omega_2], \end{aligned} \quad (8.43)$$

$$\begin{aligned}
\langle \rho^2 \rangle &= \frac{\hbar}{m_e (\Omega_1^2 - \Omega_2^2) (\Omega_1^2 - w^2) (w^2 - \Omega_2^2)} \\
&\times [\Omega_1^3 (w^2 - \Omega_2^2) \coth(\hbar\Omega_1\beta/2) \\
&+ \Omega_2^3 (\Omega_1^2 - w^2) \coth(\hbar\Omega_2\beta/2)].
\end{aligned} \tag{8.44}$$

Numerical calculation shows that for ripplon polarons in an MEB the inequality $\Omega_1 \gg w$ is fulfilled ($w/\Omega_1 \approx 10^{-3}$ to 10^{-2}) so that the strong-coupling regime is realized. Owing to this inequality, we find from Eqs. (8.43),(8.44) that

$$\langle \mathbf{R}_{cms}^2 \rangle \ll \langle \rho^2 \rangle. \tag{8.45}$$

So, the destruction of the ripplon polaron Wigner lattice in an MEB occurs through the dissociation of ripplon polarons, since the second criterion (8.41) will be fulfilled before the first (8.40). The results for the melting of the ripplon polaron Wigner lattice are summarized in the phase diagram shown in Fig. 21.

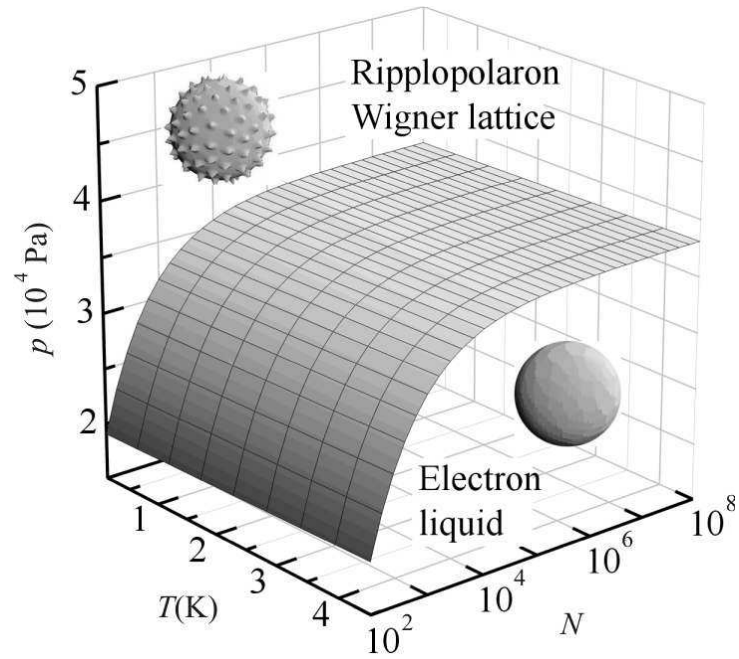


FIG. 21: The phase diagram for the spherical 2D layer of electrons in the MEB. Above a critical pressure, a ripplopolaron solid (a Wigner lattice of electrons with dimples in the helium surface underneath them) is formed. Below the critical pressure, the ripplopolaron solid melts into an electron liquid through dissociation of ripplopolarons. (From Ref. [111].)

For every value of N , pressure p and temperature T in an experimentally accessible range, this figure shows whether the ripplopolaron Wigner lattice is present (points above the surface) or molten (points below the surface). Below a critical pressure (on the order of 10^4 Pa) the ripplopolaron solid will melt into an electron liquid. This critical pressure is nearly independent of the number of electrons (except for the smallest bubbles) and is weakly temperature dependent, up to the helium critical temperature 5.2 K. This can be understood since the typical lattice potential well in which the ripplopolaron resides has frequencies of the order of THz or larger, which correspond to ~ 10 K.

The new phase that we predict, the ripplopolaron Wigner lattice, will not be present for electrons on a flat helium surface. At the values of the pressing field necessary to obtain a strong enough electron-ripplon coupling, the flat helium surface is no longer stable against long-wavelength deformations [120]. Multielectron bubbles, with their different ripplon dispersion and the presence of stabilizing factors such as the energy barrier against fissioning [121], allow for much larger electric fields pressing the electrons against the helium surface. The regime of N , p , T parameters suitable for the creation of a ripplopolaron Wigner lattice lies within the regime that would be achievable in recently proposed experiments aimed at stabilizing multielectron bubbles [114]. The ripplopolaron Wigner lattice and its melting transition might be detected by spectroscopic techniques [118, 122] probing for example the transverse phonon modes of the lattice [123].

Acknowledgments

I thank S. N. Klimin for discussions in the course of the preparation of the third edition of the Lectures.

Appendix A: Optical conductivity of a strong-coupling Fröhlich polaron [*S. N. Klimin and J. T. Devreese, Phys. Rev. B 89, 035201 (2014)*]

1. Introduction

The optical conductivity of the Fröhlich polaron model attracted attention for years [125]. In the regime of weak coupling, the optical absorption of a polaron was calculated using different methods, e. g., Green's function method [71], the Low-Lee-Pines formalism [73, 80], perturbation expansion of the current-current correlation function [126]. The strong-coupling polaron optical conductivity was calculated taking into account one-phonon [49] and two-phonon [75] transitions from the polaron ground state to the polaron relaxed excited state (RES). In fact the present work finalizes the project started in Ref. [49]. Using the path integral response formalism, the impedance function of an all-coupling polaron was calculated by FHIP [47] on the basis of the Feynman polaron model [43]. Developing further the FHIP approach, the optical conductivity was calculated in the path-integral formalism at zero temperature [50] and at finite temperatures [76]. In Ref. [127], the extension of the method of Ref. [50] accounting for the polaron damping (for the polaron coupling constant $\alpha \lesssim 8$) and the asymptotic strong-coupling approach using the Franck-Condon (FC) picture for the optical conductivity (for $\alpha \gtrsim 8$) have given reasonable results for the polaron optical conductivity at all values of α . The concept of the RES and FC polaron states played a key role in the understanding of the mechanism of the polaron optical conductivity [7, 41, 49, 50, 75, 76].

Recently, the Diagrammatic Quantum Monte Carlo (DQMC) numerical method has been developed [30, 79], which provides accurate results for the polaron characteristics in all coupling regimes. The analytic treatment [50] was intended to be valid at all coupling strengths. However, it is established in [7, 50, 75] that the linewidth of the obtained spectra [50] is unreliable for $\alpha \gtrsim 7$. Nevertheless, the position of the peak attributed to RES in Ref. [50] is close to the maximum of the polaron optical conductivity band calculated using DQMC up to very large values of α (see Fig. 1).

An extension of the path-integral approach [50] performed in Ref. [127] gives a good agreement with DQMC for weak and intermediate coupling strengths. In the strong-coupling limit, in Ref. [127] the adiabatic strong-coupling expansion was applied. That expansion,

however, is not exact in the strong-coupling limit because of a parabolic approximation [35] for the adiabatic potential.

In the present work, the strong-coupling approach of Ref. [127] is extended in order to obtain the polaron optical conductivity which is *asymptotically exact in the strong-coupling limit*. We develop the multiphonon strong-coupling expansion using numerically accurate in the strong-coupling limit polaron energies and wave functions and accounting for non-adiabaticity.

2. Optical conductivity

We consider the electron-phonon system with the Hamiltonian written down in the Feynman units ($\hbar = 1$, the carrier band mass $m_b = 1$, and the LO-phonon frequency $\omega_{\text{LO}} = 1$)

$$H = \frac{\mathbf{p}^2}{2} + \sum_{\mathbf{q}} \left(b_{\mathbf{q}}^{\dagger} b_{\mathbf{q}} + \frac{1}{2} \right) + \frac{1}{\sqrt{V}} \sum_{\mathbf{q}} \frac{\sqrt{2\sqrt{2}\pi\alpha}}{q} (b_{\mathbf{q}} + b_{-\mathbf{q}}^{\dagger}) e^{i\mathbf{q}\cdot\mathbf{r}}. \quad (\text{A1})$$

where \mathbf{r}, \mathbf{p} represent the position and momentum of an electron, $b_{\mathbf{q}}^{\dagger}, b_{\mathbf{q}}$ denote the creation and annihilation operators for longitudinal optical (LO) phonons with wave vector \mathbf{q} , and $V_{\mathbf{q}}$ describes the amplitude of the interaction between the electrons and the phonons. For the Fröhlich electron-phonon interaction, the amplitude of the electron – LO-phonon interaction is

$$V_{\mathbf{q}} = \frac{1}{\sqrt{V}} \frac{\sqrt{2\sqrt{2}\pi\alpha}}{q} \quad (\text{A2})$$

with the crystal volume V , and the electron-phonon coupling constant α .

The polaron optical conductivity describes the response of the system with the Hamiltonian (5.2) to an applied electromagnetic field (along the z -axis) with frequency ω . This optical response is expressed using the Kubo formula with a dipole-dipole correlation function:

$$\text{Re } \sigma(\omega) = \frac{n_0 \omega}{2} (1 - e^{-\beta\omega}) \int_{-\infty}^{\infty} e^{i\omega t} \langle d_z(t) d_z \rangle dt, \quad (\text{A3})$$

where $\mathbf{d} = -e_0 \mathbf{r}$ is the electric dipole moment, e_0 is the unit charge, $\beta = \frac{1}{k_B T}$, n_0 is the electron density. In the zero-temperature limit, the optical conductivity (A3) measured in units of e_0^2 becomes

$$\text{Re } \sigma(\omega) = \frac{\omega}{2} \int_{-\infty}^{\infty} e^{i\omega t} f_{zz}(t) dt, \quad (\text{A4})$$

with the correlation function

$$f_{zz}(t) \equiv \langle z(t)z(0) \rangle = \langle \Psi_0 | e^{itH} z e^{-itH} z | \Psi_0 \rangle, \quad (\text{A5})$$

where $|\Psi_0\rangle$ is the ground-state wave function of the electron-phonon system.

Within the strong-coupling approach, the ground-state wave function is chosen as the product of a trial wave function of an electron $|\psi_0^{(e)}\rangle$ and of a trial wave function of a phonon subsystem $|\Phi_{ph}\rangle$:

$$|\Psi_0\rangle = |\psi_0^{(e)}\rangle |\Phi_{ph}\rangle. \quad (\text{A6})$$

The phonon trial wave function is written as the strong-coupling unitary transformation applied to the phonon vacuum

$$|\Phi_{ph}\rangle = U |0_{ph}\rangle. \quad (\text{A7})$$

with the unitary operator

$$U = e^{\sum_{\mathbf{q}} (f_{\mathbf{q}} b_{\mathbf{q}} - f_{\mathbf{q}}^* b_{\mathbf{q}}^+)}, \quad (\text{A8})$$

and the variational parameters $\{f_{\mathbf{q}}\}$. The transformed Hamiltonian $\tilde{H} \equiv U^{-1} H U$ takes the form

$$\tilde{H} = \tilde{H}_0 + W \quad (\text{A9})$$

with the terms

$$\tilde{H}_0 = \frac{\mathbf{p}^2}{2} + \sum_{\mathbf{q}} |f_{\mathbf{q}}|^2 + V_a(r) + \sum_{\mathbf{q}} \left(b_{\mathbf{q}}^+ b_{\mathbf{q}} + \frac{1}{2} \right), \quad (\text{A10})$$

$$W = \sum_{\mathbf{q}} (W_{\mathbf{q}} b_{\mathbf{q}} + W_{\mathbf{q}}^* b_{\mathbf{q}}^+). \quad (\text{A11})$$

Here, $W_{\mathbf{q}}$ are the amplitudes of the renormalized electron-phonon interaction

$$W_{\mathbf{q}} = \frac{\sqrt{2\sqrt{2}\pi\alpha}}{q\sqrt{V}} (e^{i\mathbf{q}\cdot\mathbf{r}} - \rho_{\mathbf{q}}), \quad (\text{A12})$$

where $\rho_{\mathbf{q}}$ is the expectation value of the operator $e^{i\mathbf{q}\cdot\mathbf{r}}$ with the trial electron wave function $|\psi_0^{(e)}\rangle$:

$$\rho_{\mathbf{q}} = \langle \psi_0^{(e)} | e^{i\mathbf{q}\cdot\mathbf{r}} | \psi_0^{(e)} \rangle, \quad (\text{A13})$$

and $V_a(r)$ is the self-consistent potential energy for the electron,

$$V_a(r) = - \sum_{\mathbf{q}} \frac{4\sqrt{2}\pi\alpha}{q^2 V} \rho_{-\mathbf{q}} e^{i\mathbf{q}\cdot\mathbf{r}}. \quad (\text{A14})$$

Averaging the Hamiltonian (A9) with the phonon vacuum $|0\rangle$ and with the trial electron wave function $|\psi_0\rangle$, we arrive at the following variational expression for the ground-state energy

$$E_0 = \langle \Psi_0 | H | \Psi_0 \rangle = \left\langle \psi_0 \left| \frac{\mathbf{p}^2}{2} \right| \psi_0 \right\rangle + \sum_{\mathbf{q}} |f_{\mathbf{q}}|^2 - \sum_{\mathbf{q}} (V_{\mathbf{q}} f_{\mathbf{q}}^* \rho_{\mathbf{q}} + V_{\mathbf{q}}^* f_{\mathbf{q}} \rho_{-\mathbf{q}}), \quad (\text{A15})$$

After minimization of the polaron ground-state energy (A15), the parameters $f_{\mathbf{q}}$ acquire their optimal values

$$f_{\mathbf{q}} = V_{\mathbf{q}} \rho_{\mathbf{q}}. \quad (\text{A16})$$

The ground-state energy with $\{f_{\mathbf{q}}\}$ given by Eq. (A16) takes the form

$$E_0 = \left\langle \psi_0 \left| \frac{\mathbf{p}^2}{2} \right| \psi_0 \right\rangle - \sum_{\mathbf{q}} |V_{\mathbf{q}}|^2 |\rho_{\mathbf{q}}|^2. \quad (\text{A17})$$

With the strong-coupling Ansatz (A6) for the polaron ground-state wave function and after the application of the unitary transformation (A8), the correlation function (A5) takes the form

$$f_{zz}(t) = \left\langle 0_{ph} \left| \left\langle \psi_0 \left| e^{it\tilde{H}} z e^{-it\tilde{H}} z \right| \psi_0 \right\rangle \right| 0_{ph} \right\rangle. \quad (\text{A18})$$

This correlation function can be expanded using a complete orthogonal set of intermediate states $|j\rangle$ and the completeness property:

$$\sum_j |j\rangle \langle j| = 1. \quad (\text{A19})$$

In the present work, we use the intermediate basis of the Franck-Condon (FC) states. The FC states correspond to the equilibrium phonon configuration for the ground state. Thus the FC wave functions are the exact eigenstates of the Hamiltonian \tilde{H}_0 . Further on, the FC wave functions are written in the spherical-wave representation as $|\psi_{n,l,m}\rangle = R_{n,l}(r) Y_{l,m}(\theta, \varphi)$ where $R_{n,l}(r)$ are the radial wave functions, and $Y_{l,m}(\theta, \varphi)$ are the spherical harmonics, l is the quantum number of the angular momentum, m is the z -projection of the angular momentum, and n is the radial quantum number⁸. The energy levels for the eigenstates of the Hamiltonian \tilde{H}_0 are denoted $E_{n,l}$.

⁸In this classification, the ground-state wave function is $|\psi_{0,0,0}\rangle \equiv |\psi_0\rangle$.

Using (A19) with that complete and orthogonal basis , we transform (A18) to the expression

$$f_{zz}(t) = \sum_{\substack{n,l,m, \\ n',l',m', \\ n'',l'',m''}} \langle \psi_{n,l,m} | z | \psi_{n'',l'',m''} \rangle \langle \psi_{n',l',m'} | z | \psi_0 \rangle \\ \times \left\langle 0_{ph} \left| \left\langle \psi_0 \left| e^{it\tilde{H}} \right| \psi_{n,l,m} \right\rangle \left\langle \psi_{n'',l'',m''} \left| e^{-it\tilde{H}} \right| \psi_{n',l',m'} \right\rangle \right| 0_{ph} \right\rangle. \quad (\text{A20})$$

So far, the only approximation made in (A20) is the strong-coupling Ansatz for the polaron ground-state wave function. However, in order to obtain a numerically tractable expression for the polaron optical conductivity, an additional approximation valid in the strong-coupling limit must be applied to the matrix elements of the evolution operator $e^{-it\tilde{H}}$ with the Hamiltonian of the electron-phonon system \tilde{H} given by formula (A9). According to Ref. [128], in the strong-coupling limit, the matrix elements of the Hamiltonian of the electron-phonon system between states corresponding to different energy levels are of order of magnitude α^{-4} . Therefore in the strong-coupling regime these matrix elements can be neglected; this is called the adiabatic or the Born-Oppenheimer (BO) approximation [128], because of its strict analogy with the Born-Oppenheimer adiabatic approximation in the theory of molecules and crystals ([129], p. 171). Consequently, in the further treatment we neglect the matrix elements $\left\langle \psi_{n,l,m} \left| e^{-it\tilde{H}} \right| \psi_{n',l',m'} \right\rangle$ for the FC states with different energies, $E_{n,l} \neq E_{n',l'}$. The same scheme was used in the theory of the multi-phonon optical processes for bound electrons interacting with phonons [23, 130].

Strictly speaking, the summation over the excited polaron states in Eq. (A20) must involve the transitions to both the discrete and continuous parts of the polaron spectrum. A transition to the states of the continuous spectrum means that the electron leaves the polaron potential well. Therefore these transitions can be attributed to the ‘‘polaron dissociation’’. The transitions to the continuous spectrum are definitely beyond the adiabatic approximation. As shown in Ref. [23], the transition probability to the states of the continuous spectrum is very small compared with the transition probability between the ground and the first excited state (which belongs to the discrete part of the polaron energy spectrum). We neglect here the contribution to the polaron optical conductivity due to the transitions to the continuous spectrum.

The matrix elements neglected within the adiabatic approximation correspond to the transitions between FC states with different energies due to the electron-phonon interac-

tion. Hence these transitions can be called non-adiabatic. The adiabatic approximation is related to the matrix elements of the evolution operator $e^{-it\tilde{H}}$. On the contrary, the matrix elements of the transitions between different FC states for the electric dipole moment are, in general, not equal to zero. Moreover, these transitions can be accompanied by the emission of phonons. The electron FC wave functions constitute a complete orthogonal set. However, the corresponding phonon wave functions can be non-orthogonal because of a different shift of phonon coordinates for different electron states. This makes multi-phonon transitions possible [130]. It is important to note that in our treatment we neglect only the non-adiabatic transitions between the electron states with *different* energies. On the contrary, the transitions within one and the same degenerate level can be non-adiabatic. This *internal non-adiabaticity* (i. e., the non-adiabaticity of the transitions within one and the same degenerate level) is taken into account in the subsequent treatment.

It is useful to stress the difference between the strong-coupling Ansatz and the adiabatic approximation. The strong-coupling Ansatz consists of the choice of the trial variational ground state wave function for the electron-phonon system in the factorized form (A6). The adiabatic approximation means neglecting the matrix elements of the evolution operator between internal polaron states with different energies. These two approximations are not the same, but they both are valid in the strong-coupling regime and consistent with each other.

The correlation function (A20) is transformed in the following way. The exponents $e^{it\tilde{H}}$ and $e^{-it\tilde{H}}$ are disentangled:

$$e^{-it\tilde{H}} = e^{-it\tilde{H}_0} \text{T exp} \left(-i \int_0^t ds W(s) \right), \quad (\text{A21})$$

$$e^{it\tilde{H}} = e^{it\tilde{H}_0} \text{T exp} \left(i \int_0^t ds W(-s) \right) \quad (\text{A22})$$

where $W(s)$ is the renormalized electron-phonon interaction Hamiltonian W in the interaction representation,

$$W(s) \equiv e^{is\tilde{H}_0} W e^{-is\tilde{H}_0}. \quad (\text{A23})$$

This gives us the result

$$\begin{aligned}
f_{zz}(t) &= \sum_{\substack{n,l,m, \\ n',l',m', \\ n'',l'',m''}} \langle \psi_{n,l,m} | z | \psi_{n'',l'',m''} \rangle \langle \psi_{n',l',m'} | z | \psi_0 \rangle e^{it(E_0 - E_{n'',l'',m''})} \\
&\times \left\langle 0_{ph} \left| \left\langle \psi_0 \left| \text{T exp} \left(i \int_0^t ds W(-s) \right) \right| \psi_{n,l,m} \right\rangle \right. \\
&\times \left. \left\langle \psi_{n'',l'',m''} \left| \text{T exp} \left(-i \int_0^t ds W(s) \right) \right| \psi_{n',l',m'} \right\rangle \right| 0_{ph} \right\rangle. \tag{A24}
\end{aligned}$$

Within the adiabatic approximation, the optical conductivity is simplified. The full details of the derivation are described in the Appendix A. First, using the selection rules for the dipole matrix elements, the spherical symmetry of the Hamiltonian \tilde{H} and the adiabatic approximation, the correlation function (A24) is reduced to the form

$$\begin{aligned}
f_{zz}(t) &= \sum_n D_n e^{-i\Omega_{n,0}t} \\
&\times \left\langle \psi_{n,1,0} \left| \left\langle 0_{ph} \left| \text{T exp} \left[-i \int_0^t ds W(s) \right] \right| 0_{ph} \right\rangle \right| \psi_{n,1,0} \right\rangle \tag{A25}
\end{aligned}$$

where $\Omega_{n,0}$ is the FC transition frequency

$$\Omega_{n,0} \equiv E_{n,1} - E_0, \tag{A26}$$

and D_n is the squared modulus of the dipole transition matrix element

$$D_n = |\langle \psi_0 | z | \psi_{n,1,0} \rangle|^2. \tag{A27}$$

Within the adiabatic approximation, the partial (with the electron wave functions) averaging of the operator T-exponent in (A25) can be exactly performed (see details in Appendix A). As a result, the optical conductivity is transformed to the expression

$$\begin{aligned}
\text{Re } \sigma(\omega) &= \frac{\omega}{6} \sum_n D_n \int_{-\infty}^{\infty} e^{i(\omega - \Omega_{n,0})t} \\
&\times \left\langle 0_{ph} \left| \text{Tr} \left(\text{T exp} \left[-i \int_0^t ds \mathbb{W}^{(n)}(s) \right] \right) \right| 0_{ph} \right\rangle dt. \tag{A28}
\end{aligned}$$

The T-exponent in (A28) contains the finite-dimensional matrix $\mathbb{W}^{(n)}(s)$ depending on the phonon coordinates:

$$\left(\mathbb{W}_{k,l,m}^{(n)} \right)_{m_1, m_2} = \langle \psi_{n,1,m_1} | W_{k,l,m} | \psi_{n,1,m_2} \rangle \tag{A29}$$

where $W_{k,l,m}$ are the amplitudes of the electron-phonon interaction in the basis of spherical wave functions.

Because the kinetic energy of the phonons is of order α^{-4} compared to the leading term of the Hamiltonian [128], we neglect this kinetic energy in the present work, because the treatment is related to the strong-coupling regime. As a result, $Q_{k,l,m}$ commute with the Hamiltonian \tilde{H}_0 , so that in (A28), $\mathbb{W}^{(n)}(s) = \mathbb{W}^{(n)}$. Furthermore, in a finite-dimensional basis $\{|\psi_{n,l,m}\rangle\}$ for a given level (n, l) , all eigenvalues of the Hamiltonian \tilde{H}_0 are the same. Therefore the T-exponent entering (A28) in that finite-dimensional basis turns into a usual exponent. As a result, the strong-coupling polaron optical conductivity (A28) takes the form

$$\text{Re } \sigma(\omega) = \frac{\omega}{6} \sum_n D_n \int_{-\infty}^{\infty} e^{i(\omega - \Omega_{n,0})t} \langle 0_{ph} | \text{Tr} \exp(-i\mathbb{W}^{(n)}t) | 0_{ph} \rangle dt. \quad (\text{A30})$$

The matrix interaction Hamiltonian (A29) depends on the phonon coordinates, and the matrices $\mathbb{W}_{k,l,m}^{(n)}$ with different m for one and the same degenerate energy level do not commute with each other. According to the Jahn – Teller theorem [131], for a degenerate level there does not exist a unitary transformation which simultaneously diagonalizes all matrices $\mathbb{W}_{k,l,m}^{(n)}$ in a basis that does not depend on the phonon coordinates. The manifestations of that theorem are attributed to the Jahn – Teller effect. Therefore, because we neglect the non-commutation of the matrices $\mathbb{W}_{k,l,m}^{(n)}$, the Jahn – Teller effect is omitted.

In fact, neglecting the Jahn – Teller effect is not necessary. The averaging in Eq. (A30) is performed exactly using the effective phonon modes similarly to Ref. [133] (see the details in Appendix B). As a result, we arrive at the following expression for the strong-coupling polaron optical conductivity

$$\text{Re } \sigma(\omega) = \frac{\omega}{3\pi^2} \sum_n \frac{D_n}{a_0^{(n)}} \int_{-\infty}^{\infty} dx_0 \int_{-\infty}^{\infty} dx_1 \int_{-\infty}^{\infty} dx_2 \int_{-\infty}^{\infty} dy_1 \int_{-\infty}^{\infty} dy_2 \\ \times \sum_{j=1}^3 \exp \left\{ -\frac{1}{2} \left[x_0^2 + \sum_{m=1,2} (x_m^2 + y_m^2) + \frac{\left(\omega - \Omega_{n,0} - \frac{a_2^{(n)}}{2\sqrt{5}\pi} \lambda_j(Q_2) \right)^2}{\left(a_0^{(n)} \right)^2} \right] \right\}. \quad (\text{A31})$$

Here, $\lambda_j(Q_2)$ are the eigenvalues for the matrix interaction Hamiltonian, which are explicitly determined in the Appendix B by the formula (A74). The coefficients $a_0^{(n)}$ and $a_2^{(n)}$ are given by (A65) and (A66), respectively. The polaron optical conductivity given by the expression (A31), is in fact an envelope of the multiphonon polaron optical conductivity band with

the correlation function (A28) provided by the phonon-assisted transitions from the polaron ground state to the polaron RES. This result is consistent with Ref. [49], where the same paradigm of the phonon-assisted transitions to the polaron RES was exploited, but the calculation was limited to the one-phonon transition.

In order to reveal the significance of the Jahn – Teller effect for the polaron, we alternatively calculate $\langle 0_{ph} | \text{Tr} \exp(-i\mathbb{W}^{(n)}t) | 0_{ph} \rangle$ neglecting the non-commutation of the matrices $\mathbb{W}_{k,l,m}^{(n)}$, as described in the Appendix B. 2. The resulting expression for the polaron optical conductivity is much simpler than formula (A31) and is similar to the expression (3) of Ref. [127]:

$$\text{Re } \sigma(\omega) = \omega \sum_n \sqrt{\frac{\pi}{2\omega_s^{(n)}}} D_n \exp\left(-\frac{(\omega - \Omega_{n,0})^2}{2\omega_s^{(n)}}\right), \quad (\text{A32})$$

with the parameter (often called the Huang-Rhys factor)

$$\omega_s^{(n)} = \frac{1}{2} \left(a_0^{(n)}\right)^2 + \frac{1}{4\pi} \left(a_2^{(n)}\right)^2. \quad (\text{A33})$$

The strong-coupling electron energies and wave functions in Eq. (A28) can be calculated using different approximations. For example, within the Landau-Pekar (LP) approximation [35], the trial wave function $|\psi_0\rangle$ is chosen as the ground state of a 3D oscillator. Within the Pekar approximation [23], $|\psi_0\rangle$ is chosen in the form

$$|\psi_0(r)\rangle = C e^{-ar} (1 + ar + br^2) \quad (\text{A34})$$

with the variational parameters a and b . Finally, the trial ground state wave function can be determined numerically exactly following Miyake [40] (see also [132], Chap. 5.22). Within the LP approximation, formula (A32) reproduces the polaron optical conductivity obtained in Ref. [127].

In the LP approximation, the matrix elements $\langle \psi_0 | z | \psi_{n,1,0} \rangle$ are different from zero only for $n = 1$, i. e. only for the $1s \rightarrow 2p$ transition. Beyond the LP approximation, also the transitions to other excited states are allowed because of the nonparabolicity of the self-consistent potential $V_a(r)$. The use of exact strong-coupling wave functions, instead of the LP wave functions, may significantly influence the optical conductivity. In the present treatment we use the numerically exact electron energies and wave functions of both ground and first excited states according to Ref. [40]. The FC transition energies $\Omega_{n,0}$ to leading order of the strong-coupling approximation are determined according to (A26). In order to

account for the corrections of the FC energy with accuracy up to α^0 , we add to $\Omega_{n,0}$ the correction $\Delta\Omega_{\text{FC}} \approx -3.8$ from Ref. [127]. Because we use the numerically accurate strong-coupling wave functions and energies corresponding to Miyake [40], the formula (A24) is *asymptotically exact in the strong-coupling limit, at least in its leading term in powers of α^{-2} .*

3. Results and discussion

In Figs. 2 to 3, we have plotted the polaron optical conductivity spectra calculated for different values of the coupling constant α . The optical conductivity spectra calculated within the present strong-coupling approach taking into account the Jahn – Teller effect are shown by the solid curves. The optical conductivity derived neglecting the Jahn – Teller effect is shown by the dashed curves. It is worth mentioning that there is little difference in the optical conductivity spectra between those calculated with and without the Jahn – Teller effect. The optical conductivity obtained in Ref. [127] with the Landau-Pekar (LP) adiabatic approximation is plotted with dash-dotted curves. The full dots show the numerical Diagrammatic Quantum Monte Carlo (DQMC) data [79, 127]. The FC transition frequency for the transition to the first excited FC state $\Omega_{1,0} \equiv \Omega_{\text{FC}}$ and the RES transition frequency Ω_{RES} are explicitly indicated in the figures.

The polaron optical conductivity spectra calculated within the present strong-coupling approach are shifted to lower frequencies with respect to the optical conductivity spectra calculated within the LP approximation of Ref. [127]. This shift is due to the use of the numerically accurate strong coupling energy levels and wave functions of the internal polaron states, and of the numerically accurate self-consistent adiabatic polaron potential.

According to the selection rules for the matrix elements of the electron-phonon interaction, there is a contribution to the polaron optical conductivity from the phonon modes with angular momentum $l = 0$ (s -phonons) and with angular momentum $l = 2$ (d -phonons). The s -phonons are fully symmetric, therefore they do not contribute to the Jahn – Teller effect, while the d -phonons are active in the Jahn – Teller effect. The contribution of the d -phonons to the optical conductivity spectra is not small compared to the contribution of the s -phonons. However, the distinction between the optical conductivity spectra calculated with and without the Jahn – Teller effect is relatively small.

For $\alpha = 8$ and $\alpha = 8.5$, the maxima of the polaron optical conductivity spectra, calculated within the present strong-coupling approach are positioned to the low frequency side of the maxima of those calculated using the DQMC method. The agreement between our strong-coupling polaron optical conductivity spectra and the numerical DQMC data improves with increasing alpha. This is in accordance with the fact that the present strong-coupling approach for the polaron optical conductivity is asymptotically exact in the strong-coupling limit.

The total polaron optical conductivity must satisfy the sum rule [82]

$$\int_0^\infty \text{Re} \sigma(\omega) d\omega = \frac{\pi}{2}. \quad (\text{A35})$$

In the weak- and intermediate-coupling regimes at $T = 0$, there are two contributions to the left-hand side of that sum rule: (1) the contribution from the polaron optical conductivity for $\omega > \omega_{\text{LO}}$ and (2) the contribution from the “central peak” at $\omega = 0$, which is proportional to the inverse polaron mass [82]. In the asymptotic strong-coupling regime, the inverse to the polaron mass is of order α^{-4} , and hence the contribution from the “central peak” to the polaron optical conductivity is beyond the accuracy of the present approximation (where we keep the terms $\propto \alpha^{-2}$ and $\propto \alpha^0$).

As discussed above, in the present work the transitions from the ground state to the states of the continuous part of the polaron energy spectrum are neglected. Therefore the integral over the frequency [the left-hand side of (A35)] for the optical conductivity calculated within the present strong-coupling approximation can be (relatively slightly) smaller than $\pi/2$. The relative contribution of the transitions to the continuous part of the polaron spectrum, Δ_c , can be therefore estimated as

$$\Delta_c \equiv 1 - \frac{2}{\pi} \int_0^\infty \text{Re} \sigma(\omega) d\omega, \quad (\text{A36})$$

where the right-hand side is obtained by a numerical integration of $\text{Re} \sigma(\omega)$ calculated within the present strong-coupling approach. This numeric estimation shows that for $\alpha > 8$, $\Delta_c < 0.01$. Moreover, with increasing α , the relative contribution of the transitions to the continuous part of the polaron spectrum falls down. This confirms the accuracy of the present strong-coupling approach.

In Refs. [95, 134], the optical conductivity of a strong-coupling polaron was calculated assuming that in the strong-coupling regime the polaron optical response is provided mainly

by the transitions to the continuous part of the spectrum (these transitions are called there “the polaron dissociation”). This concept is in contradiction both with the early estimation by Pekar [23] discussed above and with the very small weight of those transitions shown in Fig. 4. The approach of Ref. [95] in fact takes into account only a small part of the strong-coupling polaron optical conductivity – namely, the high-frequency “tail” of the optical conductivity spectrum.

When comparing the polaron optical conductivity spectra calculated in the present work with the DQMC data [79, 127], we can see that the present approach, with respect to DQMC, underestimates the high-frequency part of the polaron optical conductivity. This difference, however, gradually diminishes with increasing α , in accordance with the fact that the present method is an asymptotic strong-coupling approximation.

Because the optical conductivity spectra calculated in the present strong-coupling approximation using the expressions (A31) and (A32) represent the envelopes of the RES peak with the multi-phonon satellites, the separate peaks are not explicitly seen in those spectra. The FC and RES peaks are indicated in the figures by the arrows. The FC transition frequency $\Omega_{1,0}$ in the strong-coupling case is positioned close to the maximum of the polaron optical conductivity band (both calculated within the present approach and within DQMC). The RES transition frequency is positioned one ω_{LO} below the onset of the LO-sidebands. Note that the strong-coupling polaron optical conductivity derived in Refs. [135] contains only the zero-phonon (RES) line and no phonon satellites at all. In contrast, in the present calculation, the maximum of the polaron optical conductivity spectrum shifts to higher frequencies with increasing α , so that the multiphonon processes invoking large number of phonons become more and more important, in accordance with predictions of Refs. [49, 50].

It is worth noting the following important point: the maximum of the polaron optical conductivity band can be hardly interpreted as a broadened transition to an FC state on the following reasons. Formula (A28) describes a set of multi-phonon peaks. In the simplifying approximation which neglects the Jahn – Teller effect (see Ref. [127]), those peaks are positioned at the frequencies $\omega = \tilde{\Omega}_{n,0} + k$, where k is the number of emitted phonons and is the frequency of the zero-phonon line. The frequencies $\tilde{\Omega}_{n,0}$ do not coincide with the FC transition frequencies but are determined by

$$\tilde{\Omega}_{n,0} = \Omega_{n,0} - \omega_s^{(n)}, \quad (\text{A37})$$

where the Huang-Rhys factor $\omega_s^{(n)}$ describes the energy shift due to lattice relaxation. The physical meaning of the parameters $\omega_s^{(n)}$ obviously implies that the peaks at $\omega = \tilde{\Omega}_{n,0} + k$ should be attributed to transitions to the RES with emission of k phonons. So, the so-called “FC transition” is realized as the envelope of a series of phonon sidebands of the polaron RES but not as a transition to the FC state. The account of the Jahn-Teller effects in general makes the multiphonon peak series non-equidistant, but it changes nothing in the concept of the internal polaron states which is discussed above.

4. Conclusions

We have derived the polaron optical conductivity which is asymptotically exact in the strong-coupling limit. The strong-coupling polaron optical conductivity band is provided by the multiphonon transitions from the polaron ground state to the polaron RES and has the maximum positioned close to the FC transition frequency. With increasing the electron-phonon coupling constant α , the polaron optical conductivity band shape gradually tends to that provided by the Diagrammatic Quantum Monte Carlo (DQMC) method. This agreement demonstrates the importance of the multiphonon processes for the polaron optical conductivity in the strong-coupling regime.

The obtained polaron optical conductivity with a high accuracy satisfies the sum rule [82], what gives us an evidence of the fact that in the strong-coupling regime the dominating contribution to the polaron optical conductivity is due to the transitions to the *internal* polaron states, while the contribution due to the transitions to the continuum states is negligibly small.

Accurate numerical results, obtained using DQMC method [79], – modulo the linewidths for sufficiently large α – and the analytically exact in the strong-coupling limit polaron optical conductivity of the present work, as well as the analytical approximation of Ref. [127] confirm the essence of the mechanism for the optical absorption of Fröhlich polarons, which were proposed in Refs. [7, 50].

5. Appendix 1. Correlation function

The dipole-dipole correlation function $f_{zz}(t)$ given by (A24) is further simplified within the adiabatic approximation and using the selection rules for the dipole transition matrix elements and the symmetry properties of the polaron Hamiltonian. First, according to the selection rules, the matrix element $\langle \psi_0 | z | \psi_{n,l,m} \rangle$ is

$$\langle \psi_{n',l',m'} | z | \psi_0 \rangle = \delta_{l',1} \delta_{m',0} \langle \psi_{n',1,0} | z | \psi_0 \rangle \quad (\text{A38})$$

Second, the interaction Hamiltonian W (and hence, also the evolution operator which involves W) is a scalar of the rotation symmetry group. The matrix elements $\langle \psi_{n,l,m} | W(s) | \psi_{n',l',m'} \rangle$ for $l \neq l'$ and $m \neq m'$ are then exactly equal to zero. Therefore, in the adiabatic approximation and due to the symmetry of the Hamiltonian \tilde{H} , we obtain the relations

$$\begin{aligned} & \left\langle \psi_0 \left| \text{T exp} \left(i \int_0^t ds W(-s) \right) \right| \psi_{n,l,m} \right\rangle \\ & \approx \delta_{n,0} \delta_{l,0} \delta_{m,0} \left\langle \psi_0 \left| \text{T exp} \left(-i \int_0^t ds W(s) \right) \right| \psi_0 \right\rangle, \end{aligned} \quad (\text{A39})$$

$$\begin{aligned} & \left\langle \psi_{n'',l'',m''} \left| \text{T exp} \left(-i \int_0^t ds W(s) \right) \right| \psi_{n',l',m'} \right\rangle \\ & \approx \delta_{n'',n'} \delta_{l'',l'} \left\langle \psi_{n',l',m'} \left| \text{T exp} \left(-i \int_0^t ds W(s) \right) \right| \psi_{n',l',m'} \right\rangle. \end{aligned} \quad (\text{A40})$$

Furthermore, because the ground state ψ_0 is non-degenerate, we find that

$$\left\langle \psi_0 \left| \text{T exp} \left(-i \int_0^t ds W(s) \right) \right| \psi_0 \right\rangle \approx 1,$$

because within the adiabatic approximation, for any $n \geq 1$ the averages $\langle \psi_0 | W^n | \psi_0 \rangle = 0$.

The correlation function (A24) using (A38) to (A40) takes the form

$$\begin{aligned} f_{zz}(t) &= \sum_n D_n e^{-i\Omega_n t} \\ & \times \left\langle \psi_{n,1,0} \left| \left\langle 0_{ph} \left| \text{T exp} \left[-i \int_0^t ds W(s) \right] \right| 0_{ph} \right\rangle \right| \psi_{n,1,0} \right\rangle \end{aligned} \quad (\text{A41})$$

with the squared matrix elements of the dipole transitions

$$D_n \equiv |\langle \psi_{n,1,0} | z | \psi_0 \rangle|^2 = \frac{1}{3} \left(\int_0^\infty R_{n,1}(r) R_{0,0}(r) r^3 dr \right)^2, \quad (\text{A42})$$

and the FC transition frequencies

$$\Omega_{n,0} \equiv E_{n,1} - E_0. \quad (\text{A43})$$

Further on, the interaction Hamiltonian is expressed in terms of the complex phonon coordinates $Q_{\mathbf{k}}$:

$$W = \sqrt{2} \sum_{\mathbf{k}} W_{\mathbf{k}} Q_{\mathbf{k}}, \quad Q_{\mathbf{k}} = \frac{b_{\mathbf{k}} + b_{-\mathbf{k}}^+}{\sqrt{2}} \quad (\text{A44})$$

Here, we use the spherical-wave basis for phonon modes:

$$\varphi_{k,l,m}(\mathbf{r}) \equiv (-1)^{\frac{m-|m|}{2}} \phi_{k,l}(r) Y_{l,m}(\theta, \varphi), \quad (\text{A45})$$

where the radial part of the basis function is expressed through the spherical Bessel function $j_l(kr)$:

$$\phi_{k,l}(r) = \left(\frac{2}{R}\right)^{1/2} k j_l(kr), \quad R = \left(\frac{3V}{4\pi}\right)^{1/3}. \quad (\text{A46})$$

The factor $(-1)^{\frac{m-|m|}{2}}$ is chosen in order to fulfil the symmetry property

$$\varphi_{k,l,m}^*(\mathbf{r}) = \varphi_{k,l,-m}(\mathbf{r}).$$

In the spherical-wave basis, the interaction Hamiltonian is

$$W = \sqrt{2} \sum_{k,l,m} W_{k,l,m} Q_{k,l,m}, \quad (\text{A47})$$

with the complex phonon coordinates

$$Q_{k,l,m} = \frac{b_{k,l,m} + b_{k,l,-m}^+}{\sqrt{2}} \quad (\text{A48})$$

and with the interaction amplitudes

$$W_{k,l,m} = \frac{\sqrt{2\sqrt{2}\pi\alpha}}{k} (\varphi_{k,l,m}(\mathbf{r}) - \rho_{k,l,m}), \quad \rho_{k,l,m} \equiv \langle \psi_0 | \varphi_{k,l,m} | \psi_0 \rangle. \quad (\text{A49})$$

The dipole-dipole correlation function (A41) is then

$$f_{zz}(t) = \sum_n D_n e^{-i\Omega_{n,0}t} \times \left\langle \psi_{n,1,0} \left| \left\langle 0_{ph} \left| \text{T exp} \left[-i\sqrt{2} \int_0^t ds \sum_{k,l,m} W_{k,l,m}(s) Q_{k,l,m}(s) \right] \right| 0_{ph} \right\rangle \right| \psi_{n,1,0} \right\rangle. \quad (\text{A50})$$

The operators $W_{k,l,m}(s)$ in (A50) are equivalent to the $(2l+1)$ -dimensional matrices $\mathbb{W}_{k,l,m}^{(n)}$ determined in the basis of the level (n, l) . The matrix elements of these matrices are

$$\left(\mathbb{W}_{k,l,m}^{(n)}\right)_{m_1, m_2} = \langle \psi_{n,1,m_1} | W_{k,l,m} | \psi_{n,1,m_2} \rangle. \quad (\text{A51})$$

In these notations, $f_{zz}(t)$ given by (A50) can be written down as

$$f_{zz}(t) = \sum_n D_n e^{-i\Omega_{n,0}t} \left\langle 0_{ph} \left| \left(\text{T exp} \left[-i \int_0^t ds \mathbb{W}^{(n)}(s) \right] \right) \right|_{0,0} \right| 0_{ph} \rangle. \quad (\text{A52})$$

where $\mathbb{W}^{(n)}$ is the matrix electron-phonon interaction Hamiltonian expressed through the phonon complex coordinates in the spherical-wave representation as follows:

$$\mathbb{W}^{(n)} = \sqrt{2} \sum_{k,l,m} \mathbb{W}_{k,l,m}^{(n)} Q_{k,l,m}. \quad (\text{A53})$$

Here, $\mathbb{W}_{k,l,m}^{(n)}$ is a (3×3) matrix in a basis of a level $(n, l)_{l=1}$ of the Hamiltonian \tilde{H}_0 .

Because $\mathbb{W}^{(n)}$ is a scalar of the rotation group, we can replace the diagonal matrix element of the T-exponent in (A52) with the trace in the aforesaid-finite-dimensional basis. As a result, we obtain for the polaron optical conductivity (A4) with (A52) the expression

$$\begin{aligned} \text{Re } \sigma(\omega) &= \frac{\omega}{6} \sum_n D_n \int_{-\infty}^{\infty} e^{i(\omega - \Omega_{n,0})t} \\ &\times \left\langle 0_{ph} \left| \text{Tr} \left(\text{T exp} \left[-i \int_0^t ds \mathbb{W}^{(n)}(s) \right] \right) \right|_{0_{ph}} \right\rangle dt. \end{aligned} \quad (\text{A54})$$

6. Appendix 2. Effective phonon modes

In order to perform the averaging in Eq. (A30) analytically, we introduce the effective phonon modes $Q_{0,0}$ and $Q_{2,m}$ similarly to Ref. [133]. The Hamiltonian $\mathbb{W}^{(n)}$ in terms of these effective phonon modes is expressed as

$$\mathbb{W}^{(n)} = \sqrt{2} \sum_{l,m} \tilde{\mathbb{W}}_{l,m}^{(n)} Q_{l,m} \quad (\text{A55})$$

where the matrices $\tilde{\mathbb{W}}_{l,m}^{(n)}$ (depending on the vibration coordinates $Q_{l,m}$) are explicitly given by the expressions (cf. Ref. [133]),

$$\mathbb{W}^{(n)} = a_0^{(n)} \mathbb{I} Q_{0,0} + a_2^{(n)} \sum_{m=-2}^2 \mathbb{B}_m Q_{2,m} \quad (\text{A56})$$

with the matrices \mathbb{B}_j

$$\mathbb{B}_0 = \frac{1}{2\sqrt{5\pi}} \begin{pmatrix} -1 & 0 & 0 \\ 0 & 2 & 0 \\ 0 & 0 & -1 \end{pmatrix}, \quad (\text{A57})$$

$$\mathbb{B}_1 = \mathbb{B}_{-1}^+ = \frac{1}{2}\sqrt{\frac{3}{5\pi}} \begin{pmatrix} 0 & 0 & 0 \\ -1 & 0 & 0 \\ 0 & 1 & 0 \end{pmatrix}, \quad (\text{A58})$$

$$\mathbb{B}_2 = \mathbb{B}_{-2}^+ = \sqrt{\frac{3}{10\pi}} \begin{pmatrix} 0 & 0 & 0 \\ 0 & 0 & 0 \\ -1 & 0 & 0 \end{pmatrix}. \quad (\text{A59})$$

The coefficients $a_0^{(n)}$ and $a_2^{(n)}$ in Eq. (A56) are

$$a_0^{(n)} = \left(\sqrt{2}\alpha \sum_k \frac{1}{k^2} \left[\langle \phi_{k,0} \rangle_{n,1} - \langle \phi_{k,0} \rangle_{0,0} \right]^2 \right)^{1/2}, \quad (\text{A60})$$

$$a_2^{(n)} = \left(4\sqrt{2}\pi\alpha \sum_k \frac{1}{k^2} \langle \phi_{k,2} \rangle_{n,1}^2 \right)^{1/2}. \quad (\text{A61})$$

Here $\phi_{k,l}$ is the radial part of the basis function expressed through the spherical Bessel function $j_l(kr)$:

$$\phi_{k,l}(r) = \left(\frac{2}{R} \right)^{1/2} k j_l(kr), \quad R = \left(\frac{3V}{4\pi} \right)^{1/3}, \quad (\text{A62})$$

V is the volume of the crystal, and $\langle f(r) \rangle_{n,l}$ is the average

$$\langle f(r) \rangle_{n,l} = \int_0^\infty f(r) R_{n,l}^2(r) r^2 dr. \quad (\text{A63})$$

The normalization of the phonon wave functions corresponds to the condition

$$\int_0^R \phi_{k,l}(r) \phi_{k',l}(r) r^2 dr = \delta_{k,k'}. \quad (\text{A64})$$

After the straightforward calculation using (A64), we express the coefficients $a_0^{(n)}$ and $a_2^{(n)}$ through the integrals with the radial wave functions:

$$a_0^{(n)} = \left(2\sqrt{2}\alpha \int_0^\infty dr \int_0^r dr' r (r')^2 [R_{n,1}^2(r) - R_{0,0}^2(r)] [R_{n,1}^2(r') - R_{0,0}^2(r')] \right)^{1/2}, \quad (\text{A65})$$

$$a_2^{(n)} = \left(\frac{8\sqrt{2}\pi\alpha}{5} \int_0^\infty dr \int_0^r dr' \frac{(r')^4}{r} R_{n,1}^2(r) R_{n,1}^2(r') \right)^{1/2}. \quad (\text{A66})$$

a. *Exact averaging*

Let us substitute the matrix interaction Hamiltonian (A56) to the dipole-dipole correlation function (A30), what gives us the result

$$f_{zz}(t) = \frac{1}{3} \sum_n D_n e^{-i\Omega_n t} \left\langle 0_{ph} \left| \exp\left(-ita_0^{(n)} Q_0\right) \text{Tr} \exp\left(-it \frac{a_2^{(n)}}{2\sqrt{5}\pi} \mathbb{V}(Q_2)\right) \right| 0_{ph} \right\rangle. \quad (\text{A67})$$

Here, we use the matrix depending on the phonon coordinates,

$$\mathbb{V}(Q_2) \equiv 2\sqrt{5}\pi \sum_{m=-2}^2 \mathbb{B}_m Q_{2m}, \quad (\text{A68})$$

whose explicit form is

$$\mathbb{V}(Q_2) = \begin{pmatrix} -Q_{2,0} & -\sqrt{3}Q_{2,-1} & -\sqrt{6}Q_{2,-2} \\ -\sqrt{3}Q_{2,1} & 2Q_{2,0} & \sqrt{3}Q_{2,-1} \\ -\sqrt{6}Q_{2,2} & \sqrt{3}Q_{2,1} & -Q_{2,0} \end{pmatrix}. \quad (\text{A69})$$

The matrix $\mathbb{V}(Q_2)$ is analytically diagonalized. The equation for the eigenvectors $|\chi(Q_2)\rangle$ and eigenvalues $\lambda(Q_2)$ of $\mathbb{V}(Q_2)$ is

$$\mathbb{V}(Q_2) |\chi(Q_2)\rangle = \lambda(Q_2) |\chi(Q_2)\rangle. \quad (\text{A70})$$

The eigenvalues are found from the equation

$$\det(\mathbb{V}(Q_2) - \lambda(Q_2) \mathbb{I}) = 0. \quad (\text{A71})$$

We make the transformation to the real phonon coordinates,

$$Q_{2,0} \equiv x_0, \\ Q_{2,m} \equiv \frac{x_m + iy_m}{\sqrt{2}}, \quad Q_{2,-m} = Q_{2,m}^* = \frac{x_m - iy_m}{\sqrt{2}}.$$

Five variables x_0, x_1, x_2, y_1, y_2 are the independent real phonon coordinates. The l.h.s. of Eq. (A71) is expressed in terms of these coordinates as

$$\det(\mathbb{V}(Q_2) - \lambda(Q_2) \mathbb{I}) = -\lambda^3 + 3p\lambda + 2q \quad (\text{A72})$$

with the coefficients

$$p = x_0^2 + x_1^2 + x_2^2 + y_1^2 + y_2^2, \\ q = x_0^3 + \frac{3}{2}x_0(x_1^2 + y_1^2) + \frac{3\sqrt{3}}{2}x_2(x_1^2 - y_1^2) - 3x_0(x_2^2 + y_2^2) + 3\sqrt{3}x_1y_1y_2.$$

So, we have the cubic equation for λ :

$$\lambda^3 - 3p\lambda - 2q = 0. \quad (\text{A73})$$

Because the matrix $\mathbb{V}(Q_2)$ is Hermitian, all its eigenvalues are real. Therefore, $\frac{|q|}{p^{3/2}} \leq 1$ (otherwise, $\sin(3\varphi)$ is not real). Herefrom, we have three explicit eigenvalues:

$$\begin{aligned} \lambda_1(Q_2) &= 2\sqrt{p} \sin \left[\frac{\pi}{3} + \frac{1}{3} \arcsin \left(\frac{q}{p^{3/2}} \right) \right], \\ \lambda_2(Q_2) &= -2\sqrt{p} \sin \left[\frac{1}{3} \arcsin \left(\frac{q}{p^{3/2}} \right) \right], \\ \lambda_3(Q_2) &= -2\sqrt{p} \sin \left[\frac{\pi}{3} - \frac{1}{3} \arcsin \left(\frac{q}{p^{3/2}} \right) \right]. \end{aligned} \quad (\text{A74})$$

The trace in (A67) is invariant with respect to the choice of the basis. Consequently, after the diagonalization $f_{zz}(t)$ takes the form

$$f_{zz}(t) = \frac{1}{3} \sum_n D_n e^{-i\Omega_n t} \sum_{j=1}^3 \left\langle 0_{ph} \left| \exp \left(-it \left[a_0^{(n)} Q_0 + \frac{a_2^{(n)}}{2\sqrt{5}\pi} \lambda_j(Q_2) \right] \right) \right| 0_{ph} \right\rangle. \quad (\text{A75})$$

After inserting $f_{zz}(t)$ given by (A75) into (A4), the integration over time gives the delta function multiplied by 2π , and we arrive at the result

$$\text{Re } \sigma(\omega) = \frac{\pi\omega}{3} \sum_n D_n \sum_{j=1}^3 \left\langle 0_{ph} \left| \delta \left(\omega - \Omega_{n,0} - a_0^{(n)} Q_0 - \frac{a_2^{(n)}}{2\sqrt{5}\pi} \lambda_j(Q_2) \right) \right| 0_{ph} \right\rangle. \quad (\text{A76})$$

The ground-state wave function for the effective phonon modes is

$$|0_{ph}\rangle \equiv \Phi_0(Q) = \Phi_0^{(0)}(Q_0) \Phi_0^{(2)}(Q_2). \quad (\text{A77})$$

$\Phi_0^{(0)}(Q_0)$ is the one-oscillator ground-state wave function:

$$\Phi_0^{(0)}(Q_0) = \pi^{-1/4} \exp \left(-\frac{Q_0^2}{2} \right). \quad (\text{A78})$$

The ground-state wave function of phonons with $l = 2$ is:

$$\Phi_0^{(2)}(Q_2) = \pi^{-5/4} \exp \left[-\frac{1}{2} \left(x_0^2 + \sum_{m=1,2} (x_m^2 + y_m^2) \right) \right]. \quad (\text{A79})$$

The phonon ground-state wave function (A77) is then

$$\Phi_0(Q) = \frac{1}{\pi^{3/2}} \exp \left[-\frac{1}{2} \left(x_0^2 + \sum_{m=1,2} (x_m^2 + y_m^2) + Q_0^2 \right) \right]. \quad (\text{A80})$$

With these phonon wave functions, Eq. (A76) results in the following expression for the polaron optical conductivity

$$\begin{aligned} \text{Re } \sigma(\omega) &= \frac{\omega}{3\pi^2} \sum_n \frac{D_n}{a_0^{(n)}} \int_{-\infty}^{\infty} dx_0 \int_{-\infty}^{\infty} dx_1 \int_{-\infty}^{\infty} dx_2 \int_{-\infty}^{\infty} dy_1 \int_{-\infty}^{\infty} dy_2 \\ &\times \sum_{j=1}^3 \exp \left\{ -\frac{1}{2} \left[x_0^2 + \sum_{m=1,2} (x_m^2 + y_m^2) + \frac{\left(\omega - \Omega_{n,0} - \frac{a_2^{(n)}}{2\sqrt{5}\pi} \lambda_j(Q_2) \right)^2}{\left(a_0^{(n)} \right)^2} \right] \right\}. \end{aligned} \quad (\text{A81})$$

b. Averaging neglecting the Jahn-Teller effect

In order to perform the phonon averaging explicitly, we disentangle the exponent $\exp\left(-it\sqrt{2} \sum_{l,m} \tilde{\mathbb{W}}_{l,m}^{(n)} Q_{l,m}\right)$ as follows.

$$\begin{aligned} \exp\left(-it\sqrt{2} \sum_{l,m} \tilde{\mathbb{W}}_{l,m}^{(n)} Q_{l,m}\right) &= \exp\left(-it \sum_{l,m} \tilde{\mathbb{W}}_{l,-m}^{(n)} b_{l,m}^+\right) \\ &\times \text{T exp}\left(-i \int_0^t ds \sum_{l,m} e^{is \sum_{l',m'} \tilde{\mathbb{W}}_{l',-m'}^{(n)} b_{l',m'}^+} \tilde{\mathbb{W}}_{l,m}^{(n)} b_{l,m} e^{-is \sum_{l',m'} \tilde{\mathbb{W}}_{l',-m'}^{(n)} b_{l',m'}^+}\right). \end{aligned} \quad (\text{A82})$$

Neglecting non-commutation of matrices $\tilde{\mathbb{W}}_{l,m}^{(n)}$ we find that

$$\begin{aligned} &\sum_{l,m} e^{is \sum_{l',m'} \tilde{\mathbb{W}}_{l',-m'}^{(n)} b_{l',m'}^+} \tilde{\mathbb{W}}_{l,m}^{(n)} b_{l,m} e^{-is \sum_{l',m'} \tilde{\mathbb{W}}_{l',-m'}^{(n)} b_{l',m'}^+} \\ &= \sum_{l,m} \tilde{\mathbb{W}}_{l,m}^{(n)} b_{l,m} - is \sum_{l,m} \tilde{\mathbb{W}}_{l,-m}^{(n)} \tilde{\mathbb{W}}_{l,m}^{(n)}. \end{aligned} \quad (\text{A83})$$

The sum $\sum_{l,m} \tilde{\mathbb{W}}_{l,-m}^{(n)} \tilde{\mathbb{W}}_{l,m}^{(n)}$ in the basis (l, m) for a definite n is proportional to the unity matrix. Therefore, $\exp\left(-it\sqrt{2} \sum_{l,m} \tilde{\mathbb{W}}_{l,m}^{(n)} Q_{l,m}\right)$ is

$$\begin{aligned} &e^{-it\sqrt{2} \sum_{l,m} \tilde{\mathbb{W}}_{l,m}^{(n)} Q_{l,m}} \\ &= e^{-it \sum_{l,m} \tilde{\mathbb{W}}_{l,-m}^{(n)} b_{l,m}^+} e^{-it \sum_{l,m} \tilde{\mathbb{W}}_{l,m}^{(n)} b_{l,m}} e^{-\frac{t^2}{2} \sum_{l,m} \tilde{\mathbb{W}}_{l,-m}^{(n)} \tilde{\mathbb{W}}_{l,m}^{(n)}}, \end{aligned} \quad (\text{A84})$$

that gives us the result

$$\left\langle 0_{ph} \left| e^{-it\sqrt{2} \sum_{l,m} \tilde{\mathbb{W}}_{l,m}^{(n)} Q_{l,m}} \right| 0_{ph} \right\rangle = e^{-\frac{t^2}{2} \sum_{l,m} \tilde{\mathbb{W}}_{l,-m}^{(n)} \tilde{\mathbb{W}}_{l,m}^{(n)}}. \quad (\text{A85})$$

Using the explicit formulae for the matrices $\tilde{\mathbb{W}}_{l,m}^{(n)}$, the matrix sum takes the form

$$\sum_{l,m} \tilde{\mathbb{W}}_{l,-m}^{(n)} \tilde{\mathbb{W}}_{l,m}^{(n)} = \omega_s^{(n)} \mathbb{I} \quad (\text{A86})$$

with the parameter

$$\omega_s^{(n)} = \frac{1}{2} \left(a_0^{(n)} \right)^2 + \frac{1}{4\pi} \left(a_2^{(n)} \right)^2. \quad (\text{A87})$$

Using (A86), the optical conductivity (A30) is transformed to the expression

$$\text{Re } \sigma(\omega) = \omega \sum_n \sqrt{\frac{\pi}{2S_n}} D_n \exp\left(-\frac{(\omega - \Omega_{n,0})^2}{2S_n}\right). \quad (\text{A88})$$

Figures to Appendix A

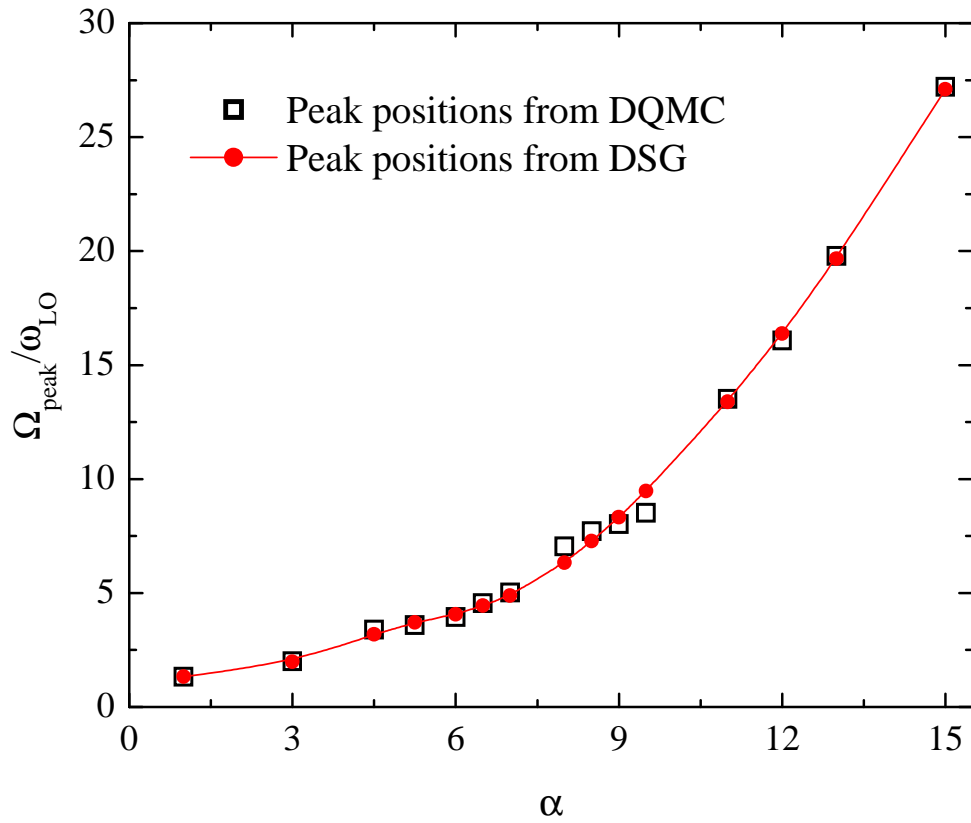


Fig. 1

Frequency of the main peak in the optical conductivity spectra calculated within the model of Ref. [50] (red dots) and the main-peak energy extracted from the DQMC data [79, 127] (black squares).

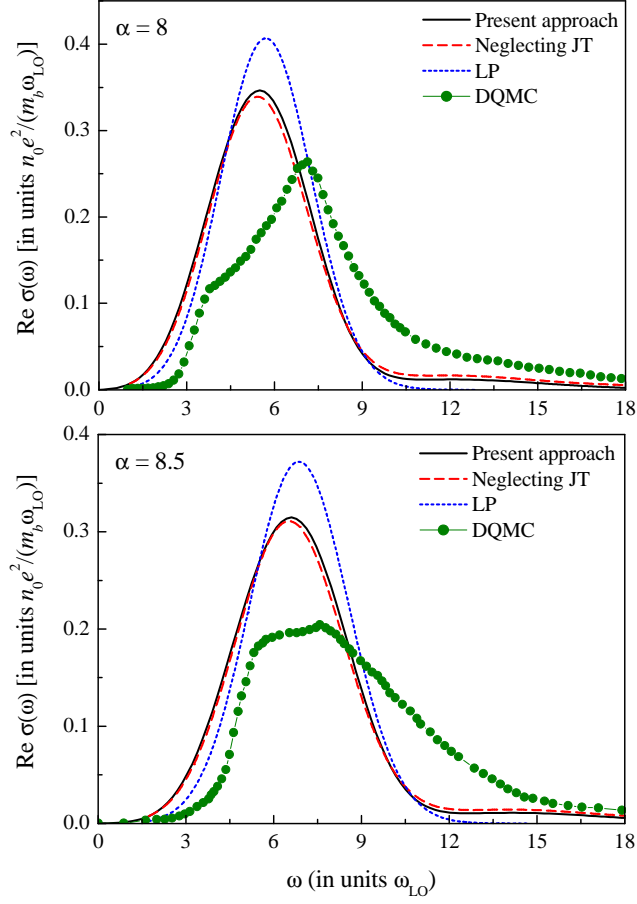


Fig. 2

The strong-coupling polaron optical conductivity calculated within the rigorous strong-coupling approach of the present work (black solid curves), within the present approach but neglecting the dynamic Jahn-Teller effect (red dashed curves), within the adiabatic approximation of Ref. [127] (blue dot-dashed curves), and the numerical Diagrammatic Monte Carlo data (full dots) for $\alpha = 8$ and 8.5.

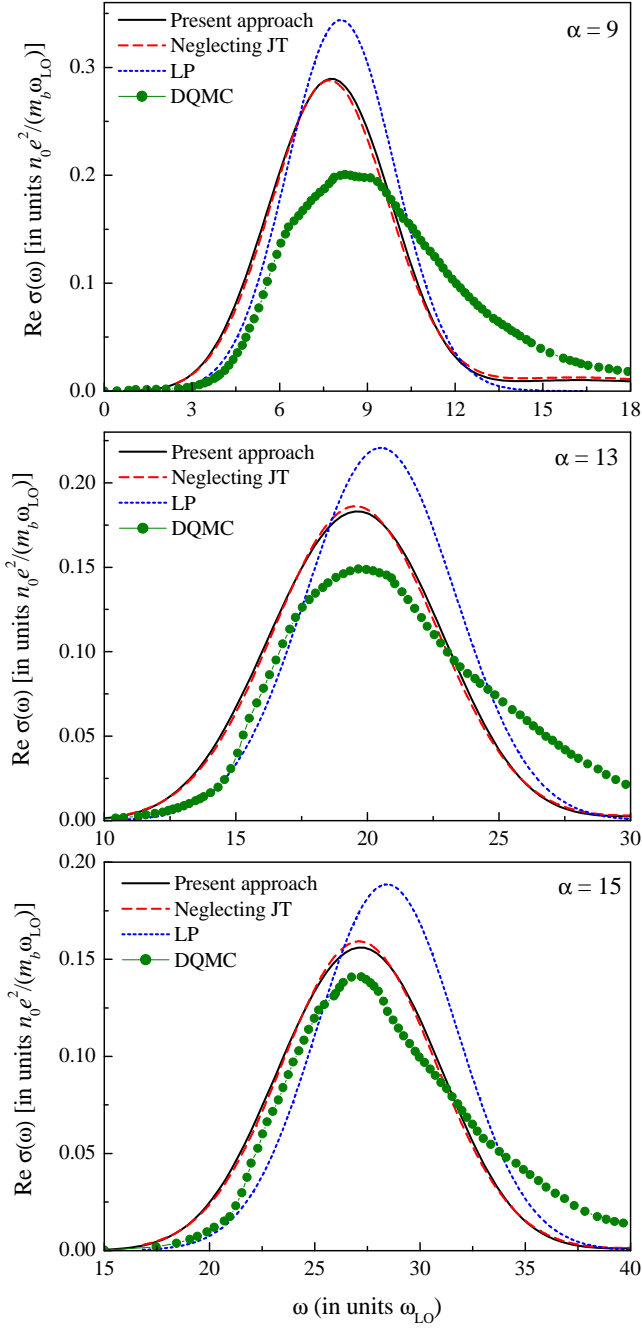


Fig. 3

The strong-coupling polaron optical conductivity calculated within the rigorous strong-coupling approach of the present work (black solid curves), within the present approach but neglecting the dynamic Jahn-Teller effect (red dashed curves), within the adiabatic approximation of Ref. [127] (blue dot-dashed curves), and the numerical Diagrammatic Monte Carlo data (full dots) for $\alpha = 9, 13$ and 15 .

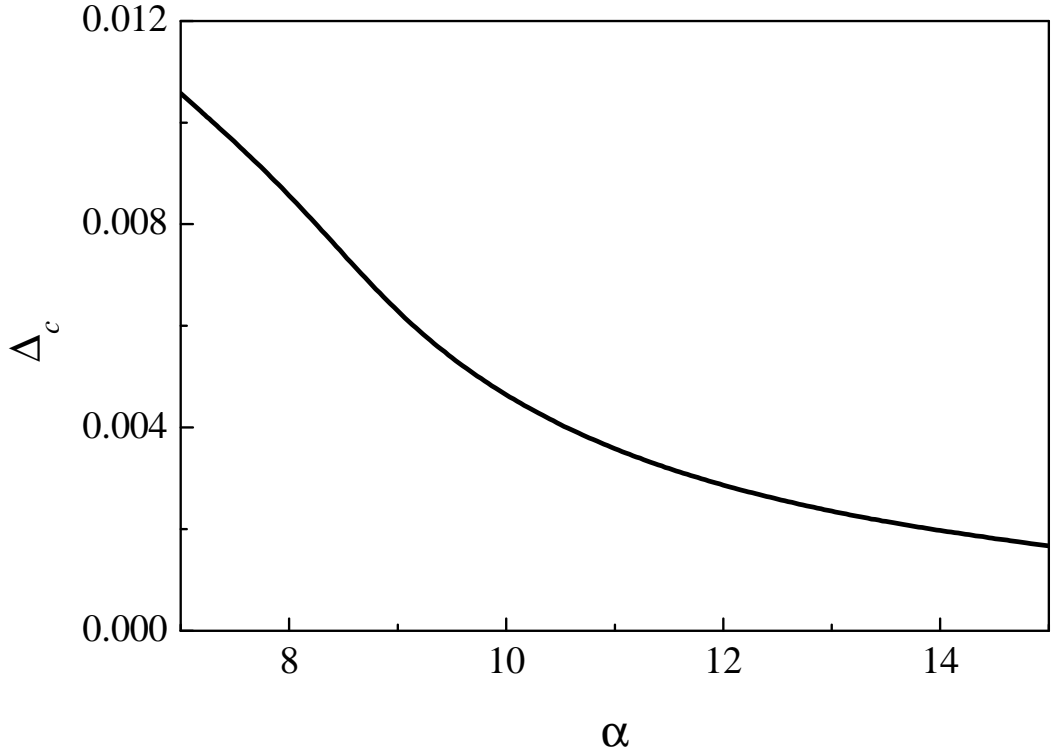


Fig. 4

Relative contribution of the transitions to the continuum polaron states to the zeroth frequency moment of the strong-coupling polaron optical conductivity as a function of the coupling constant α .

Appendix B: Feynman's path-integral polaron treatment approached using time-ordered operator calculus [*S. N. Klimin and J. T. Devreese, Solid State Communications 151, 144 (2011)*]

Several studies have been devoted to the search of a Hamiltonian formalism equivalent to Feynman's path integral approximation to polaron theory. Bogolubov [138] reproduced the Feynman result for the polaron free energy [43] using time-ordering T-products. Yamazaki [139] introduced two kinds of auxiliary vector fields to derive Feynman's ground state polaron energy expression with the operator technique, however he found no proof of the variational nature of this result. Cataudella *et al.* [140] formally re-obtained Feynman's polaron ground-

state energy expression by introducing additional degrees of freedom, but again their result could not be proved to constitute an upper bound for the polaron ground state energy.

The study of the excited polaron states is of interest i. a. for its application to the polaron response properties. In [47] a path-integral based response-formalism was introduced that was applied to derive polaron optical absorption spectra in [7]. The results for the polaron response obtained in [7] were re-derived with a Hamiltonian technique (Mori-formalism) in [76].

To the best of our knowledge, no explicit description of the polaron excited states has been derived within the “all coupling-“ Feynman approach. Only for the limiting cases of weak and strong coupling approximations (and for a 1D-model system) such excitation spectra were derived [39, 41, 125].

In principle, the spectrum of the polaron excited states can be derived indirectly – using a Laplace transform of the finite-temperature partition function. However, it is not clear how to realize this program in practice.

The polaron excitation spectrum is interesting by itself. E.g. the existence and the nature of “relaxed excited states”, “Franck-Condon states”, “scattering states” is understood from the mathematical structure of corresponding eigenstates.

In the present letter we first present a re-derivation of the original Feynman variational path integral polaron model [43] for the ground state, using a Hamiltonian formalism, and we do provide a proof of the upper bound nature of the obtained ground state energy. Furthermore, using Feynman’s (Hamiltonian-) time-ordered operator calculus (and an *ad hoc* unitary transformation) we obtain explicitly – and for the first time – the excited polaron states that correspond to the Feynman polaron model.

The novelty of the present approach consists (a) in the *direct calculation of the energies and the lifetimes of the excited polaron states* (within a Hamiltonian all-coupling approach – developed in this work – equivalent to the Feynman path integral polaron model) and (b) in the extension of the Feynman variational technique to non-parabolic trial potentials. Although the time-ordered operator calculus is formally equivalent to the path-integral formalism, it is not obvious how to directly calculate the excited polaron states using path integrals.

The present work, formulated with the (Hamiltonian) time ordered operator calculus, thus provides an (equivalent) tool complementary with respect to the Feynman path integral

approach to the polaron, to study the polaron problem. Additionally we directly study the excited polaron states.

Consider an electron-phonon system with the Fröhlich Hamiltonian

$$H = \frac{\mathbf{p}^2}{2} + H_{ph} + H_{e-ph}, \quad (\text{B1})$$

$$H_{ph} = \sum_{\mathbf{q}} \left(a_{\mathbf{q}}^+ a_{\mathbf{q}} + \frac{1}{2} \right), \quad (\text{B2})$$

$$H_{e-ph} = \frac{1}{\sqrt{V}} \sum_{\mathbf{q}} \frac{\sqrt{2\sqrt{2}\pi\alpha}}{q} (a_{\mathbf{q}} + a_{-\mathbf{q}}^+) e^{i\mathbf{q}\cdot\mathbf{r}}. \quad (\text{B3})$$

Here, the Feynman units are used: $\hbar = 1$, the band mass $m_b = 1$, the LO-phonon frequency $\omega_{\text{LO}} = 1$.

The polaron partition function after exact averaging over phonon states is

$$Z_{pol} = \text{Tr} \left[\mathbb{T} \exp \left(- \int_0^\beta \frac{\mathbf{p}_\tau^2}{2} d\tau + \hat{\Phi}[\mathbf{r}_\tau] \right) \right], \quad (\text{B4})$$

where $\beta = \frac{1}{k_B T}$. The “influence phase” of the phonons $\hat{\Phi}[\mathbf{r}_\tau]$ in the the time-ordered operator calculus has the same form as in the path-integral representation. The polaron free energy is determined as

$$F_{pol} = -\frac{1}{\beta} \ln Z_{pol}. \quad (\text{B5})$$

The trial Hamiltonian describes the electron interacting with a fictitious particle of the mass m_f through an attractive potential V_f :

$$H_{tr} = \frac{\mathbf{p}^2}{2} + \frac{\mathbf{p}_f^2}{2m_f} + V_f(\mathbf{r} - \mathbf{r}_f). \quad (\text{B6})$$

The trial potential V_f is, in general, non-parabolic. The parabolic potential with frequency parameter w corresponds to the Feynman polaron model.

Consider the “extended” partition function of the electron-phonon system

$$Z_{ext} = Z_f Z_{pol} \quad (\text{B7})$$

where Z_f is the partition function of a fictitious particle,

$$Z_f \equiv \text{Tr} \left[\mathbb{T} \exp \left(- \int_0^\beta d\tau H_{f,\tau} \right) \right], \quad (\text{B8})$$

with Hamiltonian

$$H_f = \frac{\mathbf{p}_f^2}{2m_f} + V_f(\mathbf{r}_f). \quad (\text{B9})$$

The polaron free energy is expressed as the difference

$$F_{pol} = F_{ext} - F_f, \quad (\text{B10})$$

where F_f is the free energy of the fictitious particle confined to the potential $V(\mathbf{r}_f)$. The free energies F_{ext} and F_f are determined similarly to (B5), with corresponding partition functions. In the zero-temperature limit, the free energies F_{pol} , F_{ext} and F_f become, respectively, the ground-state energies E_{pol}^0 , E_{ext}^0 and E_f^0 .

The key element of the present approach is the unitary transformation

$$U = e^{-i\mathbf{p}_f \cdot \mathbf{r}}. \quad (\text{B11})$$

Application of this canonical transformation results in the transformed ‘‘extended’’ Hamiltonian $H'_{ext} = UH_{ext}U^{-1}$,

$$\begin{aligned} H'_{ext} &= \frac{(\mathbf{p} + \mathbf{p}_f)^2}{2} + \frac{\mathbf{p}_f^2}{2m_f} + V_f(\mathbf{r}_f - \mathbf{r}) \\ &+ H_{ph} + H_{e-ph}. \end{aligned} \quad (\text{B12})$$

This Hamiltonian can be represented as a sum of an unperturbed Hamiltonian

$$H_0 \equiv H_{tr} + H_{ph} \quad (\text{B13})$$

and an interaction term

$$V \equiv \frac{1}{2}\mathbf{p}_f^2 + \mathbf{p} \cdot \mathbf{p}_f + H_{e-ph}. \quad (\text{B14})$$

Further we use the variational principle for the ground-state energy in terms of the time-ordered operators following Ref. [141]. The exact ground state $|0\rangle$ of the system with the Hamiltonian (B12) can be written in the interaction representation starting from the unperturbed ground state $|-\infty\rangle$:

$$|0\rangle = \mathcal{U}(\infty, -\infty) |-\infty\rangle \quad (\text{B15})$$

where $\mathcal{U}(\infty, -\infty)$ is the time-evolution operator,

$$\mathcal{U}(t_2, t_1) = \mathcal{T} \exp \left(-i \int_{t_1}^{t_2} e^{-\delta|t|} e^{iH_0 t} V e^{-iH_0 t} dt \right). \quad (\text{B16})$$

Here, $\delta \rightarrow +0$ and \mathcal{T} denotes time ordering.

In the exact expectation value for the ground state energy $E_{ext}^0 \equiv \langle 0 | H'_{ext} | 0 \rangle$, the phonons are eliminated using the time ordered-operator calculus as in Ref. [141]. The average of the interaction term becomes then

$$\begin{aligned} & \langle 0 | H_{e-ph} | 0 \rangle \\ &= -i \frac{\sqrt{2}\pi\alpha}{V} \int_{-\infty}^{\infty} dt e^{-i|t|-\delta|t|} \\ & \times \sum_{\mathbf{q}} \frac{1}{q^2} \langle \infty | \mathcal{T} [\mathcal{U}(\infty, -\infty) e^{i\mathbf{q}\cdot[\mathbf{r}(t)-\mathbf{r}(0)]}] | -\infty \rangle. \end{aligned} \quad (\text{B17})$$

This means that the polaron ground state energy is exactly described using a retarded potential in the interaction representation, cf. Eq. (2.16) of Ref. [141].

The ground state energy satisfies the Ritz variational principle with a trial state. Choosing the trial state as the ground state of the Hamiltonian (B13), the variational principle can be written as [141]

$$\begin{aligned} E_{ext}^0 &\leq E_{tr}^0 \\ &+ \langle \infty | \mathcal{T} \{ \mathcal{U}_{tr}(\infty, -\infty) [H'_{ext}(0) - H_0(0)] \} | -\infty \rangle, \end{aligned} \quad (\text{B18})$$

where $\mathcal{U}_{tr}(\infty, -\infty)$ is the time-evolution operator corresponding to the trial Hamiltonian (B6).

The exact polaron ground state energy is denoted here as $E^0(\mathbf{k})$, where \mathbf{k} is the polaron translation momentum. We find an upper bound for $E^0(\mathbf{k})$ substituting (B17) in (B18) and using the exact wave functions and energy levels of the trial Hamiltonian. The trial Hamiltonian (B6) can be rewritten in terms of the coordinates $(\mathbf{R}, \boldsymbol{\rho})$ and momenta $(\mathbf{P}, \vec{\pi})$ of the center-of-mass and relative (internal) motions of the trial system with the masses $M = 1 + m_f$ and $\mu = m_f / (1 + m_f)$ using the frequency $v = wM$. The energy spectrum of the trial system is the sum of the translation- and oscillation contributions,

$$E_{\mathbf{k},n} = \frac{\mathbf{k}^2}{2M} + \varepsilon_n, \quad \varepsilon_n = v \left(n + \frac{3}{2} \right). \quad (\text{B19})$$

The eigenfunctions of the Hamiltonian (B6) are products of translational- and oscillatory wave functions:

$$\psi_{\mathbf{k};l,n,m}(\mathbf{R}, \boldsymbol{\rho}) = \frac{1}{\sqrt{V}} e^{i\mathbf{k}\cdot\mathbf{R}} \varphi_{l,n,m}(\boldsymbol{\rho}), \quad (\text{B20})$$

where $\varphi_{l,n,m}(\boldsymbol{\rho})$ is the 3D harmonic-oscillator wave function with a given angular momentum.

The result is

$$E^0(\mathbf{k}) \leq \mathcal{E}_p^{(0,0)}(\mathbf{k}), \quad (\text{B21})$$

$$\begin{aligned} \mathcal{E}_p^{(0,0)}(\mathbf{k}) &= \frac{3(v-w)^2}{4v} \\ &+ \frac{1}{2} \left(1 - \frac{1}{(1+m_f)^2} \right) \mathbf{k}^2 - \frac{\sqrt{2}\alpha}{4\pi^2} \int \frac{d\mathbf{q}}{q^2} \\ &\times \sum_{\mathbf{k}',l',n',m'} \frac{|\langle \psi_{\mathbf{k};0,0,0} | e^{i\mathbf{q}\cdot\mathbf{r}} | \psi_{\mathbf{k}';l',n',m'} \rangle|^2}{\frac{1}{2(m_f+1)} ((\mathbf{k}')^2 - \mathbf{k}^2) + vn' + 1}, \end{aligned} \quad (\text{B22})$$

where $v > w$ are the Feynman variational frequencies. The functional (B22) can be reduced to the known Feynman result for the polaron ground-state energy. In the r.h.s. of (B22) at the polaron momentum $\mathbf{k} = 0$, we introduce the integral over the Euclidean time:

$$\frac{1}{\frac{(\mathbf{k}')^2}{2(m_f+1)} + vn' + 1} = \int_0^\infty e^{-\left(\frac{(\mathbf{k}')^2}{2(m_f+1)} + vn' + 1\right)\tau} d\tau. \quad (\text{B23})$$

After this, the summations and integrations in (B25) are performed analytically, and we arrive at the Feynman variational expression for the polaron ground-state energy:

$$\begin{aligned} E^0(\mathbf{k})|_{\mathbf{k}=0} &\leq \frac{3(v-w)^2}{4v} \\ &- \frac{\alpha v}{\sqrt{\pi}} \int_0^\infty \frac{e^{-\tau}}{\sqrt{w^2\tau + \frac{v^2-w^2}{v}(1-e^{-v\tau})}} d\tau. \end{aligned} \quad (\text{B24})$$

The electron-phonon contribution in (B22) is structurally similar to the second-order perturbation correction to the polaron ground-state energy due to the electron-phonon interaction (using states of the Feynman model $\psi_{\mathbf{k};l,n,m}$ as the zero-order approximation). Therefore we can estimate the energies of the excited polaron states when averaging the difference between exact and unperturbed Hamiltonians in (B18) with an excited trial state. We then arrive at the following extension for the r.h.s. of (B22):

$$\begin{aligned} \mathcal{E}_p^{(l,n)}(\mathbf{k}) &= \frac{v^2 + w^2}{2v} \left(n + \frac{3}{2} \right) - \frac{3}{2}w \\ &+ \frac{1}{2} \left(1 - \frac{1}{(1+m_f)^2} \right) \mathbf{k}^2 - \frac{\sqrt{2}\alpha}{4\pi^2} \int \frac{d\mathbf{q}}{q^2} \\ &\times \sum_{\mathbf{k}',l',n',m'} \frac{|\langle \psi_{\mathbf{k};l,n,m} | e^{i\mathbf{q}\cdot\mathbf{r}} | \psi_{\mathbf{k}';l',n',m'} \rangle|^2}{\frac{1}{2(m_f+1)} ((\mathbf{k}')^2 - \mathbf{k}^2) + v(n' - n) + 1}. \end{aligned} \quad (\text{B25})$$

In the same approach, we obtain the inverse lifetimes for the excited states of the polaron:

$$\begin{aligned} \Gamma_{l,n}(\mathbf{k}) &= \frac{\sqrt{2}\alpha}{4\pi} \sum_{\mathbf{k}',l',n',m'} \int d\mathbf{q} \frac{1}{q^2} \\ &\times |\langle \psi_{\mathbf{k};l,n,m} | e^{i\mathbf{q}\cdot\mathbf{r}} | \psi_{\mathbf{k}';l',n',m'} \rangle|^2 \\ &\times \delta \left(\frac{q^2}{2(m_f + 1)} + v(n' - n) + 1 \right). \end{aligned} \quad (\text{B26})$$

The broadening of the excited polaron “non-scattering” states must be taken into account for an analytical study of the polaron optical conductivity.

Using the above expressions, we determine the transition energies for the transitions between the ground and the first excited state $\hbar\Omega_{0 \rightarrow 1exc} \equiv E_p^{(1exc)} - E_p^{(0)}$. Let us first consider the transition energies in which $E_p^{(1exc)}$ are calculated using optimal values of the parameters of the Feynman model obtained from the minimization of the variational ground-state energy $E_p^{(0)}$. This method formally leads to the Franck-Condon (FC) excited states, with the “frozen” phonon configuration corresponding to the ground state of the polaron. Note that the existence of Franck-Condon states as eigenstates of the Fröhlich polaron Hamiltonian has not been proved: Ref [41] suggests their non-existence as eigenstates for a simplified polaron model. Nevertheless the Franck-Condon concept can be significant, e. g. for approximate treatments using a basis of Franck-Condon states, as indicative for the frequency of the maxima of phonon-sidebands, etc.

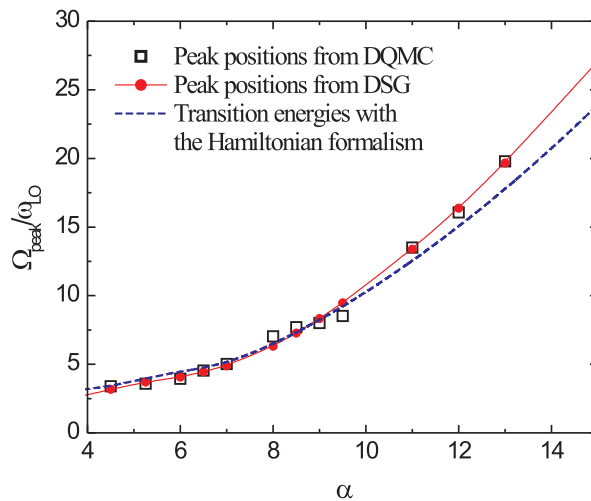


Fig. 1. Franck-Condon transition energies as a function of the coupling constant compared to the lowest-energy peak position of the polaron optical conductivity from Ref. [7] and the maximum of the polaron optical conductivity band from Ref. [79].

In Fig. 1, the FC transition energies calculated with the approach introduced in the present work for polaron momentum $\mathbf{k} = 0$ are plotted as a function of the coupling constant α . They are compared with the peak energies of the polaron optical conductivity calculated using the diagrammatic Monte Carlo method (DQMC) [79, 127] and with the peak energies attributed to polaron “relaxed excited states” (RES) in Ref. [7] (“DSG”). The DQMC and DSG main-peak energies are close to each other in the whole range of the coupling strength. In the range $4 \lesssim \alpha \lesssim 10$, the present result for the transition energy is close to the DQMC and the DSG peak energies. Furthermore, in this range of α , the non-monotonous behavior of the curvature is remarkably the same for the DQMC and DSG peak energies and for the present result.

There is a remarkable agreement between the peaks attributed to the RES in Ref. [7], the peak positions obtained within the strong-coupling approach, Eq. (3) of Ref. [127], and the positions of the maximum of the optical conductivity band calculated in Ref. [79] using DQMC. It is reasonable that the three aforesaid peaks must be interpreted in one and the same way. In order to clarify this, we can refer to Ref. [79]. In the strong-coupling regime, the dominant broad peak of the polaron optical conductivity spectrum can be considered as a “Franck-Condon sideband” of the “groundstate to RES-transition”, even if this latter transition can have a negligible oscillator strength (see also [49]). The optical conductivity spectra of Ref. [127] in the strong-coupling approximation have been calculated taking into account the polaronic shift of the energy levels. The polaronic shift in Ref. [127] has been calculated with the Franck-Condon wave functions (i. e., with the strong-coupling wave functions corresponding to the “frozen” lattice configuration for the ground state). Note that the exact excitation spectrum of the Fröhlich-Hamiltonian might be devoid of Franck-Condon eigenstates, cf. Ref. [41]). It should be remarked that the maxima of the FC-sideband structures of Ref. [7] are positioned at the frequency $\Omega = v$, i. e., at the transition frequency for the model system without the polaron shift.

The Franck-Condon peak energies calculated in the present work also take into account the polaron shift. As follows from the above analysis, in the strong-coupling limit they must correspond to the Franck-Condon peak energies of the strong-coupling expansion of Ref. [127]. The agreement of the position of the maxima of these peaks with those attributed to transitions to the RES in Ref. [7] shows that in the strong-coupling range of α , the latter should be associated to the Franck-Condon sidebands rather than to the RES.

Another approach, in which the parameters of the first excited state are determined self-consistently (Ref. [49]), was used i. a. to calculate (in the strong-coupling case) the (lowest) energy level of the relaxed excited state (RES). The transitions from the polaron ground state to the RES correspond to a zero-phonon peak in the optical conductivity.

For the study of the energies of excited states of the polaron, a variational approach requires special care, because the excited states of the polaron are not stable. A variational approach, strictly speaking, is only valid for excited states when the variational wave function of the excited state is orthogonal to the exact ground-state wave function.

For the estimation of the energy of the first RES with our present formalism, we determine a minimum of the expression (B25) in a physically reasonable range of the variational parameters. In order to determine that range, we refer to Ref. [142], where the energy of the polaron RES is calculated variationally within the Green's function formalism.

The expression for the RES energy in Ref. [142] contains the electron-phonon contribution corresponding to the second-order perturbation formula. It differs, however, from the weak-coupling second-order perturbation expression by the choice of the unperturbed states: in Ref.[142] those are variational states rather than free-electron states. There exists some analogy between our approach and that of Ref. [142]. The latter, however, does not take into account the translation invariance of the polaron problem.

In Ref. [142], the energy of the polaron RES is calculated variationally. The unperturbed wave function of the RES is chosen orthogonal (due to symmetry) to the unperturbed ground state wave function. In the present approach, this orthogonality is also exactly satisfied because of symmetry.

The expressions for the polaron RES energy of Ref. [142] contain singularities, which occur when the energies of the unperturbed ground state and that of the first excited states are in resonant with the LO-phonon energy. These singularities are related to the instability of the excited polaron with respect to the emission of LO-phonons. Using the same reasoning as in Ref. [142] we search for a local minimum of the polaron RES energy in the range where the confinement frequency ν of the Feynman model satisfies the inequality $\nu > 1$. The instability of the excited polaron state is then avoided.

The resulting numerical values of the transition energy to the first RES as a function of α are shown in Fig. 2. They are compared with the numerical-DQMC peak energies of the polaron optical conductivity band [79, 127], with the FC transition energies obtained in the

present work, and with the leading term of the strong-coupling approximation for the RES transition energy from Ref. [49].

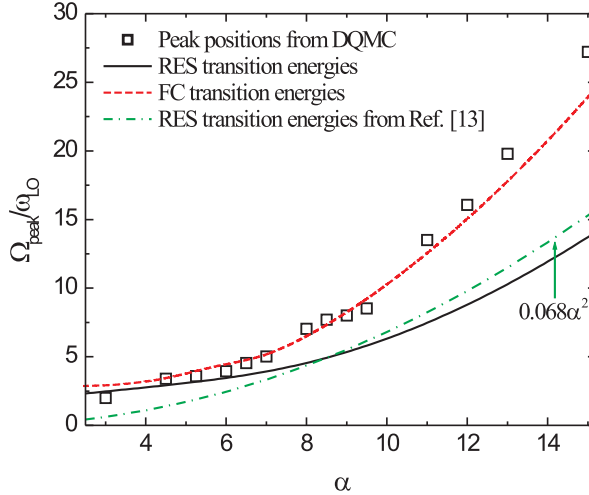


Fig. 2. The transition energy for the transition from the polaron ground state to the first RES (*solid black curve*) and to the first excited FC state (*dashed red curve*) as a function of α obtained in the present work, compared with the maximum of the polaron optical conductivity band from numerical DQMC (*black squares*, Ref. [79]). *The dashed-dot green curve*: the strong-coupling result for this transition energy as given in Ref. [49].

For $\alpha \lesssim 2.5$, there exists no minimum of $E_p^{(exc)}$ in the range $\nu > 1$. We can interpret this result as a manifestation of the fact that for decreasing coupling strength, the RES is suppressed at sufficiently weak coupling. We see that for sufficiently small α ($\alpha \lesssim 6$), the RES transition energies show good agreement with the DQMC peak energies, what confirms the concept of RES developed in Refs. [7, 49]. For higher coupling strengths, the DQMC data appear to be closer to the FC (rather than to RES) transition energies. This result can be an indication of the fact that with increasing α , the mechanism of the polaron optical absorption changes its nature as suggested in Ref. [127], from a regime with dynamic lattice relaxation (for which the RES are relevant) at weak and intermediate coupling to the Franck-Condon (“LO-phonon sidebands”-) regime at strong coupling.

In summary, we have re-formulated the Feynman all-coupling path integral method for the polaron problem within a Hamiltonian formalism using time-ordered operator calculus. This reformulation allows us to describe not only the free energy and the ground state, but also to directly determine – for the first time – the excited polaron states that correspond to the Feynman all-coupling polaron model. A variational procedure for the polaron RES

energy has been developed, within the formalism presented in this work, which provides results i.a. in agreement with the strong-coupling limit of Ref. [49]. The present treatment offers the prospect of further elucidation of the nature of the polaron resonances (“relaxed excited states” versus “Franck-Condon sidebands” [127]) at intermediate coupling.

Appendix C: Many-body large polaron optical conductivity in $\text{SrTi}_{1-x}\text{Nb}_x\text{O}_3$ [*J. T. Devreese, S. N. Klimin, J. L. M. van Mechelen, and D. van der Marel, Phys. Rev. B 81, 125119 (2010)*]

1. Introduction

The infrared optical absorption of perovskite-type materials, in particular, of copper oxide based high- T_c superconductors and of the manganites has been the subject of intensive investigations [1–10]. Insulating SrTiO_3 has a perovskite structure and manifests a metal–insulator transition at room temperature around a doping of 0.002% La or Nb per unit cell [11]. At low doping concentrations, between 0.003% and 3%, strontium titanate reveals a superconducting phase transition [12] below 0.7 K. Various optical experiments [11, 13–17] show a mid-infrared band in the normal state optical conductivity of doped SrTiO_3 which is often explained by polaronic behavior. In the recently observed optical conductivity spectra of Ref. [15], shown in Fig. 1, there is a broad mid-infrared optical conductivity band starting at a photon energy of $\hbar\Omega \sim 100$ meV, which is within the range of the LO-phonon energies of $\text{SrTi}_{1-x}\text{Nb}_x\text{O}_3$. The peaks/shoulders of the experimental optical conductivity band at $\hbar\Omega \sim 200$ to 400 meV resemble the peaks provided by the mixed plasmon-phonon excitations as described in Ref. [18]. Based on the experimental data, the authors deduce a coupling constant $3 < \alpha < 4$ and conclude the mid-infrared peaks to originate from large polaron formation. The high and narrow peaks positioned at the lower frequencies with respect to the mid-infrared band are attributed in Ref. [15] to the optical absorption of the TO-phonons.

There are different types of polaron states in solids. In the effective mass approximation for the electron placed in a continuum polarizable medium, a so-called large or continuum polaron can exist. Large polaron wave functions and the corresponding lattice distortions spread over many lattice sites. Due to the finite phonon frequencies the ion polarizations can follow the polaron motion if the motion is sufficiently slow. Hence, large polarons with a low kinetic energy propagate through the lattice as free electrons but with an enhanced effective mass. When the polaron binding energy is larger than the half bandwidth of the electron band, all states in the Bloch bands are ‘dressed’ by phonons. In this strong-coupling regime, the finite electron bandwidth becomes important, so the continuum approximation cannot be

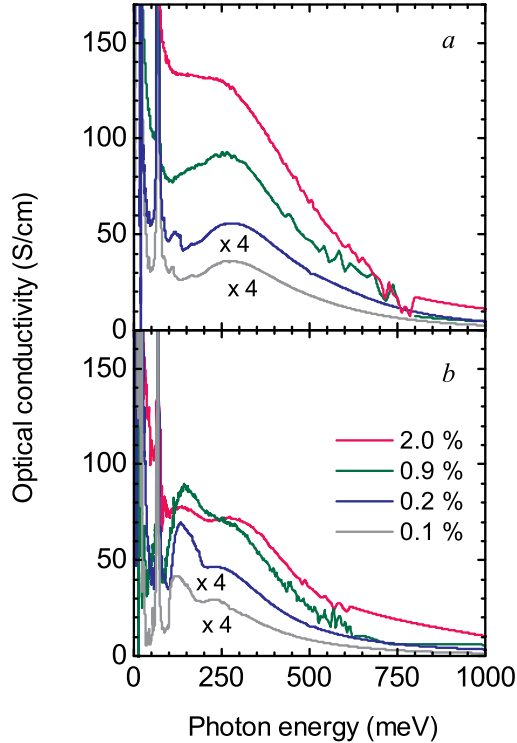


FIG. 22: Optical conductivity of $\text{SrTi}_{1-x}\text{Nb}_x\text{O}_3$ for 0.1% (grey curves), 0.2% (blue curves), 0.9% (green curves) and 2% (pink curves) at 300 K (panel a) and 7 K (panel b). For clarity, the mid-infrared conductivities of $x = 0.1\%$ and 0.2% are magnified by a factor 4. (From Ref. [15].)

applied. In this case the carriers are described as “small” or discrete (lattice) polarons that can hop between different states localized at lattice sites. A key distinction between large and small polarons is then the radius of the polaron state. For large polarons, that radius substantially exceeds the lattice constant, while for small polarons it is comparable to the lattice constant. A review of the properties of large and small polarons can be found, e. g., in Refs. [19, 20]. In the theory of “mixed” polarons [21–24] the states of the electron-phonon system are composed of a mixture of large and small polaron states.

Polaron states are formed due to the electron-phonon interaction, which is different in the cases of large and small polarons. For a large polaron, the electron-phonon interaction is provided by a macroscopic (continuum) polarization of the lattice. This interaction is characterized by the coupling constant α introduced by Fröhlich [25],

$$\alpha = \frac{1}{2} \left(\frac{1}{\varepsilon_\infty} - \frac{1}{\varepsilon_0} \right) \frac{e^2}{\hbar\omega_L} \left(\frac{2m_b\omega_L}{\hbar} \right)^{1/2}, \quad (\text{C1})$$

where ε_∞ and ε_0 are, respectively, the high-frequency and the static dielectric constants, e

is the electron charge, ω_L is the longitudinal optical (LO) phonon frequency in the Brillouin zone centre, and m_b is the band electron (or hole) mass. The large-polaron coupling constant is thus expressed through macroscopic observable parameters of a polarizable medium. On the contrary, the electron-phonon interaction for a small polaron is described through microscopic parameters.

The nature of the polaron states in $\text{SrTi}_{1-x}\text{Nb}_x\text{O}_3$ is not yet clear. Previous optical measurements on strontium titanate were interpreted in terms of small polarons [24, 26]. However, that assumption contradicts the interpretation of transport measurements [27], which rather support the large-polaron picture. Also the heat capacity measurements [28], provide effective masses similar to those of large polarons. In Ref. [13], the experimental results of Ref. [16] on the temperature-dependent plasma frequencies in $\text{SrTi}_{1-x}\text{Nb}_x\text{O}_3$ were interpreted within the theory of mixed polarons [21–24]. Thermoelectric power measurements [27] have shown that the density-of-states masses increase with increasing temperature, which can be explained by a theory of mixed polarons [21]. It has been supposed [14] that the polaron optical conductivity in $\text{SrTi}_{1-x}\text{Nb}_x\text{O}_3$ is probably provided by mixed polarons. A possible coexistence of large and small mass polarons has been suggested in Ref. [29]. In Ref. [30], coexistence of small and large polarons in the same solid is invoked to interpret experimental data on the optical absorption in oxides.

The key question is to determine the type of polarons that provide the mechanism of the polaron optical conductivity in $\text{SrTi}_{1-x}\text{Nb}_x\text{O}_3$. The optical response of large polarons in various approximations was studied, e. g., in Refs. [31–34]. The same problem for the small polaron was investigated in [26, 35]. In the large-polaron theory, the optical absorption is provided by transitions (with 0, 1, . . . phonon emission) between different continuum electron states. In the small-polaron theory, the optical absorption occurs when the self-trapped carrier is induced to transfer from its localized state to a localized state at an adjacent site, with emission of phonons. Because of the different physical mechanisms involved, the optical conductivity spectra of large and small polarons are different from each other. In the large-polaron theory the polaron optical conductivity behaves at high frequencies Ω as a power function ($\propto \Omega^{-5/2}$). In the small-polaron theory, the polaron optical conductivity at high frequencies decreases much faster than for large polarons: as a Gaussian exponent. Therefore the analysis of optical measurements can shed some light on the aforesaid question on the type of polarons responsible for the optical conductivity in $\text{SrTi}_{1-x}\text{Nb}_x\text{O}_3$.

The polaron optical conductivity band of $\text{SrTi}_{1-x}\text{Nb}_x\text{O}_3$ occupies the mid-infrared range of the photon energies $\hbar\Omega \lesssim 1$ eV, and the threshold for interband electron-hole transitions lies at the band gap energy, which is around 3.3 eV in $\text{SrTi}_{1-x}\text{Nb}_x\text{O}_3$ [15]. Therefore interband transitions do not interfere with the polaron optical conductivity. Other mechanisms of electron intraband scattering (for example, electron-phonon interaction with acoustic phonons and/or electron or hole transitions from impurity centers) may be manifested together with the polaron mechanism in the energy range $\hbar\Omega \lesssim 1$ eV. The treatment of those mechanisms is, however, beyond the scope of the present investigation.

We can make some preliminary suggestions concerning the dominating mechanism of the mid-infrared optical conductivity in the Nb doped strontium titanate. The low-frequency edge of the mid-infrared band in $\text{SrTi}_{1-x}\text{Nb}_x\text{O}_3$ at a low temperature ($T = 7$ K) lies in the range of the LO-phonon energies obtained in [16]. The maximum of the mid-infrared band lies relatively close to this low-frequency edge (the difference in frequency between the low-frequency edge and the maximum of the mid-infrared band is comparable to the LO-phonon frequencies in $\text{SrTi}_{1-x}\text{Nb}_x\text{O}_3$). This behavior is characteristic of large-polaron optical conductivity rather than of small-polaron optical conductivity. Indeed, the maximum of the small polaron optical conductivity band is expected to be shifted to considerably higher frequencies with respect to the low-frequency edge of the polaron optical conductivity band (see, e.g., Ref. [35]). Also, at sufficiently high frequencies, the experimental mid-infrared band from Ref. [15] decreases with increasing Ω rather slowly, which is characteristic for large-polaron optical conductivity rather than for small-polaron optical conductivity. We therefore can suggest that the large-polaron picture is the most appropriate for the interpretation of the mid-infrared band of $\text{SrTi}_{1-x}\text{Nb}_x\text{O}_3$ observed in Ref. [15].

In order to interpret the mid-infrared band of the experimental optical conductivity spectra of $\text{SrTi}_{1-x}\text{Nb}_x\text{O}_3$ [15] in terms of polarons, we calculate the large-polaron optical conductivity spectra for $\text{SrTi}_{1-x}\text{Nb}_x\text{O}_3$ using the model for the optical conductivity of a large-polaron gas developed in Ref. [18], adapted to take into account multiple LO-phonon branches [36]. The degeneracy and the anisotropy of the conduction band in $\text{SrTi}_{1-x}\text{Nb}_x\text{O}_3$ are taken into account.

2. Optical conductivity of a gas of large polarons

The optical absorption spectra of $\text{SrTi}_{1-x}\text{Nb}_x\text{O}_3$ are sensitive to the doping level [15]. Therefore a many-polaron description is in order. In our context, “many-polaron description” means an account of many-electron effects on the optical conductivity of a polaron gas. These effects include the influence of the electron-electron Coulomb interaction (which leads to screening effects) and of the Fermi statistics of the polaron gas on the optical conductivity spectra. In the low-density limit, those many-body effects are not important, and the optical conductivity of a polaron gas is well described by the optical conductivity of a single polaron multiplied by the electron density. The scope of the present study embraces a wide range of electron densities for which the single-polaron approach is, in general, insufficient. As shown below, even at the lowest electron density involved in the experiment [15], the shape and magnitude of the optical conductivity spectrum is strongly affected by many-body effects.

We wish to compare the experiments of Ref. [15], in particular the observed mid-infrared band, to the theoretical optical conductivity of a gas of large polarons. For that purpose we use the many-body large polaron approach of Refs. [18, 36], which takes into account the electron-electron interaction and the Fermi statistics of polarons.

Refs. [18, 36] are limited to the study of weak-coupling polarons. Up to $\alpha \approx 3$, which includes the case of $\text{SrTi}_{1-x}\text{Nb}_x\text{O}_3$, the weak coupling approximation can be expected to describe the main characteristics of the many-polaron optical response (see, e.g., Refs. [18–20]). In Ref. [36] a generalization of Ref. [18] is presented that takes into account the electron-phonon interaction with *multiple LO-phonon branches* as they exist, e. g., in complex oxides. For a single polaron, effects related to multiple LO-phonon branches were investigated in Ref. [38]. The starting point for the treatment of a many-polaron system is the Fröhlich Hamiltonian

$$\begin{aligned}
 H = & \sum_{\mathbf{k}} \sum_{\sigma=\pm 1/2} \frac{\hbar^2 k^2}{2m_b} c_{\mathbf{k},\sigma}^+ c_{\mathbf{k},\sigma} + \sum_{\mathbf{q}} \sum_{j=1}^n \hbar \omega_{L,j} a_{\mathbf{q},j}^+ a_{\mathbf{q},j} + U_{e-e} \\
 & + \frac{1}{\sqrt{V}} \sum_{\mathbf{q}} \sum_{j=1}^n \left(V_{\mathbf{q},j} a_{\mathbf{q},j} \sum_{\mathbf{k}} \sum_{\sigma=\pm 1/2} c_{\mathbf{k}+\mathbf{q},\sigma}^+ c_{\mathbf{k},\sigma} + \text{h.c.} \right), \quad (\text{C2})
 \end{aligned}$$

where $c_{\mathbf{k},\sigma}^+$ ($c_{\mathbf{k},\sigma}$) are the creation (annihilation) operators for an electron with momentum \mathbf{k} and with the spin z -projection σ , $a_{\mathbf{q},j}^+$ ($a_{\mathbf{q},j}$) are the creation (annihilation) operators for a phonon of the j -th branch with the momentum q , $\omega_{L,j}$ are the LO-phonon frequencies

(approximated here as non-dispersive), and V is the volume of the crystal. The polaron interaction amplitude $V_{\mathbf{q},j}$ is [38]

$$V_{\mathbf{q},j} = \frac{\hbar\omega_{L,j}}{q} \left(\frac{4\pi\alpha_j}{V} \right)^{1/2} \left(\frac{\hbar}{2m_b\omega_{L,j}} \right)^{1/4}, \quad (\text{C3})$$

where α_j is a dimensionless partial coupling constant characterizing the interaction between an electron and the j -th LO-phonon branch. The electron-electron interaction is described by the Coulomb potential energy

$$U_{e-e} = \frac{1}{2} \sum_{\mathbf{q} \neq 0} \frac{4\pi e^2}{\varepsilon_\infty q^2} \sum_{\mathbf{k}, \mathbf{k}', \sigma, \sigma'} c_{\mathbf{k}+\mathbf{q}, \sigma}^+ c_{\mathbf{k}'-\mathbf{q}, \sigma'}^+ c_{\mathbf{k}', \sigma'} c_{\mathbf{k}, \sigma}. \quad (\text{C4})$$

Optical phonons in SrTiO₃ show a considerable dispersion (see, e. g., Ref. [39] and references therein). The effect of the phonon dispersion is a broadening of features of the polaron optical conductivity band. The magnitude of the broadening is characterized by the dispersion parameter $\Delta\omega$ of the optical phonons, that contribute to the integrals over \mathbf{q} entering the polaron optical conductivity. In a polar crystal with a single LO-phonon branch, that range of convergence is approximately $q_0 = (m_b\omega_{LO}/\hbar)^{1/2}$. For SrTiO₃, taking $\omega_{LO} = \max\{\omega_{L,j}\}$, we obtain $q_0 \approx 1.02 \times 10^9 \text{ m}^{-1}$. The boundary of the Brillouin zone π/a_0 in SrTiO₃ (where the lattice constant $a_0 \approx 0.3905 \text{ nm}$) is at $8 \times 10^9 \text{ m}^{-1}$. Therefore the integration domain for the relevant integrals is one order smaller than the size of the Brillouin zone. In the region $0 < q < q_0$, the dispersion parameter of the LO-phonon frequencies, $\Delta\omega$, is a few percent of $\omega_{L,j}$. Consequently, $\Delta\omega$ is very small compared with the characteristic width of the polaron band. Therefore, in the present treatment, we apply the approximation of non-dispersive phonons.

For a description of a polarizable medium with n optical-phonon branches, we use the model dielectric function [40, 41]

$$\varepsilon(\omega) = \varepsilon_\infty \prod_{j=1}^n \left(\frac{\omega^2 - \omega_{L,j}^2}{\omega^2 - \omega_{T,j}^2} \right), \quad (\text{C5})$$

whose zeros (poles) correspond to the LO(TO) phonon frequencies $\omega_{L,j}$ ($\omega_{T,j}$). This dielectric function is the result of the straightforward extension of the Born-Huang approach [42] to the case where more than one optical-phonon branch exists in a polar crystal. The Born-Huang approach and its extension [40] generate expressions for the macroscopic polarization induced by the polar vibrations, and for the corresponding electrostatic potential. This electrostatic

potential is a basis element of the Hamiltonian of the electron-phonon interaction. In Ref. [40], the Hamiltonian of the electron-phonon interaction has been explicitly derived with the amplitudes

$$V_{\mathbf{q}j} = \frac{1}{\sqrt{V}} \frac{e}{iq} \left(\frac{4\pi\hbar}{\left. \frac{\partial \varepsilon(\omega)}{\partial \omega} \right|_{\omega=\omega_{L,j}}} \right)^{1/2}. \quad (\text{C6})$$

Using Eqs. (C3) and (C6) with the dielectric function (C5), we arrive at the following set of linear equations for the coupling constants α_j ($j = 1, \dots, n$):

$$\sum_{k=1}^n \hbar \omega_{L,k}^3 \left(\frac{\hbar}{2m_b \omega_{L,k}} \right)^{1/2} \frac{\alpha_k}{\omega_{L,k}^2 - \omega_{T,j}^2} = \frac{e^2}{2\varepsilon_\infty}. \quad (\text{C7})$$

Knowledge of the band mass, of the electronic dielectric constant ε_∞ and of the LO- and TO-phonon frequencies is sufficient to determine the coupling constants α_j taking into account mixing between different optical-phonon branches. In the particular case of a single LO-phonon branch, Eq. (C7) is reduced to (C1).

In order to describe the optical conductivity of a polaron gas, we refer to the work [44], where the Mori-Zwanzig projection operator technique has been used to rederive the path-integral result of Ref. [43] and the impedance of Ref. [31]. We repeat the derivations of Ref. [44] with the replacement of single-electron functions by their many-electron analogs. For example, $e^{i\mathbf{q}\cdot\mathbf{r}}$ in the Hamiltonian of the electron-phonon interaction is replaced by the Fourier component of the electron density for an N -electron system,

$$\rho(\mathbf{q}) \equiv \sum_{s=1}^N e^{i\mathbf{q}\cdot\mathbf{r}_s} = \sum_{\mathbf{k},\sigma} c_{\mathbf{k}+\mathbf{q},\sigma}^+ c_{\mathbf{k},\sigma}. \quad (\text{C8})$$

As a result, we arrive at a formula which is structurally similar to the single-polaron optical conductivity [31, 44],

$$\sigma(\Omega) = \frac{e^2 n_0}{m_b} \frac{i}{\Omega - \chi(\Omega)/\Omega}, \quad (\text{C9})$$

where $n_0 = N/V$ is the carrier density, and $\chi(\Omega)$ is the memory function. The same many-electron derivation as in the present work, to the best of our knowledge, was first performed for the polaron gas in 2D in Ref. [45] in the weak electron-phonon coupling limit.

In Refs. [31, 44] the single-polaron memory function was calculated starting from the all-coupling Feynman variational principle [46]. For a many-polaron system, an effective all-coupling extension of that variational principle has not been worked out yet. In the present

treatment, we restrict ourselves to the weak-coupling approximation for the electron-phonon interaction to derive the memory function. In this approximation, the memory function $\chi(\Omega)$ is similar to that of Ref. [45], with two distinctions: (1) the electron gas in the present treatment is three-dimensional, (2) several LO phonon branches are taken into account. The resulting form of the memory function is

$$\chi(\Omega) = \frac{4}{3\hbar m_b n_0 V} \sum_{\mathbf{q},j} q^2 |V_{\mathbf{q},j}|^2 \int_0^\infty dt (e^{i\Omega t} - 1) \times \text{Im} \left[\frac{\cos[\omega_{L,j}(t + i\hbar\beta/2)]}{\sinh(\beta\hbar\omega_{L,j}/2)} S(\mathbf{q}, t) \right], \quad (\text{C10})$$

where $\beta = 1/(k_B T)$. The dynamical structure factor $S(\mathbf{q}, t)$ is proportional to the two-point correlation function (cf. Ref. [18]),

$$S(\mathbf{q}, t) \equiv \frac{1}{2} \left\langle \sum_{i,j=1}^N e^{i\mathbf{q}\cdot[\mathbf{r}_j(t) - \mathbf{r}_i(0)]} \right\rangle = \frac{1}{2} \langle \rho(\mathbf{q}, t) \rho(-\mathbf{q}, 0) \rangle. \quad (\text{C11})$$

To obtain $\chi(\Omega)$ to order α it is sufficient to perform the averaging in the correlation function (C11) using the Hamiltonian (C2) without the electron-phonon interaction and keeping the electron-electron interaction term U_{e-e} .

We calculate the dynamical structure factor (C11) extending the method [18] to nonzero temperatures. In Ref. [18], the key advantage of the many-polaron variational approach [47] is exploited: the fact that the many-body effects are entirely contained in the dynamical structure factor $S(\mathbf{q}, t)$. The structure factor can be calculated using various approximations. Terms of order of $|V_{\mathbf{q},j}|^2$ are automatically taken into account in the memory function (C10). Consequently, up to order α for $\sigma(\Omega)$, it is sufficient to calculate $S(\mathbf{q}, t)$ without the electron-phonon coupling. In Ref. [18], $S(\mathbf{q}, t)$ was calculated within two different approximations: (i) the Hartree-Fock approximation, (ii) the random-phase approximation (RPA). As shown in Ref. [18], the RPA dynamical structure factor, contrary to the Hartree-Fock approximation, takes into account the effects both of the Fermi statistics and of the electron-electron interaction on the many-polaron optical-absorption spectra.

The dynamical structure factor is expressed through the density-density Green's functions defined as

$$\mathcal{G}(\mathbf{q}, \Omega) \equiv -i \int_0^\infty e^{i\Omega t} \langle \rho(\mathbf{q}, t) \rho(-\mathbf{q}, 0) \rangle dt, \quad (\text{C12})$$

$$G^R(\mathbf{q}, \Omega) \equiv -i \int_0^\infty e^{i\Omega t} \langle [\rho(\mathbf{q}, t), \rho(-\mathbf{q}, 0)] \rangle dt. \quad (\text{C13})$$

In terms of $G(\mathbf{q}, \Omega)$ and $G^R(\mathbf{q}, \Omega)$, the memory function (C10) takes the form:

$$\begin{aligned} \chi(\Omega) &= \sum_j \frac{\alpha_j \hbar \omega_{L,j}^2}{6\pi^2 N m_b} \left(\frac{\hbar}{2m_b \omega_{L,j}} \right)^{1/2} \\ &\times \int d\mathbf{q} \{ \mathcal{G}(\mathbf{q}, \Omega - \omega_{L,j}) + \mathcal{G}^*(\mathbf{q}, -\Omega - \omega_{L,j}) - \mathcal{G}(\mathbf{q}, -\omega_{L,j}) - \mathcal{G}^*(\mathbf{q}, -\omega_{L,j}) \\ &+ \frac{1}{e^{\beta \hbar \omega_{L,j}} - 1} [G^R(\mathbf{q}, \Omega - \omega_{L,j}) + (G^R(\mathbf{q}, -\Omega - \omega_{L,j}))^* \\ &- G^R(\mathbf{q}, -\omega_{L,j}) - (G^R(\mathbf{q}, -\omega_{L,j}))^*] \}. \end{aligned} \quad (\text{C14})$$

Taking into account the Coulomb electron-electron interaction within RPA, the retarded Green's function $G^R(\mathbf{q}, \Omega)$ is given by

$$G^R(\mathbf{q}, \Omega) = \frac{\hbar V P^{(1)}(\mathbf{q}, \Omega)}{1 - \frac{4\pi e^2}{\varepsilon_\infty q^2} P^{(1)}(\mathbf{q}, \Omega)}, \quad (\text{C15})$$

where $P^{(1)}(\mathbf{q}, \Omega)$ is the polarization function of the free electron gas, see, e.g., [48]

$$P^{(1)}(\mathbf{q}, \Omega) = \frac{1}{V} \sum_{\mathbf{k}, \sigma} \frac{f_{\mathbf{k}+\mathbf{q}, \sigma} - f_{\mathbf{k}, \sigma}}{\hbar \Omega + \frac{\hbar^2 (\mathbf{k}+\mathbf{q})^2}{2m_b} - \frac{\hbar^2 k^2}{2m_b} + i\delta}, \quad \delta \rightarrow +0 \quad (\text{C16})$$

with the electron average occupation numbers $f_{\mathbf{k}, \sigma}$. The function $\mathcal{G}(\mathbf{q}, \Omega)$ is obtained from $G^R(\mathbf{q}, \Omega)$ using the exact analytical relation

$$(1 - e^{-\beta \hbar \Omega}) \text{Im} \mathcal{G}(\mathbf{q}, \Omega) = \text{Im} G^R(\mathbf{q}, \Omega) \quad (\text{C17})$$

and the Kramers-Kronig dispersion relations for $\mathcal{G}(\mathbf{q}, \Omega)$.

The above expressions are written for an isotropic conduction band. However, the conduction band of $\text{SrTi}_{1-x}\text{Nb}_x\text{O}_3$ is strongly anisotropic and triply degenerate. The electrons are doped in three bands: d_{xy} , d_{yz} and d_{xz} , which all have their minima at $\mathbf{k} = 0$. Each of these bands has light masses along two direction (x and y for d_{xy} , etc.) and a heavy mass along the third direction. While each electron has a strongly anisotropic mass, the electronic transport remains isotropic due to the fact that 2 light masses and 1 heavy mass contribute along each crystallographic axis.

The anisotropy of the electronic effective mass of the conduction band can be approximately taken into account in the following way. We use the averaged inverse band mass

$$\frac{1}{\bar{m}_b} = \frac{1}{3} \left(\frac{1}{m_x} + \frac{1}{m_y} + \frac{1}{m_z} \right) \quad (\text{C18})$$

and the density-of-states band mass

$$m_D = (m_x m_y m_z)^{1/3}. \quad (\text{C19})$$

The mass m_D appears in the prefactor of the linear term of the specific heat. Comparing the mass m_D obtained from the experimental specific heat [28, 49] with the mass \bar{m}_b obtained using optical spectral weights [15] reveals the mass ratio of the heavy and light bands to be about 27. The expression (C18) replaces the bare mass m_b in the optical conductivity (C9) and in the memory function (C14). The polarization function of the free electron gas (C16) is calculated with the density-of-states mass m_D instead of m_b . The band degeneracy is taken into account through the degeneracy factor which is equal to 3, both in the polarization function and in the normalization equation for the chemical potential. The reduction of the polaron optical conductivity band due to screening with band degeneracy turns out to be less significant than without band degeneracy.

a. Theory and experiment

b. Material parameters

Several experimental parameters characterizing $\text{SrTi}_{1-x}\text{Nb}_x\text{O}_3$ are necessary for the calculation of the large-polaron optical conductivity (see, e.g., Refs. [14, 16]): the LO- and TO-phonon frequencies, the electron band mass, and the electronic dielectric constant ε_∞ .

The electronic dielectric constant can be obtained using reflectivity spectra of $\text{SrTi}_{1-x}\text{Nb}_x\text{O}_3$. At $T = 10$ K, the reflectivity of $\text{SrTi}_{1-x}\text{Nb}_x\text{O}_3$ is $R \approx 0.16$ for $\Omega \approx 5000$ cm^{-1} . The electronic dielectric constant can be approximated using the expression

$$R(\Omega) = \left| \frac{\sqrt{\varepsilon(\Omega)} - 1}{\sqrt{\varepsilon(\Omega)} + 1} \right|^2 \quad (\text{C20})$$

and assuming that $\Omega = 5000$ cm^{-1} is a sufficiently high frequency to characterize the electronic response. From (C20) it follows that for $\text{SrTi}_{1-x}\text{Nb}_x\text{O}_3$, $\varepsilon_\infty \approx 5.44$.

In order to determine the optical-phonon frequencies, we use the experimental data from available sources [15, 16]. In Ref. [15], three infrared active phonon modes are observed at room temperature: at 11.0 meV, 21.8 meV and 67.6 meV. With decreasing temperature, the lowest-frequency infrared-active phonon mode shows a strong red shift upon cooling,

and saturates at about 2.3 meV at 7 K. Those infrared-active phonon modes are associated with the polar TO-phonons. The TO-phonon frequencies determined in Ref. [16] for $\text{SrTi}_{1-x}\text{Nb}_x\text{O}_3$ with $x = 0.9\%$ at $T = 300$ K are 100 cm^{-1} , 175 cm^{-1} and 550 cm^{-1} . The corresponding TO-phonon energies are 12.4 meV, 21.7 meV and 68.2 meV.

Refs. [15] and [16] are used as sources for phonon parameters. In Ref. [16], the TO-phonon frequencies are calculated on the basis of reflectivity measurements using a model dielectric function to fit experimental data. In Ref. [15], the TO-phonon frequencies are obtained from an analysis of both reflectivity and transmission spectra, using inversion of the Fresnel equations of reflection and transmission coefficients and the Kramers-Kronig transformation of the reflectivity spectra. The TO-phonon energies reported in Refs. [15] and [16] are in close agreement. This confirms the reliability of both experimental data sources [15, 16]. The values of the TO-phonon frequencies used in our calculation are taken from the experiment [15] because they are directly related to the samples of $\text{SrTi}_{1-x}\text{Nb}_x\text{O}_3$ for which the comparison of theory and experiment is made in the present work.

The TO phonon frequencies from Ref. [15] can be used when they are complemented with corresponding LO phonon frequencies. However, Ref. [15] does not contain data of the LO-phonon frequencies. In the present calculation we use the LO phonon frequencies from Ref. [16].

The averaged band mass (C18) is taken to be $\bar{m}_b = 0.81m_e$ (where m_e is the electron mass in vacuum) according to experimental data from Ref. [50]. Using the ratio of the heavy mass (m_z) to the light mass ($m_x = m_y$), $m_z/m_x = 27$, we find the density-of states band mass $m_D \approx 1.65m_e$.

The TO- and LO- phonon frequencies and the resulting partial coupling constants calculated using the mass \bar{m}_b are presented in Table 1.

The effective coupling constant in Table 1 is determined following Ref. [38], as a sum of partial coupling constants α_j ,

$$\alpha_{\text{eff}} \equiv \sum_j \alpha_j \tag{C21}$$

The result $\alpha_{\text{eff}} \sim 2$ shows that the electron-phonon coupling strength in $\text{SrTi}_{1-x}\text{Nb}_x\text{O}_3$ lies in the intermediate to weak coupling range, and the conditions for small polaron formation are not fulfilled. This analysis indicates that the large-polaron picture – rather than the small-polaron description is suitable for the interpretation of the mid-infrared band of the

TABLE III: Optical-phonon frequencies and partial coupling constants of doped strontium titanate

x	$x = 0.1\%$	$x = 0.1\%$	$x = 0.2\%$	$x = 0.2\%$	$x = 0.9\%$	$x = 0.9\%$	$x = 2\%$	$x = 2\%$
T	$T = 7 \text{ K}$	$T = 300 \text{ K}$	$T = 7 \text{ K}$	$T = 300 \text{ K}$	$T = 7 \text{ K}$	$T = 300 \text{ K}$	$T = 7 \text{ K}$	$T = 300 \text{ K}$
$\hbar\omega_{T,1} \text{ (meV)}$	2.27	11.5	2.63	11.5	6.01	12.1	8.51	13.0
$\hbar\omega_{L,1} \text{ (meV)}$	21.2	21.2	21.2	21.2	21.2	21.2	21.2	21.2
α_1	0.021	0.013	0.021	0.013	0.017	0.013	0.017	0.013
$\hbar\omega_{T,2} \text{ (meV)}$	21.2	21.8	21.2	21.8	21.2	21.8	21.2	21.8
$\hbar\omega_{L,2} \text{ (meV)}$	58.4	58.4	58.4	58.4	58.4	58.4	58.4	58.4
α_2	0.457	0.414	0.457	0.414	0.452	0.414	0.447	0.409
$\hbar\omega_{T,3} \text{ (meV)}$	67.6	67.1	67.6	67.1	67.6	67.1	67.6	67.1
$\hbar\omega_{L,3} \text{ (meV)}$	98.7	98.7	98.7	98.7	98.7	98.7	98.7	98.7
α_3	1.582	1.582	1.582	1.580	1.576	1.578	1.570	1.574
α_{eff}	2.06	2.01	2.06	2.01	2.05	2.01	2.03	2.01

optical conductivity of $\text{SrTi}_{1-x}\text{Nb}_x\text{O}_3$.

We use the actual electron densities for the samples studied in Ref. [15] based on the unit cell volume (59.5 cubic angstrom) and the chemical composition (x is the doping level). These carrier densities (see Table 2) are confirmed by measurements of the Hall constants.

 TABLE IV: Electron densities of $\text{SrTi}_{1-x}\text{Nb}_x\text{O}_3$

$x \text{ (\%)}$	$n_0 \text{ (cm}^{-3}\text{)}$
0.1	1.7×10^{19}
0.2	3.4×10^{19}
0.9	1.5×10^{20}
2.0	3.4×10^{20}

3. Optical conductivity spectra

We calculate the large-polaron optical conductivity spectra for $\text{SrTi}_{1-x}\text{Nb}_x\text{O}_3$ using the approach of Ref. [18] as adapted in Ref. [36] to take into account multiple LO-phonon branches. We also include in the numerical calculation the TO-phonon contribution to the

optical conductivity, described by an oscillatory-like model dielectric function (see, e.g., Ref. [16]):

$$\text{Re } \sigma_{TO}(\Omega) = \sum_j \sigma_{0,j} \frac{\gamma_j^2}{(\Omega - \omega_{T,j})^2 + \gamma_j^2}, \quad (\text{C22})$$

where the weight coefficients $\sigma_{0,j}$ and the damping parameters γ_j for each j -th TO-phonon branch are extracted from the experimental optical conductivity spectra of Ref. [15]. The polaron- and the TO-phonon optical responses are treated as independent of each other. Consequently the polaron-(C9) and TO-phonon (C22) contributions enter the optical conductivity additively.

Following the procedure described above using the material parameters discussed above, we obtain the theoretical large-polaron optical conductivity spectra of $\text{SrTi}_{1-x}\text{Nb}_x\text{O}_3$ shown in Fig. 2 and Fig. 3 at 7 K and 300 K, respectively. In each graph also the experimental optical conductivity spectra of Ref. [15] are shown. It should be emphasized that *in the present calculation, there is no fitting of material constants for the polaron contribution to $\text{Re } \sigma(\Omega)$. Even the magnitude of the optical conductivity, which is often arbitrarily scaled in the literature, follows from first principles.*

At 7 K, the calculated optical conductivity based on the Fröhlich model and extended for a gas of large polarons as described in the present paper, shows convincing agreement with the behavior of the experimental optical conductivity for the high energy part of the spectra, i.e., $\hbar\Omega \gtrsim 300$ meV. The experimental polaron optical conductivity of $\text{SrTi}_{1-x}\text{Nb}_x\text{O}_3$ falls down at high frequencies following the power law (derived in the present work and typical for large polarons) rather than as a Gaussian exponent that would follow from the small-polaron theory. At lower photon energies $\hbar\Omega \lesssim 200$ meV, the experiment shows distinct peaks that are not explained within the polaron theory. They can be due to other scattering mechanisms as discussed below.

The minor deviations between theoretical and experimental $\text{Re } \sigma(\Omega)$ in the frequency range $\hbar\Omega \gtrsim 300$ meV may be attributed to the difference between the actual electron densities and the densities calculated on the basis of the unit cell volume and the chemical composition. However, we prefer not to fit the density.

The optical conductivity calculated for a single large-polaron absorption [31] predicts an intensity 3-4 times larger than the experimental data for the lowest doping level $x = 0.1\%$, and therefore cannot explain those data. For higher dopings, the overestimation of the

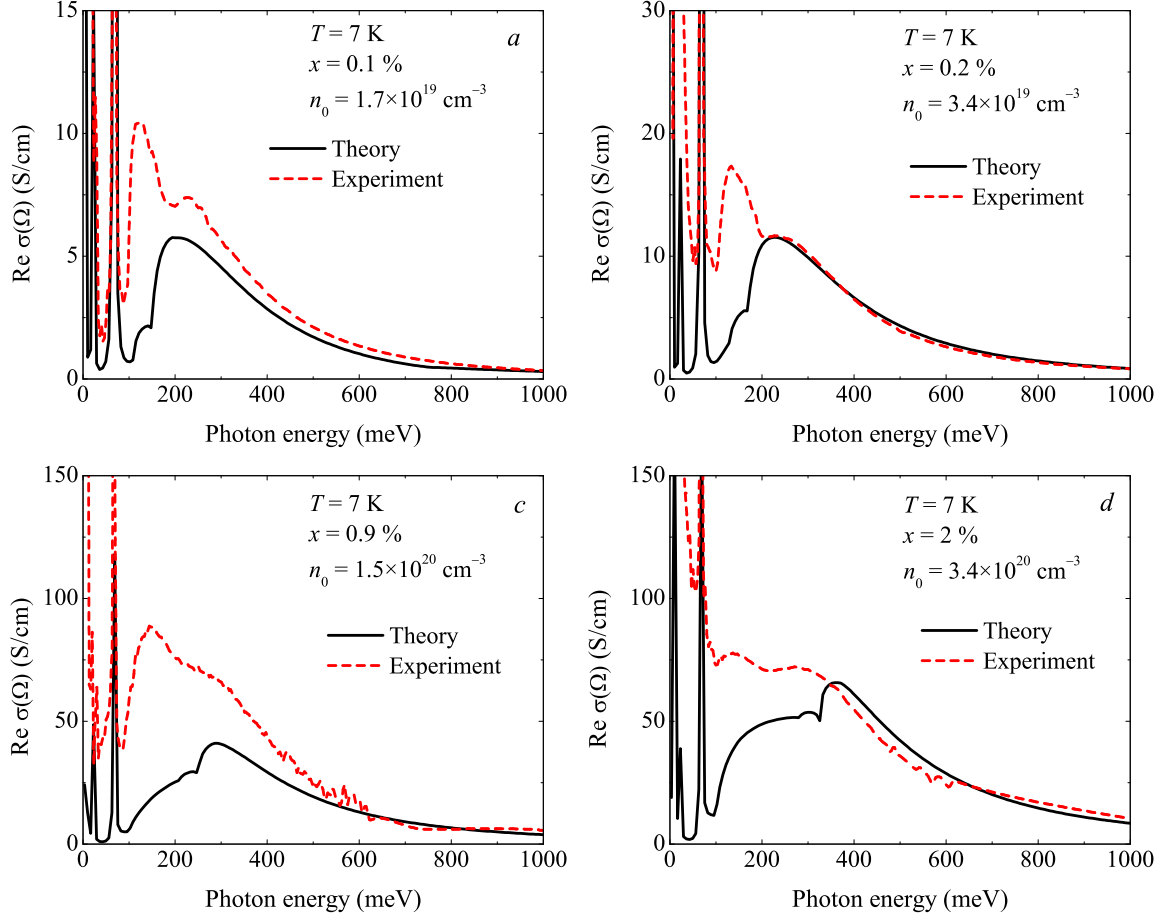


FIG. 23: The many-large-polaron optical conductivity compared with the experiment [15] at $T = 7$ K. The doping level is $x = 0.1\%$ (a), 0.2% (b), 0.9% (c) and 2% (d).

magnitude of the optical conductivity within the single-polaron theory is even larger than for $x = 0.1\%$. Therefore the many-polaron approach, used in the present work, is essential.

At 300 K, in Fig. 3 (a, b, d), the agreement between theory and experiment is qualitative. Both experimental and theoretical spectra show a maximum at the room-temperature optical conductivity spectra in the range $\hbar\Omega \sim 250$ meV. For the doping level $x = 0.9\%$ the calculated optical conductivity spectrum underestimates the experimental data, as also observed at 7 K.

Many-body effects considerably influence the optical conductivity spectra of a polaron gas. First, features related to the emission of a plasmon together with a LO phonon [18] are manifested in the optical conductivity spectra of the many-polaron gas at $T = 7$ K as separate peaks whose positions shift to higher energies with increasing doping level. At room temperature, those peaks are strongly broadened and smoothed, and only a broad

plasmon feature is apparent. Second, the mid-infrared optical conductivity (per particle) in $\text{SrTi}_{1-x}\text{Nb}_x\text{O}_3$ is decreasing at higher doping levels due to the screening of the polar interactions, which is accounted for in the present approach in which $S(\mathbf{q}, t)$ is based on RPA. The effect of screening can be illustrated by the fact that for $n_0 \sim 10^{20} \text{ cm}^{-3}$, the many-polaron optical conductivity *per particle* is reduced by about an order of magnitude compared to the single-polaron optical conductivity. The reduction in intensity of the polaron optical conductivity band can be interpreted as a decrease of the overall electron-phonon coupling strength due to many-body effects. Correspondingly, at high doping levels, the polaron mass m^* , determined by the sum rule introduced in Ref. [51]

$$\frac{\pi e^2 n_0}{2m^*} + \int_{\omega_L}^{\infty} \text{Re}(\Omega) d\Omega = \frac{\pi e^2 n_0}{2\bar{m}_b} \quad (\text{C23})$$

is reduced, compared to the single-polaron effective mass. As shown in Refs. [18, 52], the sum rule [51] remains valid for an interacting polaron gas.

The large-polaron theory of the optical absorption based on Ref. [18] explains without any fitting parameters the main characteristics and trends of the observed spectra of Ref. [15] in $\text{SrTi}_{1-x}\text{Nb}_x\text{O}_3$, including doping- and temperature dependence. Nevertheless, some features of the experimental spectra remain to be explained. In particular, at $T = 7 \text{ K}$, the pronounced peak at $\hbar\Omega \sim 130 \text{ meV}$ in the experimental optical conductivity is not accounted for by the present theoretical analysis. In the theoretical spectra, peaks of much smaller intensity appear at about the same frequency. In the large-polaron theory, those peaks are provided by the interaction between electrons and the LO-phonon branch with energy $\hbar\omega_{L,2} \approx 58.4 \text{ meV}$, accompanied by the emission of a plasmon as described in Ref. [18].

The intensity of the experimentally observed absorption peak at $\hbar\Omega \sim 130 \text{ meV}$ is considerably higher than described by the large-polaron theory. In the low density limit, the experimental optical data more rapidly approach the single polaron limit [31] than the theoretical predictions based on Eq. (C10). This absorption peak at $\hbar\Omega \sim 130 \text{ meV}$ may be provided by other mechanisms, not controlled in the present study. E. g., electron-phonon interaction with low-frequency non-polar (e. g., acoustic) phonons may contribute to the optical conductivity. The squared modulus $|V_q|^2$, which characterizes the coupling strength, for the deformation electron-phonon interaction is $|V_q|^2 \propto q$ [53], while for the Fröhlich interaction, $|V_q|^2 \propto q^{-2}$. Consequently, for the deformation electron-phonon interaction,

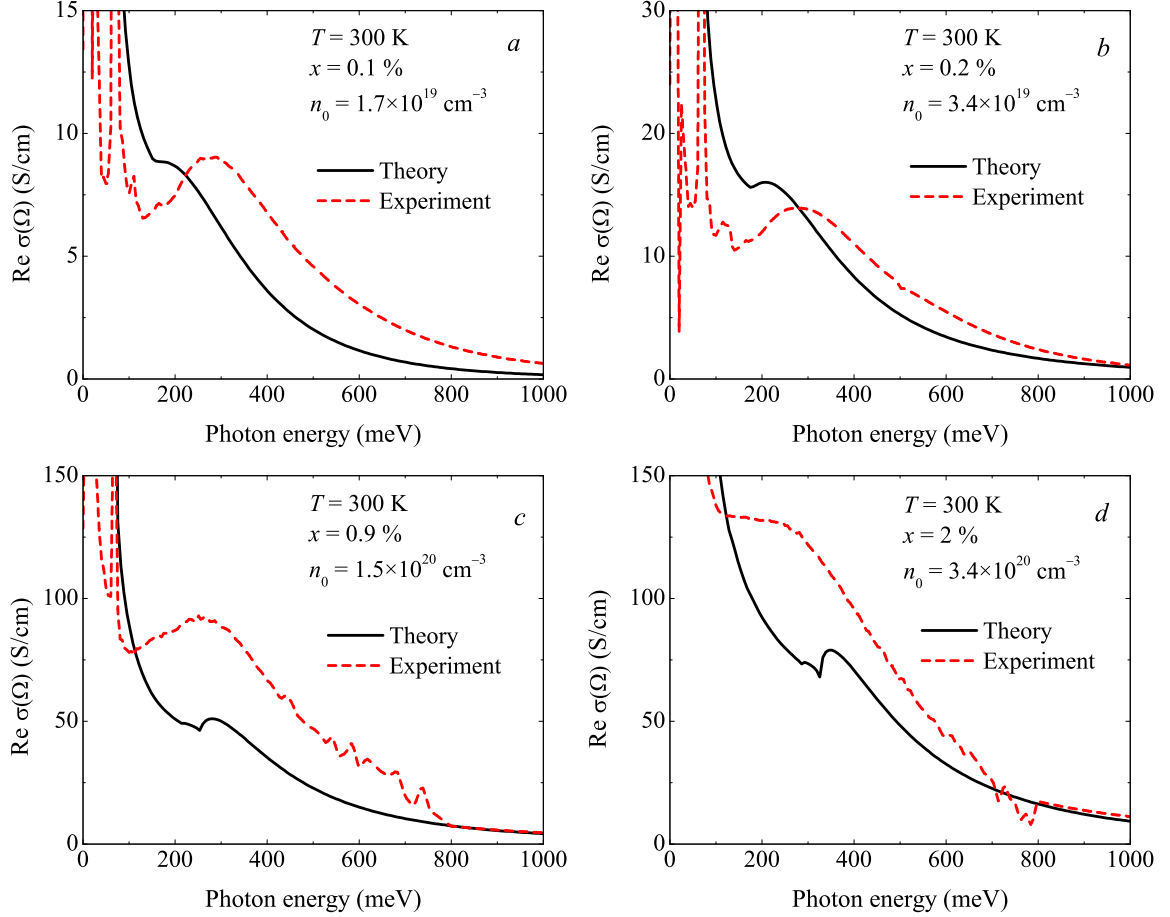


FIG. 24: The many-large-polaron optical conductivity compared with the experiment [15] at $T = 300$ K. The doping level is $x = 0.1\%$ (a), 0.2% (b), 0.9% (c) and 2% (d).

the short-wavelength phonons may provide non-negligible contributions to the optical conductivity. Also, at sufficiently large q , Umklapp scattering processes with acoustic phonons can play a role. The treatment of contributions due to acoustic phonons (and other mechanisms) is the subject of the future work. Another possible explanation of the absorption peak at $\hbar\Omega \sim 130$ meV is weakened screening in the corresponding energy range due to dynamical-exchange [54].

4. Conclusions

Many-polaron optical conductivity spectra, calculated (based on Ref. [18]) within the large-polaron picture without adjustment of material constants, explain essential characteristics of the experimental optical conductivity [15]. The intensities of the calculated many-

polaron optical conductivity spectra and the intensities of the experimental mid-infrared bands of the optical conductivity spectra of $\text{SrTi}_{1-x}\text{Nb}_x\text{O}_3$ (from Ref. [15]) are comparable for all considered values of the doping parameter. The doping dependence of the intensity of the mid-infrared band in the theoretical large-polaron spectra is similar to that of the experimental data of Ref. [15]. In the high-frequency range, the theoretical absorption curves describe well the experimental data (especially at low temperature). A remarkable difference between the present theoretical approach and experiment is manifested on the low frequency side of the mid-infrared range, where the experimental optical conductivity shows a sharp and pronounced peak for $\hbar\Omega \sim 130$ meV at 7 K. Although the theoretical curve also shows a feature around the same frequency, its intensity is clearly underestimated. This peak in the absorption spectrum at $\hbar\Omega \sim 130$ meV remains to be explained. The value of the effective electron-phonon coupling constant obtained in the present work ($\alpha_{eff} \approx 2$) corresponds to the intermediate coupling strength of the large-polaron theory.

The alternative small-polaron and mixed-polaron models for the optical conductivity require several fitting parameters. Furthermore, we find that the mixed-polaron model would need a major adjustment of the overall intensity in order to fit experimental spectra.

Contrary to the case of the large polaron, the small-polaron parameters cannot be extracted from experimental data. Moreover, the small-polaron model, for any realistic choice of parameters, shows a frequency dependence in the high-frequency range which is different from that of the experimental optical conductivity. Both the experimental and the theoretical large-polaron optical conductivity decrease as a power function at high frequencies, while the small-polaron optical conductivity falls down exponentially for sufficiently high Ω .

In summary, the many-body large-polaron model based on the Fröhlich interaction accounts for the essential characteristics (except – interestingly – for the intensity of a prominent peak at $\hbar\Omega \sim 130$ meV, that constitutes an interesting challenge for theory) of the experimental mid-infrared optical conductivity band in $\text{SrTi}_{1-x}\text{Nb}_x\text{O}_3$ without any adjustment of material parameters. The large-polaron model gives then a convincing interpretation of the experimentally observed mid-infrared band of $\text{SrTi}_{1-x}\text{Nb}_x\text{O}_3$.

[1] S. Lupi, P. Maselli, M. Capizzi, P. Calvani, P. Giura, and P. Roy, Phys. Rev. Lett. **83**, 4852 (1999).

- [2] L. Genzel, A. Wittlin, M. Bayer, M. Cardona, E. Schonherr, and A. Simon, Phys. Rev. B **40**, 2170 (1989).
- [3] P. Calvani, M. Capizzi, S. Lupi, P. Maselli, A. Paolone, and P. Roy, Phys. Rev. B **53**, 2756 (1996).
- [4] S. Lupi, M. Capizzi, P. Calvani, B. Ruzicka, P. Maselli, P. Dore, and A. Paolone, Phys. Rev. B **57**, 1248 (1998).
- [5] J.-G. Zhang, X.-X. Bi, E. McRae, P. C. Ecklund, B. C. Sales, M. Mostoller, Phys. Rev. B **43**, 5389 (1991).
- [6] C. C. Homes, B. P. Clayman, J. L. Peng, R. L. Greene, Phys. Rev. B **56**, 5525 (1997).
- [7] M. K. Crawford, G. Burns, G. V. Chandrashekar, F. H. Dacol, W. E. Farneth, E. M. McCarron, III, and R. J. Smalley, Phys. Rev. B **41**, 8933 (1990).
- [8] J. P. Falck, A. Levy, M. A. Kastner, and R. J. Birgeneau, Phys. Rev. B **48**, 4043 (1993).
- [9] H. M. Rønnow, Ch. Renner, G. Aepli, T. Kimura and Y. Tokura, Nature **440**, 1025 (2006).
- [10] Ch. Hartinger, F. Mayr, J. Deisenhofer, A. Loidl and T. Kopp, Phys. Rev. B **69** 100403R (2004); Ch. Hartinger, F. Mayr, and A. Loidl, Phys. Rev. B **73**, 024408 (2006).
- [11] P. Calvani, M. Capizzi, F. Donato, S. Lupi, P. Maselli, and D. Peschiaroli, Phys. Rev. B **47**, 8917 (1993).
- [12] J. F. Schooley, W. R. Hosler, and M. L. Cohen, Phys. Rev. Lett. **12**, 474 (1964).
- [13] D. M. Eagles, M. Georgiev and P. C. Petrova, Phys. Rev. B **54**, 22 (1996).
- [14] C. Z. Bi, J. Y. Ma, J. Yan, X. Fang, B. R. Zhao, D. Z. Yao and X. G. Qiu, J. Phys.: Condens. Matter **18**, 2553 (2006).
- [15] J. L. M. van Mechelen, D. van der Marel, C. Grimaldi, A. B. Kuzmenko, N. P. Armitage, N. Reyren, H. Hagemann, and I. I. Mazin, Phys. Rev. Lett. **100**, 226403 (2008).
- [16] F. Gervais, J. L. Servoin, A. Baratoff, J. G. Bednorz and G. Binnig, Phys. Rev. B **47**, 8187 (1993).
- [17] C. Ang, Z. Yu, Z. Jing, P. Lunkenheimer and A. Loidl, Phys. Rev. B **61**, 3922 (2000).
- [18] J. Tempere and J. T. Devreese, Phys. Rev. B **64**, 104504 (2001).
- [19] J. T. Devreese and A. S. Alexandrov, Rep. Prog. Phys. **72**, 066501 (2009).
- [20] A. S. Alexandrov and J. T. Devreese, *Advances In Polaron Physics* (Springer, 2009).
- [21] D. M. Eagles, Phys. Rev. **181**, 1278 (1969).
- [22] D. M. Eagles, J. Phys. C **17**, 637 (1984).

- [23] D. M. Eagles and P. Lalouis, *J. Phys. C* **17**, 655 (1984).
- [24] D. M. Eagles, in *Physics of Disordered Materials*, edited by D. Adler (Plenum, New York, 1985), p. 357.
- [25] H. Fröhlich, *Adv. Phys.* **3**, 325 (1954).
- [26] H. G. Reik, *Z. Phys.* **203**, 346 (1967); in *Polarons in Ionic Crystals and Polar Semiconductors* (North-Holland, Amsterdam, 1972).
- [27] H. P. R. Frederikse, W. R. Thurber and W. R. Hosler, *Phys. Rev.* **134**, A442 (1964).
- [28] E. Ambler, J. H. Colwell, W. R. Hosler and J. F. Schooley, *Phys. Rev.* **148**, 280 (1966).
- [29] G. Iadonisi, V. Cataudella, G. De Filippis, and D. Ninno, *Europhys. Lett.*, **41**, 309 (1998).
- [30] D. M. Eagles, R. P. S. M. Lobo, and F. Gervais, *Phys. Rev. B* **52**, 6440 (1995).
- [31] J. Devreese, J. De Sitter, and M. Goovaerts, *Phys. Rev. B* **5**, 2367 (1972).
- [32] V. L. Gurevich, I. G. Lang, and Yu. A. Firsov, *Sov. Phys. Solid State* **4**, 918 (1962).
- [33] J. Devreese, W. Huybrechts, and L. Lemmens, *Phys. Status Solidi B* **48**, 77 (1971).
- [34] E. Kartheuser, R. Evrard, and J. Devreese *Phys. Rev. Lett.* **22**, 94-97 (1969).
- [35] D. Emin, *Phys. Rev. B* **48**, 13691 (1993).
- [36] S. N. Klimin, V. M. Fomin, and J. T. Devreese, *to be published*.
- [37] S. N. Klimin, V. M. Fomin, F. Brosens, and J. T. Devreese, *Phys. Rev. B* **69**, 235324 (2004).
- [38] G. Verbist, F. M. Peeters, J. T. Devreese, *Ferroelectrics* **130**, 27 (1992).
- [39] N. Choudhury, E. J. Walter, A. I. Kolesnikov, and C.-K. Loong, *Phys. Rev. B* **77**, 134111 (2008).
- [40] Y. Toyozawa, in: *Polarons in Ionic Crystals and Polar Semiconductors*, North-Holland, Amsterdam (1972), pp. 1 – 27.
- [41] R. Zheng, T. Taguchi, and M. Matsuura, *Phys. Rev. B* **66**, 075327 (2002).
- [42] M. Born and K. Huang, *Dynamical Theory of Crystal Lattices* (Clarendon, Oxford, 1954).
- [43] R. P. Feynman, R. W. Hellwarth, C. K. Iddings, and P. M. Platzman, *Phys. Rev.* **127**, 1004 (1962).
- [44] F. M. Peeters and J. T. Devreese, *Phys. Rev. B* **28**, 6051 (1983).
- [45] X. Wu, F. M. Peeters, and J. T. Devreese, *Phys. Rev. B* **34**, 2621 (1986).
- [46] R. P. Feynman, *Phys. Rev.* **97**, 660 (1955).
- [47] L. F. Lemmens, J. T. Devreese, and F. Brosens, *Phys. Stat. Sol. (b)* **82**, 439 (1977).
- [48] G. D. Mahan, *Many-Particle Physics*, second edition (Plenum Press, 1990).

- [49] N.E. Phillips, B.B. Triplett, R.D. Clear, H.E. Simon, J.K. Hulm, C.K. Jones and R. Mazelsky, *Physica* **55**, 571 (1971).
- [50] J.L.M. van Mechelen (*to be published*)
- [51] J. T. Devreese, L. F. Lemmens, and J. Van Royen, *Phys. Rev. B* **15**, 1212 (1977).
- [52] J. Tempere and J. T. Devreese, *Eur. Phys. J. B* **20**, 27 (2001).
- [53] F. M. Peeters and J. T. Devreese, *Phys. Rev. B* **32**, 3515 (1985).
- [54] J. T. Devreese, F. Brosens, and L. F. Lemmens, *Phys. Rev. B* **21**, 1349 (1980); *Phys. Rev. B* **21**, 1363 (1980).

Appendix D: Notes on the polaron mobility

J. T. Devreese and S. N. Klimin

Here, we are focused on some important issues related to the polaron mobility. First, we discuss the polaron mobility in the weak-coupling regime on the basis of Ref. [143]. Several theoretical methods have been applied to study the transport properties of the Fröhlich polaron. The polaron mobility was calculated using various approaches: the calculation of the scattering amplitude [64], the kinetic equation [65], the Green's function technique, the Kubo formula [63, 66], the path-integral formalism [47, 48, 150].

A challenging difficulty is that, even for weak coupling and in the ohmic regime, there is a remarkable difference in the mobility as obtained via a relaxation-time approximation [62–65, 144], and as obtained via the path-integral formalism, worked out by Thornber and Feynman [48], and which is based on the Feynman polaron model [43].

At weak coupling and small electric field, the relaxation time result for the mobility [66] seems more reliable than the Thornber-Feynman result. This might be partly due to the deviation of the electron velocity distribution from a drifted Maxwellian as shown analytically [145] from the Boltzmann equation at weak electron-phonon coupling and low temperature in the steady state regime.

Because the Boltzmann equation is valid at weak electron-phonon coupling, and because of its intuitively transparent structure, this equation is an important tool to study transport properties of polarons for weak coupling. In Ref. [143], its solution is discussed in the ohmic regime and for the steady state. The mobility in the zero temperature limit from Ref. [143] is given by:

$$\mu|_{T \rightarrow 0} \rightarrow \frac{e}{2\alpha} \bar{N}^{-1}, \quad (\text{D1})$$

where \bar{N} is the average number of phonons. This is equivalent to the result from the relaxation-time approximation [65], which therefore holds in the zero-temperature limit.

An analytical solution of the Boltzmann equation at $T = 0$ was obtained in Ref. [146]. In Fig. 25, the mobility of a polaron in the weak-coupling regime, calculated using the exact solution of the Boltzmann equation [146] is calculated for InSb at $T = 77$ K and compared to the mobility from Ref. [48]. For weak electric fields the result of Ref. [146] is quite close to that of the polaron theory with a relaxation time but differs by the factor

$\frac{3}{2} \frac{k_B T}{\hbar \omega_0} \frac{1}{2.5}$ from [48]. These results seem to confirm the validity of a relaxation time approach for the electric field $E \rightarrow 0$ (at least for InSb at 77 K). Nevertheless, as pointed out in [147], a system of non-interacting polarons is not ergodic and this point should be examined carefully before definite conclusions can be drawn when $E \rightarrow 0$. In Ref. [148], arbitrary temperature and electric field are considered, and an exact recursion relation is obtained for the time-dependent expansion coefficients of the electron distribution function in terms of Legendre polynomials.

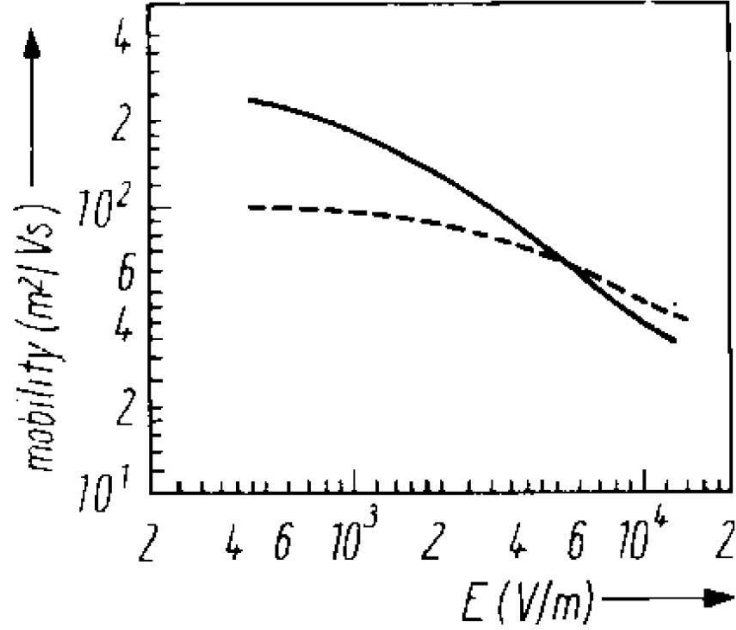


FIG. 25: Mobility of weak-coupling polarons, obtained from the exact solution of the Boltzmann equation [146] (solid line) and from [48] (dashed line). (After Ref. [147].)

The DC mobility of a polaron in the strong-coupling regime was investigated by Volovik *et al.* [149]. They showed that the interaction Hamiltonian corresponding to scattering of a phonon by a polaron can be separated in the strong-coupling limit with the aid of the transformations of Bogoliubov and Tyablikov in conjunction with the LLP canonical transformation. In the leading order in powers of the inverse coupling constant α^{-1} , the principal role in the scattering is played by two-phonon processes. In the system of units with $\hbar = 1$, the following result for the strong-coupling polaron mobility has been obtained:

$$\mu = \frac{\gamma}{m\omega_{\text{LO}}\alpha^2} \frac{T}{\omega_0} e^{\omega_0/T}, \quad (\text{D2})$$

with a numerical temperature-independent coefficient $\gamma \sim 1$.

The “ $\frac{3}{2}k_B T$ ” problem reveals a key distinction between the polaron mobility obtained in Refs. [47, 48, 150] and the other approaches. Also the other problem is worth discussing. The results of the approaches [63, 65, 66] are in agreement with each other. Therefore during a long time they were recognized well-established. Several works appeared in which the polaron mobility at low temperatures differs from the Kadanoff result by the numerical factor 3, e. g., Refs. [151, 152]. However, they have not yet attract a proper attention.

In the work by V. F. Los [151], the polaron mobility was calculated on the basis of Kubo’s formula using a Green’s superoperator technique. As stated in Ref. [151], the relaxation-time approximation [65] does not take into account the change in the electron velocity in all the electron-phonon scattering processes allowed by the energy and momentum conservation laws. The polaron mobility obtained in Ref. [151] gives the correct temperature dependence of the polaron mobility but exceeds the expression obtained by Kadanoff exactly by a factor 3.

Recently, this “factor 3” has been again confirmed using a rigorous derivation. An approach to the polaron mobility has been proposed by F. Brosens and D. Sels [153], based on the dynamics of the Wigner distribution function, using the kinetic equations derived in Refs. [154, 155].

In the paper [153], the mobility of the Fröhlich polaron is calculated within approach, based on the dynamics of the Wigner distribution function. The approach proposed by the authors is based on a path integral description of the Wigner distribution function. The time evolution of the electron distribution function $f(\mathbf{p}, t)$ in the electron-phonon system under an external time-dependent uniform electric field $\mathbf{E}(t)$ is governed by the generalized kinetic equation

$$\begin{aligned}
& \left(\frac{\partial}{\partial t} + e\mathbf{E}(t) \cdot \frac{d}{d\mathbf{p}} \right) f(\mathbf{p}, t) \\
&= \sum_{\mathbf{k}} \frac{2|\gamma(k)|^2}{\hbar^2} \iiint dt' d\mathbf{x}' d\mathbf{p}' \Theta(t' \leq t) f(\mathbf{p}', t') \\
& \times \left(\begin{array}{c} \left(\begin{array}{c} (n_B(\omega_k) + 1) \cos(\mathbf{k} \cdot (\mathbf{x} - \mathbf{x}') + \omega_k(t - t')) \\ + n_B(\omega_k) \cos(\mathbf{k} \cdot (\mathbf{x} - \mathbf{x}') - \omega_k(t - t')) \end{array} \right) \\ \times (K_0(\mathbf{x}, \mathbf{p} - \frac{\hbar\mathbf{k}}{2}, t | \mathbf{x}', \mathbf{p}' + \frac{\hbar\mathbf{k}}{2}, t') - K_0(\mathbf{x}, \mathbf{p} + \frac{\hbar\mathbf{k}}{2}, t | \mathbf{x}', \mathbf{p}' + \frac{\hbar\mathbf{k}}{2}, t')) \end{array} \right) \quad (D3)
\end{aligned}$$

with the propagator

$$K_0(\mathbf{x}, \mathbf{p}, t | \mathbf{x}', \mathbf{p}', t') = \delta \left(\mathbf{p} - \mathbf{p}' - \int_{t'}^t e \mathbf{E}(\sigma) d\sigma \right) \\ \times \delta \left(\mathbf{x} - \mathbf{x}' - \frac{\mathbf{p}'}{m} (t - t') - \int_{t'}^t \frac{e \mathbf{E}(\sigma)}{m} (t - \sigma) d\sigma \right). \quad (\text{D4})$$

Here, ω_k is the phonon frequency, $\gamma(k)$ is the amplitude of the electron-phonon interaction, and $n_B(\omega_k)$ is the free-phonon distribution function,

$$n_B(\omega_k) = \frac{1}{e^{\beta \hbar \omega_k} - 1}. \quad (\text{D5})$$

The key result of Ref. [153] is the mobility of a weak-coupling polaron given by formula (IV.4):

$$\sigma_{DC} = \frac{3e^2}{2\alpha m \omega_{LO}} e^{\beta \hbar \omega_{LO}}. \quad (\text{D6})$$

This expression differs by the factor 3 from the result by Kadanoff and Osaka [63, 65, 66]. Also the critical re-derivation of the polaron optical conductivity on the basis of the Feynman polaron model results in the optical conductivity

$$\sigma_{DC} = \frac{3e^2}{2\alpha m^* \omega_{LO}} e^{\beta \hbar \omega_{LO}} \quad (\text{D7})$$

that differs by the factor $\frac{2\hbar\omega_{LO}}{k_B T}$ from the FHIP polaron mobility.

V. F. Los derived the polaron mobility [151] on the basis of the Kubo formula and the Bogoliubov technique of an exact elimination of the phonon operators. The mobility was obtained in Ref. [151] both in the weak-coupling approximation and using the Feynman polaron model. The weak-coupling expression given in Ref. [151] by formula (18) is the same as (D3), i. e. three times larger than the Kadanoff polaron mobility.

The polaron mobility obtained in Ref. [151] using the Feynman polaron model, formula (36),

$$\mu^F = \frac{3e}{2\alpha} e^{\beta} \frac{e^{m_f/v}}{(m_f + 1)^{3/2}} \quad (\text{D8})$$

differs from (D7). However, the factor 3 with respect to the Kadanoff result is definitely present in (D8).

The key distinction between the derivation of the polaron mobility in Refs. [151, 153], on the one hand, and in Refs. [63, 65, 66] is the relaxation-time approximation (RTA) (see Ref. [60]). The RTA consists in disregarding the contribution of the so called ‘‘re-population term’’ (using terminology of Ref. [60]) in the kinetic equation. RTA is used

in Refs. [63, 65, 66]. On the contrary, in Refs. [151, 153] there is no relaxation-time approximation. In Ref. [151], the parameter attributed to the relaxation time appears in a natural way quite rigorously. Moreover, in Ref. [153], the relaxation time does not appear at all.

The difference of the results by Los from the theory by Kadanoff and Osaka appears already at an intermediate stage. Los derived the evolution equation for the correlation function velocity-velocity $\langle v_\nu(0) v_\mu(\tau) \rangle$ [formula (9)], with the kernel function

$$\Gamma_\nu(\mathbf{p}) = 2\pi \sum_{\mathbf{k}} |V_{\mathbf{k}}|^2 \left(1 - \frac{v_\nu(\mathbf{p} - \mathbf{k})}{v_\nu(\mathbf{p})} \right) \times \{ (1 + N_{\mathbf{k}}) \delta(T(\mathbf{p}) - T(\mathbf{p} - \mathbf{k}) - \omega_{\mathbf{k}}) + N_{\mathbf{k}} \delta(T(\mathbf{p}) - T(\mathbf{p} - \mathbf{k}) + \omega_{\mathbf{k}}) \} \quad (\text{D9})$$

(the notations are in Ref. [151]).

The factor $[1 - v_\nu(\mathbf{p} - \mathbf{k})/v_\nu(\mathbf{p})]$ in the kernel function is an essential difference between the theory by Los and the theory by Osaka/Kadanoff. Without this factor, as checked in Ref. [151], the theory by Los would give the same result as the Kadanoff theory. This factor describes the change in the electron velocity in the electron-phonon scattering processes allowed by the energy and momentum conservation laws. It is important to note that in relaxation times of the kinetic equations corresponding to elastic scattering mechanisms (e. g., impurity scattering) or approximately elastic mechanisms (e. g., acoustic phonons), the factor $(1 - v'_\nu/v_\nu)$ is always present. In those kinetic equations, the second (subtracted) part, v'_ν/v_ν , comes from the aforesaid “re-population” term. This “re-population” term was neglected in Refs. [63, 65, 66]. It appears that the “re-population” term is in fact non-negligible. The analogous reasoning is developed in Ref. [153], where the “re-population” contribution to the kinetic equation is taken into account. It is shown in Ref. [153] that the neglect of the re-population term in the kinetic equation is an unwarranted approximation, because it *violates the particle number conservation*. The conclusions of Refs. [151, 153] are contrary to the assumption made in Refs. [63, 65, 66], where that term is neglected.

In Ref. [151], the expression (D9) for $\Gamma_\nu(\mathbf{p})$ arises here from the rigorous microscopic treatment. It is important to note that such a relaxation time was introduced phenomenologically in 1939 in [156], but in subsequent studies the expression without the factor describing the change in the velocity was obtained.

In Ref. [156], the relaxation time has been phenomenologically defined by:

$$\frac{1}{\tau} = - \sum_{\mathbf{q}} \left(\frac{\Delta k}{k} \right)_x \phi_{\mathbf{q}}(\mathbf{k}) \quad (\text{D10})$$

where $\phi_{\mathbf{q}}(\mathbf{k})$ is the probability per unit time that an electron with the wave number \mathbf{k} makes a collision with a lattice wave of wave number \mathbf{q} , and Δk is the average change of the x -component of the wave number k_x on each collision.

The factor

$$- \left(\frac{\Delta k}{k} \right)_x = \frac{k_x - k'_x}{k_x} = 1 - \frac{k'_x}{k_x}$$

entering (D10) has exactly the same meaning as the factor $\left(1 - \frac{v_{\nu}(\mathbf{p}-\mathbf{k})}{v_{\nu}(\mathbf{p})} \right)$ which appears in the work by Los [151] and ensures the particle number conservation. Without this factor, the formula

$$\frac{1}{\tau} = \sum_{\mathbf{q}} W_{\mathbf{q}}(\mathbf{k}) \quad (\text{D11})$$

gives the result of Refs. [63, 65, 66]. With this factor, the derivation reproduced in Ref. [158] gives the same relaxation time and mobility as in Ref. [151].

In the paper by B. I. Davydov and I. M. Shmushkevich [157], the derivation of the mean free path and the electron mobility in ionic crystal is performed using the parameters of the medium which are not immediately measurable. Later, Born and Huang in their *Dynamical Theory of Crystal Lattices* [129] introduced the description of optical phonons and the electron-LO phonon interaction using only observable parameters, such as high-frequency and static dielectric constants. At present, these notations are of common use. In the monograph by A. Anselm [158], the theory by Davydov and Shmushkevich has been reproduced using these contemporary notations. The physics of the approach by Davydov and Shmushkevich is described in Ref. [158] in the following way.

“At low temperatures the scattering is inelastic, and, therefore, general the relaxation time cannot be introduced with the aid of Boltzmann equation ... However, as was demonstrated by B. I. Davydov and I. M. Shmushkevich in 1940, in the low-temperature case as well the relaxation time can be introduced, provided a correct calculation procedure is followed.

Qualitatively this can be explained as follows. At low temperatures, when $k_B T \ll \hbar \omega_0$ the absolute majority of the electrons are able only to absorb the phonons. Such absorption of a phonon results in the electron going over to the energy interval from $\hbar \omega_0$ to $2\hbar \omega_0$. Such

an electron will immediately emit a phonon, because the ratio of the emission probability to the absorption probability is equal, according to (6.1), to $\frac{N_q+1}{N_q} \approx \exp\left(\frac{\hbar\omega_0}{k_B T}\right) \gg 1$. The variation of the electron energy in the result of such an absorption and an almost immediate emission of a phonon will be very small (only at the expense of the ω_0 vs q dependence), but the variation of wave vector will be substantial. This makes it possible to regard the electron scattering in a definite sense as elastic and to introduce the relaxation time.”

Remarkably, the phenomenological definition (D10) coincides with the Davydov-Shmushkevich formula for the inverse relaxation time. The resulting low-temperature relaxation time within the approach by Davydov and Shmushkevich is given by:

$$\tau = \frac{3\sqrt{2}}{2} \frac{\hbar^2 \varepsilon^*}{e^2 m_b^{1/2} (\hbar\omega_0)^{1/2}} \exp\left(\frac{\hbar\omega_0}{k_B T}\right). \quad (\text{D12})$$

with ε^* defined through the high-frequency and static dielectric constants:

$$\frac{1}{\varepsilon^*} = \frac{1}{\varepsilon_\infty} - \frac{1}{\varepsilon_0}. \quad (\text{D13})$$

The mobility is expressed through the relaxation time in the standard way:

$$\mu = \frac{e}{m_b} \tau. \quad (\text{D14})$$

Hence the mobility is:

$$\mu = \frac{3\sqrt{2}}{2} \frac{\hbar^2 \varepsilon^*}{e m_b^{3/2} (\hbar\omega_0)^{1/2}} \exp\left(\frac{\hbar\omega_0}{k_B T}\right). \quad (\text{D15})$$

Using the Fröhlich coupling constant α ,

$$\alpha = \frac{1}{2\varepsilon^*} \frac{e^2}{\hbar\omega_0} \left(\frac{2m_b\omega_0}{\hbar}\right)^{1/2}, \quad (\text{D16})$$

the mobility is transformed to the expression

$$\mu = \frac{3e}{2m_b\alpha\omega_0} \exp\left(\frac{\hbar\omega_0}{k_B T}\right). \quad (\text{D17})$$

This result is three times larger than the mobility obtained by many authors, e. g., Kadanoff.

In the recent paper [159], the alternative representation has been found for the optical conductivity described by the Kubo formula. The treatment is based on the expression for the optical conductivity:

$$\sigma(z) = \frac{i}{zV} [\Pi(z) - e^2\Gamma] \quad (z = \Omega + i\delta, \delta \rightarrow +0) \quad (\text{D18})$$

where V is the system volume, e is the electronic charge, $\Pi(z)$ is the current-current correlation function,

$$\Pi(z) = -i \int_0^\infty dt e^{izt} \langle [J(t), J(0)] \rangle \quad (\text{D19})$$

and the coefficient Γ is determined through the correlation function in the Euclidean time:

$$e^2\Gamma = - \int_0^\beta d\tau \langle J(\tau) J(0) \rangle, \quad \beta = \frac{1}{k_B T}. \quad (\text{D20})$$

Here, the current operator is

$$J = -ev_x = -\frac{e}{m_b} p_x. \quad (\text{D21})$$

In the known expressions for the Kubo formula, Γ is given by explicit constants:

$$e^2\Gamma = -\frac{e^2}{m_b} \quad (\text{D22})$$

for a single electron with the band mass m_b (see, e. g., Ref. [50]).

In the memory-function representation, the polaron optical conductivity is given by formula (7) of Ref. [159]:

$$\sigma(z) = -\frac{i}{V} \frac{e^2\Gamma}{z + iM(z)}. \quad (\text{D23})$$

with the memory function $M(z)$. The equivalence relation (D22) is important for the sum rule [82] due to the following reasons. On the one hand, it is easily checked by hand that the expression (5.77) explicitly satisfies the sum rule given by formula (6) of Ref. [159]:

$$\int_{-\infty}^{\infty} \text{Re} \sigma(\Omega + i\delta) d\Omega = -\frac{\pi e^2\Gamma}{V}. \quad (\text{D24})$$

On the other hand, the polaron optical conductivity must satisfy the f -sum rule [82]:

$$\int_{-\infty}^{\infty} \text{Re} \sigma(\Omega + i\delta) d\Omega = \frac{1}{V} \frac{\pi e^2}{m_b}. \quad (\text{D25})$$

Thus the relation (D22) ensures the fulfilment of the f -sum rule for the polaron optical conductivity. When using exact polaron states, the integral in (D20) gives analytically e^2/m_b . However, any approximation for the polaron states may violate (D22) and consequently violate the f -sum rule.

The DC mobility of a Fröhlich polaron is obtained in Ref. [159] in the weak-coupling regime at low temperatures as $\mu = \frac{10}{3}\mu_{FHIP}$, i.e., the mobility differs by a numerical factor 10/3 from the result of FHIP [47] and by $5k_B T / (\hbar\omega_0)$ from the value obtained by Kadanoff.

Accounting for the above discussion, the fulfilment of the f -sum rule within the theory [159] and, consequently, the DC mobility need further verification.

In summary, the most reliable results for the mobility of a Fröhlich polaron are obtained in Refs. [151, 153]. It is proven in those works that the “re-population” term in the kinetic equation cannot be neglected, that leads to a significant change of the polaron mobility. Consequently, the results obtained in Refs. [151, 153] bring an important correction to the theory of the polaron response.

Appendix E: All-coupling polaron optical response: analytic approaches beyond the adiabatic approximation [*S. N. Klimin, J. Tempere, and J. T. Devreese, Phys. Rev. B 94, 125206 (2016)*]

1. Introduction

The polaron, first proposed as a physical concept by L. D. Landau [1]⁹ in the context of electrons in polar crystals, has become a generic notion describing a particle interacting with a quantized bosonic field. The polaron problem has consequently been used for a long time as a testing ground for various analytic and numerical methods with applications in quantum statistical physics and quantum field theory. In condensed matter physics, the polaron effect coming from the electron-phonon interaction is a necessary ingredient in the description of the DC mobility and the optical response in polar crystals (see Ref. [2]). Polaronic effects are manifest in many interesting systems, such as magnetic polarons [3], polarons in semiconducting polymers [4], and complex oxides [5, 6] which are described in terms of the small-polaron theory [7]. *Large-polaron* theory has recently been stimulated by the possibility to study polaronic effects using highly tunable quantum gases: the physics of an impurity immersed in an atomic Bose-Einstein condensate [8] can be modeled on the basis of a Fröhlich Hamiltonian. Another recent development in large-polaron physics stems from the experimental advances in the determination of the band structure of highly polar oxides [9], relevant for superconductivity, where the optical response of complex oxides explicitly shows the large-polaron features [10, 11].

Diagrammatic Quantum Monte Carlo (DQMC) methods have been applied in recent years to numerically calculate the ground state energy and the optical conductivity of the Fröhlich polaron [12, 13]. Advances in computational techniques such as DQMC inspired renewed study of the key problem in polaron theory – an *analytic* description of the polaron response. For the *small-polaron* optical conductivity, the all-coupling analytic theory has been successfully developed [14] showing good agreement with the numeric results of the DQMC. However, the optical response problem for a *large polaron* is not yet completely solved analytically. It should be noted that we call here “analytic” methods which in fact

⁹The bibliography to this Appendix is in a separate list.

can require massive computations (e. g., the Feynman variational method and the methods used in the present work) in order to distinguish between them and the purely numerical methods, such as DQMC.

Asymptotically exact analytic solutions for the polaron optical conductivity have been obtained in the limits of weak [15–17] and strong coupling [18, 19]. A first proposal for an all-coupling approximation for the polaron optical conductivity has been formulated in Ref. [20] (below referred to as DSG), further developing the Feynman-Hellwarth-Iddings-Platzman theory [21] (FHIP) and using the Feynman variational approach [22]. However, in Ref. [20], it was already demonstrated that FHIP is inconsistent at large α with the Heisenberg uncertainty relations. This inconsistency is revealed in Ref. [20] through extremely narrow peaks of the optical conductivity at large α . Nevertheless, the peak positions for the polaron optical conductivity as obtained in Ref. [20] have been confirmed with high accuracy [19] by the DQMC calculation [13]. This inspired further attempts to develop analytical methods for the polaron optical response, especially at intermediate and strong coupling. Among these analytic methods, an extension of the DSG method has been proposed in Ref. [18] introducing an extended memory function formalism with a relaxation time determined from the additional sum rule for the polaron optical conductivity. Alternatively, for the strong coupling regime, the strong coupling expansion (SCE) based on the Franck-Condon scheme for multiphonon optical conductivity has been developed in Refs. [18, 19].

In the limit of small α , the optical conductivity derived within the memory-function formalism (both DSG and extended methods [18, 20]) analytically tends to the asymptotically exact perturbation results of Refs. [15–17]. As seen from the comparison of the memory-function polaron optical conductivity with numerically accurate DQMC data [13, 18], they agree well to each other for $\alpha \lesssim 4$ (for DSG) and for $\alpha \lesssim 6$ (the extended memory-function formalism). As written above, the conclusion that the memory-function formalism based on the Feynman polaron model failed at large α due to inconsistency with the Heisenberg uncertainty relations was already formulated in Ref. [20].

The alternative method, strong-coupling expansion of Refs. [18, 19], is based on the adiabatic approximation for electron-phonon states which is asymptotically exact in the strong-coupling limit. In summary, the memory-function formalism is well-substantiated for small and intermediate values of α , and the strong coupling expansion adequately describes the opposite limit of large α . Consequently, the extended memory-function formalism

and the strong coupling expansion are complementary to each other. The quantitative comparison of these two methods with each other and with DQMC performed in Ref. [18] shows that they only qualitatively agree with each other and with the DQMC data in the range of intermediate coupling strengths ($6 \lesssim \alpha \lesssim 10$). On the one hand, the memory function formalism explicitly disagrees with DQMC at large α . On the other hand, the strong-coupling expansion only qualitatively reproduces the shape of the optical conductivity and fails at intermediate α [18, 19].

The main aim of the work [Phys. Rev. B **94**, 125206 (2016)] is *to extend both the memory function formalism and the strong coupling expansion in order to bridge the gap that remains between their regions of validity*, such that the combination of both methods allows to find analytical results in agreement with the numeric DQMC results at all coupling. In the present work, as in Ref. [19], the $T = 0$ case is considered. We have added the following new elements in the theory which lead to an overlapping of the areas of applicability for two aforesaid analytic methods. For weak and intermediate coupling strengths, an extension of the Feynman variational principle and the memory-function method for a polaron with a non-quadratic trial action has been developed. As distinct from the memory function formalism of Ref. [18], we do not use additional sum rules and relaxation times, and perform the calculation *ab initio*. For intermediate and strong coupling strengths, the strong coupling expansion of Ref. [19] is extended beyond the adiabatic approximation in the following way.

In the strong-coupling approximation for polaron optical conductivity [18, 19], the matrix elements for the electron-phonon interaction between electron states with different energies are neglected. This is consistent with the adiabatic approximation, as described below in detail. The similar approach is well recognized in the theory of multiphonon transitions in deep centers [23, 24]. In the present work, also transitions between different excited polaron states due to the electron-phonon interaction are taken into account. Because these transitions are beyond the adiabatic approximation, they are referred to as “non-adiabatic transitions”. The incorporation of non-adiabatic transitions in the treatment leads to a substantial expansion of the range of validity for the strong-coupling expansion towards smaller α and to an overall improvement of its agreement with DQMC.

2. Analytic methods for the polaron optical conductivity

a. Memory function formalism with a non-parabolic trial action

To generalize the memory function formalism, we start by extending Feynman's variational approach to translation invariant non-Gaussian trial actions. The electron-phonon system is described by the Fröhlich Hamiltonian, using the Feynman units with $\hbar = 1$, the LO-phonon frequency $\omega_{\text{LO}} = 1$, and the band mass $m_b = 1$,

$$\hat{H} = \frac{\hat{\mathbf{p}}^2}{2} + \sum_{\mathbf{q}} \left(\hat{a}_{\mathbf{q}}^{\dagger} \hat{a}_{\mathbf{q}} + \frac{1}{2} \right) + \frac{1}{\sqrt{V}} \sum_{\mathbf{q}} \frac{\sqrt{2\sqrt{2}\pi\alpha}}{q} (\hat{a}_{\mathbf{q}} + \hat{a}_{-\mathbf{q}}^{\dagger}) e^{i\mathbf{q}\cdot\hat{\mathbf{r}}}, \quad (\text{E1})$$

where $\hat{\mathbf{r}}$ is the position operator of the electron, $\hat{\mathbf{p}}$ is its momentum operator; $\hat{a}_{\mathbf{q}}^{\dagger}$ and $\hat{a}_{\mathbf{q}}$ are, respectively, the creation and annihilation operators for longitudinal optical (LO) phonons of wave vector \mathbf{q} . The electron-phonon coupling strength is described by the Fröhlich coupling constant α . As this Hamiltonian is quadratic in the phonon degrees of freedom, they can be integrated out analytically in the path-integral approach. The remaining electron degree of freedom is described via an action functional where the effects of electron-phonon interaction are contained in an influence phase $\Phi[r_e(\tau)]$ [22]:

$$S[\mathbf{r}_e(\tau)] = \frac{1}{2} \int_0^{\beta} \dot{\mathbf{r}}_e^2(\tau) d\tau - \Phi[\mathbf{r}_e(\tau)]. \quad (\text{E2})$$

Here $\mathbf{r}_e(\tau)$ is the path of the electron, expressed in imaginary time so as to obtain the euclidean action, and $\beta = 1/(k_B T)$ with T the temperature. The influence phase corresponding to (E1) depends on the difference in electron position at different times, resulting in a retarded action functional. In the path-integral formalism, thermodynamic potentials (such as the free energy) are calculated via the partition sum, which in turn is written as a sum over all possible paths $\mathbf{r}_e(\tau)$ of the electron that start and end in the same point, weighted by the exponent of the action.

Feynman's original variational method considers a quadratic trial action $S_{\text{quad}}[\mathbf{r}_e(\tau), \mathbf{r}_f(\tau)]$ where the phonon degrees of freedom are replaced by a fictitious particle with coordinate $\mathbf{r}_f(\tau)$, interacting with the electron through a harmonic potential.

Feynman restricted his trial action to a quadratic action, since only for case one can calculate the influence phase analytically.

Using the Feynman variational approach with the Gaussian trial action, excellent results are obtained for the polaron ground-state energy, free energy, and the effective mass. Moreover, this approach has been effectively used to derive the DSG all-coupling theory for the polaron optical conductivity, Ref. [20]. However, as mentioned in the introduction, the DSG and DQMC results contradict to each other in the range of large α . The most probable source of this contradiction is the Gaussian form of the trial action used in the DSG theory. Indeed, the model system contains only a single frequency, leading to unphysically sharp peaks in the spectrum, subject to thermal broadening only [25, 26]. Extensions to the formalism [18] have tried to overcome this problem by including an ad-hoc broadening of the energy level, chosen in such a way as to comply with the sum rules. A remarkable success in the problem of the polaron optical response has been achieved in the recent work [27], where the all-coupling polaron optical conductivity is calculated using the general quadratic trial action instead of the Feynman model with a single fictitious particle. The resulting optical conductivity is in good agreement with DQMC results [13] in the weak- and intermediate-coupling regimes and is qualitatively in line with DQMC even at extremely strong coupling, resolving the issue of the linewidth in the FHIP approach. However, there is a quantitative difference between the results of [27] and DQMC in the strong-coupling regime, which is overcome in the present work.

In the literature, there are attempts to re-formulate the Feynman variational approach avoiding retarded trial actions. For example, Cataudella et al. [28] introduce an extended action which contains the coordinates of the electron, the fictitious particle, and the phonons. This action, however, is not exactly equivalent to the action of the electron-phonon system, and hence the results obtained in [28] need verification. In Ref. [29], we introduced an extended action/Hamiltonian for an electron-phonon system and reformulated the Feynman variational method in the Hamiltonian representation. This method leads to the same result as the Feynman variational approach. However the method of Ref. [29] reproduces the strong coupling limit for the polaron energy only when using a Gaussian trial action.

In the current work, we propose to extend the Feynman variational approach to trial systems with non-parabolic interactions between an electron and a fictitious particle. The difficulty with using non-gaussian trial actions is that the path integrals with the influ-

ence phase can only be computed analytically for quadratic action functionals. However, quantum-statistical expectation values (such as the one in the Jensen-Feynman inequality) can be calculated for non-quadratic model systems by other means, in particular if the spectrum of eigenvalues and eigenfunctions can be found. So, what we propose is to focus on keeping the influence phase for a quadratic model system in the expressions, while at the same time allowing for non-Gaussian potentials for the expectation values.

The present variational method uses the following identical transformation as a starting point. Let us equivalently rewrite the partition function of the true electron-phonon system

$$\mathcal{Z} = \int \mathcal{D}\mathbf{r}_e e^{-S[\mathbf{r}_e(\tau)]} \quad (\text{E3})$$

as the extended path integral

$$\begin{aligned} \mathcal{Z} &= \frac{1}{\mathcal{Z}_f} \int \mathcal{D}\mathbf{r}_e \exp \{ \Phi[\mathbf{r}_e(\tau)] - \Phi_{\text{quad}}[\mathbf{r}_e(\tau)] \} \\ &\times \int \mathcal{D}\mathbf{r}_f \exp \left\{ - \int_0^\beta \left[\frac{m\dot{\mathbf{r}}_e^2}{2} + \frac{m_f\dot{\mathbf{r}}_f^2}{2} + U_{\text{quad}}(\mathbf{r}_f - \mathbf{r}_e) \right] d\tau \right\} \end{aligned} \quad (\text{E4})$$

with the partition function Z_f for a fictitious particle with the mass m_f in a harmonic potential $U_{\text{quad}}(\mathbf{r}_f) = m_f^2\omega^2 r_f^2/2$. Indeed, performing the path integration for the fictitious particle cancels $\Phi_{\text{quad}}[\mathbf{r}_e(\tau)]$ as well as the factor Z_f , and leaves the kinetic energy contribution, restoring the action function of the true electron-phonon system. Hence (E3) and (E4) are equivalent. The usefulness of the above transformation lies in the fact that (E4) can be interpreted as an expectation value with respect to the model system. To the best of our knowledge, this identity transformation was not yet used in the polaron problem.

In order to demonstrate the effectiveness of the transformation (E4), consider a non-quadratic variational trial action

$$S_{\text{var}}[\mathbf{r}_e(\tau), \mathbf{r}_f(\tau)] = \int_0^\beta \left[\frac{m\dot{\mathbf{r}}_e^2}{2} + \frac{m_f\dot{\mathbf{r}}_f^2}{2} + U(\mathbf{r}_f - \mathbf{r}_e) \right] d\tau \quad (\text{E5})$$

with a general potential U . We can rewrite (E4) to the partition function:

$$\begin{aligned} \mathcal{Z} &= \frac{\mathcal{Z}_{\text{var}}}{\mathcal{Z}_f} \left\langle \exp \{ \Phi[\mathbf{r}_e(\tau)] - \Phi_{\text{quad}}[\mathbf{r}_e(\tau)] \right. \\ &\quad \left. - \int_0^\beta [U_{\text{quad}}(\mathbf{r}_f - \mathbf{r}_e) - U(\mathbf{r}_f - \mathbf{r}_e)] d\tau \right\rangle_{\text{var}}, \end{aligned} \quad (\text{E6})$$

where Z_{var} is the partition function for a trial system with the action S_{var} . With $Z_{\text{var}}/Z_f = e^{-\beta F_{\text{var}}}$ and using the Jensen-Feynman variational inequality, we arrive at:

$$F \leq F_{\text{var}} + \frac{1}{\beta} \langle \Phi_{\text{quad}}[\mathbf{r}_e(\tau)] - \Phi[\mathbf{r}_e(\tau)] \rangle_{\text{var}} + \langle U_{\text{quad}}(\mathbf{r}_f - \mathbf{r}_e) - U(\mathbf{r}_f - \mathbf{r}_e) \rangle_{\text{var}} \quad (\text{E7})$$

When $U = U_{\text{quad}}$, this restores the original Jensen-Feynman variational principle for the polaron [22].

Introducing a non-quadratic potential leads to two changes. First, there is an additional term corresponding to the expectation value of the difference between the chosen variational potential and the quadratic one. Second, the expectation values are to be calculated with respect to the chosen variational potential U rather than with respect to the quadratic potential. Thus the variational inequality (E7) is a non-trivial extension of the Feynman – Jensen inequality.

It is important for the calculations that S_{var} is translation invariant but non-retarded action, so that all expressions in the variational functional (E7) have the same form in both representations – path integral and standard quantum mechanics. Apart from the parameters appearing in the trial action S_{var} , the inequality (E7) still contains as variational parameters m_f and ω , inherited from the “auxiliary” quadratic action S_{quad} and appearing in Φ_{quad} and $U_{\text{quad}}(\mathbf{r}_f - \mathbf{r}_e)$.

A physically reasonable choice of the trial interaction potential $U(\rho)$ with $\rho = |\mathbf{r}_f - \mathbf{r}|$ is no longer restricting to a single frequency oscillator. According to Refs. [23, 30], the self-consistent potential for an electron induced by the lattice polarization is parabolic near the bottom and Coulomb-like at large distances. Therefore, for the calculation of the optical conductivity, we choose a trial potential in the piecewise form, stitching together a parabolic and a Coulomb-like potential,

$$U(\rho) = \begin{cases} -U_0 + \frac{1}{2}\mu v^2 \rho^2, & \rho \leq r_0, \\ -\frac{\alpha_0}{\rho}, & \rho > r_0, \end{cases} \quad (\text{E8})$$

with the variational parameters: the reduced mass $\mu = mm_f/(m + m_f)$, the bottom energy U_0 , the confinement frequency v , and the parameter α_0 characterizing the Coulomb-like potential. The number of independent variational parameters is reduced, because we impose the boundary conditions for $U(\rho)$ to be continuous and smooth at $\rho = r_0$. This leads to

the following relations:

$$U_0 = \frac{3}{2}\mu v^2 r_0^2, \quad \alpha_0 = \mu v^2 r_0^3. \quad (\text{E9})$$

Thus the independent parameters for the present model are μ, ω, v, r_0 .

In Table V, we represent optimal variational parameters for several values of α corresponding to the spectra of the optical conductivity calculated below within the memory-function formalism. The frequency v is the analog of the first variational frequency parameter v of the Feynman model, and ω has some similarity with the second one, w . Fig. 26 shows the trial potential corresponding to these parameters. As can be seen from the figure, the potential becomes gradually deeper when α increases. Also the radius r_0 separating the parabolic and Coulomb-like fits for $U(r)$ decreases with an increasing coupling strength.

TABLE V: Parameters used for the calculation of the polaron optical conductivity within the memory function formalism

α	μ	ω	v	r_0
1	0.1035	3.139	3.882	2.499
3	0.3080	5.570	7.860	1.018
5.25	0.5255	5.189	8.885	0.733
6.5	0.6209	4.938	9.483	0.653

Because of using an auxiliary parabolic potential, the extended Jensen-Feynman inequality (E7), despite having more variational parameters, does not lead in general to a lower polaron free energy than the original Feynman result, except in the extremely strong coupling regime, where the present variational functional analytically tends (for $T = 0$) to the exact strong coupling limit obtained by Miyake [30]. However, its advantage with respect to the original Feynman treatment is in calculating the optical conductivity. The spectrum of internal states of the model system with the chosen potential necessarily consists of an infinite number non-equidistant energy levels with the energies $E_n < 0$ (counted from the potential energy at the infinity distance from the polaron) and a continuum of energies $E > 0$. Accounting for transitions between all these levels, one must expect a significant broadening of the peak absorption.

The polaron optical conductivity is calculated following the scheme of Ref. [31], where the memory-function expression for the polaron optical conductivity is derived using the Mori-

Zwanzig projection operator formalism [32]. We repeat the derivation up to formula (17) of Ref. [31], which is still formally exact. In the subsequent approximation, we extend the approach of Ref. [31], considering the density-density correlation function $\langle e^{i\mathbf{q}\cdot\mathbf{r}(t)}e^{-i\mathbf{q}\cdot\mathbf{r}(0)} \rangle_{\text{var}}$ where averaging is performed with the non-quadratic trial action/Hamiltonian. Note that these derivations in Ref. [31] and in the present work do not utilize the weak-coupling condition. As a result, the polaron optical conductivity takes the form,

$$\sigma(\Omega) = \frac{e^2 n_0}{m_b} \frac{i}{\Omega - \chi(\Omega)/\Omega}, \quad (\text{E10})$$

where $n_0 = N/V$ is the carrier density. The memory function in the non-quadratic setting is given by

$$\begin{aligned} \chi(\Omega) &= \frac{2}{3\hbar m_b} \int \frac{d\mathbf{q}}{(2\pi)^3} q^2 |V_{\mathbf{q}}|^2 \int_0^\infty dt e^{-\delta t} (e^{i\Omega t} - 1) \\ &\times \text{Im} \left[\frac{\cos[\omega_0(t + i\hbar\beta/2)]}{\sinh(\beta\hbar\omega_0/2)} \langle e^{i\mathbf{q}\cdot\mathbf{r}(t)}e^{-i\mathbf{q}\cdot\mathbf{r}(0)} \rangle_{\text{var}} \right], \end{aligned} \quad (\text{E11})$$

where $\delta \rightarrow +0$, $r(t)$ and $r(0)$ are electron coordinate vectors in the Heisenberg representation with the Hamiltonian of the trial system, ω_0 is the LO phonon frequency, and the correlation function $\langle e^{i\mathbf{q}\cdot\mathbf{r}(t)}e^{-i\mathbf{q}\cdot\mathbf{r}(0)} \rangle_{\text{var}}$ is calculated with the quantum states of the trial Hamiltonian corresponding to S_{var} . In the quadratic setting, $\chi(\Omega)/\Omega$ exactly reproduces the function $\Sigma(\Omega)$ of Ref. [31]. Further on, we consider the case $T = 0$ and apply the formula following from (E11),

$$\begin{aligned} \chi(\Omega) &= \frac{1}{3\pi^2\hbar m_b} \lim_{\delta \rightarrow 0^+} \int_0^\infty dq |V_{\mathbf{q}}|^2 q^4 \int_0^\infty dt e^{-\delta t} (e^{i\Omega t} - 1) \\ &\times \text{Im} (e^{-i\omega_0 t} \langle e^{i\mathbf{q}\cdot\mathbf{r}(t)}e^{-i\mathbf{q}\cdot\mathbf{r}(0)} \rangle_{\text{var}}). \end{aligned} \quad (\text{E12})$$

Rather than computing the correlation function $\langle e^{i\mathbf{q}\cdot\mathbf{r}(t)}e^{-i\mathbf{q}\cdot\mathbf{r}(0)} \rangle_{\text{var}}$ as a path integral, we choose to evaluate it in the equivalent Hamiltonian formalism. In this Hamiltonian framework, (E12) is written as a sum over the eigenstates of the trial Hamiltonian for the electron and the fictitious particle interacting through the potential U ,

$$\hat{H}_{\text{var}} = \frac{\hat{\mathbf{p}}^2}{2} + \frac{\hat{\mathbf{p}}_f^2}{2m_f} + U(\hat{\mathbf{r}}_f - \hat{\mathbf{r}}). \quad (\text{E13})$$

The quantum numbers for the Hamiltonian \hat{H}_{var} are the momentum k , the quanta l, m related to angular momentum, and a nodal quantum number n for the relative motion wavefunction. The quantum numbers l, n determine the energy $\varepsilon_{l,n}$ associated with

the relative motion between electron and fictitious particle (including both the discrete and continuous parts of the energy spectrum). The eigenfunctions $|\psi_{\mathbf{k};l,n,m}\rangle$ of the trial Hamiltonian (E13) are factorized as a product of a plane wave for the center-of-mass motion (with center-of-mass coordinate R) and a wave function for the relative motion $|\varphi_{l,n,m}\rangle$ (with the coordinate vector ρ of the relative motion),

$$|\psi_{\mathbf{k};l,n,m}\rangle = \frac{1}{\sqrt{V}} e^{i\mathbf{k}\cdot\mathbf{R}} |\varphi_{l,n,m}\rangle, \quad (\text{E14})$$

$$|\varphi_{l,n,m}\rangle = \mathcal{R}_{l,n}(\rho) Y_{l,m}(\theta, \varphi). \quad (\text{E15})$$

The density-density correlation function at $T = 0$ is therefore the average with the ground state of the trial system, which can be expanded in the basis of eigenfunctions $|\psi_{\mathbf{k};l,n,m}\rangle$:

$$\begin{aligned} \langle e^{i\mathbf{q}\cdot\mathbf{r}(t)} e^{-i\mathbf{q}\cdot\mathbf{r}(0)} \rangle_{\text{var}} &= \langle \psi_{\mathbf{0};0,0,0} | e^{\frac{i}{\hbar} \hat{H}_{\text{var}} t} e^{i\mathbf{q}\cdot\mathbf{r}} e^{-\frac{i}{\hbar} \hat{H}_{\text{var}} t} e^{-i\mathbf{q}\cdot\mathbf{r}} | \psi_{\mathbf{0};0,0,0} \rangle \\ &= \sum_{\mathbf{k};l,n,m} e^{i\frac{t}{\hbar} (\varepsilon_{0,0} - \varepsilon_{l,n} - \frac{\hbar^2 \mathbf{k}^2}{2M})} |\langle \psi_{\mathbf{0};0,0,0} | e^{i\mathbf{q}\cdot\mathbf{r}} | \psi_{\mathbf{k};l,n,m} \rangle|^2, \end{aligned} \quad (\text{E16})$$

where $M = 1 + m_f$ is the total mass of the trial system. Further on, the Feynman units are used, where $\hbar = 1$, $\omega_0 = 1$, and the band mass $m_b = 1$. In these units, the squared modulus $|V_{\mathbf{q}}|^2$ is:

$$|V_{\mathbf{q}}|^2 = \frac{2\sqrt{2}\pi\alpha}{q^2}.$$

When substituting (E16) into the memory function, we arrive at the result,

$$\begin{aligned} \chi(\Omega) &= \frac{2\sqrt{2}\alpha}{3\pi} \int_0^\infty dq q^2 \sum_{\mathbf{k};l,n,m} |\langle \psi_{\mathbf{0};0,0,0} | e^{i\mathbf{q}\cdot\mathbf{r}} | \psi_{\mathbf{k};l,n,m} \rangle|^2 \\ &\quad \times \int_0^\infty dt e^{-\delta t} (e^{i\Omega t} - 1) \text{Im} \left(e^{-it(\varepsilon_{l,n} - \varepsilon_{0,0} + \frac{\mathbf{k}^2}{2M} + 1)} \right). \end{aligned} \quad (\text{E17})$$

Using analytic summations as described in Appendix 1 and the integration over time, the memory function takes the form

$$\begin{aligned} \chi(\Omega) &= \frac{\sqrt{2}\alpha}{3\pi} \int_0^\infty dq q^2 \sum_{l,n} (2l+1) S_q^2(0, 0 | l | l, n) \\ &\quad \times \left(\frac{1}{\Omega - \Omega_{q,l,n} + i\delta} - \frac{1}{\Omega + \Omega_{q,l,n} + i\delta} + \frac{2}{\Omega_{q,l,n}} \right). \end{aligned} \quad (\text{E18})$$

$(\delta \rightarrow +0)$

with the transition frequency for transitions between the ground and excited states of the trial system accompanied by an emission of a phonon:

$$\Omega_{q,l,n} \equiv \frac{q^2}{2M} + \varepsilon_{l,n} - \varepsilon_{0,0} + 1, \quad (\text{E19})$$

and the matrix element with radial wave functions for the trial system $S_q(l, n | l', n')$ determined by (E51).

The limiting transition $\delta \rightarrow +0$ in (E18) is performed analytically using the relation $\lim_{\delta \rightarrow +0} (x + i\delta)^{-1} = P/x - i\pi\delta(x)$, where P/x is the Cauchy principal value and $\delta(x)$ is the delta function. This separates explicitly the real and imaginary parts of the memory function and eliminates the integration over q for the imaginary part. The obtained expressions are used then for the numerical calculation of the polaron optical conductivity within the extended memory function formalism.

b. Non-adiabatic strong coupling expansion

Next, we describe the strong coupling approach and its extension beyond the adiabatic approximation, denoted below as the non-adiabatic SCE. Here, the goal is to take non-adiabatic transitions between different excited levels of a polaron into account in the formalism. The notations in this subsection are the same as in Ref. [19]. The polaron optical conductivity in the strong coupling regime is represented by the Kubo formula,

$$\text{Re } \sigma(\Omega) = \frac{\Omega}{2} \int_{-\infty}^{\infty} e^{i\Omega t} f_{zz}(t) dt, \quad (\text{E20})$$

with the dipole-dipole correlation function

$$\begin{aligned} f_{zz}(t) = & \sum_{n,l,m} \sum_{n',l',m'} \sum_{n'',l'',m''} \langle \psi_{n,l,m} | \hat{z} | \psi_{n'',l'',m''} \rangle \langle \psi_{n',l',m'} | \hat{z} | \psi_0 \rangle \\ & \times \langle 0_{ph} | \langle \psi_0 | e^{it\hat{H}'} | \psi_{n,l,m} \rangle \langle \psi_{n'',l'',m''} | e^{-it\hat{H}'} | \psi_{n',l',m'} \rangle | 0_{ph} \rangle. \end{aligned} \quad (\text{E21})$$

where $|\psi_{n,l,m}\rangle$ are the polaron states as obtained within the strong coupling ansatz in Ref. [19]. The transformed Hamiltonian \hat{H}' of the electron-phonon system after the strong coupling unitary transformation [19] takes the form

$$\hat{H}' = \hat{H}'_0 + \hat{W} \quad (\text{E22})$$

with the terms

$$\hat{H}'_0 = \frac{\hat{\mathbf{p}}^2}{2} + \sum_{\mathbf{q}} |f_{\mathbf{q}}|^2 + V_a(\hat{\mathbf{r}}) + \sum_{\mathbf{q}} \left(\hat{b}_{\mathbf{q}}^+ \hat{b}_{\mathbf{q}} + \frac{1}{2} \right), \quad (\text{E23})$$

$$\hat{W} = \sum_{\mathbf{q}} \left(\hat{w}_{\mathbf{q}} \hat{b}_{\mathbf{q}} + \hat{w}_{\mathbf{q}}^* \hat{b}_{\mathbf{q}}^+ \right). \quad (\text{E24})$$

Here, $w_{\mathbf{q}}$ are the amplitudes of the renormalized electron-phonon interaction

$$\hat{w}_{\mathbf{q}} = \frac{\sqrt{2\sqrt{2}\pi\alpha}}{q\sqrt{V}} \left(e^{i\mathbf{q}\cdot\hat{\mathbf{r}}} - \rho_{\mathbf{q},0} \right), \quad (\text{E25})$$

where $\rho_{\mathbf{q},0}$ is the expectation value of the operator $e^{i\mathbf{q}\cdot\hat{\mathbf{r}}}$ with the trial electron wave function $|\psi_0\rangle$:

$$\rho_{\mathbf{q},0} = \langle \psi_0 | e^{i\mathbf{q}\cdot\hat{\mathbf{r}}} | \psi_0 \rangle, \quad (\text{E26})$$

and $V_a(\hat{\mathbf{r}})$ is the self-consistent potential energy for the electron,

$$V_a(\hat{\mathbf{r}}) = - \sum_{\mathbf{q}} \frac{4\sqrt{2}\pi\alpha}{q^2 V} \rho_{-\mathbf{q},0} e^{i\mathbf{q}\cdot\hat{\mathbf{r}}}. \quad (\text{E27})$$

The eigenstates of the Hamiltonian \hat{H}'_0 are the products of the electron wave functions and those of the phonon vacuum $|\psi_{n,l,m}\rangle |0_{ph}\rangle$. The dipole-dipole correlation function $f_{zz}(t)$ given by (E21) is simplified within the adiabatic approximation for the ground state and using the selection rules for the dipole transition matrix elements and the symmetry properties of the polaron Hamiltonian, as in Ref. [19]. The correlation function, using the interaction representation takes the form,

$$\begin{aligned} f_{zz}(t) &= \sum_{n',n} \langle \psi_0 | \hat{z} | \psi_{n,1,0} \rangle \langle \psi_{n',1,0} | \hat{z} | \psi_0 \rangle e^{-i\Omega_{n,0}t} \\ &\times \left\langle \psi_{n,1,0} \left| \left\langle 0_{ph} \left| \text{T exp} \left[-i \int_0^t ds \hat{W}(s) \right] \right| 0_{ph} \right\rangle \right| \psi_{n',1,0} \right\rangle \end{aligned} \quad (\text{E28})$$

with the Franck-Condon transition frequency

$$\Omega_{n,0} \equiv \varepsilon_{n,1} - \varepsilon_{1,0},$$

and the interaction Hamiltonian in the interaction representation,

$$\hat{W}(s) = e^{i\hat{H}'_0 s} \hat{W} e^{-i\hat{H}'_0 s}.$$

As found in early works on the strong-coupling Fröhlich polaron (see, for review, Refs. [23, 33]), the energy differences between different excited FC states for a strong coupling polaron

are much smaller than the energy difference between the ground and lowest excited FC state. For the illustration, the self-consistent potential for the electron in the strong-coupling approximation $V_a(r)$ given by (E27) and energy levels for an electron in this potential have been plotted for a polaron in the strong-coupling regime in Fig. 27. In the strong-coupling limit, the scaling invariance appears for energies, which are proportional to α^2 , and for the length scale, which decreases in the strong-coupling regime as α^{-1} . Therefore for sufficiently strong couplings, the energy diagrams plotted in units $(E/\alpha^2, \alpha r)$ extremely slightly depend on α , tending to an α -independent picture when $\alpha \rightarrow \infty$. Thus we restricted the strong-coupling energy diagrams to one chosen α , e. g., here $\alpha = 15$. As can be seen from the figure, the difference $\varepsilon_{1,1} - \varepsilon_{1,0}$ is indeed large with respect to differences between excited levels. Therefore we keep here the adiabatic approximation for the ground state and, consequently, for the transition between the ground and excited states. On the contrary, the adiabatic approximation for the transitions between different excited states is not applied in (E28), as distinct from the calculation in Ref. [19].

The matrix elements for the dipole transitions from the ground state to other excited states than $|\psi_{1,1,0}\rangle$ (i. e., $\langle \psi_0 | z | \psi_{n,1,0} \rangle$ with $n \neq 1$) have small relative oscillator strengths with respect to $\langle \psi_0 | z | \psi_{1,1,0} \rangle$ (of order $\sim 10^{-2}$). Therefore further on we consider the next-to-leading order nonadiabatic corrections for the contribution to (E28) with $n = n' = 1$ and the adiabatic expression for the contribution with other (n, n') . In other words, for $n = n' = 1$, the treatment will account for non-adiabatic effects, while for other $n, n' \neq 1$, we apply the adiabatic approximation to (E28). Consequently, the terms with $n' \neq n$, which are beyond this adiabatic approximation, are neglected in the next expression,

$$f_{zz}(t) = \sum_n |\langle \psi_0 | \hat{z} | \psi_{n,1,0} \rangle|^2 e^{-i\Omega_{n,0}t} \times \left\langle \psi_{n,1,0} \left| \left\langle 0_{ph} \left| T \exp \left[-i \int_0^t ds \hat{W}(s) \right] \right| 0_{ph} \right\rangle \right| \psi_{n,1,0} \right\rangle, \quad (\text{E29})$$

where T is the time-ordering symbol. The exact averaging over the phonon variables is performed by the disentangling of the evolution operator (in analogy with [34]). As a result, we obtain the formula

$$f_{zz}(t) = \sum_n |\langle \psi_0 | z | \psi_{n,1,0} \rangle|^2 e^{-i\Omega_{n,0}t} \left\langle \psi_{n,1,0} \left| T_e \exp \left(\hat{\Phi} \right) \right| \psi_{n,1,0} \right\rangle \quad (\text{E30})$$

with the ‘‘influence phase’’ (assuming $\hbar = 1$ and $\omega_0 = 1$)

$$\hat{\Phi} = - \int_0^t ds \int_0^s ds' e^{-i(s-s')} \sum_{\mathbf{q}} \hat{w}_{\mathbf{q}}(s) \hat{w}_{\mathbf{q}}^+(s'), \quad (\text{E31})$$

and T_e the time-ordering symbol with respect to the electron degrees of freedom. The correlation function (E30) is the basis expression for the further treatment.

The next approximation is the restriction to the leading-order semi-invariant expansion:

$$\langle \psi_{n,1,0} | T_e \exp(\hat{\Phi}) | \psi_{n,1,0} \rangle \approx \exp \langle \psi_{n,1,0} | T_e (\hat{\Phi}) | \psi_{n,1,0} \rangle. \quad (\text{E32})$$

As shown in Ref. [19], this approximation accounts of the static Jahn-Teller effect, and it works well, because the dynamic Jahn-Teller effect appears to be very small. The influence phase is invariant under spatial rotations so that

$$\langle \psi_{n,1,0} | T_e (\hat{\Phi}) | \psi_{n,1,0} \rangle = \langle \psi_{n,1,1} | T_e (\hat{\Phi}) | \psi_{n,1,1} \rangle = \langle \psi_{n,1,-1} | T_e (\hat{\Phi}) | \psi_{n,1,-1} \rangle.$$

Hence the correlation function (E30) can be simplified to

$$\begin{aligned} f_{zz}(t) &= \sum_n |\langle \psi_0 | \hat{z} | \psi_{n,1,0} \rangle|^2 \\ &\times \exp \left(-i\Omega_{n,0}t - \frac{1}{3} \sum_{\mathbf{q}} \sum_{n',l',m',m} |\langle \psi_{n,1,m} | \hat{w}_{\mathbf{q}} | \psi_{n',l',m'} \rangle|^2 \frac{1 - i\omega_{n',l';n,1}t - e^{-i\omega_{n',l';n,1}t}}{\omega_{n',l';n,1}^2} \right). \end{aligned} \quad (\text{E33})$$

with the notation

$$\omega_{n',l';n,1} \equiv 1 + \varepsilon_{n',l'} - \varepsilon_{n,1}. \quad (\text{E34})$$

In our previous treatments of the strong coupling polaron optical conductivity, we neglected the matrix elements for $\hat{w}_{\mathbf{q}}$ between the electron energy levels with different energies, that corresponds to the adiabatic approximation.

As described above, the correlation function (E28) goes beyond this approximation, taking into account the transitions between different excited states but still assuming that the adiabatic approximation holds for the transitions between the ground and excited states. The physical picture beyond this approximation consists in the fact that the ground state is far below other states. Therefore, to be consistent with the above reasoning, we can keep in (E33) the matrix elements $\langle \psi_{n,1,m} | \hat{w}_{\mathbf{q}} | \psi_{n',l',m'} \rangle$ only with the excited states, neglecting those matrix elements which contain the ground state. To summarize, we keep here the adiabatic

approximation for the ground state and, consequently, for the transition between the ground and excited states. On the contrary, the adiabatic approximation for the transitions between different excited states is not assumed in (E28) and (E33), as distinct from the calculation in Ref. [19].

Introducing parameters related to the extension of the Huang-Rhys factor used in Ref. [19]:

$$S_{n',l;n,1} \equiv \frac{1}{3\omega_{n',l;n,1}^2} \sum_{\mathbf{q}} \sum_{m',m} |\langle \psi_{n,1,m} | \hat{w}_{\mathbf{q}} | \psi_{n',l,m'} \rangle|^2, \quad (\text{E35})$$

the correlation function is rewritten as follows:

$$f_{zz}(t) = \sum_n |\langle \psi_0 | z | \psi_{n,1,0} \rangle|^2 \exp \left[-i\Omega_{n,0}t - \sum_{n',l} S_{n',l;n,1} (1 - i\omega_{n',l;n,1}t - e^{-i\omega_{n',l;n,1}t}) \right]. \quad (\text{E36})$$

The states $|\psi_{n',l,m'}\rangle$ can be subdivided to two groups: (1) the states $|\psi_{1,1,m'}\rangle$ with the energy level $\varepsilon_{1,1}$, (2) the higher energy states with $(n',l) \neq (1,1)$. The first group of states were already taken into account in our previous treatments and in Ref. [19]. Taking into account the second group of states provides the step beyond the adiabatic approximation – this is the focus of the present treatment. We denote the parameters corresponding to the adiabatic approximation by

$$S_n \equiv S_{n,1;n,1} \equiv \frac{1}{3} \sum_{\mathbf{q}} \sum_{m',m} |\langle \psi_{n,1,m} | \hat{w}_{\mathbf{q}} | \psi_{n,1,m'} \rangle|^2. \quad (\text{E37})$$

Correspondingly, the correlation function (E36) is rewritten as

$$f_{zz}(t) = \sum_n |\langle \psi_0 | z | \psi_{n,1,0} \rangle|^2 \times \exp \left[-i\Omega_{n,0}t - S_n (1 - it - e^{-it}) - \sum_{(n',l) \neq (n,1)} S_{n',l;n,1} (1 - i\omega_{n',l;n,1}t - e^{-i\omega_{n',l;n,1}t}) \right]. \quad (\text{E38})$$

When performing the Taylor expansion of this correlation function in powers of S_n and $S_{n',l;n,1}$ and substituting it into (E20), the spectrum of the optical conductivity will give us a set of δ -like peaks, similarly to formula (2) of Ref. [18], which is a Poissonian distribution. For sufficiently large coupling strengths, it is relevant to consider an envelope of this distribution, which is obtained in the following way. In the strong coupling regime, the phonon frequency is small with respect to the Franck-Condon frequency $\Omega_{1,0}$, which increases as

$\Omega_{1,0} \propto \alpha^2$ at large α . Therefore at a strong coupling, the range of convergence for the integral over time in (E20) is of order $t \propto 1/\Omega_{1,0} \ll 1$. Consequently, at large α we can expand the factor $(1 - it - e^{-it})$ in powers of t up to the second order,

$$1 - it - e^{-it} = \frac{1}{2}t^2 + O(t^3). \quad (\text{E39})$$

In the particular case when non-adiabatic terms are not taken into account, the expansion (E39) provides a Gaussian envelope of the optical conductivity spectrum obtained in [18, 19]. The other factor, $(1 - i\omega_{n',l;n,1}t - e^{-i\omega_{n',l;n,1}t})$, should not be expanded in the same way, because the frequencies $\omega_{n',l;n,1}$ ($n', l \neq (1, 1)$) also increase in the strong coupling limit as α^2 . Therefore we keep the non-adiabatic contribution as is, without expansion. As a result, in the strong coupling regime we arrive at the correlation function:

$$f_{zz}(t) = \sum_n |\langle \psi_0 | z | \psi_{n,1,0} \rangle|^2 \times \exp \left(-\delta S_n - i\tilde{\Omega}_{n,0}t - \frac{1}{2}S_n t^2 + \sum_{(n',l) \neq (n,1)} S_{n',l;n,1} e^{-i\omega_{n',l;n,1}t} \right). \quad (\text{E40})$$

with the parameters:

$$\delta S_n \equiv \sum_{(n',l) \neq (1,1)} S_{n',l;n,1}, \quad (\text{E41})$$

$$\delta \Omega_n \equiv \sum_{(n',l) \neq (1,1)} S_{n',l;n,1} \omega_{n',l;n,1}, \quad (\text{E42})$$

$$\tilde{\Omega}_{n,0} \equiv \Omega_{n,0} - \delta \Omega_n. \quad (\text{E43})$$

The parameter δS_n plays a role of the Debye-Waller factor and ensures the fulfilment of the f -sum rule for the optical conductivity. The parameter $\delta \Omega_n$ is the shift of the Franck-Condon frequency to a lower value due to phonon-assisted transitions to higher energy states. The exponent can be expanded, yielding a description in terms of multiphonon processes:

$$\exp \left(\sum_{(n',l) \neq (n,1)} S_{n',l;n,1} e^{-i\omega_{n',l;n,1}t} \right) = \sum_{\{p_{n',l} \geq 0\}} \left(\prod_{(n',l) \neq (n,1)} \frac{S_{n',l;n,1}^{p_{n',l;n,1}}}{p_{n',l;n,1}!} \right) e^{-i \sum_{n',l} p_{n',l;n,1} \omega_{n',l;n,1} t}, \quad (\text{E44})$$

where the sum $\sum_{\{p_{n',l}\}}$ is performed over all combinations $\{p_{n',l} \geq 0\}$.

With the expansion (E44), the polaron optical conductivity takes the form:

$$\begin{aligned} \text{Re } \sigma(\Omega) = & \Omega \sum_n |\langle \psi_0 | z | \psi_{n,1,0} \rangle|^2 e^{-\delta S_n} \sqrt{\frac{\pi}{2S_n}} \\ & \times \sum_{\{p_{n',l;n,1} \geq 0\}} \left(\prod_{(n',l) \neq (n,1)} \frac{S_{n',l;n,1}^{p_{n',l;n,1}}}{p_{n',l;n,1}!} \right) \exp \left[-\frac{(\tilde{\Omega}_{n,0} + \sum_{n',l} p_{n',l;n,1} \omega_{n',l;n,1} - \Omega)^2}{2S_n} \right]. \end{aligned} \quad (\text{E45})$$

In formula (E45), the term where all $p_{n',l;n,1} = 0$ corresponds to the adiabatic approximation and exactly reproduces the result of Ref. [19]. The other terms represent the non-adiabatic contributions to $\text{Re } \sigma(\Omega)$, and are correction terms to the previously found results.

3. Results and discussions

The polaron optical conductivity derived in the above section is in line with the physical understanding of the underlying processes for the polaron optical response, achieved in early works [20, 35] and summarized in Ref. [36]. It is based on the concept of the polaron excitations of three types:

- Relaxed Excited States (RES) [35] for which the lattice polarization is adapted to the electronic distribution;
- Franck-Condon states (FC) where the lattice polarization is “frozen”, adapted to the polaron ground state;
- Scattering states characterized by the presence of real phonons along with the polaron.

These polaron excitations are schematically shown in Fig. 28. The polaron RES can be formed when the electron-phonon coupling is strong enough, for $\alpha \gtrsim 4.5$. At weak coupling, the polaron optical response at zero temperature is due to transitions from the polaron ground state to scattering states. In other words, the optical absorption spectrum of a weak-coupling polaron is determined by the absorption of radiation energy, which is re-emitted in the form of LO phonons. At stronger couplings, the concept of the polaron relaxed excited states first introduced in Ref. [35] becomes of key importance. In the range of sufficiently large α when the polaron RES are formed, the absorption of light by a

polaron occurs through transitions from the ground state to RES which can be accompanied by the emission of different numbers $n \geq 0$ of free phonons. These transitions contribute to the shape of a multiphonon optical absorption spectrum. At very large coupling, lattice relaxation processes become too slow and the Franck-Condon states determine the optical response.

We analyze polaron optical conductivity spectra both with the memory function formalism and with the strong-coupling expansion, and compare these to the DQMC numerical data [13]. Within the framework of formalisms based on the memory function (MF), we compare the following theories:

- The original DSG method of Ref. [20], where the expectation value in E17 is calculated with respect to a gaussian trial action. This will be denoted by MF-1 in the figures.
- The extended MF formalism of [18], where an ad-hoc broadening with a strength determined from sum rules is included in (E10). This will be denoted by MF-2.
- The current non-quadratic MF formalism, based on the extension of the Jensen-Feynman inequality introduced in this paper, denoted by MF-new.

Among the strong-coupling expansions (SCE), we distinguish:

- The strong-coupling result in the adiabatic approximation, as obtained in Ref. [18]. This will be denoted here by SCE-1.
- The adiabatic approximation of Ref. [19], which uses more accurate trial polaron states. This will be denoted by SCE-2.
- The current non-adiabatic strong coupling expansion, denoted by SCE-new.

The subsequent figures show the results for increasing α . In Figure 29, the optical conductivity is shown for small coupling, $\alpha = 1$, and for $\alpha = 3, \alpha = 5.25$ which correspond to the dynamic regime where the RES starts to play a role. In this regime, analytic solutions are provided by the various memory function formalisms listed above, and we compare them to DQMC numeric data [13]. At weak coupling ($\alpha = 1$, panel (a)), all the approaches based on the memory function give results in agreement with DQMC. For $\alpha = 3$ (panel (b)), the current method gives a better fit to the DQMC result than the other two methods. For a

stronger coupling, $\alpha = 5.25$ (panel (c)) the MF-2 approach substantially improves the original result MF-1, but the optical conductivity spectrum calculated within the new non-quadratic MF formalism lies closer to the DQMC data than either of the other two.

Fig. 30 demonstrates the behavior of the polaron optical conductivity spectra in the intermediate coupling regime, for $\alpha = 6.5$ and $\alpha = 7$. In this regime, the existing memory function approaches (MF-1, MF-2) as well as the existing strong coupling expansions (SCE-1, SCE-2) do not provide satisfactory results. The new memory function approach and the new strong coupling expansion are in much better agreement with the DQMC data.

This range of coupling parameters is where one would want to cross over from using a memory function based approach to a strong coupling expansion. Whereas the existing methods do not allow to bridge this gap at intermediate coupling, the extensions that we have proposed here are suited to implement such a cross-over. The present memory-function approach with the non-parabolic trial action leads to a relatively small extension of the range of α where the polaron optical conductivity compares well with the DQMC data, namely from $\alpha \approx 4.5$ to $\alpha \approx 6.5$. For $\alpha \gtrsim 6.5$, the memory-function approach with the non-parabolic trial action provides a better agreement with DQMC than all other known approximations. Remarkably, the optical conductivity spectra as given by the non-quadratic MF formalism and the non-adiabatic SCE are both in better agreement with the Monte Carlo data than any of the preceding analytical methods. For $\alpha = 6.5$, the polaron optical conductivity calculated within non-quadratic MF formalism and the non-adiabatic SCE lie rather close to each other. We can conclude therefore that the ranges of validity of those two approximations overlap, despite the fact that these approximations are based on different assumptions.

The maximum of the optical conductivity spectrum provided by the non-quadratic MF formalism for $\alpha = 6.5$ is positioned at slightly higher frequency than that for the maximum of the optical conductivity obtained in the strong coupling approximation with non-adiabatic corrections. They lie remarkably close to two features of the DQMC optical conductivity spectrum: the higher-frequency peak, which is the maximum of the spectrum, and the lower-frequency shoulder. The similar comparative behavior of the memory-function and strong coupling results was noticed in Ref. [18], where it was suggested that these two features in the DQMC spectra can correspond physically to the dynamic (RES) and the Franck-Condon contributions. The present results are in line with that physical picture.

In Fig. 30 (b), the arrows indicate the FC transition frequency for the transition to the first excited FC state $\Omega_{1,0} \equiv \Omega_{\text{FC}}$ and the RES transition frequency Ω_{RES} for a strong coupling polaron as calculated in Ref. [35]. We can see that both the shape and the position of the maximum of the optical conductivity band obtained within the adiabatic approximation in Refs. [18, 19] are rather far from those for the DQMC data. Taking into account non-adiabatic transitions drastically improves the agreement of the strong coupling approximation with DQMC, even for $\alpha = 7$, which, strictly speaking, is not yet the strong coupling regime. The value $\alpha = 7$ can be rather estimated as an intermediate coupling. However, even at this intermediate coupling strength, the results of present approach lie much closer to the DQMC data than those obtained within all other aforesaid analytic methods. Also a substantial improvement of the agreement between the strong coupling expansion and DQMC is clearly expressed in Fig. 31, where the polaron optical conductivity spectra are shown for the strong coupling regime for $\alpha = 8$ to $\alpha = 9$. For strong couplings, the non-adiabatic SCE accurately reproduces both the peak position and the overall shape of the DQMC spectra. Finally, we see that the results of the non-adiabatic SCE remain accurate also in the extremely strong coupling regime, as shown in Fig. 32.

4. Conclusions

In the present work, we have modified two basic analytic methods for the polaron optical conductivity in order to extend their ranges of applicability for the electron-phonon coupling constant in such a way that these ranges overlap. The memory function formalism using a trial action for a model two-particle system has been extended to work with non-quadratic interaction potentials in the model system. This method combines the translation invariance of the trial system, which is one of the main advantages of the Feynman variational approach, with a more realistic interaction between the electron and the fictitious particle. This extension leads to a substantial improvement of the polaron optical conductivity for small and intermediate coupling strengths with respect to the preceding known versions of the memory function approach.

The other method is the strong-coupling expansion, and we have extended it beyond the Franck-Condon adiabatic approximation by taking into account non-adiabatic transitions between different excited polaron states. As a result, the modified non-adiabatic strong-

coupling expansion appears now to be in good agreement with the numerical DQMC data in a wide range of α from intermediate coupling strength to the strong coupling limit. For the intermediate coupling value $\alpha = 6.5$, the two methods that we propose, i.e. the non-quadratic MF formalism and the non-adiabatic SCE, result in optical conductivity spectra which are remarkably close to each other and to the DQMC results. Thus, both methods can be combined to provide all-coupling, accurate analytic results for the polaron optical absorption.

For larger α the agreement between the results of the non-adiabatic SCE and DQMC becomes gradually better. At very strong coupling, even the preceding adiabatic SCE [19] is already sufficiently good, so that the improvement due to the non-adiabatic transitions, e. g., for $\alpha = 15$, is relatively small. However, for a slightly weaker coupling, e. g., for $\alpha = 9$, we can observe a drastically improved agreement with DQMC for the present non-adiabatic SCE as compared to the adiabatic approximation. We can conclude that at present, the strong coupling approximation taking into account non-adiabatic contributions provides the best agreement with the DQMC results for $\alpha \gtrsim 6.5$ with respect to all other known analytic approaches for the polaron optical conductivity. We find that the non-adiabatic transitions lead to a substantial change of the spectral shape with respect to the optical conductivity derived within the adiabatic approximation. The non-adiabatic effects are non-negligible in the whole range of the coupling strength, at least for $\alpha \leq 15$, available for DQMC.

As discussed in Ref. [33], at strong coupling the distances between different polaron energy levels rise as $\propto \alpha^2$, and hence the matrix elements of the electron-phonon interaction diminish. Thus the small parameter in the strong-coupling approximation for a polaron is $1/\alpha$. The contribution to the optical conductivity taking into account non-adiabatic transitions represent in fact the next-to-leading order correction in powers of this small parameter. Consequently, this correction is more significant at weaker couplings, and is relatively small at strong coupling. The comparison of the calculated optical conductivity with DQMC confirms this prediction.

In summary, extending the MF and SCE formalisms leads to an overlapping of the areas of α where these two analytic methods are applicable. These analytic methods have been verified, appearing to be in good agreement with numeric DQMC data at all α available for DQMC. We therefore possess the analytic description of the polaron optical response which embraces the whole range of the coupling strength.

Appendix 1: Analytic summations

The matrix element in (E17) is a particular case of the product of two matrix elements:

$$\langle \psi_{\mathbf{k};l,n,m} | e^{i\mathbf{q}\cdot\mathbf{r}} | \psi_{\mathbf{k}';l',n',m'} \rangle = \frac{1}{V} \langle e^{-i\mathbf{k}\mathbf{R}} | e^{i\mathbf{q}\cdot\mathbf{R}} | e^{i\mathbf{k}'\mathbf{R}} \rangle \langle \varphi_{l,n,m} | e^{i\mu\mathbf{q}\cdot\boldsymbol{\rho}} | \varphi_{l',n',m'} \rangle, \quad (\text{E46})$$

where μ is the reduced mass of the trial system. The first matrix element is

$$\frac{1}{V} \langle e^{-i\mathbf{k}\mathbf{R}} | e^{i\mathbf{q}\cdot\mathbf{R}} | e^{i\mathbf{k}'\mathbf{R}} \rangle = \delta_{\mathbf{k}',\mathbf{k}-\mathbf{q}}. \quad (\text{E47})$$

This eliminates the integration over the final electron momentum k' and reduces the memory function to the expression

$$\begin{aligned} \chi(\Omega) &= \frac{2\sqrt{2}\alpha}{3\pi} \int_0^\infty dq q^2 \sum_{l',n',m'} |\langle \varphi_{0,0,0} | e^{i\mu\mathbf{q}\cdot\boldsymbol{\rho}} | \varphi_{l',n',m'} \rangle|^2 \\ &\times \int_0^\infty dt e^{-\delta t} (e^{i\Omega t} - 1) \text{Im} \left(e^{-it \left(\frac{q^2}{2M} + \varepsilon_{l',n'} - \varepsilon_{0,0} + 1 \right)} \right). \end{aligned} \quad (\text{E48})$$

For a more general expression $|\langle \varphi_{l,n,m} | e^{i\mu\mathbf{q}\cdot\boldsymbol{\rho}} | \varphi_{l',n',m'} \rangle|^2$, the summation over m and m' is performed explicitly:

$$\begin{aligned} &\sum_{m,m'} |\langle \varphi_{l,n,m} | e^{i\mu\mathbf{q}\cdot\boldsymbol{\rho}} | \varphi_{l',n',m'} \rangle|^2 \\ &= \frac{(2l+1)(2l'+1)}{2} \int_0^\infty \rho^2 d\rho \int_0^\infty (\rho')^2 d\rho' \mathcal{R}_{l,n}(\rho) \mathcal{R}_{l',n'}(\rho) \mathcal{R}_{l,n}(\rho') \mathcal{R}_{l',n'}(\rho') \\ &\times \int_0^{2\pi} \frac{\sin(\mu q |\boldsymbol{\rho} - \boldsymbol{\rho}'|)}{\mu q |\boldsymbol{\rho} - \boldsymbol{\rho}'|} P_l(\cos \theta) P_{l'}(\cos \theta) \sin \theta d\theta. \end{aligned} \quad (\text{E49})$$

The modulus $|\boldsymbol{\rho} - \boldsymbol{\rho}'|$ is expressed as

$$|\boldsymbol{\rho} - \boldsymbol{\rho}'| = \sqrt{\rho^2 + (\rho')^2 - 2\rho\rho' \cos \theta}. \quad (\text{E50})$$

Hence we can use the expansion of $\frac{\sin(\mu q |\boldsymbol{\rho} - \boldsymbol{\rho}'|)}{\mu q |\boldsymbol{\rho} - \boldsymbol{\rho}'|}$ through the Legendre polynomials $P_l(z)$ and spherical Bessel functions $j_l(z)$:

$$\frac{\sin(\mu q |\boldsymbol{\rho} - \boldsymbol{\rho}'|)}{\mu q |\boldsymbol{\rho} - \boldsymbol{\rho}'|} = \sum_{l''=0}^{\infty} (2l''+1) j_{l''}(\mu q \rho) j_{l''}(\mu q \rho') P_{l''}(\cos \theta).$$

The integral of the product of three Legendre polynomials is expressed through the $3j$ -symbol:

$$\int_0^{2\pi} P_{l''}(\cos \theta) P_l(\cos \theta) P_{l'}(\cos \theta) \sin \theta d\theta = 2 \begin{pmatrix} l & l' & l'' \\ 0 & 0 & 0 \end{pmatrix}^2.$$

Therefore we find that

$$\sum_{m,m'} |\langle \varphi_{l,n,m} | e^{i\mu\mathbf{q}\cdot\boldsymbol{\rho}} | \varphi_{l',n',m'} \rangle|^2 = \sum_{l''=0}^{\infty} (2l+1)(2l'+1)(2l''+1) \times \begin{pmatrix} l & l' & l'' \\ 0 & 0 & 0 \end{pmatrix}^2 S_q^2(l, n | l'' | l', n'),$$

where $S_q(l, n | l'' | l', n')$ is the matrix element with radial wave functions for the trial system,

$$S_q(l, n | l'' | l', n') \equiv \int_0^{\infty} \mathcal{R}_{l,n}(\rho) \mathcal{R}_{l',n'}(\rho) j_{l''}(\mu q \rho) \rho^2 d\rho. \quad (\text{E51})$$

For $l = 0$ the result of the summation over intermediate states is reduced to the formula

$$\sum_{m'} |\langle \varphi_{0,n,0} | e^{i\mu\mathbf{q}\cdot\boldsymbol{\rho}} | \varphi_{l',n',m'} \rangle|^2 = (2l'+1) S_q^2(0, 0 | l' | l', n'), \quad (\text{E52})$$

which is used in our calculations.

Figure 33 shows radial wave functions $R_{l,n}(\rho)$ entering the matrix elements. The wave functions are plotted for several lowest values of the quantum numbers l, n . The figure corresponds to the intermediate-coupling regime with $\alpha = 5.25$. These radial wave functions represent analytically exact solutions of the Schrödinger equation for a particle with the reduced mass μ in the trial potential $U(\rho)$ given by (E8).

-
- [1] L. D. Landau, *Phys. Z. Sowjetunion* **3**, 664 (1933) [English translation in *Collected Papers*, Gordon and Breach, New York, 1965, pp. 67-68].
 - [2] A. S. Alexandrov and J. T. Devreese, *Advances in Polaron Physics* (Springer, 2009).
 - [3] R. von Helmolt, J. Wecker, B. Holzapfel, L. Schultz, and K. Samwer, *Phys. Rev. Lett.* **71**, 2331 (1993).
 - [4] H. Sirringhaus *et al.*, *Nature (London)* **401**, 685 (1999).
 - [5] M. Setvin, C. Franchini, X. Hao, M. Schmid, A. Janotti, M. Kaltak, C. G. Van de Walle, G. Kresse, and U. Diebold, *Phys. Rev. Lett.* **113**, 086402 (2014).
 - [6] X. Hao, Z. Wang, M. Schmid, U. Diebold, and C. Franchini, *Phys. Rev. B* **91**, 085204 (2015).
 - [7] T. Holstein, *Ann. Phys. (N.Y.)* **8**, 325 (1959).
 - [8] J. Vlietinck, W. Casteels, K. Van Houcke, J. Tempere, J. Ryckebusch, and J. T. Devreese, *New J. Phys.* **17**, 033023 (2015).

- [9] W. Meevasana, X. J. Zhou, B. Moritz, C.-C. Chen, R. H. He, S.-I. Fujimori, D. H. Lu, S.-K. Mo, R. G. Moore, F. Baumberger, T. P. Devereaux, D. van der Marel, N. Nagaosa, J. Zaanen and Z.-X. Shen, *New Journal of Physics* **12**, 023004 (2010).
- [10] J. L. M. van Mechelen, D. van der Marel, C. Grimaldi, A. B. Kuzmenko, N. P. Armitage, N. Reyren, H. Hagemann, and I. I. Mazin, *Phys. Rev. Lett.* **100**, 226403 (2008).
- [11] J. T. Devreese, S. N. Klimin, J. L. M. van Mechelen, and D. van der Marel, *Phys. Rev. B* **81**, 125119 (2010).
- [12] A. S. Mishchenko, N. V. Prokof'ev, A. Sakamoto, and B. V. Svistunov, *Phys. Rev. B* **62**, 6317 (2000).
- [13] A. S. Mishchenko, N. Nagaosa, N. V. Prokof'ev, A. Sakamoto, and B. V. Svistunov, *Phys. Rev. Lett.* **91**, 236401 (2003).
- [14] G. L. Goodvin, A. S. Mishchenko, and M. Berciu, *Phys. Rev. Lett.* **107**, 076403 (2011).
- [15] V. L. Gurevich, I. G. Lang, and Yu. A. Firsov, *Sov. Phys. Solid State* **4**, 918 (1962).
- [16] J. Devreese, W. Huybrechts, and L. Lemmens, *Phys. Status Solidi B* **48**, 77 (1971).
- [17] B. E. Sernelius, *Phys. Rev. B* **48**, 7043 (1993).
- [18] G. De Filippis, V. Cataudella, A. S. Mishchenko, C. A. Perroni, and J. T. Devreese, *Phys. Rev. Lett.* **96**, 136405 (2006).
- [19] S. N. Klimin and J. T. Devreese, *Phys. Rev. B* **89**, 035201 (2014).
- [20] J. Devreese, J. De Sitter, and M. Goovaerts, *Phys. Rev. B* **5**, 2367 (1972).
- [21] R. P. Feynman, R. W. Hellwarth, C. K. Iddings, and P. M. Platzman, *Phys. Rev.* **127**, 1004 (1962).
- [22] R. P. Feynman, *Phys. Rev.* **97**, 660 (1955).
- [23] S. I. Pekar, *Untersuchungen über die Elektronentheorie der Kristalle* (Akademie-Verlag, Berlin, 1954).
- [24] K. Huang and A. Rhys, *Proc. R. Soc. London, Ser. A* **204**, 406 (1950).
- [25] D. Sels and F. Brosens, *Phys. Rev. E* **89**, 012124 (2014).
- [26] D. Sels and F. Brosens, *Phys. Rev. E* **89**, 042110 (2014).
- [27] D. Sels, *arXiv:1605.04998* (2016).
- [28] V. Cataudella, G. De Filippis, and C.A. Perroni, "Single Polaron Properties in Different Electron-Phonon Models", in: *Polarons in Advanced Materials*, ed. by A. S. Alexandrov, Springer Series in Materials Science, Volume 103, 2007, pp. 149-189.

- [29] S. N. Klimin and J. T. Devreese, *Solid State Communications* **151**, 144 (2011).
- [30] S. J. Miyake, *J. Phys. Soc. Japan* **38**, 181 (1975).
- [31] F. M. Peeters and J. T. Devreese, *Phys. Rev. B* **28**, 6051 (1983).
- [32] H. Mori, *Prog. Theor. Phys.* **33**, 423 (1965); **34**, 399 (1965).
- [33] G. R. Allcock, in *Polarons and Excitons*, edited by C. G. Kuper and G. D. Whitfield (Oliver and Boyd, Edinburgh, 1963), pp. 45 – 70.
- [34] R. P. Feynman, *Phys. Rev.* **84**, 108 (1951).
- [35] E. Kartheuser, R. Evrard, and J. Devreese *Phys. Rev. Lett.* **22**, 94-97 (1969).
- [36] J. T. Devreese, in *Polarons in Ionic Crystals and Polar Semiconductors* (North-Holland, Amsterdam, 1972), pp. 83 – 159.

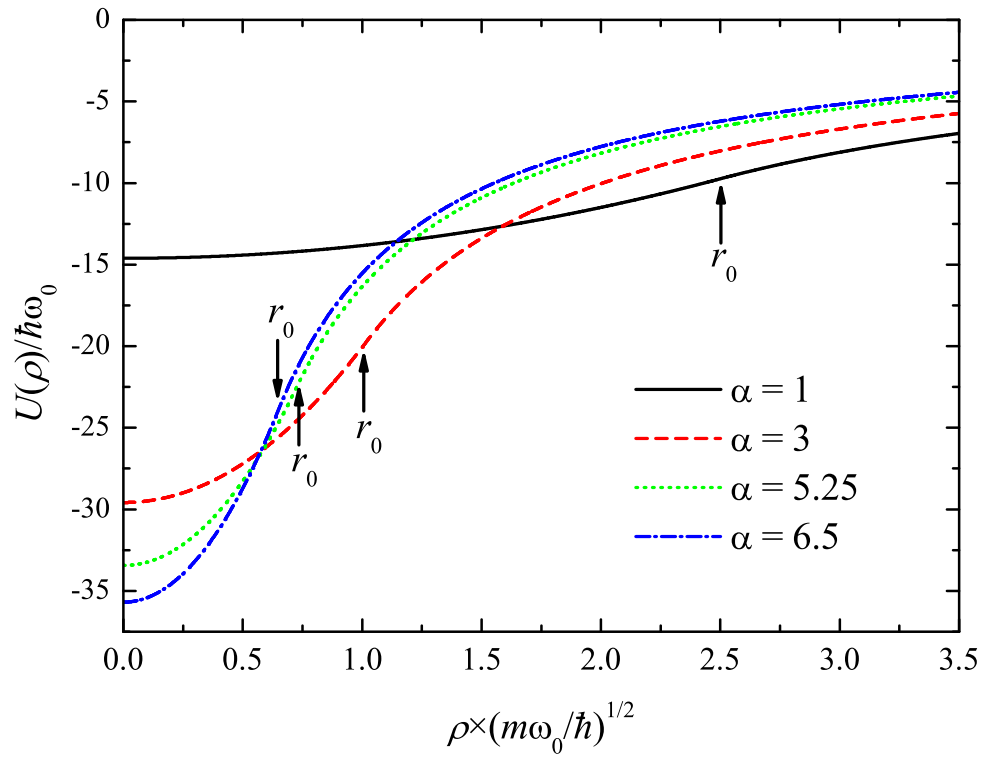


FIG. 26: Trial potential $U(\rho)$ calculated for parameters of the polaron model listed in Table V.

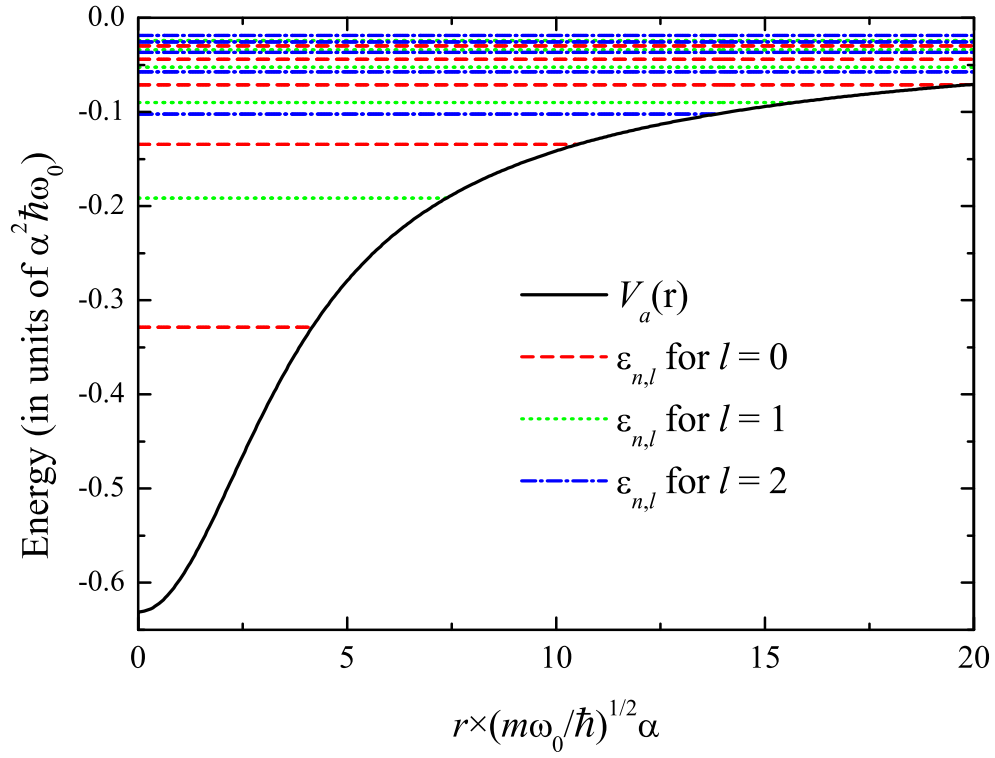


FIG. 27: Self-consistent potential $V_a(r)$ determined by (E27) and energy levels for a polaron in the strong-coupling regime at $\alpha = 15$.

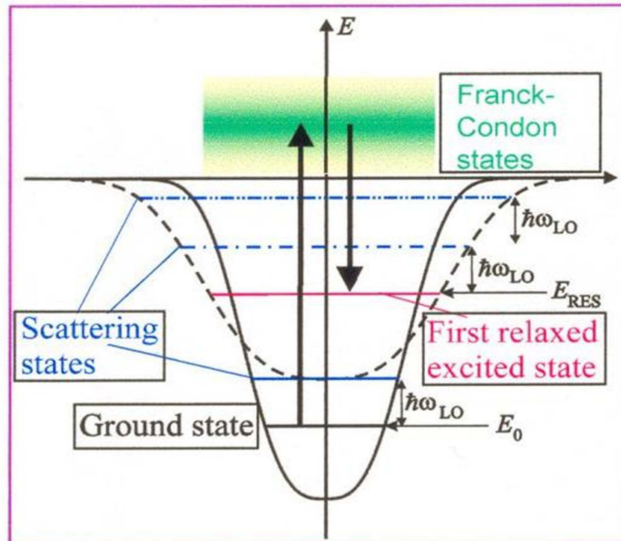


FIG. 28: Structure of the energy spectrum of a polaron at strong coupling.

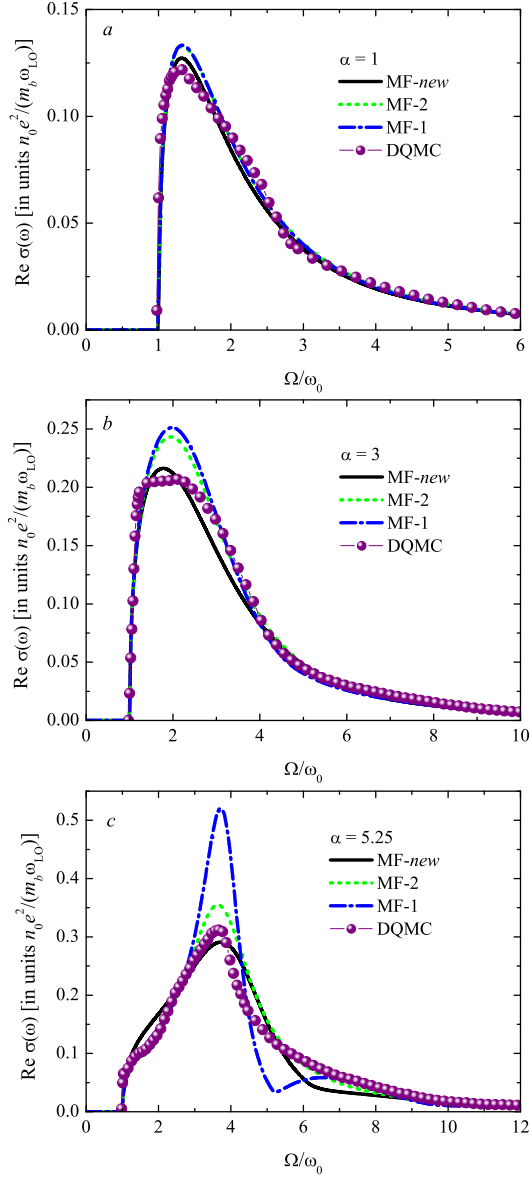


FIG. 29: Polaron optical conductivity calculated for $\alpha = 1$ (a), $\alpha = 3$ (b) and $\alpha = 5.25$ (c) within the present non-quadratic MF formalism (denoted in the figure as MF-*new*), compared with the polaron optical conductivity calculated within the extended memory-function formalism (MF-2) of Ref. [18], the results of the memory-function approach using the Feynman parabolic trial action [20] (MF-1), and the diagrammatic quantum Monte Carlo (DQMC) [13, 18].

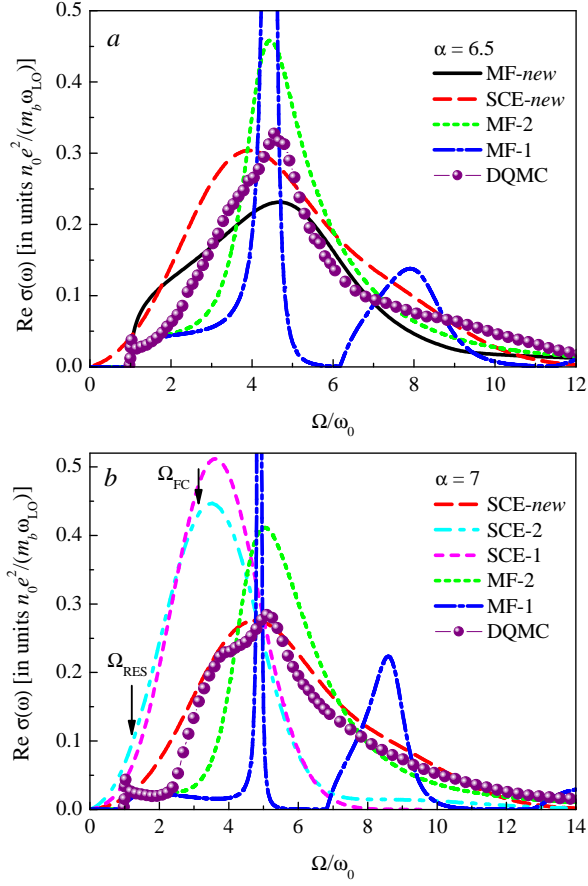


FIG. 30: Polaron optical conductivity calculated for $\alpha = 6.5$ (a) and $\alpha = 7$ (b) using different analytic approaches: the non-quadratic MF formalism (MF-*new*), the extended memory-function formalism of Ref. [18] (MF-2), the memory-function approach with the Feynman parabolic trial action [20] (MF-1), the non-adiabatic strong-coupling expansion (denoted at the figure as SCE-*new*), the adiabatic strong-coupling expansions of Refs. [18, 19] (SCE-1 and SCE-2). The results are compared to DQMC data of Refs. [13, 18].

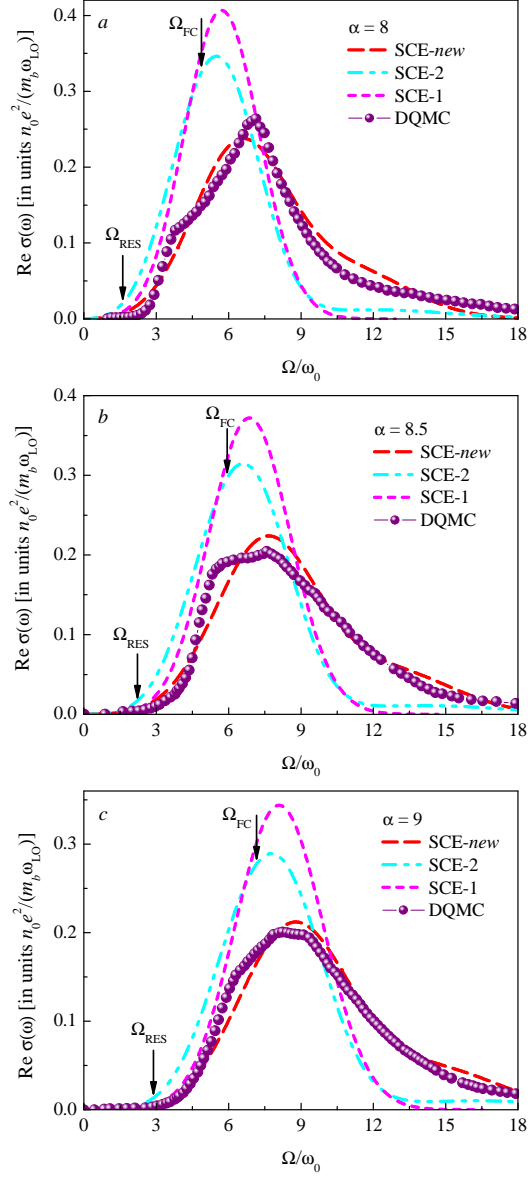


FIG. 31: Polaron optical conductivity calculated for $\alpha = 8$ (a), $\alpha = 8.5$ (b) and $\alpha = 9$ (c) within several analytic strong coupling approaches and compared to DQMC data of Refs. [13, 18]. The notations are the same as in Fig. 30.

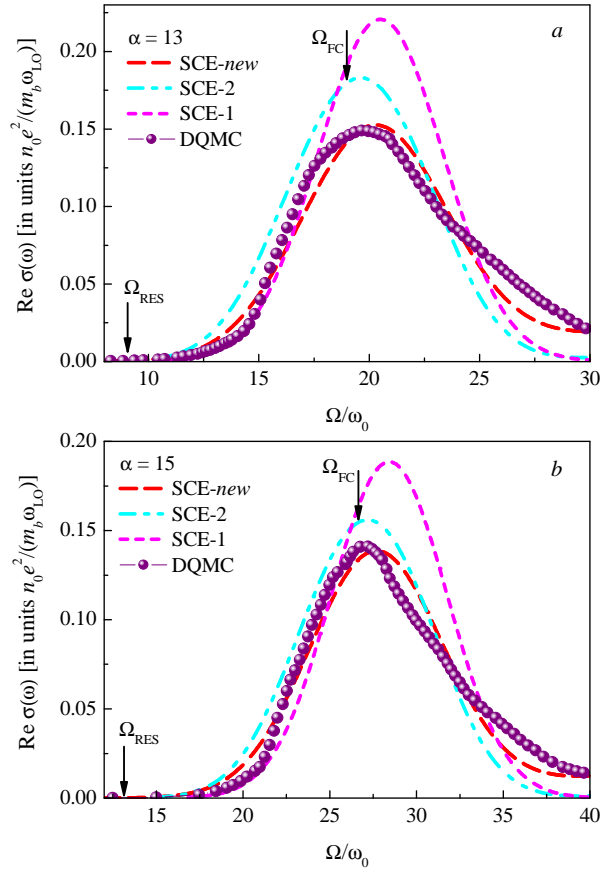


FIG. 32: Polaron optical conductivity in the extremely strong coupling regime, for $\alpha = 13$ (a) and $\alpha = 15$ (b). The notations are the same as in Fig. 30.

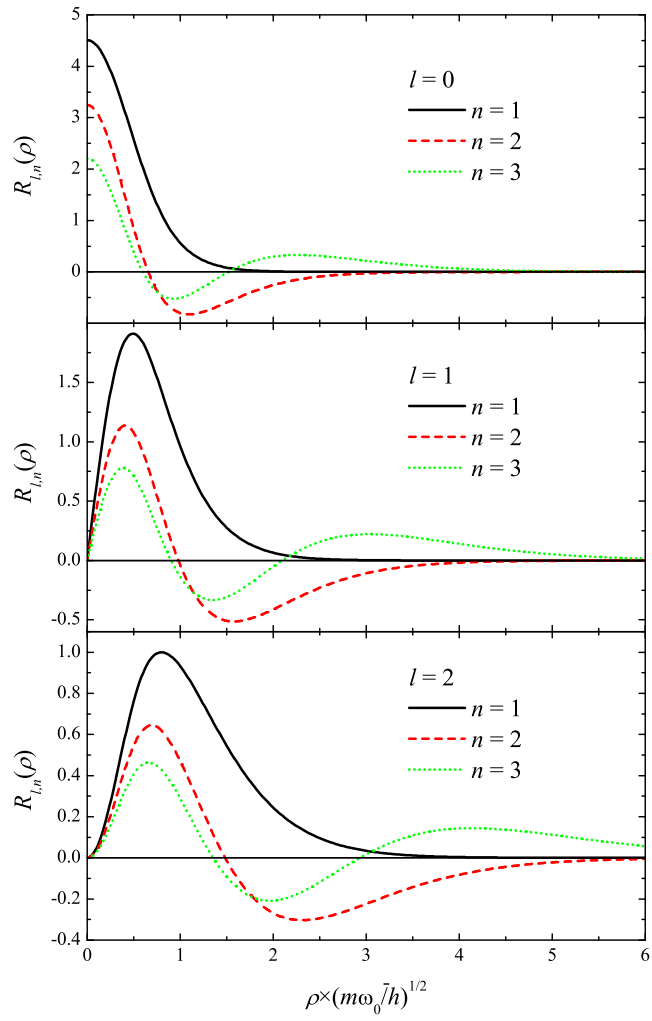


FIG. 33: Radial wave functions $\mathcal{R}_{l,n}(\rho)$ calculated for several values of the quantum numbers l, n .

Appendix F: Diagrammatic Monte Carlo study of the Fröhlich polaron dispersion in 2D and 3D [*T. Hahn, S. N. Klimin, J. Tempere, J. T. Devreese, and C. Franchini, Phys. Rev. B 97, 134305 (2018)*]

1. Introduction

Ever since the emergence of polaron theory in the 1930s [1]¹⁰, the concept of polarons has been applied to a wide variety of physical systems in which a particle is coupled to its environment, e.g. spin or magnetic polarons [2], exciton polarons [3], BEC-impurity polarons [4], ripplonic polaron [5] etc. The polaron problem in its original form considers a single electron in a polar crystal interacting with the surrounding lattice. Due to Coulomb forces, the electron distorts the ions in its neighbourhood, which creates a polarization that follows the electron as it moves through the crystal. This generated polarization acts back on the electron and so renormalizes electronic properties. The resulting quasiparticle consisting of the electron surrounded by the distorted lattice was termed a “polaron”. Nowadays (cf. the review by Alexandrov and Devreese [6]) a more quantum mechanical picture of a polaron is used in which the electron dresses itself with a cloud of phonons.

Polarons may be classified according to the strength of the electron-phonon coupling (weak/strong) and the extension of the lattice distortion around the electron (small/large) [6, 7]. Weak-coupling polarons dress themselves with only a small number of phonons $\bar{N} \ll 1$ leading to a slightly enhanced effective mass compared to the “bare” electron ($m_* - m \ll m$). Strong-coupling polarons have more phonons in the cloud $\bar{N} \gg 1$ and a much larger effective mass $m_*/m \gg 1$. By \bar{N} we denote the average number of phonons in the cloud, m_* is the effective mass of the polaron and m the mass of the “bare” electron without coupling. Furthermore, a polaron is called a small polaron when the lattice distortion induced by the electron is of the same size as the lattice constant and a large polaron when the distortion extends over several lattice sites. Typically, the description of small polarons requires the treatment of short-range electron-phonon interaction and an explicit account of the lattice periodicity. Instead, the theory of large polarons assumes long-range forces and relies on the continuum approximation.

¹⁰The bibliography to this section is in a separate list.

Studies of polarons are historically conducted in the framework of quantum field theory using effective quantum Hamiltonians [8, 9]. More recently, first principles methods based on density functional theory turned out to provide an accurate microscopic description of both large and small polarons [10, 11]. The most famous model Hamiltonians go back to the 1950s to Fröhlich [8] and Holstein [9]. Both contain a term for a free particle H_e , a free phonon field H_{ph} and for the particle-phonon interaction $H_{e\text{-ph}}$. While the Holstein Hamiltonian models small polarons, the Fröhlich Hamiltonian, which is the focus of the present study, describes large polarons and is given as

$$H = H_e + H_{\text{ph}} + H_{e\text{-ph}}, \quad (\text{F1})$$

$$H_e = \sum_{\mathbf{k}} \frac{k^2}{2} a_{\mathbf{k}}^\dagger a_{\mathbf{k}}, \quad (\text{F2})$$

$$H_{\text{ph}} = \sum_{\mathbf{q}} b_{\mathbf{q}}^\dagger b_{\mathbf{q}}, \quad (\text{F3})$$

$$H_{e\text{-ph}} = \sum_{\mathbf{k}, \mathbf{q}} \left[V_d(\mathbf{q}) b_{\mathbf{q}}^\dagger a_{\mathbf{k}-\mathbf{q}}^\dagger a_{\mathbf{k}} + V_d^\dagger(\mathbf{q}) b_{\mathbf{q}} a_{\mathbf{k}+\mathbf{q}}^\dagger a_{\mathbf{q}} \right]. \quad (\text{F4})$$

Here $a_{\mathbf{k}}$ and $b_{\mathbf{q}}$ are destruction operators for a particle with wave vector \mathbf{k} and a phonon with wave vector \mathbf{q} , respectively. $V_d(\mathbf{q})$ is the coupling function for a system in d dimensions and takes the form

$$V_3(\mathbf{q}) = i \left(\frac{2\sqrt{2}\pi\alpha}{A} \right)^{\frac{1}{2}} \frac{1}{q} \quad (\text{F5})$$

in 3 dimensions and

$$V_2(\mathbf{q}) = i \left(\frac{\sqrt{2}\pi\alpha}{A} \right)^{\frac{1}{2}} \frac{1}{\sqrt{q}} \quad (\text{F6})$$

in 2 dimensions [12]. In Eq. F5 and F6, A is the d -dimensional volume of the system and α is the coupling constant which is material dependent and determines the strength of the electron-phonon interaction. Typical values for real materials are in the range $0 < \alpha < 5$ [13]. Units are chosen such that energy is measured in units of $\hbar\omega_0$ and length in units of $\sqrt{\hbar/m\omega_0}$ which leads to $\hbar = \omega_0 = m = 1$. In deriving and solving the Fröhlich Hamiltonian, it is a common practice to assume certain approximations: (i) the energy dispersion for the electron is parabolic with a band mass m , (ii) the phonon frequency $\omega(\mathbf{q}) = \omega_0$ is dispersionless and constant, (iii) the interaction is only between the electron and long-wavelength optical, longitudinal phonons and (iv) the spatial extension of the polaron is larger than the lattice constant. In this paper, we exclusively focus on the Fröhlich model and we study the polaron

dispersion law, i.e. the dependence of the ground-state energy $E_0(k, \alpha)$ on the modulus of the total polaron momentum $k = |\mathbf{k}|$.

A large body of work [6] exists on solving the Fröhlich Hamiltonian, and most of it concerns the energy of the polaron at rest, $E_0(0, \alpha)$. Yet, so far no exact analytic solution was found. The most successful approach to calculate $E_0(0, \alpha)$ is Feynman's path integral formalism [14, 15], a variational treatment that provides a very accurate upper bound for the polaron ground state energy for all coupling strengths as well as approximate values for the polaron effective mass. Early work on the behavior of the dispersion curve [16, 17] allowed to conclude that the energy-momentum relation starts off quadratically at low k (thus allowing to define a polaron mass) but bends over when approaching the continuum edge $E_c(\alpha) = E_0(0, \alpha) + \hbar\omega_0$. Later it was found that in 3D the dispersion hits the continuum edge whereas for 2D it approaches it asymptotically, and upper and lower bounds for the dispersion were obtained [18–20]. These bounds, as well as some analytically known limits, constitute good benchmarks for any theory of the polaron dispersion.

More recently, the Diagrammatic Monte Carlo method (DMC) was developed and applied to the 3-dimensional Fröhlich polaron [21, 22]. It makes use of diagrammatic expansions of Green's functions and a Metropolis sampling algorithm to perform a random walk in the space of all Feynman diagrams. The DMC not only allows for the calculation of the ground state energies but as well as the polaron dispersion curves, Z-factors (quasiparticle weights) and phonon statistics. However, the DMC results [21, 22] were criticized [19, 20]: the reported results disagree with the analytically known second order coefficient in α for the polaron ground state energy, as well as the large- α expansion coefficient.

The aim of the present paper is the application of our newly implemented DMC code to the solution of the Fröhlich Hamiltonian in both the 3-dimensional (3D) and the 2-dimensional (2D) case. To our knowledge, there do not exist any DMC results for the 2D Fröhlich polaron in the literature. We find that the present DMC results, both in 2D and 3D, agree with the analytically known limits, thus refuting the critique of the DMC method formulated in [19, 20]. In addition, we compare the obtained dispersion relations with analytic upper and lower bounds (where available) and a fitting function [20].

The structure of the paper is as follows. The DMC program is based on the seminal works of Prokof'ev [21] and Mishchenko [22], and is described in Sec. F 2. The numerical outcome is presented and discussed in Sec. F 3. We first benchmark our results for the 3D

case with the reference data of Prokof'ev *et al.* [21] and Mishchenko *et al.* [22] as well as with results obtained from Feynman's path integral approach [15]. Furthermore, we show ground state energies $E_0(0, \alpha)$, polaron dispersions $E_0(k, \alpha)$ and effective masses $m_*(\alpha)$ for the 2D Fröhlich polaron and compare them to various scaling relations derived by Peeters and Devreese [23]. We also provide values for the exactly known weak- and strong coupling coefficients. Finally, conclusive remarks are drawn in Sec. F 4.

2. Theory and Methodology

In this section, we introduce the concepts of many-body Green's functions, diagrammatic expansions and corresponding Feynman diagrams as well as the basic concepts of the Diagrammatic Monte Carlo method. Necessary computational details of our code are also given in this section.

a. Green's functions and Feynman diagrams

To solve the Fröhlich Hamiltonian from Eq. F1 for the lowest energy eigenvalues, we make use of the Green's function formalism from many-body physics. In particular, we are interested in the one-electron- N -phonon Green's function in the momentum $(\mathbf{k}, \tilde{\mathbf{q}}_i)$ - imaginary time (τ) representation at zero-temperature, where we assume $\tau > 0$:

$$G^{(N)}(\mathbf{k}, \tau, \{\tilde{\mathbf{q}}_i\}) = \langle 0 | b_{\tilde{\mathbf{q}}_N}(\tau) \dots b_{\tilde{\mathbf{q}}_1}(\tau) a_{\mathbf{k}_1}(\tau) a_{\mathbf{k}_1}^\dagger(0) b_{\tilde{\mathbf{q}}_1}^\dagger(0) \dots b_{\tilde{\mathbf{q}}_N}^\dagger(0) | 0 \rangle. \quad (\text{F7})$$

The ket $|0\rangle$ in Eq. F7 is the electron and phonon vacuum state [24] and the operators are in the Heisenberg picture $a_{\mathbf{k}}(\tau) = e^{\tau H} a_{\mathbf{k}} e^{-\tau H}$. The total or polaron wave vector is given by $\mathbf{k} = \mathbf{k}_1 + \sum_i \tilde{\mathbf{q}}_i$ and is a conserved quantity [8].

By adding a complete set of polaron eigenstates $|\beta(\mathbf{k})\rangle$ to Eq. F7, with $H |\beta(\mathbf{k})\rangle = E_\beta(\mathbf{k}) |\beta(\mathbf{k})\rangle$ and $H |0\rangle = E_v |0\rangle = 0$, the Green's function becomes

$$\begin{aligned} G^{(N)}(\mathbf{k}, \tau, \{\tilde{\mathbf{q}}_i\}) &= \sum_{\beta} |\langle \beta(\mathbf{k}) | a_{\mathbf{k}_1}^\dagger b_{\tilde{\mathbf{q}}_1}^\dagger \dots b_{\tilde{\mathbf{q}}_N}^\dagger | 0 \rangle|^2 e^{-(E_\beta(\mathbf{k}) - E_v)\tau} \\ &= \sum_{\beta} Z_{\beta}^{(N)}(\mathbf{k}, \{\tilde{\mathbf{q}}_i\}) e^{-E_\beta(\mathbf{k})\tau}. \end{aligned} \quad (\text{F8})$$

The $Z_\beta^{(N)}$ -factor measures the squared overlap between the polaron eigenstate $|\beta(\mathbf{k})\rangle$ and a state with one free electron and N free phonons. If $\tau \rightarrow \infty$, Eq. F8 shows that the term which contains the state with the lowest energy eigenvalue $E_0(\mathbf{k})$ is the dominant one in the sum. Therefore it is possible to retrieve $E_0(\mathbf{k})$ and the corresponding $Z_0^{(N)}(\mathbf{k}, \{\tilde{\mathbf{q}}_i\})$ -factor for given \mathbf{k} and $\{\tilde{\mathbf{q}}_i\}$ values from the asymptotic behaviour of the Green's function at long imaginary-times:

$$G^{(N)}(\mathbf{k}, \tau \rightarrow \infty, \{\tilde{\mathbf{q}}_i\}) = Z_0^{(N)}(\mathbf{k}, \{\tilde{\mathbf{q}}_i\}) e^{-E_0(\mathbf{k})\tau}. \quad (\text{F9})$$

To calculate $G^{(N)}$, we expand the Green's function in a perturbation series [25]. Formally, this leads to an expression of the form

$$G^{(N)}(\mathbf{k}, \tau, \{\tilde{\mathbf{q}}_i\}) = \sum_{n=0}^{\infty} \sum_{\xi_n} \int \cdots \int \mathcal{D}_{n,\xi_n}(\mathbf{k}, \tau, \{\tilde{\mathbf{q}}_i\}; \mathbf{x}) d\mathbf{x}, \quad (\text{F10})$$

where n labels the order of the perturbation expansion, ξ_n indexes different terms of the same order and $\mathbf{x} = (\tau_1, \dots, \tau_n, \mathbf{q}_1, \dots, \mathbf{q}_k)$ is a vector of integration variables (times of interaction vertices and internal phonon wave vectors). Note the difference between external phonon wave vectors $\{\tilde{\mathbf{q}}_i\}$ appearing in the definition of $G^{(N)}$ and internal phonon wave vectors $\{\mathbf{q}_i\}$ over which is integrated. The integrands \mathcal{D}_{n,ξ_n} are given as a product of free electron Green's functions $G_0(\mathbf{k}, \tau_i - \tau_j)$, free phonon Green's functions $W_0(\mathbf{q}, \tau_i - \tau_j)$ and squared interaction vertices $|V_d(\mathbf{q})|^2$. With the following simple rules it is possible to map all \mathcal{D}_{n,ξ_n} functions to Feynman diagrams:

$$G_0(\mathbf{k}, \tau_i - \tau_j) = e^{-k^2/2(\tau_i - \tau_j)}, \quad (\text{F11})$$

$$W_0(\mathbf{q}, \tau_i - \tau_j) = e^{-\omega_0(\tau_i - \tau_j)}, \quad (\text{F12})$$

$$|V_d(\mathbf{q})|^2 = \frac{(d-1)\sqrt{2}\pi\alpha}{Aq^{d-1}}. \quad (\text{F13})$$

This allows us to write the Green's function as an infinite series over Feynman diagrams. Odd orders in the perturbation series evaluate to zero because phonon operators appear linear in the interaction term of the Hamiltonian (Eq. F4). A typical diagram is presented in Fig. 34. It shows a 8th-order diagram of $G^{(2)}(\mathbf{k}, \tau, \tilde{\mathbf{q}}_1, \tilde{\mathbf{q}}_2)$. All diagrams of $G^{(N)}$ have N external phonon propagators attached to the diagram end. The rules from Eq. F11 - F13 can be used to translate a diagram back into its functional form. Integration has to be performed over all internal phonon wave vectors $\{\mathbf{q}_i\}$ and over all times $\{\tau_i\}$ so that their chronological order is maintained, e.g. $0 < \tau_1 < \tau_2 < \dots < \tau_8 < \tau$ in Fig. 34. The total wave

vector \mathbf{k} is always conserved at interaction vertices. For example, the electron propagator between τ_1 and τ_2 in Fig. 34 must have the wave vector $\mathbf{k}_2 = \mathbf{k}_1 + \tilde{\mathbf{q}}_1$ so that $\mathbf{k} = \mathbf{k}_2 + \tilde{\mathbf{q}}_2$.

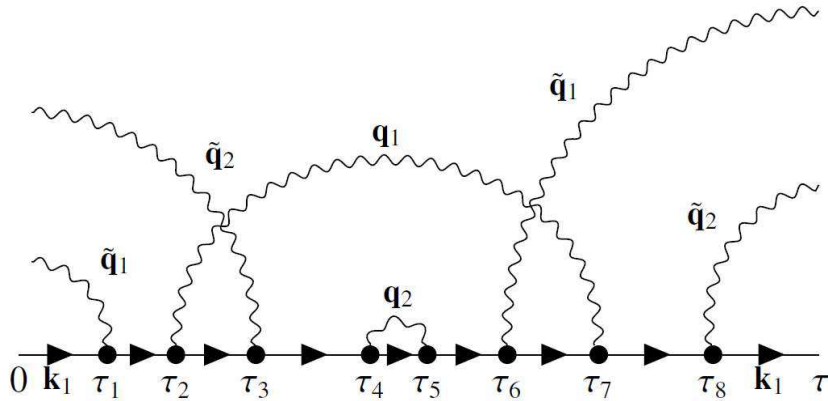


FIG. 34: 8th-order diagram for $G^{(2)}(\mathbf{k}, \tau, \tilde{\mathbf{q}}_1, \tilde{\mathbf{q}}_2)$. Note that diagrams in the expansion of $G^{(2)}$ have two phonon propagators attached to the diagram end. The total polaron wave vector $\mathbf{k} = \mathbf{k}_1 + \tilde{\mathbf{q}}_1 + \tilde{\mathbf{q}}_2$ is conserved at the vertices.

Expressing the Green's function in terms of Feynman diagrams doesn't solve the problem. It merely is a way to rewrite the expansion in a more accessible way. It is still necessary to sum the infinite series of integrals from Eq. F10.

b. Diagrammatic Monte Carlo

In Ref. [21, 22, 26] it was shown how to use the DMC method to numerically calculate a function $Q(\{y\})$ which is given in a diagrammatic expansion of the form

$$Q(\{y\}) = \sum_{n=0}^{\infty} \sum_{\xi_n} \int \cdots \int \mathcal{D}_{n, \xi_n}(\{y\}; x_1, \dots, x_n) dx_1 \dots dx_n. \quad (\text{F14})$$

The overall idea behind the DMC method is to interpret $Q(\{y\})$ as a distribution function for the external variables $\{y\}$ [21]. It then uses a Markov chain Monte Carlo (MCMC) procedure to simulate $Q(\{y\})$ by generating diagrams stochastically. This is achieved with a Metropolis-Hastings update scheme to accept or reject new diagrams in which the numerical values of \mathcal{D}_{n, ξ_n} serve as statistical weights. The function $Q(\{y\})$ is obtained by collecting statistics for the external variables $\{y\}$, e.g. in the form of a histogram. At the heart of the DMC algorithm are updates that allow the Markov chain to explore the whole space

of Feynman diagrams, i.e. the Markov chain has to be ergodic. It is therefore necessary to implement updates which change the order n , the topology ξ_n , external variables $\{y\}$ and internal variables x_i . Details on basic updating procedures and acceptance probabilities can be found in the Refs. [21, 22, 26, 27].

```

Input: initial diagram  $\mathcal{D}^{(0)} \leftarrow (\{y^{(0)}\}; x_1^{(0)}, \dots, x_n^{(0)}, n^{(0)}, \xi_n^{(0)})$ ,
        update procedures  $\{U_1, \dots, U_k\}$ ,
        update probabilities  $\{p(U_1), \dots, p(U_k)\}$ ;
Output: histogram of  $Q(\{y\})$ ;

initialize histogram[];
initialize diagram  $\mathcal{D}_{cur} \leftarrow \mathcal{D}^{(0)}$ ;
while not converged do
    choose an update  $U_i$  from  $\{U_1, \dots, U_k\}$  with probability  $p(U_i)$ ;
    propose a new diagram  $\mathcal{D}_{new} \leftarrow (\{y'\}; x'_1, \dots, x'_{n'}, n', \xi'_{n'})$  ac-
    cording to  $U_i$ ;
    calculate acceptance ratio  $R$ ;
    draw random uniform number  $r$ ;
    if  $R \geq r$  then
        accept the proposed diagram:  $\mathcal{D}_{cur} \leftarrow \mathcal{D}_{new}$ ;
    else
        reject the proposed diagram:  $\mathcal{D}_{cur} \leftarrow \mathcal{D}_{cur}$ ;
    end if
    histogram[ $\{y\}$ ]  $\leftarrow$  histogram[ $\{y\}$ ] + 1;
end while
return histogram;

```

FIG. 35: General workflow of the DMC algorithm. The algorithm returns the histogram of the function $Q(\{y\})$.

A general workflow of a DMC application is sketched in Fig. 35. Necessary requirements are a diagrammatic expansion of $Q(\{y\})$, updates $\{U_1, \dots, U_k\}$ and probabilities $\{p(U_1), \dots, p(U_k)\}$ with which the updates are chosen. The current diagram in each step is denoted by \mathcal{D}_{cur} and characterized by its parameters values $\mathbf{z} = (\{y\}; x_1, \dots, x_n, n, \xi_n)$. The proposed diagram is called \mathcal{D}_{new} with new parameters $\mathbf{z}' = (\{y'\}; x'_1, \dots, x'_{n'}, n', \xi'_{n'})$. At the beginning, an initial diagram $\mathcal{D}^{(0)}$, e.g. a free electron propagator, is defined and the grid for the histogram is generated. During each Monte Carlo step an update U_i gets selected with probability $p(U_i)$. The update U_i proposes a new diagram \mathcal{D}_{new} by changing one or more of the current parameters of \mathbf{z} to \mathbf{z}' . Then a Metropolis-Hastings accept/reject step is

performed with the following acceptance ratio (detailed balance is assumed)

$$R = \frac{p(U_i^\dagger) \mathcal{D}_{new} P(\mathbf{z}' \rightarrow \mathbf{z})}{p(U_i) \mathcal{D}_{cur} P(\mathbf{z} \rightarrow \mathbf{z}')}, \quad (\text{F15})$$

where $p(U_i^\dagger)$ is the probability of selecting the inverse update U_i^\dagger of U_i and $P(\mathbf{z} \rightarrow \mathbf{z}')$ is an arbitrary probability density from which the new parameters \mathbf{z}' are chosen. If $R \geq r$, where r is a uniform random number, \mathcal{D}_{new} is accepted otherwise rejected. Finally, the histogram at position $\{y\}$ is updated. These steps are repeated until convergence is achieved. Normalizing the resulting histogram leads to an estimation for $Q(\{y\})$.

c. DMC for the Fröhlich polaron

With the general procedure of the DMC algorithm at hand, it is fairly easy to apply it to the Fröhlich polaron. Comparing Eq. F10 with F14 leads to the following identifications:

- (i) $Q \leftrightarrow G^{(N)}$
- (ii) $\{y\} \leftrightarrow \{\mathbf{k}, \tau, \{\tilde{\mathbf{q}}_i\}\}$
- (iii) $\{x_1, \dots, x_n\} \leftrightarrow \{\tau_1, \dots, \tau_n, \mathbf{q}_1, \dots, \mathbf{q}_k\}$

The most straightforward way to obtain the lowest energy eigenvalues $E_0(k, \alpha)$ of the Fröhlich Hamiltonian for a given \mathbf{k} and α with the DMC method is to simulate $G^{(0)}(\mathbf{k}, \tau)$ and fit an exponential function to its long imaginary time behaviour, as can be seen in Eq. F9. This was done in the original paper by Prokof'ev [21].

Mishchenko *et al.* [22] provided some improvements to this method. They simulated all $G^{(N)}(\mathbf{k}, \tau, \{\tilde{\mathbf{q}}_i\})$ up to some maximum value $N < N_{max}$ in a single run. It allowed them to introduce direct Monte Carlo estimators for the energy, effective mass, group velocity and Z-factors and to obtain results up to $\alpha = 20$.

In the present paper, we follow the approach by Mishchenko using estimators for the energy $e_{est}(\mathcal{D})$ and inverse effective polaron mass $m_{est}(\mathcal{D})$ making the curve fitting procedure obsolete. A detailed exposition of the workflow can be found in Fig. 36. Values for the coupling constant α and the polaron wave vector \mathbf{k} are defined as inputs before the simulation starts. The parameter μ is used as part of a guiding function of the form $e^{\mu\tau}$ to improve

the sampling in τ -space. In practice this means that each diagram is multiplied by $e^{\mu\tau}$ or simply by changing the value of the free electron Green's function to

$$G_0(\mathbf{k}, \tau_i - \tau_j, \mu) = e^{-(k^2/2 - \mu)(\tau_i - \tau_j)}. \quad (\text{F16})$$

For our calculations, we set μ slightly smaller than the true ground state energy, as recommended in Ref. [21]. We also have specified maximum values for the diagram length τ_{max} , the order n_{max} and for the number of phonon propagators attached to the diagram end N_{max} . The value τ_{min} is used as a cut off, in the sense that we only accumulate estimators if the current diagram length τ is greater than τ_{min} . In our case, $\tau_{max} = 50$ and $\tau_{min} = 5$. Values for n_{max} and N_{max} are dependent on the coupling strength α , τ_{max} and μ and should be chosen sufficiently higher than the average diagram order and average number of external phonons per diagram. The most important ingredients are the updates U_i . We implemented updates for adding and removing internal as well as external phonon propagators, changing the diagram length τ , stretching the diagram as a whole, shifting a single vertex in imaginary time and swapping the phonon propagators of two adjacent vertices. All these updates and a derivation of the estimators are explained in detail in Ref. [22]. We only changed the arbitrary proposal probability distribution $P(\mathbf{z} \rightarrow \mathbf{z}')$ for some of the updates (see Eq. F15). Updates are addressed with the same probability $p(U_i) = p(U_j)$.

The basic concept is the same as in the general DMC algorithm, except that we accumulate estimators instead of a histogram (cf. Fig. 35 and 36). We start from an initial diagram $\mathcal{D}^{(0)}$. The accumulators for the energy E_0^{MC} and inverse effective mass m_*^{MC} as well as the counter c , for the number of diagrams with $\tau > \tau_{min}$, are set to zero. In the main loop, an update U_i is chosen with probability $p(U_i)$ and a new diagram \mathcal{D}_{new} is proposed. It is accepted with probability $\min\{1, R\}$. After the accept/reject step, we check if the current diagram length is greater than τ_{min} . If $\tau > \tau_{min}$, c is increased by 1 and the energy and inverse effective mass estimator for the current diagram \mathcal{D}_{cur} are accumulated. The effective mass is calculated near $\mathbf{k} = 0$ using the quadratic approximation:

$$m_*(\alpha) = \left[\frac{\partial^2 E_0(k, \alpha)}{\partial k^2} \right]_{k=0}^{-1}. \quad (\text{F17})$$

The loop is repeated until the energy and inverse effective mass estimates have converged. The final estimates are obtained by dividing the accumulators by c .

Input: initial diagram $\mathcal{D}^{(0)} \leftarrow (\mathbf{k}, \tau^{(0)}, \{\tilde{\mathbf{q}}_i^{(0)}\}; \{\tau_i^{(0)}\}, \{\mathbf{q}_i^{(0)}\}, n^{(0)}, \xi_n^{(0)})$,
 update procedures $\{U_1, \dots, U_k\}$,
 update probabilities $\{p(U_1), \dots, p(U_k)\}$,
 values for: α, μ, \mathbf{k} ,
 parameters: $\tau_{max}, \tau_{min}, n_{max}, N_{max}$;

Output: energy $E_0^{MC}(k, \alpha)$,
 inverse effective polaron mass $m_*^{MC}(\alpha)$;

initialize diagram $\mathcal{D}_{cur} \leftarrow \mathcal{D}^{(0)}$;
 $E_0^{MC} \leftarrow 0, m_*^{MC} \leftarrow 0$;
 $c \leftarrow 0$;

while not converged **do**
 choose an update U_i from $\{U_1, \dots, U_k\}$ with probability $p(U_i)$;
 propose a new diagram $\mathcal{D}_{new} \leftarrow (\mathbf{k}, \tau', \{\tilde{\mathbf{q}}'_i\}; \{\tau'_j\}, \{\mathbf{q}'_k\}, n', \xi'_{n'})$ according to U_i ;
 calculate acceptance ratio R ;
 draw random uniform number r ;
if $R \geq r$ **then**
 accept the proposed diagram: $\mathcal{D}_{cur} \leftarrow \mathcal{D}_{new}$;
else
 reject the proposed diagram: $\mathcal{D}_{cur} \leftarrow \mathcal{D}_{cur}$;
end if
if $\tau > \tau_{min}$ **then**
 $c \leftarrow c + 1$;
 $E_0^{MC} \leftarrow E_0^{MC} + e_{est}(\mathcal{D}_{cur})$;
 $m_*^{MC} \leftarrow m_*^{MC} + m_{est}(\mathcal{D}_{cur})$;
end if
end while
return $E_0^{MC}/c, m_*^{MC}/c$;

FIG. 36: Detailed workflow of the DMC algorithm as it was used in this paper. The algorithm returns estimates for the lowest eigenenergy $E_0(k, \alpha)$ and the inverse of the effective polaron mass $1/m_*(\alpha)$ for given \mathbf{k} and α values.

In Fig. 37, we reproduced some of the results from Ref. [22] to verify the correctness of our code. The top graph shows the polaron ground state energy and the bottom graph shows the logarithm of the effective mass as a function of α . Our data are in very good agreement with Mishchenko's data which lets us assume that our code gives reliable DMC results. The figure also displays results obtained with Feynman's variational treatment [15].

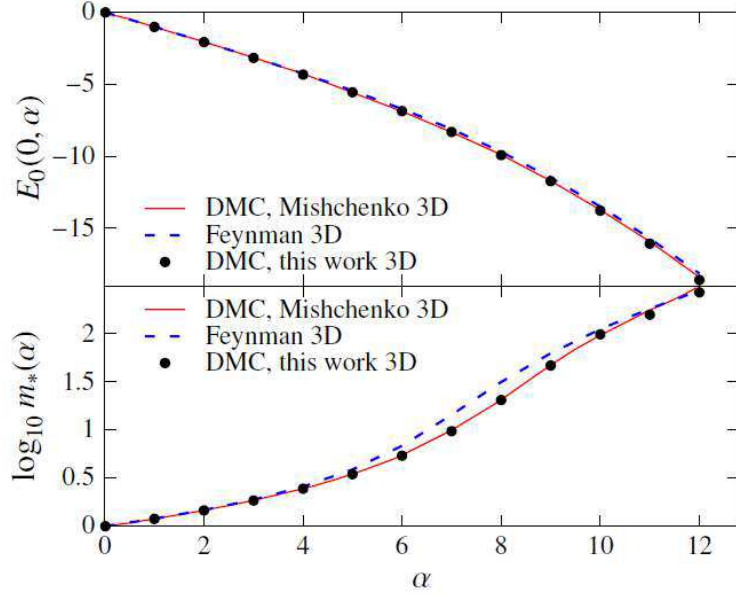


FIG. 37: Comparison of our results (circles) with previous DMC results by Mishchenko [22] (continuous lines) and with results obtained with Feynman’s approach [15] (dashed lines). The top graph shows the polaron ground state energy $E_0(0, \alpha)$ and the bottom graph the logarithm of the polaron effective mass $\log m_*(\alpha)$ as a function of α .

3. Results and discussion

In this section, we provide a more extensive discussion of the DMC results for the Fröhlich polaron in 3D and 2D. We show and discuss polaron ground state energies, effective polaron masses and polaron dispersions for different coupling strengths and prove that DMC correctly accounts for the 3D→2D scaling relations. All energies are given in units of $\hbar\omega_0$ and lengths in units of $\sqrt{\hbar/m\omega_0}$.

a. Polaron ground state energy and effective mass

We first focus on our results for the polaron ground state energy $E_0(0, \alpha)$ (Fig. 38), i.e. the minimum of the polaron energy band, and for the effective polaron mass $m_*(\alpha)$ (Fig. 39) as a function of α for 3D and 2D systems. Both cases are compared to Feynman’s approach [15] and with available DMC results in 3D [22] (Fig. 37). The corresponding numerical values are written in Table VI (3D) and Table VII (2D).

Feynman results in 2D have been obtained from the 3D results via scaling relations [23,

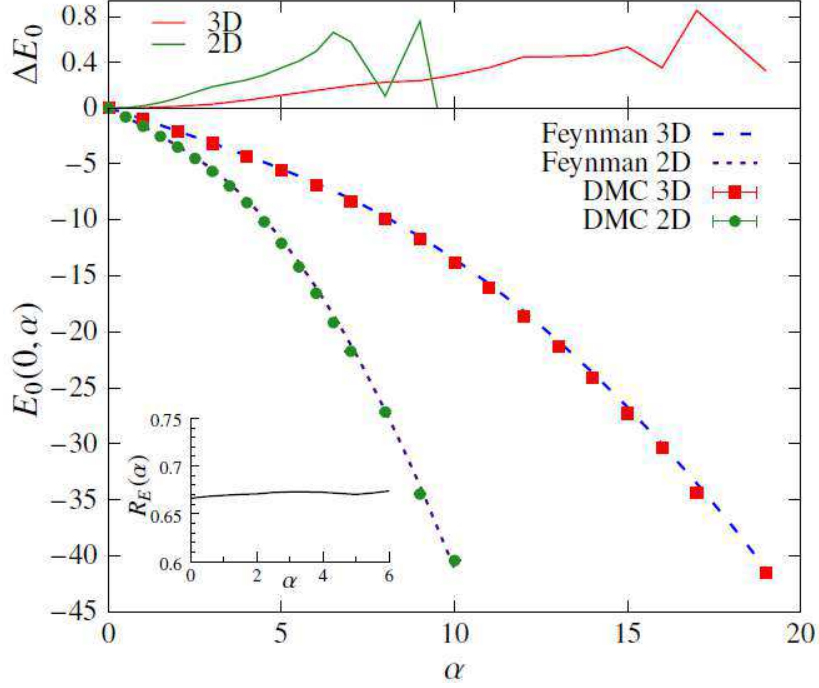


FIG. 38: Polaron energy $E_0(0, \alpha)$ as a function of the coupling constant α . The modulus of the total wave vector is $k = 0$. Results from the Feynman approach are shown as dashed lines. DMC results for 3D systems are depicted as squares and for 2D as circles. ΔE_0 is the difference between Feynman and DMC results. The inset shows the scaling ratio $R_E(\alpha) = E_0^{2D}(0, \alpha)/E_0^{3D}(0, 3\pi\alpha/4)$ between our 2D and 3D DMC results.

28, 29]. These scaling relations are exact for the Feynman polaron energy and Feynman polaron mass:

$$E_0^{2D}(0, \alpha) = \frac{2}{3}E_0^{3D}(0, 3\pi\alpha/4), \quad (\text{F18})$$

$$\frac{m_*^{2D}(\alpha)}{m^{2D}} = \frac{m_*^{3D}(3\pi\alpha/4)}{m^{3D}}. \quad (\text{F19})$$

For $\alpha = 0$ the polaron does not form and therefore $E_0 = 0$ and $m_*(0) = m$. As expected, with increasing electron-phonon coupling the polaron energy $E_0(0, \alpha)$ decreases and the effective mass increases as a consequence of the progressive localization of the polaron band. This effect is stronger in 2D than in 3D and explains the steeper curves in 2D.

Overall, our DMC data agree very well with the Feynman results in the entire range of coupling strength, in particular for what concerns the polaron energy (Fig. 38). The only sizeable deviation is observed for the effective mass in the intermediate coupling regime, for which Feynman's approach gives considerably higher values than the DMC (Fig. 39).

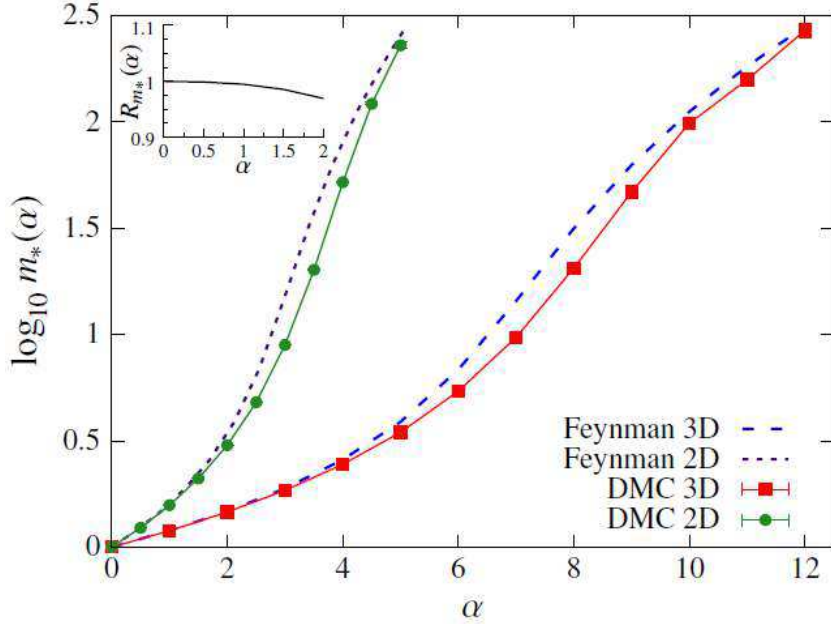


FIG. 39: Logarithm of the polaron effective mass $m_*(\alpha)$ as a function of the coupling constant α . Results from the Feynman approach are shown as dashed lines. DMC results for 3D systems are depicted as squares and for 2D as circles. The inset shows the scaling ratio $R_{m_*}(\alpha) = m_*^{2D}(\alpha)/m_*^{3D}(3\pi\alpha/4)$ between our 2D and 3D DMC results.

Both the DMC results and the variational results obey the scaling laws (F18) and (F19). This can be seen in the insets of Figs. 38 and 39 where we show the ratios $R_E(\alpha) = E_0^{2D}(0, \alpha)/E_0^{3D}(0, 3\pi\alpha/4)$ and $R_{m_*}(\alpha) = m_*^{2D}(\alpha)/m_*^{3D}(3\pi\alpha/4)$ between our DMC results in 2D and 3D. However, the uncertainty in the Monte Carlo calculations of m_*^{2D} for $\alpha > 2$ worsens the stability of the scaling relation of the effective mass at large α . The reason for this low performance is that the effective mass estimator actually calculates the inverse of the effective mass rather than the effective mass itself [22]. Since the polaron mass grows very fast with increasing coupling, its inverse becomes very small, which unavoidably worsens the accuracy of the results.

To test the accuracy of our calculations, we have also retrieved values for the exactly known weak-coupling coefficients q_1 and q_2

$$E_0(0, \alpha) = -q_1\alpha - q_2\alpha^2 + \mathcal{O}(\alpha^3) \quad (\text{F20})$$

and the strong-coupling coefficient γ

$$\lim_{\alpha \rightarrow \infty} E_0(0, \alpha)/\alpha^2 = -\gamma. \quad (\text{F21})$$

TABLE VI: Ground state energies $E_0(0, \alpha)$ and effective masses $m_*(\alpha)$ in 3D from the DMC and Feynman method [15]. Values in brackets stand for the uncertainty in the DMC simulation, e.g $-1.01662(47)$ has a sample standard error of 4.7×10^{-4} .

α	E_0 DMC	E_0 Feynman	m_* DMC	m_* Feynman
1	-1.01662(47)	-1.0130308	1.19396(2)	1.1955147
2	-2.06957(84)	-2.0553559	1.46166(7)	1.4718919
3	-3.16829(136)	-3.1333335	1.85047(13)	1.8889540
4	-4.32490(211)	-4.2564809	2.45196(57)	2.5793104
5	-5.55297(296)	-5.4401445	3.47194(180)	3.8856197
6	-6.86647(287)	-6.7108710	5.41952(625)	6.8383564
7	-8.31039(309)	-8.1126875	9.7130(268)	14.394070
8	-9.92206(606)	-9.6953709	20.55(14)	31.569255
9	-11.72535(701)	-11.485786	46.90(78)	62.751527
10	-13.7820(136)	-13.490437	98.8(3.3)	111.81603
11	-16.0660(127)	-15.709808	158.2(4.6)	183.12497
12	-18.5943(240)	-18.143395	270.1(20.0)	281.62189
13	-21.2434(249)	-20.790681	/	412.78190
14	-24.1151(369)	-23.651278	/	582.58390
15	-27.2629(359)	-26.724904	/	797.49838

The exact [19, 28] and DMC values for these coefficients, listed in Table VIII, are in very good agreement. However, a word of caution is needed here: the coefficients are obtained with a simple curve fitting procedure and the final numerical values are highly sensitive to the range of α values included in the fitting process. We have computed q_1 and q_2 using $\alpha < 0.85$ and $\alpha < 0.2$, in 3D and 2D respectively, whereas for γ we have included values in the range $9 \leq \alpha < 18$ (3D) and $4 \leq \alpha < 9$ (2D).

Gerlach, Kalina and Smondyrev [19] correctly point out that the (3D) second order perturbative result $q_2 = 0.0126$ obtained by Mishchenko using DMC [22] deviates from Röseler's [30] exact result $q_2 = 0.01592\dots$, but we surmise that they incorrectly concluded that the DMC results $E_0(0, \alpha)$ are incompatible with Röseler's results. Here, we resolve this

TABLE VII: Ground state energies $E_0(0, \alpha)$ and effective masses $m_*(\alpha)$ in 2D from the DMC and Feynman method [15]. Values in brackets stand for the uncertainty in the DMC simulation, e.g $-1.64348(23)$ has a sample standard error of 2.3×10^{-4} .

α	E_0 DQMC	E_0 Feynman	m_* DQMC	m_* Feynman
1	-1.64348(23)	-1.62321	1.57437(8)	1.59966
2	-3.48333(62)	-3.39482	3.01609(21)	3.40982
3	-5.66337(46)	-5.47667	8.94191(730)	15.2085
4	-8.45543(149)	-8.20738	52.108(341)	81.1684
5	-12.08288(610)	-11.7281	229.3(7.8)	257.452
6	-16.5403(269)	-16.0402	601.9(46.0)	609.244
7	-21.7231(566)	-21.1408	/	/
8	-27.1346(802)	-27.0283	/	/
9	-34.4669(370)	-33.7021	/	/
10	-40.4139(379)	-41.1602	/	/

TABLE VIII: Exactly known (exact) vs. calculated (calc.) expansion coefficients of $E_0(0, \alpha)$ for the weak- and strong coupling limit. The coefficients were obtained using different ranges of α in 2D and 3D. In 2D, we have included $\alpha < 0.2$ for computing q_1 and q_2 and $4 \leq \alpha < 9$ for γ . The corresponding 3D ranges are $\alpha < 0.85$ (q_1 and q_2) and $9 \leq \alpha < 18$ (γ).

	q_1 exact	q_1 calc.	q_2 exact	q_2 calc.	γ exact	γ calc.
3D	1.0	$0.9999 \pm 3.8 \times 10^{-4}$	0.01592	$0.01588 \pm 9.1 \times 10^{-4}$	0.1085	$0.10805 \pm 7.7 \times 10^{-4}$
2D	1.5708	$1.57084 \pm 1.7 \times 10^{-4}$	0.06397	$0.06483 \pm 2.8 \times 10^{-3}$	0.4047	$0.40236 \pm 3.8 \times 10^{-3}$

issue by providing the calculated DMC values explicitly, showing that there is no discrepancy. Both for the 3D and the 2D case, it can be seen in Table VIII that the DMC technique yields accurate estimates for q_2 , as well as for the other analytically known expansion coefficients q_1 and γ .

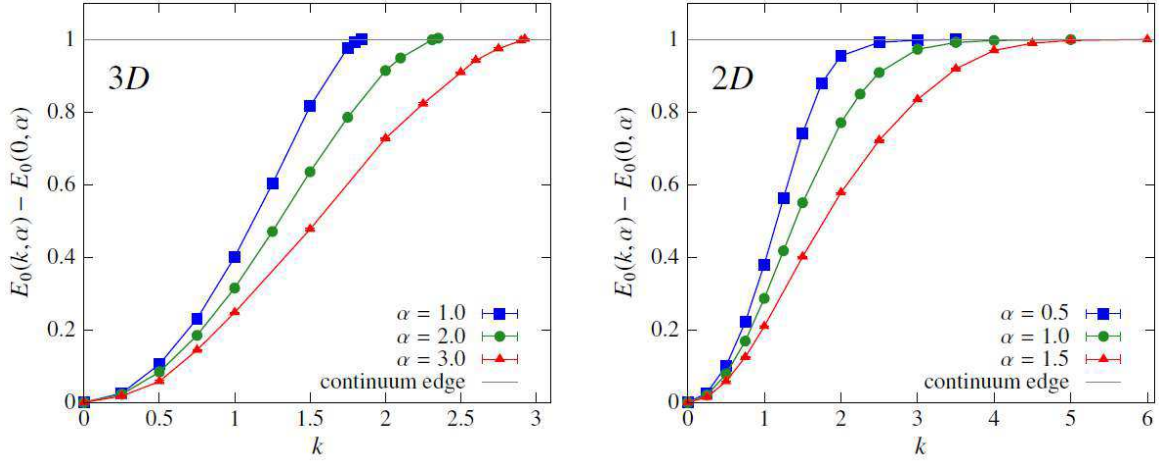


FIG. 40: Polaron energy $E_0(k, \alpha) - E_0(0, \alpha)$ as a function of the modulus of the total wave vector k in 3D (left, for coupling constants $\alpha = 1.0, 2.0$ and 3.0) and 2D (right, $\alpha = 0.5, 1.0$ and 1.5). The continuum edge is shown at $E_c(k) = 1$.

b. Polaron dispersion

In Fig. 40, we display some dispersion curves in 3D and 2D for selected values of α . The results have been shifted so that the ground state energy at $k = 0$ is $E_0(0, \alpha) = 0$. This makes a comparison between different α values easier. As expected, $E_0(k, \alpha)$ increases monotonically as a function of k and becomes more flat with increasing coupling. This reflects the tendency to form more localized bands as the electron-phonon coupling strength becomes stronger, an effect that is more intense in the more-localized 2D limit, where the dispersion curves bend over more sharply. Clearly, this behavior correlates with the polaron effective mass since it is defined as the inverse of the curvature of the energy band at $k = 0$ (see Fig. 39).

For large k , the energy curve approaches the so called "continuum edge" $E_c(\alpha)$ defined as the energy value:

$$E_c(\alpha) = E_0(0, \alpha) + \hbar\omega_0 = E_0(0, \alpha) + 1, \quad (\text{F22})$$

i.e. the energy value which is one phonon excitation quantum or unity (in our units) above the ground state energy. An important difference between the 3D and 2D case is that in 3D the dispersion curve crosses the continuum edge at a finite critical wave vector length $k_c(\alpha)$. Instead, in 2D, it has been proven that this edge constitutes an asymptote and is approximated from below as $k \rightarrow \infty$ [18–20].

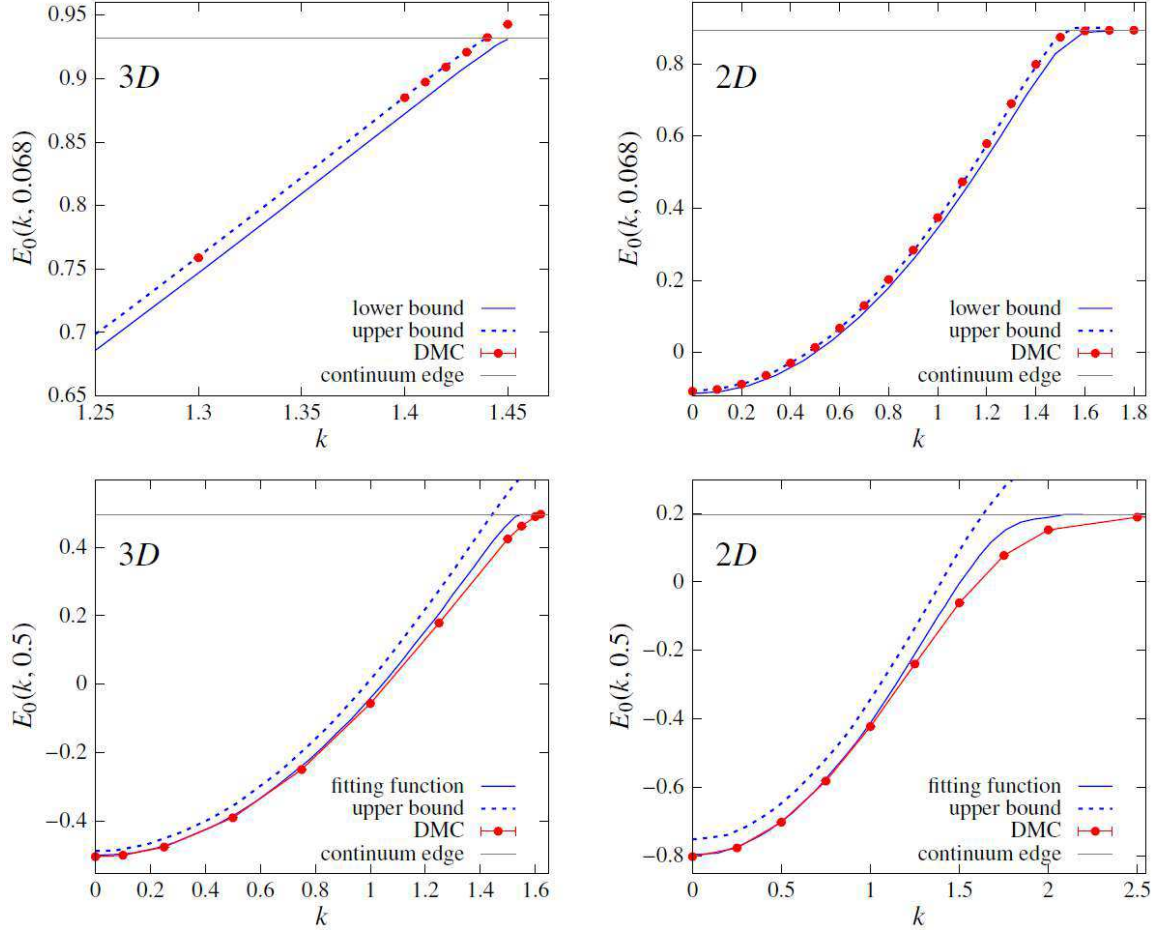


FIG. 41: Polaron energy $E_0(k, \alpha)$ in 3D (left) and 2D (right) as a function of the modulus of the total wave vector k for coupling constant $\alpha = 0.068$ (top row) and $\alpha = 0.5$ (bottom row). Lower and upper bounds, and a fitting function to the dispersion are taken from Ref. [20].

For small α , there exist rigorous upper and lower bounds for the polaron dispersion [20] that restrict this dispersion to a narrow domain. In the top row of Fig. 41, the DMC results are shown together with these bounds for $\alpha = 0.068$, the value of the coupling strength for GaAs. Our results lie in between the bounds, close to the upper bound, both in 3D (upper left panel of Fig. 41) and 2D (upper right panel). The strict lower bound only exists for small values of the coupling strength: $\alpha = 0.5$ already lies outside the range where this lower bound can be found.

Gerlach and Smondyrev [20] propose a fitting function for the dispersion. This fit is based on a re-scaling of the upper bound formula, to obtain the correct gap between bottom of the band and the continuum edge, while maintaining the effective mass. As shown in the

TABLE IX: Critical wave vectors $k_c(\alpha)$ for coupling constants $\alpha = 0.068$, $\alpha = 0.5$ and $\alpha = 1.0$. Listed are results from our DMC calculations, from Eq. F23 which is valid up to first order in α , as well as from the fitting function from Ref. [20].

	$\alpha = 0.068$	$\alpha = 0.5$	$\alpha = 1.0$
DMC, this work	1.440	1.615	1.833
Result to order α , Eq. (F23)	1.442	1.616	1.818
Gerlach and Smondyrev, Ref. [20]	1.442	1.570	1.697

lower left panel of Fig. 41, the DMC results for the 3D case for $\alpha = 0.5$ lie below both the variational upper bound and the Gerlach-Smondryev dispersion. The same conclusion can be drawn for the 2D case, shown in the lower right panel of Fig. 41.

We now focus on the 3D case, in which the dispersion reaches the continuum edge at a given k_c . Up to lowest order in α ,

$$k_c(\alpha) = \sqrt{2} + \left(\frac{\pi}{2} - 1\right) \frac{\alpha}{\sqrt{2}} + \mathcal{O}(\alpha^2). \quad (\text{F23})$$

In Table IX, we compare for several α values the critical wavenumber obtained (i) with DMC, (ii) with the first order approximation, Eq. F23, and (iii) using the Gerlach-Smondryev dispersion. At small coupling strength $\alpha = 0.068$, all three approaches yield the same result. However, as α is increased slightly (remaining in the regime where the lowest order approximation can be expected to be valid), the result obtained from the Gerlach-Smondryev dispersion drops below the value found by the other two approaches. The value of k_c in the Gerlach-Smondryev approach is 3% resp. 8% smaller than the DMC result for $\alpha = 0.5$ and 1.

Previously [20], this discrepancy was blamed on the fact that the DMC method supposedly failed to reproduce even the known q_2 parameter (the coefficient of α^2), whereas the fitting function is claimed to be good up to order α^3 . However, as we have shown in the previous subsection, this explanation cannot hold since contrary to what was believed earlier, the DMC does reproduce the q_2 value with high accuracy. The Gerlach-Smondryev dispersion is not the result of variational minimization, nor is it a rigorous lower bound: rather it is an ad hoc proposal that rescales the best variational upper bound to give the correct known limits. Keeping in mind that the DMC calculation takes many phonons into

account (i.e. goes well beyond order α in the diagrams), we can conclude that the DMC results indicate that this fitting procedure is not appropriate for $\alpha \geq 0.5$.

4. Summary and Conclusion

The Diagrammatic Monte Carlo is a powerful method which has proven to work in many applications for many different systems [31–36]. For this paper, we have implemented a DMC code based on the Refs. [21, 22] and applied it to the solution of the large polaron Fröhlich Hamiltonian in 3D and 2D. We benchmarked our code with existing DMC results for the 3D case to verify its correctness and then computed polaron ground state energies, effective polaron masses and polaron dispersion curves in 2D and 3D.

In summary, our data confirm that the effect of electron-phonon coupling is enhanced in 2D compared to 3D, and this is reflected in all computed physical quantities. Concerning the ground state energies, the DMC results are in very good agreement with those obtained by Feynman’s approach [15] and we have demonstrated that they obey the scaling relations between 3D and 2D [23]. The reliability of the DMC procedure is further corroborated by the calculations of the coefficients used for the weak- and strong-coupling regime, which are almost identical to the exactly known values. This refutes a claim [19] that the DMC technique is not able to correctly obtain the q_2 coefficients. Regarding the effective polaron mass, the DMC performance becomes slightly less satisfactory at stronger coupling. This inaccuracy should be traced back to the numerical errors involved in the calculation of the inverse of the effective mass. Alternative definitions of the polaron effective mass have been proposed in literature, which could be possibly tested in future work to assess and compare the performance of DMC and path-integrals approaches [37, 38].

One of the most interesting outcomes of the present study are the polaron dispersion curves. The DMC calculations reproduce very well the different behaviour seen in 2D and 3D: in 2D the energy curve approaches the continuum edge asymptotically from below, whereas in 3D it reaches the continuum edge at a finite critical k_c . For small α ($=0.068$, a realistic value for a material like GaAs), the DMC dispersion as well as the k_c are in very good agreement with the known lower and upper limits derived from the variational approach of Gerlach and Smondyrev [20]. For larger α ($\alpha= 0.5, 1.0$), the DMC data agree well with the first order expansion results, but deviate from the values based on a proposed

fitting function for the dispersion. While the DMC technique cannot validate the fitting procedure proposed by Gerlach and Smondyrev for $\alpha \geq 0.5$, it does suggest that up to $\alpha \approx 1$ the first order expansion result of Eq. F23 already provides an accurate estimate of k_c .

-
- [1] L. Landau, Phys. Z. Sowjet. **3**, 664 (1933).
 - [2] E. L. Nagaev, physica status solidi (b) **65**, 11 (1974).
 - [3] H. Haken, in Polarons and Excitons, edited by C. Kuper and G. Whitfield (Plenum, New York, 1963) pp. 295 – 322.
 - [4] A. Miller, D. Pines, and P. Nozières, Phys. Rev. **127**, 1452 (1962).
 - [5] S. A. Jackson and P. M. Platzman, Phys. Rev. B **24**, 499 (1981).
 - [6] A. S. Alexandrov and J. T. Devreese, *Advances in Polaron Physics*, Springer Series in Solid-State Sciences (Springer-Verlag, Berlin, 2010).
 - [7] E. Rashba, in *Encyclopedia of Condensed Matter Physics*, edited by F. Bassani, G. L. Liedl, and P. Wyder (Elsevier, Oxford, 2005) pp. 347 – 355.
 - [8] H. Fröhlich, Advances in Physics **3**, 325 (1954).
 - [9] T. Holstein, Ann. Phys. NY **8**, 325 (1959).
 - [10] M. Setvin, C. Franchini, X. Hao, M. Schmid, A. Janotti, M. Kaltak, C. G. Van de Walle, G. Kresse, and U. Diebold, Phys. Rev. Lett. **113**, 086402 (2014).
 - [11] K. Miyata, D. Meggiolaro, M. T. Trinh, P. P. Joshi, E. Mosconi, S. C. Jones, F. De Angelis, and X.-Y. Zhu, Science Advances **3** (2017), 10.1126/sciadv.1701217.
 - [12] F. M. Peeters, W. Xiaoguang, and J. T. Devreese, Phys. Rev. B **33**, 3926 (1986).
 - [13] J. T. Devreese, Physica Scripta **T25**, 309 (1989).
 - [14] R. P. Feynman, Phys. Rev. **97**, 660 (1955).
 - [15] R. Rosenfelder and A. W. Schreiber., Phys. Lett. A **284**, 63 (2001).
 - [16] G. Whitfield and R. D. Pu , Phys. Rev. **139**, A338 (1965).
 - [17] J. Appel, in Solid State Physics (Advances in Research and Applications), Vol. 21, edited by F. Seitz, D. Turnbull, and H. Ehrenreich (Academic, New York, 1968) pp. 193 – 391.
 - [18] B. Gerlach and F. Kalina, Phys. Rev. B **60**, 10886 (1999).
 - [19] B. Gerlach, F. Kalina, and M. Smondyrev, physica status solidi (b) **237**, 204 (2003).

- [20] B. Gerlach and M. A. Smondyrev, Phys. Rev. B **77**, 174303 (2008).
- [21] N. V. Prokof'ev and B. V. Svistunov, Phys. Rev. Lett. **81**, 2514 (1998).
- [22] A. S. Mishchenko, N. V. Prokof'ev, A. Sakamoto, and B. V. Svistunov, Phys. Rev. B **62**, 6317 (2000).
- [23] F. M. Peeters and J. T. Devreese, Phys. Rev. B **36**, 4442 (1987).
- [24] D. Pines, in Polarons and Excitons, edited by C. Kuper and G. Whitfield (Plenum, New York, 1963) pp. 155 – 170.
- [25] G. Mahan, Many-Particle Physics, Physics of Solids and Liquids (Springer US, 2000).
- [26] A. S. Mishchenko, Physics-Uspekhi **48**, 887 (2005).
- [27] K. V. Houcke, E. Kozik, N. Prokof'ev, and B. Svistunov, Physics Procedia **6**, 95 (2010).
- [28] W. Xiaoguang, F. M. Peeters, and J. T. Devreese, Phys. Rev. B **31**, 3420 (1985).
- [29] F. M. Peeters, X. Wu, and J. T. Devreese, Phys. Rev. B **37**, 933 (1988).
- [30] J. Röseler, Phys. Stat. Sol. **26**, 311 (1968).
- [31] J. Vlietinck, J. Ryckebusch, and K. Van Houcke, Phys. Rev. B **87**, 115133 (2013).
- [32] E. A. Burovski, A. S. Mishchenko, N. V. Prokof'ev, and B. V. Svistunov, Phys. Rev. Lett. **87**, 186402 (2001).
- [33] A. S. Mishchenko, N. Nagaosa, and N. Prokof'ev, Phys. Rev. Lett. **113**, 166402 (2014).
- [34] A. S. Mishchenko, N. Nagaosa, N. V. Prokof'ev, A. Sakamoto, and B. V. Svistunov, Phys. Rev. Lett. **91**, 236401 (2003).
- [35] J. Vlietinck, J. Ryckebusch, and K. Van Houcke, Phys. Rev. B **89**, 085119 (2014).
- [36] J. Vlietinck, W. Casteels, K. V. Houcke, J. Tempere, J. Ryckebusch, and J. T. Devreese, New Journal of Physics **17**, 033023 (2015).
- [37] D. C. Khandekar, K. V. Bhagwat, and S. V. Lawande, Phys. Rev. B **37**, 3085 (1988).
- [38] V. Sa-yakanit and K. Tayanasaki, Phys. Rev. B **57**, 8739 (1998).

Appendix G: Selected publications on polarons in high-rating journals (Nature, Science, Physical Review Letters – 2005-2020)

1. *Method for Analyzing Second-Order Phase Transitions: Application to the Ferromagnetic Transition of a Polaronic System*, J. A. Souza, Yi-Kuo Yu, J. J. Neumeier, H. Terashita, and R. F. Jardim, Phys. Rev. Lett. **94**, 207209 (2005).

Abstract

A new method for analyzing second-order phase transitions is presented and applied to the polaronic system $\text{La}_{0.7}\text{Ca}_{0.3}\text{MnO}_3$. It utilizes heat capacity and thermal expansion data simultaneously to correctly predict the critical temperature's pressure dependence. Analysis of the critical phenomena reveals second-order behavior and an unusually large heat capacity exponent.

2. *Validity of the Franck-Condon Principle in the Optical Spectroscopy: Optical Conductivity of the Fröhlich Polaron*, G. De Filippis, V. Cataudella, A. S. Mishchenko, C. A. Perroni, and J. T. Devreese, Phys. Rev. Lett. **96**, 136405 (2006).

Abstract

The optical absorption of the Fröhlich polaron model is obtained by an approximation-free diagrammatic Monte Carlo method and compared with two new approximate approaches that treat lattice relaxation effects in different ways. We show that: (i) a strong coupling expansion, based on the Franck-Condon principle, well describes the optical conductivity for large coupling strengths ($\alpha > 10$); (ii) a memory function formalism with phonon broadened levels reproduces the optical response for weak coupling strengths ($\alpha < 6$) taking the dynamic lattice relaxation into account. In the coupling regime $6 < \alpha < 10$, the optical conductivity is a rapidly changing superposition of both Franck-Condon and dynamic contributions.

3. *Remanent Zero Field Spin Splitting of Self-Assembled Quantum Dots in a Paramagnetic Host*, C. Gould, A. Slobodskyy, D. Supp, T. Slobodskyy, P. Grabs, P. Hawrylak, F. Qu, G. Schmidt, and L. W. Molenkamp, Phys. Rev. Lett. **97**, 017202 (2006).
4. *Quantum Transport of Slow Charge Carriers in Quasicrystals and Correlated Systems*, Guy Trambly de Laissardière, Jean-Pierre Julien, and Didier Mayou, Phys. Rev. Lett. **97**, 026601 (2006).

Abstract

We show that the semiclassical model of conduction breaks down if the mean free path of charge carriers is smaller than a typical extension of their wave function. This situation is realized for sufficiently slow charge carriers and leads to a transition from a metalliclike to an insulatinglike regime when scattering by defects increases. This explains the unconventional conduction properties of quasicrystals and related alloys. The conduction properties of some heavy fermions or polaronic systems, where charge carriers are also slow, present a deep analogy.

5. *Occurrence of Intersubband Polaronic Repellons in a Two-Dimensional Electron Gas*, Stefan Butscher and Andreas Knorr, Phys. Rev. Lett. **97**, 197401 (2006).
6. *Subsecond Spin Relaxation Times in Quantum Dots at Zero Applied Magnetic Field Due to a Strong Electron-Nuclear Interaction*, R. Oulton, A. Greilich, S. Yu. Verbin, R. V. Cherbunin, T. Auer, D. R. Yakovlev, M. Bayer, I. A. Merkulov, V. Stavarache, D. Reuter, and A. D. Wieck, Phys. Rev. Lett. **98**, 107401 (2007).
7. *Exciton Dephasing in Quantum Dots due to LO-Phonon Coupling: An Exactly Solvable Model*, E. A. Muljarov and R. Zimmermann, Phys. Rev. Lett. **98**, 187401 (2007)
8. *Electron-Phonon Interaction and Charge Carrier Mass Enhancement in SrTiO₃*, J. L. M. van Mechelen, D. van der Marel, C. Grimaldi, A. B. Kuzmenko, N. P. Armitage, N. Reyren, H. Hagemann, and I. I. Mazin, Phys. Rev. Lett. **100**, 226403 (2008).

Abstract

We report a comprehensive THz, infrared and optical study of Nb-doped SrTiO₃ as well as dc conductivity and Hall effect measurements. Our THz spectra at 7 K show the presence of an unusually narrow ($< 2\text{meV}$) Drude peak. For all carrier concentrations the Drude spectral weight shows a factor of three mass enhancement relative to the effective mass in the local density approximation, whereas the spectral weight contained in the incoherent midinfrared response indicates that the mass enhancement is at least a factor two. We find no evidence of a particularly large electron-phonon coupling that would result in small polaron formation.

9. *Orbital and Charge-Resolved Polaron States in CdSe Dots and Rods Probed by Scanning Tunneling Spectroscopy*, Zhixiang Sun, Ingmar Swart, Christophe Delerue, Daniël Vanmaekelbergh, and Peter Liljeroth, Phys. Rev. Lett. **102**, 196401 (2009).

10. *Dynamical Response and Confinement of the Electrons at the LaAlO₃/SrTiO₃ Interface*, A. Dubroka, M. Rössle, K. W. Kim, V. K. Malik, L. Schultz, S. Thiel, C. W. Schneider, J. Mannhart, G. Herranz, O. Copie, M. Bibes, A. Barthélémy, and C. Bernhard, Phys. Rev. Lett. **104**, 156807 (2010).

Abstract

With infrared ellipsometry and transport measurements we investigated the electrons at the interface between LaAlO₃ and SrTiO₃. We obtained a sheet carrier concentration of $N_s \approx 5 - 9 \times 10^{13} \text{ cm}^{-2}$, an effective mass of $m^* = 3.2 \pm 0.4m_e$, and a strongly frequency dependent mobility. The latter are similar as in bulk SrTi_{1-x}Nb_xO₃ and therefore suggestive of polaronic correlations. We also determined the vertical concentration profile which has a strongly asymmetric shape with a rapid initial decay over the first 2 nm and a pronounced tail that extends to about 11 nm.

11. *Bipolaron and N-Polaron Binding Energies*, Rupert L. Frank, Elliott H. Lieb, Robert Seiringer, and Lawrence E. Thomas, Phys. Rev. Lett. **104**, 210402 (2010).

Abstract

The binding of polarons, or its absence, is an old and subtle topic. Here we prove two things rigorously. First, the transition from many-body collapse to the existence of a thermodynamic limit for N polarons occurs precisely at $U = 2\alpha$, where U is the electronic Coulomb repulsion and α is the polaron coupling constant. Second, if U is large enough, there is no multipolaron binding of any kind. Considering the known fact that there is binding for some $U > 2\alpha$, these conclusions are not obvious and their proof has been an open problem for some time.

12. *Polaronic Conductivity in the Photoinduced Phase of 1T-TaS₂*, N. Dean, J. C. Petersen, D. Fausti, R. I. Tobey, S. Kaiser, L. V. Gasparov, H. Berger, and A. Cavalleri, Phys. Rev. Lett. **106**, 016401 (2011).

13. *Spectroscopy of Single Donors at ZnO(0001) Surfaces*, Hao Zheng, Jörg Kröger, and Richard Berndt, Phys. Rev. Lett. **108**, 076801 (2012)

14. *Polarons in Suspended Carbon Nanotubes*, I. Snyman, and Yu. V. Nazarov, Phys. Rev. Lett. **108**, 076805 (2012)

15. *Two-Dimensional Polaronic Behavior in the Binary Oxides m-HfO₂ and m-ZrO₂*, K.

- P. McKenna, M. J. Wolf, A. L. Shluger, S. Lany, and A. Zunger, Phys. Rev. Lett. **108**, 116403 (2012)
16. *Polaron-to-Polaron Transitions in the Radio-Frequency Spectrum of a Quasi-Two-Dimensional Fermi Gas*, Y. Zhang, W. Ong, I. Arakelyan, and J. E. Thomas, Phys. Rev. Lett. **108**, 235302 (2012)
- Abstract**
- We measure radio-frequency spectra for a two-component mixture of a ${}^6\text{Li}$ atomic Fermi gas in a quasi-two-dimensional regime with the Fermi energy comparable to the energy level spacing in the tightly confining potential. Near the Feshbach resonance, we find that the observed resonances do not correspond to transitions between confinement-induced dimers. The spectral shifts can be fit by assuming transitions between noninteracting polaron states in two dimensions.
17. *Model of the Electron-Phonon Interaction and Optical Conductivity of $\text{Ba}_{1-x}\text{K}_x\text{BiO}_3$* , R. Nourafkan, F. Marsiglio, and G. Kotliar, Phys. Rev. Lett. **109**, 017001 (2012)
18. *p-Wave Polaron*, Jesper Levinsen, Pietro Massignan, Frédéric Chevy, and Carlos Lobo, Phys. Rev. Lett. **109**, 075302 (2012)
19. *Effect of Electron-Phonon Interaction Range for a Half-Filled Band in One Dimension*, Martin Hohenadler, Fakher F. Assaad, and Holger Fehske, Phys. Rev. Lett. **109**, 116407 (2012)
20. *Digital Quantum Simulation of the Holstein Model in Trapped Ions*, A. Mezzacapo, J. Casanova, L. Lamata, and E. Solano, Phys. Rev. Lett. **109**, 200501 (2012)
21. *Bilayers of Rydberg Atoms as a Quantum Simulator for Unconventional Superconductors*, J. P. Hague and C. MacCormick, Phys. Rev. Lett. **109**, 223001 (2012)
22. *Relaxation Dynamics of the Holstein Polaron*, Denis Golež, Janez Bonča, Lev Vidmar, and Stuart A. Trugman, Phys. Rev. Lett. **109**, 236402 (2012)
23. *Quantum Simulation of Small-Polaron Formation with Trapped Ions*, Vladimir M. Stojanović, Tao Shi, C. Bruder, and J. Ignacio Cirac, Phys. Rev. Lett. **109**, 250501 (2012)

24. *Condensed-matter physics: Repulsive polarons found*, P. Hanneford, Nature **485**, 588 (2012)

Abstract

Quasiparticles known as repulsive polarons are predicted to occur when 'impurity' fermionic particles interact repulsively with a fermionic environment. They have now been detected in two widely differing systems. See Letters p.615 & p.619

25. *Quantum Breathing of an Impurity in a One-Dimensional Bath of Interacting Bosons*, Sebastiano Peotta, Davide Rossini, Marco Polini, Francesco Minardi, and Rosario Fazio, Phys. Rev. Lett. **110**, 015302 (2013)

Abstract

By means of the time-dependent density-matrix renormalization-group (TDMRG) method we are able to follow the real-time dynamics of a single impurity embedded in a one-dimensional bath of interacting bosons. We focus on the impurity breathing mode, which is found to be well described by a single oscillation frequency and a damping rate. If the impurity is very weakly coupled to the bath, a Luttinger-liquid description is valid and the impurity suffers an Abraham-Lorentz radiation-reaction friction. For a large portion of the explored parameter space, the TDMRG results fall well beyond the Luttinger-liquid paradigm.

26. *Measurement of Coherent Polarons in the Strongly Coupled Antiferromagnetically Ordered Iron-Chalcogenide $Fe_{1.02}Te$ using Angle-Resolved Photoemission Spectroscopy*, Z. K. Liu, R.-H. He, D. H. Lu, M. Yi, Y. L. Chen, M. Hashimoto, R. G. Moore, S.-K. Mo, E. A. Nowadnick, J. Hu, T. J. Liu, Z. Q. Mao, T. P. Devereaux, Z. Hussain, and Z.-X. Shen, Phys. Rev. Lett. **110**, 037003 (2013)

27. *Decoherence of a Single-Ion Qubit Immersed in a Spin-Polarized Atomic Bath*, L. Ratschbacher, C. Sias, L. Carcagni, J. M. Silver, C. Zipkes, and M. Köhl, Phys. Rev. Lett. **110**, 160402 (2013)

28. *Tunable Polaronic Conduction in Anatase TiO_2* , S. Moser, L. Moreschini, J. Jaćimović, O. S. Barišić, H. Berger, A. Magrez, Y. J. Chang, K. S. Kim, A. Bostwick, E. Rotenberg, L. Forró, and M. Grioni, Phys. Rev. Lett. **110**, 196403 (2013)

29. *Investigating Polaron Transitions with Polar Molecules*, Felipe Herrera, Kirk W. Madison, Roman V. Krems, and Mona Berciu, Phys. Rev. Lett. **110**, 223002 (2013)

Abstract

We determine the phase diagram of a polaron model with mixed breathing-mode and Su-Schrieffer-Heeger couplings and show that it has two sharp transitions, in contrast to pure models which exhibit one (for Su-Schrieffer-Heeger coupling) or no (for breathing-mode coupling) transition. We then show that ultracold molecules trapped in optical lattices can be used as a quantum simulator to study precisely this mixed Hamiltonian, and that the relative contributions of the two couplings can be tuned with external electric fields. The parameters of current experiments place them in the region where one of the transitions occurs. We also propose a scheme to measure the polaron dispersion using stimulated Raman spectroscopy.

30. *Electronic Instability in a Zero-Gap Semiconductor: The Charge-Density Wave in $(\text{TaSe}_4)_2$* , C. Tournier-Colletta, L. Moreschini, G. Autès, S. Moser, A. Crepaldi, H. Berger, A. L. Walter, K. S. Kim, A. Bostwick, P. Monceau, E. Rotenberg, O. V. Yazyev, and M. Grioni, Phys. Rev. Lett. **110**, 236401 (2013).

31. *Itinerant Ferromagnetism in a Polarized Two-Component Fermi Gas*, Pietro Massignan, Zhenhua Yu, and Georg M. Bruun, Phys. Rev. Lett. **110**, 230401 (2013).

32. *Suppression of the Hanle Effect in Organic Spintronic Devices*, Z. G. Yu, Phys. Rev. Lett. **111**, 016601 (2013).

33. *Energy and Contact of the One-Dimensional Fermi Polaron at Zero and Finite Temperature*, E. V. H. Doggen and J. J. Kinnunen, Phys. Rev. Lett. **111**, 025302 (2013).

34. *Measurement of the Femtosecond Optical Absorption of $\text{LaAlO}_3/\text{SrTiO}_3$ Heterostructures: Evidence for an Extremely Slow Electron Relaxation at the Interface*, Yasuhiro Yamada, Hiroki K. Sato, Yasuyuki Hikita, Harold Y. Hwang, and Yoshihiko Kanemitsu, Phys. Rev. Lett. **111**, 047403 (2013)

Abstract

The photocarrier relaxation dynamics of an n-type $\text{LaAlO}_3/\text{SrTiO}_3$ heterointerface is investigated using femtosecond transient absorption (TA) spectroscopy at low temperatures. In both $\text{LaAlO}_3/\text{SrTiO}_3$ heterostructures and electron-doped SrTiO_3 bulk crystals, the TA

spectrum shows a Drude-like free carrier absorption immediately after excitation. In addition, a broad absorption band gradually appears within 40 ps, which corresponds to the energy relaxation of photoexcited free electrons into self-trapped polaron states. We reveal that the polaron formation time is enhanced considerably at the LaAlO₃/SrTiO₃ heterointerface as compared to bulk crystals. Further, we discuss the interface effects on the electron relaxation dynamics in conjunction with the splitting of the t_{2g} subbands due to the interface potential.

35. *Pauli Spin Blockade and the Ultrasmall Magnetic Field Effect*, Jeroen Danon, Xuhui Wang, and Aurélien Manchon, Phys. Rev. Lett. **111**, 066802 (2013)
36. *Tkachenko Polarons in Vortex Lattices*, M. A. Caracanhas, V. S. Bagnato, and R. G. Pereira, Phys. Rev. Lett. **111**, 115304 (2013).
37. *Impurity Problem in a Bilayer System of Dipoles*, N. Matveeva and S. Giorgini, Phys. Rev. Lett. **111**, 220405 (2013).
38. *Single-Polariton Optomechanics*, Juan Restrepo, Cristiano Ciuti, and Ivan Favero, Phys. Rev. Lett. **112**, 013601 (2014)
39. *Ferromagnetism of a Repulsive Atomic Fermi Gas in an Optical Lattice: A Quantum Monte Carlo Study*, S. Pilati, I. Zintchenko, and M. Troyer, Phys. Rev. Lett. **112**, 015301 (2014)
40. *Ultrafast Photoemission Spectroscopy of the Uranium Dioxide UO₂ Mott Insulator: Evidence for a Robust Energy Gap Structure*, Steve M. Gilbertson, Tomasz Durakiewicz, Georgi L. Dakovski, Yinwan Li, Jian-Xin Zhu, Steven D. Conradson, Stuart A. Trugman, and George Rodriguez, Phys. Rev. Lett. **112**, 087402 (2014).
41. *Direct View at Excess Electrons in TiO₂ Rutile and Anatase*, Martin Setvin, Cesare Franchini, Xianfeng Hao, Michael Schmid, Anderson Janotti, Merzuk Kaltak, Chris G. Van de Walle, Georg Kresse, and Ulrike Diebold, Phys. Rev. Lett. **113**, 086402 (2014)

Abstract

A combination of scanning tunneling microscopy and spectroscopy and density functional theory is used to characterize excess electrons in TiO₂ rutile and anatase, two prototypical

materials with identical chemical composition but different crystal lattices. In rutile, excess electrons can localize at any lattice Ti atom, forming a small polaron, which can easily hop to neighboring sites. In contrast, electrons in anatase prefer a free-carrier state, and can only be trapped near oxygen vacancies or form shallow donor states bound to Nb dopants. The present study conclusively explains the differences between the two polymorphs and indicates that even small structural variations in the crystal lattice can lead to a very different behavior.

42. *Diagrammatic Monte Carlo Method for Many-Polaron Problems*, Andrey S. Mishchenko, Naoto Nagaosa, and Nikolay Prokof'ev, Phys. Rev. Lett. **113**, 166402 (2014)

Abstract

We introduce the first bold diagrammatic Monte Carlo approach to deal with polaron problems at a finite electron density nonperturbatively, i.e., by including vertex corrections to high orders. Using the Holstein model on a square lattice as a prototypical example, we demonstrate that our method is capable of providing accurate results in the thermodynamic limit in all regimes from a renormalized Fermi liquid to a single polaron, across the nonadiabatic region where Fermi and Debye energies are of the same order of magnitude. By accounting for vertex corrections, the accuracy of the theoretical description is increased by orders of magnitude relative to the lowest-order self-consistent Born approximation employed in most studies. We also find that for the electron-phonon coupling typical for real materials, the quasiparticle effective mass increases and the quasiparticle residue decreases with increasing the electron density at constant electron-phonon coupling strength.

43. *Polaron spin current transport in organic semiconductors*, Shun Watanabe, Kazuya Ando, Keehoon Kang, Sebastian Mooser, Yana Vaynzof, Hidekazu Kurebayashi, Eiji Saitoh, and Henning Sirringhaus, Nature Physics **10**, 308 (2014)
44. *Real Space Imaging of Spin Polarons in Zn-Doped SrCu₂(BO₃)₂*, M. Yoshida, H. Kobayashi, I. Yamauchi et al., Phys. Rev. Lett. **114**, 056402 (2015)
45. *Crossover from Super- to Subdiffusive Motion and Memory Effects in Crystalline Organic Semiconductors*, G. De Filippis, V. Cataudella, A. S. Mishchenko, N. Nagaosa, A. Fierro, and A. de Candia, Phys. Rev. Lett. **114**, 086601 (2015)

Abstract

The transport properties at finite temperature of crystalline organic semiconductors are investigated, within the Su-Schrieffer-Heeger model, by combining an exact diagonalization technique, Monte Carlo approaches, and a maximum entropy method. The temperature-dependent mobility data measured in single crystals of rubrene are successfully reproduced: a crossover from super- to subdiffusive motion occurs in the range $150 < T < 200\text{K}$, where the mean free path becomes of the order of the lattice parameter and strong memory effects start to appear. We provide an effective model, which can successfully explain features of the absorption spectra at low frequencies. The observed response to slowly varying electric field is interpreted by means of a simple model where the interaction between the charge carrier and lattice polarization modes is simulated by a harmonic interaction between a fictitious particle and an electron embedded in a viscous fluid.

46. *Mobility of Holstein Polaron at Finite Temperature: An Unbiased Approach*, A.S. Mishchenko, N. Nagaosa, G. De Filippis, A. de Candia, and V. Cataudella, Phys. Rev. Lett. **114**, 146401 (2015).

Abstract

We present the first unbiased results for the mobility μ of a one-dimensional Holstein polaron obtained by numerical analytic continuation combined with diagrammatic and worldline Monte Carlo methods in the thermodynamic limit. We have identified for the first time several distinct regimes in the $\lambda - T$ plane including a band conduction region, incoherent metallic region, an activated hopping region, and a high-temperature saturation region. We observe that although mobilities and mean free paths at different values of λ differ by many orders of magnitude at small temperatures, their values at T larger than the bandwidth become very close to each other.

47. *Band Structures of Plasmonic Polarons*, F. Caruso, H. Lambert, and F. Giustino, Phys. Rev. Lett. **114**, 146404 (2015)

Abstract

Using state-of-the-art many-body calculations based on the “GW plus cumulant” approach, we show that electron-plasmon interactions lead to the emergence of plasmonic polaron bands in the band structures of common semiconductors. Using silicon and group IV transition-metal dichalcogenide monolayers ($\text{AX}(2)$ with $\text{A} = \text{Mo, W}$ and $\text{X} = \text{S, Se}$) as prototypical examples, we demonstrate that these new bands are a general feature of systems charac-

terized by well-defined plasmon resonances. We find that the energy versus momentum dispersion relations of these plasmonic structures closely follow the standard valence bands, although they appear broadened and blueshifted by the plasmon energy. Based on our results, we identify general criteria for observing plasmonic polaron bands in the angle-resolved photoelectron spectra of solids.

48. *Long-lived photoinduced polaron formation in conjugated polyelectrolyte-fullerene assemblies*, R. C. Huber, A. S. Ferreira, R. Thompson *et al.*, *Science* **348**, 1340 (2015).

49. *Electron-Phonon Interactions, Metal-Insulator Transitions, and Holographic Massive Gravity*, M. Baggioli and O. Pujolas, *Phys. Rev. Lett.* **114**, 251602 (2015)

Abstract

Massive gravity is holographically dual to “realistic” materials with momentum relaxation. The dual graviton potential encodes the phonon dynamics, and it allows for a much broader diversity than considered so far. We construct a simple family of isotropic and homogeneous materials that exhibit an interaction-driven metal-insulator transition. The transition relates to the formation of polarons – phonon-electron quasibound states that dominate the conductivities, shifting the spectral weight above a mass gap. We characterize the polaron gap, width, and dispersion.

50. *Electron-Phonon Coupling in the Bulk of Anatase TiO₂ Measured by Resonant Inelastic X-Ray Spectroscopy*, S. Moser, S. Fatale, P. Krueger *et al.*, *Phys. Rev. Lett.* **115**, 096404 (2015).

Abstract

We investigate the polaronic ground state of anatase TiO₂ by bulk-sensitive resonant inelastic x-ray spectroscopy (RIXS) at the Ti L-3 edge. We find that the formation of the polaron cloud involves a single 95 meV phonon along the c axis, in addition to the 108 meV ab-plane mode previously identified by photoemission. The coupling strength to both modes is the same within error bars, and it is unaffected by the carrier density. These data establish RIXS as a directional bulk-sensitive probe of electron-phonon coupling in solids.

51. *Impurity in a Bose-Einstein Condensate and the Efimov Effect*, J. Levinsen, M. M. Parish, and G. M. Bruun, *Phys. Rev. Lett.* **115**, 125302 (2015).

52. *Decoherence of Impurities in a Fermi Sea of Ultracold Atoms*, M. Cetina, M. Jag, R. S. Lous, et al., Phys. Rev. Lett. **115**, 135302 (2015).

53. *Impurities in Bose-Einstein Condensates: From Polaron to Soliton*, S. Shadkhoo and R., Shahriar, Phys. Rev. Lett. **115**, 135305 (2015).

Abstract

We propose that impurities in a Bose-Einstein condensate which is coupled to a transversely laser-pumped multimode cavity form an experimentally accessible and analytically tractable model system for the study of impurities solvated in correlated liquids and the breakdown of linear-response theory. As the strength of the coupling constant between the impurity and the Bose-Einstein condensate is increased, which is possible through Feshbach resonance methods, the impurity passes from a large to a small polaron state, and then to an impurity-soliton state. This last transition marks the breakdown of linear-response theory.

54. *Quasiparticle Properties of a Mobile Impurity in a Bose-Einstein Condensate*, R. S. Christensen, J. Levinsen, and G. M. Bruun, Phys. Rev. Lett. **115**, 160401 (2015).

Abstract

We develop a systematic perturbation theory for the quasiparticle properties of a single impurity immersed in a Bose-Einstein condensate. Analytical results are derived for the impurity energy, effective mass, and residue to third order in the impurity-boson scattering length. The energy is shown to depend logarithmically on the scattering length to third order, whereas the residue and the effective mass are given by analytical power series. When the boson-boson scattering length equals the boson-impurity scattering length, the energy has the same structure as that of a weakly interacting Bose gas, including terms of the Lee-Huang-Yang and fourth order logarithmic form. Our results, which cannot be obtained within the canonical Frohlich model of an impurity interacting with phonons, provide valuable benchmarks for many-body theories and for experiments.

55. *Ab initio Lattice Results for Fermi Polarons in Two Dimensions*, Shahin Bour, Dean Lee, H.-W. Hammer, and Ulf-G. Meissner, Phys. Rev. Lett. **115**, 185301 (2015);

56. *Field Effect and Strongly Localized Carriers in the Metal-Insulator Transition Material VO₂*, K. Martens, J.W. Jeong, N. Aetukuri, C. Rettner, N. Shukla, E. Freeman, D.N. Esfahani, F.M. Peeters, T. Topuria, P.M. Rice, A. Volodin, B. Douhard, W.

Vandervorst, M. G. Samant, S. Datta, and S. S. P. Parkin, Phys. Rev. Lett. **115**, 196401 (2015).

57. *Tunable Polarons of Slow-Light Polaritons in a Two-Dimensional Bose-Einstein Condensate*, Fabian Grusdt and Michael Fleischhauer, Phys. Rev. Lett. **116**, 053602 (2016).

Abstract

When an impurity interacts with a bath of phonons it forms a polaron. For increasing interaction strengths the mass of the polaron increases and it can become self-trapped. For impurity atoms inside an atomic Bose-Einstein condensate (BEC) the nature of this transition is not understood. While Feynman's variational approach to the Fröhlich model predicts a sharp transition for light impurities, renormalization group studies always predict an extended intermediate-coupling region characterized by large phonon correlations. To investigate this intricate regime and to test polaron physics beyond the validity of the Fröhlich model we suggest a versatile experimental setup that allows us to tune both the mass of the impurity and its interactions with the BEC. The impurity is realized as a dark-state polariton (DSP) inside a quasi-two-dimensional BEC. We show that its interactions with the Bogoliubov phonons lead to photonic polarons, described by the Bogoliubov-Fröhlich Hamiltonian, and make theoretical predictions using an extension of a recently introduced renormalization group approach to Fröhlich polarons.

58. *Spontaneous Charge Carrier Localization in Extended One-Dimensional Systems*, Vojtěch Vlček, Helen R. Eisenberg, Gerd Steinle-Neumann, Daniel Neuhauser, Eran Rabani, and Roi Baer, Phys. Rev. Lett. **116**, 186401 (2016).

59. *Cavity-Controlled Chemistry in Molecular Ensembles*, Felipe Herrera and Frank C. Spano, Phys. Rev. Lett. **116**, 238301 (2016).

60. *Giant Optical Polarization Rotation Induced by Spin-Orbit Coupling in Polarons*, Blai Casals, Rafael Cichelero, Pablo Garcia Fernandez, Javier Junquera, David Pesquera, Mariano Campoy-Quiles, Ingrid C. Infante, Florencio Sánchez, Josep Fontcuberta, and Gervasi Herranz, Phys. Rev. Lett. **117**, 026401 (2016).

61. *Observation of Attractive and Repulsive Polarons in a Bose-Einstein Condensate*, Nils B. J. Jørgensen, Lars Wacker, Kristoffer T. Skalmstang, Meera M. Parish, Jesper

Levinsen, Rasmus S. Christensen, Georg M. Bruun, and Jan J. Arlt, Phys. Rev. Lett. **117**, 055302 (2016).

Abstract

The problem of an impurity particle moving through a bosonic medium plays a fundamental role in physics. However, the canonical scenario of a mobile impurity immersed in a Bose-Einstein condensate (BEC) has not yet been realized. Here, we use radio frequency spectroscopy of ultracold bosonic ^{39}K atoms to experimentally demonstrate the existence of a well-defined quasiparticle state of an impurity interacting with a BEC. We measure the energy of the impurity both for attractive and repulsive interactions, and find excellent agreement with theories that incorporate three-body correlations, both in the weak-coupling limits and across unitarity. The spectral response consists of a well-defined quasiparticle peak at weak coupling, while for increasing interaction strength, the spectrum is strongly broadened and becomes dominated by the many-body continuum of excited states. Crucially, no significant effects of three-body decay are observed. Our results open up exciting prospects for studying mobile impurities in a bosonic environment and strongly interacting Bose systems in general.

62. *Bose Polarons in the Strongly Interacting Regime*, Ming-Guang Hu, Michael J. Van de Graaff, Dhruv Kedar, John P. Corson, Eric A. Cornell, and Deborah S. Jin, Phys. Rev. Lett. **117**, 055301 (2016).

Abstract

When an impurity is immersed in a Bose-Einstein condensate, impurity-boson interactions are expected to dress the impurity into a quasiparticle, the Bose polaron. We superimpose an ultracold atomic gas of ^{87}Rb with a much lower density gas of fermionic ^{40}K impurities. Through the use of a Feshbach resonance and radio-frequency spectroscopy, we characterize the energy, spectral width, and lifetime of the resultant polaron on both the attractive and the repulsive branches in the strongly interacting regime. The width of the polaron in the attractive branch is narrow compared to its binding energy, even as the two-body scattering length diverges.

63. *Quantum Dynamics of Ultracold Bose Polarons*, Yulia E. Shchadilova, Richard Schmidt, Fabian Grusdt, and Eugene Demler, Phys. Rev. Lett. **117**, 113002 (2016).

Abstract

We analyze the dynamics of Bose polarons in the vicinity of a Feshbach resonance between the impurity and host atoms. We compute the radio-frequency absorption spectra for the case when the initial state of the impurity is noninteracting and the final state is strongly interacting with the host atoms. We compare results of different theoretical approaches including a single excitation expansion, a self-consistent T-matrix method, and a time-dependent coherent state approach. Our analysis reveals sharp spectral features arising from metastable states with several Bogoliubov excitations bound to the impurity atom. This surprising result of the interplay of many-body and few-body Efimov type bound state physics can only be obtained by going beyond the commonly used Fröhlich model and including quasiparticle scattering processes. Close to the resonance we find that strong fluctuations lead to a broad, incoherent absorption spectrum where no quasiparticle peak can be assigned.

64. *Engineering Polarons at a Metal Oxide Surface*, C. M. Yim, M. B. Watkins, M. J. Wolf, C. L. Pang, K. Hermansson, and G. Thornton, Phys. Rev. Lett. **117**, 116402 (2016).

Abstract

Polarons in metal oxides are important in processes such as catalysis, high temperature superconductivity, and dielectric breakdown in nanoscale electronics. Here, we study the behavior of electron small polarons associated with oxygen vacancies at rutile TiO₂(110), using a combination of low temperature scanning tunneling microscopy (STM), density functional theory, and classical molecular dynamics calculations. We find that the electrons are symmetrically distributed around isolated vacancies at 78 K, but as the temperature is reduced, their distributions become increasingly asymmetric, confirming their polaronic nature. By manipulating isolated vacancies with the STM tip, we show that particular configurations of polarons are preferred for given locations of the vacancies, which we ascribe to small residual electric fields in the surface. We also form a series of vacancy complexes and manipulate the Ti ions surrounding them, both of which change the associated electronic distributions. Thus, we demonstrate that the configurations of polarons can be engineered, paving the way for the construction of conductive pathways relevant to resistive switching devices.

65. *Lightwave-driven quasiparticle collisions on a subcycle timescale*, F. Langer, M. Hohenleutner, C. P. Schmid *et al.*, Nature **533**, 225 (2016).
66. *Screening in crystalline liquids protects energetic carriers in hybrid perovskites*, H. Zhu, K. Miyata, Y. Fu *et al.*, Science **353**, 1409 (2016).

67. Magnon Polarons in the Spin Seebeck Effect. By: Kikkawa, Takashi; Shen, Ka; Flebus, Benedetta et al., Phys. Rev. Lett. **117**, 207203 (2016).

68. Interplay of Site and Bond Electron-Phonon Coupling in One Dimension. By: Hohenadler, Martin, Phys. Rev. Lett. **117**, 206404 (2016).

Abstract

The interplay of bond and charge correlations is studied in a one-dimensional model with both Holstein and Su-Schrieffer-Heeger (SSH) couplings to quantum phonons. The problem is solved exactly by quantum Monte Carlo simulations. If one of the couplings dominates, the ground state is a Peierls insulator with long-range bond or charge order. At weak coupling, the results suggest a spin-gapped and repulsive metallic phase arising from the competing order parameters and lattice fluctuations. Such a phase is absent from the pure SSH model even for quantum phonons. At strong coupling, evidence for a continuous transition between the two Peierls states is presented.

69. Repulsive Fermi Polarons in a Resonant Mixture of Ultracold Li-6 Atoms. By: Scazza, F.; Valtolina, G.; Massignan, P.; et al., Phys. Rev. Lett. **118**, 083602 (2017).

Abstract

We employ radio-frequency spectroscopy to investigate a polarized spin mixture of ultracold Li-6 atoms close to a broad Feshbach scattering resonance. Focusing on the regime of strong repulsive interactions, we observe well-defined coherent quasiparticles even for unitarity-limited interactions. We characterize the many-body system by extracting the key properties of repulsive Fermi polarons: the energy E_+ , the effective mass m^* , the residue Z , and the decay rate Γ . Above a critical interaction, E_+ is found to exceed the Fermi energy of the bath, while m^* diverges and even turns negative, thereby indicating that the repulsive Fermi liquid state becomes energetically and thermodynamically unstable.

70. Fermi polaron-polaritons in charge-tunable atomically thin semiconductors. By: Sildler, Meinrad; Back, Patrick; Cotlet, Ovidiu; et al., Nature Physics **13**, 255 (2017).

Abstract

The dynamics of a mobile quantum impurity in a degenerate Fermi system is a fundamental problem in many-body physics. The interest in this field has been renewed due to recent ground-breaking experiments with ultracold Fermi gases(1-5). Optical creation of an exciton or a polariton in a two-dimensional electron system embedded in a microcavity constitutes a

new frontier for this field due to an interplay between cavity coupling favouring ultralow-mass polariton formation(6) and exciton-electron interactions leading to polaron or trion formation(7,8). Here, we present cavity spectroscopy of gatetunable monolayer MoSe₂ (ref. 9) exhibiting strongly bound trion and polaron resonances, as well as non-perturbative coupling to a single microcavity mode(10,11). As the electron density is increased, the oscillator strength determined from the polariton splitting is gradually transferred from the higher-energy repulsive exciton-polaron resonance to the lower-energy attractive exciton-polaron state. Simultaneous observation of polariton formation in both attractive and repulsive branches indicates a new regime of polaron physics where the polariton impurity mass can be much smaller than that of the electrons. Our findings shed new light on optical response of semiconductors in the presence of free carriers by identifying the Fermi polaron nature of excitonic resonances and constitute a first step in investigation of a new class of degenerate Bose-Fermi mixtures(12,13).

71. Stationary Phonon Squeezing by Optical Polaron Excitation. By: Papenkort, T.; Axt, V. M.; Kuhn, T., Phys. Rev. Lett. **118**, 097401 (2017).

Abstract

We demonstrate that a stationary squeezed phonon state can be prepared by a pulsed optical excitation of a semiconductor quantum well. Unlike previously discussed scenarios for generating squeezed phonons, the corresponding uncertainties become stationary after the excitation and do not oscillate in time. The effect is caused by two-phonon correlations within the excited polaron. We demonstrate by quantum kinetic simulations and by a perturbation analysis that the energetically lowest polaron state comprises two-phonon correlations which, after the pulse, result in an uncertainty of the lattice momentum that is continuously lower than in the ground state of the semiconductor. The simulations show the dynamics of the polaron formation process and the resulting time-dependent lattice uncertainties.

72. Homogeneous Atomic Fermi Gases. By: Mukherjee, Biswaroop; Yan, Zhenjie; Patel, Parth B.; et al., Phys. Rev. Lett. **118**, 123401 (2017).

Abstract

We report on the creation of homogeneous Fermi gases of ultracold atoms in a uniform potential. In the momentum distribution of a spin-polarized gas, we observe the emergence of the Fermi surface and the saturated occupation of one particle per momentum state: the

striking consequence of Pauli blocking in momentum space for a degenerate gas. Cooling a spin-balanced Fermi gas at unitarity, we create homogeneous superfluids and observe spatially uniform pair condensates. For thermodynamic measurements, we introduce a hybrid potential that is harmonic in one dimension and uniform in the other two. The spatially resolved compressibility reveals the superfluid transition in a spin-balanced Fermi gas, saturation in a fully polarized Fermi gas, and strong attraction in the polaronic regime of a partially polarized Fermi gas.

73. Evidence for a Nematic Phase in $\text{La}_{1.75}\text{Sr}_{0.25}\text{NiO}_4$. By: Zhong, Ruidan; Winn, Barry L.; Gu, Genda; et al., Phys. Rev. Lett. **118**, 177601 (2017).|

Abstract

Determining the nature of electronic states in doped Mott insulators remains a challenging task. In the case of tetragonal $\text{La}_{2-x}\text{Sr}_x\text{NiO}_4$, the occurrence of diagonal charge and spin stripe order in the ground state is now well established. In contrast, the nature of the high-temperature "disordered" state from which the stripe order develops has long been a subject of controversy, with considerable speculation regarding a polaronic liquid. Following the recent detection of dynamic charge stripes, we use neutron scattering measurements on an $x = 0.25$ crystal to demonstrate that the dispersion of the charge-stripe excitations is anisotropic. This observation provides compelling evidence for the presence of electronic nematic order.

74. Visualizing the Efimov Correlation in Bose Polarons. By: Sun, Mingyuan; Zhai, Hui; Cui, Xiaoling, Phys. Rev. Lett. **119**, 013401 (2017).

75. Momentum-Resolved View of Electron-Phonon Coupling in Multilayer WSe₂. By: Waldecker, L.; Bertoni, R.; Huebener, H.; et al., Phys. Rev. Lett. **119**, 036803 (2017).

Abstract

We investigate the interactions of photoexcited carriers with lattice vibrations in thin films of the layered transition metal dichalcogenide (TMDC) WSe₂. Employing femtosecond electron diffraction with monocrystalline samples and first-principles density functional theory calculations, we obtain a momentum-resolved picture of the energy transfer from excited electrons to phonons. The measured momentum-dependent phonon population dynamics are compared to first-principles calculations of the phonon linewidth and can be rationalized

in terms of electronic phase-space arguments. The relaxation of excited states in the conduction band is dominated by intervalley scattering between Sigma valleys and the emission of zone boundary phonons. Transiently, the momentum-dependent electron-phonon coupling leads to a nonthermal phonon distribution, which, on longer time scales, relaxes to a thermal distribution via electron-phonon and phonon-phonon collisions. Our results constitute a basis for monitoring and predicting out of equilibrium electrical and thermal transport properties for nanoscale applications of TMDCs.

76. *Ultrafast Excited-State Dynamics of V3O5 as a Signature of a Photoinduced Insulator-Metal Phase Transition.*

By: Kumar, Nardeep; Rua, Armando; Lu, Junqiang; et al., Phys. Rev. Lett. **119**, 057602 (2017).

Abstract

The ultrafast elastic light scattering technique is applied to reveal the strong nonlinearity of V3O5 associated with a photoinduced insulator-metal phase transition. Observation of time-domain relaxation dynamics suggests several stages of structural transition. We discuss the nonequilibrium processes in V3O5 in terms of photoinduced melting of a polaronic Wigner crystal, coalescence of V-O octahedra, and photogeneration of acoustical phonons in the low-T and high-T phases of V3O5. A molecular dynamics computation supports experimentally observed stages of V3O5 relaxation dynamics.

77. *Correlation of Fe-Based Superconductivity and Electron-Phonon Coupling in an FeAs/Oxide Heterostructure.* By: Choi, Seokhwan; Johnston, Steven; Jang, Won-Jun; et al., Phys. Rev. Lett. **119**, 107003 (2017).

Abstract

Interfacial phonons between iron-based superconductors (FeSCs) and perovskite substrates have received considerable attention due to the possibility of enhancing preexisting superconductivity. Using scanning tunneling spectroscopy, we studied the correlation between superconductivity and e-ph interaction with interfacial phonons in an iron-based superconductor Sr2VO3FeAs (T-c approximate to 33 K) made of alternating FeSC and oxide layers. The quasiparticle interference measurement over regions with systematically different average superconducting gaps due to the e-ph coupling locally modulated by O vacancies in the VO2 layer, and supporting self-consistent momentum-dependent Eliashberg calculations pro-

vide a unique real-space evidence of the forward-scattering interfacial phonon contribution to the total superconducting pairing.

78. *Theory of Thermal Relaxation of Electrons in Semiconductors.*

By: Sadasivam, Sridhar; Chan, Maria K. Y.; Darancet, Pierre, Phys. Rev. Lett. **119**, 136602 (2017).

Abstract

We compute the transient dynamics of phonons in contact with high energy “hot” charge carriers in 12 polar and nonpolar semiconductors, using a first-principles Boltzmann transport framework. For most materials, we find that the decay in electronic temperature departs significantly from a single-exponential model at times ranging from 1 to 15 ps after electronic excitation, a phenomenon concomitant with the appearance of nonthermal vibrational modes. We demonstrate that these effects result from slow thermalization within the phonon subsystem, caused by the large heterogeneity in the time scales of electron-phonon and phonon-phonon interactions in these materials. We propose a generalized two-temperature model accounting for phonon thermalization as a limiting step of electron-phonon thermalization, which captures the full thermal relaxation of hot electrons and holes in semiconductors. A direct consequence of our findings is that, for semiconductors, information about the spectral distribution of electron-phonon and phonon-phonon coupling can be extracted from the multiexponential behavior of the electronic temperature.

79. *Charged Polaron Polaritons in an Organic Semiconductor Microcavity.*

By: Cheng, Chiao-Yu; Dhankar, Rijul; Gray, Christopher L. *et al.*, Phys. Rev. Lett. **120**, 017402 (2018).

Abstract

We report strong coupling between light and polaron optical excitations in a doped organic semiconductor microcavity at room temperature. Codepositing MoO₃ and the hole transport material 4, 4'-cyclohexylidenebis[N, N-bis(4-methylphenyl) benzenamine] introduces a large hole density with a narrow linewidth optical transition centered at 1.8 eV and an absorption coefficient exceeding 104 cm⁻¹. Coupling this transition to a Fabry-Perot cavity mode yields upper and lower polaron polariton branches that are clearly resolved in angle-dependent reflectivity with a vacuum Rabi splitting $\hbar\Omega(R) > 0.3$ eV. This result establishes a path to electrically control polaritons in organic semiconductors and may lead to increased polariton-

polariton Coulombic interactions that lower the threshold for nonlinear phenomena such as polariton condensation and lasing.

80. *Polaron Polaritons in the Integer and Fractional Quantum Hall Regimes.*

By: Ravets, Sylvain; Knuppel, Patrick; Faelt, Stefan, *et al.*, Phys. Rev. Lett. **120**, 057401 (2018).

Abstract

Elementary quasiparticles in a two-dimensional electron system can be described as exciton polarons since electron-exciton interactions ensures dressing of excitons by Fermi-sea electron-hole pair excitations. A relevant open question is the modification of this description when the electrons occupy flat bands and electron-electron interactions become prominent. Here, we perform cavity spectroscopy of a two-dimensional electron system in the strong coupling regime, where polariton resonances carry signatures of strongly correlated quantum Hall phases. By measuring the evolution of the polariton splitting under an external magnetic field, we demonstrate the modification of polaron dressing that we associate with filling factor dependent electron-exciton interactions.

81. *Bose Polarons at Finite Temperature and Strong Coupling.*

By: Guenther, Nils-Eric; Massignan, Pietro; Lewenstein, Maciej, *et al.*, Phys. Rev. Lett. **120**, 050405 (2018).

Abstract

A mobile impurity coupled to a weakly interacting Bose gas, a Bose polaron, displays several interesting effects. While a single attractive quasiparticle is known to exist at zero temperature, we show here that the spectrum splits into two quasiparticles at finite temperatures for sufficiently strong impurity-boson interaction. The ground state quasiparticle has minimum energy at T_c , the critical temperature for Bose-Einstein condensation, and it becomes overdamped when $T \gg T_c$. The quasiparticle with higher energy instead exists only below T_c , since it is a strong mixture of the impurity with thermally excited collective Bogoliubov modes. This phenomenology is not restricted to ultracold gases, but should occur whenever a mobile impurity is coupled to a medium featuring a gapless bosonic mode with a large population for finite temperature.

82. *Creation of Rydberg Polarons in a Bose Gas.*

By: Camargo, F.; Schmidt, R.; Whalen, J. D., *et al.*, Phys. Rev. Lett. **120**, 083401

(2018).

Abstract

We report spectroscopic observation of Rydberg polarons in an atomic Bose gas. Polarons are created by excitation of Rydberg atoms as impurities in a strontium Bose-Einstein condensate. They are distinguished from previously studied polarons by macroscopic occupation of bound molecular states that arise from scattering of the weakly bound Rydberg electron from ground-state atoms. The absence of a p-wave resonance in the low-energy electron-atom scattering in Sr introduces a universal behavior in the Rydberg spectral line shape and in scaling of the spectral width (narrowing) with the Rydberg principal quantum number, n . Spectral features are described with a functional determinant approach (FDA) that solves an extended Frohlich Hamiltonian for a mobile impurity in a Bose gas. Excited states of polyatomic Rydberg molecules (trimers, tetrameters, and pentamers) are experimentally resolved and accurately reproduced with a FDA.

83. *Bipolarons in a Bose-Einstein Condensate.*

By: Camacho-Guardian, A.; Ardila, L. A. Pena; Pohl, T.; *et al.*, Phys. Rev. Lett. **121**, 013401 (2018).

Abstract

Mobile impurities in a Bose-Einstein condensate form quasiparticles called polarons. Here, we show that two such polarons can bind to form a bound bipolaron state. Its emergence is caused by an induced nonlocal interaction mediated by density oscillations in the condensate, and we derive using field theory an effective Schrodinger equation describing this for an arbitrarily strong impurity-boson interaction. We furthermore compare with quantum Monte Carlo simulations finding remarkable agreement, which underlines the predictive power of the developed theory. It is found that bipolaron formation typically requires strong impurity interactions beyond the validity of more commonly used weak-coupling approaches that lead to local Yukawa-type interactions. We predict that the bipolarons are observable in present experiments, and we describe a procedure to probe their properties.

84. *Carrier Lifetimes and Polaronic Mass Enhancement in the Hybrid Halide Perovskite $\text{CH}_3\text{NH}_3\text{PbI}_3$ from Multiphonon Frohlich Coupling.*

By: Schlipf, Martin; Ponce, Samuel; Giustino, Feliciano, Phys. Rev. Lett. **121**, 086402 (2018).

Abstract

We elucidate the nature of the electron-phonon interaction in the archetypal hybrid perovskite $\text{CH}_3\text{NH}_3\text{PbI}_3$ using ab initio many-body calculations and an exactly solvable model. We demonstrate that electrons and holes near the band edges primarily interact with three distinct groups of longitudinal-optical vibrations, in order of importance: the stretching of the Pb-I bond, the bending of the Pb-I-Pb bonds, and the libration of the organic cations. These polar phonons induce ultrafast intraband carrier relaxation over timescales of 6-30 fs and yield polaron effective masses 28% heavier than the bare band masses. These findings allow us to rationalize previous experimental observations and provide a key to understanding carrier dynamics in halide perovskites.

85. *Electron-Phonon Systems on a Universal Quantum Computer.*

By: Macridin, Alexandru; Spentzouris, Panagiotis; Amundson, James; *et al.*, Phys. Rev. Lett. **121**, 110504 (2018).

Abstract

We present an algorithm that extends existing quantum algorithms for simulating fermion systems in quantum chemistry and condensed matter physics to include bosons in general and phonons in particular. We introduce a qubit representation for the low-energy subspace of phonons which allows an efficient simulation of the evolution operator of the electron-phonon systems. As a consequence of the Nyquist-Shannon sampling theorem, the phonons are represented with exponential accuracy on a discretized Hilbert space with a size that increases linearly with the cutoff of the maximum phonon number. The additional number of qubits required by the presence of phonons scales linearly with the size of the system. The additional circuit depth is constant for systems with finite-range electron-phonon and phonon-phonon interactions and linear for long-range electron-phonon interactions. Our algorithm for a Holstein polaron problem was implemented on an Atos quantum learning machine quantum simulator employing the quantum phase estimation method. The energy and the phonon number distribution of the polaron state agree with exact diagonalization results for weak, intermediate, and strong electron-phonon coupling regimes.

86. *Longitudinal Optical Phonons Modified by Organic Molecular Cation Motions in Organic-Inorganic Hybrid Perovskites.*

By: Nagai, Masaya; Tomioka, Takuya; Ashida, Masaaki; *et al.*, Phys. Rev. Lett. **121**,

145506 (2018).

Abstract

We performed terahertz time-domain spectroscopy for methylammonium (MA) lead halide perovskite single crystals and characterized the longitudinal optical (LO) phonons directly. We found that the effective LO phonon wave number does not change in the wide temperature range between 10 and 300 K. However, the coupling between MA cation modes and the LO phonon mode derived from lead halide cages induces a mode splitting at low temperatures and a damping of the LO phonon mode at high temperatures. These results influence the interpretation of electron-LO phonon interactions in perovskite semiconductors, as well as the interpretations of mobility, carrier diffusion, and polaron formation.

87. *Diagrammatic Monte Carlo Approach to Angular Momentum in Quantum Many-Particle Systems.*

By: Bighin, G.; Tscherbul, T., V; Lemeshko, M., Phys. Rev. Lett. **121**, 165301 (2018).

Abstract

We introduce a diagrammatic Monte Carlo approach to angular momentum properties of quantum many particle systems possessing a macroscopic number of degrees of freedom. The treatment is based on a diagrammatic expansion that merges the usual Feynman diagrams with the angular momentum diagrams known from atomic and nuclear structure theory, thereby incorporating the non-Abelian algebra inherent to quantum rotations. Our approach is applicable at arbitrary coupling, is free of systematic errors and of finite-size effects, and naturally provides access to the impurity Green function. We exemplify the technique by obtaining an all-coupling solution of the angulon model; however, the method is quite general and can be applied to a broad variety of systems in which particles exchange quantum angular momentum with their many-body environment.

88. *Spin Pumping Driven by Magnon Polarons.*

By: Hayashi, Hiroki; Ando, Kazuya, Phys. Rev. Lett. **121**, 237202 (2018)

Abstract

We report the observation of a resonant enhancement of spin pumping induced by magnon-phonon coupling at room temperature. We show that the spin pumping driven by microwave parametric excitation is enhanced, compared to its purely magnonic value, when

the microwave excites dipole-exchange magnons in the proximity of the intersection of the uncoupled magnon and phonon dispersions. This observation is consistent with a model of the spin pumping driven by hybridized magnon-phonon modes, magnon polarons, where the spin-pumping efficiency depends on the relative scattering strengths of the magnons and phonons in a magnetic insulator.

89. *Impurity-Induced Multibody Resonances in a Bose Gas*

By: Shi, Zhe-Yu; Yoshida, Shuhei M.; Parish, Meera M.; *et al.*, Phys. Rev. Lett. **121**, 243401 (2018)

Abstract

We investigate the problem of N identical bosons that are coupled to an impurity particle with infinite mass. For noninteracting bosons, we show that a dynamical impurity-boson interaction, mediated by a closed-channel dimer, can induce an effective boson-boson repulsion which strongly modifies the bound states consisting of the impurity and N bosons. In particular, we demonstrate the existence of two universal “multibody” resonances, where all multibody bound states involving any N emerge and disappear. The first multibody resonance corresponds to infinite impurity-boson scattering length, $a \rightarrow +\infty$, while the second corresponds to the critical scattering length $a^* > 0$ beyond which the trimer ($N = 2$ bound state) ceases to exist. Crucially, we show that the existence of a^* ensures that the ground-state energy in the multibody boundstate region, $\infty > a > a^*$, is bounded from below, with a bound that is independent of N . Thus, even though the impurity can support multibody bound states, they become increasingly fragile beyond the dimer state. This has implications for the nature of the Bose polaron currently being studied in cold-atom experiments.

90. *Light Bipolarons Stabilized by Peierls Electron-Phonon Coupling*

By: Sous, John; Chakraborty, Monodeep; Krems, Roman V.; *et al.*, Phys. Rev. Lett. **121**, 247001 (2018)

Abstract

It is widely accepted that phonon-mediated high-temperature superconductivity is impossible at ambient pressure, because of the very large effective masses of polarons or bipolarons at strong electron-phonon coupling. Here we challenge this belief by showing that strongly bound yet very light bipolarons appear for strong Peierls coupling. These bipolarons also exhibit many other unconventional properties; e.g., at strong coupling there are two low-

energy bipolaron bands that are stable against strong Coulomb repulsion. Using numerical simulations and analytical arguments, we show that these properties result from the specific form of the phonon-mediated interaction, which is of “pair hopping” instead of regular density-density type. This unusual effective interaction is bound to have nontrivial consequences for the superconducting state expected to arise at finite carrier concentrations and should favor a large critical temperature.

91. *Interplay between Adsorbates and Polarons: CO on Rutile TiO₂(110)*

By: Reticcioli, Michele; Sokolovic, Igor; Schmid, Michael; et al., Phys. Rev. Lett. **122**, 016805 (2019)

Abstract

Polaron formation plays a major role in determining the structural, electrical, and chemical properties of ionic crystals. Using a combination of first-principles calculations, scanning tunneling microscopy, and atomic force microscopy, we analyze the interaction of polarons with CO molecules adsorbed on the reduced rutile TiO₂(110) surface. Adsorbed CO shows attractive coupling with polarons in the surface layer, and repulsive interaction with polarons in the subsurface layer. As a result, CO adsorption depends on the reduction state of the sample. For slightly reduced surfaces, many adsorption configurations with comparable adsorption energies exist and polarons reside in the subsurface layer. At strongly reduced surfaces, two adsorption configurations dominate: either inside an oxygen vacancy, or at surface Ti-5c sites, coupled with a surface polaron. Similar conclusions are predicted for TiO₂(110) surfaces containing near-surface Ti interstitials. These results show that polarons are of primary importance for understanding the performance of polar semiconductors and transition metal oxides in catalysis and energy-related applications.

92. *Enhanced Superconducting State in FeSe/SrTiO₃ by a Dynamic Interfacial Polaron Mechanism*

By: Zhang, Shuyuan; Wei, Tong; Guan, Jiaqi; et al., Phys. Rev. Lett. **122**, 066802 (2019)

Abstract

The observation of substantially enhanced superconductivity of single-layer FeSe films on SrTiO₃ has stimulated intensive research interest. At present, conclusive experimental data on the corresponding electron-boson interaction is still missing. Here we use inelastic electron

scattering spectroscopy and angle resolved photoemission spectroscopy to show that the electrons in these systems are dressed by the strongly polarized lattice distortions of the SrTiO₃, and the indispensable nonadiabatic nature of such a coupling leads to the formation of dynamic interfacial polarons. Furthermore, the collective motion of the polarons results in a polaronic plasmon mode, which is unambiguously correlated with the surface phonons of SrTiO₃ in the presence of the FeSe films. A microscopic model is developed showing that the interfacial polaron-polaron interaction leads to the superconductivity enhancement.

93. *Boiling a Unitary Fermi Liquid*

By: Yan, Zhenjie; Patel, Parth B.; Mukherjee, Biswaroop; et al., , Phys. Rev. Lett. **122**, 093401 (2019)

Abstract

We study the thermal evolution of a highly spin-imbalanced, homogeneous Fermi gas with unitarity limited interactions, from a Fermi liquid of polarons at low temperatures to a classical Boltzmann gas at high temperatures. Radio-frequency spectroscopy gives access to the energy, lifetime, and short-range correlations of Fermi polarons at low temperatures T . In this regime, we observe a characteristic T^{-2} dependence of the spectral width, corresponding to the quasiparticle decay rate expected for a Fermi liquid. At high T , the spectral width decreases again towards the scattering rate of the classical, unitary Boltzmann gas, proportional to $T^{-1/2}$. In the transition region between the quantum degenerate and classical regime, the spectral width attains its maximum, on the scale of the Fermi energy, indicating the breakdown of a quasiparticle description. Density measurements in a harmonic trap directly reveal the majority dressing cloud surrounding the minority spins and yield the compressibility along with the effective mass of Fermi polarons.

94. *Antidoping in Insulators and Semiconductors Having Intermediate Bands with Trapped Carriers*

By: Liu, Qihang; Dalpian, Gustavo M.; Zunger, Alex, Phys. Rev. Lett. **122**, 106403 (2019)

Abstract

Ordinary doping by electrons (holes) generally means that the Fermi level shifts towards the conduction band (valence band) and that the conductivity of free carriers increases. Recently, however, some peculiar doping characteristics were sporadically recorded in dif-

ferent materials without noting the mechanism: electron doping was observed to cause a portion of the lowest unoccupied band to merge into the valence band, leading to a decrease in conductivity. This behavior, that we dub as “antidoping”, was seen in rare-earth nickel oxides SmNiO_3 , cobalt oxides $\text{SrCoO}_{2.5}$, Li-ion battery materials, and even MgO with metal vacancies. We describe the physical origin of antidoping as well as its inverse problem—the “design principles” that would enable an intelligent search of materials. We find that electron antidoping is expected in materials having preexisting trapped holes and is caused by the annihilation of such “hole polarons” via electron doping. This may offer an unconventional way of controlling conductivity.

95. *Ultrafast THz Probe of Photoinduced Polarons in Lead-Halide Perovskites*

By: Cinquanta, Eugenio; Meggiolaro, Daniele; Motti, Silvia G.; et al., Phys. Rev. Lett. **122**, 166601 (2019)

Abstract

We study the nature of photoexcited charge carriers in CsPbBr_3 nanocrystal thin films by ultrafast optical pump-THz probe spectroscopy. We observe a deviation from a pure Drude dispersion of the THz dielectric response that is ascribed to the polaronic nature of carriers; a transient blueshift of observed phonon frequencies is indicative of the coupling between photogenerated charges and stretching-bending modes of the deformed inorganic sublattice, as confirmed by DFT calculations.

96. *Quench Dynamics and Orthogonality Catastrophe of Bose Polarons*

By: Mistakidis, S., I.; Katsimiga, G. C.; Koutentakis, G. M.; et al., Phys. Rev. Lett. **122**, 183001 (2019)

Abstract

We monitor the correlated quench induced dynamical dressing of a spinor impurity repulsively interacting with a Bose-Einstein condensate. Inspecting the temporal evolution of the structure factor, three distinct dynamical regions arise upon increasing the interspecies interaction. These regions are found to be related to the segregated nature of the impurity and to the Ohmic character of the bath. It is shown that the impurity dynamics can be described by an effective potential that deforms from a harmonic to a double-well one when crossing the miscibility-immiscibility threshold. In particular, for miscible components the polaron formation is imprinted on the spectral response of the system. We further illustrate that for

increasing interaction an orthogonality catastrophe occurs and the polaron picture breaks down. Then a dissipative motion of the impurity takes place leading to a transfer of energy to its environment. This process signals the presence of entanglement in the many-body system.

97. *Observation of Coherent Multiorbital Polarons in a Two-Dimensional Fermi Gas*

By: Opong, N. Darkwah; Riegger, L.; Bettermann, O.; et al., Phys. Rev. Lett. **122**, 193604 (2019)

Abstract

We report on the experimental observation of multiorbital polarons in a two-dimensional Fermi gas of Yb-173 atoms formed by mobile impurities in the metastable P-3(0) orbital and a Fermi sea in the ground-state S-1(0) orbital. We spectroscopically probe the energies of attractive and repulsive polarons close to an orbital Feshbach resonance and characterize their coherence by measuring the quasiparticle residue. For all probed interaction parameters, the repulsive polaron is a long-lived quasiparticle with a decay rate more than 2 orders of magnitude below its energy. We formulate a many-body theory, which accurately treats the interorbital interactions in two dimensions and agrees well with the experimental results. Our work paves the way for the investigation of many-body physics in multiorbital ultracold Fermi gases.

98. *Polarons from First Principles, without Supercells*

By: Sio, Weng Hong; Verdi, Carla; Ponce, Samuel; et al., Phys. Rev. Lett. **122**, 246403 (2019)

Abstract

We develop a formalism and a computational method to study polarons in insulators and semiconductors from first principles. Unlike in standard calculations requiring large supercells, we solve a secular equation involving phonons and electron-phonon matrix elements from density-functional perturbation theory, in a spirit similar to the Bethe-Salpeter equation for excitons. We show that our approach describes seamlessly large and small polarons, and we illustrate its capability by calculating wave functions, formation energies, and spectral decomposition of polarons in LiF and Li₂O₂.

99. *Single Photons by Quenching the Vacuum*

By: Sanchez-Burillo, E.; Martin-Moreno, L.; Garcia-Ripoll, J. J.; et al., Phys. Rev.

Lett. **123**, 013601 (2019)

Abstract

Heisenberg's uncertainty principle implies that the quantum vacuum is not empty but fluctuates. These fluctuations can be converted into radiation through nonadiabatic changes in the Hamiltonian. Here, we discuss how to control this vacuum radiation, engineering a single-photon emitter out of a two-level system (2LS) ultrastrongly coupled to a finite-band waveguide in a vacuum state. More precisely, we show the 2LS nonlinearity shapes the vacuum radiation into a non-Gaussian superposition of even and odd cat states. When the 2LS bare frequency lays within the band gaps, this emission can be well approximated by individual photons. This picture is confirmed by a characterization of the ground and bound states, and a study of the dynamics with matrix-product states and polaron Hamiltonian methods.

100. *Polarons leave a trace*

By: Schauss, Peter, Science **365**, 218 (2019)

101. *Self-Trapping of Exciton-Polariton Condensates in GaAs Microcavities*

By: Ballarini, Dario; Chestnov, Igor; Caputo, Davide; et al. Phys. Rev. Lett. **123**, 047401 (2019)

Abstract

The self-trapping of exciton-polariton condensates is demonstrated and explained by the formation of a new polaronlike state. Above the polariton lasing threshold, local variation of the lattice temperature provides the mechanism for an attractive interaction between polaritons. Because of this attraction, the condensate collapses into a small bright spot. Its position and momentum variances approach the Heisenberg quantum limit. The self-trapping does not require either a resonant driving force or a presence of defects. The trapped state is stabilized by the phonon-assisted stimulated scattering of excitons into the polariton condensate. While the formation mechanism of the observed self-trapped state is similar to the Landau-Pekar polaron model, this state is populated by several thousands of quasiparticles, in a striking contrast to the conventional single-particle polaron state.

102. *Polaron Mobility in the “Beyond Quasiparticles” Regime*

By: Mishchenko, Andrey S.; Pollet, Lode; Prokof'ev, Nikolay, V; et al. Phys. Rev. Lett. **123**, 076601 (2019)

Abstract

In a number of physical situations, from polarons to Dirac liquids and to non-Fermi liquids, one encounters the “beyond quasiparticles” regime, in which the inelastic scattering rate exceeds the thermal energy of quasiparticles. Transport in this regime cannot be described by the kinetic equation. We employ the diagrammatic Monte Carlo method to study the mobility of a Frohlich polaron in this regime and discover a number of nonperturbative effects: a strong violation of the Mott-Ioffe-Regel criterion at intermediate and strong couplings, a mobility minimum at T similar to Ω in the strong-coupling limit (Ω is the optical mode frequency), a substantial delay in the onset of an exponential dependence of the mobility for $T < \Omega$ at intermediate coupling, and complete smearing of the Drude peak at strong coupling. These effects should be taken into account when interpreting mobility data in materials with strong electron-phonon coupling.

103. *Imaging magnetic polarons in the doped Fermi-Hubbard model*

By: Koepsell, Joannis; Vijayan, Jayadev; Sompet, Pimonpan; et al., *Nature* **572**, 358 (2019)

Abstract

Polarons-electronic charge carriers ‘dressed’ by a local polarization of the background environment-are among the most fundamental quasiparticles in interacting many-body systems, and emerge even at the level of a single dopant. In the context of the two-dimensional Fermi-Hubbard model, polarons are predicted to form around charged dopants in an antiferromagnetic background in the low-doping regime, close to the Mott insulating state; this prediction is supported by macroscopic transport and spectroscopy measurements in materials related to high-temperature superconductivity. Nonetheless, a direct experimental observation of the internal structure of magnetic polarons is lacking. Here we report the microscopic real-space characterization of magnetic polarons in a doped Fermi-Hubbard system, enabled by the single-site spin and density resolution of our ultracold-atom quantum simulator. We reveal the dressing of doublons by a local reduction-and even sign reversal-of magnetic correlations, which originates from the competition between kinetic and magnetic energy in the system. The experimentally observed polaron signatures are found to be consistent with an effective string model at finite temperature. We demonstrate that delocalization of the doublon is a necessary condition for polaron formation, by comparing this setting with

a scenario in which a doublon is pinned to a lattice site. Our work could facilitate the study of interactions between polarons, which may lead to collective behaviour, such as stripe formation, as well as the microscopic exploration of the fate of polarons in the pseudogap and ‘bad metal’ phases.

104. *Few Versus Many-Body Physics of an Impurity Immersed in a Superfluid of Spin 1/2 Attractive Fermions*

By: Pierce, M.; Leyronas, X.; Chevy, F. Phys. Rev. Lett. **123**, 080403 (2019)

Abstract

In this Letter we investigate the properties of an impurity immersed in a superfluid of strongly correlated spin 1/2 fermions and we calculate the beyond-mean-field corrections to the energy of a weakly interacting impurity. We show that these corrections are divergent and have to be regularized by properly accounting for three-body physics in the problem and that our approach naturally provides a unifying framework for Bose and Fermi polaron physics.

105. *Polaron imaging*

By: Li, Yun

NATURE PHYSICS Volume: 15 Issue: 9 Pages: 878-878 Published: SEP 2019

Abstract

Polarons are quasiparticles resulting from the coupling between a single impurity, usually an electronic charge carrier, and a surrounding bath of particles. The impurity repelling or attracting nearby particles modifies the background potential, which, in turn, affects the physical properties of the impurity. Although the presence of polarons has been inferred from macroscopic transport and spectroscopic measurements of various materials, their microscopic details, such as the internal structure, have never been confirmed experimentally. This goal has now been achieved by Joannis Koepsell and co-workers who have reported a direct observation of magnetic polarons in a doped Fermi–Hubbard system realized by an ultracold-atom quantum simulator. The full single-site spin and density resolution on the lattice allowed the tracking of a local distortion of the magnetic correlations upon impurity doping, yielding a kind of real-space image of the polaron. The authors were able to derive the size of the polaron based on the range within which the impurity retains its impact on the environment.

106. *Fundamental Limits to Coherent Photon Generation with Solid-State Atomlike Transitions*

By: Koong, Z. X.; Scerri, D.; Rambach, M.; et al.

PHYSICAL REVIEW LETTERS Volume: 123 Issue: 16 Article Number: 167402

Published: OCT 16 2019

Abstract

Coherent generation of indistinguishable single photons is crucial for many quantum communication and processing protocols. Solid-state realizations of two-level atomic transitions or three-level spin- Λ systems offer significant advantages over their atomic counterparts for this purpose, albeit decoherence can arise due to environmental couplings. One popular approach to mitigate dephasing is to operate in the weak-excitation limit, where the excited-state population is minimal and coherently scattered photons dominate over incoherent emission. Here we probe the coherence of photons produced using two-level and spin- Λ solid-state systems. We observe that the coupling of the atomlike transitions to the vibronic transitions of the crystal lattice is independent of the driving strength, even for detuned excitation using the spin- Λ configuration. We apply a polaron master equation to capture the non-Markovian dynamics of the vibrational manifolds. These results provide insight into the fundamental limitations to photon coherence from solid-state quantum emitters.

107. *Roton-Induced Bose Polaron in the Presence of Synthetic Spin-Orbit Coupling*

By: Wang, Jia; Liu, Xia-Ji; Hu, Hui

PHYSICAL REVIEW LETTERS Volume: 123 Issue: 21 Article Number: 213401

Published: NOV 19 2019

Abstract

We predict the existence of a roton-induced Bose polaron for an impurity immersed in a three-dimensional Bose-Einstein condensate with Raman-laser-induced spin-orbit coupling, where the condensate is in a finite-momentum plane-wave state with an intriguing roton minimum in its excitation spectrum. This novel polaron is formed by dressing the impurity with roton excitations, instead of phonon excitations as in a conventional (i.e., phonon-induced) Bose polaron, and acquires a significant center-of-mass momentum and highly anisotropic effective mass. We find that the roton-induced polaron evolves from a phonon-induced polaron, as the interaction between impurity and atoms increases across a Feshbach resonance. The

evolution is not smooth, and a first-order phase transition from a phonon- to roton-induced polaron is observed at a critical interaction strength.

108. *Topological Magnon-Phonon Hybrid Excitations in Two-Dimensional Ferromagnets with Tunable Chern Numbers*

By: Go, Gyungchoon; Kim, Se Kwon; Lee, Kyung-Jin

PHYSICAL REVIEW LETTERS Volume: 123 Issue: 23 Article Number: 237207

Published: DEC 5 2019

Abstract

We theoretically investigate magnon-phonon hybrid excitations in two-dimensional ferromagnets. The bulk bands of hybrid excitations, which are referred to as magnon polarons, are analytically shown to be topologically nontrivial, possessing finite Chern numbers. We also show that the Chern numbers of magnon-polaron bands and the number of band-crossing lines can be manipulated by an effective magnetic field. For experiments, we propose to use the thermal Hall conductivity as a probe of the finite Berry curvatures of magnon-polarons. Our results show that a simple ferromagnet on a square lattice supports topologically nontrivial magnon polarons, generalizing topological excitations in conventional magnetic systems.

109. *Spectroscopic Signatures of Quantum Many-Body Correlations in Polariton Microcavities*

By: Levinsen, Jesper; Marchetti, Francesca Maria; Keeling, Jonathan; et al.

PHYSICAL REVIEW LETTERS Volume: 123 Issue: 26 Article Number: 266401

Published: DEC 26 2019

Abstract

We theoretically investigate the many-body states of exciton polaritons that can be observed by pump-probe spectroscopy in high-Q inorganic microcavities. Here, a weak-probe "spin-down" polariton is introduced into a coherent state of "spin-up" polaritons created by a strong pump. We show that the down arrow impurities become dressed by excitations of the down arrow medium, and that they form new polaronic quasiparticles that feature two-point and three-point many-body quantum correlations that, in the low density regime, arise from coupling to the vacuum biexciton and triexciton states, respectively. In particular, we find that these correlations generate additional branches and avoided crossings in the down arrow optical transmission spectrum that have a characteristic dependence on the

up arrow-polariton density. Our results thus demonstrate a way to directly observe correlated many-body states in an exciton-polariton system that go beyond classical mean-field theories.

110. *Discovery of the soft electronic modes of the trimeron order in magnetite*

By: Baldini, Edoardo; Belvin, Carina A.; Rodriguez-Vega, Martin; et al.

NATURE PHYSICS Volume: 16 Issue: 5 Pages: 541-+ Published: MAY 2020

Abstract

Spectroscopic study of the low-energy excitations in magnetite Fe_3O_4 shows the signatures of its charge-ordered structure involved in the metal-insulator transition, whose building blocks are the three-site small polarons, termed trimerons.

The Verwey transition in magnetite (Fe_3O_4) is the first metal-insulator transition ever observed and involves a concomitant structural rearrangement and charge-orbital ordering. Owing to the complex interplay of these intertwined degrees of freedom, a complete characterization of the low-temperature phase of magnetite and the mechanism driving the transition have long remained elusive. It was demonstrated in recent years that the fundamental building blocks of the charge-ordered structure are three-site small polarons called trimerons. However, electronic collective modes of this trimeron order have not been detected to date, and thus an understanding of the dynamics of the Verwey transition from an electronic point of view is still lacking. Here, we discover spectroscopic signatures of the low-energy electronic excitations of the trimeron network using terahertz light. By driving these modes coherently with an ultrashort laser pulse, we reveal their critical softening and hence demonstrate their direct involvement in the Verwey transition. These findings shed new light on the cooperative mechanism at the origin of magnetite's exotic ground state.

111. *Unidirectional Charge Transport via Ripplonic Polarons in a Three-Terminal Microchannel Device*

By: Badrutdinov, A. O.; Rees, D. G.; Lin, J. Y.; et al.

PHYSICAL REVIEW LETTERS Volume: 124 Issue: 12 Article Number: 126803

Published: MAR 23 2020

Abstract

We study the transport of surface electrons on superfluid helium through a microchannel structure in which the charge flow splits into two branches, one flowing straight and one

turned at 90 degrees. According to Ohm's law, an equal number of charges should flow into each branch. However, when the electrons are dressed by surface excitations (ripples) to form polaronlike particles with sufficiently large effective mass, all the charge follows the straight path due to momentum conservation. This surface-wave induced transport is analogous to the motion of electrons coupled to surface acoustic waves in semiconductor 2DEGs.

112. *Polaron Photoconductivity in the Weak and Strong Light-Matter Coupling Regime*

By: Krainova, Nina; Grede, Alex J.; Tsokkou, Demetra; et al.

PHYSICAL REVIEW LETTERS Volume: 124 Issue: 17 Article Number: 177401

Published: APR 30 2020

Abstract

We investigate the potential for cavity-modified electron transfer in a doped organic semiconductor through the photocurrent that arises from exciting charged molecules (polarons). When the polaron optical transition is strongly coupled to a Fabry-Perot microcavity mode, we observe polaron polaritons in the photoconductivity action spectrum and find that their magnitude depends differently on applied electric field than photocurrent originating from the excitation of uncoupled polarons in the same cavity. Crucially, moving from positive to negative detuning causes the upper and lower polariton photocurrents to swap their field dependence, with the more polaronlike branch resembling that of an uncoupled excitation. These observations are understood on the basis of a phenomenological model in which strong coupling alters the Onsager dissociation of polarons from their dopant counterions by effectively increasing the thermalization length of the photoexcited charge carrier.

113. *Probing Nonequilibrium Dynamics of Photoexcited Polarons on a Metal-Oxide Surface with Atomic Precision*

By: Guo, Chaoyu; Meng, Xiangzhi; Fu, Huixia; et al.

PHYSICAL REVIEW LETTERS Volume: 124 Issue: 20 Article Number: 206801

Published: MAY 19 2020

Abstract

Understanding the nonequilibrium dynamics of photoexcited polarons at the atomic scale is of great importance for improving the performance of photocatalytic and solar-energy materials. Using a pulsed-laser-combined scanning tunneling microscopy and spectroscopy,

here we succeeded in resolving the relaxation dynamics of single polarons bound to oxygen vacancies on the surface of a prototypical photocatalyst, rutile TiO₂ (110). The visible-light excitation of the defect-derived polarons depletes the polaron states and leads to delocalized free electrons in the conduction band, which is further corroborated by ab initio calculations. We found that the trapping time of polarons becomes considerably shorter when the polaron is bound to two surface oxygen vacancies than that to one. In contrast, the lifetime of photogenerated free electrons is insensitive to the atomic-scale distribution of the defects but correlated with the averaged defect density within a nanometer-sized area. Those results shed new light on the photocatalytically active sites at the metal-oxide surface.

114. *Evidence of Large Polarons in Photoemission Band Mapping of the Perovskite Semiconductor CsPbBr₃*

By: Puppini, M.; Polishchuk, S.; Colonna, N.; et al.

PHYSICAL REVIEW LETTERS Volume: 124 Issue: 20 Article Number: 206402

Published: MAY 20 2020

Abstract

Lead-halide perovskite (LHP) semiconductors are emergent optoelectronic materials with outstanding transport properties which are not yet fully understood. We find signatures of large polaron formation in the electronic structure of the inorganic LHP CsPbBr₃ by means of angle-resolved photoelectron spectroscopy. The experimental valence band dispersion shows a hole effective mass of $0.26 \pm 0.02 m(e)$, 50% heavier than the bare mass $m(0) = 0.17 m(e)$ predicted by density functional theory. Calculations of the electron-phonon coupling indicate that phonon dressing of the carriers mainly occurs via distortions of the Pb-Br bond with a Frohlich coupling parameter $\alpha = 1.81$. A good agreement with our experimental data is obtained within the Feynman polaron model, validating a viable theoretical method to predict the carrier effective mass of LHPs ab initio.

115. *Dynamical Variational Approach to Bose Polarons at Finite Temperatures*

By: Dzsotjan, David; Schmidt, Richard; Fleischhauer, Michael

PHYSICAL REVIEW LETTERS Volume: 124 Issue: 22 Article Number: 223401

Published: JUN 2 2020

Abstract

We discuss the interaction of a mobile quantum impurity with a Bose-Einstein condensate

of atoms at finite temperature. To describe the resulting Bose polaron formation we develop a dynamical variational approach applicable to an initial thermal gas of Bogoliubov phonons. We study the polaron formation after switching on the interaction, e.g., by a radio-frequency (rf) pulse from a noninteracting to an interacting state. To treat also the strongly interacting regime, interaction terms beyond the Frohlich model are taken into account. We calculate the real-time impurity Green's function and discuss its temperature dependence. Furthermore we determine the rf absorption spectrum and find good agreement with recent experimental observations. We predict temperature-induced shifts and a substantial broadening of spectral lines. The analysis of the real-time Green's function reveals a crossover to a linear temperature dependence of the thermal decay rate of Bose polarons as unitary interactions are approached.

116. *Superfluid Flow of Polaron Polaritons above Landau's Critical Velocity*

By: Nielsen, K. Knakkegaard; Camacho-Guardian, A.; Bruun, G. M.; et al.

PHYSICAL REVIEW LETTERS Volume: 125 Issue: 3 Article Number: 035301 Published: JUL 14 2020

Abstract

We develop a theory for the interaction of light with superfluid optical media, describing the motion of quantum impurities that are created and dragged through the liquid by propagating photons. It is well known that a mobile impurity suffers dissipation due to phonon emission as soon as it moves faster than the speed of sound in the superfluid-Landau's critical velocity. Surprisingly we find that in the present hybrid light-matter setting, polaritonic impurities can be protected against environmental decoherence and be allowed to propagate well above the Landau velocity without jeopardizing the superfluid response of the medium.

117. *Vibrational Dressing in Kinetically Constrained Rydberg Spin Systems*

By: Mazza, Paolo P.; Schmidt, Richard; Lesanovsky, Igor

PHYSICAL REVIEW LETTERS Volume: 125 Issue: 3 Article Number: 033602 Published: JUL 14 2020

Abstract

Quantum spin systems with kinetic constraints have become paradigmatic for exploring collective dynamical behavior in many-body systems. Here we discuss a facilitated spin system which is inspired by recent progress in the realization of Rydberg quantum simulators. This

platform allows to control and investigate the interplay between facilitation dynamics and the coupling of spin degrees of freedom to lattice vibrations. Developing a minimal model, we show that this leads to the formation of polaronic quasiparticle excitations which are formed by many-body spin states dressed by phonons. We investigate in detail the properties of these quasiparticles, such as their dispersion relation, effective mass, and the quasiparticle weight. Rydberg lattice quantum simulators are particularly suited for studying this phonon-dressed kinetically constrained dynamics as their exaggerated length scales permit the site-resolved monitoring of spin and phonon degrees of freedom.

118. *Radio-Frequency Response and Contact of Impurities in a Quantum Gas*

By: Liu, Weizhe Edward; Shi, Zhe-Yu; Levinsen, Jesper; et al.

PHYSICAL REVIEW LETTERS Volume: 125 Issue: 6 Article Number: 065301 Published: AUG 5 2020

Abstract

We investigate the radio-frequency spectroscopy of impurities interacting with a quantum gas at finite temperature. In the limit of a single impurity, we show using Fermi's golden rule that introducing (or injecting) an impurity into the medium is equivalent to ejecting an impurity that is initially interacting with the medium, since the "injection" and "ejection" spectral responses are simply related to each other by an exponential function of frequency. Thus, the full spectral information for the quantum impurity is contained in the injection spectral response, which can be determined using a range of theoretical methods, including variational approaches. We use this property to compute the finite-temperature equation of state and Tan contact of the Fermi polaron. Our results for the contact of a mobile impurity are in excellent agreement with recent experiments and we find that the finite-temperature behavior is qualitatively different compared to the case of infinite impurity mass.

119. *Evidence of Rotational Frohlich Coupling in Polaronic Trions*

By: Trushin, Maxim; Sarkar, Soumya; Mathew, Sinu; et al.

PHYSICAL REVIEW LETTERS Volume: 125 Issue: 8 Article Number: 086803 Published: AUG 20 2020

Abstract

Electrons commonly couple through Frohlich interactions with longitudinal optical phonons to form polarons. However, trions possess a finite angular momentum and should therefore

couple instead to rotational optical phonons. This creates a polaronic trion whose binding energy is determined by the crystallographic orientation of the lattice. Here, we demonstrate theoretically within the Frohlich approach and experimentally by photoluminescence emission that the bare trion binding energy (20 meV) is significantly enhanced by the phonons at the interface between the two-dimensional semiconductor MoS₂ and the bulk transition metal oxide SrTiO₃. The low-temperature binding energy changes from 60 meV in [001]-oriented substrates to 90 meV for [111] orientation, as a result of the counterintuitive interplay between the rotational axis of the MoS₂ trion and that of the SrTiO₃ phonon mode.

120. *Large Polarons as Key Quasiparticles in SrTiO₃ and SrTiO₃-Based Heterostructures*

By: Geondzhian, Andrey; Sambri, Alessia; De Luca, Gabriella M.; et al.

PHYSICAL REVIEW LETTERS Volume: 125 Issue: 12 Article Number: 126401

Published: SEP 15 2020

Abstract

Despite its simple structure and low degree of electronic correlation, SrTiO₃(STO) features collective phenomena linked to charge transport and, ultimately, superconductivity, that are not yet fully explained. Thus, a better insight into the nature of the quasiparticles shaping the electronic and conduction properties of STO is needed. We studied the low-energy excitations of bulk STO and of the LaAlO₃/SrTiO₃ two-dimensional electron gas (2DEG) by Ti L-3 edge resonant inelastic x-ray scattering. In all samples, we find the hallmark of polarons in the form of intense dd + phonon excitations, and a decrease of the LO₃-mode electron-phonon coupling when going from insulating to highly conducting STO single crystals and heterostructures. Both results are attributed to the dynamic screening of the large polaron self-induced polarization, showing that the low-temperature physics of STO and STO-based 2DEGs is dominated by large polaron quasiparticles.

121. *Observation of the polaronic character of excitons in a two-dimensional semiconducting magnet CrI₃*

By: Jin, Wencan; Kim, Hyun Ho; Ye, Zhipeng; et al.

NATURE COMMUNICATIONS Volume: 11 Issue: 1 Article Number: 4780

Published: SEP 22 2020

Abstract

Exciton dynamics can be strongly affected by lattice vibrations through electron-phonon

coupling. This is rarely explored in two-dimensional magnetic semiconductors. Focusing on bilayer CrI_3 , we first show the presence of strong electron-phonon coupling through temperature-dependent photoluminescence and absorption spectroscopy. We then report the observation of periodic broad modes up to the 8th order in Raman spectra, attributed to the polaronic character of excitons. We establish that this polaronic character is dominated by the coupling between the charge-transfer exciton at 1.96eV and a longitudinal optical phonon at 120.6 cm^{-1} . We further show that the emergence of long-range magnetic order enhances the electron-phonon coupling strength by similar to 50% and that the transition from layered antiferromagnetic to ferromagnetic order tunes the spectral intensity of the periodic broad modes, suggesting a strong coupling among the lattice, charge and spin in two-dimensional CrI_3 . Our study opens opportunities for tailoring light-matter interactions in two-dimensional magnetic semiconductors.

122. *Quasiparticle Lifetime of the Repulsive Fermi Polaron*

By: Adlong, Haydn S.; Liu, Weizhe Edward; Scazza, Francesco; et al.

PHYSICAL REVIEW LETTERS Volume: 125 Issue: 13 Article Number: 133401

Published: SEP 24 2020

Abstract

We investigate the metastable repulsive branch of a mobile impurity coupled to a degenerate Fermi gas via short-range interactions. We show that the quasiparticle lifetime of this repulsive Fermi polaron can be experimentally probed by driving Rabi oscillations between weakly and strongly interacting impurity states. Using a time-dependent variational approach, we find that we can accurately model the impurity Rabi oscillations that were recently measured for repulsive Fermi polarons in both two and three dimensions. Crucially, our theoretical description does not include relaxation processes to the lower-lying attractive branch. Thus, the theory-experiment agreement demonstrates that the quasiparticle lifetime is dominated by many-body dephasing within the upper repulsive branch rather than by relaxation from the upper branch itself. Our findings shed light on recent experimental observations of persistent repulsive correlations, and have important consequences for the nature and stability of the strongly repulsive Fermi gas.

123. *Imaging Charge Localization in a Conjugated Oligophenylene*

By: Patera, Laerte L.; Queck, Fabian; Repp, Jascha

Published: OCT 23 2020

Abstract

Polaron formation in conjugated polymers has a major impact on their optical and electronic properties. In polyphenylene, the molecular conformation is determined by a delicate interplay between electron delocalization and steric effects. Injection of excess charges is expected to increase the degree of conjugation, leading to structural distortions of the chain. Here we investigated at the single-molecule level the role of an excess charge in an individual oligophenylene deposited on sodium chloride films. By combining sub-molecular-resolved atomic force microscopy with redox-state-selective orbital imaging, we characterize both structural and electronic changes occurring upon hole injection. While the neutral molecule exhibits a delocalized frontier orbital, for the cationic radical the excess charge is observed to localize, inducing a partial planarization of the molecule. These results provide direct evidence for self-trapping of the excess charge in oligophenylenes, shedding light on the interplay of charge localization and structural distortion.

124. *Perturbed Sachdev-Ye-Kitaev Model: A Polaron in the Hyperbolic Plane*

By: Lunkin, A., V; Kitaev, A. Yu; Feigel'man, M., V.

PHYSICAL REVIEW LETTERS Volume: 125 Issue: 19 Article Number: 196602

Published: NOV 3 2020

Abstract

We study the Sachdev-Ye-Kitaev (SYK4) model with a weak SYK2 term of magnitude Γ beyond the simplest perturbative limit considered previously. For intermediate values of the perturbation strength, $J/N \ll \Gamma \ll J/\sqrt{N}$, fluctuations of the Schwarzian mode are suppressed, and the SYK4 mean-field solution remains valid beyond the timescale $t(0)$ similar to N/J up to t^* similar to $\Gamma(2)$. The out-of-time-order correlation function displays at short time intervals exponential $2\pi T$, but its prefactor scales as T at low temperatures $T \ll \Gamma$.

-
- [1] L. D. Landau, *Phys. Z. Sowjetunion* **3**, 664 (1933) [English translation in *Collected Papers*, Gordon and Breach, New York, 1965, pp. 67-68].
- [2] S. I. Pekar, *Journal of Physics USSR* **10**, 341 (1946).
- [3] S. I. Pekar, *Zh. Eksper. Teor. Fiz.* **16**, 341 (1946).
- [4] J. T. Devreese, in *Lectures on the Physics of Highly Correlated Electron Systems VII*, edited A. Avella and F. Mancini Proceedings of the 7th Training Course in the Physics of Correlated Electron Systems&High-T_c Superconductors, Vietri sul Mare, Italy, October 14-16, 2002, AIP, Melville (2003), pp. 3 - 56.
- [5] H. Fröhlich, *Adv. Phys.* **3**, 325 (1954).
- [6] R. P. Feynman, R. B. Leiton and M. Sands, *The Feynman Lectures on Physics* (Addison-Wesley, 1972), Vol. II.
- [7] E. Kartheuser, in *Polarons in Ionic Crystals and Polar Semiconductors* edited J. T. Devreese, North-Holland, Amsterdam (1972), pp. 717 - 733.
- [8] M. Grynberg, S. Huant, G. Martinez, J. Kossut, T. Wojtowicz, G. Karczewski, J. M. Shi, F. M. Peeters, J. T. Devreese, *Phys. Rev. B* **54**, 1467 (1996).
- [9] The spectra of the infrared-active LO (and TO) phonons in α -Al₂O₃ (sapphire) contain six modes. The values of the LO and TO phonon frequencies and of the high-frequency dielectric constants $\epsilon_{\infty\parallel} = 3.072$, $\epsilon_{\infty\perp} = 3.077$ are taken from Ref. [10]. Using these parameters and the electron band mass $m_b = 0.25m_e$ as estimated in Ref. [11], the effective value of the electron-phonon coupling constant α in Al₂O₃ has been calculated as
- $$\alpha = \sum_j \alpha_j \left\langle \left(\mathbf{e}_j \cdot \frac{\mathbf{k}}{k} \right)^2 \right\rangle,$$
- where \mathbf{e}_j is the polarization vector of the j -th LO-phonon branch, \mathbf{k} is the phonon wave vector, $\langle \rangle$ denote the angular averaging, and the coupling constants α_j for each branch are obtained using the method [12]. The resulting value of the polaron coupling constant is $\alpha \approx 1.25$
- [10] M. Schubert, T. E. Tiwald, and C. M. Herzinger, *Phys. Rev. B* **61**, 8187 (2000).
- [11] J. Shan, F. Wang, E. Knoesel, M. Bonn, and T. F. Heinz, *Phys. Rev. Lett.* **90**, 247401 (2003).

- [12] S. N. Klimin, V. M. Fomin, and J. T. Devreese, *to be published*.
- [13] J. W. Hodby, G. P. Russell, F. Peeters, J. T. Devreese, and D. M. Larsen, *Phys. Rev. Lett.* **58**, 1471 (1987).
- [14] The spectra of the LO (and TO) phonons in α -SiO₂ contain ten modes. The values of the LO and TO phonon frequencies are taken from Refs. [15, 16]. Using these frequencies and the value $\varepsilon_\infty = 2.40$ from Ref. [17] for the high-frequency dielectric constant, the effective value of the electron-phonon coupling constant α in SiO₂ has been calculated using the method of Ref. [12] as indicated in Ref. [9]. We use the estimated value of the electron band mass $m_b = 0.5m_e$ as in Refs. [18–20]. The resulting value of the polaron coupling constant is $\alpha \approx 1.59$.
- [15] F. Gervais and B. Piriou, *Phys. Rev. B* **11**, 3944 (1975).
- [16] J. L. Duarte, J. A. Sanjurjo, and R. S. Katiyar, *Phys. Rev. B* **36**, 3368 (1987).
- [17] S. T. Pantelides and W. A. Harrison, *Phys. Rev. B* **13**, 2667 (1976).
- [18] M. V. Fischetti, D. J. DiMaria, L. Dori, J. Batey, E. Tierney, and J. Stasiak, *Phys. Rev. B* **35**, 4404 (1987).
- [19] D. Arnold, E. Cartier, and D. J. DiMaria, *Phys. Rev. B* **49**, 10278 (1994).
- [20] P. Martin, S. Guizard, Ph. Daguzan, G. Petite, P. D'Oliveira, P. Meynadier, and M. Perdrix, *Phys. Rev. B* **55**, 5799 (1997).
- [21] I. Biaggio, R. W. Hellwarth, and J. P. Partanen, *Phys. Rev. Lett.* **78**, 891 (1997) (for $m_b/m_e = 2$).
- [22] G. Verbist, F. M. Peeters, and J. T. Devreese, *Ferroelectrics*, **130**, 27 (1992) (for $m_b/m_e = 2.6$).
- [23] S. I. Pekar, *Issledovaniya po Ekelectronnoj Teorii Kristallov*, Gostekhizdat, Moskva, 1951 (in Russian) [German translation: *Untersuchungen über die Elektronentheorie der Kristalle*, Akademie Verlag, Berlin, 1951].
- [24] G. C. Kuper and G. D. Whitfield (eds.), *Polarons and Excitons*, Oliver and Boyd, Edinburgh, 1963.
- [25] J. Appel, in *Solid State Physics*, edited by F. Seitz, D. Turnbull, and H. Ehrenreich, Academic Press, New York, 1968, vol. 21, pp. 193-391.
- [26] J. T. Devreese (ed.), *Polarons in Ionic Crystals and Polar Semiconductors*, North-Holland, Amsterdam, 1972.

- [27] T. K. Mitra, A. Chatterjee, and S. Mukhopadhyay, *Phys. Rep.* **153**, 91 (1987).
- [28] J. T. Devreese, in *Encyclopedia of Applied Physics*, edited by G. L. Trigg, VCH, Weinheim, 1996, vol. 14, pp. 383 - 413.
- [29] A. S. Alexandrov and Sir Nevill Mott, *Polarons and Bipolarons*, World Scientific, Singapore, 1996.
- [30] A. S. Mishchenko, N. V. Prokof'ev, A. Sakamoto, and B. V. Svistunov, *Phys. Rev. B* **62**, 6317 (2000).
- [31] T. D. Lee, F. E. Low, and D. Pines, *Phys. Rev.* **90**, 297 (1953).
- [32] J. Röseler, *Phys. Stat. Sol.(b)* **25**, 311 (1968)
- [33] M. A. Smondyrev, *Teor. Math. Fiz.* **68**, 29 (1986) [English translation: *Theor. Math. Phys.* **68**, 653 (1986)]
- [34] O. V. Selyugin and M. A. Smondyrev, *Phys. Stat. Sol.(b)*
- [35] L. D. Landau and S. I. Pekar, *Zh. Eksper. Teor. Fiz.* **18**, 419 (1948)
- [36] N. N. Bogolubov and S. V. Tyablikov, *Zh. Eksp. i Teor. Fiz.* **19**, 256 (1949)
- [37] N. N. Bogolubov, *Ukr. Matem. Zh.* **2**, 3 (1950)
- [38] S. V. Tyablikov, *Zh. Eksp. i Theor. Phys.* **21**, 377 (1951)
- [39] R. Evrard, *Phys. Letters* **14**, 295 (1965)
- [40] S. J. Miyake, *J. Phys. Soc. Japan* **38**, 181 (1975)
- [41] J. T. Devreese and R. Evrard, *Phys. Letters* **11**, 278 (1964).
- [42] E. Kartheuser, R. Evrard, and J. Devreese, in *Optical Properties of Solids*, edited by E. D. Haidemenakis, Gordon and Breach, New York, 1970, pp. 433-459 (Table 1).
- [43] R. P. Feynman, *Phys. Rev.* **97**, 660 (1955).
- [44] J. T. Devreese and R. Evrard, in *Proceedings of the British Ceramic Society* **10**, 151 (1968).
- [45] J. T. Titantah, C. Pierleoni, and S. Ciuchi, *Phys. Rev. Lett.* **87**, 206406 (2001).
- [46] G. De Filippis, V. Cataudella, V. Marigliano Ramaglia, C. A. Perroni, and D. Bercioux, *Eur. Phys. J. B* **36**, 65 (2003).
- [47] R. P. Feynman, R. W. Hellwarth, C. K. Iddings, and P. M. Platzman, *Phys. Rev.* **127**, 1004 (1962).
- [48] K. K. Thornber and R. P. Feynman, *Phys. Rev. B* **1**, 4099 (1970)
- [49] E. Kartheuser, R. Evrard, and J. Devreese, *Phys. Rev. Lett.* **22**, 94 (1969).
- [50] J. T. Devreese, J. De Sitter, and M. Goovaerts, *Phys. Rev. B* **5**, 2367 (1972)

- [51] F. M. Peeters and J. T. Devreese *Phys. Rev. B* **34**, 7246 (1986).
- [52] V. Cataudella, G. De Filippis, and G. Iadonisi, *Eur. Phys. J. B* **12**, 17 (1999).
- [53] J. Tempere and J. T. Devreese, *Phys. Rev. B* **64**, 104504 (2001).
- [54] J. Devreese, R. Evrard, and E. Kartheuser, *Phys. Rev. B* **12** 3353 (1975).
- [55] W. Becker, B. Gerlach, H. Schliffke, *Phys. Rev. B* **28**, 5735 (1983).
- [56] F. M. Peeters, J. T. Devreese, *Phys. Rev. B* **31**, 6826 (1985).
- [57] Y. Osaka, *Prog. Theor. Phys.* **22**, 437 (1959).
- [58] J. T. Devreese, *Contribution to the polaron theory*, Ph.D. Thesis, KU Leuven, 1964.
- [59] J. T. Devreese and R. Evrard, in *Proceedings of the British Ceramic Society* **10**, 151 (1968).
Reprinted in: *Path Integrals and Their Applications in Quantum, Statistical, and Solid State Physics*, edited by G. J. Papadopoulos and J. T. Devreese, NATO ASI Series B, Physics, vol. 34, Plenum, New York, 1977, pp. 344-357.
- [60] F. M. Peeters and J. T. Devreese, in *Solid State Physics*, edited by F. Seitz and D. Turnbull, Academic Press, New York, 1984, vol. 38, pp. 81 - 133.
- [61] H. Fröhlich, *Proc. R. Soc. (London) Ser. A* **160**, 230 (1937).
- [62] D. J. Howarth and E. H. Sondheimer, *Proc. R. Soc. (London) Ser. A* **219**, 53 (1953).
- [63] Y. Osaka, *Progr. Theoret. Phys.* **25**, 517 (1961).
- [64] F. E. Low and D. Pines, *Phys. Rev.* **98**, 414 (1955).
- [65] L. P. Kadanoff, *Phys. Rev.* **130**, 1364 (1963).
- [66] D. C. Langreth and L. P. Kadanoff, *Phys. Rev.* **133**, A1070 (1964).
- [67] F.M. Peeters, J.T. Devreese, *Phys. Stat. Sol. (b)* **115**, 539 (1983).
- [68] R. W. Hellwarth and I. Biaggio, *Phys. Rev. B* **60**, 299 (1999).
- [69] F. C. Brown, in *Point Defects in Solids*, edited by J. H. Crawford and L. M. Slifkin, Plenum, New York, 1972, vol. 1, p. 537.
- [70] E. Hendry, F. Wang, J. Shan, T. F. Heinz, and M. Bonn, *Phys. Rev. B* **69**, 081101(R) (2004).
- [71] V. L. Gurevich, I. G. Lang, and Yu. A. Firsov, *Fiz. Tverd. Tela* **4**, 1252 (1962) [English translation: *Sov. Phys. — Solid St.* **4**, 918 (1962)].
- [72] G. D. Mahan, *Many-Particle Physics*, Kluwer/Plenum, New York, 2000.
- [73] J. Devreese, W. Huybrechts, and L. Lemmens, *Phys. Stat. Sol. (b)* **48**, 77 (1971).
- [74] H. Finkenrath, N. Uhle, and W. Waidelich, *Solid State Commun.* **7**, 11 (1969).
- [75] M. J. Goovaerts, J. De Sitter, and J. T. Devreese, *Phys. Rev.* **7**, 2639 (1973).

- [76] F. M. Peeters and J. T. Devreese, *Phys. Rev. B* **28**, 6051 (1983).
- [77] D. Forster, *Hydrodynamic Fluctuations, Broken Symmetry and Correlation Functions*, Benjamin, New York, 1975.
- [78] F. M. Peeters and J. T. Devreese, *Phys. Rev. B* **23**, 1936 (1981).
- [79] A. S. Mishchenko, N. Nagaosa, N. V. Prokof'ev, A. Sakamoto, and B. V. Svistunov, *Phys. Rev. Lett.* **91**, 236401 (2003).
- [80] W. Huybrechts and J.T. Devreese, *Phys. Rev. B* **8**, 5754 (1973).
- [81] D. M. Eagles, R. P. S. M. Lobo, and F. Gervais, *Phys. Rev. B* **52**, 6440 (1995).
- [82] J. T. Devreese, L. Lemmens, and J. Van Royen, *Phys. Rev. B* **15**, 1212 (1977).
- [83] L. F. Lemmens, J. De Sitter, and J. T. Devreese, *Phys. Rev. B* **8**, 2717 (1973).
- [84] F. M. Peeters, Wu Xiaoguang, J. T. Devreese, *Phys. Rev. B* **33**, 3926 (1986).
- [85] Wu Xiaoguang, F. M. Peeters, J. T. Devreese, *Phys. Rev. B* **31**, 3420 (1985).
- [86] F. M. Peeters, J. T. Devreese, *Phys. Rev. B* **36**, 4442 (1987).
- [87] F. M. Peeters, J. T. Devreese, *Phys. Rev. B* **28**, 6051 (1983).
- [88] J. T. Devreese, L. F. Lemmens, J. Van Royen, *Phys. Rev. B* **2**, 1212 (1977).
- [89] F. M. Peeters, J. T. Devreese, *Solid State Phys.* **38**, 81 (1984).
- [90] F. Brosens, S. N. Klimin, and J. T. Devreese, *Phys. Rev. B* **77**, 085308 (2008).
- [91] L. F. Lemmens, J. T. Devreese, and F. Brosens, *Phys. Stat. Sol. (b)* **82**, 439 (1977).
- [92] S. Lupi, P. Maselli, M. Capizzi, P. Calvani, P. Giura and P. Roy, *Phys. Rev. Lett.* **83**, 4852 (1999).
- [93] Ch. Hartinger, F. Mayr, J. Deisenhofer, A. Loidl, and T. Kopp, *Phys. Rev. B* **69**, 100403(R) (2004).
- [94] Ch. Hartinger, F. Mayr, A. Loidl, and T. Kopp, cond-mat/0406123.
- [95] D. Emin, *Phys. Rev. B* **48**, 13691 (1993).
- [96] G. P. Zhang, T. A. Callcott, G. T. Woods, L. Lin, B. Sales, D. Mandrus, and J. He, *Phys. Rev. Lett.* **88**, 077401 (2002).
- [97] T. Hotta, *Phys. Rev. B* **67**, 104428 (2003).
- [98] S. N. Klimin, V. M. Fomin, F. Brosens, and J. T. Devreese, *Phys. Rev. B* **69**, 235324 (2004).
- [99] L. F. Lemmens, F. Brosens, and J. T. Devreese, *Phys. Rev. E* **53**, 4467 (1996).
- [100] J. T. Devreese, S. N. Klimin, V. M. Fomin, and F. Brosens, *Solid State Communications* **114**, 305 (2000).

- [101] F. Brosens, J. T. Devreese, and L. F. Lemmens, Phys. Rev. E **55**, 227 (1997); **55**, 6795 (1997); **58**, 1634 (1998).
- [102] L. F. Lemmens, F. Brosens, and J. T. Devreese, Solid State Communications **109**, 615 (1999).
- [103] G. De Filippis, V. Cataudella and G. Iadonisi, Eur. Phys. J. B **8**, 339 (1999).
- [104] W.B. da Costa, N. Studart, Phys. Rev. B **47**, 6356 (1993).
- [105] F. Brosens, S. N. Klimin, and J. T. Devreese, Phys. Rev. B **71**, 214301 (2005).
- [106] S. N. Klimin, V. M. Fomin, F. Brosens, and J. T. Devreese, Physica E **22**, 494 (2004).
- [107] J. T. Devreese, in: *Fluctuating Paths and Fields* (World Scientific, Singapore, 2001), pp. 289-304.
- [108] G. Verbist, F. M. Peeters and J. T. Devreese, Phys. Rev. B **43**, 2712 (1991).
- [109] M. A. Smondyrev, G. Verbist, F. M. Peeters, and J. T. Devreese, Phys. Rev. B **47**, 2596 (1993).
- [110] N. I. Kashirina, V. D. Lakhno, and V. V. Sychyov, Phys. Stat. Sol. (b) **239**, 174 (2003).
- [111] J. Tempere, S. N. Klimin, I. F. Silvera, J. T. Devreese, Eur. Phys. J. **32**, 329 (2003).
- [112] A.P. Volodin, M.S. Khaikin, and V.S. Edelman, JETP Lett. **26**, 543 (1977); U. Albrecht and P. Leiderer, Europhys. Lett. **3**, 705 (1987).
- [113] V.B. Shikin, JETP Lett. **27**, 39 (1978); M.M. Salomaa and G.A. Williams, Phys. Rev. Lett. **47**, 1730 (1981).
- [114] I.F. Silvera, Bull. Am. Phys. Soc. **46**, 1016 (2001).
- [115] J. Tempere, I.F. Silvera, and J.T. Devreese, Phys. Rev. Lett. **87**, 275301 (2001).
- [116] S. Fratini and P. Quémerais, Eur. Phys. J. B **14**, 99 (2000).
- [117] F. Lindemann, Z. Phys. **11**, 609 (1910); C.M. Care and N.H. March, Adv. Phys. **24**, 101 (1975).
- [118] C.C. Grimes and G. Adams, Phys. Rev. Lett. **42**, 795 (1979).
- [119] V.M. Bedanov and F.M. Peeters, Phys. Rev. B **49**, 2667 (1994).
- [120] L.P. Gor'kov and D.M. Chernikova, Pis'ma Zh. Eksp. Teor. Fiz. **18**, 119 (1973) [JETP Lett. **18**, 68 (1973)].
- [121] J. Tempere, I.F. Silvera, and J.T. Devreese, Phys. Rev. B **67**, 035402 (2003).
- [122] D.S. Fisher, B.I. Halperin, and P.M. Platzman, Phys. Rev. Lett. **42**, 798 (1979).
- [123] G. Deville *et al.*, Phys. Rev. Lett. **53**, 588 (1984).
- [124] S. N. Klimin and J. T. Devreese (*to be published*).

- [125] J. T. Devreese and A. S. Alexandrov, Rep. Prog. Phys. **72**, 066501 (2009); A. S. Alexandrov and J. T. Devreese, *Advances in Polaron Physics* (Springer, 2009).
- [126] B. E. Sernelius, Phys. Rev. B **48**, 7043 (1993).
- [127] G. De Filippis, V. Cataudella, A. S. Mishchenko, C. A. Perroni, and J. T. Devreese, Phys. Rev. Lett. **96**, 136405 (2006).
- [128] G. R. Allcock, in *Polarons and Excitons*, edited by C. G. Kuper and G. D. Whitfield (Oliver and Boyd, Edinburgh, 1963), pp. 45 – 70.
- [129] M. Born and K. Huang, *Dynamical theory of crystal lattices* (Oxford University Press, 2007).
- [130] Yu. E. Perlin, Sov. Physics. Uspekhi. **6**, 542 (1964).
- [131] H. Jahn and E. Teller, Proc. R. Soc. London A **161**, 220 (1937).
- [132] H. Kleinert, *Path Integrals in Quantum Mechanics, Statistics, Polymer Physics, and Financial Markets* (5th edition, World Scientific, Singapore 2009).
- [133] V. M. Fomin, V. N. Gladilin, J. T. Devreese, E. P. Pokatilov, S. N. Balaban, and S. N. Klimin, Phys. Rev. B **57**, 2415 (1998).
- [134] E. N. Myasnikov, A. E. Myasnikova, and Z. P. Mastropas, Physics of the Solid State **48**, 1046 (2006).
- [135] H. Spohn, Phys. Rev. B **33**, 8906 (1986); Ann. Phys. **175**, 278 (1987).
- [136] G. Wellein, H. Röder, and H. Fehske, Phys. Rev. B **53**, 9666 (1996).
- [*] This work was presented at the 10th International Conference “Path Integrals – 2010”, July 11 – 16, 2010, Washington DC, USA.
- [138] N. N. Bogoliubov and N. N. Bogoliubov, Jr., *Some Aspects of Polaron Theory*. In: *Lecture Notes in Physics* vol. 4, World Scientific, Singapore (1988).
- [139] K. Yamazaki, J. Phys. A **16**, 3675 (1983).
- [140] V. Cataudella, G. De Filippis, and C. A. Perroni, in *Polarons in Advanced Materials*, Springer Series in Materials Science , Vol. 103, Edited by A. S. Alexandrov (Canopus and Springer, Bath, UK, 2007), pp. 149 – 189.
- [141] J. T. Devreese and F. Brosens, Phys. Rev. B **45**, 6459 (1992).
- [142] Y. Lépine and M. Charbonneau, Phys. Status Solidi B **122**, 151 (1984); Y. Frongillo and Y. Lépine, Phys. Rev. B **40**, 3570 (1989).
- [143] J. T. Devreese and F. Brosens, Phys. Stat. Sol. (b) **108**, K29 (1981).
- [144] T. D. Schultz, Phys. Rev. **116**, 596 (1959).

- [145] J. T. Devreese and R. Evrard, *Phys. Stat. Sol. (b)* **78**, 85 (1976).
- [146] J. T. Devreese, R. Evrard, and E. Kartheuser, *Phys. Stat. Sol. (b)* **90**, K73 (1978).
- [147] J. T. Devreese and R. Evrard, in: *Linear and Nonlinear Electron Transport in Solids* (Plenum Press, New York, 1978).
- [148] F. Brosens and J. T. Devreese, *Phys. Stat. Sol. (b)* **111**, 591 (1982).
- [149] G. E. Volovik, V. I. Melnikov, and V. M. Edelshtein, *JETP Letters* **18**, 138 (1973).
- [150] K. K. Thornber, *Phys. Rev. B* **3**, 1929 (1971).
- [151] V. F. Los, *Theor. and Math. Phys.* **60**, 703 (1984).
- [152] S. A. Sokolovsky, *Theoretical and Mathematical Physics*, **168**, 1150 (2011).
- [153] D. Sels and F. Brosens, *Phys. Rev. E* **89**, 012124 (2014).
- [154] D. Sels, F. Brosens, and W. Magnus, *Physica A* **392**, 326 (2013).
- [155] D. Sels and F. Brosens, *Phys. Rev. E* **88**, 042101 (2013).
- [156] H. Fröhlich and N. F. Mott, *Proc. R. Soc. London, Ser. A* **171**, 496 (1939).
- [157] B. I. Davydov and I. M. Shmushkevich, *Uspekhi Fiz. Nauk* **24**, 21 (1940).
- [158] A. Anselm, *Introduction to Semiconductor Theory* (English translation: Prentice Hall, 1981).
- [159] G. De Filippis, V. Cataudella, A. de Candia, A. S. Mishchenko, and N. Nagaosa, *Phys. Rev. B* **90**, 014310 (2014).

10th edition

Fröhlich Polarons

Lecture course including detailed theoretical derivations

Jozef T. L. Devreese

*Theory of Quantum and Complex Systems (TQC), Universiteit Antwerpen,
Universiteitsplein, 1, B-2610 Antwerpen, Belgium*

Abstract

Based on a course presented by the author at the International School of Physics Enrico Fermi, CLXI Course, "Polarons in Bulk Materials and Systems with Reduced Dimensionality", Varenna, Italy, 21.6. - 1.7.2005, including further developments since 2005.

In the present course, an overview is presented of the fundamentals of continuum-polaron physics, which provide the basis of the analysis of polaron effects in ionic crystals and polar semiconductors. These Lecture Notes deal with "large", or "continuum", polarons, as described by the Fröhlich Hamiltonian. The emphasis is on the polaron optical absorption, with detailed mathematical derivations.

Appendix A treats optical conductivity of a strong-coupling polaron.

Appendix B considers Feynman's path-integral polaron treatment approached using time-ordered operator calculus.

Appendix C is devoted to the many-body large polaron optical conductivity in Nb doped strontium titanate.

Appendix D contains summary of the present state of the problem of the polaron mobility.

Appendix E represents the all-coupling analytic description for the optical conductivity of the Fröhlich polaron.

Appendix F represents the solution of the large polaron Fröhlich Hamiltonian obtained via the Diagrammatic Monte Carlo method.

Appendix G lists recent publications on Fröhlich polarons in Nature, Science and Physical Review Letters appeared from 2005 to 2020.

Theory of Quantum- and Complex Systems

Departement Fysica

Universiteit Antwerpen

November 2020

©TQC – Departement Fysica – Universiteit Antwerpen / JTL Devreese

Printed in Belgium

Tenth edition (2020)

An electronic version of this manuscript is available on <http://arxiv.org> (Cornell University / Los Alamos National Laboratory): arXiv: 1611.06122